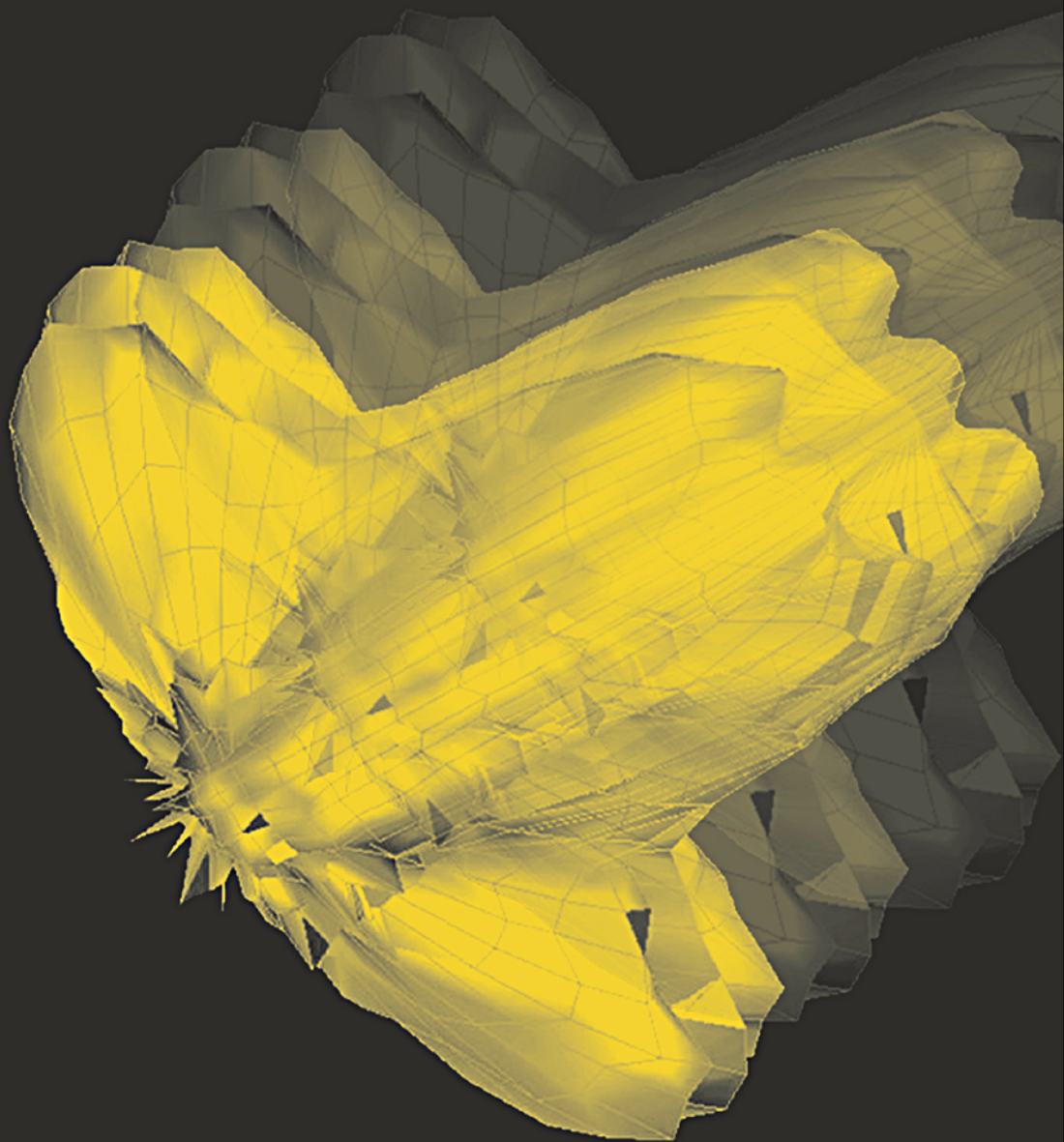


Acoustic Absorbers and Diffusers

Theory, Design and Application Trevor J. Cox and Peter D'Antonio



**Also available as a printed book
see title verso for ISBN details**

Acoustic Absorbers and Diffusers

Also available from Taylor & Francis

Understanding Active Noise Cancellation

Colin Hansen

Hb: 0-415-23191-4; Pb: 0-415-23192-2

Taylor & Francis

Room Acoustics

Heinrich Kuttruff

Hb: 0-419-24580-4

Taylor & Francis

Fundamentals of Sound and Vibration

Frank Faby and John Walker

Hb: 0-419-24180-9; Pb: 0-419-22700-8

Taylor & Francis

Active Control of Noise and Vibration

Colin Hansen and Scott Snyder

Hb: 0-419-19390-1

Taylor & Francis

Sound Reinforcement Engineering

Wolfgang Ahnert and Frank Steffen

Hb: 0-415-23870-6

Taylor & Francis

Information and ordering details

For price availability and ordering visit our website www.ergonomicsarena.com

Alternatively our books are available from all good bookshops.

Acoustic Absorbers and Diffusers

Theory, design and application

Trevor J. Cox

University of Salford, UK

and

Peter D'Antonio

RPG Diffusor Systems Inc., USA



Spon Press
Taylor & Francis Group

LONDON AND NEW YORK

First published 2004
by Spon Press
11 New Fetter Lane, London EC4P 4EE

Simultaneously published in the USA and Canada
by Spon Press
29 West 35th Street, New York, NY 10001

This edition published in the Taylor & Francis e-Library, 2005.

“To purchase your own copy of this or any of Taylor & Francis or Routledge’s collection of thousands of eBooks please go to www.eBookstore.tandf.co.uk.”

Spon Press is an imprint of the Taylor & Francis Group

© 2004 Trevor Cox and Peter D’Antonio

All rights reserved. No part of this book may be reprinted or reproduced or utilised in any form or by any electronic, mechanical, or other means, now known or hereafter invented, including photocopying and recording, or in any information storage or retrieval system, without permission in writing from the publishers.

British Library Cataloguing in Publication Data

A catalogue record for this book is available
from the British Library

Library of Congress Cataloging in Publication Data

A catalog record for this book has been requested

ISBN 0-203-49299-4 Master e-book ISBN

ISBN 0-203-57215-7 (Adobe eReader Format)

ISBN 0-415-29649-8 (Print edition)

To our families and Manfred Schroeder

Contents

<i>Preface</i>	xiv
<i>Acknowledgements</i>	xviii
<i>Glossary of frequently used symbols</i>	xix
Introduction	1
1 Applications and basic principles of absorbers	6
1.1 Reverberation control	6
1.1.1 A statistical model of reverberation	7
1.2 Noise control in factories and large rooms with diffuse fields	11
1.3 Modal control in critical listening spaces	12
1.4 Echo control in auditoria and lecture theatres – basic sound propagation models	13
1.4.1 Sound propagation – a wave approach	15
1.4.2 Impedance, admittance, reflection factor and absorption	16
1.5 Absorption in sound insulation – transfer matrix modelling	18
1.5.1 Transfer matrix modelling	19
1.6 Absorption for pipes and ducts – porous absorber characteristics	20
1.6.1 Characterizing porous absorbers	21
1.7 Summary	22
1.8 References	22
2 Applications and basic principles of diffusers	23
2.1 Echo control in auditoria	23
2.1.1 Example applications	23
2.1.2 Wavefronts and diffuse reflections	26
2.1.3 Coherence and terminology	30

2.2	Reducing colouration in small rooms	32
2.2.1	Sound reproduction	32
2.2.2	Music practice rooms	39
2.3	Controlling modes in reverberation chambers	43
2.4	Improving speech intelligibility in underground or subway stations	44
2.5	Promoting spaciousness in auditoria	44
2.6	Reducing effects of early arriving reflections in large spaces	45
2.7	Diffusers for uniform coverage with overhead stage canopies	46
2.8	Diffusers for rear and side of stage enclosures	48
2.9	Diffusers to reduce focussing effects of concave surfaces	52
2.10	Diffusion and road side barriers	53
2.11	Diffusion and street canyons	55
2.12	Conclusions	55
2.13	References	56
3	Measurement of absorber properties	58
3.1	Impedance tube or standing wave tube measurement	58
3.1.1	Standing wave method	61
3.1.2	Transfer function method	62
3.2	Two microphone free field measurement	64
3.3	Multi-microphone techniques for non-isotropic, non-planar surfaces	65
3.3.1	Multi-microphone free field measurement for periodic surfaces	66
3.4	Reverberation chamber method	68
3.4.1	Measurement of seating absorption	71
3.5	<i>In situ</i> measurement of absorptive properties	74
3.6	Internal properties of absorbents	78
3.6.1	Measurement of flow resistivity	78
3.6.2	Measurement of flow impedance	81
3.6.3	Direct measurement of wavenumber	82
3.6.4	Indirect measurement of wavenumber and characteristic impedance	82
3.6.5	Measurement of porosity	83
3.7	Summary	85
3.8	References	85
4	Measurement and characterization of diffuse reflections or scattering	87
4.1	Measurement of scattered polar responses	88
4.1.1	Near and far fields	95

4.1.2	Sample considerations	102
4.1.3	The total field and comb filtering	103
4.2	Diffusion and scattering coefficients, a general discussion	104
4.3	The need for coefficients	105
4.3.1	Diffuser manufacturer and application	105
4.3.2	Geometric room acoustic models	106
4.4	The diffusion coefficient	107
4.4.1	Principle	107
4.4.2	Obtaining polar responses	109
4.4.3	Discussion	110
4.4.4	Diffusion coefficient table	111
4.5	The scattering coefficient	112
4.5.1	Principle	112
4.5.2	Rationale and procedure	113
4.5.3	Sample considerations	116
4.5.4	Anisotropic surfaces	116
4.5.5	Predicting the scattering coefficient	118
4.6	From polar responses to scattering coefficients, the correlation scattering coefficient	120
4.6.1	Scattering coefficient table	123
4.7	Contrasting diffusion and scattering coefficient: a summary	124
4.8	Other methods for characterizing diffuse reflections	124
4.8.1	Measuring scattering coefficients by solving the inverse problem	124
4.8.2	Room diffuseness	125
4.9	Summary	126
4.10	References	127
5	Porous absorption	129
5.1	Absorption mechanisms and characteristics	129
5.1.1	Covers	131
5.2	Material types	132
5.2.1	Mineral wool and foam	132
5.2.2	Recycled materials	133
5.2.3	Curtains (drapes)	134
5.2.4	Carpets	135
5.2.5	Absorbent plaster	135
5.2.6	Coustone or quietstone	137
5.3	Basic material properties	137
5.3.1	Flow resistivity	138
5.3.2	Porosity	140
5.4	Modelling propagation within porous absorbers	141
5.4.1	Macroscopic empirical models such as Delany and Bazley	141

5.4.2	Further material properties	144
5.4.3	Theoretical models	145
5.5	Predicting the impedance and absorption of porous absorbers	148
5.5.1	Single layer porous absorber with rigid backing	149
5.6	Local and extended reaction	150
5.7	Oblique incidence	151
5.8	Biot theory for elastic-framed materials	153
5.9	Summary	155
5.10	References	155
6	Resonant absorbers	157
6.1	Mechanisms	158
6.2	Example constructions	159
6.2.1	Bass trap membrane absorber	159
6.2.2	Helmholtz absorption	160
6.2.3	Absorption and diffusion	162
6.2.4	Clear absorption	163
6.2.5	Masonry devices	164
6.3	Design equations: resonant frequency	166
6.3.1	Helmholtz resonator	166
6.3.2	Losses	172
6.4	Example calculations	178
6.4.1	Slotted Helmholtz absorber	178
6.4.2	Porous absorbent filling the cavity	179
6.5	More complicated constructions	180
6.5.1	Double resonators	180
6.5.2	Microperforation	180
6.5.3	Lateral orifices	183
6.6	Summary	184
6.7	References	184
7	Miscellaneous absorbers	186
7.1	Seating and audience	186
7.2	Absorbers from Schroeder diffusers	188
7.2.1	Energy flow mechanism	189
7.2.2	Boundary layer absorption	191
7.2.3	Absorption or diffusion	191
7.2.4	Depth sequence	193
7.2.5	Use of mass elements	194
7.2.6	Number of wells	196
7.2.7	Theoretical model	196

7.3	Summary	200
7.4	References	200
8	Prediction of scattering	202
8.1	Boundary element methods	202
8.1.1	The Helmholtz–Kirchhoff integral equation	204
8.1.2	General solution method	205
8.1.3	Thin panel solution	209
8.1.4	Periodic formulation	212
8.1.5	Accuracy of BEM modelling: thin rigid reflectors	215
8.1.6	Accuracy of BEM modelling: Schroeder diffusers	216
8.2	Kirchhoff	219
8.3	Fresnel	224
8.4	Fraunhofer or Fourier solution	225
8.4.1	Near and far field	226
8.4.2	Fraunhofer theory accuracy	227
8.5	Other methods	228
8.5.1	Transient model	228
8.5.2	FEA	229
8.5.3	Edge diffraction models	229
8.5.4	Wave decomposition and mode-matching approaches	230
8.5.5	Random roughness	230
8.5.6	Boss models	231
8.6	Summary	231
8.7	References	231
9	Schroeder diffusers	233
9.1	Basic principles	233
9.2	Design equations	234
9.3	Some limitations and other considerations	236
9.4	Sequences	239
9.4.1	Maximum length sequence diffuser	239
9.4.2	Quadratic residue sequence	242
9.4.3	Primitive root sequence	242
9.4.4	Index sequences	245
9.4.5	Huffman and beyond	245
9.5	The curse of periodicity	248
9.6	Improving base response	257
9.7	Multi-dimensional devices	260
9.8	Absorption	263

9.9	But . . .	266
9.10	Optimization	268
	9.10.1 Process	268
	9.10.2 Results	271
9.11	Summary	273
9.12	References	274
10	Geometric reflectors and diffusers	276
10.1	Plane surfaces	276
	10.1.1 Single panel response	276
	10.1.2 Panel array response: far field arc	281
	10.1.3 Panel array response: near field	282
10.2	Triangles and pyramids	284
	10.2.1 Arrays of triangles	287
10.3	Concave arcs	288
10.4	Convex arcs	290
	10.4.1 Geometric scattering theory and cut-off frequencies	291
	10.4.2 Performance of simple curved diffusers	293
10.5	Optimized curved surfaces	297
	10.5.1 Example application	297
	10.5.2 Design process	298
	10.5.3 Performance for un baffled single optimized diffusers	301
	10.5.4 Periodicity and modulation	303
	10.5.5 Stage canopies	305
10.6	Fractals	307
	10.6.1 Fourier synthesis	308
	10.6.2 Step function addition	309
10.7	Summary	311
10.8	References	311
11	Hybrid surfaces	313
11.1	Planar hybrid surface	313
11.2	Curved hybrid surface	314
11.3	Simplest theory	316
11.4	Number sequences	318
	11.4.1 One-dimensional sequences	318
	11.4.2 Two-dimensional sequences	324
11.5	Designing curved hybrid surfaces	324
11.6	Absorption	324
11.7	Accuracy of simple theories	327
11.8	Diffuse reflections	330

11.9	Boundary element modelling	332
11.10	Summary	333
11.11	References	334
12	Absorbers and diffusers in rooms and geometric models	335
12.1	Absorption coefficients: from free field to random incidence	335
12.2	From the reverberation chamber absorption coefficients to room predictions	338
12.3	Absorption in geometric room acoustic models	339
12.4	Diffuse reflections in geometric room acoustic models	343
12.4.1	Ray re-direction	345
12.4.2	Transition order using particle tracing	345
12.4.3	Diffuse energy decays with the reverberation time of the hall	346
12.4.4	Radiosity and radiant exchange	346
12.4.5	Early sound field wave model	346
12.4.6	Distributing the diffuse energy	346
12.4.7	Scattering coefficients	349
12.5	Summary	352
12.6	References	352
13	Active absorption and diffusion	355
13.1	Some principles of active control	356
13.2	An example active impedance system and a general overview	359
13.3	Active absorption in ducts	361
13.4	Active absorption in three dimensions	362
13.4.1	Low frequency modal control – example results	364
13.4.2	Low frequency modal control – alternative control regime	365
13.5	Hybrid active–passive absorption	368
13.6	Active diffusers	371
13.7	Summary	373
13.8	References	373
	<i>Appendix A</i>	375
	<i>Appendix B</i>	381
	<i>Appendix C</i>	388
	<i>Index</i>	396

Preface

Every book tells a story and there is a story behind every book. This story begins in 1980, in the conference room of the laboratory for the structure of matter at the Naval Research Laboratory (NRL) in Washington, DC, where Peter D'Antonio was employed as a diffraction physicist. Knowing Peter's interest in music, a colleague handed him the latest issue of *Physics Today* with a cover photo of Manfred Schroeder seated in an anechoic chamber. The article suggested using a number of theoretic diffusers in concert halls. While Peter's interest at the time was not in concert halls, he became fascinated with the thought of using these diffusers in a renovation of Underground Sound, a private studio he originally built in 1972 with Jerry Ressler. The acoustic renovation utilized a new concept called Live End Dead End™ proposed by Don and Carolyn Davis of Synergetic Audio Concepts (Syn-Aud-Con) and implemented successfully by Chips Davis. At that time, Peter was examining the three-dimensional (3D) structure of matter in various phases using electron and X-ray diffraction techniques. Peter shared the article with John Konnert, a colleague at NRL, and it became apparent that the 'reflection phase gratings' suggested by Schroeder were in effect two-dimensional (2D) sonic crystals, which scatter sound in the same way that 3D crystal lattices scatter electromagnetic waves. Since the diffraction theory employed in X-ray crystallographic studies was applicable to reflection phase gratings, it was straightforward to model and design the reflection phase gratings.

At this time, Peter's only link to the field of acoustics was a love of composing, recording and performing music. Having scientific backgrounds, John and Peter approached acoustics as they did the field of diffraction physics, and began researching and publishing findings in the scientific literature. The Audio Engineering Society and Syn-Aud-Con offered a unique forum and community for discussing the research. In October 1983, at the 74th AES Convention in New York, Peter met Bob Todrank following a presentation of Peter and John's first paper on Schroeder diffusers. Bob was designing a new studio for the Oak Ridge Boys in Hendersonville, TN and was interested in utilizing these new acoustical surfaces. The studio was a resounding success and turned out to be a harbinger of many exciting things to come.

In 1983, Peter and John measured quadratic residue and primitive root diffusers with a TEF 10 analyzer at a Syn-Aud-Con seminar in Dallas, Texas, with the assistance of Don Eger of Techron. Here Peter and John met Russ Berger who was a pioneer in the use of new products into his firm's recording studios. In 1984, an intensive measurement programme was carried out using Richard Heyser's time delay spectrometry implementation. Farrell Becker was very helpful in the initial evaluation of these exciting new surfaces. Not having access to an anechoic chamber, a boundary

measurement technique was developed. These measurements were initially carried out at full scale in large spaces like open fields and parking lots, eventually moving indoors to a sports arena, a motion picture sound stage, and a local high school gymnasium. The measurements enabled the theories to be validated.

The Oak Ridge Boy's Acorn Sound Recorders project was celebrated with a Syn-Aud-Con control room design workshop in 1984. This project led to many others and collaborations with a growing community of new studio designers were undertaken. Neil Grant was an early staunch proponent of the research and products. Some of his milestone designs include Peter Gabriel's Real World Studios, Box, UK; Reba McEntire's Starstruck Studios, Nashville, TN; Sony Music, New York, NY and Cinerama Theater, Seattle, WA. In 1989, John Storyk integrated diffusive technology in many of his designs, including Whitney Houston Studio, Mendham, NJ; Electronic Arts, Vancouver, BC and Jazz at Lincoln Center, NY highlighting the list. Today much of the recorded music you hear is created in music facilities utilizing RPG technology. These fledgling years established relationships that continue to this day and produced many acoustical landmarks.

Interest in recording facilities naturally spread to broadcast facilities, where diffuser technology is now commonplace. Facilities include BBC, NPR, NBC, CBC and most of the broadcast networks due to Russ Berger's innovative designs. Being musicians and audiophiles, led to significant involvement in residential high end audio listening rooms as well as production studios.

In 1989, Peter was introduced to Jack Renner, President of Telarc Records, the company that started the classical high end recording industry on a digital journey. Jack was recording the Baltimore Symphony Orchestra at the Meyerhoff Symphony Hall and asked if RPG could assist him. Following initial experimentation, Telarc graciously credited RPG[®] as Telarc's exclusive acoustical system for control room and stage use for the Berlioz *Symphonie Fantastique* in 1990. The somewhat accidental stage use and overwhelming acceptance by musicians and conductor prompted an objective and subjective investigation of stage acoustics and acoustical shells both with small ensembles and with the Baltimore Symphony Orchestra. These chamber group studies were conducted with Tom Knab at the Cleveland Institute of Music, where Peter has been adjunct professor of acoustics since 1990, at the invitation of Jack Renner. In 1989, RPG was privileged to provide a custom number theoretic surface for the rear wall of Carnegie Hall, New York. This installation, along with the new diffusive acoustical shell development, launched RPG's involvement into performing arts applications, which eventually included the Fritz Philips Muziekcentrum, Eindhoven and the Corning Glass Center, Corning, NY.

Many of the acoustical consultants involved in the design of worship spaces began to include the use of diffusers for rear wall applications and acoustical shells. While RPG has collaborated with many acousticians, the relationship with Mike Garrison is noteworthy for the sheer number and size of the successful worship spaces produced using diffusers. The crown jewel of this collaboration is the 9,000 seat South East Christian Church in Louisville, KY.

In 1990, RPG funded the DISC Project in an attempt to devise a standard methodology for evaluating diffuser quality. In 1991, Peter proposed a directional diffusion coefficient and the Audio Engineering Society invited him to chair standards committee SC-04-02 to formerly develop an information document describing these procedures.

In 1993, David Quirt Associate Editor of the *Journal of the Acoustical Society of America* asked Peter to referee a paper by Trevor Cox entitled ‘Optimization of profiled diffusers’. (Trevor’s research journey had started a few years earlier in 1989 when, under the direction of Raf Orłowski and Yiu Wai Lam he completed a PhD on Schroeder diffusers at Salford University, UK.) Trevor’s paper outlined a process that combined boundary element modelling and multi-dimensional optimization techniques to make better diffusers. In Peter’s view, this paper represented a creative milestone in diffuser development on par with Schroeder’s seminal contribution. Peter and John’s review of the paper consumed many months. It required the writing of boundary element codes and developing the first automated goniometer to measure these optimized surfaces. During the summer of 1994, Paul Kovitz helped to complete the measurement software. Trevor’s revised paper, accompanied by a refereed paper of Peter and John’s review were published in 1995. Since this was nearly three years after Trevor submitted the paper to JASA, this must have seemed to be the peer review from hell, especially as the referees’ comments were 36 pages long.

Peter finally met Trevor in Amsterdam at an AES SC-04-02 standards committee meeting in 1994 and again in Arup Acoustics’ office in London. Our strong mutual interests led to an informal collaboration. In 1995, Trevor became a research consultant to RPG Diffusor Systems, Inc. This relationship started with developing an automated program to optimize loudspeaker and listening positions in a critical listening room and blossomed to generate much of the contents of this book.

Realizing that good acoustical design results from an appropriate combination of absorptive, reflective and diffusive surfaces, as mentioned in the Introduction, Peter (and later with Trevor) began developing absorption technologies as well, including hybrid abffusive (absorptive/diffusive) systems, diffforptive (diffusing/absorbing), concrete masonry units, low frequency absorbing arena seating risers, nestable open-cell foam systems and dedicated absorptive low frequency membrane systems.

In 1995, Peter and Trevor became aware of the diffusion research of James Angus on amplitude gratings and modulated phase gratings. James has made significant contributions to the field of diffuser design and we both have great respect for his insight and enjoy our collaborations with him. Also in 1995, we met Eckard Mommertz and Michael Vorlander at the 15th ICA in Trondheim, Norway. It was at this meeting that we learned of their work developing a procedure to measure the random incidence scattering coefficient. We have maintained close collaboration to this day, especially as members of the ISO WG 25, chaired by Jens Holger Rindel.

To further the development of the diffusion coefficient, RPG co-funded a three year grant with the Engineering and Physical Sciences Research Council of the United Kingdom, beginning in 1996. Trevor, Yiu Wai Lam and Peter were the investigators and Tristan Hargreaves was the doctoral student. This research was very fruitful in that it produced the first 3D measurement goniometer and yielded a robust diffusion coefficient which has since been published as AES-4id-2001.

This diffusion coefficient has since been used as a metric to develop a range of new diffusing surfaces, including optimized welled diffusers, profile diffusers, 1D and 2D curved diffusers, baffled diffusers, genetic binary hybrid surfaces, flat and curved binary amplitude gratings, fractal and modulated surfaces, in effect many of the topics included in this book. These new optimized custom curved surfaces have found application in performance spaces like Kresge Auditorium, Boston, MA;

Hummingbird Center, Toronto, Canada; Edwina Palmer Hall, Hitchin, UK and also recording facilities like Sony Music's premier mastering room M1, in New York.

Things began falling into place and all of the relevant diffusion research was collected into a special edition of *Applied Acoustics*, entitled 'Surface Diffusion in Room Acoustics', guest edited by Yiu Wai Lam and published in June of 2000. Lam also organized a symposium in Liverpool that year. In September of 2001, a special structured session on scattering in room acoustics was organized by Michael Vorlander at the 17th ICA in Rome. Having played a pioneering role in making Schroeder's theoretical suggestions a practical reality, it was personally very gratifying for Peter to be part of a session dedicated to a topic which started as an intellectual curiosity, and has now turned into a diffuser industry and a field of research actively being studied by the leading acousticians of our time.

There have been many significant accomplishments over the past 20 years. We now know how to design, predict, optimize, measure, characterize and standardize the performance of scattering surfaces. While there is still much to do, there is a general consensus in the architectural acoustics community that a solid theoretical and experimental foundation has been laid, that diffuser performance can now be quantified and standardized and that diffusers can now be integrated into contemporary architecture, taking their rightful place along with absorbers and reflectors in the acoustical palette. The future holds many exciting possibilities.

It is a good time in the history of diffuser development to tell this story. This book has allowed us to chronicle developments with sufficient scientific detail, and to collect in one volume much of what is known about both diffusers and absorbers.

In an effort to make this book 'timeless', we are providing a website www.rpginc.com/research, at which we will provide updates, polar responses of 1D and 2D diffusers, and additional diffusion and correlation scattering coefficients for 2D diffusing surfaces. You can contact us and tell us about technology and techniques we may have inadvertently missed in the book. So stay tuned and 'Listen to the Music, Not the Room'.

Peter D'Antonio
Trevor Cox

Acknowledgements

We would like to acknowledge the worldwide architectural acoustics community for their continuing support and specification of our research, designs and products, thereby enabling the growth of a diffusion industry and allowing diffusion to take its rightful place along with absorption and reflection. We would also like to thank the Audio Engineering Society and other professional bodies for offering a peer review forum and community to share our research. Thanks are also due to the members of AES SC-04-02 and ISO WG 25. Many people have helped and contributed to the book. Colleagues from Salford University kindly proof read chapters, and people contributed data and pictures from their research. We have been fortunate to have collaborated with some of the best scientists of our generation – Dr Jerome Karle, Chief Scientist and Nobel Laureate 1985 Chemistry, Peter’s supervisor at the Naval Research Laboratory; Dr John H. Konnert, co-founder of RPG Diffusor Systems, Inc. and author of the restrained macromolecular least squares program, and Prof. Manfred Schroeder, a true visionary and the inspiration for our career in acoustics.

Glossary of frequently used symbols

Vectors are denoted in bold

a	Half diffuser or reflector width (m)
a	Fibre radius (m)
A	Total absorption of a room (m^2)
A	Scaling constant
A_n	Coefficients for grating lobes (Pa)
b	Half diffuser length (m)
c	Speed of sound (ms^{-1}), in air unless otherwise stated. Subscript 0 denotes value in air where ambiguity might arise otherwise ($\approx 343 \text{ms}^{-1}$).
c_p	Specific heat capacity of air at constant pressure ($\approx 1.01 \text{JKg}^{-1} \text{K}^{-1}$).
d	Slot width for slotted Helmholtz absorbers (m)
d	Diffusion coefficient
d	Thickness of materials (m)
d_n	Depth of the n th well in a Schroeder diffuser (m)
D	Cell width for Helmholtz absorbers (m)
E	Perimeter of absorption samples (m)
f	Frequency (Hz)
f_0	Design frequency (Hz)
g	Acceleration due to gravity (ms^{-2})
G	Green's function
$H_0^{(1)}$	Hankel function of the first kind of order zero
H	Transfer function
FT()	Fourier Transform
\mathbf{j}	$\sqrt{-1}$
k	Wavenumber (m^{-1}). Subscript 0 denotes value in air where ambiguity might arise otherwise
k_x	Wavenumber component in x -direction, similar expressions for y and z (m^{-1}).
k_s	Tortuosity
K_e	Effective bulk modulus
l	Depth of materials (m)
m	Mass per area (kg m^{-2})
m	Order of diffraction or grating lobes
m	Energy attenuation coefficient for absorption in air
m	Constant relating finite to infinite sample absorption coefficients
\mathbf{n}	Normal to surface, for BEM modelling this is pointing out of the surface
N	Number of wells per period

N	Length of pseudorandom sequence
N_p	Prandtl number (≈ 0.77)
p	Pressure (Pa or Nm^{-2}). Subscript 0 denotes value in air where ambiguity might arise otherwise
p_1	Pressure from a single diffuser/reflector (Pa)
p_a	Pressure from an array (Pa)
p_i	Pressure incident direct from a source (Pa)
p_m	Pressure of m th order diffraction lobe (Pa)
P_0	Atmospheric pressure (≈ 101320 Pa).
p_s	Pressure scattered from a surface (Pa)
PRD	Primitive Root Diffuser
QRD [®]	Quadratic Residue Diffuser
r	Distance (m)
r	Primitive root of N
r'	Distance from image source (m)
\mathbf{r}	Receiver position
\mathbf{r}_0	Source position
\mathbf{r}_s	Point on diffuser surface
R	Pressure reflection coefficient
s, s_n	Number sequence
s	Diffuser surface
s	Standing wave ratio
s	Scattering coefficient
S	Surface area of a room (m^2)
S	Area of holes in Helmholtz resonator (m^2)
$\text{sinc}(x)$	$= \sin(x)/x$
S_{xxm}	Maximum energy in autocorrelation side lobes
S_{xym}	Maximum energy in crosscorrelation
t	Sheet thickness for Helmholtz and membrane absorbers (m)
t_a	Resistive layer thickness for Helmholtz and membrane absorbers (m)
T_{60}	Reverberation time (s)
V	Volume (m^3)
w	Well width (m)
W	Repeat distance or periodicity width (m)
x	Cartesian coordinate (m)
y	Cartesian coordinate (m)
z	Specific acoustic impedance (Pa s m^{-1} or MKS rayl)
z	Cartesian coordinate (m)
z_c	Characteristic impedance of a medium (MKS rayl)
z_f	Flow impedance (MKS rayl)
z_n	Normalised specific acoustic impedance ($= z/\rho c$)
α	Absorption coefficient
α_s	Random incidence absorption coefficient
α_∞	Random incidence absorption coefficient for an infinite sized sample
β	Admittance (rayl^{-1})
β'	Admittance with outward pointing normal (rayl^{-1})
β_n	Normalised admittance ($= \beta\rho c$)
ε	Porosity or fractional open area

δ	End correction factor (i.e. ≈ 0.85 if baffled)
δ	Delta function
δ_v	Size of viscous boundary layer (m)
δ_h	Size of thermal boundary layer (m)
γ	Ratio of specific heat capacities (≈ 1.4 in air)
η	Viscosity of air (1.84×10^{-5} poiseuille)
κ	Thermal conductivity of air ($\approx 2.41 \times 10^{-2} \text{ WmK}^{-1}$)
λ	Wavelength (m)
λ_0	Design wavelength (m)
ν	Kinematic viscosity of air ($15 \times 10^{-6} \text{ m}^2 \text{ s}^{-1}$)
θ	Angle of reflection
ρ	Density (kgm^{-3})
ρ_e	Effective density in porous absorber
σ	Flow resistivity (MKS rayl m^{-1})
σ_s	Flow resistance (MKS rayl)
ω	Angular frequency (s^{-1})
ψ	Angle of incidence
Λ, Λ'	Characteristic dimensions for porous absorber modelling (m)

Introduction

The sound that is heard in most environments is a combination of the direct sound straight from the source or sources and the indirect reflections from surfaces and other objects. For instance, in room acoustics, both the direct sound and the reflections from the walls, ceiling and floor are key in determining the quality of the acoustic. Hence, one of the central topics in acoustics is how to manipulate these reflections that affect the way the sound propagates, and ultimately perceived.

Sound striking a surface is transmitted, absorbed or reflected; the amount of energy going into transmission, absorption or reflection depends on the surface's acoustic properties. The reflected sound can either be redirected by large flat surfaces (specularly reflected) or scattered by a diffusing surface. When a significant portion of the reflected sound is spatially and temporally dispersed, this is a diffuse reflection, and the surface involved is often termed a diffuser. Figure 1 illustrates temporal and spatial characteristics of absorbing, specularly reflecting and diffusing surfaces, which form the acoustical palette. In addition to the surface types shown in Figure 1, there are hybrid surfaces, which can both absorb and diffuse to varying degrees.

Over the past 100 years, since the founding of architectural acoustics by Sabine, there has been considerable effort devoted to studying surface absorption. Over this time, a considerable library of absorption coefficients has been tabulated based on accepted standards of measurement and a reasonable understanding of how absorbers should be designed and applied has been achieved. This development continues, and in recent decades many innovative absorber designs have been developed, and new ways to predict and measure absorptive materials have been found. In contrast, significant scientific knowledge about the role of scattering (diffusely reflecting) surfaces has only been developed much more recently. Over the past 20–30 years, significant research on methods to design, predict, measure and quantify diffusing surfaces has resulted in a growing body of scientific knowledge and understanding. All these issues, and many more, are covered in this book.

Good architectural acoustic design requires the right room volume, the right room shape and surface treatments, utilizing an appropriate combination and placement of absorbers, diffusers and flat surfaces. Architectural acoustic spaces can be loosely divided into sound production, sound reproduction and noise control environments.

An example of a sound production room is the performing arts facility such as concert halls for classical music or a theatre for speech. The room acoustic contributes greatly to the perceived sound of the music or speech. The arrival time, direction and temporal density, and level of the early reflections, coupled with the balance of the early to late energy, decay time, temporal and spatial density of the late reflections,

2 Introduction

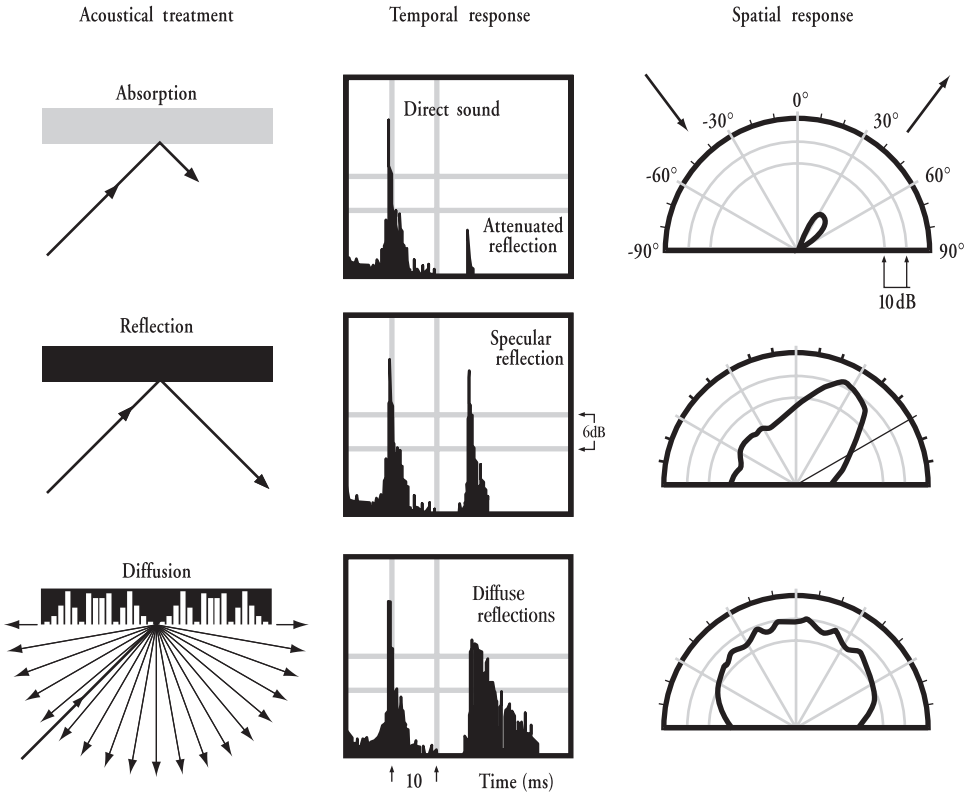


Figure 1 The temporal and spatial characteristics of absorbing, specularly reflecting and diffusing surfaces.

define the quality of sound that is heard. In large sound production rooms, reflection and diffuse reflection are the primary acoustic tools. This is schematically illustrated in Figure 2. Absorption may be used to control reverberance, but the unavoidable absorption due to paying customers must also be considered.

In contrast, the acoustics of sound reproduction rooms, like recording studios and home theatres, should be neutral. All of the spectral, timbre and spatial information is pre-recorded on the playback media, and the reproduction room is only there to allow a listener to hear what has been recorded, as is was recorded. In a sound reproduction room, absorption and diffuse reflection play a key role, and specular reflection is a minor contributor. This is illustrated in Figure 3. Absorption and diffusion are used to control the colouration that would otherwise occur in the space from early arriving reflections and low frequency modes.

In noise control situations, like gymnasiums, swimming pools and factories, the objective is simply to reduce the reverberance and sound level. This might be done to reduce sound levels to prevent hearing damage or to improve the intelligibility of speech. Uniform distribution of absorption is the primary acoustic tool, and specular reflection and diffuse reflection have more minor roles. This is illustrated in Figure 4.

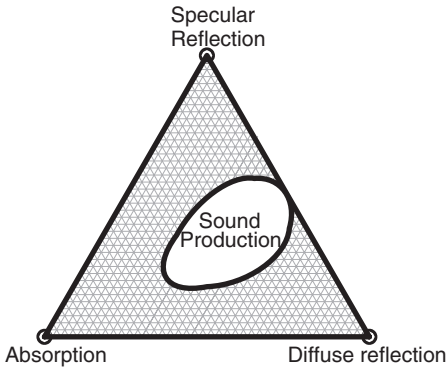


Figure 2 The relative importance of three acoustic treatments for sound production rooms such as concert halls, recital halls, auditoria, theatres, conference halls, courtrooms and worship spaces.

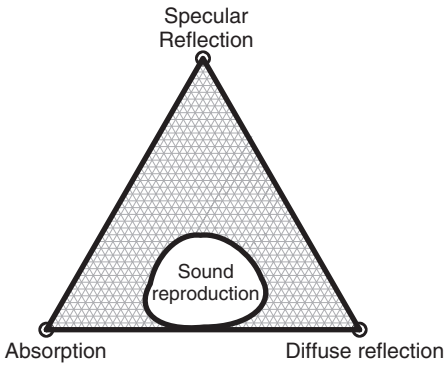


Figure 3 The relative importance of three acoustic treatments for sound reproduction rooms such as recording and broadcast studios, video conferencing rooms and home theatres.

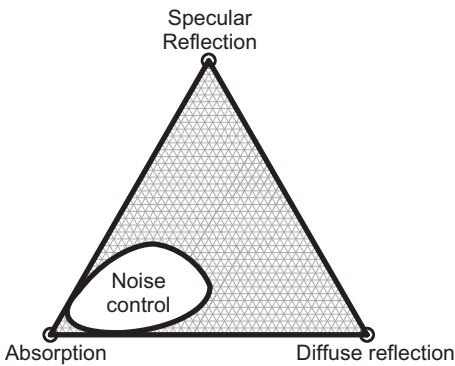


Figure 4 The relative importance of three acoustic treatments for noise control such as for factories, gymnasiums, swimming pools, libraries, atria and road side barriers.

4 Introduction

(Although it has been suggested that diffusers can play a useful role in disproportionate spaces, but then Figures 2–4 are all generalizations of the true situation.)

Surface acoustic treatment also plays an important role outdoors. For instance, the absorption of the ground can have a significant impact on sound levels from ambient noise sources such as roads and industrial premises. The treatment of noise levels might involve the use of noise barriers, and these might be treated with absorption, or less commonly, diffusers to reduce the noise levels.

This introductory description has sketched out a few of the issues concerning where and why absorbers and diffusers are applied. More detailed descriptions can be found in Chapter 1 for absorbers and Chapter 2 for diffusers. The following section, however, tries to give an overview of the relative merits of absorption and diffuse reflections.

1 Absorption versus diffuse reflections

Both absorbers and diffusers can be used to prevent acoustic distortion. For example, both can be effective in controlling echoes, colouration and image shift caused by high level reflections. This raises the question as to which is the best treatment in which situation.

Whether absorbers or diffusers are best depends to a considerable degree on other acoustic factors, primarily on whether a decrease in reverberation and/or sound level is desirable. If a wall is causing an echo or colouration problem, and the designer wishes to conserve the reverberation time and sound energy in the space, then a diffuser is the best solution. The diffuser is placed on the wall to disperse the reflection and to reduce the distortion without removing sound energy from the space. For this reason, in concert halls, where acoustic energy is at a premium, diffusers are to be preferred. In smaller rooms, say a lecture theatre, where intelligibility is important, a balance must be reached in which absorption is used to adjust the reverberation time and level, and diffusers are used to ensure that early reflections which constructively contribute to support speech do not produce distortion. When reflections cannot be constructively used for intelligibility, then absorption would be the normal choice.

In critical listening rooms, a mixture of absorbers and diffusers is used to control the acoustics of a space. Treatment is placed to control first-order reflections. When absorbers are used, the sonic images forming the soundstage are points in space. When diffusers are used, these images take on a more natural width and depth. Which material is correct, absorbers or diffusers, is a matter of personal taste. If all the treatment is absorption, then the room turns out to be rather dead. While some people favour this for mixing audio, others do not, and for a listening room a very absorbent environment is not best. Consequently, if some liveliness is to be left in the room, a combination of absorbers and diffusers must be used. The current trend is to use absorption at the points where first-order reflection occurs, between the listener and the loudspeakers, to minimize interference with the source imaging. Diffusers are used in other locations to provide a natural ambience for all of the musical playback formats, ranging from stereo to surround, for example, by placing the diffusers on the rear wall.

Where low frequency acoustic problems are being treated, both absorbers and diffusers require considerable depth to work, and the depths of acoustic treatments are often limited because of space constraints and cost. Because of this, resonant

structures are often used to deal with the problems in a space efficient manner. For example, a membrane or Helmholtz absorber might be used. The speed of sound in a porous absorber is lower than in air, and consequently a given thickness of absorber can work to a lower frequency than the same thickness of diffuser. For this reason, a partially absorbing diffuser, such as a hybrid structure, or a full resonant absorber is usually favoured to treat low frequencies where space is a premium. Furthermore, most spaces naturally lack bass absorption, and so additional absorbers are useful in dealing with low frequency reverberance.

Diffusers have the advantage of generally being more robust than absorbers. Most absorber technologies involve fibrous materials which do not stand up well to the effects of wind, rain and toxic environments. For example, in railway stations or on streets a large amount of particulate pollution may be generated, which over time can clog the pores of fibrous absorbents. There is a great risk with outdoor installations that fibrous absorbents will wash away over time. Consequently, if it is possible to meet the acoustic requirement using a hard diffuser, it is possible to generate a much more robust treatment than with many absorbents.

Both absorbers and diffusers have a role to play in good acoustic design. They have complementary functions, which means when they are used appropriately, better acoustics can be achieved.

1 Applications and basic principles of absorbers

This chapter is intended to introduce the basic principles of absorption, along with a basic explanation of the physics behind the absorption processes and some fundamental formulations which will be used in later chapters. Since the book is aimed at practitioners and researchers, most chapters begin with an application-driven, qualitative description, followed by a quantitative description of the technology and design. Following this type of philosophy, this introductory chapter on absorption is written from an application or case study perspective. The style is intended to make the more theoretical sections more palatable. Rather than start with a section labelled ‘A little light mathematics’ – which in most books is anything but light – the mathematical explanations will be formed around application examples. The chapter will also introduce some of the issues concerning the design, prediction and measurement of absorbers that will be treated in more detail in future chapters.

This chapter naturally introduces principles of airborne acoustics related to absorbers, such as some principles of room acoustics. Readers familiar with these principles can skip these sections. Readers very unfamiliar with the subject should refer to the appropriate references. The first application example concerns the control of reverberance.

1.1 Reverberation control

Readers should be familiar with excessively reverberant spaces; this might be a restaurant or railway station where the sound echoes around the space make it noisy and difficult to communicate. In these types of spaces, people tend to slow down their speech, talk louder and try to pronounce words more precisely in an effort to make the received speech intelligible.

For some reason, many restaurateurs seem to think that to create the right atmosphere, it is necessary to make speech communication virtually impossible. The issue here is reverberation.

Reverberation is the decay of sound after a sound source has stopped and it is a key feature in room acoustics [1]. Reverberation is most audible in large spaces with hard surfaces, such as cathedrals, where the sound echoes around long after the sound was emitted from the source. In small spaces, with plenty of soft acoustically absorbent materials, such as living rooms, the absorbent materials quickly absorb the sound energy, and the sound dies away rapidly. When people talk about rooms being ‘live’ or ‘dead’ this is usually a description of the perception of reverberance.

The amount of reverberation in a space depends on the size of the room and the amount of sound absorption. The solution to the reverberant restaurant is to add

acoustic absorbent. This will reduce the reflected sound energy in the room and so reduce the reverberance and sound level. Problems arise in dining rooms, because any surfaces close to eating or preparation areas need to be robust and washable, and many acoustic absorbers are soft and so are inherently unsuitable.

Consequently, the best place for absorption is the ceiling or high up on the walls. Figure 1.1 shows such an absorbent ceiling. This room has a special absorbent plaster ceiling which has the advantage of being flat and monolithic and so does not visually impose on the space. The absorbent plaster is discussed in more detail in Chapter 5. A less expensive solution would be standard absorbent ceiling tile made of materials such as compressed mineral wool, mounted in a t-bar grid; but this is not as elegant.

Getting the correct amount of reverberation in a space is vital to the design of most rooms, whether the aim is to make music sound beautiful, to make speech intelligible, to reduce noise levels or simply to make a space a pleasant place to be in. The primary technique for reverberation control is absorption. In discussing the design, application and measurement of absorbers, it is necessary to understand a statistical model of sound within an enclosure [1, 2]. This is discussed in the next section.

1.1.1 A statistical model of reverberation

A simple model of sound propagation in a room is of particles of energy bouncing around the room in an analogous way to a snooker ball bouncing around a billiard



Figure 1.1 Absorbent plaster ceiling applied to a restaurant (photo courtesy of BASWA acoustic, AG).

8 Applications and principles of absorbers

table. The room can be characterized by the impulse response, an example of which is shown in Figure 1.2. The impulse response is a pressure versus time graph showing the response at a receiver position when somewhere else in the room a short impulse is created. For example, a balloon burst or a starting pistol might generate the short impulse, and the response might be measured with a microphone. First of all the direct sound from the source to receiver is received. Soon after, a series of reflections arrive, the level of these reflections generally decaying with time due to absorption at the room surfaces. The effects of the boundaries dominate the behaviour of sound in rooms, and it is at the boundaries where absorption is normally found. (Only in large rooms does absorption by the air become important.) There is an increase in reflection density with time, and when the reflections become very dense this is termed the reverberant field. The energy of the reverberant reflections around the room is roughly constant and can be readily predicted provided the sound field is diffuse [3].

The reverberation time T_{60} measures the time taken for the sound pressure level to decay by 60 dB when a sound stops. From the impulse response, the Schroeder curve must be calculated first by backwards integration before evaluating the reverberation time [4]. Sabine showed that the reverberation time could be calculated from the room volume and absorption by [5]:

$$T_{60} = \frac{55.3V}{cA} \quad (1.1)$$

where V is the room volume, c the speed of sound and A the total absorption of all room surfaces.

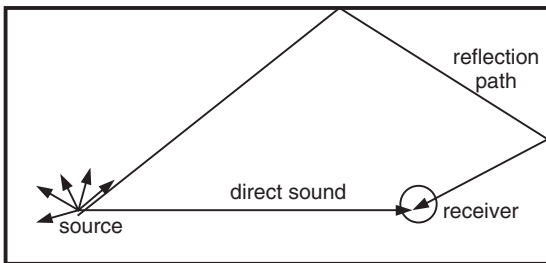
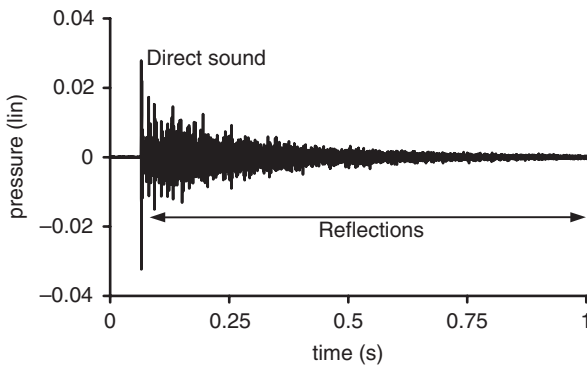


Figure 1.2 The generation of an impulse response in a room, and a typical example impulse response from a concert hall.

The total absorption of the room can be calculated from the individual absorption coefficients of the room surfaces using the following expression:

$$\begin{aligned} A &= \sum_{i=1}^N S_i \alpha_i \\ &= S \bar{\alpha} \end{aligned} \quad (1.2)$$

where S_i is the surface area of i th surface element in the room, S the total surface area of the room, α_i the absorption coefficient of the i th surface element in the room, and $\bar{\alpha}$ the average absorption coefficient of the room.

The absorption coefficient of a surface is the ratio of the energy absorbed by a surface to the energy incident. It typically lies between 0 and 1, which represent non-absorbing and totally absorbing surfaces, respectively. Values greater than 1 are often found in random incidence measurements, although theoretically impossible. This usually occurs due to diffraction/edge effects – see Chapter 3 for further details. The absorption coefficient can be defined for a specific angle of incidence or random incidence as required.

Equations 1.1 and 1.2 form the basis for the standard method for measuring a random incidence absorption coefficient. The reverberation time in a reverberation chamber is measured with and without the test sample. The test sample adds absorption to the room and so reduces the reverberation time. From the change in reverberation time, the absorption coefficient can be obtained. This technique is described in detail in Chapter 3.

For large rooms, the absorption of air should also be accounted for. The total air absorption A_{air} in a room of volume V is given by:

$$A_{\text{air}} = 4Vm \quad (1.3)$$

where m is the energy attenuation coefficient. This can be calculated from [2]:

$$m = 5.5 \times 10^{-4} \frac{50}{h} \left(\frac{f}{1000} \right)^{1.7} \quad (1.4)$$

where h is the relative humidity as a per cent and f the frequency. This formulation is applicable for $20 < h < 70$ per cent and $1.5 < f < 10$ kHz.

To allow for air absorption in the reverberation time predictions, the additional absorption calculated from Equation 1.3 should be added to the denominator of Equation 1.1 to give:

$$T_{60} = \frac{55.3V}{cA + 4mV} \quad (1.5)$$

Sabine's formulation does not correctly predict the reverberation time for rooms with a large amount of absorption. Over the years many new formulations have been

developed, the most popular of these being the Eyring equation [6], also known as the Eyring-Norris equation:

$$T_{60} = \frac{55.3V}{-cS \ln(1 - \bar{\alpha})} \quad (1.6)$$

where $\ln()$ signifies the natural logarithm. A little used formulation, but one needed in Chapter 12 is the Millington equation [7]:

$$T_{60} = \frac{55.3V}{-c \sum S_i \ln(1 - \alpha_i)} \quad (1.7)$$

Alternate reverberation time equations are the topic of considerable interest. Many formulations attempt to be catch-all equations for reverberation time estimation, but it is often difficult to know a priori, whether a formulation will work in a particular room. It is conceivable that better equations can be developed by analyzing rooms in more detail (surface size and orientation statistics, absorption and diffuser distribution, etc.), but any such attempt would require a computer model of the room to be made for the analysis. As geometric models exist (ray tracing and variants thereof), where the impulse response of a room can be predicted, there is little need nowadays to search for ever complex reverberation time formulations.

The relative advantages of the reverberation time formulations given in Equations 1.1, 1.6 and 1.7 will become important when discussing absorption measurement in Chapter 3. In recent years, researchers have also been revisiting alternative reverberation time formulations in an effort to improve the accuracy of predictions in geometric room acoustics models; this is discussed in Chapter 12. Using geometric models for reverberation time estimation also requires diffuse reflections to be taken into account, which is still the subject of standardization and investigation, as discussed in Chapters 4 and 12.

Despite many studies, the application of absorption coefficients in computer models is fraught with difficulty, mainly because it is difficult to know what the absorption coefficients are for surfaces, and this is a key input to the model. The accuracy of absorption coefficients is particularly important when a significant portion of the surface area of a room is very reflective, for instance if much of the room is made from concrete, glass or wood. Furthermore, when the absorption is restricted to one plane, as typically is the case in concert halls, swimming pools, sports halls and classrooms, this means that the late decay is very dependent on the exact value of the absorption coefficient selected for the reflective surfaces. Even in a room entirely made of one material, such as a room made only of concrete, accurate absorption coefficients are critical. Changing the absorption coefficient of the concrete from 0.02 to 0.01 in such a room will double the reverberation time (except at higher frequencies where air absorption will dominate in a large room). In other words, when a hard material is dominating, a very accurate estimate of the absorption coefficient is necessary for purely numerical reasons. Consequently, while there are tables of absorption coefficients in the literature and Appendix A of this book, these cannot be blindly applied. The measured absorption coefficients can vary greatly from laboratory to laboratory, even for the same sample. Furthermore, for some products the absorption can vary greatly from manufacturer to manufacturer – an example being carpets as discussed in Chapter 5. Consequently, there is great interest concerning *in situ* methods for

measuring absorption both within rooms and for outdoor applications, and these methods are discussed in Chapter 3.

The reverberation time formulations are statistical models of room acoustic behaviour, and are only applicable where there are a large number of reflections and the sound field is diffuse. For instance, at low frequencies the modal behaviour of the room make the sound field non-diffuse. Consequently, there is a lower frequency bound on the applicability of statistical absorption formulations. The lower bound is usually taken to be the Schroeder frequency [8] given by:

$$f \geq 2000 \sqrt{\frac{T_{60}}{V}} \quad (1.8)$$

Although this formal limit has been known for many years, it does not prevent many practitioners and researchers still defining and using absorption coefficients below the Schroeder frequency as it is convenient, even if not strictly physically correct. Geometric models are also used below this limit, although they have difficulties in predicting at frequencies where there is a low modal density where correct modelling of phase is needed.

1.2 Noise control in factories and large rooms with diffuse fields

The noise levels within working environments must be controlled to allow safe working, as excessive levels can cause hearing loss. Consequently, noise levels in working environments are subject to regulations to limit the exposure of workers. There are several methods for controlling noise exposure. The most efficient of which is usually to control the noise at the source, but this may not always be possible. Another technique that can be employed is to reduce the reverberant sound level within a space. This is only effective if the noise levels have a significant contribution from the reverberant field. For instance, it is ineffective if the worker is close to a noisy machine. The reverberant field level is reduced by the addition of absorption and hence the noise exposure is decreased. Typically, porous or bulk absorber such as mineral wool is used as it is inexpensive, light and effective.

The porous absorber often has to be protected from dust, and so is frequently wrapped in plastic, but this decreases high frequency absorption. There are situations where the absorbent needs to be washable, and there are a few types of porous absorber that achieves this. There are also situations where the absorbent needs to be fibreless to prevent contamination. Chapter 5 discusses the design and modelling of porous absorbents including some innovative materials. Porous absorbers are only effective at mid- to high frequencies, but this is where the ear is most sensitive, and consequently where noise control is most needed in the working environment.

Factories tend to be very disproportionately dimensioned; they have very low ceilings compared to their widths and lengths. This means that the simple diffuse field equations, such as Equations 1.1 and 1.3, are unlikely to work. For statistical room acoustics to hold, the space needs to be diffuse. A diffuse field is one where there is uniform reflected energy density across the whole room, and all directions of propagation are equally probable. There are many reasons why real rooms do not have even energy density and equally probable propagation directions.

12 Applications and principles of absorbers

- 1 At low frequencies there are standing wave modes similar to those found in ducts – see Section 1.3.
- 2 If the room's dimensions are very dissimilar, there is a tendency to get different reverberation times in different directions as happens with many factories. Sound will decay faster if it is propagating perpendicular rather than parallel to the floor, as the perpendicular propagating sound will reflect more often, and it is at the reflections that absorption occurs.
- 3 The absorption in a room should ideally be evenly distributed across all surfaces. For many cases this is not true; for example, the factory absorption might all be on the ceiling, a swimming pool may also have all the absorption in the ceiling, a reverberation chamber with a test sample has all of the absorption on the floor, a classroom usually has absorption on the ceiling and floor but not on the walls, etc.
- 4 If the room has a distinctive shape, e.g. cylindrical, the curved surfaces can focus sound to a point like a curved mirror does with light. The result will be an uneven sound field – see Section 2.9.

The relevance of the diffuseness of the space to absorption technologies is as follows. The absorption coefficient of a building element will be measured in a reverberation chamber using Sabine's reverberation time formulation – see Section 3.4. When the absorption is applied, however, the acoustic conditions might be dramatically different, for instance non-diffuse, which means that the anticipated changes in noise levels and reverberance might not occur. The absorption might be more or less effective than predicted; this is discussed in Chapter 12. A special example of the problem is considered in Section 7.1 when auditorium seating is considered. Chapter 12 discusses the application of absorption coefficients to room acoustic models where the issue of non-diffuseness is again important.

1.3 Modal control in critical listening spaces

Small rooms, like recording/broadcast studios, home theatres and conference rooms, usually suffer from problems due to low frequency modes. At low frequencies, the standing wave modes of the room are separated in frequency. Figure 1.3 shows the frequency response for a small room. The frequency response is uneven meaning that

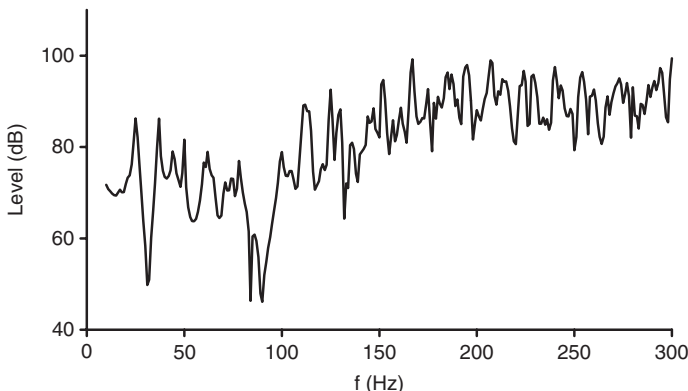


Figure 1.3 Low frequency response in a small room.

some frequencies are emphasized, where mode(s) are strong, and some suppressed, where mode(s) are weak, leading to colouration of the received sound. This is most critical for music applications, particularly with the increasingly widespread use of sub-woofer technology and reproduction of modern music with high bass content. Common solutions include choosing appropriate room dimensions, loudspeaker locations and listening positions, to flatten the frequency response of the room as much as possible and avoid degenerate modes [9]. Even when the room dimensions have been carefully chosen, however, the frequency response of the room will still be uneven and acoustic treatment is needed.

Particularly prominent modes are usually treated with bass absorption, often referred to as bass traps or bins. (It is not usually possible to treat this problem with diffusion because the sizes of the diffusers become prohibitively large.) Porous absorbers are not usually used, as they would have to be extremely thick to provide significant bass absorption. Porous absorption is most effective when it is placed at a distance from a room boundary where the particle velocity is maximum. This is at the quarter wavelength position. For a 100 Hz tone this would be roughly 1 m from the boundary. Placing porous absorbers directly on a room boundary, while the most practical, is not efficient because the particle velocity at a boundary is zero. In practice, many people place porous absorption in corners of rooms thinking this will absorb the modes since all modes have a 'contribution' in the corners. However, while the modes have a maximum pressure in the corners, the particle velocity is very low and so the absorption is ineffective. For these reasons, resonant absorbers are preferred for low frequency modal treatments.

Resonant absorbers are mass spring systems with damping to provide absorption at the resonant frequency of the system. The mass might come in the form of a membrane made of plywood or mass-loaded vinyl. Alternatively, the vibrating air in the neck of a hole might form the mass, as is the case for a Helmholtz resonant absorber. The spring usually comes from an air cavity. Damping is most often provided by sound being forced through a porous resistive material: mineral wool, fiberglass or acoustic foam.

The problem with resonant absorbers is that they usually only provide narrow band absorption. To cover a wide bandwidth, a series of absorbers are required, each tuned to a different frequency range. Alternatively, double-layered absorbers can be used, but are expensive to construct. Resonant absorbers are discussed in Chapter 6. An alternative, but expensive solution is to use active absorbers. Active absorbers have much in common with active noise control systems, and are discussed in Chapter 13.

One problem with modal control using resonant absorption is knowing how much resonant absorption to use. Although the theories set out in Chapter 6 allow the absorption coefficient for Helmholtz absorbers to be estimated, the meaning of absorption coefficient at low frequencies is problematical. (Even more problematical is the lack of good prediction models for membrane absorbers, but that is another story.) At low frequency the sound field is not diffuse, and consequently the effect that the absorber has is not calculable through simple statistical laws.

1.4 Echo control in auditoria and lecture theatres – basic sound propagation models

A late arriving reflection appears as an echo if its level is significantly above the general reverberation level. In a large auditorium, the reflection from the rear wall is

14 Applications and principles of absorbers

a common source of echo problems for audience members near the front of the stalls (main level seating) or performers on the stage. Echoes are very likely if the rear wall forms a concave arc which focusses the reflections at the front of the hall. The physical and subjective processes are the same as for echoes heard in mountain ranges or in cities with large building facades. One technique for removing the echo is to apply absorption to the rear wall. The absorption attenuates the reflection and so making it inaudible as a separate acoustic source. Figure 1.4 shows the Royal Festival Hall where such a solution was used. The problem with using absorption in this case is that it removes acoustic energy, which is at a premium in large spaces for orchestral performance, and so diffusion is currently the preferred solution – see Section 2.1.

For small spaces, where absorption is being used anyway for reverberation control, absorption is a possible treatment for echo problems. The absorption needs to act at mid- to high frequencies as echoes are most notable for directional instruments. Consequently, a layer of porous absorber can be used. Alternatively, hybrid surfaces controlling reverberation at mid-low frequencies, but providing diffuse reflections at mid-high frequencies might be used; these are discussed in Chapter 11.

Flutter echoes can occur in spaces with two large parallel walls. The regular pattern of reflections caused by sound bouncing back and forth between the parallel walls causes colouration. By colouration, it is meant that the frequency response of the sound is detrimentally altered. If you go into many staired wells with parallel walls



Figure 1.4 The Royal Festival Hall, London (photo courtesy of Bridget Shield).

and clap your hands, a high frequency ringing will be heard; this is the flutter echo. Flutter echoes are common in lecture theatres. One remedial measure available is to apply absorbent to at least one of the two parallel walls to absorb the reflections. Again, a relatively thin layer of porous absorber can achieve this, as it is mid- to high frequency treatment that is needed. Alternatively, diffusers may be used.

Porous absorbers are any material where sound propagation occurs in a network of interconnected pores in such a way that viscous effects cause acoustic energy to be dissipated as heat. Common examples are mineral wools, fibreglass, open cell foams, acoustic tiles, carpets and curtains. To gain a proper theoretical understanding of porous absorbers, it is necessary to understand the theories of sound propagating in a medium. Some basic models of sound propagation, which are the basis for much of the absorber and diffuser modelling in the book, are presented in the next section.

1.4.1 Sound propagation – a wave approach

To understand and design absorbers, it is necessary to have a basic understanding of the terminology used and the fundamental mathematical constructs used for sound propagation. This section introduces some basic constructs, concepts and terms.

A complex number representation of waves will be adopted throughout the book. The pressure of a plane propagating in a direction \mathbf{r} is:

$$p(t, \mathbf{r}) = A e^{j(\omega t - \mathbf{k} \cdot \mathbf{r})} = A e^{j(\omega t - k_x x - k_y y - k_z z)} \quad (1.9)$$

where $\mathbf{k} = \{k_x, k_y, k_z\}$ is the wavenumber (\propto propagation constant) with k_x being the component in the x -direction, $k^2 = |\mathbf{k}|^2 = k_x^2 + k_y^2 + k_z^2$, A is a constant related to the magnitude of the wave, $\mathbf{r} = \{x, y, z\}$ the location of the observation point, t the time, and $\omega = 2\pi f = kc$ the angular frequency, where f is the frequency and c the speed of sound.

The same conventions as used in Reference 2 are being adopted, so this forms a useful background reading for those who find this introduction too brief. Some texts and papers used a propagation constant, $\gamma = jk$, in their equations instead of the wavenumber, but this will not be often used in this book.

Consider a plane wave propagating through an acoustic medium, this could be air or a porous absorber. The plane wave will be taken to propagate in the x -direction for convenience. The pressure and particle velocity are given by:

$$p = A e^{j(\omega t - kx)} \quad (1.10)$$

$$\mathbf{u} = \frac{A}{\rho c} e^{j(\omega t - kx)} \quad (1.11)$$

where ρ is the density of the medium and c the speed of sound in the acoustic medium. The ratio of pressure to velocity gives the characteristic specific acoustic impedance of the medium, z_c :

$$z_c = \rho c \quad (1.12)$$

The characteristic acoustic impedance is a very useful property of the material when calculating the transmission of acoustic waves within and between different acoustic media.

The characteristic impedance of plane waves in air is purely real with a value of about 415 MKS rayl. In other acoustic medium it will often be complex, with a characteristic resistance and reactance which are the real and imaginary parts of the impedance, respectively. The characteristic impedance is analogous to the characteristic impedance of an electronic transmission line.

Once the characteristic impedance and wavenumber within an acoustic medium are known, it is possible to predict the sound propagation. While it is possible to characterize a medium with the characteristic impedance and the wavenumber, it is also possible to use two other variables, the effective density ρ_e and bulk modulus K_e . The term effective is used to signify that this is the density experienced by the acoustic waves rather than the more normal definition. The bulk modulus is the ratio of the pressure applied to a material to the resultant fractional change in volume it undergoes. It is the reciprocal of the compressibility. For a porous absorber the effective density and bulk modulus can be related to the characteristic impedance and wavenumber by the following formulations. The characteristic impedance is given by:

$$z_c = \sqrt{K_e \rho_e} \quad (1.13)$$

and the propagation wavenumber by:

$$k = \omega \sqrt{\frac{\rho_e}{K_e}} \quad (1.14)$$

Where possible, this book will work just with impedance and wavenumber, as multi-interrelated parameters are a potential source of confusion. Some porous absorbent prediction formulas, however, explicitly give values for the bulk modulus and the effective density, so these terms will sometimes be met in the literature.

1.4.2 *Impedance, admittance, reflection factor and absorption*

The effect that a surface has on an acoustic wave can be characterized by four interrelated acoustic quantities: the impedance, the admittance, the pressure reflection factor and the absorption coefficient. The first three (impedance, admittance and pressure reflection factor) give information about both the magnitude and phase change on reflection. The absorption coefficient does not contain phase data, but only gives information about the energy change on reflection.

Understanding these four acoustic quantities is fundamental to understanding the absorption sections of this book. These will now be defined mathematically by considering a wave propagating between two media. Consider a plane wave incident at an angle ψ to a boundary between two acoustic media at $x=0$ as illustrated in Figure 1.5. A simple model for a porous absorber assumes that it behaves as an acoustic medium like air, only with a different speed of sound c_1 and density ρ_1 . The incident p_i , reflected p_r and transmitted p_t pressures are given by:

$$p_i = A_i e^{j[\omega t - kx \cos(\psi) - ky \sin(\psi)]} \quad (1.15)$$

$$p_r = A_r e^{j[\omega t + kx \cos(\theta) - ky \sin(\theta)]} \quad (1.16)$$

$$p_t = A_t e^{j[\omega t - k_1 x \cos(\phi) - k_1 y \sin(\phi)]} \quad (1.17)$$

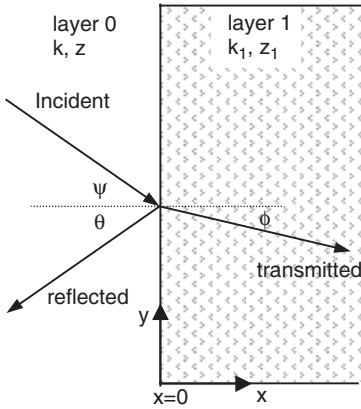


Figure 1.5 Sound hitting a surface.

where A_i , A_r and A_t are the magnitudes of the plane waves incident, reflected and transmitted, respectively, and the angles are defined in Figure 1.5.

Applying continuity of pressure gives the following relationship:

$$A_r e^{j[\omega t + kx \cos(\theta) - ky \sin(\theta)]} + A_i e^{j[\omega t - kx \cos(\psi) - ky \sin(\psi)]} = A_t e^{j[\omega t - k_1 x \cos(\phi) - k_1 y \sin(\phi)]} \quad (1.18)$$

This must be true for all times and for all values of y as this is a plane wave. Consequently, we obtain a relationship between the angles of propagation, more commonly known as Snell's law:

$$\sin(\psi) = \sin(\theta) \quad (1.19)$$

$$\frac{\sin(\psi)}{c} = \frac{\sin(\phi)}{c_1}$$

or

$$K \sin(\psi) = K_1 \sin(\phi) \quad (1.20)$$

The behaviour of the sound wave therefore depends on the relative size of the speed of sounds in the two media. For most absorbers, the speed of sound is much less than that in air. Consequently, the angle of propagation in the medium is smaller than in the air. In fact for many absorbers, the angle of propagation can be assumed to be normal to the surface, i.e. $\phi \rightarrow 0$.

The pressure reflection coefficient, R , gives the ratio of the reflected and incident pressure, i.e.:

$$R = \frac{p_r}{p_i} \quad (1.21)$$

The pressure reflection coefficient therefore includes both magnitude and phase information about the reflection of sound. There is also an intensity reflection coefficient, but this is not used in this book.

The continuity of particle velocity normal to the surface should also be considered to enable the derivation of an expression for the specific acoustic impedance of the surface. The relationships between pressure reflection factor and impedance will be used repeatedly in the book. For oblique incidence, these are:

$$R = \frac{\frac{z_1}{\rho c} \cos(\psi) - 1}{\frac{z_1}{\rho c} \cos(\psi) + 1} \quad (1.22)$$

$$\frac{z_1}{\rho c} \cos(\psi) = \frac{1 + R}{1 - R} \quad (1.23)$$

The admittance is the reciprocal of the impedance:

$$\beta = \frac{1}{z_1} \quad (1.24)$$

Often the surface admittance and impedance are normalized to the characteristic impedance of air, and these are denoted with a subscript of n .

The surface impedance is often split into the real term (resistance) and imaginary term (reactance). In general, the real term of surface impedance is associated with energy losses, and the imaginary term with phase changes. So a simple inspection of the surface acoustic impedance can give more insight into the absorbing properties of a material than the absorption coefficient.

Remembering from Section 1.1.1 that the absorption coefficient, α , is a ratio of the absorbed and incident energy enables the following expression to be derived:

$$\alpha = 1 - |R|^2 \quad (1.25)$$

where $|R|$ is the magnitude of the pressure reflection coefficient.

This section has described a number of key terms for sound propagation fundamental to absorber and diffuser modelling. These will be used throughout the theoretical sections of this book. But for now, it is time for some light relief by returning to some applications.

1.5 Absorption in sound insulation – transfer matrix modelling

Porous absorbent material is widely used in sound insulation. Lightweight constructions are often based on double leaf partitions with an air gap in between as shown in Figure 1.6. It is normal for the air gap to contain a porous absorber. The porous absorber is used to prevent a resonance of the air cavity. If cavity resonances are not removed by damping, at the resonant frequency sound will pass easier through the partitions, and so the sound insulation will be poorer. It is important that the applied absorber is lightly packed; otherwise it can form a vibration path bridging between the two partitions, which could greatly reduce the performance of the system. Most

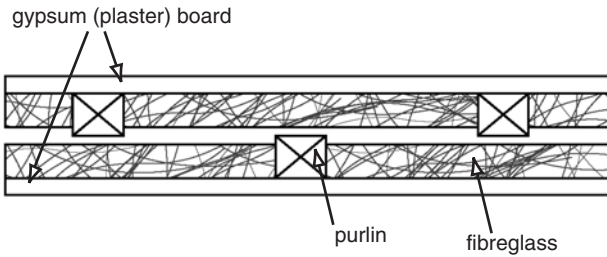


Figure 1.6 Mineral wool in a partition.

porous absorbers will be effective in partition, this is not the most critical application for the design of absorbers.

As the issue of transmission is being discussed, it seems appropriate to discuss the transfer function matrix approach to modelling transmission through, and absorption from, porous and resonant absorbers. The transfer matrix approach is the basis for many of the prediction techniques given in this book. A similar process is used in transducer modelling, where the method is called a two-port network.

1.5.1 Transfer matrix modelling

The transfer matrix approach to modelling sound propagation is a very powerful technique most often applied to porous absorption with and without membrane or perforated facings. It enables the surface impedance of single and multiple layers of absorbent to be calculated. For instance, it enables the case of a rigidly backed porous absorbent to be considered. This is the most important acoustic case, because it represents an absorbent placed on a wall, floor or ceiling.

Consider the situation shown in Figure 1.7. It is assumed that only plane waves exist within the layers. It is further assumed that the propagation is entirely contained in the x - y plane. By considering the continuity of pressure and velocity at the boundaries, it is possible to relate the surface pressure of one layer to the next.

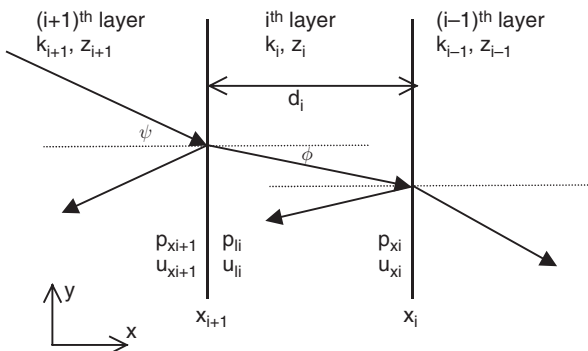


Figure 1.7 Geometry for transfer matrix modelling of a multi-layer absorbent.

$$\begin{Bmatrix} p_{li} \\ u_{li} \end{Bmatrix} = \begin{Bmatrix} p_{xi+1} \\ u_{xi+1} \end{Bmatrix} = \begin{Bmatrix} \cos(k_{xi}d_i) & j \frac{\omega \rho_i}{k_{xi}} \sin(k_{xi}d_i) \\ j \frac{k_{xi}}{\omega \rho_i} \sin(k_{xi}d_i) & \cos(k_{xi}d_i) \end{Bmatrix} \begin{Bmatrix} p_{xi} \\ u_{xi} \end{Bmatrix} \quad (1.26)$$

where p_{xi} and u_{xi} are the pressure and particle velocity at the bottom of the i th layer, for velocity this is defined to be in the x -direction, p_{xi+1} and u_{xi+1} the pressure and particle velocity at the bottom of the $(i+1)$ th layer, p_{li} and u_{li} the pressure and particle velocity at the top of the i th layer, d_i the thickness of the i th layer, ρ_i the density of i th layer, and k_{xi} the x -direction component of the complex wavenumber for the i th layer.

The x -component of the wavenumber is calculated by considering Snell's law (Equation 1.20):

$$k_{xi} = k_i \sqrt{1 - \sin^2(\phi)} = \sqrt{k_i^2 - k_{i+1}^2 \sin^2(\psi)} \quad (1.27)$$

Many porous absorbents have a small speed of sound in comparison to air, and so often $k_{xi} \approx k_i$ as $\phi \approx 0$.

This is a recursive equation from which the pressure and velocity of any layer can be determined from boundary and incident sound wave conditions. Although this process can be used to determine absolute values for the pressure and velocity, the technique is most powerful in determining surface impedance values. The surface impedance is calculated for the top of the i th layer, this is then used to calculate the impedance at the top of the $(i+1)$ th layer. The process is then repeated until all layers have been evaluated. The relationship that enables this process, relates the surface impedance at $x = x_{i+1}$ to the impedance at $x = x_i$ [10]:

$$z_{si+1} = \frac{-jz_{si}z_i \frac{k_i}{k_{xi}} \cot(k_{xi}d_i) + \left(z_i \frac{k_i}{k_{xi}}\right)^2}{z_{si} - jz_i \frac{k_i}{k_{xi}} \cot(k_{xi}d_i)} \quad (1.28)$$

where z_{si} is the impedance at $x = x_i$, z_{si+1} the impedance at $x = x_{i+1}$, k_i the wave-number in the i th layer, and x_i and x_{i+1} are defined in Figure 1.7.

To illustrate the application of Equation 1.28, consider the most common case which is a rigidly backed single layer. In this case, $z_{si} \rightarrow \infty$, and Equation 1.28 reduces to give the surface impedance of the rigid back absorbent as:

$$z_{si+1} = -jz_i \frac{k_i}{k_{xi}} \cot(k_{xi}d_i) \quad (1.29)$$

1.6 Absorption for pipes and ducts – porous absorber characteristics

Air conditioning ducts and other pipelines are a common source of noise [11]. Break-out noise radiates from the sides of the pipelines and ducts. The most effective treatment will be to reduce the noise at the source, but where this is not possible, application of absorbent within or external to the duct can be effective. For ventilation ducts, internal lining of the duct with porous absorbent is most effective. Internal duct liners are generally made of porous absorbent, the type is not that important from an

acoustic perspective. It is often necessary to use a protective coating, which can be a spray-on polyurethane coating, impervious lightweight plastic sheet, perforated metal, etc. The protective coating can have a significant effect on the absorption obtained.

For pipelines internal treatment is not often possible, and in this case external lagging can be done. The external lagging is often a combination of mineral wool and a heavy limp mass jacket made of metal, although the evidence is that foam is more effective. Below 300 Hz, the lagging of pipelines is not effective, and indeed around 300 Hz it can often result in increased noise breakout. Reference 11 gives design charts to enable the effectiveness of pipeline and duct lagging to be calculated, although the prediction can be inaccurate unless proper manufacturer's data is known.

1.6.1 Characterizing porous absorbers

To theoretically model the sound propagation through a porous absorber, it is necessary first to have measurements characterizing the acoustic properties of the absorber acoustic medium. So far in this chapter, the wavenumber and characteristic impedance have been discussed, but these cannot be directly measured. There are other parameters which are needed by absorber designers. Given a piece of porous absorbent material to characterize, often a researcher would start by measuring the flow resistivity σ and porosity ε . The flow resistivity gives a measure of the resistance to flow that the porous absorber offers and porosity the amount of open volume in the absorber. Chapter 3 outlines measurement methods for obtaining these values, although for many porous absorbents it is possible to assume a porosity of 1. These are probably the two most important determining parameters for porous absorbents. Once the flow resistivity and porosity are known, it is then possible to get the characteristic impedance and wavenumber via empirical laws, such as those outlined in Chapter 5, and predict the absorption properties of the sample.

It is possible to go to a more refined model of porous absorbers, which need further measurements of properties. There are a variety of models in the literature, but the one outlined in Chapter 5 uses three additional parameters, two characteristic lengths and tortuosity. These are more complete models of porous absorbents, but suffer from the problem that the characteristic lengths have to be fitted empirically, and consequently the verification of the accuracy of the theories is rather circular.

It is possible to directly measure the surface impedance, pressure reflection factor or absorption coefficient of a sample. This is often done in the development of prediction models for absorbents. As mentioned previously, the absorption coefficient can be measured through a reverberation chamber method, but this is problematical as the diffuse field absorption coefficient is often influenced by edge effects. Furthermore, it is not possible to get phase information from the reverberation chamber, and this is very useful in understanding how an absorber works or why a theory succeeds or fails. To get phase information, a measurement for a particular incident angle needs to be made. The easiest system is to measure the impedance in a tube, where only normal incidence plane waves exist. To get oblique incidence coefficients, it is necessary to use large samples in an anechoic chamber; the most common technique is a two-microphone method, which is limited to homogeneous, isotropic, planar samples. All these techniques are discussed in Chapter 3.

1.7 Summary

This chapter has outlined some absorber applications and touched on some of the issues that will be important in future chapters. It has also introduced some necessary mathematical principles. The remaining chapters concerning absorption are as follows:

- Chapter 3 discusses measuring absorber properties from the microscopic to the macroscopic.
- Chapter 5 discusses the application, design and theoretical modelling of porous absorbers.
- Chapter 6 discusses the application, design and theoretical modelling of resonant absorption, especially Helmholtz and membrane devices.
- Chapter 7 sets out some miscellaneous absorbers, which did not obviously fit into Chapters 5 and 6. Seating in auditoria and absorption from diffusers are considered.
- Chapter 11 discusses hybrid diffusers, and as these cause absorption, they are also an interesting absorber technology.
- Chapter 12 discusses how to get from predictions of single absorbent properties (mainly absorption coefficients) to full room predictions, especially the role of absorption coefficients in geometric room acoustic models.
- Chapter 13 rounds off the absorption work by looking at active absorber technologies.

The next chapter introduces surface diffusion.

1.8 References

- 1 H. Kuttruff, *Room Acoustics*, 4th edn, Spon Press (2000).
- 2 L. E. Kinsler, A. R. Frey, A. B. Coppens and J. V. Sanders, *Fundamentals of Acoustics*, 4th edn, John Wiley & Sons (2000).
- 3 M. Barron and L.-J. Lee, "Energy relations in concert auditoriums, I", *J. Acoust. Soc. Am.*, **84**(2), 618–628 (1988).
- 4 M. R. Schroeder, "New method of measuring reverberation time", *J. Acoust. Soc. Am.*, **37**, 409–412 (1965).
- 5 W. C. Sabine, *Collected Papers on Acoustics*, Harvard University Press (1922), republished, Acoustical Society of America (1993).
- 6 C. F. Eyring, "Reverberation time in 'dead' rooms", *J. Acoust. Soc. Am.*, **1**, 217–226 (1930).
- 7 G. Millington, "A modified formula for reverberation", *J. Acoust. Soc. Am.*, **4**, 69–81 (1932).
- 8 M. R. Schroeder and H. Kuttruff, "On frequency response curves in rooms. Comparison of experimental, theoretical, and Monte Carlo results for the average frequency spacing between maxima", *J. Acoust. Soc. Am.*, **34**(1), 76–80 (1962).
- 9 T. J. Cox and P. D'Antonio, "Determining optimum room dimensions for critical listening environments: a new methodology", *Proc. 110th Convention Audio Eng. Soc.*, preprint 5353 (2000).
- 10 J. F. Allard, *Propagation of Sound in Porous Media: Modelling Sound Absorbing Materials*, Elsevier Applied Science (1993).
- 11 D. A. Bies and C. H. Hansen, *Engineering Noise Control: Theory and Practice*, E&FN Spon, 2nd edn (1996).

2 Applications and basic principles of diffusers

In this chapter the basic principles of diffusers will be developed. Following the same style of Chapter 1, the chapter will be driven by application. In many respects, the right and wrong places to use diffusers are still being defined [1, 2]. There are places, such as rear walls of large auditoria, where there is a general consensus that diffusers are a good treatment to prevent echoes and better than traditional absorptive approaches. The case for using diffusers in some other places is less clear cut, and until further research is undertaken, some applications of diffusers are going to be based more on precedence and intuition, rather than scientific fact. Having said this, much has been learned in recent decades which can help to ensure that diffusers are used where they are needed.

This chapter will outline how diffusers can be applied and the effects their application will have on the physical acoustics and the listener response. It will also be used as an opportunity to introduce some basic physics, which will be needed to understand the more detailed chapters on diffuser prediction, design, measurement and characterization later in the book.

2.1 Echo control in auditoria

In Section 1.4 the problems of echoes and flutter echoes in room acoustics were discussed. To recap, echoes are caused by late arriving reflections with a level significantly above the general reverberance. For instance, they are often heard at the front of badly designed auditoria, with the echo being a reflection from the rear wall. The echo might also come from a balcony front or many other multiple reflection paths. Flutter echoes are caused by repeated reflections from parallel walls and are often heard in lecture theatres, corridors, meeting rooms, etc.

In Chapter 1, the suggested treatment for echoes was absorption, but diffusers can also be used. Using diffusers can be advantageous because they do not remove energy from the sound field. This is important in large auditoria with an orchestra, because every part of the sound power generated by the musicians should be preserved and not lost by avoidable absorption. In other cases, the choice between diffusers and absorbers will rest on whether the energy lost to absorption will detract or improve other aspects of the acoustics, such as the reverberance, envelopment and intelligibility.

2.1.1 Example applications

Figure 2.1 shows quadratic residue diffusers (QRDs) applied to the rear wall of Carnegie Hall in New York. QRDs are a type of Schroeder diffuser described in



Figure 2.1 Schroeder diffusers (QRDs[®]) applied to the rear wall of Carnegie hall to prevent echoes (after D’Antonio and Cox [2]).

Chapter 10. This form of reflection phase grating was the starting catalyst for modern diffuser research about three decades ago. The diffusers were installed in Carnegie Hall because a long delayed reflection from the rear wall caused an echo to be heard on the stage making it difficult for musicians to play in time with each other. Adding diffusers dispersed the reflection, reducing the reflection level arriving on the stage and consequently making the reflection inaudible. The diffusers also improved spaciousness on the main floor by uniformly diffusing rear wall reflections and masking echoes from the boxes [3].

Figure 2.2 shows the application of optimized curved diffusers to side walls of the Hummingbird Centre in Toronto (Consultant John O’Keefe, Aercoustics Engineering Ltd). A refurbishment of the hall was going to involve adding a reverberation enhancement system. The reverberation enhancement system added additional reflections from loudspeakers mounted in the side walls. Unfortunately, this was a shallow splay, fan-shaped hall, and as is common with many auditoria of this shape, if sources are on the side walls, echoes across the width of the audience area are heard. This was not a problem while the sound was being generated from the stage, but would have been a problem when the artificial reflections were generated from the side walls. It made no sense to treat the echoes with absorption, since this would just remove sound energy, which would have rather defeated the point of having the artificial enhancement system installed in the first place. The solution was therefore to use diffusers, which break up lateral propagating reflections in the audience area.

The original design for the diffusers in the Hummingbird Centre was for Schroeder diffusers, which were to be cloth covered to hide their visual appearance. This is a common story in diffuser design. The acoustical treatment needs to complement the visual appearance of the room to be acceptable to architects. If the visual aesthetic is not agreeable, the treatment will have to be hidden behind fabric, but as discussed in

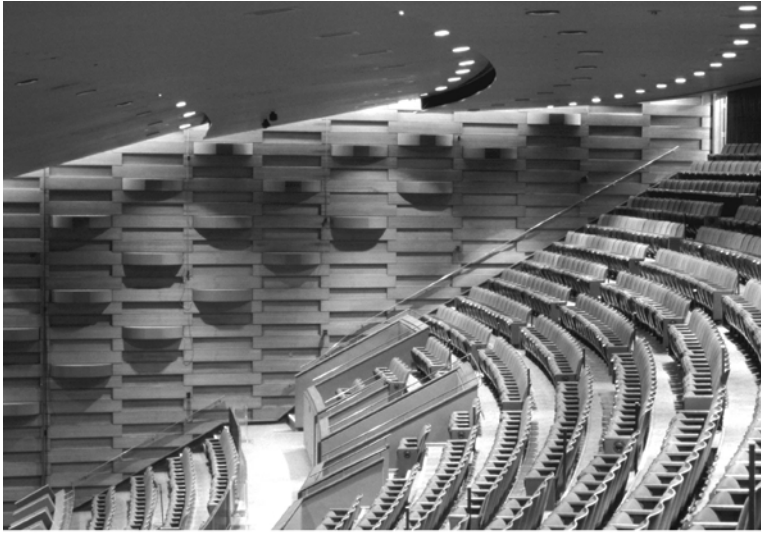


Figure 2.2 Application of optimized curved diffusers (OptiCurve™) in the Hummingbird Centre, Toronto (after D'Antonio and Cox [1]).

Chapters 7 and 9, this would have turned the side wall diffusers into absorbers. (Another solution architects often apply to acoustical treatment that does not fit with the visual requirement of a space, is to remove the treatment completely. This not only solves the visual aesthetic problem, but it saves money!) In the Hummingbird Centre, the designers were encouraged to try a new method for designing optimized curved surfaces, which will be outlined in Chapter 10. The finished design then complemented

the appearance of the space, and so the diffusers were left exposed. By choosing a curved shape, the diffuser could meet the visual requirements of the architect. The concept was a basket weave that would thread in and out of the cherry wood side walls. ‘The renovated room and, in particular, the enhancement system have been well received by the owners and their tenants, including the National Ballet and the Canadian Opera Company.’ [4]

2.1.2 *Wavefronts and diffuse reflections*

This section is an introduction to how diffusers disperse reflections. A standard construction to explain the effects of diffraction in physics was devised by Huygen. It is not exact for acoustic diffusers, but helps explain some of the phenomena happening with wave scattering. Figure 2.3 shows a plane wave reflected from a planar hard surface using Huygen’s construct, the incident wave is omitted for clarity. The construction involves placing a set of secondary sources, shown as stars on the surface, which are generated by the incident waves. These secondary sources hemispherically radiate, forming concentric waves which interfere and thereby model the reflected sound. Lines are drawn through points on the reflected wave which are in phase with each other, as shown on the lower figure. These lines are the wavefronts which show the direction and propagation of the reflected sound. Figure 2.3 shows the effect of a plane wave incident normal to a flat surface. This produces a reflected

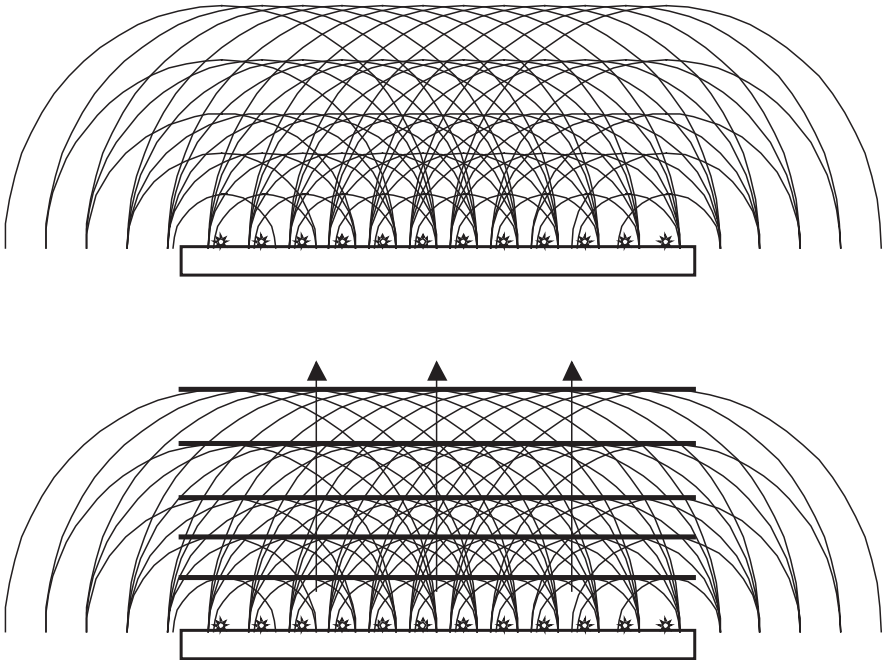


Figure 2.3 Huygen’s construct for a plane wave reflected from a flat surface. Normal incidence source. The incident wavefronts are excluded for clarity. The secondary sources are shown as stars on the surface.

plane wave in the specular reflection direction, where the angle of incidence equals the angle of reflection.

The reflected wavefront is spatially unaltered from the incident sound. Consequently, the sound from the source reflects straight back and is unchanged and not dispersed. This could lead to the reflection being perceived as an echo, especially if the source is a directional instrument such as a trumpet. Therefore, the role of a diffuser is to break up or diffuse the reflection, so that the sound energy is dispersed around the auditoria, and sound from directional instruments does not remain in narrow beams.

Figure 2.4 shows the effect of adding surface roughness to disperse the reflection. In this case a semicylinder is used. It can be seen that the reflected wavefront is no longer planar, but is now semicircular. The semicylinder has generated a virtual point source at the middle of itself. Consequently, a semicylinder will generate spatial dispersion. The wavefronts generated are still very ordered; however, so although semicylinders are good at spatial dispersion, they are not the best diffusers because temporal dispersion is not achieved; this will be discussed further in Chapter 10.

Figure 2.5 shows the effect of using a simplified Schroeder diffuser. A Schroeder diffuser changes the phase of the reflected wavefronts. The waves radiated by the

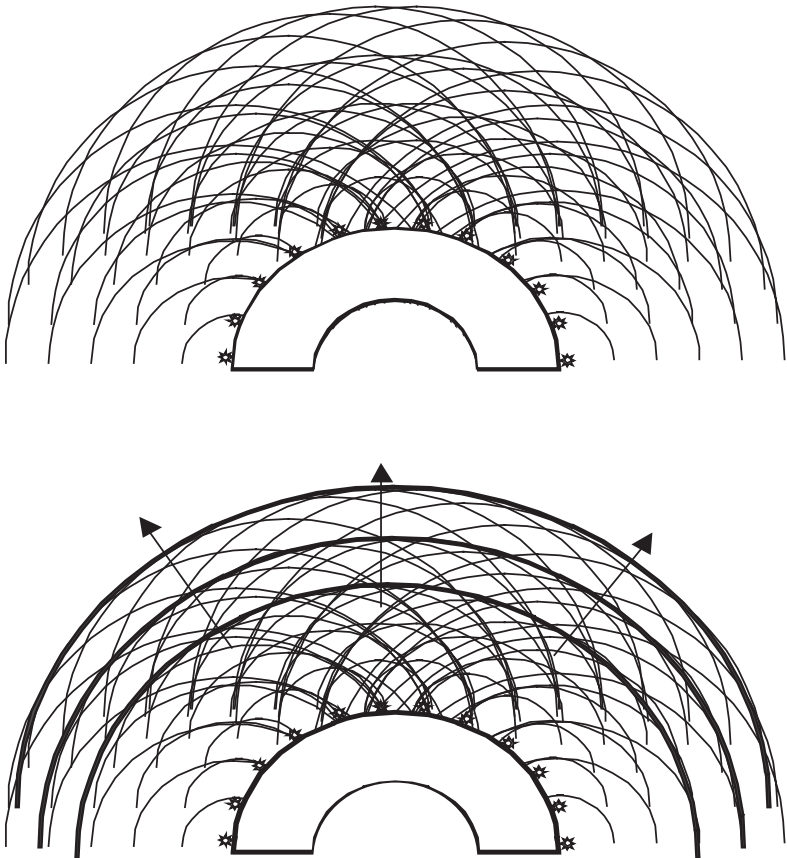


Figure 2.4 Huygen's construct for a plane wave reflected from a cylinder surface.

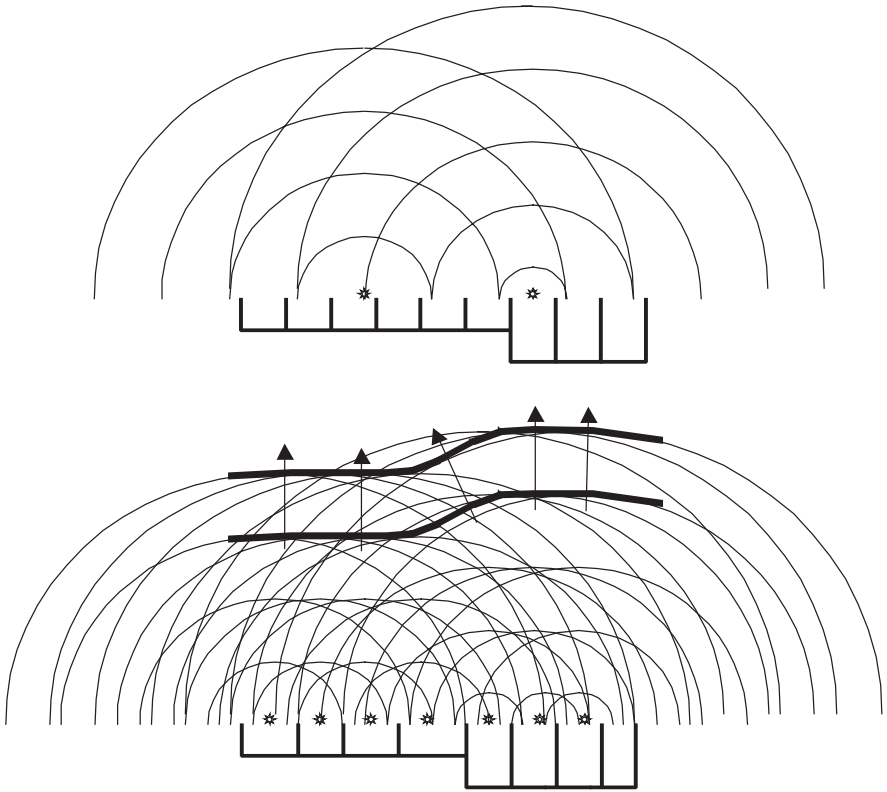


Figure 2.5 A Huygen's construct for a plane wave reflected from a simplified Schroeder diffuser. The top diagram shows the wavefronts from two wells only for clarity.

secondary sources are complicated, and it is difficult to pick out clear cut wavefronts. As well as generating spatial dispersion, reflection phase grating diffusers generate temporal dispersion. This can be seen in Figure 2.6.

The consequences of temporal dispersion can be seen in the frequency domain. In Figure 2.7 the temporal and frequency response of a single specular reflection from a flat surface and a diffuse reflection from a diffuser are shown. In Figure 2.7a, the direct sound, a specular reflection and the room interference are shown. In Figure 2.7b, the frequency response of the specular reflection alone is given. (The time window is illustrated by the two vertical lines in Figure 2.7c.) The specular reflection frequency response is characterized by a high pass filter response, characterized by the size and shape of the reflecting surface (see Chapter 10 for discussions of flat reflectors). In Figure 2.7c, where the reflection from a diffuser is given, the specular reflection is now temporally dispersed and shown as a diffuse reflection. The diffuser frequency response in Figure 2.7d is characterized by a random distribution of irregularly spaced nulls and peaks. Many heuristic diffuser designs assume that any temporal distribution will provide a satisfactory frequency spectrum, when in fact colouration is often inadvertently introduced.

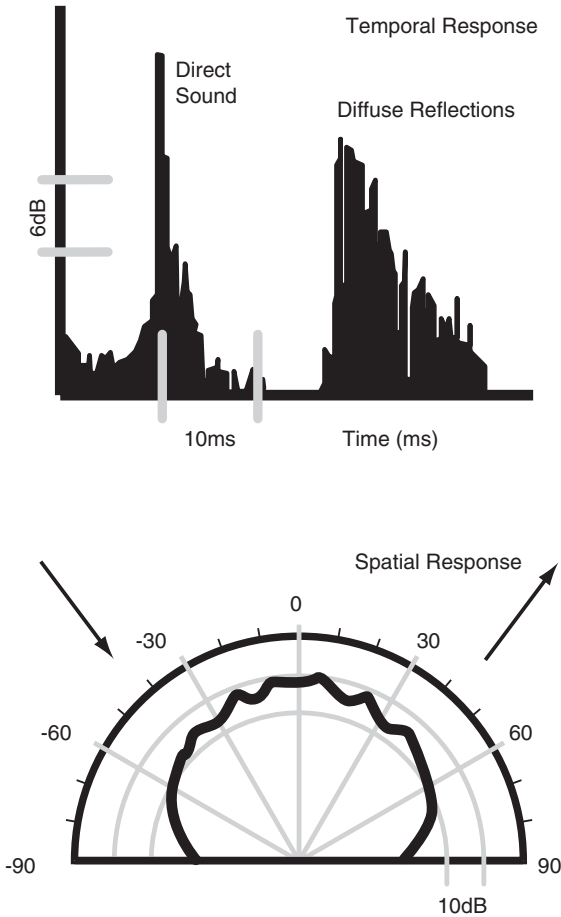


Figure 2.6 Measured spatial and temporal dispersion generated by a reflection phase grating.

In Figure 2.8 the temporal and frequency responses of the total fields, consisting of the direct sound and the reflection(s), are shown. When the direct sound and a specular reflection combine, they form a comb filter. The frequency spacing of the pattern is related to the time delay between, and the notch depth is related to the relative amplitude of, the direct sound and specular reflection. This is an effect that should be avoided in critical listening rooms and performance spaces. It can happen if large flat reflectors and nearby walls are not treated with absorbers or diffusers. When the direct sound combines with a diffuse reflection, the regularity of the comb filtering is removed and the variation in levels reduced. The spectral content of the direct sound can be more fully perceived. In addition to providing uniform spatial dispersion, reducing comb filtering is a principal reason for using diffusers in many applications.

Another way of forming a diffuser is to combine reflection and absorption. By putting patches of absorbent on a wall, some of the secondary sources will be absent,

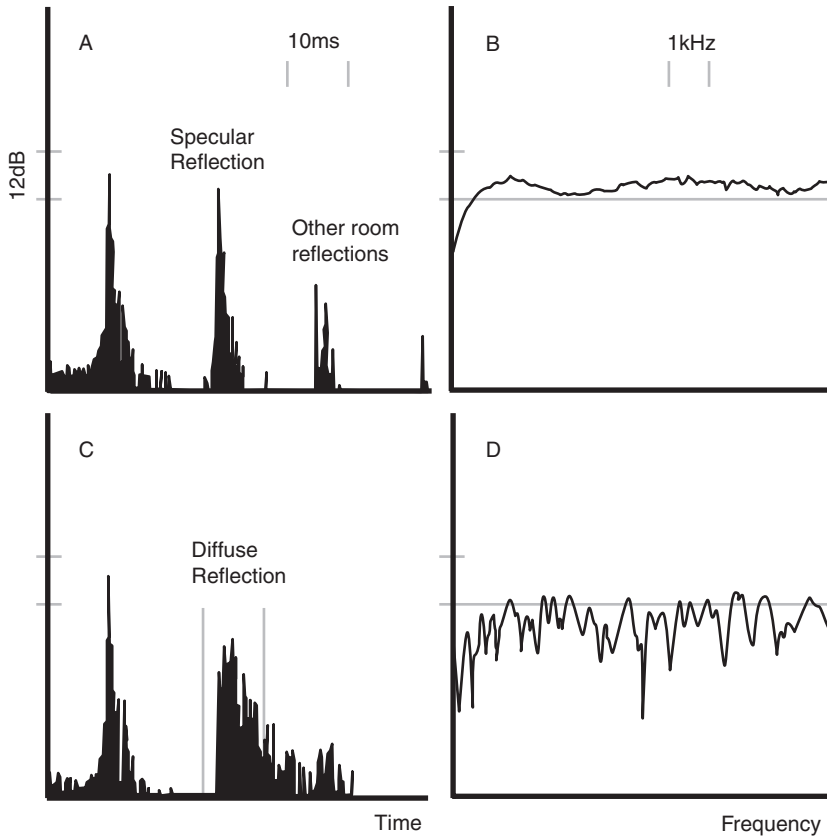


Figure 2.7 Measured temporal and frequency responses for a flat surface (top) and a diffuser (bottom). The frequency responses are for the reflected sound only (after D'Antonio and Cox [1]).

and dispersion is generated. Figure 2.9 shows a simple wavefront construction for this case. Traditionally, acousticians have utilized patches of absorption on wall surfaces to obtain dispersion. But this only leads to modest dispersion below frequencies where the dimension of the panel is roughly half a wavelength. To obtain high frequency diffuse reflections, the dimension of the patches must be much smaller and the distribution of the patches is important. This approach forms a hybrid surface, which partially absorbs and diffuses reflected sound, i.e. providing difforsorption. This type of surface is discussed in more detail in Chapter 11. These types of hybrid surfaces cause partial absorption, therefore they need to be used where reverberation control and dispersion are simultaneously needed.

2.1.3 *Coherence and terminology*

Many might describe the plane surface reflection as being coherent, and the reflections from diffusers as being incoherent, but this is actually a misleading use of terminology. From a purely physical standpoint, coherence occurs when there is a

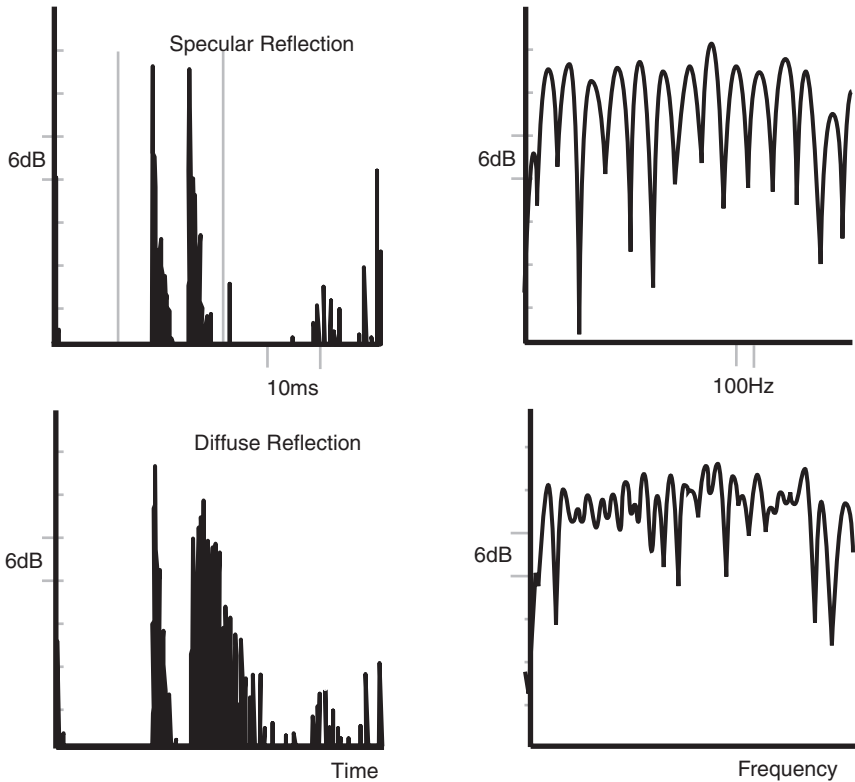


Figure 2.8 Measured temporal and frequency response of the total field, consisting of the direct and reflected sound. Top case is for specular reflection, the bottom case is for diffuse reflection (after D'Antonio and Cox [1]).

fixed, time invariant phase relationship between separate parts of a wavefront. For both plane surfaces and complex diffusers there is a fixed phase relationship. In this linear system, there is time variance. The wavefront from a diffuser is just complicated; it is not incoherent. To achieve physical incoherence, the surface would have to move or change in a random fashion over time.

Another terminology commonly used is to say the reflection is diffuse. There is no formal definition of this, but it refers to the case where the reflection is dispersed both spatially and temporally. Many modern designs are designed by examining the spatial dispersion and assuming that this will be accompanied by temporal dispersion. In addition, many diffusers are designed simply assuming that any temporal variation will produce uniform spatial dispersion and an acceptable frequency response; however, this is not necessarily the case.

It might be appropriate here to discuss and contrast surface diffusion and volume diffusion. For surfaces, the diffusion being discussed here is that generated by surface reflections in terms of the spatial and temporal dispersion. Whether these diffuse reflections then contribute to make a sound field more diffuse, is not what is being referred to. Indeed, diffusers might be applied simply to treat first reflection

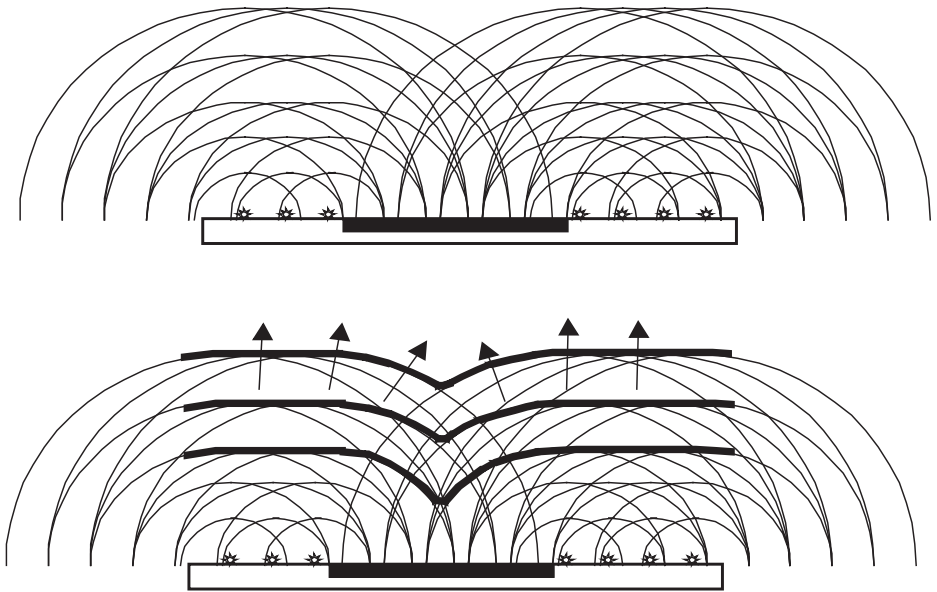


Figure 2.9 A simplified Huygen's construct for a plane wave reflected from a hybrid surface. The black patch is completely absorbing.

problems, such as echoes, and the effect these have on the reverberant field in the space might be of little concern. Both surface and volume diffusion refer to cases where the sound field, or surface reflections, become more complex. The effect of surface roughness and impedance changes is to generate diffraction, i.e. the breaking up of sound wavefronts due to edges and other effects. Acousticians do not seem to favour the term diffraction, however, but prefer diffusion, diffuse reflection or scattering. To complicate matters further, the use of these terms is inconsistent between different disciplines in acoustics. The only place where some clear differentiation has been set is with surface scattering and diffusion coefficients. A scattering coefficient refers to the ability of a surface to remove energy from the specular reflection direction, the diffusion coefficient refers to a measure of quality referring to the spatial uniformity of the reflections from a surface. Measuring and characterizing surface reflections is discussed in Chapter 4. This is also relevant to Chapter 12, where the application of scattering coefficients to geometric models is discussed.

Finally, it might be appropriate to discuss the spelling of diffusers. Schroeder and D'Antonio chose to use the spelling 'diffusor' to distinguish between acoustic and other diffusers such as those used for lighting and air dispersion. However, common usage has drifted towards diffuser, and this will be employed throughout this book.

2.2 Reducing colouration in small rooms

2.2.1 *Sound reproduction*

It is often useful to consider the extremes of boundary conditions when attempting to solve a room acoustic problem. In the case of a critical listening room, one extreme is

an anechoic chamber, and the other a reverberation chamber. Anyone who has spent any time in these rooms realizes that neither is an exciting place to listen to music. An ideal critical listening room will usually lie somewhere between the two extremes. It is also important to realize that since this is a sound reproduction room, the room can only corrupt what is being reproduced by the playback system. The unwanted artefacts added by the room are acoustic distortion.

In the early 1980s, there was an interest in improving the design of stereo listening rooms. It is difficult to underplay the importance that modern diffuser design has had on state-of-the-art sound reproduction facilities, whether these are listening rooms, recording or broadcast control rooms, teleconferencing or distance learning rooms. A major catalyst for this work was the pioneering research of D'Antonio [5] initially utilizing diffuser designs suggested by Schroeder [6] and also room design concepts such as live end dead end (LEDE[®]) [7] and reflection free zone (RFZ[™]) [8].

An RFZ design strives to minimize the influence of the room acoustic on the sound reproduction and so provides a neutral two-channel critical listening room. The design creates a spatial and temporal RFZ surrounding the primary mixing or listening position(s). The zone is spatial, because it only exists within a certain area in the room; and it is temporal, because the interfering reflections are only controlled over a certain time window, between the arrival of the direct sound, and prior to reflections arriving from the rest of the room.

It is well established that early reflections affect the characteristics of the sound at the listening position [9, 10]. One solution is to use absorption to control first-order reflections between the source and the listener and so remove early arriving high level reflections, which produce colouration and image shift. (Image shift meaning that the sound source appears to be coming from the wrong place.) Applying large numbers of absorbers leads to a dead room, and so diffusers are used as a way of preserving the energy, but providing it delayed and temporally dispersed to minimized distortion caused by interference with the direct sound. Diffusers on the rear wall essentially provided a passive surround sound that provides ambience in the room and envelopment.

Figure 2.10 shows the energy time curves measured before and after treatment in a small critical listening room. At the top of Figure 2.10, the direct sound and interfering side wall, floor, ceiling and sparse reflections from the room are identified. The early specular reflections cause colouration, image shifting and broadening of the image width and depth. The sparse specular reflections from the rear of the room also interfere with the direct sound further colouring the reproduction. These problems can be addressed by controlling the competing early reflections from the walls, floor and ceiling by application of absorbers and diffusers. This creates an initial time delay gap before the onset of the reflections from the rear wall forming the RFZ described above; this extends to roughly 18 ms, see lower graph in Figure 2.10. If absorption is used, psychoacoustic experiments indicate that the sonic images in the soundstage will be extremely small, as if sound comes from a point in space. If diffusers are used, the sonic images take on greater size and appear more realistic. Following the application of diffusers on the rear wall, the effects of which are shown in the lower part of Figure 2.10, the sparse room reflections more resemble a reverberant field of a larger room, with increased spatial and temporal reflection density. Using this technique, it is also possible to create a reverberant sound field with a linear slope.

D'Antonio *et al.* [11] carried out a study on a recording control room. A drawing of the room can be seen in Figure 2.11. In this example, an RFZ is achieved by flush

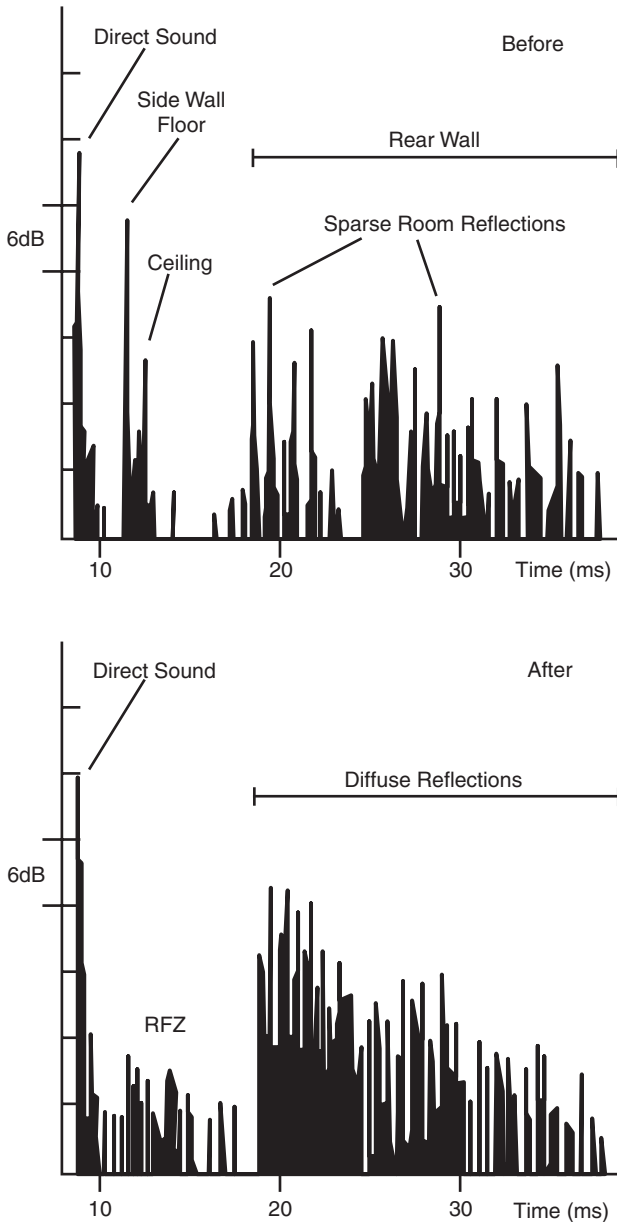


Figure 2.10 The impulse response in an untreated small critical listening room before (top) and after treatment (bottom) (after D'Antonio and Cox [1]).

mounting the loudspeakers (L) with the woofers close to the front trihedral corners of the room. The massive front walls are splayed outward and treated with porous absorption to provide broadband control of first-order reflections. The rear wall surfaces are treated with broadband diffusers (QRD) to disperse first-order rear wall

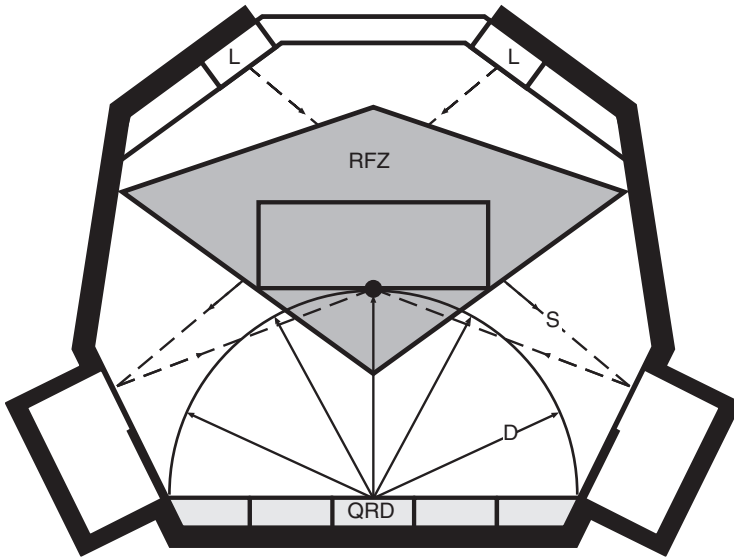


Figure 2.11 A sound reproduction room, with a designed reflection free zone (RFZ) shown shaded (after D'Antonio and Cox [1]).

reflections away from the listeners, while providing ambience and envelopment. The shaded area represents the spatial RFZ, 24 dB below the direct sound, with an initial time delay gap of approximately 17 ms, where the predominant energy is from the monitor loudspeakers. Two types of reflections are indicated in Figure 2.11. An undesirable specular reflection from the glass doors forming the machine room (S), and diffuse reflections which arise from 7 m² of diffusers located on the rear wall (D).

The rear wall diffusers reduce the level of the reflections reaching the listener early and so colouration effects are reduced. Figure 2.8 (top row) shows the time and frequency response for a listener close to a large plane surface with no other surfaces present. The similarity between the incident and reflected time responses can be seen. (Some minor differences are seen because the measured surface was finite in extent.) The incident and reflected sounds interfere to cause the well-known comb filtered response, shown to the right. A comb filter gives emphasis to some frequency components, while others are absent. This will change the relative magnitude of the harmonics in music and so lead to a coloured sound where the timbre is not true. Figure 2.8 (bottom row) shows the case for a listener close to a diffuser. The diffuser introduces temporal diffusion of the reflected sound, which leads to a more complicated frequency response. The regularity of the comb filtering is minimized, and consequently its audibility is diminished.

Unfortunately, although the colouration will be reduced, there is no formal method for evaluating the audibility of comb filtering. Some have suggested relating the frequency response to critical bands [12], although a more complex model is required to allow for masking effects which occur due to other room reflections.

In a small critical listening room, the boundary surfaces are usually rather close to the listener. The most efficient placement for a diffuser (or an absorber for that matter), is at the points where the first-order specular reflections are produced – the geometric reflection points. Consider a room in which all of the surfaces are mirrors. The geometric reflection points would be at all of those locations on the boundary surfaces at which a listener can see the sources.

The number of diffusers that should be used depends on what a listener's personal preference is. If interfering reflections are absorbed, then one experiences the highest resolution sonic images which are essentially points in space. If diffusers are used to control these reflections, the apparent size of the image is broadened. If done properly, some have described this as a more natural size image, similar to what might be experienced in the presence of an actual sound source. So a balance has to be reached in which the desired apparent source width and depth is achieved, while creating the desired ambience. While some people favour very dead spaces for mixing audio, others do not. Some studio designers like to create a non-environment where only the direct sound is received by the sound engineer. Whether this is a desirable acoustic or not seems to be a matter of taste. This personal preference aspect of critical listening is what makes acoustics a science and an art. High levels of absorption remove most of the room effects such as colouration, but lead to a very dead room that some would find oppressive. It leaves the sound engineer the tricky job of interpolating between the dead mixing room and normal listening environments such as living rooms, but does ensure that the engineer receives a very pure sound where detail can be easily detected.

If some liveliness is to be left in the room, a combination of absorbers and diffusers is better than absorption and flat walls which generate specular reflections. Consequently, many of the industry's leading mastering facilities use rooms with a combination of absorbers and diffusers. To take a couple of examples, one of the industry's most successful mastering rooms is Gateway Mastering + DVD, Portland, ME, shown in Figure 2.12 and one of the most successful recording studios is the Hit Factory, New York, shown in Figure 2.13.

How far away should a listener be positioned from the diffusers? The distance from listener to diffuser can be determined by considering the scattered and total field. First consider the scattered field, i.e. just the reflections from the diffuser. A diffuser requires a certain time or distance to form a wavefront. There is an analogy to loudspeakers that can be made here. A listener would not consider sitting 30 cm from a multi-way loudspeaker, because the listener would be in the near field of one of the drivers. At some distance from the loudspeaker, all individual high, mid- and low frequency waves from the individual drivers will combine to form a coherent wavefront. The same holds true for scattering surfaces. They also can be thought of in terms of near and far field, although the situation is a bit more complex than for loudspeakers.

It is common to describe the scattered field by its spatial response. This is similar to the far field polar response of a loudspeaker; however, the polar response of a diffuser is much more difficult to measure and this has been the subject of extensive research as reported in Chapter 4. In the far field, the polar response of an ideal diffuser is invariant to the angle of incidence, the angle of observation and the frequency, within its operational bandwidth. Unfortunately, in most critical listening rooms, it is usual for sources and receivers to be in the near rather than the far field, as the far field is



Figure 2.12 Gateway Mastering, Portland, ME showing a fractal diffusing rear wall Diffraactal[®] (photo courtesy of Gateway Mastering + DVD).

outside the room. Consequently, listeners should be positioned as far from scattering surfaces as possible. Precedence has shown that it is best if the listener is at least three wavelengths away from diffusers. Since diffusers used in listening room applications have a lower frequency limit of roughly 300–500 Hz, this means a minimum distance of 3 m is recommended. In some situations this distance may have to be compromised.

A listener positioned near a multi-way loudspeaker with their ear close to the mid-range driver hears sonic anomalies, and the same is true when the listener gets too close to a diffuser. Many of the phasing anomalies reported by room designers are due to the fact that they are listening too close to the diffuser and they are hearing near field comb filtering effects. Some listeners have even put their heads in the wells of large low frequency diffusers, and then claim something is wrong because it sounds odd! Furthermore, getting too close to a diffuser means that the temporal response is overly dominated by the surface close to the ear, which means the temporal dispersion generated by the diffuser is not heard. The direct and reflected sounds are then rather similar and comb filtering gets worse. This naturally leads us to a consideration of the total field.

When listening to music in a room, the total field is heard, which is a combination of the direct sound and reflections. If the scattered sound predominates, aberrations are heard. Just as room reflections affect the size and directionality of sonic images, they also can introduce colouration by changing the frequency response, distorting the spectral content or timbre of the direct sound. Studying the total field offers some insight into why scattering surfaces may introduce colouration.



Figure 2.13 Hit Factory, New York (photo courtesy of The Hit Factory, New York and Pilchner Schoustal Associates).

Consider a listener approximately 1 m from a scattering surface. If the reflection comes from a flat surface, the reflected and direct sound are comparable in level and the result is a comb filter (Figure 2.8 top). This is not very representative of the content of the direct sound. While this looks rather bad, the comb filtering may or may not be perceived depending on the relationship between the frequency of the nulls/peaks and auditory critical bands. In addition, masking by other reflections affects the audibility of the colouration. If the reflection comes from a diffuser, the scattered energy is dispersed in time, and the frequency response consists of an irregular spacing of null and peaks as in a diffuse sound field (Figure 2.8 bottom). The frequency response of the total field more closely resembles the direct sound, since the diffuse reflections have minimized the interference. Importantly, the listener no longer picks up the regularity of the peaks and troughs that were seen for the flat surface, and so the spectral changes introduced may be less noticeable. Figure 2.8 shows the case for a diffuser which scatters in one plane. Diffusers which scatter hemispherically, will direct more energy away from the listener and so will further reduce the comb filtering.

Recent research has now led to hybrid surfaces, which consist of reflective and absorptive areas. These surfaces provide both absorption and diffuse reflection, and may allow the listener to get even closer to the scattering surface. These surfaces are described in Chapter 11.

The level of the scattered sound and the resulting interference in the total field decreases in the following order: flat surface, curved surface, 1D phase grating, 2D phase grating, 1D amplitude grating, 2D amplitude grating, absorber. In light of these remarks, it is important to consider the temporal, spatial and spectral response of a sound diffusing surface. Casual or arbitrary shaping of surfaces is unwise and designers should solicit theoretical or experimental proof of performance characteristics for diffusers.

To conclude, the design of modern critical listening rooms is heavily dependent on how one controls strong specular reflections between the sources and listeners. The diffusers in RFZ spaces provided passive surround sound enhancing envelopment. Today, with surround sound reproduction formats such as 5.1 finding acceptance, the concepts are still valid but are employed differently. The rooms are not polarized between live and dead zones, and tend to be more uniform, with diffusers being used to enhance the envelopment and immersion of the surround speakers and to provide the desired degree of ambience. Absorbers and diffusers can still control strong specular reflections, which cause spectral and spatial distortion. One approach to designing a surround critical listening room, suggested by D'Antonio, utilizes broad-band absorption down to the modal frequencies in the corners (using a combination of membrane and porous absorption). Absorbers or hybrid surfaces of 50–100 mm deep are used on the walls between speakers and listener, to control first-order reflections, and diffusers are used in the middle of the four walls to enhance envelopment. Diffusing clouds, with broad bandwidth absorption down to the modal frequencies placed above the listeners, provide surround reflections and additional modal control.

2.2.2 Music practice rooms

Individual practice rooms play an essential role in music education. For all the extensive hours students spend in them, they are usually very uninviting and uninspiring cubicles. They usually are small rectangular rooms, 8–25 m³, fabricated from concrete block, with traditional compressed acoustic ceiling tile, some curtains to allow the acoustics to be varied, concrete floors and a full length mirror, which students use to monitor their posture and fingering. In other words, a low cost, functional and student proof space. Since the surfaces are usually concrete and the volume is small, the rooms typically have audible modal frequency problems. Some designs feature non-parallel walls to minimize flutter echoes. In addition to awareness of the unwanted buzzes and squeaks, students study articulation, tone production and intonation, and this is hampered by poor room acoustics. Another approach used is a prefabricated isolation cubicle. These rooms are typically small with absorptive surface treatment making the space relatively dead. As with other small acoustically critical rooms, these spaces can benefit from diffusers to give the musician some reverberance while minimizing colouration.

Consider a candidate room, which was 4.5 m long, 2.1 m wide on one end, 2.4 m wide on the other and 2.7 m high. The room had a conventional compressed acoustical ceiling glued to drywall, concrete floor, cinder block walls and a thin curtain to allow the acoustics to be varied somewhat. A series of objective measurements and subjective musician impressions before and after acoustical changes were carried out. The study introduced three acoustical elements: (i) an acoustical concrete masonry

block; (ii) a hemispherical ceiling diffuser, and (iii) a wall-mounted hemispherical hybrid diffuser-absorber. The first two of these elements are shown in Figure 2.14. The acoustical concrete masonry block [13] provided low frequency modal control via resonant absorption, structural walls and diffuse reflections in a single plane to promote ambience, intonation, tone production and support. In this connection the



Figure 2.14 A music practice room treated with diffusers (Skyline[®] on the ceiling [14] and DiffusorBlox[®] on rear wall [13]) and absorbers (after D'Antonio and Cox [1]).

word ambience is used to denote a high spatial impression and envelopment. The hemispherical ceiling diffuser [14] provided ambience, enhanced intonation control and a more diffuse sound field in the room. The hemispherical hybrid diffuser provided partial absorption, with any reflected energy being diffused. This provided the desired amount of articulation control for critical listening. Thus, the practice room provided detailed resolution, space or ambience, improved feedback for intonation and tone production, support, reduced modal colouration and lessened playing fatigue.

The impulse response of the room was measured during various stages of treatment, Figures 2.15 and 2.16. The time response shows the sound decay becoming more

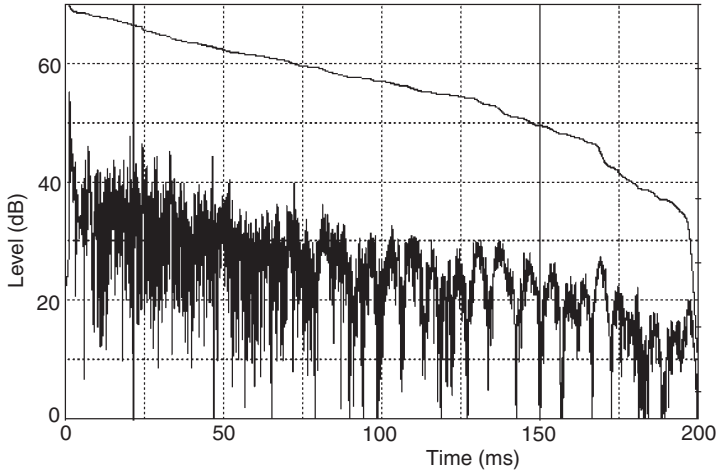


Figure 2.15 Impulse response of the music practice room shown in Figure 2.14 at early stages of treatment (after D'Antonio and Cox [1]).

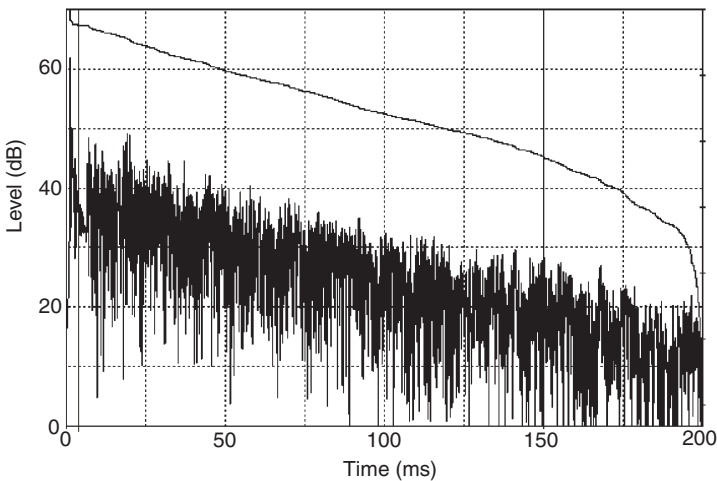


Figure 2.16 Impulse response of the music practice room shown in Figure 2.14 at end of treatment (after D'Antonio and Cox [1]).

even. Low frequency modal measurements were made before and after the addition of acoustical masonry units. The masonry units made a significant improvement in reducing the unevenness in the frequency response produced by the modes as seen in Figure 2.17. Figure 2.18 shows the decrease in the reverberation time in the frequency range where the masonry units are tuned for maximum absorption.

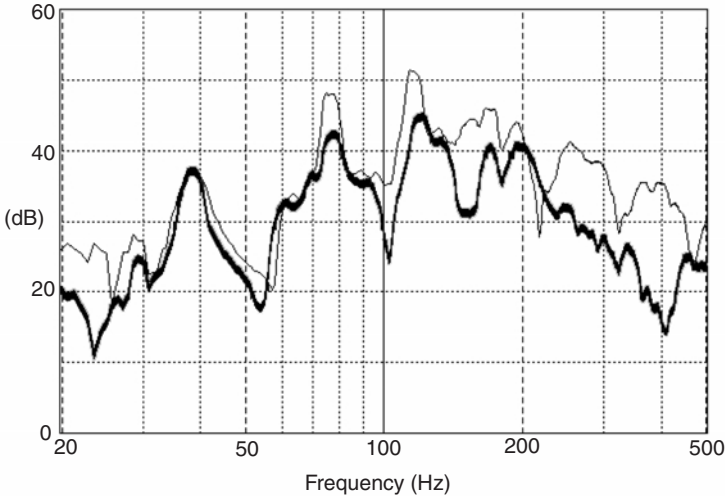


Figure 2.17 Frequency response of the music practice room. — Before bass treatment; — After bass treatment (after D’Antonio and Cox [1]).

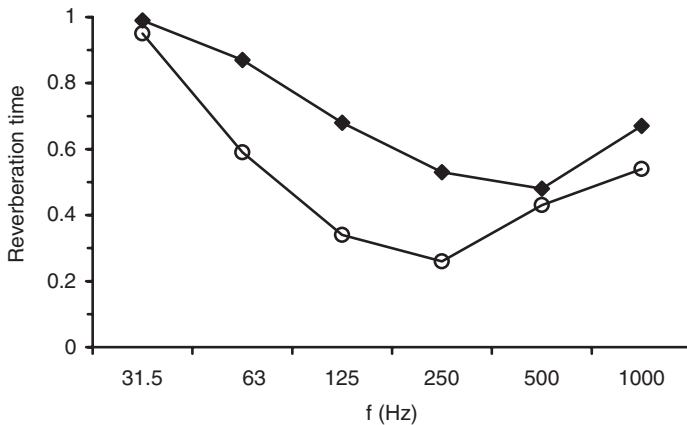


Figure 2.18 Change in reverberation time caused by adding absorbing/diffusing masonry units in the music practice room. —◆— Without masonry units; —○— With masonry units (after D’Antonio and Cox [1]).

The experiments verified that by utilizing limited diffraction, hemispherical ceiling diffusion and lateral wall diffusion, along with modal absorption, a very functional and enjoyable practice room could be attained.

2.3 Controlling modes in reverberation chambers

Reverberation chambers are designed to produce a diffuse sound field. This is a sound field where the reflected energy density is the same throughout the room and all directions of propagation are equally probable. Reverberation chambers need to achieve this condition because they are a fixed, reference, test environment providing repeatable results which can be interpreted and matched by other laboratories. Unfortunately, a completely diffuse field is not achievable, and this is one of the reasons that round robin tests on reverberation chamber methods usually show significant anomalies, see Chapter 3.

One of the methods used to achieve a diffuse field is surface or volume diffusers. Standing wave modes in the reverberation chamber cause the energy density to be uneven. Placing diffusers in the paths of modal propagation creates additional modes, which make the sound field more uniform. Surface diffusers need to be of the order of half a wavelength or deeper to have a significant effect on the sound field. The diffusers must also be applied to at least three of the boundaries, so that opposite surface pairs have at least one surface treated (e.g. treat the floor or ceiling). Consequently, the size of surface diffusers needed is often prohibitively large and expensive. A more economic solution is to hang diffusers in the volume of the room. Surface diffusers can only influence a hemisphere of sound, as they only receive sound from 2π space. Volume diffusers, on the other hand, can influence a full sphere, and so it is possible to get greater diffusion from this type. Figure 2.19 shows a typical application in



Figure 2.19 A small reverberation chamber (photo courtesy of RPG Diffusor Systems Inc.).

a reverberation chamber. A final option is to use rotating elements, but these will presumably become less common as test signals which require time invariance, such as maximum length sequences (MLS) and swept sine waves, become more popular.

There have been discussions about using diffusers to deal with modal problems in small rooms [15, 16]. This would be an alternative solution to the absorption treatment discussed in Section 1.3. If the walls of the rooms are hung with diffusers, then additional sound propagation paths are creating, generating additional room modes. These new room modes have the potential to smooth out the low frequency room response where the number of modes is small. Unfortunately, this solution requires very deep diffusers, and consequently, this is not a very practical solution. A solution might be to use active diffusers as discussed in Chapter 13.

2.4 Improving speech intelligibility in underground or subway stations

Many underground (subway) stations are non-diffuse spaces. The long and narrow shape means that mean free paths along the length of the station are much longer than those for transverse propagation (where the mean free path is the average time between reflections). Consequent, the sound decays much faster for transversely propagating sound, than for sound travelling up and down the length of the station. This results in a double decay and two reverberations times in the space. The long reverberation time causes problems with speech intelligibility, as the reverberance causes words to run into each other and become difficult to distinguish. Kang [17] showed that by applying diffusers to the side walls of the station, more transverse propagation can be promoted to decrease the reverberance of the space and improve speech intelligibility.

2.5 Promoting spaciousness in auditoria

One of the pioneering applications of Schroeder diffusers was by Marshall and Hyde in the Michael Fowler Centre, New Zealand [18, 19]. Figure 2.20 illustrates the application. Marshall and Hyde used large overhead reflectors to provide early reflections to the audience in the balconies. This was a method whereby a hall could have good clarity and yet maintain a large volume for reverberance. The large volume partly comes from the space behind the diffusers.

Not many years before the design of the hall, it had been established that lateral reflections were important in concert halls as these promote a sense of envelopment or spatial impression in rooms [20]. Music outdoors may be popular when accompanied with fireworks, but the quality of the sound is usually poor. Move indoors and the sound comes alive, enveloping and involving the listener in the music-making process. Outdoors, listeners receive sound straight from the orchestra, there are no reflections from walls, and the sound appears distant. When music is played in a room, reflections from the walls, ceiling and floor embellish the sound, especially if there are plenty of reflections arriving from the side. When sound reaches the listener from the stage, the same sound signal is received at both ears, because the head is symmetrical and the sound to both ears travels an identical path. When reflections come from the side, the sound at each ear is different, as sound to the furthest ear has to bend around

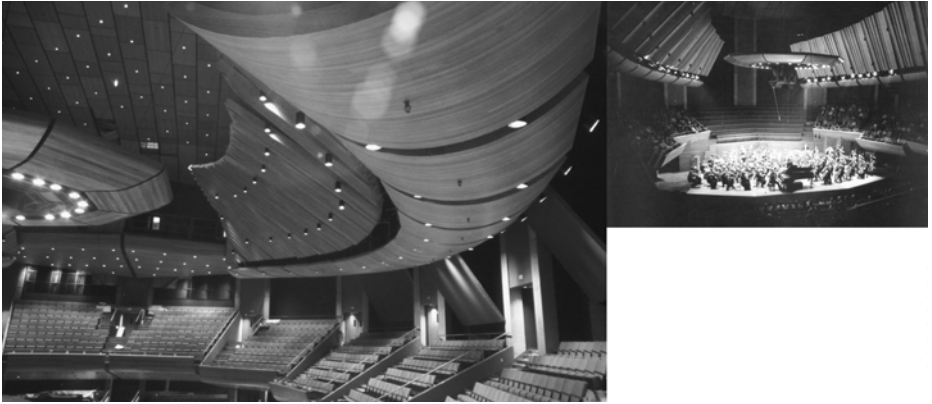


Figure 2.20 Schroeder diffusers in the Michael Fowler Centre, New Zealand (photo courtesy of Dr Harold Marshall of Marshall Day Acoustics).

the head. This means the sound arrives later and is significantly altered. The brain senses it is in a room because of the differences between the ear signals, and a feeling of being enveloped by the music occurs.

This need for lateral reflections influenced Marshall and Hyde to apply diffusers to the large overhead surfaces shown in Figure 2.20. The diffusers promote early arriving lateral reflections for spatial impression and clarity.

2.6 Reducing effects of early arriving reflections in large spaces

In Section 2.2 it was discussed how early arriving reflections can cause problems in small spaces due to colouration. Problems also arise in large rooms, for example in rooms with low ceilings. The ceiling reflection can arrive soon after the direct sound for audience members at the rear of the room, and this can lead to colouration as comb filtering may result. Figure 2.21 shows an application of diffusers in the Cinerama Theatre, Seattle, WA. Mainstream cinemas tend to be very dead spaces with the room effects added artificially through the surround sound reproduction system. The design brief for Cinerama, by Grant of Harris-Grant Associates, was to generate an acoustic with high envelopment and some reverberance, a first in modern commercial cinema design, by using diffusers on the ceiling and walls. While there is an extensive use of surface diffusion, experimental measurements showed that the cinema satisfied THX design criteria. The curved diffusers were used to disperse reflections from the relatively low ceiling to minimize comb filtering. The diffuser used on the ceiling is an optimized curved diffuser, a design process discussed in more detail in Chapter 10.

A secondary effect of using ceiling diffusers can be to reduce the level of early arriving non-lateral reflections from the ceiling. This can increase the spatial impression, but whether this happens depends on the geometry of the room and the diffusers used.

Another situation where overhead reflections can cause problems is overhead stage canopies, especially if the canopy effectively covers the whole stage area. Overhead canopies might be used to hide the presence of a fly tower, or may simply be an



Figure 2.21 Cinerama Theatre, Seattle, WA with a diffusing ceiling (OptiCurve™) (photo courtesy of University of Salford).

integral part of the stage canopy design. Figure 2.22 shows a typical case at Kresge Auditorium, Boston, MA (Acoustician: Rein Pirn, Acentech, Boston). The canopy provides reflections back to the stage area, which are necessary for the musicians to hear themselves and others. Without early reflections from the stage shells, musicians will find it difficult to create a good balance among themselves and keep in time. Canopies with little open area provide plenty of overhead reflections back to the musicians, but if the canopy elements are flat, there is a risk that the overhead reflections will be too strong and specular, and so cause colouration. The solution to this is to shape the canopy, so that some breaking up of the reflected wavefronts occurs. The diffusers spatially and temporally disperse the reflections and so reduce colouration. The design of overhead stage canopies is discussed in more detail in Chapter 10.

2.7 Diffusers for uniform coverage with overhead stage canopies

Overhead stage canopies can have a much greater open area than that shown in Figure 2.22. Figure 2.23 shows a typical example, where the canopy serves both the performers and the audience at Rivercenter for the Performing Arts, Columbus, GA (Acoustician, Jaffe, Holden Acoustics). Again the canopy is likely to be designed to promote better communication between musicians across the orchestral stage, leading to better ensemble among musicians and consequently



Figure 2.22 Overhead stage canopy at Kresge Auditorium, Boston, MA (Waveform™) (photo courtesy of RPG Diffusor Systems Inc.).

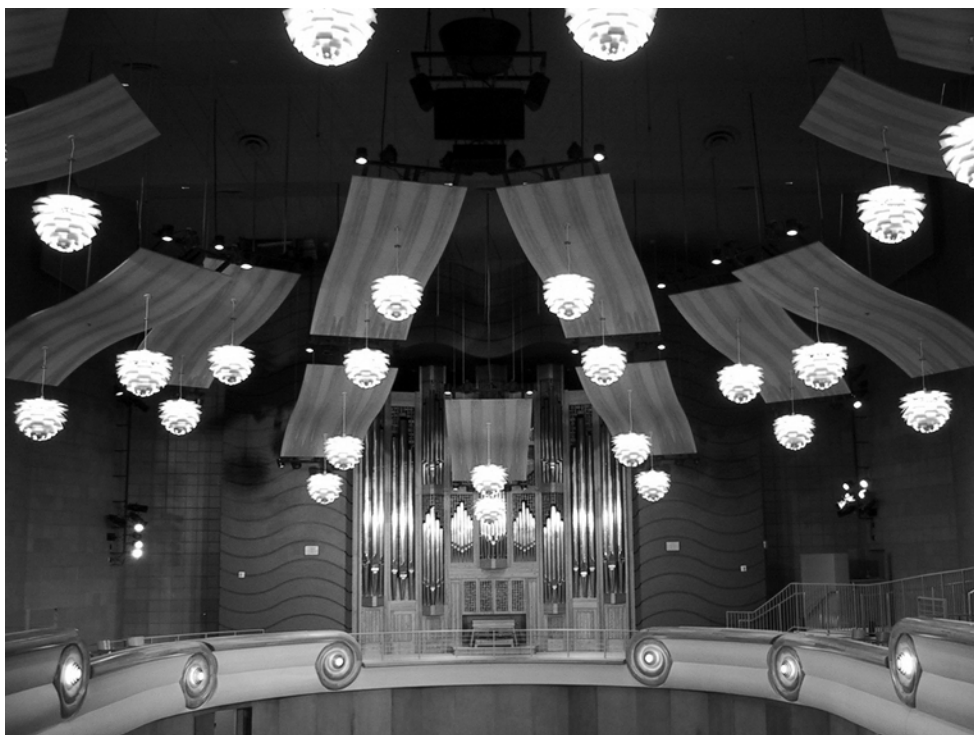


Figure 2.23 Rivercenter for the Performing Arts, Columbus, GA (photo Courtesy of Steve Haas).

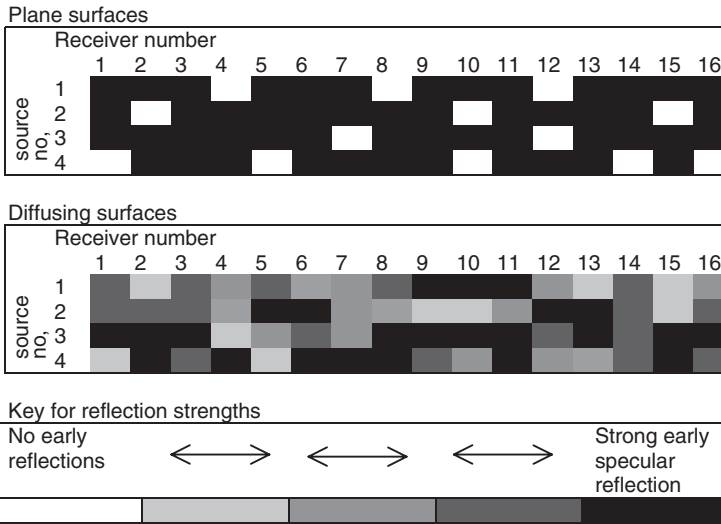


Figure 2.24 Schematic of pressure distribution from fairly open canopies with different surface treatments (adapted from Dalenback *et al.* [22]).

better quality concerts. This is achieved by ensuring an even distribution of reflected energy from each of the musicians’ instruments on the stage to other musicians, with the reflected energy being delayed by about 20–30 ms [21]. A canopy may also be used to reflect sound towards audience areas lacking sound energy.

There is risk, however, that providing extra overhead reflections from the stage canopy could lead to comb filtering and image shift. Canopies with large open areas are usually designed so much of the sound will go through the stage canopy to the void above, to be returned to the audience or stage from the true ceiling of the auditoria, and so provide reverberance.

If the canopy elements are flat, then the pressure distribution will be uneven. For some receiver positions there will be specular reflections from a canopy element, and so at mid-high frequency a strong reflection level results. For other receiver position, the geometric reflection point misses the canopy elements, and a low reflection level results. Figure 2.24 shows a comparative sound pressure level distribution from a canopy with open areas and plane surfaces and a canopy with open areas and diffusing surfaces after Dalenback *et al.* [22]. Consequently, canopies with spaces between the reflectors benefit from using diffusing elements, as they enable a more uniform coverage over the stage area, by scattering sound to receivers which would otherwise lack reflections due to the gaps between the canopy. Chapter 10 discusses stage canopy design in more detail.

2.8 Diffusers for rear and side of stage enclosures

During musical performances there is a need for surfaces or enclosures, conventionally called acoustical shells, that surrounds the musicians. The acoustical shell reinforces and blends the sound that is projected toward the audience. It also heightens the ability of the musicians to hear themselves and others. Acoustical shells typically

incorporate a rear wall, flared side walls and an overhead canopy. In addition to the orientation of the shell surfaces with respect to the performers, the nature of the acoustical surfaces is critical to good performance. A shell can contain reflecting and diffusing surfaces [23] and less often absorption.

Marshall *et al.* [24] suggested that early reflections among musicians greatly improve their sensation of playing as a group if the reflections:

- a Occur within a temporal window that is dependent on the nature of the musical program material, typically between 17 and 35 ms after the direct sound.
- b Include high frequency content roughly between 500 and 2,000 Hz, containing the attack transients that are cues for rhythm and expression.
- c Contain a balance of all the parts in the ensemble at all performance positions.

Condition (a) is easily met by spacing the shell an appropriate distance from the performers, while (b) and (c) depend more on the surface topology. Acoustical shells have used a wide variety of surfaces ranging from flat reflecting panels to various forms of surface irregularity, such as curved surfaces, polycylinders and fluted columns, and reflection phase gratings. The current state-of-the-art is to utilize multi-dimensional optimization to obtain the optimal shape and orientation, a technique discussed in Chapter 10. In Figure 2.25, the reflections from a flat and diffuse shell are

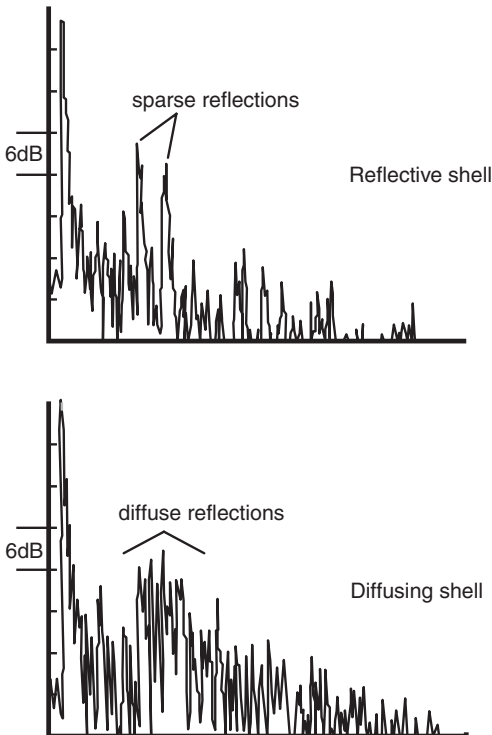


Figure 2.25 The reflections from a flat and diffusely reflecting hall.

compared. The diffuse reflections are spread over time and are of reduced level, lowering the chances of colouration and harshness due to comb filtering. The diffusion also satisfied the requirements (b) and (c).

D'Antonio [25] carried out a series of experiments using objective measures as well as musician's perceptual evaluations, to determine the appropriate combination and orientation of reflecting, diffusing and absorbing surfaces to optimize performance. The study began by looking at small groups chamber groups. An example of the test arrangement with a string ensemble is shown in Figure 2.26. Five different microphone systems were used for each playing environment to obtain five simultaneously recorded signals:

- 1 A mannequin with microphones at the entrance to the ear canal, was placed within the group to determine ensemble blend without self masking.
- 2 Probe microphones, Figure 2.27, were inserted into the ear canal to determine ensemble blend with self masking of the musician's instrument.
- 3 Headband microphones, located at the entrance to the ear canal, were also used to monitor ensemble blend with self masking.
- 4 An omnidirectional microphone was placed within the group as a monophonic control.
- 5 Spaced omnidirectional microphones were placed at the front of the house.

The string ensemble preferred a mixed orientation shell with lower vertical wells and upper horizontal wells, producing lateral and vertical diffusion, respectively. Some



Figure 2.26 Cavani string quartet performing in front of VAMPS[®] shell [23] at the Cleveland Institute of Music (after D'Antonio and Cox [2]).



Figure 2.27 In the ear probe microphone inserted into the ear canal of the 1st violinist. Microphone is inserted to a point just in front of the ear drum (after D'Antonio [22]).

musicians preferred flat surfaces on the lower surfaces for better bass coupling. Mutual and self-hearing was unanimously improved. The general reaction was that the diffusive shell provides warmth and intimacy and minimizes harshness. The preferred shell distance for warmth and intimacy was approximately 0.9–1.8 m. The preferred shell distance for projected sound quality was 2.7–3.7 m. There was unanimous agreement that a height of 4.9 m was better than 2.4 m.

A brass quintet experienced harshness from a completely reflective shell and preferred lower diffusers with vertical wells and upper diffusers with horizontal wells. The preferred distance for mutual and self-hearing as well as projected sound quality was 2.7 m. A horn duo preferred a mixture of flat surfaces and diffusers at approximately 1.8 m.

Following the chamber group research, the requirements of a symphony orchestra were investigated. There is an inherent imbalance in an orchestra, because the percussion and brass are naturally louder than the strings and woodwinds. Many traditional shells employ an average acoustic solution to satisfy a majority of the players, using fixed acoustical elements designed for existing musical formats and orchestral arrangements. Since each musician and musical section has a different preference for its own local acoustical environment, and since musical formats, orchestral arrangements, and conductor's preferences change, the benefit of a variable acoustical design was explored. The result was an open architecture modular framework, which would allow local acoustical environments in the rear of the orchestra, where the loudest and most problematic instruments are located. A study was done



Figure 2.28 Diffusers around the stage of the Corning Glass Centre, NY (photo © Paul Warchol Photography, www.warcholphotography.com).

with the Baltimore Symphony Orchestra at the Meyerhoff Symphony Hall, Baltimore, USA, using questionnaires and experimental measurements.

The shell was placed around the entire perimeter of the stage, similar to the shell shown in Figure 2.28. The shell consisted of a lower open support that allowed sound to reflect from the hard existing wall behind the shell. The next 0.6 m high tier consisted of horizontally diffusing single plane Schroeder diffusers with the centre of this level at seated ear height. The next 0.6 m in height contained all vertical diffusion, resulting from the wells being oriented horizontally. A 0.6 m cantilever canopy was oriented atop the vertically diffusing diffusers, at an angle of 45° with respect to the face of the diffusers. The purpose of the experiment was to blend the outer strings into the woodwinds, decrease the harshness of the brass, intensify the fullness and warmth of the strings and control strong specular reflections to enhance the sense of ensemble and rhythmic performance of the musicians. Musicians reported improved ensemble playing through the questionnaires.

2.9 Diffusers to reduce focussing effects of concave surfaces

Concave surfaces can cause focussing in a similar manner to concave mirrors. This can lead to uneven sound levels around a room, which is usually undesirable. Furthermore, as the concave surface concentrates energy in particular locations, there is a risk that this reflection will be significantly above the general reverberation of the space and so cause echo problems or colouration. A famous example of this is the Royal Albert Hall, where the large dome caused problems with long delayed and focussed reflections. The solution to this was to place volume scatterers, the well-known mushrooms, to disperse sound and also to provide earlier reflections to the audience. Assuming the concave surface cannot be removed, the only treatments

available are absorbers or diffusers. Both the treatments will work; the choice depends on other acoustic considerations, such as reverberance.

Figure 2.29 shows the polar response near a concave wall, which was to be part of a music rehearsal room, at the Edwina Palmer Hall, Hitchin, England. The concentration of sound at the focus is clear. To overcome this problem, a diffuser was specified by Orłowski of Arup Acoustics, UK. An optimized diffuser was developed and applied as shown in Figure 2.30, and Figure 2.29 shows that the dispersion of the focussed energy is quite dramatic. It would have been possible to remove the echo with absorbers, but then the musicians would not have received reflections from this wall. This would potentially have a detrimental effect on ensemble. In this case, the wall reflection had to be preserved, but the focussing removed, and hence diffusers were preferred over absorbers. Orłowski commented that ‘For architectural reasons, a concave form was developed for the hall, which obviously gave rise to concerns about focussing. Curve shape optimization was used to minimize focussing by the concave wall using a geometrical motif based on an amplitude modulated wave. Subjective listening tests to piano and clarinet music in the hall indicated a very uniform sound field with no evidence of focussing. Furthermore, both instruments produced an expansive sound with a very good balance between clarity and reverberance. Musicians found the hall easy to play in. The success of this project has led Arup Acoustics to consider curve optimization for providing diffusion for other projects, including a rehearsal hall with curvature in two dimensions.’ See Chapter 10 for detailed discussions of geometric diffusers and optimized diffuser design.

2.10 Diffusion and road side barriers

Traffic noise barriers are used to reduce noise propagation from the road to neighbouring houses. One problem that road side barriers suffer from is double reflections from high sided vehicles enable some of the noise to bypass barriers, as shown in Figure 2.31a. Another problem is reflections from barriers on one side of the road, which then pass over barriers on the other side, as shown in Figure 2.31b. One solution to this problem is to apply absorption. The problem with absorption is that it tends to wear badly under the harsh conditions of high winds, salt and water, which are common next to busy roads. Consequently, absorber performance is likely to decrease over time unless specialized and expensive durable absorbers are used. Diffusers may offer a solution to this problem, as shown in Figure 2.31c. By dispersing the sound, the reflection problems are decreased. The difficulty with this solution is that sound energy has not been removed by the diffusers, just scattered into other directions. There is a risk that wind and other meteorological conditions could cause the scattered noise to be blown or refracted to noise sensitive areas. Consequently, there is a need to make this solution robust under a wide range of weather conditions. Recent studies have indicated that trees can be used to reduce turbulence around roadside barriers, and so natural wind breaks might enable the performance of diffusing barriers to be more robust to changing metrology [26]. (Recently, phase gratings have been optimized to provide absorption, utilizing a perforated metal screen on the face acting as a resistive element. These new absorbers may offer a durable alternative to porous absorption.)

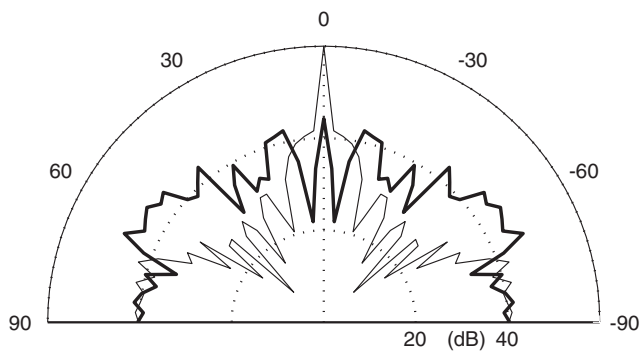


Figure 2.29 Scattering from a concave arc compared to an optimized curved diffuser at 3 kHz. ——— concave arc; ————— optimized curved diffuser.



Figure 2.30 Optimized curved surface (OptiCurve™) in the Edwina Palmer Hall (photo courtesy of Arup Acoustics).

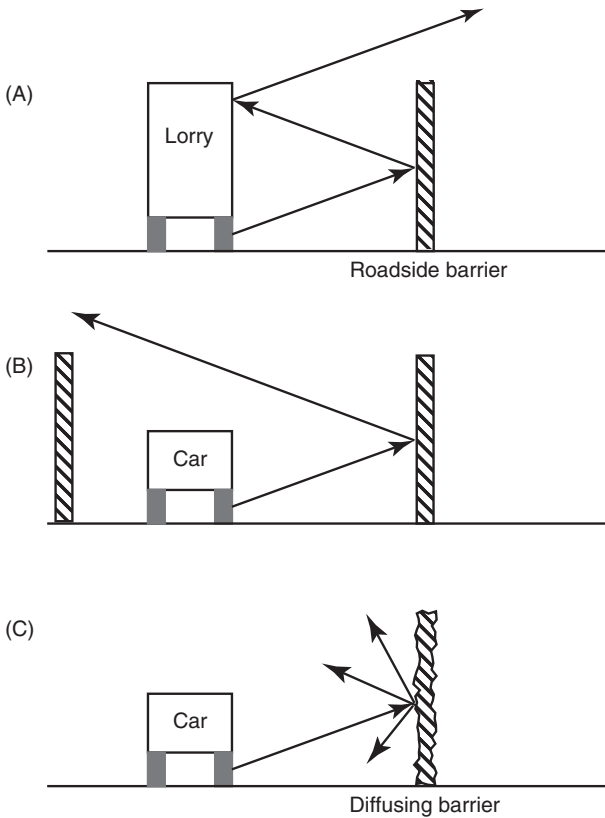


Figure 2.31 Schematic illustrating diffusers to reduce reflection problems with noise barriers.

2.11 Diffusion and street canyons

Street canyons are streets with high sided buildings on both sides, which form a semi-enclosed space where sound levels can build up and noise levels can become unacceptable. The surface structures of the buildings forming the street canyon influence the sound levels. For example, balcony fronts can have the unfortunate effect of reflecting sound back down to street level and so exacerbating noise problems. On the other hand, diffusers may have a role in breaking up the reflected sound on the building fronts, causing it to disperse and therefore be minimized at street level. Kang [27] used a geometric computer model to compare the influence of the building faces on noise levels in streets. He found that diffusely reflecting surfaces reduced the sound level from traffic by 2–4 dB provided the listener is not too close to the traffic sources.

2.12 Conclusions

In recent decades, an understanding of where and why diffusers should be used has been created. While this knowledge is still incomplete, in many common applications it is now well established how diffusers should be used. This chapter has detailed

some of these applications, as well as presenting some of the key principles to be further developed later in the book. The remaining chapters concerning diffusers are as follows:

- *Chapter 4* discusses the measurement of reflections from surfaces, and the characterization in terms of scattering and diffusion coefficients.
- *Chapter 8* deals with the methods for predicting diffuser scattering, presenting both complex and simple methods.
- *Chapters 9, 10 and 11* deal with the design of key diffuser types: Schroeder, geometric and hybrid diffusers.
- *Chapter 12* discusses the role of scattering coefficients in geometric room acoustic models.
- *Chapter 13* rounds off the diffuser chapters by looking at active diffuser technologies.

2.13 References

- 1 P. D'Antonio and T. J. Cox, "Diffusor application in rooms", *Appl. Acoust.*, **60**(2), 113–142 (2000).
- 2 P. D'Antonio and T. J. Cox, "Two decades of sound diffusor design and development part 1: applications and design", *J. Audio Eng. Soc.*, **46**(11), 955–976 (1998).
- 3 L. L. Beranek, *Concert and Opera Halls: How They Sound*, Acoustical Society of America, 69–74 (1996).
- 4 J. P. O'Keefe, T. J. Cox, N. Muncy and S. Barbar, "Modern measurements, optimized diffusion, and electronic enhancement in a large fan-shaped auditorium", *J. Acoust. Soc. Am.*, **103**(5), 3032–3033 (1998) also *Proc. 16th ICA* (1998).
- 5 P. D'Antonio and J. H. Konnert, "The reflection phase grating diffusor: design theory and application", *J. Audio Eng. Soc.*, **32**(4) (1984).
- 6 M. R. Schroeder, "Binaural dissimilarity and optimum ceilings for concert halls: more lateral sound diffusion", *J. Acoust. Soc. Am.*, **65**, 958–963 (1979).
- 7 D. David and C. Davis, "The LEDE concept for the control of acoustic and psychoacoustic parameters in recording control rooms", *J. Audio Eng. Soc.*, **28**, 585–595 (1980).
- 8 P. D'Antonio and J. H. Konnert, "The RFZ/RPG approach to control room monitoring", *Proc. Audio Eng. Soc.*, preprint 2157 (I-6) (October 1984).
- 9 J. Blauert, *Spatial Hearing*, MIT Press, Cambridge, MA (1983).
- 10 S. E. Olive and F. E. Toole, "The detection of reflections in typical rooms", *J. Audio Eng. Soc.*, **37**(7/8), 539–553 (1989).
- 11 P. D'Antonio, F. Becker and C. Bilello, "Sound intensity and interaural cross-correlation measurements using time delay spectrometry", *J. Audio Eng. Soc.*, **37**(9), 659–673 (1989).
- 12 F. A. Everest, *Master Handbook of Acoustics*, 4th edn, McGraw-Hill (2001).
- 13 P. D'Antonio, *Acoustical Diffusing and Absorbing Cinder Blocks*, US patent 5, 193, 318 (1993).
- 14 P. D'Antonio, *Two-dimensional Primitive Root Diffusor*, US patent 5, 401, 921 (1995).
- 15 P. D'Antonio, "New types of acoustical materials simplify room designs", *Proc. 81st Convention Audio Eng. Soc.*, preprint 2365 (1986).
- 16 J. Angus, A. C. Marvin and J. Clegg, "The effect of acoustic diffusers on room mode density", *Proc. 96th Audio Eng. Soc. Convention*, preprint 3851 (1994).
- 17 J. Kang, "Experimental approach to the effect of diffusers on the sound attenuation in long enclosures", *Bldg. Acoust.*, **2**, 391–402 (1995).
- 18 A. H. Marshall and J. R. Hyde, "Some practical considerations in the use of quadratic residue diffusing surfaces", *Proc. 10th ICA*, Sydney, paper E7.3 (1980).

- 19 A. H. Marshall, J. R. Hyde and M. F. E. Barron, “The acoustical design of Wellington Town Hall: design development, implementation and modelling results”, *Proc. IoA (UK)*, Edinburgh (1982).
- 20 M. Barron, “The subjective effects of first reflections in concert halls – the need for lateral reflections”, *J. Sound Vib.*, **15**, 475–494 (1971).
- 21 M. Barron, *Auditorium Acoustics and Architectural Design*, E&FN Spon, 55 (1993).
- 22 B.-I. Dalenbäck, M. Kleiner and P. Svensson, “A macroscopic view of diffuse reflection”, *J. Audio Eng. Soc.*, **42**, 793–807 (1994).
- 23 P. D’Antonio, *Variable Acoustics Modular Performance Shell*, US Patent 5, 168, 129 (1992).
- 24 A. H. Marshall, D. Gottlob and H. Alrutz, “Acoustical conditions preferred for ensemble”, *J. Acoust. Soc. Am.*, **64**(5), 1437–1422 (1978).
- 25 P. D’Antonio, “Performance acoustics: the importance of diffusing surfaces and the variable acoustics modular performance shell”, *Proc. 91st Audio Eng. Soc. Convention*, New York, preprint 3118 (B-2) (October 1991).
- 26 T. Van Renterghem, D. Botteldooren, W. M. Cornelis *et al.*, “Reducing screen-induced refraction of noise barriers in wind by vegetative screens”, *Acta AcusticaAcustica*, **88**(2), 231–238 (2002).
- 27 J. Kang, “Sound propagation in street canyons: comparison between diffusely and geometrically reflecting boundaries”, *J. Acoustic. Am. Soc.*, **107**(3), 1394–1404 (2000).

3 Measurement of absorber properties

This chapter covers a variety of methods used to measure and characterize acoustic absorbers. For many practitioners, the only important measurement is to gain the random incidence absorption coefficient in a reverberation chamber. While this may be the absorption coefficient that is needed for performance specifications in room design, other measurements are needed to understand and model absorptive materials. This is particularly true, because the prediction of random incidence absorption coefficient is problematic, and consequently it is necessary to measure materials in a more controlled environment to allow direct comparison between theory and measurements.

The more controlled environment that is often used is the impedance tube, which allows normal incidence impedance and absorption to be determined. Less often, but nevertheless valuable, are the free field measurements on large area samples done in hemi-anechoic spaces. The most common free field method uses a two-microphone approach, but this is often only applicable to isotropic, homogeneous samples. Consequently, attention has recently turned to using more than two microphones; however, the measurements appear to be problematic and very noise sensitive.

The next subject for this chapter is *in situ* measurements for obtaining acoustic absorption and impedance. There has been recent interest in these techniques to allow the true absorption properties of materials after construction and in their final in use condition to be determined.

There is also a need to be able to characterize the propagation within the absorbent material, to enable theoretical modelling of the absorption properties. For instance, the well-known Delaney and Bazley empirical model outlined in Chapter 5 requires the flow resistivity and porosity of the absorptive material to be known. For this reason, methods to measure key parameters that characterize the propagation within the absorbent are outlined.

The intention of the chapter is to provide information on the different measurement techniques. It is not intended that each description is a comprehensive standard with a foolproof description of how to carry out the measurements. What is intended is that the reader should be able to make an informed decision about the different techniques described, understand the advantages and disadvantages, and supplement the descriptions given here with that available in the referenced literature.

3.1 Impedance tube or standing wave tube measurement

The standing wave tube enables both the normal incidence absorption coefficient and surface impedance to be measured. This is a very useful test method as it enables the

absorption coefficient and impedance to be measured under well-defined and controlled conditions. Consequently, it is frequently used in validating prediction models for absorptive materials. This method has the advantage of only needing small samples (a few centimetres in diameter); this makes it ideal for developers of absorptive materials, as the alternative is construction of large samples for reverberation chamber tests, which are more difficult and expensive. The final key advantage is that the impedance tube method can be carried out with relatively simple apparatus in a normal room and does not need specialist test chambers. Problems with the method arise when the absorption from the small sample is not representative of the behaviour of a large sample, as would happen with many resonant absorbers. For this reason, the method is most used with local reacting porous absorbers.

Figure 3.1 shows some typical set-ups, and the concept is as follows. A loudspeaker generates plane wave propagation in the impedance tube, the plane wave propagates down the tube before reflecting from the sample. A standing wave is set up within the tube. The impedance of the sample alters the reflected wave, and by measuring the resulting standing wave, it is possible to calculate the normal incidence absorption coefficient and surface impedance of the sample. This is such a common technique in acoustics, that it has been enshrined in international standards [1, 2].

The necessity for plane wave propagation imposes many limitations on the system which are discussed as follows.

- 1 The losses into and through the tube should be minimized so that the plane waves propagate without significant attenuation. Consequently, thick metal is a common

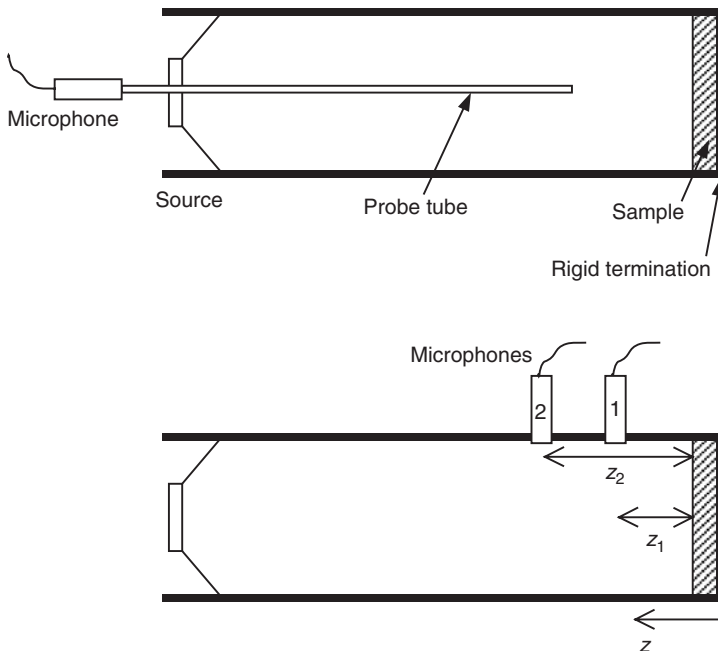


Figure 3.1 Set-ups for impedance tube measurement. Top, probe tube for standing wave method, bottom, two-microphone technique.

construction material for the mid- to high frequency ranges of most concern in building design. For impedance tubes that are to work at bass frequencies, more extreme construction is needed to prevent significant losses from the tube. For example, steel-lined concrete tubes can work down to the limit of human hearing (20 Hz). Whatever the size, to minimize losses the tube should be smooth on the inside and clean.

- 2 The tube should have constant cross-section over the measurement region where the sample and microphone positions are located. The actual shape is not that important; square and circular tubes are most popular. Although circular tubes seem to be less prone to cross-mode problems within porous absorbents, square tubes are useful, as in some cases square samples are easier to construct.
- 3 The loudspeaker should be a few tube diameters (or widths) from the first microphone position so that any cross modes generated by the loudspeaker have decayed away.
- 4 The microphone positions should not be too close to the sample so that any evanescent waves generated on reflection have had time to die away. For a homogeneous, isotropic sample that means the first measurement microphone should be at least half a tube diameter (or width) away. For samples that are structured and anisotropic, no microphones closer than two diameters away from the sample surface should be used.
- 5 The highest frequency, f_u , that can be measured in a tube is then determined by:

$$f_u = \frac{c}{2d} \quad (3.1)$$

where d is the tube diameter or maximum width and c the speed of sound. This is a statement that there should not be any cross modes in the tube; the first mode appears when half a wavelength fits across the tube. The limitation imposed by Equation 3.1 means that to cover a wide frequency range, several different impedance tubes with different diameters or widths are required.

It is possible to measure at higher frequencies if multiple microphones are used across the width of the tube. The sound field within the tube can be considered to be a sum of the plane wave and higher modes, in a similar way to a room sound field that can be decomposed into modes. In a circular tube and an isotropic sample, one additional microphone enables the impedance of the sample for the plane wave and first cross mode to be determined (circular symmetry can be exploited to reduce the number of additional microphone measurements in this case). The disadvantage of the multi-microphone method, is that for frequencies where the first cross mode dominates the sample is not receiving plane waves, so the absorption coefficient measured may be hard to relate to prediction models.

An experimental detail that is most critical is the requirement for the sample to be cut and mounted correctly. It is vital that the sample fits snugly into the tube. Any gaps around the edge must be filled and sealed, otherwise the gaps will allow absorption by the edge of the sample and the measured absorption will be too high. Worse still, if the small gaps open up to an air cavity behind, a Helmholtz device could be formed, and the absorption overestimated by a large margin. The normal way of providing proper sealing is to use petroleum jelly (Vaseline[®]), Plasticene[®] or mastic to fill the edges of the sample. It is also important,

however, not to wedge porous absorbers into the tube – this changes the mechanics of the absorber frame and so can lead to incorrect absorption being measured due to the mass spring action of the absorber frame. It is also important that the rear of the absorber is properly terminated. Air gaps between the absorber and the backing plate will lead to excess absorption being measured, unless of course it is planned to mount the absorber with an air gap, in which case the measurement would be correct.

The impedance tube is not often useable for extended reaction absorbers, unless the impedance tube happens to coincidentally be the same size as the extended reaction device. For instance, the performance of a membrane absorber is usually dependent on the mounting of the membrane. It is not possible just to mount a smaller membrane absorber in an impedance tube, and expect the same performance as the larger device.

3.1.1 Standing wave method

The advantage of the standing wave method is that it is very dependable, and relatively idiot proof. Unfortunately, it only measures one frequency at a time, so only spot frequency information is available. The procedure for locating minima in the standing wave, which is needed to get phase information, is rather slow, and so measuring a large number of frequencies is tedious. It is, however, more robust and reliable than the transfer function method discussed in Section 3.1.2 and is a useful second check on results from that method.

If plane waves are assumed to propagate in the tube, then the theories outlined in Chapter 1 for the reflection of sound from a plane infinite absorbent can be used. The steady state pressure in the tube is given by:

$$p = A \left[e^{jkz} + R e^{-jkz} \right] \quad (3.2)$$

where R is the reflection factor, k is the wavenumber, the sample is assumed to be at $z = 0$, and A is a complex constant.

The first term represents the incident wave and the second the reflected wave.

There are two methods for sampling the pressure within the tube, the first is the standing wave ratio method, and the second is the transfer function method. For the standing wave method, the minimum and maximum pressures are measured. The maximum pressure p_{\max} occurs when the first and second terms in Equation 3.2 are in phase, and the minimum pressure p_{\min} occurs when they are out of phase. In terms of equations:

$$\begin{aligned} p_{\max} &= 1 + |R| \\ p_{\min} &= 1 - |R| \end{aligned} \quad (3.3)$$

The standing wave ratio s is defined as the ratio of p_{\max} to p_{\min} and is given by:

$$s = \frac{p_{\max}}{p_{\min}} = \frac{1 + |R|}{1 - |R|} \quad (3.4)$$

Equation 3.4 can then be rearranged to allow the magnitude of the reflection factor to be obtained:

$$|R| = \frac{s - 1}{s + 1} \quad (3.5)$$

From the reflection factor it is possible to get the absorption coefficient as $\alpha = 1 - |R|^2$ – see Section 1.4.2.

To find the pressure maximum and minimum, it is necessary to have a probe microphone mounted on a moving trolley. The advantage of this formulation is that no pressure calibration is needed provided the equipment remains time invariant, as any factors relating the acoustic pressure to the voltage monitored by the measurement equipment, such as the effects of the probe tube, cancel out.

By noting the distance of the first minimum from the sample, z_{\min} , and considering the necessity for the incident and reflected phase to be different by exactly π at this position, it is possible to also calculate the impedance of the sample at the test frequency. The phase angle of the reflection factor is given by:

$$\angle R = 2kz_{\min} - \pi \quad (3.6)$$

Using Equation 1.23, it is then possible to obtain the normal incidence surface impedance.

Moving back from the sample, the first minimum met should be measured, and then the next maximum. This minimizes the effect of tube losses. It is possible to add loss factors into Equation 3.2 if the tube absorption is significant, and equations are given in the standard [1] to do this. It is far better, however, to make sure the losses are negligible in the first place. For samples with low absorption, this measurement becomes rather inaccurate as the measured standing wave ratio has a large error associated with it, as the pressure minimum becomes too small to be accurately measured.

3.1.2 *Transfer function method*

Equation 3.2 has two unknowns, the magnitude and phase of the reflection factor. By measuring the pressure at two points in the tube, it is possible to set up and solve simultaneous equations for the reflection factor and from there get the impedance and absorption coefficient. This is the principle of the transfer function, often called the two-microphone method. (Although, as this is often used with one microphone which is moved, calling this a two-microphone method is nowadays rather misleading.)

The primary advantage of using this method is that it obtains the absorption and impedance of the surface for all frequencies (within limits) with only a couple of quick measurements. It is therefore much more efficient than the standing wave tube method.

The transfer function between two microphone positions in the tube is measured as shown in Figure 3.1. Remembering that the transfer function is simply the ratio of pressures, and applying Equation 3.2, the transfer function between microphone positions 1 and 2 is given by:

$$H = \frac{e^{jkz_2} + Re^{-jkz_2}}{e^{jkz_1} + Re^{-jkz_1}} \quad (3.7)$$

where z_1 and z_2 are the positions of the microphones shown in Figure 3.1. Rearrangement then directly leads to the complex pressure reflection factor:

$$R = \frac{He^{jkz_1} - e^{jkz_2}}{e^{-jkz_2} - He^{-jkz_1}} \quad (3.8)$$

Using the equations set out in Section 1.4.2, the absorption coefficient and surface impedance are then obtained.

There are restrictions on the microphone spacing. If the microphones are too close together, the transfer function measured will be inaccurate because the change in pressure will be too small to be accurately measured. This leads to a lower frequency limit, f_l , for a given microphone spacing $|z_1 - z_2|$:

$$f_l > \frac{c}{20|z_1 - z_2|} \quad (3.9)$$

If the microphone spacing becomes too wide problems arise. As the spacing approaches a wavelength, the simultaneous equations become impossible to resolve as the pressure measured at both microphones is identical. This leads to an upper frequency limit f_u due to microphone spacing given by:

$$f_u < \frac{0.45c}{|z_1 - z_2|} \quad (3.10)$$

Consequently, there are two upper frequency limits given by Equations 3.1 and 3.10, and the lowest figure should be taken.

The lower and upper frequency limits mean that to cover a reasonable number of octaves it is often necessary to use more than two microphone positions in a tube; three positions are typically used. Three positions give three possible microphone spacings, and by appropriately setting the frequency ranges for each of the spacings, it is possible to cover a wider frequency range.

There are a choice of methods for measuring the transfer function in Equation 3.7. A dual channel FFT analyser can be used with a matched pair of microphones using a white noise source. In that case it is necessary to compensate for differences in the microphone responses by measuring once, then interchanging the microphones and measuring again. A more efficient method is to use a deterministic signal such as a maximum length sequence [3] or swept sine wave [4]. This means one microphone can be used to measure the transfer function to each microphone position, and ratios of these transfer functions taken to obtain Equation 3.7. This negates the need for matched microphones. Using a deterministic signal rather than white noise also removes the need for time-consuming averaging.

It is important that any unused holes are blocked, and that microphones are mounted flush to the tube sides. Better results appear to be obtained for fixed microphones than for a probe microphone. The likely reason is that microphone positioning accuracy is crucial, and this is harder to obtain with a probe. This

problem can be overcome by measuring many different microphone positions along the impedance tube with the probe and averaging the different results, but this is rather slow.

3.2 Two microphone free field measurement

The disadvantage of the impedance tube is that it does not readily allow oblique incidence measurement. A method is therefore needed for oblique incident sound to allow the angle dependence of absorption to be found. The two-microphone free-field method allows this to be done. By its very nature, the test method needs a large sample, which can be difficult to produce. It also needs an anechoic or hemi-anechoic space for the measurement. This method, like the impedance tube, is of most use to porous absorber designers or modellers.

The method can be thought of as an extension of the transfer function, impedance tube method. Readers unfamiliar with the impedance tube method should read Section 3.1 before proceeding here. The technique is most straightforward for homogeneous, isotropic materials. Consider a large sample of absorbent being irradiated by a loudspeaker a long way from the surface as shown in Figure 3.2. The measurement can be done in an anechoic or hemi-anechoic chamber. It can even be done in a large room providing that time windowing is used to remove unwanted reflections from other boundaries. It is assumed that plane waves are incident on the surface. Furthermore, for large isotropic, homogeneous samples, it can be assumed that the reflected wave is also a plane wave. In which case the equations set out in Section 3.1.2 for the transfer function measurement in the impedance tube can be applied directly to the free-field case.

Some practical details need careful consideration. Although in theory the sample should be infinite, in reality the sample will be finite in extent and so edge diffraction becomes important. The diffraction from the edges at low frequencies causes the reflected wave to no longer be planar, and so the simple theories no longer apply. A rough lower frequency limit is when half a wavelength fits across the smallest sample dimension. Consequently, samples are typically several square metres in area. When

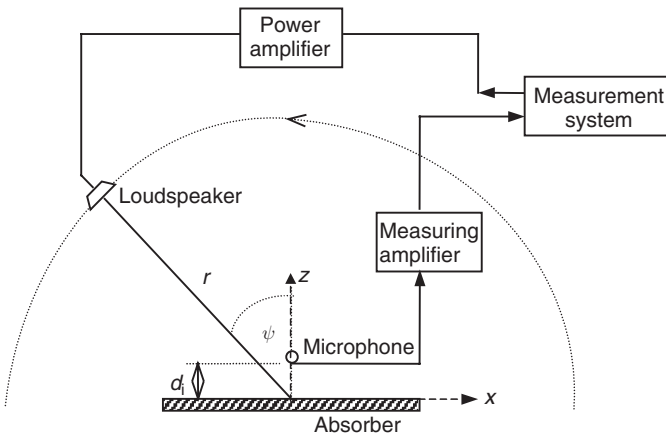


Figure 3.2 Experimental set-up for two or multi-microphone free-field measurement.

large samples are not available, one solution is to bring the source close to the surface, say 20 cm away, so the edge waves become less significant [5]. In which case, it is necessary to use spherical wave equations rather than the plane wave equations given above. The drawback of using spherical wave formulations is that the interpretation of the measured impedance becomes less straightforward.

Returning to the plane wave case, the first microphone is typically 5 mm from the surface, and the second 15 mm from the surface; the lower and upper frequency limits discussed for the impedance tube related to microphone spacing are still relevant. The microphones must be small enough that they do not cause significant disturbance to the acoustic sound field. While it is possible to use two microphones, one microphone that is moved may be preferred as it disturbs the sound field less significantly than a microphone pair. It also removes the need for calibration. A deterministic test signal such as a maximum length sequence or swept sine must be used in this case.

The method can be extended to deal with oblique incidence in which case the equations should be re-derived. For an incident angle of ψ , the transfer function between the two microphones positions is given by:

$$H = \frac{e^{jkz_2 \cos(\psi)} + Re^{-jkz_2 \cos(\psi)}}{e^{jkz_1 \cos(\psi)} + Re^{-jkz_1 \cos(\psi)}} \quad (3.11)$$

where it has been assumed that the two microphone positions have the same x and y displacement in the coordinate system defined in Figure 3.2. A rearrangement of Equation 3.11 leads directly to the reflection factor:

$$R = \frac{He^{jkz_1 \cos(\psi)} - e^{jkz_2 \cos(\psi)}}{e^{-jkz_2 \cos(\psi)} - He^{-jkz_1 \cos(\psi)}} \quad (3.12)$$

The impedance can then be calculated using Equation 1.23 and from Equation 1.25 the absorption coefficient at that particular angle of incidence can be found.

Problems arise for large angles of incidence. As the angle of incidence increases, the effects of edge diffraction become more significant at higher frequencies. Consequently, very large angles of incidence are difficult to measure due to the effects of edge scattering unless very large sample sizes are available.

3.3 Multi-microphone techniques for non-isotropic, non-planar surfaces

For non-isotropic or non-planar surfaces, it is still possible to carry out a free-field measurement using a method similar to that detailed in Section 3.2, although the system becomes more elaborate and rather sensitive to measurement error. The formulations for the two-microphone free-field method have assumed that the dominant reflected wave is a plane wave, which is true for isotropic, homogeneous, infinitely large planar scatterers. As soon as the surface becomes rough, or there are impedance variations, then there is potential for non-plane wave propagation. For example, if a periodic impedance variation is considered, a set of grating or diffraction lobes in non-specular directions are generated. (See for example Figure 9.3, where the

Schroeder diffuser generates 11 lobes.) To measure the absorption in the periodic case, it is necessary to measure the magnitude and phase of each of these reflected waves. This requires the measurement using more than two microphone positions because there are additional unknowns – the magnitude and phase of each of the grating lobe waves – to be resolved. To measure the 11 propagating waves seen in Figure 9.3, 12 microphone positions would be needed. In reality, it is unlikely that this case could be measured, as the number of microphones increase, multi-microphone systems become prone to measurement of noise and errors [6, 7].

The next section details a multi-microphone method for surfaces with periodic impedance variation [6] to give an idea of how such a multi-microphone system might work. Although it is difficult to implement and get accurate measurements, it does enable incident angle dependent absorption to be measured.

3.3.1 *Multi-microphone free field measurement for periodic surfaces*

There will be multiple reflected waves, not just the plane waves considered in the two-microphone method. By using more than two microphone positions, it is possible to measure the amplitude and phase of these reflected waves. The pressure in front of the absorber $p(x, z)$, shown in Figure 3.2, is decomposed into the incident plane wave $p_i(x, z)$ and scattered (reflected) pressure $p_s(x, z)$:

$$\begin{aligned} p(x, z) &= p_i(x, z) + p_s(x, z) \\ p_i(x, z) &= P_i e^{j(-xk_x + zk_z)} \\ p_s(x, z) &= \sum_{n=-\infty}^{\infty} A_n e^{j(-x\beta_n - z\gamma_n)} \end{aligned} \quad (3.13)$$

where $k_x = k \sin(\psi)$, $k_z = k \cos(\psi)$, $\beta_n = k_x + n2\pi/W$, $\gamma_n = -jk \sqrt{(\sin(\psi) + n\lambda/W)^2 - 1}$, A_n are complex coefficients describing each of the reflected waves, P_i a constant, ψ the incident angle, k the wavenumber in air, λ the wavelength in air, and W the width of one period.

The surface is periodic and (assumed) infinite so that a Fourier representation of the reflected sound field is used. Readers are referred to Chapter 7 for more details of the theory.

The scattered pressure is an infinite sum of waves, with complex coefficients A_n . Not all of these waves will propagate into the far field. The waves which are confined to the near field, the evanescent waves, need not be modelled, which means the sum over n is finite. The upper and lower limits for the sum in Equation 3.13 are determined by:

$$\left[\sin(\psi) + n \frac{\lambda}{W} \right]^2 \leq 1 \quad (3.14)$$

Let the lower limit be denoted n_1 and the upper limit n_2 (they must be integers). The number of coefficients to be determined must be small for this measurement to work.

The absorption coefficient is found by taking one minus the ratio of the reflected to incident energy, which gives:

$$\alpha(\psi) = 1 - \left| \frac{A_0}{P_i} \right|^2 - \frac{1}{\cos(\psi)} \sum_{n=n_1, \neq 0}^{n_2} \left| \frac{A_n}{P_i} \right|^2 \sqrt{1 - (\sin(\psi) + n\lambda/W)^2} \quad (3.15)$$

When only the $n = 0$ term exists, then a two-microphone approach can be used as the only radiating wave is the plane wave term. When more than one term is present, $|n_1| \vee |n_2| > 0$, more microphones are needed. In this case $N = (|n_1| + |n_2| + 2)$ points need to be measured since the transfer functions between two measured positions will be used.

At m th measurement point (x_m, z_m) , where m runs from 1 to N , the sound pressure can be calculated as:

$$p_m(x_m, z_m) = P_i e^{j(-x_m k_x + z_m k_z)} + \sum_{n=n_1}^{n_2} A_n e^{j(-x_m \beta_n - z_m \gamma_n)} \quad (3.16)$$

In the data processing, it is convenient to use the transfer functions between adjacent measurement positions $H_{m, m+1} = p_m/p_{m+1}$. Using Equation 3.16, this is given by:

$$H_{m, m+1} \frac{p_m}{p_{m+1}} = \frac{P_i e^{j(-x_m k_x + z_m k_z)} + \sum_{n=n_1}^{n_2} A_n e^{j(-x_m \beta_n - z_m \gamma_n)}}{P_i e^{j(-x_{m+1} k_x + z_{m+1} k_z)} + \sum_{n=n_1}^{n_2} A_n e^{j(-x_{m+1} \beta_n - z_{m+1} \gamma_n)}} \quad (3.17)$$

This means a $N - 1$ set of simultaneous equations can be obtained in terms of (A_n/P_i) :

$$\sum_{n=n_1}^{n_2} \left(\frac{A_n}{P_i} \right) (e^{j(-x_m \beta_n - z_m \gamma_n)} - H_{m, m+1} e^{j(-x_{m+1} \beta_n - z_{m+1} \gamma_n)}) = H_{m, m+1} e^{j(-x_{m+1} k_x + z_{m+1} k_z)} - e^{j(-x_m k_x + z_m k_z)} \quad (3.18)$$

Once the simultaneous equations have been formed, these can be solved to give A_n/P_i , which can be substituted into Equation 3.16, and gives the absorption coefficient after a little manipulation.

The choice of measurement positions is critical. If the microphone is only allowed to traverse the z -direction, then critical frequencies occur where there are insufficient unique simultaneous equations to resolve the coefficients. These critical frequencies manifest themselves as frequencies for which non-sensical absorption coefficients are obtained. These critical frequencies can be avoided by changing the microphone position in z and x . The typical spacings used give microphones 5–10 cm apart.

The multi-microphone method is very sensitive to evanescent (non-propagating) waves. The microphone must be far enough from sample not to measure evanescent waves as these have been neglected in the above theories, but if the microphone is too far from the surface, diffraction from the sample edges will cause the measured

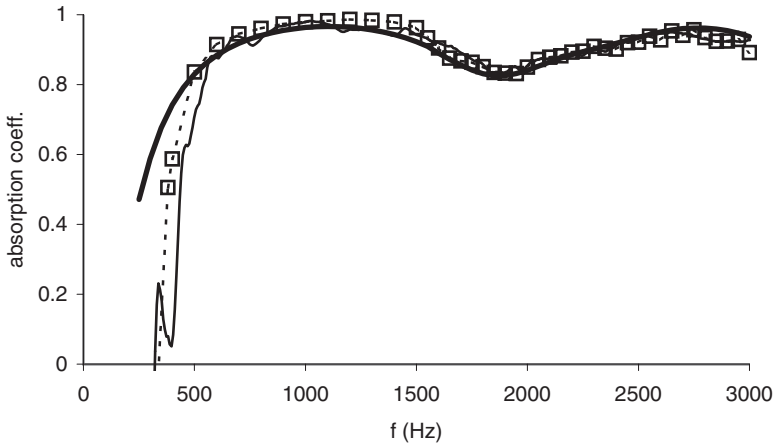


Figure 3.3 Measurement and prediction of absorption for a periodic profiled absorber. — Multi-microphone measurement; — Infinite sample prediction;□..... Boundary element method (BEM) prediction (adapted from Wu *et al.* [6]).

pressures to be inaccurate. The multi-microphone method is much more noise sensitive than the two-microphone method. Very accurate microphone positioning is needed. Others looking at multiple microphone techniques have found similar noise sensitivity [7].

Figure 3.3 shows an example measurement result for an incident angle of 30° . It is compared to two prediction models. Good accuracy is achieved with the multi-microphone measurement system in this case. At low frequencies only two microphone positions are used as there is only one plane wave reflection, at mid-high frequencies three microphone positions are needed as an additional reflected wave is present.

3.4 Reverberation chamber method

In most applications, the sound will be incident on an absorptive material from a multitude of incident angles at once. It is not efficient to laboriously measure the absorption coefficients for all angles of incidence in the free field and reconstruct these into a random incidence absorption coefficient (although this can be done as discussed in Chapter 12). Consequently a quicker method is needed, and this is afforded by the reverberation chamber method [8]. The random incidence absorption coefficient is the parameter used most in the design of spaces to specify the absorption performance of materials. It is well known and defined; however, it is notoriously difficult to predict. So while the random incidence absorption coefficient is needed to enable room design, it is not very useful for those interested in validating prediction models.

The reverberation chamber test requires large sample sizes and a specialist test room, and so is expensive to undertake. It also only gives absorption coefficients; the impedance cannot be measured. Consequently, developers of absorptive material will often use the impedance tube to build up an understanding of the material properties on small samples, before undertaking reverberation tests.

The reverberation time of a room is dependent on the total absorption in the room – see Equation 1.1. Consequently, by measuring the reverberation time of a room before and after a sample of absorbent is introduced, it is possible to calculate the random incidence absorption coefficient. It is necessary to have defined acoustic conditions for the test, and the normal technique is to try and generate a diffuse field. A diffuse field can be roughly defined as requiring the reflected sound energy to be the same across the whole room and the energy to be propagating evenly in all directions. To achieve this, reverberation chambers often use diffusers in the volume of the room, and the chamber walls are often skewed (splayed). Furthermore, the room should be of a certain minimum size, and room dimensions should be irrationally related to reduce the influence of room modes. The minimum requirements are given in the appropriate standard [8].

Despite these measures, a diffuse field is not completely achieved, and consequently the reverberation time is position dependent. For this reason, it is normal to use multiple source and receiver positions and to average the results to reduce the effect of non-diffuseness. The source is normally placed in the corner of a room, pointing into the corner, because it maximally excites the modes of the room and reduces the amount of direct radiation from the loudspeaker to the absorbent sample. Receivers should be at least 1 m from the room boundaries, room diffusers and the sample, and should be chosen to obtain a diverse sampling of the room volume. Even with all these measures, the measured absorption coefficients are often more inaccurate at low than high frequencies due to modal effects.

The reverberation time before the sample is introduced is given by:

$$T_0 = \frac{55.3V}{c\alpha_0 S} \quad (3.19)$$

where V is the room volume, c the speed of sound, α_0 the average absorption coefficient of the empty room and S the surface area of the room.

The reverberation time after the sample is introduced is given by:

$$T_1 = \frac{55.3V}{c(\alpha_0[S - S_s] + \alpha_s S_s)} \quad (3.20)$$

where S_s is the surface area and α_s the absorption coefficient of the sample. By rearranging Equations 3.19 and 3.20 it is possible to obtain the absorption coefficient of the sample. If ISO 354:1985 is followed, the factor $[S - S_s]$ is approximated to S , which simplifies the end formulation.

The current international standards are based on Sabine's formulations as used above. It is well known that this formula becomes inaccurate for large absorption coefficients, in which case other formulations like the ones derived by Eyring and Millington can be used; these were given in Equations 1.6 and 1.7. Indeed, Chapter 12 discusses how some geometric room acoustic modellers are advocating the use of alternative reverberation time formulations to give better room predictions. While it can be argued that using alternative reverberation time formulations produces more correct answers, the databases of absorption coefficients available to designers have been derived from Sabine's formulation. Consequently, while it is known that Sabine's equation produces systematic (or bias) errors, it continues to be industry

practice to use this formulation. Appendix A gives a table of typical measured absorption coefficients for common materials.

The reverberation times can be measured by interrupted noise, MLS or swept sine waves. MLS allow rapid measurement, but problems in getting sufficiently long decays can arise due to non-linearities in loudspeakers [9].

To get an accurate measurement, it is necessary to have a wide difference between T_0 and T_1 . This necessitates a large sample of 10–12 m² to be used. Even with such a large sample, the accuracy is compromised due to edge effects. Sound is diffracted around the edges of the sample, which usually leads to excess absorption. It is a normal practice to cover the edges of the sample and to use rectangular samples to reduce edge effects. Nevertheless, even with the edges covered, absorption coefficients greater than one can be measured. Chapter 12 discusses how these edge effects might be compensated for in real room predictions.

In newer revisions of the standard, Equations 3.17 and 3.18 will be corrected to allow for changing air absorption. If the air temperature and humidity change between the empty and with sample measurement, this can produce a bias error. By adding formulations for air absorption on the denominator of the equations, it is possible to reduce the error introduced. The revised formula to do this can be deduced from Equation 1.3.

It is also possible to measure discrete objects, for example persons. They are arranged randomly around the room and a total absorption per object calculated from the reverberation times.

Given the standard deviations of the reverberation times T_0 and T_1 , it is possible to calculate the random experimental error. The standard deviations are calculated from the set of reverberation times for all source and receiver combinations. If the standard deviation of the reverberation time measure T_0 is σ_0 , then the 95 per cent confidence limit is given by:

$$\delta_0 = \frac{2\sigma_0}{\sqrt{n}} \quad (3.21)$$

where n is the number of source and receiver pairs. (It is assumed that n is sufficiently large that two standard errors is equivalent to the 95 per cent confidence limit.) A similar relationship exists for T_1 . The accuracy (95 per cent confidence limit) of the empty room average absorption coefficient is given by:

$$\delta_{\alpha_0} = \left| \frac{55.3V}{cT_0^2S_0} \right| \delta_0 \quad (3.22)$$

and the accuracy of sample absorption is given by:

$$\delta_{\alpha_s} = \sqrt{\left| \frac{55.3V}{cT_1^2S_s} \right|^2 \delta_1^2 + \left(\frac{c[S_0 - S_s](\delta\alpha_0)^2}{S_s} \right)^2} \quad (3.23)$$

While good repeatability within a laboratory can be achieved, there are reproducibility problems between laboratories. The measured absorption coefficients can

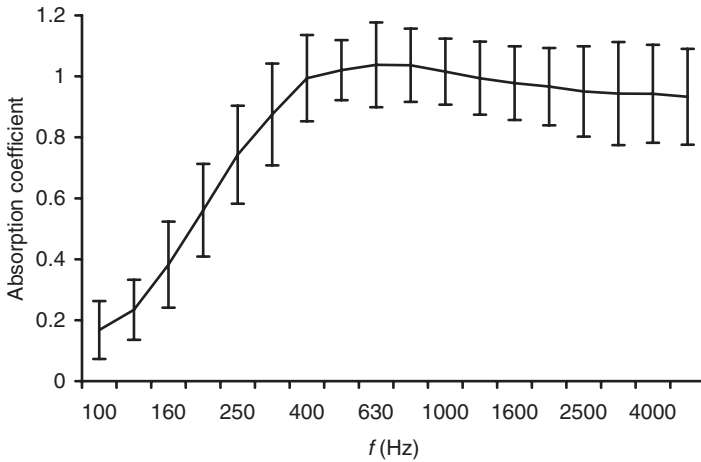


Figure 3.4 Comparison of measured absorption coefficients for a single sample in 24 laboratories. The mean absorption coefficient across all laboratories is shown, along with error bars indicating the 95 per cent confidence limit in any one laboratory measurement.

vary greatly from laboratory to laboratory. Figure 3.4 shows the average absorption coefficient for an identical fibreglass sample measured in 24 reverberation chambers. The error bars indicate the 95 per cent confidence limits in one of the laboratory measurements. To explain this figure further, when the sample was sent to one laboratory, 95 per cent of the time the absorption coefficient was found to be within ± 0.2 of the mean value at 1 kHz. This indicates that the absorption coefficients could vary by as much as 0.4 between two different laboratories, a huge error in the absorption coefficient.

3.4.1 Measurement of seating absorption

The reverberation time in a concert hall is dominated by the absorption of the seating and audience, it is essential that these can be measured or predicted accurately in the early stages of design. The wrong estimation of seating absorption has been blamed for acoustic problems in many halls, and consequently a measurement procedure is given here. Davies, Orłowski and Lam [10] compared seating absorption coefficients in a reverberation chamber and in concert halls for ten different cases, and showed that the Kath and Kuhl method [11] is an accurate method for estimating seating absorption in a real hall. Beranek [12] showed that it is best to calculate seating absorption coefficients based on absorption per unit floor area rather than by absorption per seat.

The aim of measuring the random incidence absorption coefficients of a small sample of seats in a reverberation chamber is to predict the total absorption that a larger area of the same seats will exhibit when installed in an auditorium. There are problems, however, in that the small sample of chairs in the reverberation chamber (say 24), is unrepresentative of a large block of seating, because the edge effect is overemphasized in the reverberation chamber measurements.

The Kath and Kuhl method involves placing the seating in the corner of the reverberation chamber in rows with their intended row spacing. The exposed edges are obscured with barriers for some of the measurements. The barriers need to be massive and stiff to reduce low frequency absorption. The barriers should be at least as high as the seating, and higher if any audience is present for an occupied measurement. Excessive extra height (say, more than 100 mm above the top of the seating for the unoccupied case) should be avoided. The set-up is schematically shown in Figure 3.5. Though it seems that the array is mirrored in the adjacent walls of the chamber, thus effectively increasing its size, it is not effectively infinite as Kath and Kuhl thought. Diffraction effects will still be present and so the measured absorption coefficient may still vary with sample size.

The concept is to separately measure three absorption coefficients by carrying out measurements with and without barriers:

- for an infinite array with no edges, yields an absorption coefficient α_∞ , with side and front barriers in place;
- for the front edges, α_f , by measuring with the side barrier only in place and combining the result for α_∞ ; and
- for the side edges, α_s , by measuring with the front barrier only in place, and combining with the result for α_∞ .

Then in the hall, if the areas of the front edges S_f , side edges S_s and plan area S_p are known, the absorption coefficient of the audience block is given by:

$$\alpha = \alpha_\infty + \alpha_f \frac{S_f}{S_p} + \alpha_s \frac{S_s}{S_p} \quad (3.24)$$

In the reverberation chamber the absorption coefficients α_∞ , α_f and α_s are determined by the following formulations. First with both the front and side barriers in place the infinite array absorption coefficient is obtained:

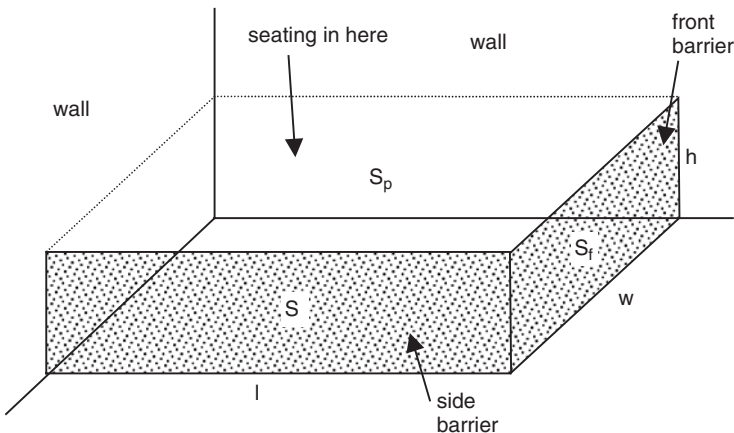


Figure 3.5 Set-up for Kath and Kuhl seating absorption measurement.

$$\alpha_{\infty} = \frac{A_1}{(l + \lambda/8)(w + \lambda/8)} \quad (3.25)$$

where A_1 is the total absorption of the sample with both barriers in place, and the $\lambda/8$ terms correct for pressure doubling at the chamber walls, where λ is the wavelength of the centre frequency in the octave band, as discussed later, l and w are defined in Figure 3.5.

With an additional measurement of the total absorption A_2 with the front barrier missing, the absorption of the front edge is determined.

$$\alpha_f = \frac{A_2 - A_1}{b(w + \lambda/8)} \quad (3.26)$$

where b is the barrier height.

Finally, with an additional measurement of the total absorption with the side barrier missing A_3 , the absorption of the side edge is determined.

$$\alpha_s = \frac{A_3 - A_1}{b(l + \lambda/8)} \quad (3.27)$$

The corner placing of the seats is advantageous because it increases the effective size of the array. However, there is a disadvantage: the pressure in a reverberant field is increased at the boundaries [13] so the absorption coefficients measured will be higher than those found when the sample is in the centre of the chamber. To compensate for this, Kath and Kuhl proposed [14] that the absorber areas used in the calculations should be increased by strips of width $\lambda/8$. This extra absorbing area accounts for the increase in measured total absorption due to the increase of up to 3 dB in sound pressure level close to the wall. In a corner, there is an increase of up to 6 dB, and a correction of $(\lambda/8)^2$ is needed. This is the reason for the extra terms in the denominators of Equations 3.25–3.27.

Figure 3.6 shows a comparison of the measured absorption coefficient in an auditorium and a prediction from the reverberation chamber results from Davies

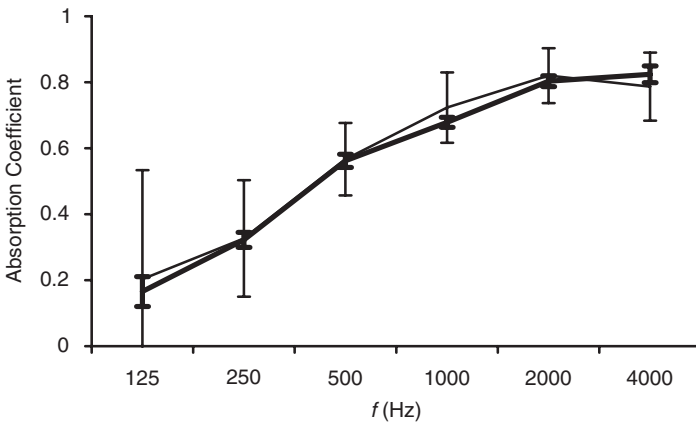


Figure 3.6 Absorption coefficient measured in an auditorium compared to a prediction based on a Kath and Kuhl reverberation chamber method. — Prediction for full auditorium seating based on reverberation chamber measurement; — Full auditorium measurement (data from Davies *et al.* [10]).

et al. [10]. Good prediction accuracy is achieved for this case. Discrepancies found by Davies *et al.* [10] for other halls were likely to be due to the non-diffuseness of the auditoria and indefinable changes in the hall between the without and with seating measurements.

Bradley [15] also suggested a seating absorption measurement method which attempts to take account of the variation of seating absorption with sample size. This involves making measurements on five or six differently sized arrays of seats and then extrapolating to the expected absorption for large seating blocks in auditoria. Although this is accurate, it requires more tests than the Kath and Kuhl method, and so the Kath and Kuhl method is more efficient.

3.5 *In situ* measurement of absorptive properties

There is great interest in being able to measure the absorption coefficient and surface impedance of products *in situ*. To take one example, in geometric room acoustic models the absorption coefficients of surfaces are required, but how can these be determined if the room is already built? It is for this sort of problem that *in situ* techniques have been developed. Indeed, *in situ* techniques for absorption measurement can be traced back as far as 1934 [16]. For those interested in the historical context of *in situ* measurement, the paper by Nocke and Mellert [16] gives a comprehensive reference list of the important literature.

One possible technique is to use the two-microphone free-field method outlined in Section 3.2. If the surface to be tested is large, homogeneous, isotropic and planar, and the unwanted reflections from other surfaces can be removed by time gating (windowing), then this process has been shown to work [17]. This process will fail if the unwanted reflections cannot be removed, or non-plane wave reflections are significant, which might arise if the surface is too small, or if the surface to be tested is inhomogeneous. This technique is accurate, provided the sample restrictions are followed and the unwanted reflections can be removed.

Other techniques try to separate the incident and reflected sound from a surface by arrival times. This is schematically shown in Figure 3.7. An impulse response is measured and the reflected and incident sound isolated by applying rectangular time windows. From this the reflection coefficient is calculated. To achieve this, however, requires considerable distance between the microphone and the surface, which means that problems often arise because of edge reflections from the test surface and unwanted reflections from other surfaces. Very large surfaces are needed, otherwise there is poor accuracy at low frequencies. Consequently, while this technique is potentially accurate, its range of applicability is limited.

A more promising technique was developed by Mommertz [18, 19], as this exploits a subtraction technique which enables the microphone to be placed close to the test surface. This allows measurement from 250 Hz to 8 kHz for normal incidence on plane surfaces greater than 4 m². The low frequency accuracy is compromised for oblique incidence or smaller samples. The test arrangement is that shown in Figure 3.7. The sound source is connected to the microphone by an anchored tube to ensure that the distance between the source and microphone remains constant. This distance precision is vital if the measurement method is to be accurate. The impulse response between the source and microphone is measured with the microphone close to the test surface, and separately in the free field. These two impulses can be

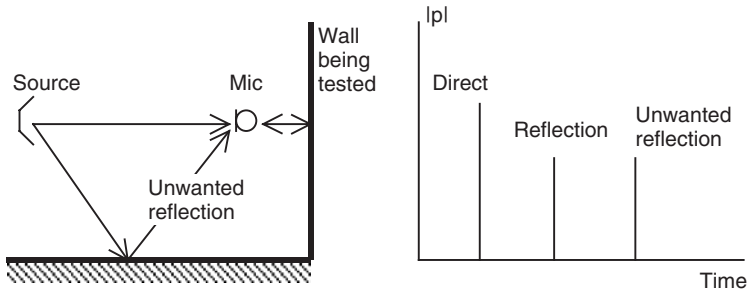


Figure 3.7 Measurement of *in situ* absorptive properties using time gating.

subtracted, which leaves the reflected sound and unwanted interfering reflections. These parasitic reflections can be removed by time windowing. To allow the subtraction, a deterministic test signal such as MLS or swept sine must be used.

Placing the microphone very close to the surface ensures that the interfering reflections are maximally spaced from the wanted reflections, consequently allowing more accurate measurements. By de-convolving the loudspeaker's free-field impulse response from the *in situ* measured impulse response, the length of the direct and reflected sound in the impulse responses can be shortened. This can help make the gating process more accurate. Mommertz advocates doing this de-convolution by pre-emphasizing the test signal – the inverse of the loudspeaker impulse response is used to pre-filter the maximum length sequence signal before it is sent to the loudspeaker. Alternatively this de-convolution could be done as part of the post-processing before the windows are applied. If overlap still exists between the wanted and parasitic reflections, then a window with a smooth transition should be used, like a half-Hanning.

If the microphone is very close to the surface, a simple ratio of the reflected and incident spectra can be taken to give the complex pressure reflection factor and from there absorption coefficients and surface impedance. If the microphone is not close to the surface, a correction for spherical spreading and propagation phase must be made to the incident and reflected spectra before the ratio is taken.

Figure 3.8 shows a typical result. For normal incidence, the absorption coefficients of the sample obtained using the *in situ* method match those obtained using a standing wave method in an impedance tube. For oblique incidence and at low frequencies (<800 Hz), the method fails with the absorption coefficient exceeding one. This occurs because there is an implicit assumption of plane waves in the methodology. At low frequencies, the edges of the test sample create other types of reflected waves which then render the technique inaccurate. One solution to this is to consider spherical wave theories [20].

Problems arise with this *in situ* method if the acoustic medium changes between the free field and sample measurement. For instance, Mommertz gives an example of a temperature change of 1 °C leading to an error of 0.03 in absorption coefficient.

The final *in situ* method detailed uses an alternative approach. No attempt is made to separate the incident and reflected sound; this removes some of the

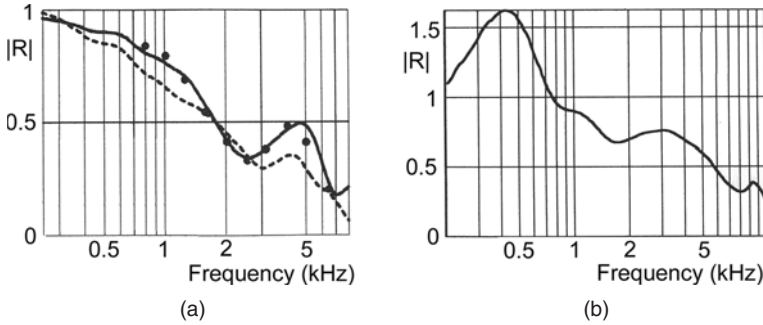


Figure 3.8 Measurements of reflection factor. Left figure: ——— *In situ* method, $\psi = 0^\circ$; - - - - - *In situ* method, $\psi = 45^\circ$; ● Standing wave tube method. Right figure: $\psi = 81^\circ$ (after Mommertz [19]).

geometric restrictions on the measurement system. To make it work accurately, however, requires a good theoretical model of the sound field close to the test surface. The idea is this, given measurements of the sound field in the vicinity of the test surface and a theoretical model for the sound propagation, it is possible to apply a numerical optimization to derive the unknown properties of the test sample.

Figure 3.9 shows a typical set-up used by Nocke [21]. The transfer function between the source and receiver is measured, and from this the angle-dependent impedance and absorption coefficient is derived by numeric inversion.

To simplify the description, consider a plane homogeneous sample. The pressure above the absorber is given by:

$$p(\mathbf{r}) = p_i(\mathbf{r}) - F(k, \mathbf{r}, \mathbf{r}_0, R(\mathbf{r}_s), p_i(\mathbf{r}_s)) \tag{3.28}$$

where $p_i(\mathbf{r})$ is the pressure direct from the source to the receiver, \mathbf{r} the receiver position, \mathbf{r}_0 the source position, \mathbf{r}_s the position of a point on the surface, $F()$ a function which gives the pressure at the microphone due to reflections from the surface, k the wavenumber, and R the surface reflection factor.

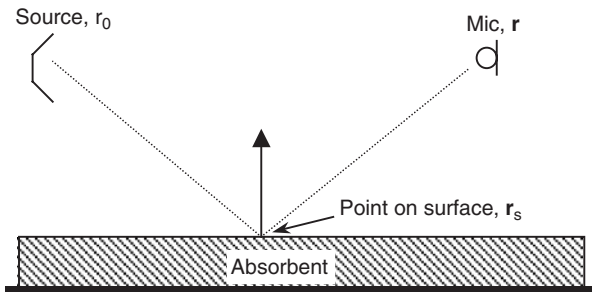


Figure 3.9 Typical set-up for *in situ* measurement (after Nocke [21]).

There are various prediction theories that can be used to model the function $F()$ which gives the reflected energy. For instance, it would be possible to use the theories outlined in Chapter 8. Nocke advocates using a spherical wave reflection theory. It would also be possible (and easier) to use simple plane wave formulations, provided the surface is large so that the edge diffraction is not significant.

Given that the incident and reflected pressures have been measured, that the receiver and source positions given in Equation 3.28 are known, the only unknown in the equation is the complex reflection factor R as a function of the vector on the surface \mathbf{r}_s . This complex reflection factor can therefore be found by using iterative procedure. For simplicity, assume that R is the same for the whole surface. If the measured pressure is $p_m(\mathbf{r})$ and the predicted pressure $p(\mathbf{r})$, then a numerical optimizer can be tasked with the procedure of minimizing the mean square error between the measured and predicted pressures, $|p_m(\mathbf{r}) - p(\mathbf{r})|^2$ by finding the value of R which gives minimal error. There are a variety of numerical methods that can be used for this process, the most trendy at the time of writing being genetic algorithms.

In theory this could work for samples where R varies across the surface. As a number of different surface reflection factors have to be derived, more microphone positions are needed. In this case, the optimization problem becomes slower to solve, and the risk of getting incorrect solutions by the optimizer increases. The experience with multiple microphone techniques, is that the more microphones, the more problems with noise sensitivity and evanescent waves. Consequently, it might be anticipated that resolving a large number of different surface reflection factors might prove to be problematical.

Nocke [21] restricts himself to deriving an average absorption coefficient for inhomogeneous surfaces. Figure 3.10 shows a typical result showing the *in situ* method compared to impedance tube measurements. By using the spherical wave formulation, accurate results are achieved down to 80 Hz, but this requires a very large sample of 16 m² to prevent edge effects being significant. The upper frequency limit he measured was 4 kHz, presumably limited by the accuracy of the microphone positioning.

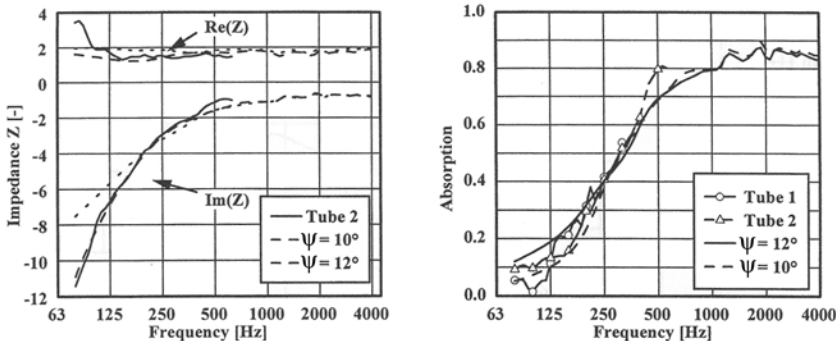


Figure 3.10 Comparison of *in situ* measurement by Nocke and measurements in impedance tube for a fibrous absorber. The transfer function was measured at angles ψ as shown in legend (after Nocke [21]).

3.6 Internal properties of absorbers

The remaining sections of the chapter are devoted to the measurement of properties within absorbers, characterizing the sound propagation within the absorber either in terms of propagation constants and characteristic impedances, or finding key parameters such as flow resistivity and porosity. These are key measurements for those involved in the development or modelling of porous materials.

3.6.1 *Measurement of flow resistivity*

The flow resistivity of a porous absorber is one of the most important defining acoustic characteristics. Once the flow resistivity is known, simple empirical models for porous absorbers can be used to find the characteristic impedance and wave-number, and from there, the surface impedance and absorption coefficient can be obtained. The importance of this parameter is discussed in more detail in Chapter 5, for now three techniques for measurement will be considered. The measurement techniques presented here follow directly from the definition of flow resistivity. Consider a slice of the porous material of thickness d subject to a mean steady flow velocity U . The pressure drop across the sample ΔP is measured, and from these quantities the flow resistivity σ is given by:

$$\sigma = \frac{\Delta P}{Ud} \quad (3.29)$$

The measurement of flow resistivity has been enshrined into International Standards [22], where more details of the measurement procedure can be found. In the direct flow method, a steady air supply pushes air through the porous material. Sensors are used to measure the air flow and pressure drop to atmospheric pressure, and hence the flow resistivity is obtained. This is shown in Figure 3.11.

It is important that flow rates are kept small because otherwise the relationship between the pressure drop and velocity becomes non-linear. Flow rates between

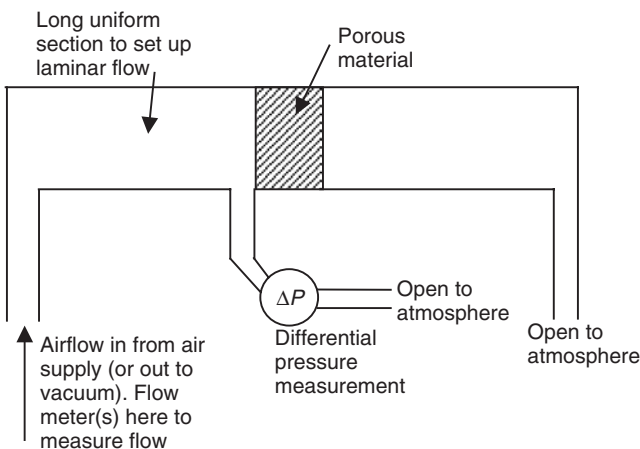


Figure 3.11 Set-up for direct airflow method for measuring flow resistivity.

5×10^{-4} and $5 \times 10^{-2} \text{ ms}^{-1}$ are recommended by Bies and Hansen [23]. Ingard [24] produces results that show that the flow rate should not be greater than 0.1 ms^{-1} , to get results consistent with the velocity amplitude of typical sound waves in absorbers (0.01 ms^{-1}). The flow resistivity is calculated from:

$$\sigma = \frac{\rho_0 \Delta P A}{m d} \quad (3.30)$$

where ρ_0 is the density of air, A is the cross-sectional area of the specimen, m the air mass flow rate (kgs^{-1}), and d is the specimen thickness.

In the alternative airflow method, a piston is used to generate a low frequency alternating airflow through the test specimen; the piston should move at a frequency of $f = 2 \text{ Hz}$. The set-up is shown in Figure 3.12. The rms airflow velocity is then:

$$u_{\text{rms}} = \frac{\pi f b A_p}{\sqrt{2} A} \quad (3.31)$$

where b is the peak-peak displacement of the piston, A_p the cross-sectional area of the piston, and A the cross-sectional area of the porous material. The standard recommends $0.5 < u_{\text{rms}} < 4 \text{ mms}^{-1}$. A condenser microphone is used to measure the rms pressure relative to atmospheric pressure.

The problem with these measurement techniques is that many have found a great variation between measurements by different laboratories. Garai and Pompoli [25] found that repeatability within a laboratory is good, with an error of about 2.5 per cent with repeat measurements on one sample, and about 5 per cent with five samples cut from the same material. Reproducibility between laboratories, on the other hand, is a problem with errors around 15 per cent.

There are alternative methods for obtaining the flow resistance. Ingard [24] devised a measurement system which does not require blowers and flow instrumentation and so greatly simplifies the apparatus required. The set-up is shown in Figure 3.13. A piston within a tube falls under gravity and pushes air through the porous absorber. When the piston has reached terminal velocity, the pressure drop ΔP across the sample is given by:

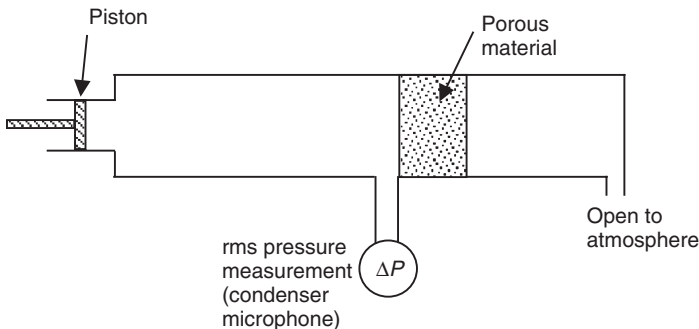


Figure 3.12 Set-up for alternating airflow method for measuring flow resistivity.

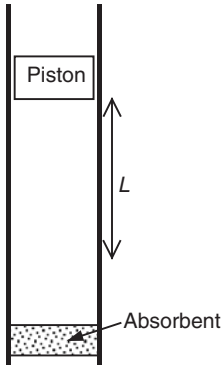


Figure 3.13 Set-up for Ingard's method for measuring flow resistivity.

$$\Delta P = \frac{Mg}{A_p} \quad (3.32)$$

where M is the mass of the piston, g is gravity and A_p the cross-sectional area of the piston or tube. The flow velocity U is given by:

$$U = \frac{A_p}{S_s} \nu \quad (3.33)$$

where S_s is the cross-sectional area of the sample, and ν is the terminal velocity of the piston found by timing how long it takes the piston to travel a set length. Equations 3.32 and 3.33 can be combined with Equation 3.29 to give the flow resistivity. It is first necessary, however, to include a calibration factor. There will be frictional forces between the piston and the tube walls, and there will be leakage between the piston and the tube wall. Consequently, it is necessary to calibrate for these. This involves two calibration measurements, and so in total three timed falls of the piston are made as summarized in Table 3.1.

The time taken for the piston to fall in the tube with no sample over a set length is measured in two cases. First with the tube open, t_0 , and second with one end of the tube closed (it does not matter which), t_1 . Then a calibration factor is found:

$$C = \frac{1 - t_0/t}{1 - t/t_1} \quad (3.34)$$

Table 3.1 Measurements needed for flow resistivity measurement

<i>Time measured</i>	<i>Condition</i>
t	Sample in tube, both ends of tube open
t_0	No sample in tube, both ends of tube open
t_1	No sample in tube, one end of tube closed (either end)

where t is the time it takes the piston to drop over the same measurement distance L with the sample present. Then the flow resistance is given by:

$$\sigma = \frac{CMg \cos(\psi)S_s t}{LA_p^2} \quad (3.35)$$

where ψ is the angle of the tube to the vertical.

Ingard [24] reports using a tube with an inner diameter of 0.08 m and 1.2 m long, and $L = 0.6$ m. The piston was 264 g and 10 cm long. The gap between the cylinder and the tube wall was about 0.2 mm. The system does not work for materials with very small or large flow resistivities due to problems with accurate timing and calibration.

3.6.2 Measurement of flow impedance

Strictly speaking, porous materials are not just resistive but contain some reactance as well [24]. The reactance comes from additional mass due to viscous boundary layer effects and constrained flow. Consequently, while Section 3.6.1 has given methods for flow resistance, there is also interest in measuring the flow impedance to get the flow reactance. As the resistive term dominates, this type of measurement is not that commonly undertaken. However, it does give an alternative method for getting the flow resistivity if apparatus presented in Section 3.6.1 is not available.

This flow impedance is measured within an impedance tube [26]. Figure 3.14 shows an arrangement that can be used, the tube is about 5 cm in diameter. A pure tone plane wave is produced by the sound source. The frequency is adjusted so that the distance w is an odd integer multiple of a quarter wavelengths:

$$w = \frac{n\lambda}{4} \quad (3.36)$$

where n is the number of quarter wavelengths in the length w and n must be odd. There are an infinite set of frequencies which satisfy this condition, but the frequency should also be a low frequency (say less than 100 Hz), to get accurate results as the sample should be thin compared to wavelength. This forces the pressure and surface impedance at the rear of the sample to be zero. The flow impedance z_f is then a ratio of the pressures measured at microphones 1 and 2 [24]:

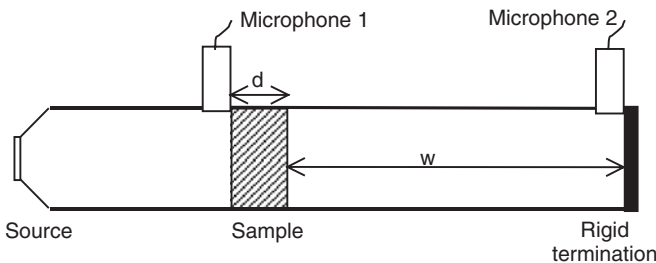


Figure 3.14 Apparatus for determining flow impedance using an impedance tube (after Ingard and Dear [26]).

$$z_f = j\rho_0 c_0 (-1)^{(n-1)/2} \frac{p_1}{p_2} \quad (3.37)$$

where p_1 and p_2 are the complex pressures for microphones 1 and 2. This formulation can be derived as follows. As the impedance at the rear of the sample is zero, the flow impedance equals the impedance at the front face of the sample. This impedance can be derived using the transfer matrix method outlined in Section 1.5.1.

The calculation yields a complex impedance, of which the real part is the flow resistance and the imaginary part the flow reactance; the latter is generally small.

3.6.3 *Direct measurement of wavenumber*

The wavenumber (or propagation constant) for a porous medium can be directly measured [27]. It is a crucial parameter describing how sound propagates in a medium and was defined in Section 1.4.1. The direct measurement process is rather slow, but accurate and robust. An impedance tube is filled with the material to be tested. A loudspeaker at one end of the tube generates sound waves which propagate through the absorbent. If it is assumed that no reflection happens from the opposite end of the tube from the loudspeaker, the steady state pressure in the tube is given by:

$$p = Ae^{-jkz} \quad (3.38)$$

where z is the distance along the tube, and A is a constant. Remembering that the wavenumber k is complex, this can be rewritten as:

$$p = Ae^{\text{Im}(k)z} e^{-j\text{Re}(k)z} \quad (3.39)$$

By measuring the decay in the amplitude of the sound wave, and plotting the log of the amplitude versus distance, the imaginary part of the wavenumber can be obtained. By measuring the changing phase of the sound wave and plotting another log-linear graph yields the real part of the wavenumber.

It is necessary to ensure there are no reflections from the tube end remote from the loudspeaker. This necessitates a long length of absorbent to ensure full absorption – it is not sufficient just to leave the end of the tube open. Typically 0.5 m of the test absorbent might be used, followed by another 0.5 m of loosely packed porous absorber such as mineral wool to give an anechoic termination.

The sensing microphone must be placed in the bulk of the absorbent in the tube, this can be achieved by using a probe tube microphone similar to that shown in Figure 3.1. The probe tube moves within a hole pre-drilled through the centre of the absorbent material.

3.6.4 *Indirect measurement of wavenumber and characteristic impedance*

Given a theoretical model for the propagation of sound in a porous absorbent and some measurements on a simple experimental set-up, it is possible to derive the wavenumber and the characteristic impedance of porous absorbers [28–30]. For example, a numerical fit can be carried out between the experimental data and the theoretical model to find values for unknown parameters in the theoretical model.

Such a technique is similar to that used for *in situ* measurements discussed at the end of Section 3.5. There are various arrangements that can be used for this measurement. The most convenient methods are probably those that use the impedance tube, as this is readily available to many. The advantage of these methods over the direct measurement of wavenumber described in Section 3.6.3 is that it yields the characteristic impedance as well as the wavenumber.

Smith and Parrott [28] review two possible methods, of which the two thicknesses method is the most convenient and so will be described here. The surface impedance is measured for two different thicknesses of the absorbent with a rigid backing. For a thickness of d_1 the surface impedance is z_1 :

$$z_1 = -jz_c \cot(kd_1) \quad (3.40)$$

where z_c is the characteristic impedance of the sample. A similar relationship gives the surface impedance $z_2 = -jz_c \cot(kd_2)$ for a depth d_2 . These relationships were derived in Section 1.5.1. For simplicity, assume that $d_2 = 2d_1$; typically d_1 would be a couple of centimetres. The equations for z_1 and z_2 can then be rearranged using trigonometric identities and solved to give the characteristic impedance z_c and wavenumber k :

$$z_c = \sqrt{z_1(2z_2 - z_1)} \quad (3.41)$$

$$k = \frac{-j}{2d_2} \ln \left(\frac{1 + \sqrt{\frac{2z_2 - z_1}{z_1}}}{1 - \sqrt{\frac{2z_2 - z_1}{z_1}}} \right) \quad (3.42)$$

It is necessary to choose depths so that $z_1 \neq z_2$, otherwise the results become unreliable. This happens when $kd_1 = kd_2 \pm n\pi$, where n is an integer. Unfortunately, there is no way to test for this before measurement as the wavenumber is not known. Consequently, this must be checked for in analyzing the measurements, and if necessary another set of thicknesses measured.

3.6.5 Measurement of porosity

The porosity is a measure of the ratio of pore volume involved in sound propagation to total volume. For specialist absorbers, such as mineral wool, the porosity is close to one, and so the value is often assumed rather than measured. Table 5.1 gives a table of typical porosities and Section 5.3.2 discusses the significance of this parameter in more detail. If measurements are done, it is best if it is measured using air saturation rather than by liquid saturation of the sample, as it cannot be guaranteed that the liquid will fill all the available pores. Figure 3.15 shows a set-up used by Beranek [31] which uses the isothermal compression of the air volume within and external to a porous absorber. This summary is partly taken from Cremer and Müller [32].

There is a chamber of known volume connected to a U-shaped manometer. The material to be tested is placed in the chamber. The valve at the top of the chamber can be open or closed. With the valve open, the liquid in both legs will have the same

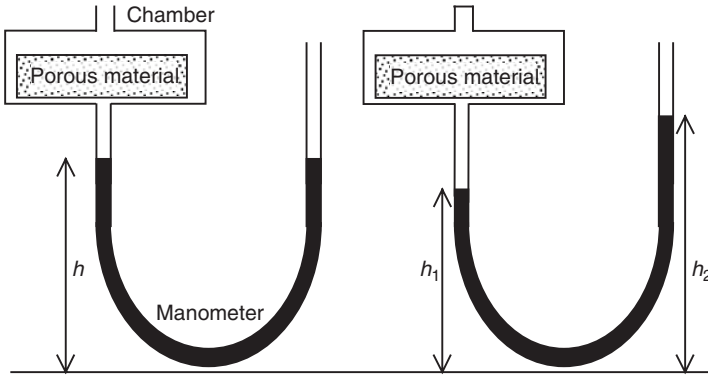


Figure 3.15 Apparatus for measuring porosity (after Beranek [31]).

height, h . This height is measured. The valve is then closed, and the pressure in the vessel is increased by raising the right leg of the manometer. The surface of the liquids is now at h_1 and h_2 in the two legs, and these heights are measured. The difference in the liquid levels in the two legs ($h_2 - h_1$) is the increase in pressure in the sample in metres of water ΔP . This needs to be converted to SI units:

$$\Delta P = \rho_w (h_2 - h_1) g \quad (3.43)$$

where ρ_w is the density of the liquid in the manometer and g is gravity. The height difference multiplied by the cross-sectional area of the manometer tube S_s is the reduction in the volume, ΔV , in the chamber:

$$\Delta V = S_s (h_2 - h_1) \quad (3.44)$$

Assuming this is an isothermal system, the product of the pressure and volume is constant ($PV = nRT$). This gas law is needed in a differential form for the derivation:

$$\Delta PV + \Delta VP = 0 \quad (3.45)$$

By considering the volumes of air being compressed within the chamber, both within and external to the test sample, and remembering that the porosity ε gives the ratio of the pore volume to total volume of the sample, Equation 3.45 can be expanded to:

$$\Delta P (V - V_a + \varepsilon V_a) + \Delta V P_0 = 0 \quad (3.46)$$

where P_0 is atmospheric pressure, V_a the volume of the material being tested in the chamber and V the volume of the chamber. Rearranging then gives the porosity:

$$\varepsilon = \frac{P_0 \Delta V}{V_a \Delta p} + 1 - \frac{V}{V_a} \quad (3.47)$$

3.7 Summary

This chapter has reviewed the methods used to measure and thereby characterize absorbing materials. There are a few other parameters concerned with porous absorber models that have not been mentioned, the characteristic lengths and the tortuosity. Measurement of these will be covered in Chapter 5 when porous absorber models are presented. The next chapter details the measurement of diffusion.

3.8 References

- 1 ISO 10534-2:1998, "Acoustics – determination of sound absorption coefficient and impedance in impedance tubes. Part 1: Method using standing wave ratio".
- 2 ISO 10534-2:1998, "Acoustics – determination of sound absorption coefficient and impedance in impedance tubes. Part 2: Transfer-function method".
- 3 D. D. Rife and J. Vanderkooy, "Transfer function measurement with maximum-length sequences", *J. Audio Eng. Soc.*, **37**(6), 491–438 (1989).
- 4 A. Farina, "Simultaneous measurement of impulse response and distortion with a swept-sine technique", *108th Audio Eng. Soc. Convention*, Paris 18–22 (2000).
- 5 J. F. Allard, *Propagation of Sound in Porous Media: Modelling Sound Absorbing Materials*, Elsevier Applied Science (1993).
- 6 T. Wu, Y. W. Lam and T. J. Cox, "Measurement of non-uniform impedance surface by the two microphone method", *17th ICA Rome* (2001).
- 7 W. Lauriksa, G. Jansensa, J. F. Allard, L. De Geeterea and G. Vermeira, "Evaluation of free field techniques for the measurement of the surface impedance of sound absorbing materials", *17th ICA Rome* (2001).
- 8 ISO 354:1985, "Acoustics – measurement of sound absorption in a reverberation room".
- 9 J. S. Bradley, "Optimizing the decay range in room acoustics measurements using maximum-length-sequence techniques", *J. Audio Eng. Soc.*, **44**(4), 266–273 (1996).
- 10 W. J. Davies, R. J. Orłowski and Y. W. Lam, "Measuring auditorium seat absorption", *J. Acoust. Soc. Am.*, **96**, 879–888 (1994).
- 11 U. Kath and W. Kuhl, "Messungen zur schallabsorption von personen auf ungepolsterten stuhlen", *Acustica*, **14**, 49–55 (1964).
- 12 L. L. Beranek, "Audience and chair absorption in large halls. II", *J. Acoust. Soc. Am.*, **45**, 13–19 (1969).
- 13 R. V. Waterhouse, "Interference patterns in reverberant sound fields", *J. Acoust. Soc. Am.*, **27**, 247–258 (1955).
- 14 U. Kath and W. Kuhl, "Einfluss von streufläche und hallraumdimensionen auf den gemessenen schallabsorptionsgrad", *Acustica*, **11**, 50–64 (1961).
- 15 J. S. Bradley, "Predicting theater chair absorption from reverberation chamber measurements", *J. Acoust. Soc. Am.*, **91**, 1514–1524 (1992).
- 16 C. Nocke and V. Mellert, "Brief review on *in situ* measurement techniques of impedance or absorption", Forum Acusticum, Sevilla (2002).
- 17 G. Dutilleux, T. E. Vigran and U. R. Kristiansen, "An *in situ* transfer function technique for the assessment of the acoustic absorption of materials in buildings", *Appl. Acoust.*, **62**(5), 555–572 (2001).
- 18 E. Mommertz, "Untersuchung akustischer wandeigenschaften und modellierung der schallrückwürfe in der binauralen raumsimulation", Dissertation RWTH Aachen, Shaker Verlag (1996).
- 19 E. Mommertz, "Angle-dependent *in situ* measurements of reflection coefficients using a subtraction technique", *Appl. Acoust.*, **46**(3), 251–264 (1995).

- 20 C. Nocke, V. Mellert, T. Waters-Fuller, K. Attenborough and K. M. Li, "Impedance deduction from broad-band point-source measurements at grazing incidence", *Acustical Acta Acustica*, **83**(6), 1085–1090 (1997).
- 21 C. Nocke, "In situ acoustic impedance measurement using a free-field transfer function method", *Appl. Acoust.*, **59**(3), 253–264 (2000).
- 22 ISO 9053:1991, "Acoustics-materials for acoustical applications – determination of air-flow resistance".
- 23 D. A. Bies and C. H. Hansen, *Engineering Noise Control: Theory and Practice*, E&FN Spon, 2nd edn (1996).
- 24 U. K. Ingard, *Notes on Sound Absorption Technology*, Noise Control Foundation (1994).
- 25 M. Garai and F. Pompoli, "An intercomparison of laboratory measurements of flow resistance", *17th ICA Rome*, 5a-08-02 (2001).
- 26 U. K. Ingard and T. A. Dear, "Measurement of acoustic flow resistance", *J. Sound Vib.*, **103**, 567–572 (1985).
- 27 R. A. Scott, "The absorption of sound in a homogenous medium", *Proc. Phys. Soc.*, London, **58**, 165–183 (1946).
- 28 C. D. Smith and T. L. Parrott, "Comparison of three methods for measuring acoustic properties of bulk materials", *J. Acoust. Soc. Am.*, **74**, 1577–1582 (1983).
- 29 C. K. Amédin, Y. Champoux and A. Berry, "Acoustical characterisation of absorbing porous materials through transmission measurements in the free field", *J. Acoust. Soc. Am.*, **102**(2), 1982–1994 (1997).
- 30 J. Tran-vana, X. Olnyb, F. C. Sgard and Y. Gervais, "Global inverse methods for determining the acoustical parameters of porous materials", *17th ICA Rome* (2001).
- 31 L. L. Beranek, "Acoustic impedance of porous materials", *J. Acoust. Soc. Am.*, **13**, 248–260 (1942).
- 32 L. Cremer and H. A. Müller, *Principles and Applications of Room Acoustics*, Applied Science Publishers translated by T. J. Schultz (1978).

4 Measurement and characterization of diffuse reflections or scattering

While surface scattering elements have been used accidentally or by design in rooms for centuries, it is only in recent decades that a concerted effort has been made into developing methods for measuring and characterizing the scattering from these surfaces. Without measurements of the scattering produced by surfaces, it is impossible to confidently design and apply diffusers. Consequently, this chapter starts by describing methods for measuring the scattering produced by a surface. This mainly concentrates on measurements in terms of polar responses, as this is the primary way that the scattering from surfaces has been measured for diffuser design and evaluation.

The polar response of a source, like a loudspeaker, can be determined by measuring the sound energy distribution on a polar arc or hemisphere surrounding the source. With care, this concept can be translated from loudspeaker measurements, to be used for backscattering from architectural surfaces. While polar responses tell designers much about how a surface reflects sound, they contain a considerable amount of data and a different polar response is required for each frequency band and angle of incidence. This is one of the reasons why the focus of recent years has been on developing single figure parameters, which condense the polar data and allow characterization in terms of diffusion coefficients.

The reflection from a surface can also be characterized using a scattering coefficient, which is different from a diffusion coefficient. The differences between the coefficients will be discussed in some depth later in this chapter, but for now, it is opportune to give the contrasting definitions of diffusion and scattering coefficients.

Diffusion coefficient (d), is a measure of the uniformity of the reflected sound. The purpose of this coefficient is to enable the design of diffusers, and to also allow acousticians to compare the performance of surfaces for room design and performance specifications.

Scattering coefficient (s), is a ratio of sound energy scattered in a non-specular manner to the total reflected sound energy. The purpose of this coefficient is to characterize surface scattering for use in geometrical room modelling programs.

Both the coefficients are simplified representations of the true reflection behaviour. It is necessary to come up with simple metrics, rather than trying to evaluate the reflection characteristics for all possible source and receiver positions, because the amount of data soon becomes too large to deal with. The coefficients attempt to represent the reflection by a single parameter, maximizing the information carried by that single number. The difference between diffusion and scattering coefficients is the emphasis on which information is most important to be preserved in the data reduction. For diffuser designers, it is the uniformity of all reflected energy which is most

important; for room acoustic modelling, it is the amount of energy scattered away from specular angles. The difference between the definitions may appear subtle, but it is significant.

In this chapter, diffusion and scattering coefficients are described after a discussion of the direct ways of measuring the scattered energy from surfaces. For example, given the source and receiver positions, what are the best ways of obtaining the scattered and total sound fields? The chapter concludes by describing some other techniques for characterizing surfaces which have yet to find great favour, but may in the future be useful techniques.

4.1 Measurement of scattered polar responses

In order to characterize a diffuser's performance, it is necessary to be able to both measure and/or predict how the diffuser scatters sound. Currently, this is most often done by looking at how the scattered energy is spatially distributed. This spatial distribution is conventionally described by polar responses in one-third octaves, for a given angle of incidence. An ideal diffuser produces a polar response that is invariant to the angle of incidence, the angle of observation and the frequency (within its operational bandwidth). Figure 4.1 shows a measured polar response for normal incidence, at 2 kHz, from an array of 2D number theoretic diffusers, one of which is also shown in the figure. There are various techniques for measuring such a scattered polar distribution which is discussed below. (Chapter 8 details some possible prediction methods.)

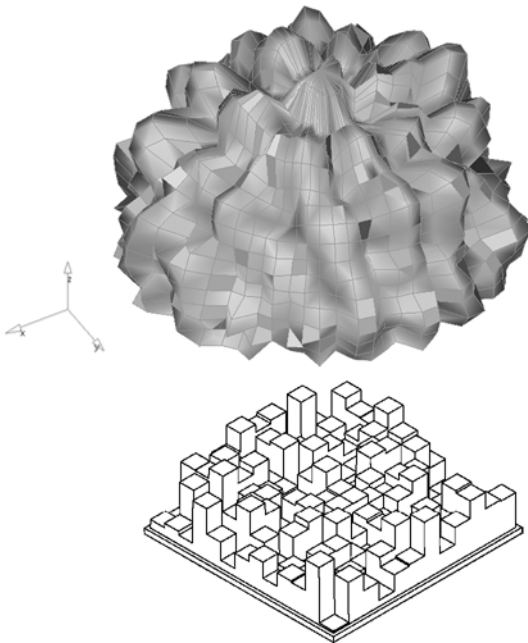


Figure 4.1 3D polar balloon measured from a Skyline[®] diffuser, which is shown below the polar response.

Systems for measuring the reflections from surfaces have been based on techniques which use a source to irradiate the test surface, and measurement microphones at radial positions in front of the surface, to record the pressure impulse response. The microphone positions usually map out a semicircle or hemisphere, for a single plane or hemispherical measurement, respectively. Once the pressure impulse responses are measured, time gating is used to separate the reflections from the incident sound.

There are various ways of measuring the impulse responses. The most common uses a maximum length sequence signal. Other signal possibilities include swept sine waves, time delay spectroscopy and pulses. As time variance and non-linearity are not an issue, MLS are currently the most efficient to use.

Polar response measurements can be made in a single plane using a 2D goniometer on a semicircle [1], as shown in Figure 4.2, or over a hemisphere using a 3D goniometer, as shown in Figure 4.3. The choice of single plane or hemispherical measurement depends on the type of diffuser. Figure 4.4 illustrates that an extruding diffuser (known as a single plane or 1D diffuser) produces scattering in one plane, and consequently a single plane evaluation is appropriate [2]. If the surface produces scattering in multiple planes, as shown in Figure 4.4 right, then a hemispherical evaluation will be needed. Figures 4.2 and 4.3 show 1:5 scale measurement systems. Scale model measurements are needed, because otherwise the source and receiver radii become too large.

In the single plane measurement goniometer shown, a fixed microphone array is used. In the hemispherical measurement goniometer, a single microphone is moved on a lightweight scaffolding, which then traces out a hemisphere. It is also possible to use a boom arm to rotate a microphone on a single arc as shown in Figure 4.5.

The single plane measurement can be made in an anechoic chamber [3], but it is also possible to use a boundary layer technique [1]. This latter technique is in

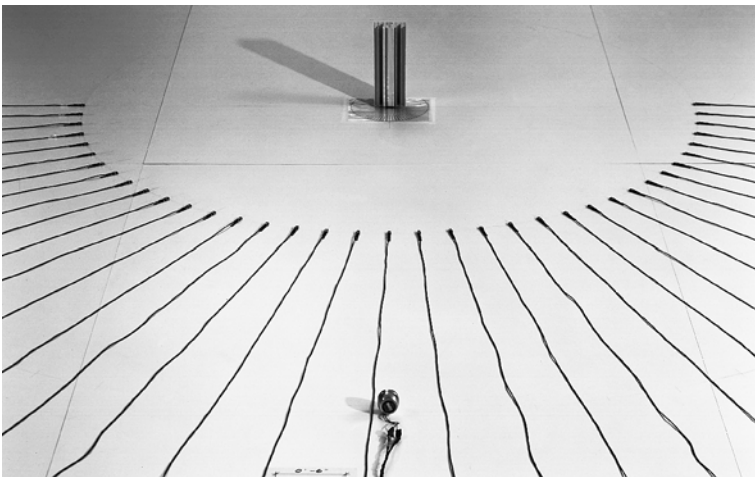


Figure 4.2 A system for measuring the scattering from a surface in a plane using a boundary plane measurement. The diffuser (a Schroeder diffuser) is shown top middle. There are 37 microphones arranged on an arc. The source loudspeaker is at the bottom middle of the picture (after AES [6], photo courtesy of RPG Diffusor Systems Inc.).



Figure 4.3 A system for measuring the scattering from a surface over a hemisphere. The diffuser being tested is the small pyramid in the centre. The source arc is most obvious, the receiver arc is acoustically transparent and so is difficult to see (after AES [6], photo courtesy of University of Salford).

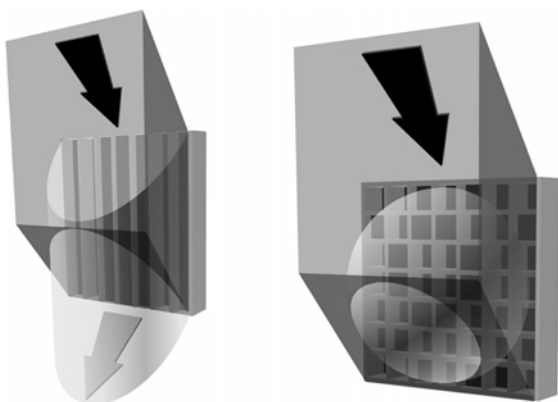


Figure 4.4 Scattering from a single plane (left) and hemispherical diffuser (right) (after D'Antonio and Cox [2]).

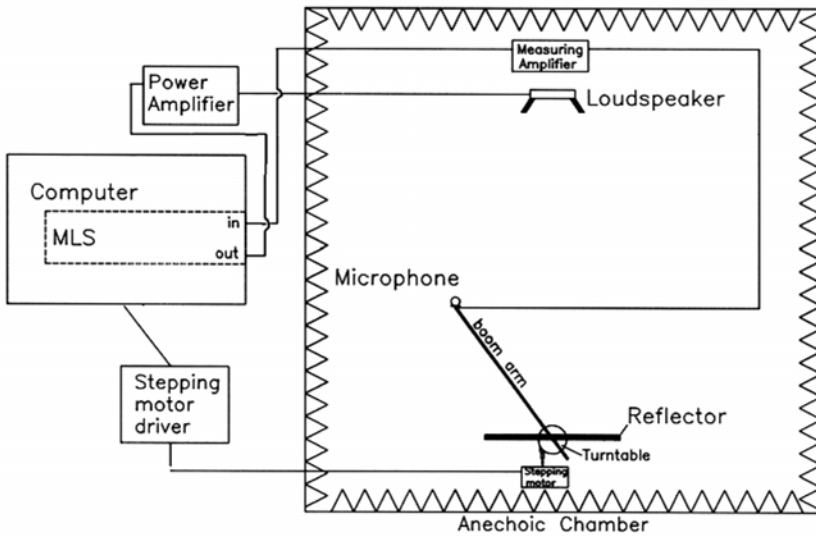


Figure 4.5 A schematic of a measurement system.

Figure 4.2. This can be done in a large room, provided that the ceiling and walls are sufficiently far away from the test set-up. The scattering sample is shown in the top middle, along with 37 pressure zone microphones arranged on a semicircle 1 m from the sample. The source loudspeaker, for normal incidence, at the bottom middle is located 2 m from the sample. The measurement geometry is shown in plan view in Figure 4.6, and from this geometry it is possible to calculate the size of non-anechoic room needed for the measurement. In this case, the loudspeaker (L), microphone (M) and diffuser (D) are placed on a flat, hard surface on the

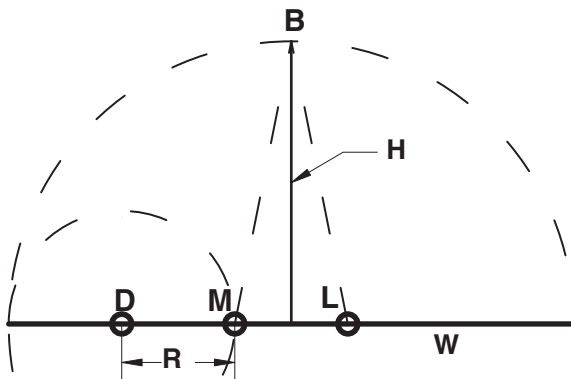


Figure 4.6 Plan view of reflection free zone geometry for diffusion coefficient boundary measurement technique. Loudspeaker (L), microphone (M), diffuser (D), microphone radius (R), room boundary (B), ellipse axes (H) and (W).

floor. The microphone radius is denoted by R and the loudspeaker radius is $2R$. Figure 4.6 illustrates the ellipsoidal area (dashed) necessary to make a reflection free zone measurement. What is the reflection free zone? Consider the respective sound paths of the direct sound ($LM = R$), the scattered sound ($LSM = 3R$) and the limiting reflection from the second order reflection from the speaker ($LSLM = 5R$). Therefore, the reflection free zone, which measures only scattering from the sample, is $4R$. It is possible to determine the ellipsoidal area from the measurement geometry. If the limiting path is $5R$, then the total travel path from the loudspeaker to the room boundary, B , and back to the microphone is also equal to $5R = LBM$ ($LB + BM$). The minor axis of the ellipsoid, H , equals $2.45R$ and the major axis, W , equals $2.5R$. If $R = 5$ m, then this requires a room 12.2 m high, 24.4 m wide and 25 m long. Since this is an unreasonably large room, measurements have been done at 1:5 scale in which $R = 1$ m.

In the boundary layer measurement, the boundary layer acts as an mirror image and what is measured is effectively the diffuser paired with a mirror image of the diffuser, as illustrated in Figure 4.7 where a section is shown. In Figure 4.7 (left) a diffuser is shown in a real test condition and its image source equivalent. The diffuser is

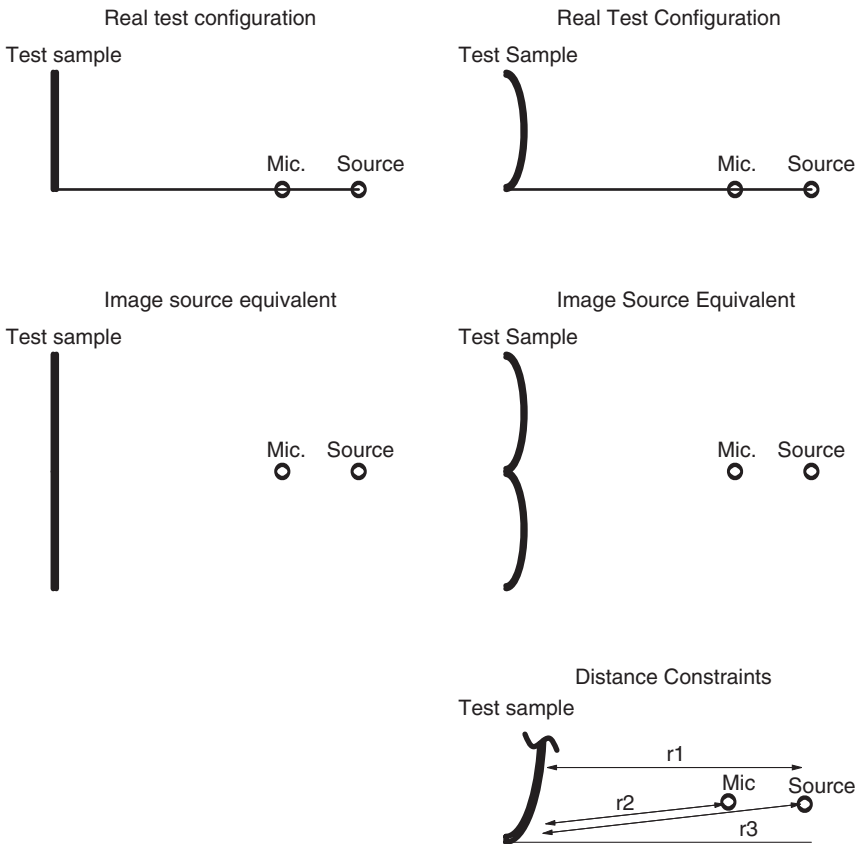


Figure 4.7 Boundary plane measurement and equivalent configuration using images for two types of surface.

extruded in the vertical direction, and so it can be seen that what is actually measured is a sample twice as high, with the source and receiver at the midpoint. In Figure 4.7 (right) a non-extruded shape (arc) is shown in the real test configuration and its image source equivalent. For this sample, the actual sample and its mirror image are being measured.

As the source and receivers are not located exactly on the boundary, there is an upper frequency limit on this measurement. The longest and shortest propagation paths must not differ by more than half a wavelength. In terms of the geometry shown in Figure 4.7, the path difference $|r_1 - r_2 - r_3| \ll \lambda/2$, where r_1 , r_2 and r_3 are defined in Figure 4.7.

A potential problem with this measurement process is that the microphone(s) will get in the way of the sound propagating from the source to the panel. For this reason, the fixed microphone array or the boom arm used to move a single microphone, must be small enough not to cause significant reflections or disturbance to the sound field. Where possible, supports should be located not in a direct line between source and diffuser, and be covered in absorbent material or be acoustically transparent. Fixed microphone arrays have been constructed using small pressure zone microphones. This potential interference by the microphones on the sound field makes diffuser measurements more awkward than measuring the polar responses from loudspeakers, because for loudspeakers it is possible just to rotate the loudspeaker.

The single plane measurement is quick and easy to carry out. Measurements in a hemispherical goniometer, however, require considerably more complex engineering to achieve the acoustically transparent microphone positioning and source positioning in an anechoic chamber. Hemispherical measurements are also more time-consuming, due to the great increase in the number of measurements required. A spatial resolution of 5° in azimuth and elevation has been used between receivers for the set-up shown in Figure 4.3, resulting in 1,296 measurement positions for a single angle of incidence. (Five degrees was chosen because tests have shown that this is a sufficient resolution to gain the polar response accurately without overburdening measurements with excessive sampling points.)

Consequently, for hemispherical evaluation, it is much easier to use validated prediction models. Farina [4] has suggested evaluating along selected semicircles (say two or three) rather than measuring the whole hemisphere to reduce the burden of measurement. If symmetry in the sample exists, and the source lies in the plane of symmetry, it is possible to reduce the number of measurements. For the hemispherical measurement, symmetry is certainly worth exploiting.

Figure 4.8 illustrates the sequence of events to determine the scattered impulse response at a particular observation angle, for a given angle of incidence for the set-up shown in Figure 4.2. To obtain the impulse response of a sample under test, it is necessary to de-convolve the loudspeaker–microphone response at each scattering angle, $h_3(t)$. It is also necessary to minimize any room interference and reflections from microphone supports and wires within the time window of interest. To obtain the ‘loudspeaker/microphone response’ (top panel in Figure 4.8) at each scattering angle, the loudspeaker is placed at the sample position and rotated, so its on-axis response is coincident with the on-axis response of each microphone for each angle.

The loudspeaker is then placed in its normal source position, without any sample present, and the ‘background response without sample’, $h_2(t)$, at each angle is automatically measured via computer control by emitting 37 impulses and sequentially

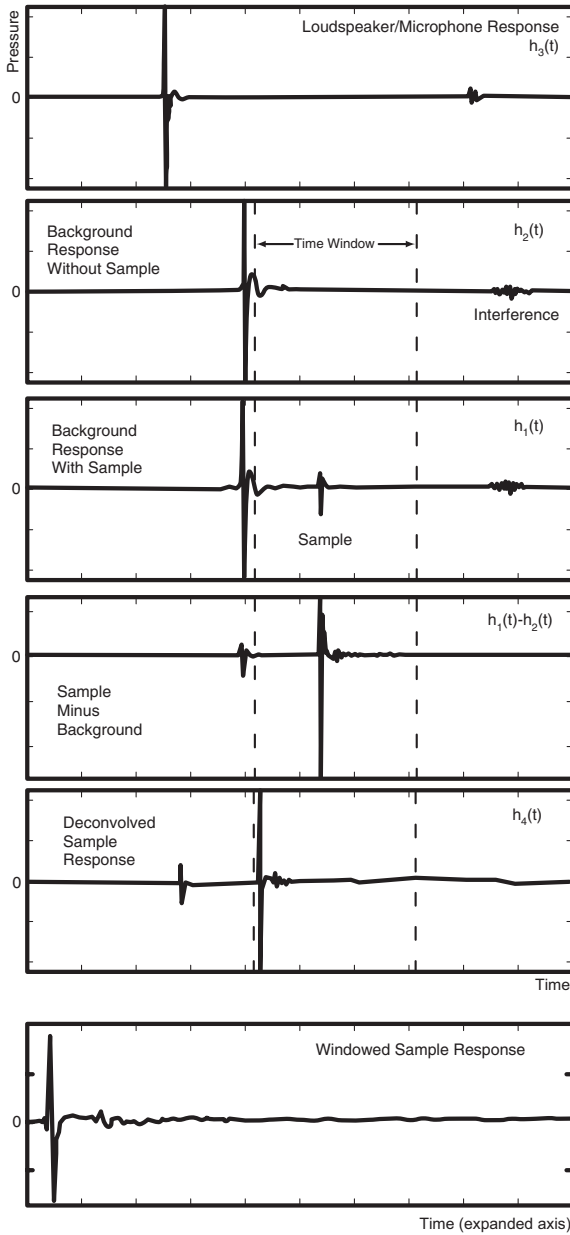


Figure 4.8 Data reduction process to extract the scattered impulse response from a test sample at a given observation angle.

switching each microphone on. A vertical dotted line representing the ‘time window’ of 10 ms used to isolate the reflections is also shown. The sample under test is then placed in position, and the scattered sound is measured obtaining the ‘background response with sample’, $h_1(t)$, in Figure 4.8.

Data are collected at 5° intervals. Higher resolution, for example 2.5° , is possible by combining another data set with the sample rotated by 2.5° . The measurement system selects a microphone, emits a selected maximum length sequence stimulus, records the data, selects the next microphone position, etc. Since the microphones are stationary and the measurement process is rapid, the respective background response can be subtracted from each microphone position, prior to de-convolution. This is illustrated as ‘sample minus background’ in Figure 4.8. The direct sound is significantly decreased and is not providing interference in the time window with the scattered sound. The room interference is also decreased. The speaker–microphone response can now be de-convolved as illustrated in ‘de-convolved sample response’, $h_4(t)$, where $h_4(t)$ is calculated using:

$$h_4(t) = \text{IFT} \left\{ \frac{\text{FT}[h_1(t) - h_2(t)]}{\text{FT}[h_3(t)]} \right\} \quad (4.1)$$

where FT and IFT are the forward and inverse Fourier transforms. The data within the time window is gated to isolate the ‘windowed sample response’.

The data are further post-processed to provide frequency responses, polar responses and finally diffusion coefficients, as shown in Figure 4.9.

The top of Figure 4.9a, shows the 2D boundary measurement geometry with the exciting loudspeaker at an angle of incidence of -60° , with respect to the normal. Also shown are the 37 receiving microphones. A flat non-absorbing sample is being measured. Below that, Figure 4.9b, the impulse response at 0° is shown, with the scattered data outlined in a box, corresponding to the time window in Figure 4.8. The scattered data are windowed for all of the angles of observation, of which five are highlighted at -60° , -30° , 0° , 30° and 60° and concatenated in Figure 4.9c in the form of a temporal angular impulse response. A Fourier transform is then applied to each part of the impulse response to get the frequency responses, Figure 4.9d. Five of the 37 frequency responses are only shown for clarity. The frequency response energy is summed over one-third octave bands, and three of the polar responses are shown in Figure 4.9d. The visible polar response at high frequency is narrow and directed in the specular direction of $+60^\circ$ as would be expected. The polar responses can then be further processed to give a diffusion coefficient, which is plotted versus frequency to obtain the diffusion response, Figure 4.9e. As the frequency increases, one can see a drop in the diffusion coefficient, as the width of the panel becomes increasingly large compared to the wavelength.

In Figure 4.10, the same procedure is shown for a diffusing sample for -60° incidence. The polar responses are more semicircular and the diffusion coefficient closer to 1, the value for complete diffuse reflection.

Figure 4.11 compares the measured and predicted scattering from a surface measured both on a single plane and a hemisphere. The agreement between theory and measurement is good – this is a measurement process that yields accurate results.

4.1.1 Near and far fields

All free field measurements suffer from the problem that the relative levels within the polar response are dependent on the source and receiver distances from the surface, unless the source and receivers are in the far field. (The far field being where the scattered pressure falls by 6 dB per distance doubling for 3D geometries, and 3 dB per

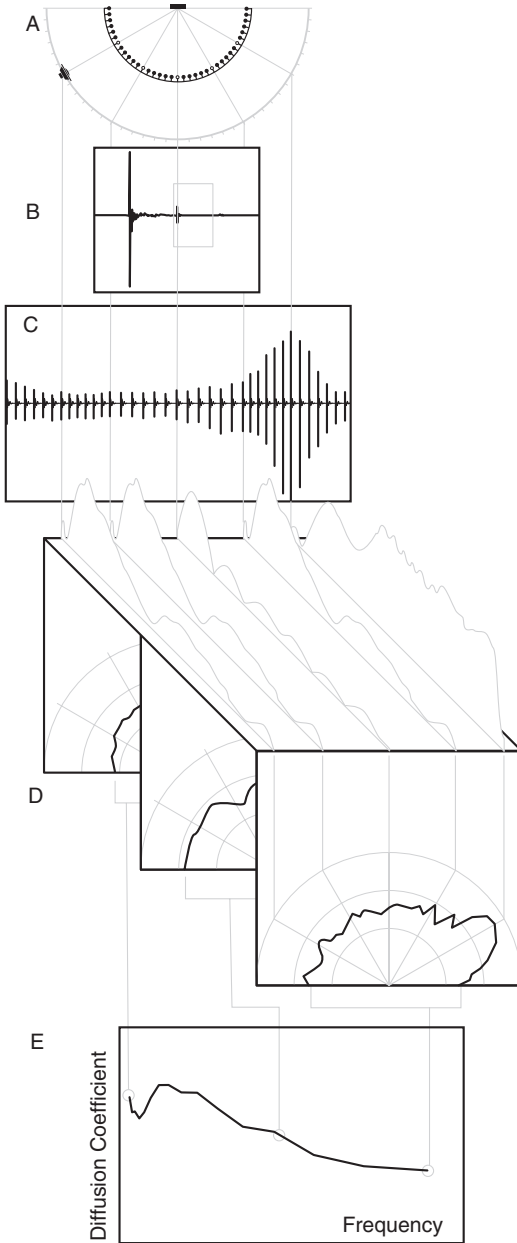


Figure 4.9 Summary of data processing technique from a flat reflector at -60° incidence.

distance doubling in 2D geometries.) Unfortunately, in most room applications, it is usual for sources and receivers to be in the near rather than the far field unless the test surface is small. Figure 4.12 shows the scattering from a plane surface for a variety of receiver distances. As the receiver approaches the surface, the scattered pressure is more evenly distributed over the polar response. A plane surface appears to be a very

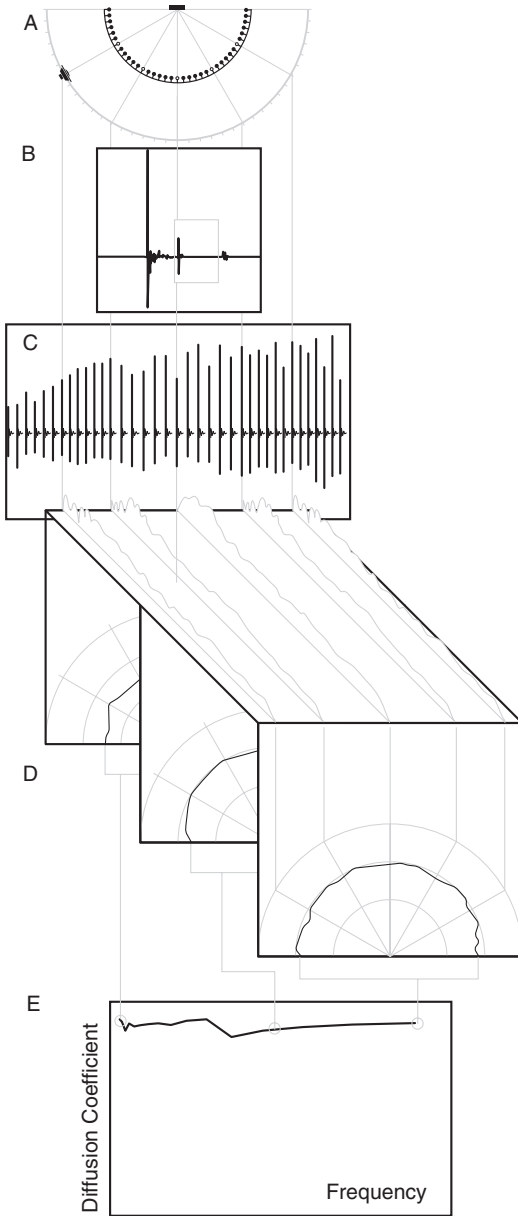


Figure 4.10 Summary of data processing technique from a diffuser at -60° incidence (after AES [6]).

good diffuser when measurements are made close to the surface. In fact, close enough to the surface, the reflection is provided by an approximate image source that radiates the same energy to all receivers except for minor effects due to spherical spreading due to the differences in path lengths. This seemingly contradicts conventional wisdom in room design that a plane surface is a poor diffuser.

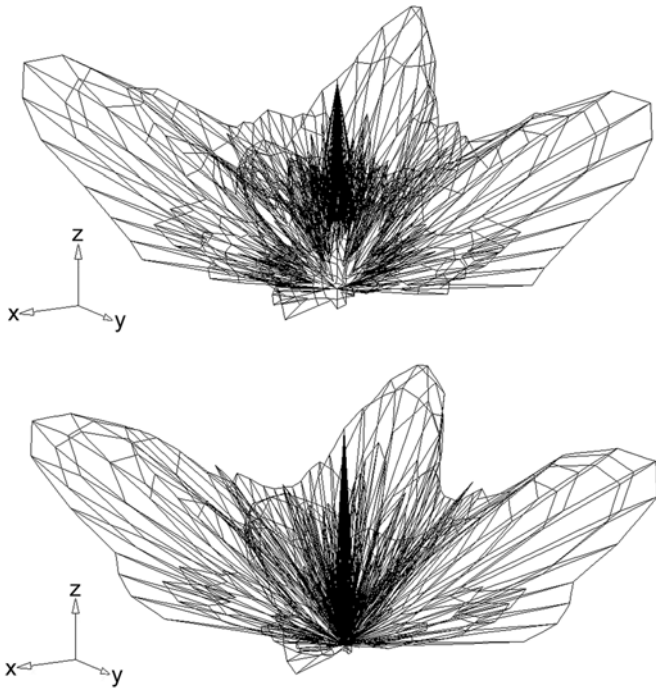
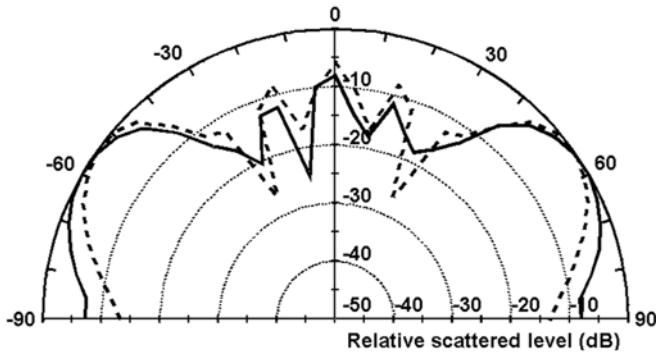


Figure 4.11 Comparison of measured and predicted polar responses. Top: — Measurement (2D) using boundary plane; - - - Single plane boundary element method (BEM) prediction; (Square-based pyramid, 1 kHz, normal incidence.) middle: 3D measurements at the University of Salford; (Square-based pyramid, 2 kHz, normal incidence.) bottom: 3D BEM prediction; (Square-based pyramid, 2 kHz, normal incidence.) (after Hargreaves *et al.* [12]).

To understand this contradiction it is necessary to understand why plane surfaces can cause problems in real applications. Problems can occur with plane surfaces with directional sources such as trumpets. The reflected energy will be concentrated over a narrow solid angle, leading to a risk of detrimental effects such as echoes, colouration or image shift for receivers within this solid angle. The results shown in Figure 4.12

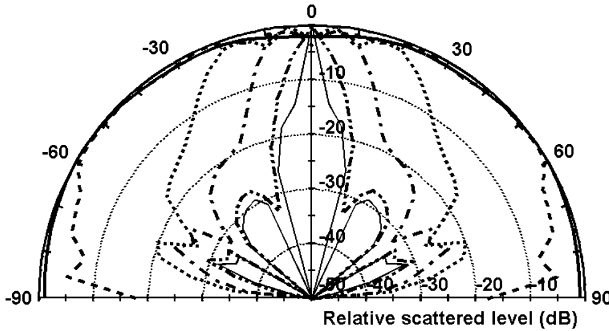


Figure 4.12 Effect of receiver arc radius on the polar response of a 1 m square plane panel. Single plane BEM prediction, 5 kHz, normal incidence, source distance = 100 m. Receiver distances ——— 0.1 m; - - - - 0.5 m; 1 m; - · - · - 2 m; - - - - - 5 m; - · - · - · - 100 m (after Hargreaves *et al.* [12]).

were produced using an omnidirectional source. Furthermore, the plane surface does not produce any temporal diffusion in the polar response, and as discussed in Chapter 10, this is another reason why it is a poor diffuser. These polar responses are neglecting to look at the wavefront phase.

The solution usually adopted is for scattering measurements based on polar distributions to be taken in the far field, even when this is further than any real listeners would ever be. Then some receivers will be outside the specular zone (the specular zone is defined in Figure 4.13), and it is possible to measure the energy dispersed from receivers in the specular zone to receivers outside the specular zone. In the spatial domain and in the far field, the effect of a diffuser should be to move energy from the specular zone to other positions. So unless receivers are placed both outside and within the specular zone, measuring energy levels alone will not detect the effects of diffuse reflections.

There are standard formulations for approximately calculating the required distance for measurements to be in the far field [5]. These criteria apply to both sources and receivers, but for now only receivers are considered to simplify explanations – the source will be assumed to be at infinity. There are two criteria to satisfy: the receiver radius should be large compared to wavelength, and the differences between path lengths from points on the surface to the receiver should be small compared to wavelength. With the geometries and frequencies used for measuring acoustic diffuser scattering, it is the latter criterion that is most exacting.

Unfortunately, the common far field formulations are not applicable to the case of oblique receivers where significant destructive interference occurs. Problems arise because the amount of destructive interference is very sensitive to the relative magnitudes of the waves coming from the secondary sources on the scattering surface (assuming the scattering is modelled following Huygen's principle). Consequently, the receiver distance required to achieve the true far field for oblique receivers is often so large that measurements cannot be accommodated in normal test facilities. Figure 4.14 shows the scattering from a surface as a function of distance, it takes a receiver distance of hundreds or even thousands of metres to reach a completely stable far field polar response!

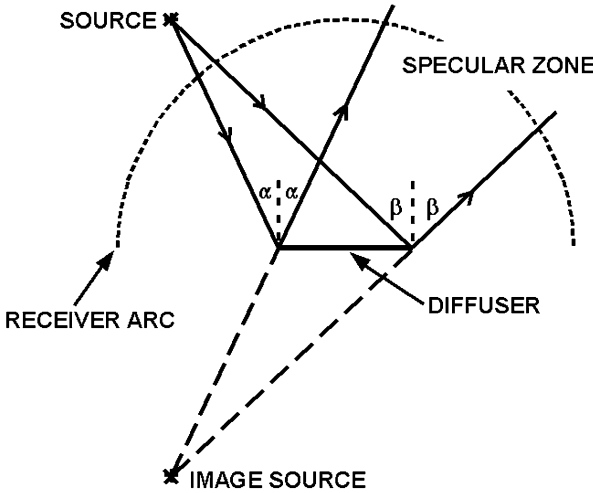


Figure 4.13 Definition of the specular zone – the region over which a geometric reflection occurs (Although the specular zone is strictly a high frequency construction, practice has shown it to be a useful concept for the geometries and frequencies typically used in diffuser design.) (after Hargreaves *et al.* [12]).

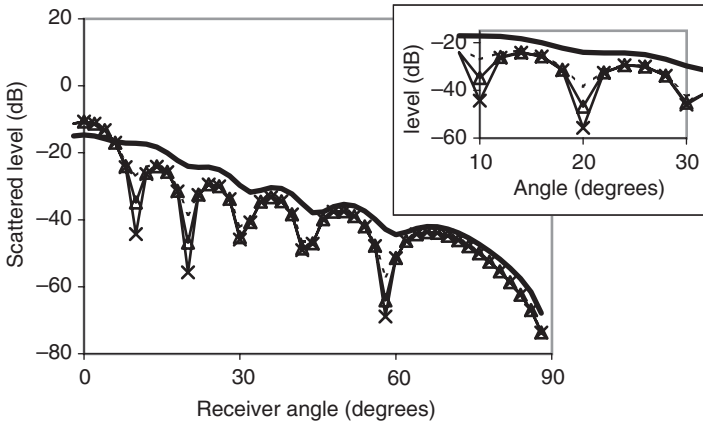


Figure 4.14 Variation of scattered polar response with receiver distance to illustrate extent of near field. Receiver angle on a linear scale for clarity; insert graph is an enlargement of a section of the main graph. 1 m plane surface at 1 kHz using BEM predictions. A distance correction of $1/\sqrt{r}$ has been used to correct for cylindrical wave spreading. — 2.94; - - - - - 12; —△— 32; —×— 100 m (after Hargreaves *et al.* [12]).

Fortunately, a pragmatic approach may be taken, as knowing the minima in a polar response to very exact detail is not that necessary. This is particularly true if diffusion coefficients are going to be evaluated, as the calculation of the diffusion coefficients involves reducing the many scattered pressure values in a polar response to a single figure of merit.

Consequently, errors from the slight misrepresentation of notches in the polar response will be negligible in the diffusion coefficient value. The situation is also less critical when one-third octave bandwidths are used, as is normal practice. So, the true far field does not have to be obtained, it is sufficient to ensure that the majority of receivers are outside the specular zone so that the diffuser's ability to move energy out of the specular zone can be measured. Then a reasonable approximation to the far field polar response can be obtained.

AES-4id-2001 [6] recommends that 80 per cent of receivers are outside the specular zone, ideally in revisions of the standard this figure should be referenced to Fresnel zones or panel-critical frequencies [7]. In Figure 4.15 the diffusion coefficients (the single figure of merit derived from the polar responses) for two surfaces as a function of receiver distance are shown. The point where 80 per cent of the receivers are outside the specular zone is shown. The plane panel case shown is one of the worst case scenarios, and the error introduced into the diffusion coefficient is only 0.1. Furthermore, this is a single frequency prediction. Once summing across one-third octave bands is used, this error approximately halves. Consequently, a reasonable approximation to the true far field polar responses and diffusion coefficients can be obtained.

An alternative solution is to use near field acoustic holography [8] to enable near field measurements to be projected into the far field, but this method has disadvantages such as the problems of mounting the surface in an application-realistic manner. Another solution is to use validated numerical models as predicting in the far field is always possible.

For some surfaces, however, it is not sufficient just to measure in the far field. For concave surfaces, and others that might have significant aberrations closer to the surface, it is necessary to monitor in the near field as well as the far field to ensure that effects such as focussing are found. This is illustrated in Figure 4.16 where the scattering from a concave surface is shown as a function of distance. It can be seen that receivers very close to the surface detect a good diffuser, but a little further out the reflected sound is highly focussed. In the far field, some diffusion is created. In summary, a pragmatic approach requires receivers to be both inside and outside the specular zone, and measurements at application-realistic distances are also needed to check whether concave surfaces focus far field aberrations into the near field.

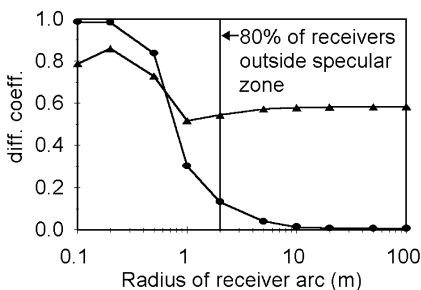


Figure 4.15 Effect of receiver arc radius on the diffusion coefficient. Single plane BEM predictions, normal incidence, source distance = 100 m. —●— 1 m wide plane panel, 5 kHz; —▲— 1 m wide random binary panel, 400 Hz (after Hargreaves *et al.* [12]).

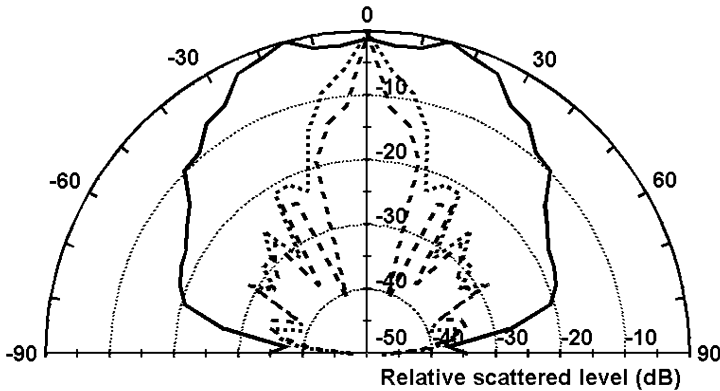


Figure 4.16 Effect of receiver arc radius on the polar response of a concave prism. Single plane BEM predictions, 2 kHz, normal incidence, source distance = 10 m. ——— Near field; - - - - - Focal distance; Far field (after Hargreaves *et al.* [12]).

4.1.2 *Sample considerations*

It is important to test a sample as close to the entire structure to be applied in a real application as possible. For instance, one period of a Schroeder diffuser should not be tested alone if the intention is to apply the surface periodically. This is because the scattering from the periodic and single diffuser will be very different. Where the whole sample cannot be tested, because of geometric constraints on source and receiver distance, the following techniques are suggested in AES-4id-2001 [6]: for a periodic sample at least four complete repeat sequences should be included, so that the effects of lobing from repetition is measured. (Although the width of the diffraction lobes depends somewhat on the number of repeat units in the sample [9].) Figure 4.17 shows the diffusion coefficient from four different sets of semicylinders. It is shown that one semicylinder is not representative of the scattering from an array of semicylinders. For random surfaces, representative samples of the surface roughness should be tested, large enough so that surface rather than edge effects are more prominent in the scattering.

Some have said that the diffusion coefficient method will not work for large surfaces with small surface roughness, and it is intended to be used for single diffusers only. This is not true, and the evaluation method can theoretically be used on any sized surface. The problem is that when the surface becomes large, the measurement becomes impractical, because it is impossible to get far enough away from the surface. In this case, the evaluation can still be done, but using prediction models.

When scale models are used, it is important that a proper scale model is constructed. For scale models, the absorption properties shall be the same for both the full-scale surface at full-scale frequencies and the test surface at the equivalent model scale frequency. When considering absorption from samples, losses due to viscous boundary layer effects should be included. This consideration can limit the usable model scales because viscous boundary layer effects do not scale in the same way as physical dimensions.

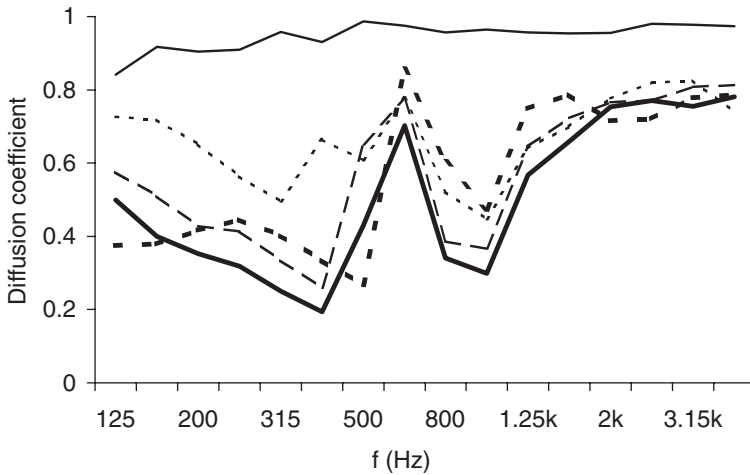


Figure 4.17 The diffusion coefficient for various sets of semicylinders. The number of cylinders in each set is: — 1; 2; - - - 3; ——— 4; 8.

The method measures the diffraction effects of the edges and surface roughness together. While it may be possible to separate edge and surface diffraction effects for large surfaces with small roughness, for the majority of surfaces, such a separation is problematic.

4.1.3 The total field and comb filtering

The above discussion has only investigated the sound energy scattered from the diffuser. This has disregarded several important issues. With a single cylinder or hemisphere, it is possible to produce good spatial dispersion, but without temporal dispersion. With most diffusers, on the other hand, good spatial dispersion also means temporal dispersion is generated. Consequently, while current diffuser evaluation concentrates on energy dispersion, in the future it might also become necessary to look at the phase in the polar response. Pertinent comments about this point can be found in Chapter 10 where the scattering from cylinders is discussed.

In reality, the listener hears a fusion of the direct sound from the source and the reflection from the surface. This has led some to suggest that the total field (direct plus scattered) is an appropriate way of measuring the effect of surfaces. It certainly gets around all the problems of having to separate the direct and reflected sound by measuring impulse responses. The problem with the total sound field evaluation is that it is so dependent on the geometry. The dominating feature of the total sound field frequency response is comb filtering, examples of which can be found in Figure 2.8. The depth and frequencies of the minima and maxima, in the comb filtering, are strongly dependent on the delay time and relative level between the direct and reflected sound and hence on the source and receiver distances. Consequently,

evaluating the total sound field is problematical, but maybe sometime in the future a robust method will be achieved.

4.2 Diffusion and scattering coefficients, a general discussion

While measuring polar responses can give much information about the scattering from the surface, the problem is that it can yield too much detail. There is a need to reduce the large amount of data in a polar response to a single value, to allow a more ready comparison of diffuser quality. This then helps diffuser designers to evaluate the worth of a product, and room designers to produce product specifications for surface designs. Furthermore, there is a need for a scattering coefficient to evaluate the amount of dispersion generated by a surface and so allow accurate predictions using geometric room acoustic models.

Unfortunately, there does not appear to be one ideal coefficient which meets the needs of all interest groups – the room modellers, diffuser manufacturers and room designers. There are no diffusion or scattering coefficients currently in the literature that do not have flaws in their use. While on first examination it appears possible to produce a watertight definition of a coefficient, detailed analysis reveals problems. For this reason, two different coefficient definitions are, or are about to be, enshrined in international standards. While this may appear unsatisfactory, it should be remembered that room acoustics has used an absorption coefficient for a century which has well-defined limitations in application. For example, there are two primary techniques for measuring absorption – the impedance tube and reverberation chamber methods – and each measurement method has advantages and disadvantages and is used for different reasons. In an analogous manner, the methods for characterizing diffusion can be classified either as free or diffuse field.

Diffuse field methods have the advantage of quickly obtaining a random incidence coefficient, but are difficult to predict. A measurement method for obtaining a random incidence scattering coefficient is due to be standardized by the ISO based on the Mommertz and Vorländer technique [10, 11]. Free field measurements are often more laborious to carry out, but can be readily predicted. A free-field method for a diffusion coefficient, based on the Cox and D’Antonio technique has recently been published in an Audio Engineering Society standard information document AES-4id-2001 [6]. At the time of writing, the technique is also being considered by an ISO working group.

The terms scattering and diffusion are used in different ways and are interchanged in different subject fields. It would be possible to have a long argument about whether diffusion or scattering is a better terminology for a given coefficient, but it would be impossible to get a unanimous agreement on nomenclature. Consequently, in this book the nomenclature that is being used in the standards development will be used, even if some readers may disagree with the terminology. This defines the diffusion and scattering coefficients as follows:

- A diffusion coefficient measures the quality of reflections produced by a surface, in the case of the AES coefficient, by measuring the similarity between the scattered polar response and a uniform distribution.

- A scattering coefficient is a measure of the amount of sound scattered away from a particular direction or distribution. This has the greatest similarity to the coefficients required as inputs to geometric room acoustic models.

4.3 The need for coefficients

4.3.1 Diffuser manufacturer and application

When Schroeder introduced his revolutionary design of diffusers, which are described in Chapter 9, he also introduced a possible measure for complete diffuse scattering. This was different from Lambert law. Schroeder defined optimum diffuse scattering as being when all the scattering lobes produced by periodic phase gratings have the same energy. Since the 1970s, many other types of diffusers have been produced, and to enable the merits of these designs to be evaluated, it is necessary to have a better measure of the quality of the diffuse reflections than lobe energy. The idea of measuring the similarity of the lobe energy is not a useful criterion because surfaces do not have to be periodic, and so did not necessarily have periodicity lobes. Consequently, new definitions to measure the diffuseness of reflections have been developed.

For a diffusion coefficient to be useful to designers, the primary characteristic of the coefficient is that it must rank diffusers correctly according to quality. This will not necessarily be achieved by the scattering coefficient, and this is why a separate coefficient has been developed for quality. An ideal diffusion coefficient would [12]:

- have a solid physical basis;
- be clear in definition and concept, and related to the current and future roles of diffuse reflections in airborne acoustics, especially in rooms;
- consistently evaluate and rank the performance of diffusers;
- apply to all the different surfaces and geometries found in rooms;
- be measurable by a simple process;
- be bounded; and
- be easy to predict.

This turns out to be like searching for the Holy Grail, but it is possible to produce a diffusion coefficient that does satisfy most of the above criteria.

The current state of the art in diffuser design is numerical optimization as described in Chapters 9 and 10. Using diffusion coefficients in a numerical optimization has enabled designs to move away from the rigid geometric constructs imposed by phase grating diffusers. This has enabled designs where both acoustic and visual requirements can be considered and their conflicting requirements resolved. It is now possible to make diffusers which blend in with architectural forms rather than appearing as add-ons, and this is important for acoustic treatments to be acceptable to architects. This shape optimization capability allows architects to design the form or motif and the acoustic consultant to define the acoustic performance criteria. The result is a surface treatment or suspended element, which simultaneously satisfies the architecture, the acoustics and the aesthetics. The process strives to provide acoustical scattering surfaces that complement contemporary architecture in the same way that columns, statuary, coffered ceilings and relief ornamentation complemented classic architecture. It also offers an opportunity to create a new generation of vernacular

scattering surfaces in contemporary architecture. Enabling this technique of optimization has been one of the main drivers behind the development of a diffusion coefficient.

When a designer requires absorbing surfaces in a space, a performance specification in terms of the absorption coefficient is currently used to ensure quality and compliance with design requirements. One of the aims of research into diffusion coefficients was to facilitate the use of defined scattering ability in performance specifications; this can now be done by specifying diffusion coefficients measured or predicted according to AES-4id-2001. Without standardization, the industry is vulnerable to published performance data, which have no basis in fact and diffusers that do not perform as intended. The evaluation criteria developed do not just have to be applied to especially designed surfaces, they can also be used to monitor the diffusion by accidental diffusers. It appears that surface diffusion is often applied in a haphazard fashion because there is not a good understanding of when to apply diffusers, and when not to use diffusers. For instance, discussions with consultants produce examples where it is claimed that too much or too little surface diffusion resulted in acoustic aberrations. A priori to developing a better understanding of where diffusers are needed, is an index to measure their quality. This measure is now provided by the uniformity diffusion coefficient.

4.3.2 Geometric room acoustic models

Originally, geometric room acoustic models did not include the effects of scattering due to edge effects and surface roughness. In recent decades, however, evidence has been produced to show that incorporating scattering into the geometric models enhances prediction accuracy. For instance, it has been shown that without surface scattering, geometric room acoustic models tend to over predict reverberation time [13–15]. This is especially true in spaces where absorption is unevenly distributed, as happens in many concert halls, or where rooms are highly disproportionate, as happens in many factories. Moreover, for acoustic parameters that are highly dependent on early reflection prediction accuracy, such as early lateral energy fraction and clarity, there can be great sensitivity to a correct diffuse modelling technique and correct scattering coefficients [16]. In the first round robin study of room acoustic models [15], three models were found to perform significantly better than others. These three models produced results approximately within one subjective difference limen, while the less successful models produced predictions inaccurate by many difference limen. What differentiated the three best models from the others was the inclusion of a method to model surface scattering. Scattering in geometric room acoustic models is discussed in detail in Chapter 12.

There are many different methods for incorporating diffuse reflections into a geometric room acoustic model [17] – see Chapter 12. This process is inevitably approximate, because the geometric models cannot explicitly model the true wave nature of sound. The geometric models use a scattering coefficient to determine the proportion of the reflected energy that is reflected in a specular manner and the proportion that is scattered. (In the computer models, these coefficients are usually referred to as diffusion coefficients just to confuse matters further.) Problems arise because until recently there has not been a procedure for determining the values of the scattering coefficients except for trial and error and through precedence.

Consequently, a key driving force behind the ISO process was to standardize a method to enable scattering coefficients to be determined in a rigorous manner.

The scattered energy in a geometric model is usually distributed according to Lambert's cosine law [18]. Lambert's law is used because it fits with the philosophy of the geometric models which are based on high frequency modelling techniques. The law is correct for high frequency, point, incoherent scattering. As shall be discussed below, diffusion coefficients used by diffuser designers are based on uniform energy distribution. Uniform energy distribution is possible because the reflected sound from surfaces display coherent interference effects at the important acoustic frequencies. Indeed, this coherence is explicitly exploited in many diffuser designs. Try and explain how a Schroeder diffuser works without referring to interference. Consequently, Lambert's law is inapplicable for evaluating diffusers, and despite what some have claimed, diffuser designers are not violating the second law of thermodynamics! Conversely, using the diffusion coefficients measured according to AES-4id-2001 in geometric room acoustic models is likely to produce incorrect results, unless the model has been explicitly designed to use this coefficient.

4.4 The diffusion coefficient

4.4.1 Principle

The general method for evaluating diffuser quality is as follows. First the scattering from a surface is measured or predicted in terms of a polar distribution as discussed in Section 4.1. Then the diffusion coefficient is a frequency dependent, single figure of merit derived from the polar distribution. This is evaluated in one-third octave bandwidths, which has the advantage of smoothing out some of the local variations in the polar responses, so the diffusion coefficient is based more on the overall envelope. There have been various statistical operations suggested to calculate a diffusion coefficient from the polar distributions: standard deviation [19–21] directivity [22, 23], specular zone levels [24, 25] and spherical harmonics [26], percentiles and autocorrelation [12]. In any such data reduction, there is a risk of losing essential detail. It has been shown that the autocorrelation coefficient seems to offer significant advantages over other published statistical techniques.

The autocorrelation function is commonly used to measure the similarity between a signal and a delay version of itself, looking for self similarity in time. It is also possible to use the autocorrelation to measure the scattered energy's spatial similarity, i.e. with receiver angle. A surface which scatters sound uniformly to all receivers, will produce high values in the spatial autocorrelation function, conversely surface which concentrates scattered energy in one direction will give low values. To form a single figure diffusion coefficient, the circular autocorrelation function is first calculated, and then an average taken. This is a rather laborious process, but fortunately the whole calculation can be simplified to a single equation. For a fixed source position, the autocorrelation diffusion coefficient, d_ψ , can be calculated from:

$$d_\psi = \frac{\left(\sum_{i=1}^n 10^{L_i/10}\right)^2 - \sum_{i=1}^n (10^{L_i/10})^2}{(n-1) \sum_{i=1}^n (10^{L_i/10})^2} \quad (4.2)$$

where L_i are a set of sound pressure levels in decibels, n is the number of receivers in the polar response, and ψ is the angle of incidence. This equation is only valid when each receiver position samples the same measurement area. This is automatically achieved for single plane measurements on a semicircle with an even angular spacing between receivers. (The fact that receiver positions at $\pm 90^\circ$ actually sample half the area of the other receivers can be ignored, as applying a correction makes an insignificant difference to the diffusion coefficient.)

For some measurements, the area sampled by a receiver will vary with position. In that case, the following formulation should be used:

$$d_\psi = \frac{\left(\sum_{i=1}^n 10^{L_i/10} N_i\right)^2 - \sum_{i=1}^n N_i (10^{L_i/10})^2}{\left(\sum_{i=1}^n N_i - 1\right) \sum_{i=1}^n N_i (10^{L_i/10})^2} \quad (4.3)$$

where N_i is proportional to the area sampled by receiver point i and should be calculated from the following equations:

$$\begin{aligned} A_i &= \frac{4\pi}{\Delta\phi} \sin^2(\Delta\theta/4) & \theta &= 0^\circ \\ A_i &= 2 \sin(\theta) \sin(\Delta\theta/2) & \theta &\neq 0^\circ, |\theta| \neq 90^\circ \\ A_i &= \sin(\Delta\theta/2) & |\theta| &= 90^\circ \end{aligned} \quad (4.4)$$

$$N_i = \frac{A_i}{A_{\min}} \quad (4.5)$$

where ϕ is the azimuth angle and θ elevation angle for the receiver. $\Delta\phi$ and $\Delta\theta$ are the angular spacing in azimuth and elevation between adjacent receivers, usually 5° . A_{\min} is the smallest value of A_i for $i = 1 \dots n$. The equations assume a single measurement at $\theta = 0^\circ$.

This uneven sampling will arise for hemispherical measurements using an even angular spacing in azimuth and elevation. An uneven sampling of the hemisphere with respect to area results, with more receiver points nearer the normal to the surface. Equation 4.3 adds additional dummy samples into the calculation to make the sampling linear with respect to area. This usually makes a relatively small difference to the diffusion coefficient values.

The concern with diffusion measurement is to measure the ability of diffusers to uniformly scatter in all directions, rather than with just the ability of a surface to move energy away from the specular angles. This restriction is placed because of experiences of diffuser designers. From the standpoint of the diffuser designer, it is important that a diffusion coefficient differentiates between redirection and dispersion. Figure 4.18 shows the scattering from a plane surface, and a plane surface which has been rotated by 20° to redirect the specular reflection in another direction. The diffusion coefficient measures the dispersion capabilities to be the same in both cases. The scattering coefficient, however, sees the redirection of energy from the specular reflection angles as scattering, and there gives a high coefficient for the rotated plane surface, even though this is only achieving redirection, not dispersion. Diffusers are often applied

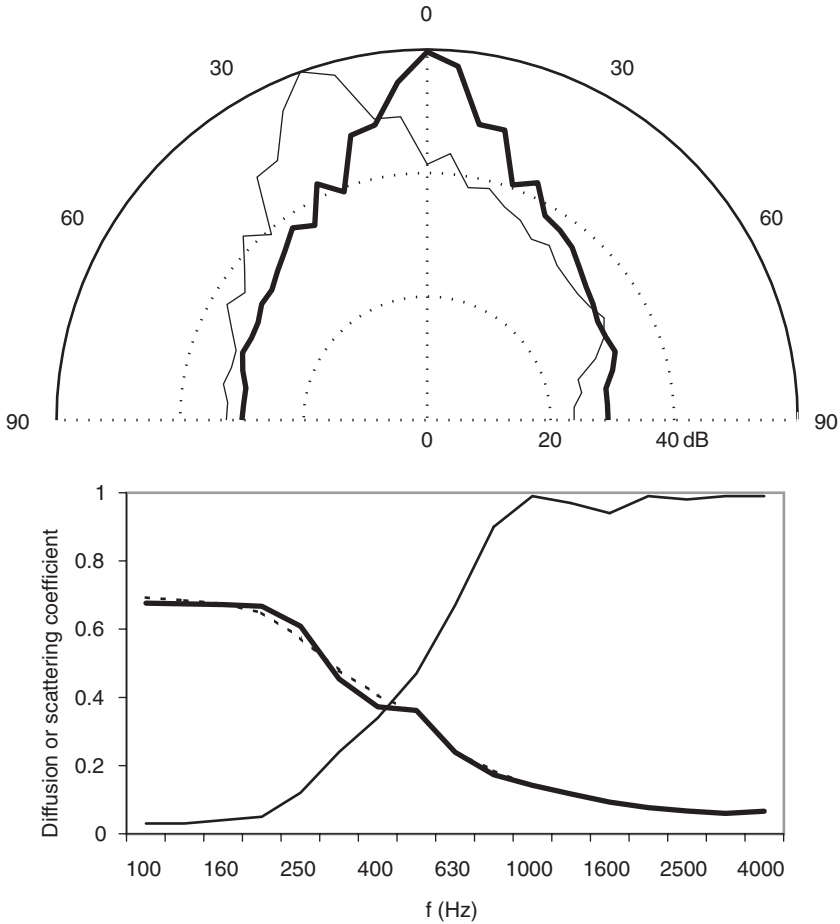


Figure 4.18 Top, the polar responses for a **—————** plane surface and a **—————** rotated plane surface. Bottom, the diffusion and scattering coefficient frequency responses. **—————** Correlation scattering coefficient; **.....** Diffusion coefficient, plane surface; **—————** Diffusion coefficient, rotated plane surface (adapted from Cox and D'Antonio [32]).

to treat first-order reflections, for example to prevent echoes from the rear wall of concert halls. If all the diffuser achieves is redirection, there is a risk that the echo problem will simply move to another place in the hall. On the other hand, if the diffuser achieves spatial dispersion, this has the potential to reduce the echo problem without creating new difficulties elsewhere. This is the reason why the Mommertz and Vorländer [10, 11] free-field method has not found favour with diffuser designers.

4.4.2 Obtaining polar responses

Section 4.1 already discussed how measurements might be made to obtain the polar responses. Predictions can also be used. AES-4id-2001 [6] recommends a receiver

every 5° , with the source at 10 m and receiver arc radii 5 m (equivalent full scale). It recommends that to obtain a random incidence diffusion coefficient, source positions should be measured with a maximum angular separation of 10° , covering a semicircle or hemisphere measured about the reference normal. Random incidence is achievable for single plane measurements, but the number of measurements in the hemispherical case is unrealistically large (0.5 million source and receiver combinations). To overcome this, the standard suggests that when time is limited, the directional diffusion coefficients can be obtained for normal and 55° angles of incidence only.

In many applications the source position is well known. In performance spaces, for example, this is the location of the stage. In that case, it makes most sense to evaluate the diffusion coefficient for this specific angle of incidence, as the first-order effects of a diffuser are of primary importance, especially if the concern is to remove echoes or colouration.

AES-4id-2001 stipulates that different radii polar responses might be used to check for focussing effects. If measurements are made at different radial distances from the surface, it is necessary to apply a correction to allow for the normal drop in level due to spherical or cylindrical spreading. Otherwise the diffusion coefficient is overly biased by drops in levels that naturally occur due to effects that are not related to a surface's ability to diffuse.

4.4.3 *Discussion*

In Figure 4.19 the autocorrelation diffusion coefficient for different surfaces is illustrated as a function of frequency. It can be seen to be ranking the diffusers correctly and separating the different surfaces along the diffusion axis. The coefficient has a clear physical basis in the autocorrelation function, but has the drawback that only the extreme values of uniform diffusion and specular reflection are truly defined. The meaning of intermediate values cannot be easily found, but over time, an understanding for what intermediate values mean should naturally develop. It is also unknown how exactly the diffusion coefficient values relate to subjective response, which would be useful in evaluating the merits of diffusers.

The experimentally measured and theoretically predicted diffusion coefficient values tend to be small. This can be seen by glancing at the coefficient values given in Appendix C. Values for the autocorrelation coefficient can in theory spread over the entire range from 0 to 1. A value of close to 0 has been measured for a concave surface designed to focus sound on a single receiver. A value of 1 can be measured for a small single hemisphere or semicylinder, but a single semicylinder on its own is not of much use because it cannot cover a wide area. As soon as more complex surfaces are introduced, such as a set of semicylinders, the diffusion coefficient is reduced because of the lobing introduced. This lobing is unavoidable in extended structures, and so the diffusion coefficient is rarely close to 1 for usable and realistic diffusers. A single semicylinder may produce complete diffusion, but to cover a wall a set of semicylinders are needed. This is why it is important to measure application-realistic samples as the scattering from a single object is not representative of the response from a periodic or modulated array.

It would be possible to distribute the diffusion coefficient values differently along the axis to obtain larger values for common surfaces. For instance, this could be done by calculating the autocorrelation based on levels rather than energies. Calculating

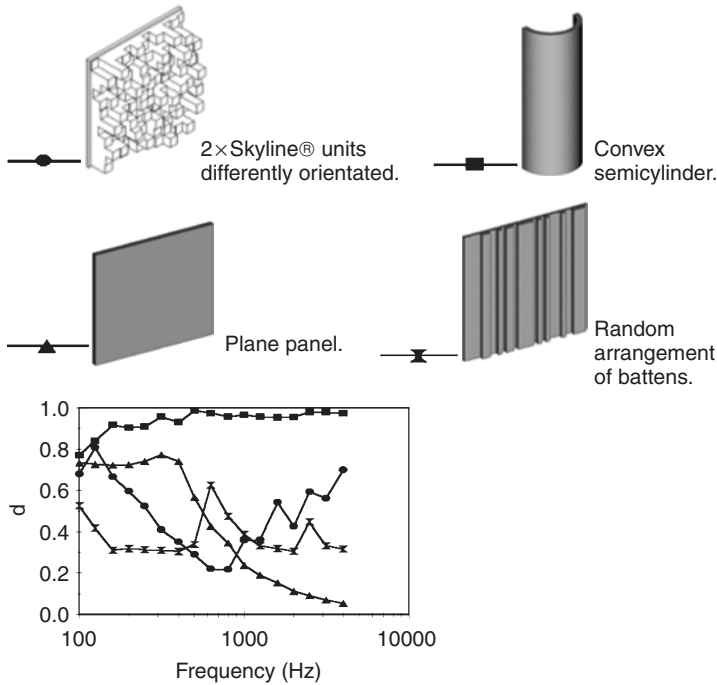


Figure 4.19 Variation of diffusion coefficient with frequency for a selection of samples. Measurements using boundary plane system, normal incidence (after Hargreaves *et al.* [12]).

the autocorrelation from energies, greatly penalises uneven responses, maybe it over penalises uneven responses, as the ear response is better matched to a decibel scale than linear energy.

4.4.4 Diffusion coefficient table

Appendix C gives values for diffusion coefficients for various surfaces by calculation following the procedure in AES-4id-2001. The predictions were carried out using a 2D boundary element model as described in Chapter 8. All surfaces were modelled as thin panel extrusions, the rear of the surfaces was not enclosed in a box or similar. These therefore represent the diffusion coefficient for single plane devices such as semicylinders. The source and receiver were 100 and 50 m, respectively from the surface. Each one-third octave band polar response was found by averaging seven single frequency responses. The random incidence diffusion coefficient values were found by an arithmetic average of the diffusion coefficient values for ten different angles of incidence (Paris' formulation was not applied). The table reports three incident angles, normal, 57° and random incidence.

The first part of the table shows the effect of changing the number of diffusers in an array, illustrating that the diffusion coefficients for single and multiple devices are very different. The results for planar surfaces of different width show how the

diffusion coefficient is dependent on the test sample size. The rest of the table keeps all the test sample widths the same at about 3.6 m to allow ready comparison. When comparing other diffusers in the table, it is important to compare like with like, for example to ensure that the diffusers being compared have the same maximum depth.

The second section shows the effect of diffuser depth on the diffusion coefficient. To do this a set of semi-ellipses are used. As might be expected, as the semi-ellipses get deeper, they start diffusing at a lower frequency – although period width becomes a limiting factor for deeper devices as discussed in Chapter 10. The third section shows the diffusion coefficients for different triangles – the scattering from triangles is discussed in detail in Chapter 10. The fourth section gives examples of what happens when ellipses are mounted on a flat baffle with spaces between, as might be expected this reduces the dispersion generated at high frequencies.

The fifth part shows the performance that can be obtained from optimized curved surfaces, the design of which is discussed in detail in Chapter 10. The table values illustrate that the optimization design process is very effective. The sixth part gives results for flat and planar hybrid surfaces, where absorptive patches are used to generate dispersion; these diffusers are discussed in detail in Chapter 11. The seventh and last part gives data for a variety of reflection phase gratings: simple Schroeder diffusers, fractal designs and optimized surfaces. These designs are discussed in Chapter 9. The Schroeder surfaces were modelled by meshing the entire surface, so the predictions are valid above (and below) the limit where plane wave propagation becomes less dominant in the wells.

4.5 The scattering coefficient

4.5.1 Principle

The principle of a scattering coefficient is to separate the reflected sound into specular and scattered components. The specular component is the proportion of energy which is reflected in the same way as would happen for a plane surface, large compared to wavelength. The scattered components give the energy reflected in a non-specular manner. This is illustrated in Figure 4.20. The coefficient has a clear physical meaning, and the definition is very useful for geometric room acoustic models because these tend to have separate algorithms dealing with specular and scattered components, and so the separation of terms mimics the modelling methods. With this definition it is then possible to define a scattering coefficient, s , as the proportion of energy not reflected in a specular manner.

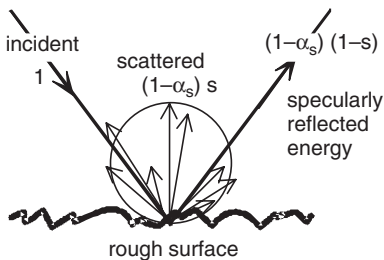


Figure 4.20 Definitions used for scattering coefficient (after Vorländer and Mommertz [11]).

This definition takes no account of how the scattered energy is distributed, but assumes that in most room acoustic applications there is a large amount of mixing of different reflections, and so any inaccuracies that arise from this simplification will average out. This is probably a reasonable assumption for the reverberant field, where there are many reflections, but could well be troublesome for the early sound field, where the impulse response is dominated by a few isolated reflections, and the correct modelling of these is essential to gaining accurate predictions. Section 4.4.1 has already illustrated how scattering coefficients can give misleading results for redirecting surfaces.

The scattering coefficient, like the diffusion coefficient, generally depends on frequency and angle of incidence. Similar to the random incidence absorption coefficient obtained in reverberation rooms, an angular average of the scattering coefficient – the random incidence scattering coefficient – can be defined as well. As a general assumption, the surface under test is assumed to be large and not too rough. The method will not work for isolated items and deep surfaces as it is trying to measure the scattering from the surface roughness and not the edges. It also has problems when the surface absorption is high as the coefficient estimation becomes inaccurate.

4.5.2 Rationale and procedure

The energies of reflections (normalized with respect to a reflection from a non-absorbing flat surface) are expressed as follows [10]:

$$E_{\text{spec}} = (1 - \alpha_s)(1 - s) \equiv (1 - \alpha_{\text{spec}}), \quad E_{\text{total}} = 1 - \alpha_s \quad (4.6)$$

where E_{spec} is the specular reflected energy, E_{total} the total reflected energy, s the scattering coefficient, α_s the absorption coefficient, and α_{spec} is the apparent specular absorption coefficient.

The apparent specular absorption coefficient warrants further description. It is the energy dispersed from specular reflection directions. This energy is not dissipated to heat, it is reflected into non-specular directions. From these equations the scattering coefficient can be determined from:

$$s = \frac{\alpha_{\text{spec}} - \alpha_s}{1 - \alpha_s} = 1 - \frac{E_{\text{spec}}}{E_{\text{total}}} \quad (4.7)$$

The measurement of this quantity is easiest to explain in the free field, although it is in the diffuse field measurement where this process is useful and powerful. The set-up is shown in Figure 4.21. The specular absorption coefficient is found by rotating the test sample while phase lock averaging the reflected pulses. Figure 4.22 shows three band pass filtered pulses for different orientations of a corrugated surface. The initial parts of the reflections are highly correlated; these are the specular components of the reflection and remain unaltered as the sample is rotated. In contrast, the later parts of the three reflected pulses are not in phase and depend strongly on the specific orientation; this is the scattered component. By averaging the reflected pulse pressure while rotating the sample, the scattered components are averaged to zero and only the specular energy remains.

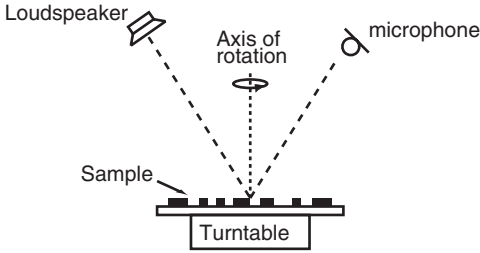


Figure 4.21 Set-up used for measuring scattering coefficient (after Vorländer and Mommertz [11]).

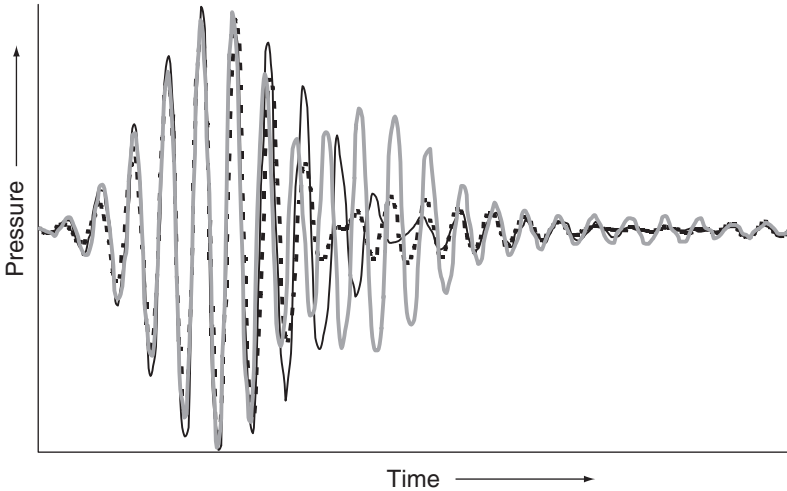


Figure 4.22 Band limited reflected pulses for different sample orientations (after Vorländer and Mommertz [11]).

Transferring this procedure to the reverberation chamber, the measurement technique is as follows. A circular test sample is placed on a turntable and rotated. While the turntable is rotated the impulse response is repeatedly measured. The latter parts of the impulse response, which are due to the scattering from the surface, will cancel out, and the averaged impulse response only contains the specular reflection component. This impulse response is then backward integrated to give the reverberation time due to the specular reflection component. The reverberation time with the sample stationary (not-rotating) can also be obtained, and this decay is due to the total scattering – specular plus diffuse. By manipulating these reverberation times, it is possible to derive the specular and total reflected energy, and from Equation 4.7 the scattering coefficient.

Table 4.1 The measurement conditions for the four different reverberation times

Reverberation time	Test sample	Turntable
T_1	Not present	Not rotating
T_2	Present	Not rotating
T_3	Not present	Rotating
T_4	Present	Rotating

In reality, four reverberation times are needed. It is difficult to get a perfectly flat and circular turntable; this is especially true for full scale measurements [27, 28]. Consequently, the imperfections in the turntable must be compensated for by additional measurements. The four reverberation times that must be measured are shown in Table 4.1.

Once these reverberation times are measured, the following formulations are used to get the scattering coefficient. The random incidence absorption coefficient α_s of the sample is calculated using:

$$\alpha_s = 55.3 \frac{V}{S} \left(\frac{1}{c_2 T_2} - \frac{1}{c_1 T_1} \right) - \frac{4V}{S} (m_2 - m_1) \quad (4.8)$$

where V is the volume of the reverberation room, S the area of the test sample, c_1 the speed of sound in air during the measurement of T_1 , c_2 the speed of sound in air during the measurement of T_2 , m_1 the energy attenuation coefficient of air in m^{-1} during the measurement of T_1 , see Section 1.1.2, and m_2 the energy attenuation coefficient of air during the measurement of T_2 .

The specular absorption coefficient α_{spec} is calculated using the following formulation:

$$\alpha_{\text{spec}} = 55.3 \frac{V}{S} \left(\frac{1}{c_4 T_4} - \frac{1}{c_3 T_3} \right) - \frac{4V}{S} (m_4 - m_3) \quad (4.9)$$

where c_3 is the speed of sound in air during the measurement of T_3 , c_4 the speed of sound in air during the measurement of T_4 , m_3 the energy attenuation coefficient of air during the measurement of T_3 , and m_4 the energy attenuation coefficient of air during the measurement of T_4 . Finally, the random incidence scattering coefficient s is calculated using Equation 4.7.

These reverberation times are measured using the standard procedures in ISO 354 [29], so multiple source receiver pairs are needed to average out spatial variation within the reverberation chamber. The measurement must use a deterministic source signal to allow the phase locked pressure averaging. In the original work, MLS were favoured. The problem with maximum length sequences is that they are rather sensitive to time variance, which means the measurement of the reverberation times with the turntable rotating must be done quickly. This is not a problem at model scale, but at full scale the turntable must move slowly. The signal periodicity must be longer than the reverberation time in the room, which means full scale measurements take a long time, as typically 72 measurements in a single rotation are needed. For this reason, some have favoured the use of swept sine waves which are less prone to time variance problems [27].

At full scale, the measurement is rather slow and laborious. There are some considerable logistical problems in fabricating a 3.6 m diameter flat turntable. For instance, the doors of the reverberation chamber are probably too small for the turntable to go through in one piece and so it needs to be dismantled, yet a completely flat and strong turntable when assembled must be made. Furthermore, a powerful, yet quiet motor is required [27]. For these reasons, model scale measurements are to be preferred for speed and efficiency.

4.5.3 Sample considerations

Since the measurement method is intended to measure surface roughness, the results are only reliable when the structural depth of the sample is small compared to the size of the specimen (approximately $b \leq d/16$, where d is the diameter of the turntable, and b the structural depth). Examination of the reliability of measurements of different sample depths has enabled the empirical derivation of this depth limit. If variations of the structural depth along the edges of the samples are too large, excess scattering from the edge is measured. Even with shallow surfaces, the edge effects cause measured scattering coefficients to be larger than 1 at high frequencies.

The measured scattering coefficients are very sensitive to edge conditions [30]. If a square sample is placed on top of a round base plate, the scattering from the square edges results in excessive scattering and misleading results. The solution is to recess square samples within the circular base plate as shown in Figure 4.23. Figure 4.24 shows example scattering for the different mounting conditions, indicating that the recessed sample mounting gives the best results.

4.5.4 Anisotropic surfaces

The scattering coefficients give potentially misleading values when a surface is anisotropic. This is illustrated by Figure 4.25 where the scattering coefficients for a single plane and hemispherical diffusers are compared. The single plane diffuser produces a high value for the scattering coefficient, even though it is plane and extruded in one direction. To use a simplistic analysis, even if the scattering coefficient in the plane of

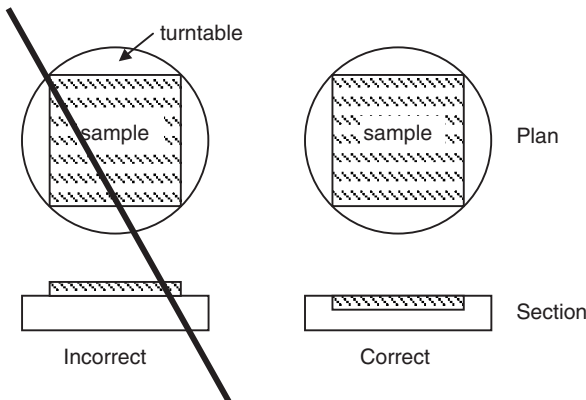


Figure 4.23 Mounting condition for non-circular samples.

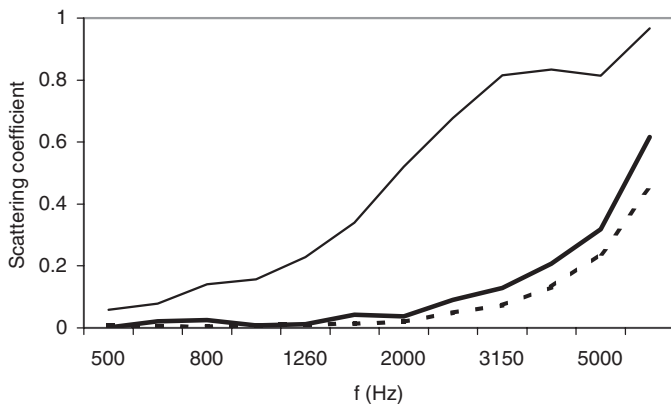


Figure 4.24 Scattering from a sinusoidal shaped sample with different mounting conditions and sample shapes. — Square sample, proud edges; — Square sample, recessed edges; - - - - - Circular sample (modified from Gomes *et al.* [30]).

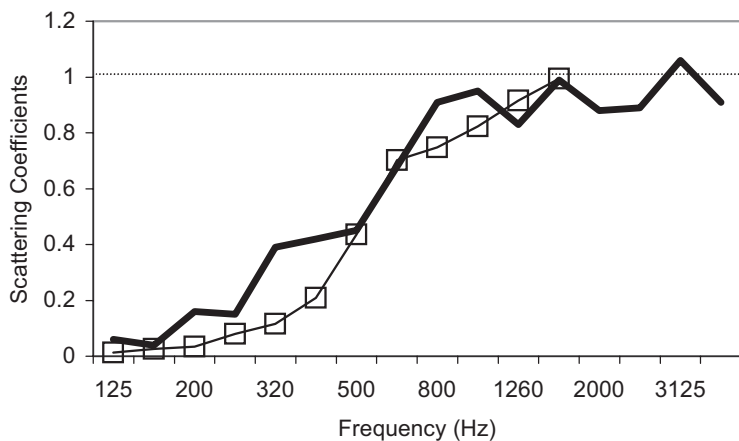
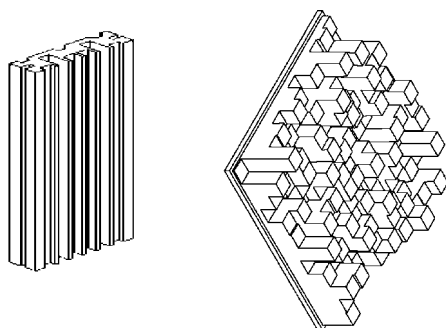


Figure 4.25 Scattering coefficients for two different diffusers and also the diffuser shapes. Left diffuser is single plane device (FlutterFree[®]), right diffuser is hemispherical device (Skyline[®]). Multiple periods of each were used. — Single plane; —□— Hemispherical.

maximum dispersion was 1, the scattering coefficient in the extruded direction must be close to 0, and so it might be expected that the hemispherical coefficient would be somewhere around 0.5. Yet a value of 1 is obtained. This happens because the topology changes dramatically when the surface is rotated, and consequently the surface is seen as being very good at scattering.

The ISO method often (if not always) produces high scattering coefficients for anisotropic surfaces. A more strict measure of diffusion ability would be two coefficients in two orthogonal directions as is done for the AES diffusion coefficient. But then current room acoustic models can only deal with hemispherical scattering coefficients, so this more strict evaluation is incompatible with current geometric models. Some geometric models are planning to introduce several distribution functions to be used in conjunction with the scattering coefficient, and this may help in more accurately distributing the randomly directed diffuse rays.

4.5.5 *Predicting the scattering coefficient*

It is awkward to predict the random incidence scattering coefficient. The necessity to carry out the predictions for a large number of sample orientations makes the prediction tedious with a boundary element model. Furthermore, it would be anticipated that the reverberation chamber would introduce inaccuracies due to non-diffuse and other effects commonly seen in absorption measurement. Nevertheless, it is possible to carry out predictions for the free-field scattering coefficient as a function of incidence angle, and use Paris' formula (Equation 12.1) to get approximate random incidence value.

The free field scattering coefficient follows a similar principle to the random incidence coefficient. The measurement is done in an anechoic chamber, and the receiver is placed in the specular reflection direction as was shown in Figure 4.21. The surface is again rotated and the reflected pulses phase locked averaged. The energy remaining after the averaging is the specular energy. From this the scattering coefficient is obtained.

This measurement process can be mimicked in a boundary element method (BEM), although as noted above it is rather tedious to do. Hargreaves [31] did this for a sample of rectangular battens and obtained accurate predictions, but this was only done for a few spot frequencies.

If a simpler numerical model is used, the prediction time can be greatly decreased. Indeed, for Schroeder diffusers, it is possible to draw up a very simple formulation for the scattering coefficient. The far field scattering from a Schroeder diffuser can be predicted using a simple Fourier model as described in Chapters 8 and 9. The Fourier model is not exact, but it does give reasonably accurate predictions of the scattering from the surfaces except at low frequencies and large angles of incidence or reflection. Under this approximate model, the pressure scattered from the surface, p_s , is given by:

$$p_s(\psi, \theta) \approx A \sum_{np=1}^{N_p} \sum_{n=1}^N e^{-2jkd_n} e^{jknw[\sin(\theta)+\sin(\psi)]} \quad (4.10)$$

where ψ is the angle of incidence, θ the angle of reflection, N_p the number of periods, N the number of wells in a period, w the well width, k the wavenumber, d_n the depth of the n th well, and A is a constant.

This approximate theory enables a simple formulation for the scattering coefficient to be derived. In addition, the polar response can also be calculated from Equation 4.10 and so the diffusion coefficient can be found. Hence, a comparison of the diffusion and scattering coefficients can be made [32]. The scattering coefficient is not the ISO coefficient, however. Instead, it is a free-field version of the Mommertz and Vorländer coefficient [10, 11] derived following a similar philosophy.

The free-field scattering coefficient is evaluated by finding the invariant energy, E_{spec} , in the specular direction ($\psi = -\theta$), when the surface is moved. Equation 4.10 is a single plane formulation, so it is natural to translate the surface. The surface has been assumed infinitely large so that edge effects are not significant. In this case, the averaging is done by translation over a complete period as this then gives the population statistics for the problem. In this ideal case, the scattering does not change with translation because the receiver is in the specular reflection direction and all the terms which vary when the surfaces moves cancel out. The specular or invariant energy can be shown to be:

$$E_{\text{spec}} \approx \left| A' \sum_{np=1}^{N_p} \sum_{n=1}^N e^{-2jk d_n} \right|^2 \quad (4.11)$$

where A' is a constant.

The invariant energy is put in a ratio with the energy from a flat plane surface for normalization purposes [10]. This then gives a specular reflection coefficient, R_{spec} :

$$R_{\text{spec}} = \frac{\left| A' \sum_{np=1}^{N_p} \sum_{n=1}^N e^{-2jk d_n} \right|^2}{\left| A' N_p N \right|^2} \quad (4.12)$$

This then represents the proportion of energy that is reflected in a specular manner by the surface, and so the scattering coefficient can be readily evaluated:

$$s = 1 - \left| \frac{1}{N} \sum_{n=1}^N e^{-2jk d_n} \right|^2 \quad (4.13)$$

The scattering coefficient is independent of angle of incidence, and so averaging over multiple angles of incidence is not needed. Consequently, applying Paris' formulation to Equation 4.13 would yield a random incidence coefficient numerically identical to the free-field case. This is similar to the prediction model produced for Gaussian rough surfaces by Embrechts *et al.* [33].

Equation 4.13 shows that to get the greatest scattering, the sum of the reflection coefficients ($e^{-2jk d_n}$) must be evenly spaced around the unit circle. This is achieved for the modified versions of the primitive root diffuser [34, 35] at integer multiples of a design frequency as discussed in Chapter 9. This is illustrated in Figure 4.26 (the line labelled correlation scattering coefficient can be ignored for now). At multiples of the design frequency, the scattering coefficient using Equation 4.13 is one. (Except at the flat plate or critical frequency of $(N-1)f_0 = 3$ kHz.) This complete scattering at the design frequency and multiples thereof, simply means no energy is in the specular

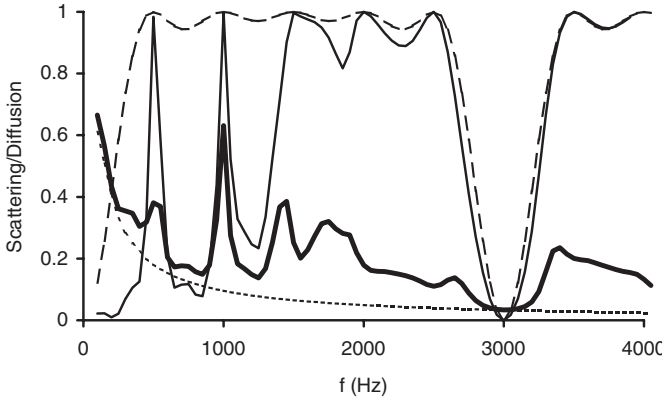


Figure 4.26 Various scattering and diffusion coefficients for a primitive root diffuser with a design frequency of 500 Hz. ----- Scattering coefficient using Equation 4.13; **————** Diffusion coefficient, diffuser; Diffusion coefficient, plane surface; ——— Correlation scattering coefficient (modified from Cox and D’Antonio [32]).

direction, it does not necessarily say how good the dispersion produced is. This is why diffusion coefficients are numerically less than the free field scattering coefficient.

The free field scattering coefficient is given by the sum of the reflection coefficients squared – there is no dependence on the order of the wells in the diffuser. Although the distribution of polar response energy changes with the order of the wells, the energy actually moved from the specular reflection direction does not. Consequently, while the diffusion coefficient will vary if the order of the wells is changed, the scattering coefficient will not. This is another illustration of why the diffusion coefficient is a more strict test of diffuser quality.

4.6 From polar responses to scattering coefficients, the correlation scattering coefficient

Mommertz presented a method for evaluating a scattering coefficient from polar responses. This correlates the scattered pressure polar responses from the test surface and a reference flat surface [36] to give a scattering coefficient. This will be called the correlation scattering coefficient δ_c . The coefficient is given by:

$$\delta_c = 1 - \frac{\left| \sum_{i=1}^n p_1(\theta_i) p_0^*(\theta_i) \right|^2}{\sum_{i=1}^n |p_1(\theta_i)|^2 \sum_{i=1}^n |p_0(\theta_i)|^2} \tag{4.14}$$

where p_1 is the pressure scattered from the test surface, p_0 the pressure scattered from the flat surface, *denotes complex conjugate, θ_i the receiver angle of the i th measurement position, and n the number of measurements in the polar response.

An alternative description of this coefficient was given by Embrechts *et al.* [33] who described it in terms of an LMS problem, which might be a more familiar description to anyone with a signal processing background.

This is not the same as the ISO coefficient or the free field scattering coefficient. This is illustrated in Figure 4.26 where the scattering coefficient from Equation 4.13 is compared to the correlation scattering coefficient for a primitive root diffuser. This difference arises because the coefficient definition is different. The free field Mommertz and Vorländer method measures the amount of energy moved from the specular direction when the surface is moved, the correlation scattering coefficient measures the dissimilarity between the test and flat surface scattering over a polar response. In the case of randomly rough surfaces, the two coefficients probably are similar, but for diffusers with distinct polar responses, this is not the case.

Although the correlation scattering coefficient is not identical to the ISO scattering coefficient, it does illustrate and help contrast the performance of diffusion and scattering coefficients [32]. One useful property of the correlation scattering coefficient is that it is readily predicted. Consequently, it is possible to compare prediction and measurement in a 2D polar response for a single cylinder and a set of cylinders. Predictions were carried out using a BEM (Chapter 8), and measurements in a 2D goniometer (Section 4.1). Figure 4.27 compares the predicted and measured correlation scattering coefficients and a good match is achieved. This provides evidence that the coefficient can be predicted and that the measurement system used is robust. It was feared that the measurement system might have difficulties as accurate magnitude and phase is needed, but this did not occur. Problems might occur, however, in measurements where exact microphone position replication is not achieved, for example if a moving boom arm is used, or where time variance cannot be maintained between the reference surface and diffuser measurements.

A sample of a single plane QRD[®] has also been tested at 1:5 scale. One period of the sample is shown as an insert in Figure 4.25. About four periods were used in the final sample. The sample was measured in the 2D goniometer first with the QRD wells perpendicular to the measurement arc, and then with the wells parallel to the measurement arc. For each sample orientation, three incidence angles (0° , 30° and 60°) were measured. These measurement results were then averaged to give an approximate random incidence coefficient. A similar sample was measured using the ISO method in a model

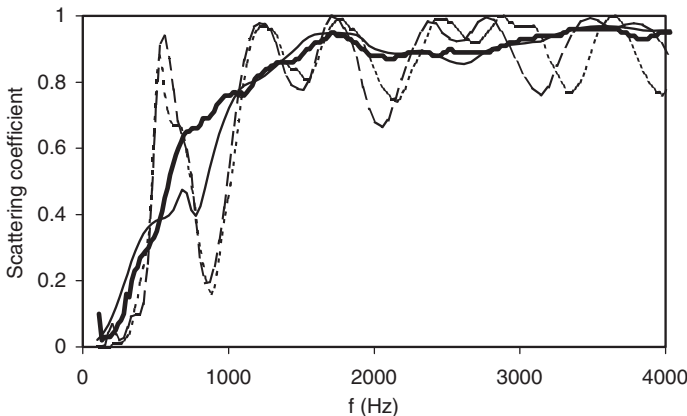


Figure 4.27 Comparison of predicted and measured correlation scattering coefficients.
 — Prediction, 1 cylinder; — Measurement, 1 cylinder;
 - - - Prediction, 4 cylinders; - - - Measurement, 4 cylinders.

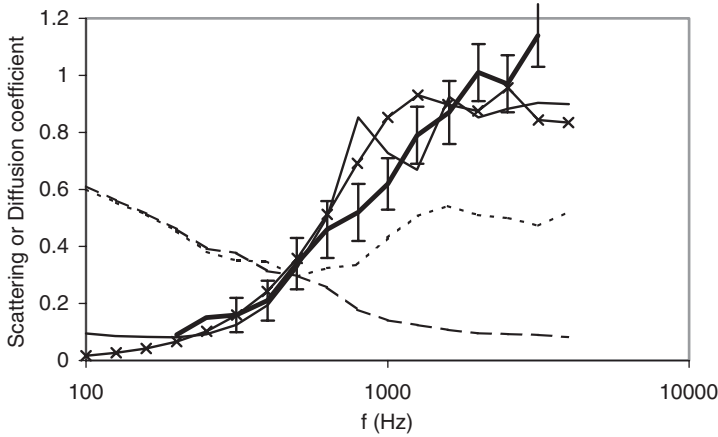


Figure 4.28 Various diffusion and scattering coefficients for a Schroeder diffuser. Diffuser was shown top left in Figure 4.25. — Correlation scattering coefficient; — Random incidence ISO scattering coefficient; - - - - - Diffusion coefficient, diffuser; - · - · - Diffusion coefficient, plane surface; —×— Scattering coefficient predicted using Equation 4.13.

reverberation chamber. The results are compared in Figure 4.28. There is reasonable correspondence between the two measured results, though in two frequency bands the results are significantly different. For example, for the 3.2 kHz octave band the random incidence measurements exceeds 1, something that cannot happen with the correlation scattering coefficient (The frequency of the octave band is non-standard because of scaling from model scale measurements.). Considering one measurement is done in a diffuse field and the other in the free field; however, the match is actually quite good, better than many have obtained when diffuse and free field absorption coefficients are compared.

Also shown in Figure 4.28 is the scattering coefficient predicted using the simplest Fourier model, Equation 4.13. The prediction accuracy is surprisingly good considering that the Fourier theory makes many assumptions which are not entirely correct for this type of surface.

Figure 4.28 also shows the diffusion coefficient for the diffuser and a plane surface. This is a single plane measurement in the plane of maximum diffusion. In this case the scattering and diffusion coefficients agree as to the frequency at which significant scattering/diffusion begins (≈ 500 Hz). Again, the diffusion coefficient is numerically less than the scattering coefficients as discussed earlier.

The polar response measurement system can also be used to illustrate some other key differences between scattering and diffusion coefficients. For example, in Section 4.4.1 the case of redirection was discussed. Another example is shown in Figure 4.29; this illustrates the effects of a focussing surface. The surface is designed to focus the sound on one microphone in the receiver arc. The diffusion coefficient interprets the focussing surface as being worse at diffusing sound than the plane surface. The correlation scattering coefficient, however, interprets the focussed polar response as being different from the plane surface and interprets this as being increased scattering. This illustrates that scattering coefficients should not be used to interpret single surface

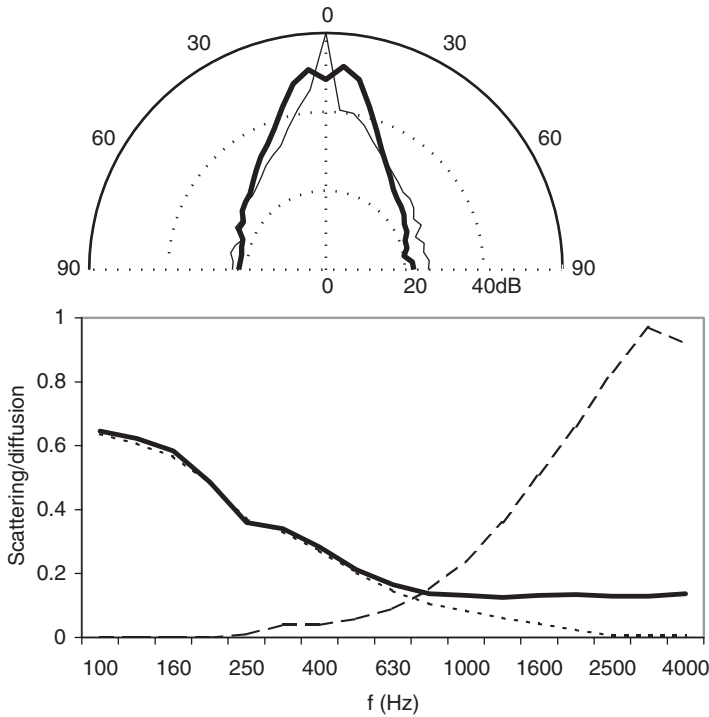


Figure 4.29 Top, polar responses for: — Flat surface; - - - Concave sample; Bottom, diffusion and scattering coefficients for these two samples: - - - - Correlation scattering coefficient, concave sample; — Diffusion coefficient, plane surface; ····· Diffusion coefficient, concave sample.

items, but should only be used for large surfaces with roughness. Furthermore, it shows that when evaluating diffusion coefficients it is necessary not only to test the far field but also to test at receiver positions where aberrations such as focussing may occur.

4.6.1 Scattering coefficient table

Appendix C gives a table of scattering coefficients for single plane diffusers. Some details of the geometry were given in Section 4.4.4, along with the rationale behind the choice of surfaces used in the prediction. The table includes all the surfaces included in the diffusion coefficient table, except hybrid surfaces. The formulation for the correlation scattering coefficient needs to be revised for surfaces which partially absorb, because the current formulation interprets any absorption as being scattering.

The random incidence values tend to have raised values at low frequencies, especially for deep surfaces; values of up to 0.2 at 100 Hz are measured for many surfaces. At oblique incidence, edge scattering becomes important, and the edges of the test samples are very different from the reference flat surface. Furthermore, because the rear of the test surfaces was not enclosed in a box, the scattering from the rear of the surface may also be having some effect.

The scattering coefficient does not discriminate between different diffusers in a consistent manner – see the values for the optimized curved surfaces compared to the semi-ellipses, for example. The coefficient also interprets redirection as scattering. For instance, a 45° triangle returns a strong reflection back to a normal source as discussed in Chapter 10, yet the scattering coefficient interprets this as dispersion. Nevertheless, this is the first published table of scattering coefficients and can be used by geometric room acoustic modellers as discussed in Chapter 12.

4.7 Contrasting diffusion and scattering coefficient: a summary

The scattering coefficient method gives a quick and rough estimate of the scattering process. It should not be used to evaluate the worth of surfaces when designing or specifying diffusers. The scattering coefficient is only concerned with how much energy is moved from the specular direction, it does not measure the quality of dispersion. For this reason, diffusing surfaces need to be evaluated using the diffusion coefficient when the quality of scattering is important. The diffusion coefficient should not, however, be blindly used in geometric room acoustic models as its definition is not compatible with the surface scattering models used in current geometric algorithms.

There are many issues surrounding these coefficients that remain to be resolved. One common question is whether there is a direct link between the coefficients and a physical property of the space. This arises because practitioners are used to a direct link between the absorption coefficient and the reverberation time. For diffusion and scattering there is no simple relationship, but maybe future research should include investigating what relationships, if any, exist between these coefficients and the room acoustic quality.

4.8 Other methods for characterizing diffuse reflections

There have been other methods developed to characterize the scattering from surfaces. They are noted here because they may yet develop into practical and used processes. The first method is a pragmatic approach, which has similarities to *in situ* absorption method – maybe it will be developed into an *in situ* measurement method for diffusion coefficients. The second method tries to characterize the effect of diffuse reflections by investigating the change in diffuseness of a space.

4.8.1 *Measuring scattering coefficients by solving the inverse problem*

This method was developed and published by Farina [37]. In the description below, the general principle is discussed so that readers can get a sense of the process used. What is presented here is a variation on Farina's approach rather than a slavish following of his exact methods.

The sound field in the vicinity of a diffuser is measured using a deterministic signal to gain the impulse response. It is necessary to make the measurements over many different spatial positions, these could be on an arc, as was done for the diffusion coefficient measurement, or if more convenient these can be done on a straight line parallel to the diffuser surface. The reflected impulse response is isolated by time windowing, as was done in Section 4.1, and then the frequency response found by

using a Fourier transform. The frequency response is then normalized to a measurement of the incident sound field without the diffuser present to make the measurement independent of the source frequency response and sound power level.

The process is to predict the measured scattering from the surface using a geometric model and compare the predicted and measured polar response. The scattering and absorption coefficients within the geometric model are varied until the error between the predicted and measured polar responses is minimized. This is a trial and error process that can be automated using a numerical optimization technique similar to that used to design diffusers in Chapters 9 and 10. A computer is tasked to search for the scattering and absorption coefficients which gives the least mean square error between the measurement and prediction. Actually, the number of combinations to be tried is small if we assume the absorption and scattering coefficients only need to be varied in increments of say 0.01, and consequently, it is possible to just do an exhaustive check of every possible combination.

This is a pragmatic approach to finding scattering coefficients. This process will probably give the scattering coefficient most appropriate within the geometric model for randomly rough surfaces. Problems may arise because the scattering coefficient will be dependent on the geometric model used, so this does not give a robust parameter for all models. The method lacks a fundamental theoretical basis, but is a possible engineering solution to obtaining the coefficients. The coefficient will only be as useful as the quality of the geometric model's diffuse reflection algorithm.

The problem arises when the scattered polar response does not match well any of the possible polar responses generated by the geometric model. Although Farina's paper shows good matches being achieved, many other diffusers have responses which do not match geometric models well. For instance, polar responses with a small number of distinct lobes, like Figure 10.11, are polar responses unlike anything that a geometric model will produce. In this case, the best matched scattering coefficient will turn out to be nonsensical. This will happen with periodic devices at low- to mid-frequencies, as well as triangles and pyramids. This could be cured, however, by using a more accurate dispersion patterns in the geometric model.

A further problem is there may be ambiguity between the effects of scattering and absorption. There may be several good fits to the polar response, resulting from different combinations of absorption and scattering coefficients. Within experimental error, there will be a range of possible coefficients which could be used.

4.8.2 Room diffuseness

When surface diffusers are applied to a non-diffuse space, the volume diffuseness of the room will alter. Consequently, by measuring acoustic characteristics of a room before and after diffusers are introduced, it is possible to try and infer the scattering coefficient of the diffusers by the effect they have on the volume acoustic [31].

Consider the room shown in Figure 4.30a. It is a reverberation chamber with one wall covered in highly absorbent material. This is a highly non-diffuse space, for example the sound decay will be non-linear. If a diffuser is placed on another surface, Figure 4.30b, then the diffuser will scatter sound onto the absorbent, the reverberation times in the room will decrease, and the sound decays will become more linear. The issue here, is what is the appropriate volume characteristic of the space to measure to monitor the change in diffuseness.

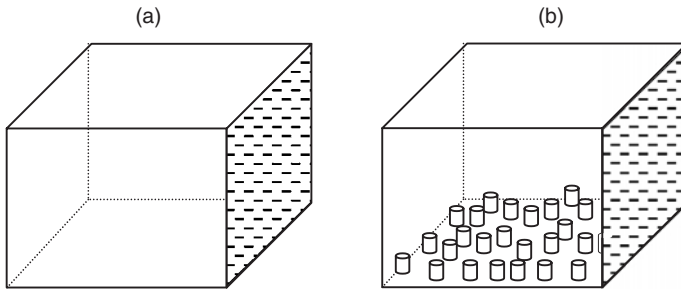


Figure 4.30 (a) A reverberation chamber with one wall made of absorbent (shown shaded) (b) Chamber with test sample on floor.

A pragmatic approach, very similar in philosophy to Farina's method from the previous section, would be to use a geometric model to predict the sound field in the space. The geometric model is used to predict the acoustic in Figure 4.30a without diffusers, and this then enables the absorption of the walls of the reverberation chamber to be set by adjusting the values in the model until measurement and prediction match. Reverberation time would be an appropriate parameter to monitor. Then the diffusers are introduced. Again the model is tuned, this time changing the absorption and scattering coefficients on the floor, until the best match between measurement and prediction is obtained. This process has the same disadvantages as that outlined for Farina's method in the previous section. The ambiguity between scattering and absorption is greater as both affect the reverberation time. But most troublesome is the reliability and robustness of the geometric model used. These models are most problematical in non-diffuse spaces, which is exactly the test space deliberately created.

Is it possible to do the measurement without a geometric model by just monitoring the reverberation time? The largest reverberation time obtained is for the test room before diffusers are applied, Figure 4.30a. This is the case where the floor has a scattering coefficient of zero. If it was possible to obtain a lower limit for the reverberation time with diffusers present, the lowest achievable reverberation time when the maximally diffusing diffuser is applied, then this could be equated to a scattering coefficient of 1 for the floor. It would be straightforward to obtain a scattering coefficient from the actual measured reverberation time with a test sample by simple scaling. The problem, however, is obtaining this lower bounding limit. In theory, this limit would be the reverberation time predicted by Eyring's equation, but this can only be achieved if diffusers are applied to at least three surfaces, so that no surface and its opposite pair are untreated. For this reason, to carry out such a test method would involve large quantities of surface diffusion, far more than would be practical.

4.9 Summary

This chapter has mapped out some of the measurement techniques used for diffuse reflections. It might be anticipated that the use of scattering and diffusion coefficients might increase in the future as practitioners want quantifiable evidence of how surfaces scatter and better predictions from geometric models. Having two coefficients

gives potential for much confusion, and it is important that practitioners and researchers are educated as to the difference, as using the wrong coefficient could lead to poor predictions or bad design.

4.10 References

- 1 P. D'Antonio, J. H. Konnert and P. Kovitz, "The disc project: experimental measurement of the directional scattering properties of architectural acoustic surfaces", *Acoust. Soc. Am.*, 1pAA2, 141–144 (June 1994).
- 2 P. D'Antonio and T. J. Cox, "Diffusor application in rooms", *Appl. Acoust.*, 60(2), 113–142 (2000).
- 3 T. J. Cox, "Objective and Subjective Evaluation of Reflection and Diffusing Surfaces in Auditoria", PhD thesis, University of Salford (1992).
- 4 A. Farina, personnel communication.
- 5 L. E. Kinsler, A. R. Frey, A. B. Coppens and J. V. Sanders, *Fundamentals of Acoustics*, John Wiley & Sons (1982).
- 6 AES-4id-2001, "AES information document for room acoustics and sound reinforcement systems – characterisation and measurement of surface scattering uniformity", *J. Audio Eng. Soc.*, 49(3), 149–165 (2001).
- 7 J. H. Rindel, "Attenuation of sound reflections due to diffraction", *Nordic Acoustical Meeting*, NAM86 (1986).
- 8 M. Kleiner, H. Gustafsson and J. Backman, "Measurement of directional scattering coefficients using near-field acoustic holography and spatial transformation of sound fields", *J. Audio Eng. Soc.*, 45(5), 331–346 (1997).
- 9 P. D'Antonio and J. H. Konnert, "The reflection phase grating diffusor: design theory and application", *J. Audio Eng. Soc.*, 32(4), 228–238 (1984).
- 10 E. Mommertz and M. Vorländer, "Measurement of scattering coefficients of surfaces in the reverberation chamber and in the free field", *Proc. 15th ICA*, II, 577–580 (1995).
- 11 M. Vorländer and E. Mommertz, "Definition and measurement of random-incidence scattering coefficients", *Appl. Acoust.*, 60(2), 187–200 (2000).
- 12 T. J. Hargreaves, T. J. Cox, Y. W. Lam and P. D'Antonio, "Surface diffusion coefficients for room acoustics: free field measures", *J. Acoust. Soc. Am.*, 108(4), 1710–1720 (2000).
- 13 Y. W. Lam, "On the parameters controlling diffusion calculation in a hybrid computer model for room acoustic prediction", *Proc. IoA(UK)*, 16, 537–544 (1994).
- 14 M. Hodgson, "Evidence of diffuse surface reflections in rooms", *J. Acoust. Soc. Am.*, 89, 765–771 (1991).
- 15 M. Vorländer, "International round robin on room acoustical computer simulations", *Proc. 15th ICA*, II, 689–692 (1995).
- 16 Y. W. Lam, "Diffuse reflection modeling methods", *J. Acoust. Soc. Am.*, 100(4), 2181–2192 (1996).
- 17 B. Dalenbäck, M. Kleiner and P. Svensson, "A macroscopic view of diffuse reflection", *J. Audio. Eng. Soc.*, 42, 793–807 (1994).
- 18 H. Kuttruff, *Room Acoustics*, 4th edn, Spon Press (2000).
- 19 T. J. Cox, "Optimization of profiled diffusers", *J. Acoust. Soc. Am.*, 97(5), 2928–2941 (1995).
- 20 T. J. Cox, "Designing curved diffusers for performance spaces", *J. Audio Eng. Soc.*, 44, 354–364 (1996).
- 21 P. D'Antonio, "The disc project: directional scattering coefficient determination and auralization of virtual environments", *Proc. Noise-Con 93*, 259–264 (1993).
- 22 J. Angus, A. C. Marvin, J. Clegg and J. F. Dawson, "A practical metric for evaluating sound diffusers", *Proc. 98th Audio Eng. Soc. Convention*, preprint 3955 (D5) (February 1995).

- 23 D. Takahashi, "Development of optimum acoustic diffusers", *J. Acoust. Soc. Am.*, **16**(2), 51–58 (1995).
- 24 T. J. Cox, "Diffusion parameters for baffled surfaces", *99th Convention Audio Eng. Soc.*, New York (October 1995).
- 25 Y. W. Lam, "A boundary integral formulation for the prediction of acoustic scattering from periodic structures", *J. Acoust. Soc. Am.*, **105**(2), 762–769 (1999).
- 26 J. A. S. Angus, "Diffuser assessment using surface spherical harmonics", *J. Acoust. Soc. Am.*, **104**(3), 1857–1858 (1998).
- 27 J.-J. Embrechts, "Practical aspects of the ISO procedure for measuring the scattering coefficient in a real-scale experiment", Forum Acusticum, Sevilla, RBA-06-001-IP (2002).
- 28 L. De Geetere and G. Vermeir, "Investigations on real-scale experiments for the measurement of the ISO scattering coefficient in the reverberation room", Forum Acusticum, Sevilla, RBA-06-004 (2002).
- 29 ISO 354:1985, "Acoustics – measurement of sound absorption in a reverberation room."
- 30 M. H. A. Gomes, M. Vorländer and S. N. Y. Gerges, "Aspects of the sample geometry in the measurement of the random-incidence scattering coefficient", Forum Acusticum, Sevilla, RBA-06-002-IP (2002).
- 31 T. J. Hargreaves, "Acoustic Diffusion and Scattering Coefficients for Room Surfaces", PhD thesis, University of Salford (2000).
- 32 T. J. Cox and P. D'Antonio, "Contrasting surface diffusion and scattering coefficients", *Proc. 17th ICA*, 6B.09.01, Italy (2001).
- 33 J. J. Embrechts, D. Archambeau and G. B. Stan, "Determination of the scattering coefficient of random rough diffusing surfaces for room acoustics applications", *Acta Acustica/Acustica*, **87**, 482–494 (2001).
- 34 E. Feldman, "A reflection grating that nullifies the specular reflection: a cone of silence", *J. Acoust. Soc. Am.*, **98**(1), 623–634 (1995).
- 35 T. J. Cox and P. D'Antonio, "Acoustic phase gratings for reduced specular reflection", *Appl. Acoust.*, **60**(2), 167–186 (2000).
- 36 E. Mommertz, "Determination of scattering coefficients from reflection directivity of architectural surfaces", *Appl. Acoust.*, **60**(2), 201–204 (2000).
- 37 A. Farina, "A new method for measuring the scattering coefficient and the diffusion coefficient of panels", *Acustica*, **86**(6), 928–942 (2000).

5 Porous absorption

Typical porous absorbers are carpets, acoustic tiles, acoustic (open cell) foams, curtains, cushions, cotton and mineral wool. They are materials where sound propagation occurs in a network of interconnected pores in such a way that viscous and thermal effects cause acoustic energy to be dissipated. As discussed in Chapter 1, they are used widely to treat acoustic problems, from reducing resonances in double partition cavities to improve sound insulation, to their application to absorb noise and reduce sound levels in factories. This chapter will detail the physical processes producing the absorption and theoretical models for predicting absorption properties.

The first section gives a qualitative description of the use of porous absorbers; this will be followed by some example materials in Section 5.2. These materials range from standard well-known materials, such as mineral wool, to more recent developments, such as absorbent plaster systems. Section 5.3 and onwards then outlines the methods needed to predict the absorption from this type of absorber. The theoretical sections start by outlining how the sound propagation within a porous absorbent might be modelled in terms of characteristic acoustic parameters of the material. There are empirical and semi-empirical approaches, and both are detailed. The chapter then proceeds to show how these acoustic parameters are combined with mounting conditions, to enable the absorption coefficient and surface impedance to be predicted, which is ultimately what is required in design.

5.1 Absorption mechanisms and characteristics

When sound propagates in small spaces, such as the interconnected pores of a porous absorber, energy is lost. This is primarily due to viscous boundary layer effects. Air is a viscous fluid, and consequently sound energy is dissipated via friction with the pore walls. The boundary layer in air is sub-millimetre in size, and consequently viscous losses occur in a sub-millimetre-sized air layer adjacent to the pore walls. As well as viscous effects, there will be losses due to thermal conduction. For the absorption mechanisms to be effective there must be interconnected air paths through the surface, so an open pore structure is needed. The difference in construction between an open and closed pore system is shown schematically in Figure 5.1 [1].

Figures 5.2 and 5.3 show the absorption coefficients for two porous absorbers illustrating the effect of material thickness. The porous absorber is mounted on a rigid backing. These curves follow the characteristic shape of porous absorption coefficients, a high pass filter response, although the curves can shift in frequency and move

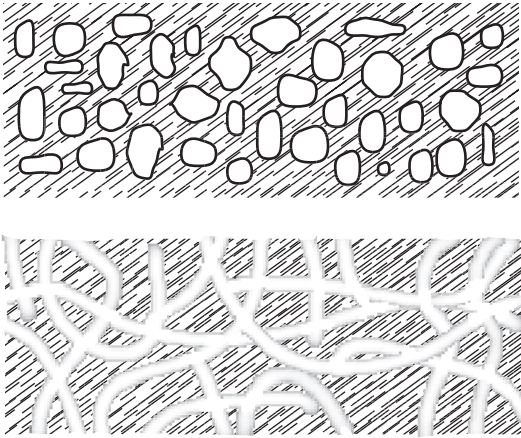


Figure 5.1 Illustration of the difference between closed (top) and open (bottom) pore structures (adapted from Cremer and Müller [1]).

up and down in absorption depending on the characteristics of the particular material and mounting.

As the porous absorber thickness increases, the absorption at low frequency usually increases. For the porous absorber to create significant absorption, it needs to be placed somewhere where the particle velocity is high. The particle velocity close to a room boundary is usually small, and so the parts of the absorbent close to the boundary are not generating much absorption. It is the parts of the absorbent furthest from the backing surface which are often most effective, and this is why thick layers of absorbent are needed to absorb low frequencies.

For low frequencies, where the wavelength is large, one has to go a considerable distance from the wall to reach a point where the particle velocity is significant.

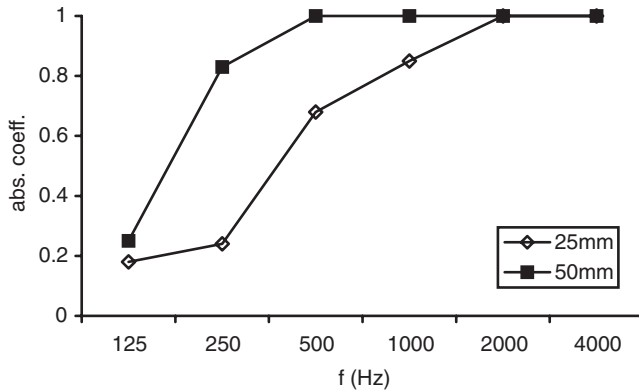


Figure 5.2 Random incidence absorption coefficient for rockwool of two different thicknesses on a rigid backing.

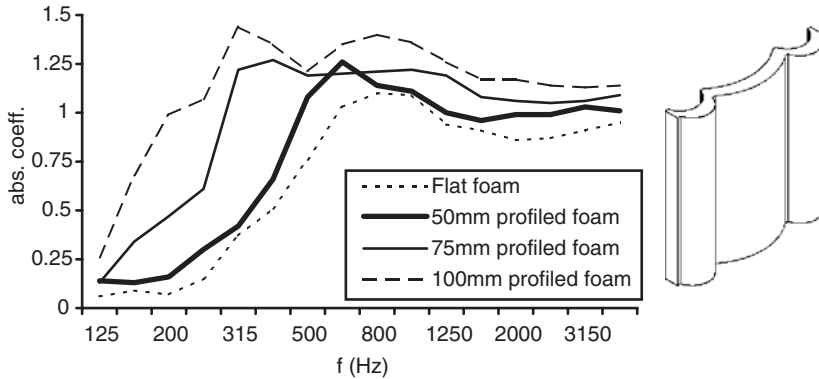


Figure 5.3 Random incidence absorption coefficients for a profiled acoustic foam on a rigid backing sold as ProFoam™ [3].

A rough figure sometimes quoted is that the absorbent needs to be at least a tenth of a wavelength thick to cause significant absorption [2], and a quarter of a wavelength to absorb all the incident sound. Consequently, substantial absorption cannot be achieved by simply applying some thin layer of paint. As the absorbent very close to the boundary is absorbing relatively little, it is possible to simply space porous absorbers away from a wall and get good performance. Figure 5.3 shows a simple way of achieving this by shaping acoustic foam into a rough sinusoidal shape [3]. The acoustic absorption achieved is also given.

The need for significant thickness compared to wavelength makes porous absorbers inefficient and not particularly useful at low frequency. At low frequencies, resonant absorption will produce greater absorption from a given depth as discussed in Chapter 6, or maybe this can be achieved through active absorbers as discussed in Chapter 13. To get broadband passive absorption across the frequencies of most interest to human acoustic design, usually requires a combination of resonant and porous absorption.

5.1.1 Covers

Often porous absorbers are covered by a thin membrane; this might be achieved by wrapping the material in thin plastic or similar. This is done to prevent the absorber being damaged or to stop fibres from the absorber being lost. The effect of the membrane will be to reduce the high frequency absorption. At low frequencies, the membrane's acoustic mass is small and the sound passes through the membrane largely unaltered – although a small increase in absorption due to the added mass of the membrane may occur. At high frequencies, however, the membrane's acoustic mass is high and it will prevent some or all of the acoustic energy entering the porous absorber. This membrane effect is why porous absorbers should not be painted except with a non-bridging paint. Most paints will block the pores, prevent sound energy entering the structure and so reduce the absorption. Consequently, porous absorbent is often finished by cloth wrapping.

Another surface treatment used for protection is to place the porous material behind perforated panels. If the perforated sheet does not have a very open structure,

with a large per cent open area, the mass effect of the holes will mean that the absorption increases at low frequency, but decreases at high frequency. Although it is commonly quoted that a greater than 20 per cent open area means that the perforated sheet has no effect [4], the results for hybrid diffuser-absorbers given in Chapter 11 illustrate that even a 50 per cent open area perforated sheet can have a significant effect on absorption. The transfer matrix techniques outlined in Chapter 6 can be used to predict the effects of perforated sheets on absorption. For membrane-wrapped porous material behind a perforated sheet, it is important that the membrane and perforated sheets are not in contact, otherwise the absorption is decreased [4].

5.2 Material types

5.2.1 *Mineral wool and foam*

There is a bewildering array of materials available for porous absorption. Mineral wool is made from sand, basaltic rock, recycled glass, etc. The raw materials are melted at high temperature and then spun or pulled into woolly filaments. These are then bonded together to give the product its physical shape, with roughly 1–5 per cent of the final product weight being binder [5]. Glass fibre is made up of the same raw ingredients as normal glass: sand, limestone, soda ash, etc.; and the manufacturing process is similar to rock or basalt wool, although rock and basalt wool products tend to be heavier. The acoustic absorption achieved is determined by the fibre composition, fibre orientation, fibre dimensions, product density, and the quantity and nature of the binder used. The mineral wool can be in the form of semi-rigid boards or loose blanket. Compressed mineral fibreboard is the basis of the ubiquitous absorbing ceiling tiles mounted in t-bar grids.

The acoustic performance of mineral wool can vary with density, and for low densities the high frequency absorption performance can be reduced. Man made mineral wools are cheap to manufacture and can be partially recycled. Mineral wool is often laid down in layers and so is anisotropic. For this reason, the acoustic properties vary depending on whether sound is incident parallel or perpendicular to the fibres.

There have been some concerns about the long-term health effects of man-made mineral fibres (MMMFs), concerns which have helped develop a market for non-MMMF and fibreless absorbers. MMMFs are known to be irritants, causing skin, eye and upper respiratory tract irritation; the irritation is usually caused by mechanical action rather than an allergic reaction. Small diameter fibres have been shown to be carcinogenic in animals, but these results cannot be directly extrapolated to human exposure [6]. The USA National Institute of Occupational Safety and Health (NIOSH) recommends precautionary measures in light of the uncertainty concerning the scientific evidence. Member States of the European Community have agreed that some forms of MMMFs (<6 mm diameter) should be classified as category 3 carcinogens under the terms of the Dangerous Substances Directive [7]. Although potentially a carcinogen, it is currently believed that the risk when exposure is taken into account is small. The UK Department of Health's Committee on the Carcinogenicity in Food, Consumer Products and the Environment [8] reviewed epidemiological data from a study involving workers at several factories producing MMMFs and experimental data from animal studies designed to assess the carcinogenic potential of some types of MMMFs. Overall, they concluded that there was no clear evidence to indicate the

carcinogenicity of MMMFs but, in view of some uncertainties, recommended that it would be prudent to assume high exposures might pose a risk of lung cancer in workers. Europe wide epidemiological studies of workers involved in the production of MMMFs are ongoing. To date, these have not provided any clear evidence for the carcinogenicity of MMMFs in the workplace. A great deal of research effort worldwide is being directed to designing laboratory tests predictive of potential toxicity and carcinogenicity of MMMFs.

Foams can have open or closed cell structures. With open cell structures the pores are interconnected and significant acoustic absorption can result. Closed cell structures, on the other hand, do not permit the passage of sound and so the absorption is rather low. It is possible, however, to perforate closed foam structures at the end of manufacture and so provide moderate absorption by interconnecting the pores. Consequently, it is important to check that acoustic foam is used where absorption is needed. The fire rating of acoustic foams needs to be checked, especially when they are used in buildings.

5.2.2 Recycled materials

There is great interest in trying to make acoustic absorbers from recycled materials, whether that be recycled cloth, metal, foams, wood, plastics or rubber. To take one example, researchers have been investigating recycling tyres as acoustic absorbers [9]. The hope is that the elastic properties of the material will also enable the rubber to cushion the effects of crashes if these are used in roadside barriers. The other advantages that tyres offer are that they can be painted, and will survive the harsh environment around roads better than standard fibrous materials. The rubber is broken up into small granules, and these are then bonded together with a binder. The key is to use enough binder to hold the granules together without blocking the air pores, which are crucial to absorption, and to get the right grain size and shape. To take another example, Swift and Horoshenkov [10] showed that loose granulated mixes of waste foam with particles sizing <5 mm, can be pressed into consolidated, elastic, porous media with a high proportion of open and interconnected pores and good absorption properties. Pfretzschner [9] tested rubber granular diameters ranging from 1.4 to 7 mm. An example of the typical absorption coefficients is shown in Figure 5.4, mostly measured in an impedance tube. They found that for a given sample thickness, the absorption coefficient increases when the diameter of the grains decreases.

The behaviour of granular materials is different from fibrous ones such as mineral wool. Differences arise because grains pack together differently from fibres, usually resulting in a lower porosity for granular materials in comparison to fibrous ones. In terms of absorption, the absorption is much more uneven in frequency for granular materials than for fibrous materials as shown in Figure 5.4 in comparison to Figures 5.1 and 5.2. There is a critical thickness for the granular material, beyond which additional thickness does not increase absorption. The broadband absorption for thick samples of the granular material shown in Figure 5.4 is limited to around 0.8, whereas with fibrous absorbent, the value would tend to unity. Consequently, mineral wool will often give better acoustic absorption, but the recycled granular materials might be favoured for other reasons such as sustainability. The performance of the recycled absorber can be improved by forming wedges rather than flat boards.

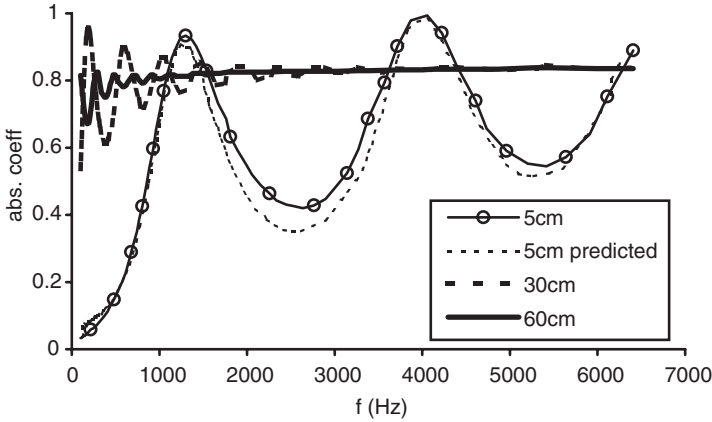


Figure 5.4 Absorption from granulated rubber 1–3 mm in size for different thicknesses. Measured in the impedance tube unless otherwise indicated in legend (modified from Pffretschner [9]).

Also included in Figure 5.4 is a prediction of the absorption coefficient using a complicated porous absorber model. This shows that good results from such theories can be obtained, and a similar theory is outlined later in this chapter.

5.2.3 Curtains (drapes)

Curtains or drapes are essentially porous absorbers. Most of the time, the deeper the folds, the greater the absorption [11], as this means there is more resistive material, and the resistive material is further from the rigid backing where the particle velocity is greater. This is illustrated in Figure 5.5 where the same curtain is hung to different fullness. It is also possible to increase the absorption by hanging the curtain away

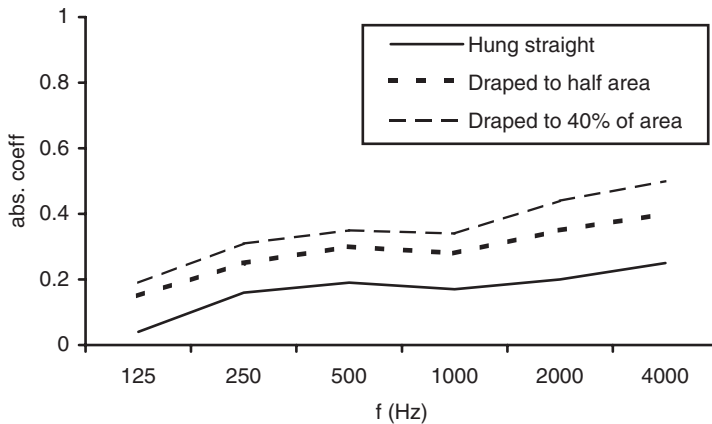


Figure 5.5 Curtain (drape) absorption with different fullness of draping (data from Harris [11]).

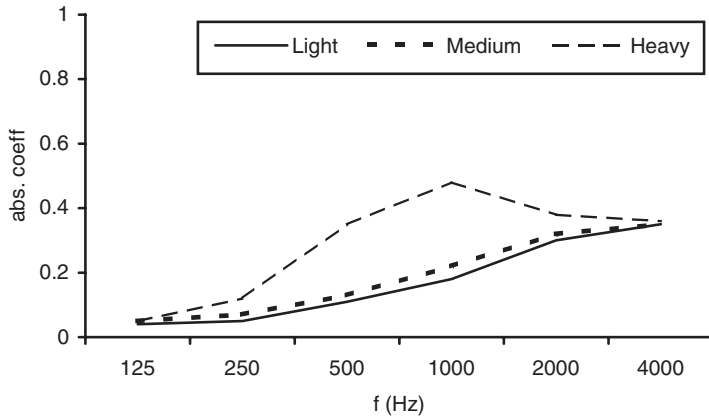


Figure 5.6 Curtain (drape) absorption for different weight material (data from Beranek [12]).

from the rigid surface and so placing the resistive material where the particle velocity is higher, and hence producing more absorption. Increasing the density of the material generally increases the absorption produced [12] as shown in Figure 5.6. Appendix A gives further typical absorption coefficients for curtains, showing that the absorption coefficient varies greatly depending on the type of curtain and mounting.

5.2.4 Carpets

If present, carpet usually contributes a large proportion of the high frequency absorption present in a room. The amount of absorption created depends on the type of carpet and also the underlay used [11, 13]. Essentially, the carpet is a porous absorber, and so it has little absorption at low frequencies, but significant absorption at high frequencies. If the underlay is open celled, then its presence increases the thickness of the absorbent layer, and so increases the absorption generated. Some underlay types are open celled, such as old-fashioned felt hair and foam rubber. Sponge rubber, however, can be open or closed cell. The absorption generated is also very dependent on the type of carpet, for instance the way the pile is constructed. Appendix A gives a large number of absorption coefficients for different carpet types taken from literature. Everest notes [13] that the absorption coefficients reported for carpet vary quite considerably between different publications. This is illustrated in Figure 5.7, where the variation in absorption coefficients in the literature is shown as the minimum, mean and maximum found. This emphasizes the need for measurement of the carpet to be used, rather than assuming that an average value from the literature will be accurate.

5.2.5 Absorbent plaster

Acousticians have long sought an absorptive, smooth, seamless and durable plastered finish to satisfy the aesthetic requirements of architects and interior designers. Architects more often than not prefer their acoustic treatment to be hidden and certainly not defining the visual aesthetic. A system which achieves this is BASWA[®] phon. A photo showing BASWA[®] phon applied to a ceiling was given in Figure 1.1.

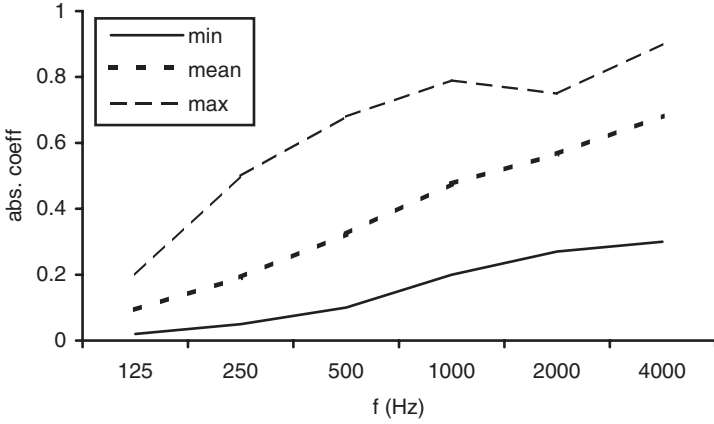


Figure 5.7 The minimum, mean and maximum values for carpet absorption from literature.

The key ingredient of the system is a proprietary emulsion of spherical mineral particles, which form a micro-porous membrane to be used on top of mineral wool. The trick is formulating and applying the plaster in such a way that the structure has open pores to allow sound energy to reach the mineral wool. This is achieved using spherical granules which will naturally form an open structure, and a binder that does not clog the pores. A succession of layers is applied, with the granule size decreasing with each layer. Figure 5.8 shows the construction. The top layer granules are so small that they provide the appearance of a smooth, seamless conventional gypsum-plastered surface. In fact, the top layer does seal the surface a little and acts as a thin membrane. As might be expected this produces additional low frequency absorption, but at the cost of a little loss of absorption at high frequencies, in comparison to the mineral wool alone. The absorption coefficient for the plaster system is shown in Figure 5.9 for two different thicknesses. The main disadvantage of this system is that it is slow to apply, and has to be applied on site, which can be a problem on building projects when completion times can be very short.

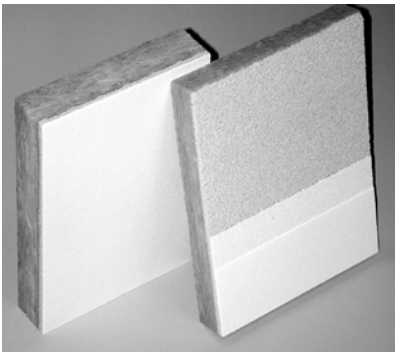


Figure 5.8 A proprietary system for achieving a flat porous plaster. The right sample shows the different layers of plaster which are used (photo courtesy of BASW Acoustic, AG).

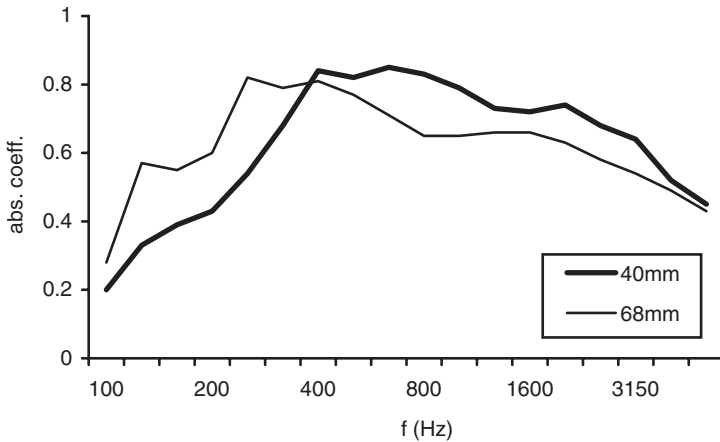


Figure 5.9 Absorption coefficient for an absorbent plaster system for two different thicknesses (data courtesy of BASWAacoustic, AG).

5.2.6 Coustone or quietstone

Porous absorbers tend to be soft and prone to damage, for instance most do not survive repeated soakings. There is a need for a material which provides absorption and allows washing. Such an absorbent is coustone (also sold as quietstone). The ability to be washed means that coustone can be used in places such as swimming centres, police interview rooms and firing ranges. The absorbent is a rigid hard wearing material with a granulated surface. It is constructed from bonded flint in such a way as to keep the structure open and so allow absorption. It is heavy so it can also provide good sound insulation, but the weight also means that it can be expensive to use.

Coustone is formed by bonding flint aggregate together with a resin. Flint aggregate around a millimetre in size has a particular shape that means when bonded together with the right resin, it forms an open pore structure. The cavities formed are of the order of millimetres in size. Furthermore, the pores are very irregularly shaped and joined; consequently the tortuosity is high. (Tortuosity, as the name suggests, is a measure of how tortuous the air paths are within the absorbent, and this influences the amount of absorption produced.) The high tortuosity is key to the high absorption; other aggregates form different pore shapes absorb less efficiently. The resin must have the right properties. It must not fill the cavities, yet be strong enough to hold the absorber together. The resin is also elastic, and so coustone can offer a degree of vibration isolation.

Figure 5.10 shows typical absorption coefficients under different conditions. The material behaves like a porous absorber. Consequently, it can be spaced from walls to produce additional absorption by moving it away from where the particle velocity is low. It can also be backed by mineral wool to provide additional absorption at a lower cost and with less weight.

5.3 Basic material properties

The rest of this chapter is devoted to the mathematical modelling of porous absorbers; given a particular material, how can the surface impedance and absorption coefficient be

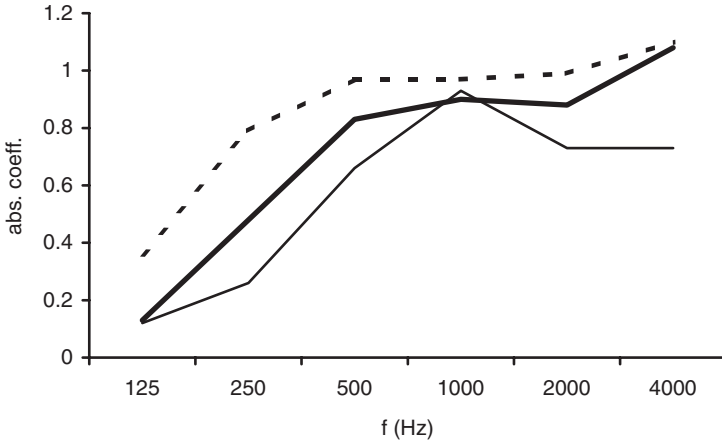


Figure 5.10 Random incidence absorption coefficient from a bonded flint absorbent. — 14 mm coustone + 50 mm air gap; — 28 mm coustone + 50 mm air gap; 28 mm coustone + 50 mm mineral wool (data courtesy of Sound Absorption UK Ltd).

estimated? The mathematical models also give insight into how absorption is produced, and enable better designs to be produced. But first it is necessary to set down the two most important and fundamental quantities that determine the acoustic behaviour of sound within porous absorbers, namely flow resistivity and porosity.

5.3.1 Flow resistivity

The flow resistivity is a measure of how easily air can enter a porous absorber and the resistance that air flow meets through a structure. It therefore gives some sense of how much sound energy may be lost due to boundary layer effects within the material. A slice of the porous material of thickness d is subject to a mean steady flow velocity U . It is assumed that the flow velocity is small. The pressure drop ΔP is measured. From these quantities the flow resistivity σ is defined as:

$$\sigma = \frac{\Delta P}{Ud} \tag{5.1}$$

The flow resistance σ_s is defined as:

$$\sigma_s = \frac{\Delta P}{U} = \sigma d \tag{5.2}$$

The flow resistivity is effectively the resistance per unit material thickness. If the flow velocity is not small, then non-linear factors must be considered.

It is important to check the units used with flow resistance and resistivity as two systems have been in use. The unit of flow resistance in MKS units is $Nm^{-3} s$, often

referred to as one rayl, and should nowadays be used. Older texts may use CGS rayls. To convert a CGS rayl to MKS rayl multiply by ten.

The flow resistivity is one of the most important parameters determining the absorption properties of a porous absorber – if not the most important. It is the parameter that varies most between common porous absorbent materials, and so is the most important to determine. Chapter 3 details how this is measured.

There are several empirical and semi-empirical formulations in the literature that can be used to estimate the flow resistivity. For fibreglass, the following empirical relationship derived by Bies and Hansen can be used [4, 14]:

$$\sigma = 27.3(1 - \varepsilon)^{1.53} \left(\frac{\eta}{4a^2} \right) \tag{5.3}$$

where a is the fibre radius, η the viscosity of air (1.84×10^{-5} poiseuille) and ε the porosity, which is defined in the next section. For mineral and glass fibre, diameters are typically 1–10 μm . Bies and Hansen showed that fibrous materials have an approximately linear relationship between flow resistivity and density, but this is not necessarily true for foam. For fibrous materials, Bies and Hansen measured samples with resistivity values ranging from 2,000 to 200,000 rayl m^{-1} , and for one type of foam with flow resistivity between 2,000 and 40,000 rayl m^{-1} .

Mechel [5] reports findings attributed to Sullivan, unfortunately reference unknown, giving an empirical relationship for flow resistivity. First consider parallel fibre materials with all fibres having the same radii. The flow resistivity parallel to the fibres is given by:

$$\sigma = \frac{3.94\eta(1 - \varepsilon)^{1.413} [1 + 27(1 - \varepsilon)^3]}{a^2\varepsilon} \tag{5.4}$$

The flow resistivity perpendicular to the fibres is given by:

$$\begin{aligned} \sigma &= \frac{10.56\eta(1 - \varepsilon)^{1.531}}{a^2\varepsilon^3} & 6 \leq a \leq 10 \mu\text{m} \\ &= \frac{6.8\eta(1 - \varepsilon)^{1.296}}{a^2\varepsilon^3} & 20 \leq a \leq 30 \mu\text{m} \end{aligned} \tag{5.5}$$

Semi-empirical results for materials made with a single fibre radius, but with random fibre orientation give the flow resistivity as:

$$\sigma = \frac{4\eta}{a^2} \left[\frac{0.55(1 - \varepsilon)^{4/3}}{\varepsilon} + \frac{\sqrt{2}(1 - \varepsilon)^2}{\varepsilon^3} \right] \tag{5.6}$$

For random fibre radius distribution with a mean radius of a , and random fibre orientation, empirical data gives the flow resistivity as:

$$\begin{aligned} \sigma &= \frac{3.2\eta(1 - \varepsilon)^{1.42}}{a^2} & \text{fibreglass} \\ \sigma &= \frac{4.4\eta(1 - \varepsilon)^{1.59}}{a^2} & \text{mineral fibre} \end{aligned} \tag{5.7}$$

Unfortunately, the range of applicability of the models is unknown, but it is probably safe to assume that the fibre diameters and types were typical of commercial materials made from man-made mineral fibres.

The above models are mostly empirical, and so will not necessarily work for materials with different construction. For instance, Garai and Pompoli [15] examined polyester fibrous materials and found the formulation of Bies and Hansen inaccurate as the diameters of their polyester fibres (33 μm) were considerably larger than the samples tested by Bies and Hansen. For Garai and Pompoli samples, the following empirical relationship was derived:

$$\sigma = \frac{28.3 \times 10^{-9}}{(2a)^2 \rho^{-1.404}} \quad (5.8)$$

where ρ is the density.

5.3.2 Porosity

Porosity gives the fractional amount of air volume within the absorbent. It is a ratio of the total pore volume to the total volume of the absorbent. Good absorbers tend to have high porosity, for example most mineral wools have a porosity of about 0.98, but in designing an absorber, it is possible to trade off porosity against flow resistivity (and to a lesser degree the structural factors outlined later). When determining the porosity, closed pores should not be included in the total pore volume as these are relatively inaccessible to sound waves (closed pores are most commonly found in foams, even ones designed to be open celled). The porosity is a key parameter, but for commonly used bulk absorbing materials, the value of porosity does not vary greatly being close to unity. Table 5.1 gives some typical porosity values.

Table 5.1 Typical porosity values for some materials from References 5 and 1

<i>Material</i>	<i>Typical porosities</i>
Mineral wool	0.92–0.99
Open cell acoustic foams	0.95–0.995
Felts	0.83–0.95
Wood fibre board	0.65–0.80
Wood wool board	0.50–0.65
Porous render	0.60–0.65
Pumice concrete	0.25–0.50
Gravel and stone chip fill	0.25–0.45
Ceramic filters	0.33–0.42
Brick	0.25–0.30
Sinter metal	0.10–0.25
Firebrick	0.15–0.35
Sandstone	0.02–0.06
Marble	≈ 0.005

5.4 Modelling propagation within porous absorbents

The modelling of the propagation within a porous absorbent is difficult. Two approaches are found to be most useful. The first is a completely empirical approach as exemplified by Delany and Bazley. They measured a large number of samples of porous material and used curve fitting to arrive at relationships describing how the characteristic impedance and propagation wavenumber vary with flow resistivity. When applied to an existing material, this type of empirical technique is the simplest to apply and can be most effective. It is detailed in Section 5.4.1.

A second approach to modelling porous absorbent is to formulate the problem using a semi-analytical approach. For instance, the propagation within the pores can be modelled in a semi-analytical way by working on a microscopic scale. This approach results in complicated theoretical models, of which there are several variants in the literature. This approach is not for the faint hearted, and runs into difficulty because it is not possible to analytically derive all the necessary parameters within the models for most porous absorbents. In particular, factors related to the pore shapes are difficult to obtain except empirically. Consequently, the verification of the accuracy of the model is rather circular as measurements are needed to tune the model, and then the same measurements are sometimes used to show that the theory worked! This is not very satisfactory. Nevertheless, it is this type of modelling which holds the best chance of enabling the development of new porous absorbers to be undertaken without resorting to a completely experimental approach. Section 5.4.2 details some of the additional material properties that are needed in this approach, and Section 5.4.3 gives details of some of the models for rigid-framed materials.

Readers looking for a simple solution to porous absorber modelling are advised to read Section 5.4.1 and to use an empirical approach, before skipping to Section 5.5 to see how these empirical models can be applied to predict the absorption of finite absorbent layers.

5.4.1 Macroscopic empirical models such as Delany and Bazley

When predicting the absorption of porous absorbents, it is necessary to know the characteristics of the material in terms of the characteristic impedance and (complex) wavenumber. These empirical models take a macroscopic view of the propagation, as the details of propagation through every pore are not considered, and the impedance and wavenumber are found empirically. For fibrous absorbent materials, Delany and Bazley [16] undertook a large number of impedance tube measurements and derived empirical relationships relating the impedance and wavenumber to the flow resistivity. These relationships are widely used as they give reasonable estimations across quite a wide frequency range.

The characteristic impedance, z_c , is given by:

$$z_c = \rho_0 c_0 (1 + 0.0571X^{-0.754} - j0.087X^{-0.732}) \quad (5.9)$$

and the wavenumber, k , by:

$$k = \frac{\omega}{c_0} (1 + 0.0978X^{-0.700} - j0.189X^{-0.595}) \quad (5.10)$$

where ρ_0 and c_0 are the density and speed of sound in air and ω angular frequency. X is given by:

$$X = \frac{\rho_0 f}{\sigma} \tag{5.11}$$

where f is the frequency and σ the flow resistivity of the fibrous material.

A good empirical match was achieved, but there are restrictions on the applicability of these formulations. These are only applicable where:

- The porosity, ε , is close to 1, which most purpose built fibrous absorbers achieve.
- $0.01 < X < 1.0$, which means the formulations only work over a defined frequency range.
- The limits of the flow resistivity in the measurements were $1,000 \leq \sigma \leq 50,000$ MKS rayl m^{-1} .

Figure 5.11 shows a large number of measurements undertaken by Mechel and Grundmann and reported in English in Reference 5 which give a visual indication of the accuracy of the empirical fit. These graphs show the normalized propagation constant k/k_0 and normalized characteristic impedance ($z_n = z_c/\rho_0 c_0$) for the measurements, alongside a thin dashed line giving the Delany and Bazley empirical values. The results shown are for glass fibre, and similar accuracy is obtained for basalt and rock wool.

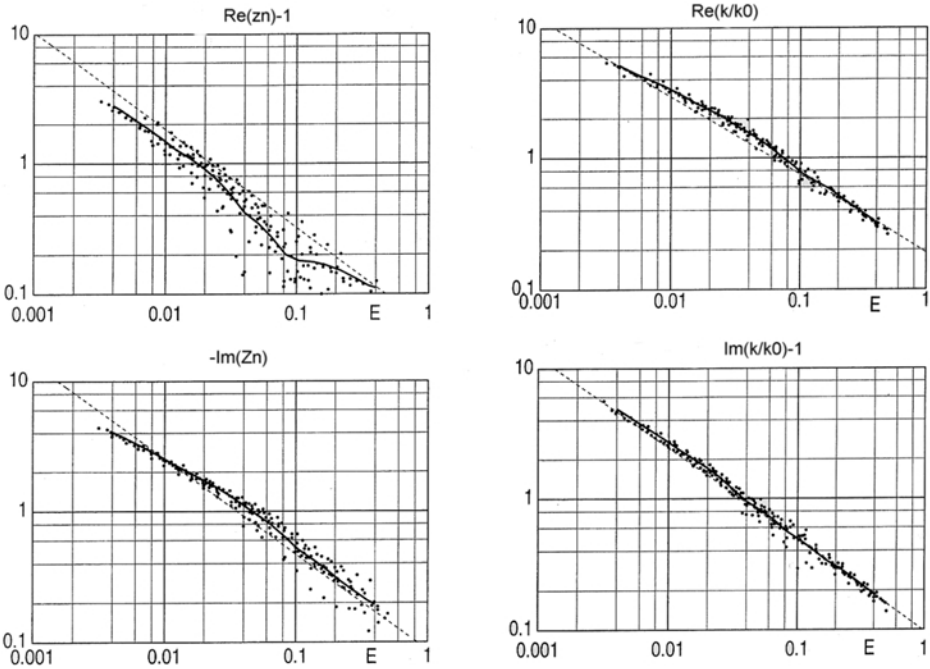


Figure 5.11 Normalized propagation constant and characteristic impedance ($z_n = z_c/\rho_0 c_0$) for fibreglass. Points show measured data, dashed line the Delany Bazley approximation and the solid line a running mean (after Mechel [5]).

It is known that the Delany and Bazley model gives erroneous low frequency behaviour [17] as this is outside its range of applicability. For this reason, several authors have attempted to produce improved relationships. For instance, Mechel and Grundmann produced a more complex set of empirical relationships [5]. They derive separate empirical relationships for mineral fibre and glass fibre, and this enables some improvement over the Delany and Bazley model. For many cases, however, the difference in the predicted quantities is relatively small. Figure 5.11 showed the floating average for the Mechel and Grundmann measurements, which is presumably close to their empirical predictions, compared to the measurements and the Delany and Bazley predictions.

The Mechel and Grundmann empirical can be most simply given as:

$$\left. \begin{matrix} -jk/k_0 \\ z_n \end{matrix} \right\} = \chi^{-1}\beta_{-1} + \chi^{-1/2}\beta_{-1/2} + \beta_0 + \chi^{1/2}\beta_{1/2} + \chi\beta_1 + \chi^{3/2}\beta_{3/2} \quad (5.12)$$

The coefficients are given in Table 5.2. The range of applicability is $0.003 < X < 0.4$. Other authors have also produced their own empirical models to update and improve on the Delany and Bazley model [18, 19].

Section 5.5 details how these empirical formulations can be used to get the surface impedance and absorption coefficient of a material.

The problem with these macroscopic empirical models is they do not readily give information about how the microscopic properties of the porous absorber, such as the pore size, orientation of the pores, etc. affect the absorption produced. This means that it is difficult to use this empirical approach to inform design, beyond finding the optimum flow resistivity required. To improve designs, more detailed models of the propagation are required. In the next section some of the key parameters needed for more physically based porous absorber models are discussed. Following on from this, some of these models are presented in Section 5.5.3.

Table 5.2 Coefficients for Mechel and Grundmann empirical model of porous absorbers, from Reference 5

Coefficients	$-jk/k_0$	z_n
<i>Mineral fibre (basalt or rockwool)</i>		
β_{-1}	$-0.003\ 557\ 57 - j\ 0.000\ 016\ 489\ 7$	$0.0026786 + j\ 0.003\ 857\ 61$
$\beta_{-1/2}$	$0.421\ 329 + j\ 0.342\ 011$	$0.135\ 298 - j\ 0.394\ 160$
β_0	$-0.507\ 733 + j\ 0.086\ 655$	$0.946\ 702 + j\ 1.476\ 53$
$\beta_{1/2}$	$-0.142\ 339 + j\ 1.259\ 86$	$-1.452\ 02 - j\ 4.562\ 33$
β_1	$1.290\ 48 - j\ 0.082\ 0811$	$4.031\ 71 + j\ 7.560\ 31$
$\beta_{3/2}$	$-0.771\ 857 - j\ 0.668\ 050$	$-2.869\ 93 - j\ 4.904\ 37$
<i>Glass fibre</i>		
β_{-1}	$-0.004\ 518\ 36 + j\ 0.000\ 541\ 333$	$-0.001\ 713\ 87 + j\ 0.001\ 194\ 89$
$\beta_{-1/2}$	$0.421\ 987 + j\ 0.376\ 270$	$0.283\ 876 - j\ 0.292\ 168$
β_0	$-0.383809 - j\ 0.353\ 780$	$-0.463\ 860 + j\ 0.188\ 081$
$\beta_{1/2}$	$-0.610\ 867 + j\ 2.599\ 22$	$3.127\ 36 + j\ 0.941\ 600$
β_1	$1.133\ 41 - j\ 1.74819$	$-2.109\ 2\ 0 - j\ 1.323\ 98$
$\beta_{3/2}$	0	0

5.4.2 Further material properties

The simplest theoretical models of porous absorbers assume that the material (or frame) of the absorbent is rigid. Then it is possible to apply some classical theories of sound propagation in small pores. It is only possible to gain analytical solutions for simple geometries such as bundles of cylindrical pores. Unfortunately, cylindrical pores are far removed from the complex geometry of the vast majority of porous absorbers. Consequently, a semi-empirical approach is often adopted, where a mixture of experiment and theory determines key properties of the material. The necessary parameters are detailed below; they are not independent.

5.4.2.1 Pore shape factor and characteristic dimensions

While the porosity and the flow resistivity are usually the most important parameters in determining the sound absorption, other secondary parameters such as the shape factor and the tortuosity (see next section) can have an important effect. The shape of the pores influences the sound propagation and hence the absorbent varies with pore shape. Different pore shapes have different surface areas and hence have different thermal and viscous effects. Analytically obtaining the shape factor for most porous absorbents is impossible as they do not usually conform to simple geometric shapes. Consequently, the pore shape factors are usually empirically found by best fitting the acoustic measurements of the effective density and bulk modulus of the material. The shape factors are therefore dependent on the model being used to predict the propagation within the absorbent. Later in this chapter, formulations for the effective density and bulk modulus are found, from which the characteristic impedance and wavenumber can be obtained, for now, the important shape factors (Λ and Λ') used in those formulations are defined. These factors are sometimes prefixed with the term 'dynamic' to emphasis that they apply to the dynamic not static case.

The characteristic dimension Λ is a weighted ratio of the volume to surface area of the pores. It is weighted according to the squared modulus of the microscopic velocity evaluated, including the effects of viscosity. It can be found for simple pore shapes using the following formulation:

$$\Lambda = \frac{1}{s} \sqrt{\frac{8\eta k_s}{\varepsilon\sigma}} \quad (5.13)$$

where s is a constant. For most porous absorbers, s lies between 0.3 and 3, s is 1, 1.07, 1.14 for circular, square and triangular pores respectively and 0.78 for slits. k_s is the tortuosity as defined in the following section, and η is the viscosity of air.

For materials with non-cylindrical pores and complicated internal structures, it is necessary to use another characteristic dimension [20]. The effective density of real porous absorbers tends to be determined by parts of the pores with smaller cross sections, whereas the bulk modulus is more determined by larger cross-sectional areas [21]. For this reason, a second characteristic dimension to supplement Λ is needed. The second characteristic dimension Λ' is given by:

$$\Lambda' = \frac{2V_p}{S_p} \quad (5.14)$$

where S_p and V_p are the surface area and volume of the pores respectively. This is the same ratio as used for Λ but without the weighting for microscopic velocity. Cylindrical pores are a special case where $\Lambda = \Lambda'$. In general $\Lambda' \geq \Lambda$, and to a first approximation $\Lambda' = 2\Lambda$ and $s = 1$ can be used in Equations 5.13 and 5.14 to derive simpler formulations for the sound propagation in rigid-framed fibrous materials [17].

The determination of these characteristic dimensions poses one of the biggest problems in the use of the theoretical models. For most absorbers, the pore shape is so complex that the characteristic dimensions must be fitted from empirical measurements on samples – which in a sense defeats the point of theoretical modelling, because it is impossible to accurately predict the absorption from a material before it is built. Further complications arise when the material is anisotropic, which is common in many materials. For instance, mineral wool is often laid down in layers, in these cases the characteristic dimensions depend on the incident angle of the sound wave.

5.4.2.2 Tortuosity

The orientation of the pores relative to the incident sound field has an effect on the sound propagation. This effect [22] is represented by the parameter tortuosity denoted k_s . Some authors use the term *structural form factor* for this property, and there are some differences in definition in the literature. Using tortuosity has the advantage that the term is almost self-explanatory. The more complex the propagation path through the absorbent, the higher is the absorption, and the complexity of the path is partly represented by the tortuosity. Furthermore, the tortuosity affects how easily sound can penetrate the absorbent. For simple cylindrical pores, all aligned in the same direction, the tortuosity is simply related to the angle between the pores and the incident sound ($k_s = 1/\cos^2(\psi)$). Real absorbents, however, are not normally that well ordered. Consequently, tortuosity needs to be measured. For a non-conducting material (non-conducting mineral wool and foams) the material can be saturated with a conducting fluid and the electrical resistivity measured [23]. From the electrical resistance, the tortuosity can be found. The electrical resistance of the conducting fluid, r_f , is measured alone and then the electrical resistance of the porous material impregnated with the conducting fluid, r_a . Then the tortuosity can be found from:

$$k_s = \frac{\varepsilon r_a}{r_f} \tag{5.15}$$

Typically k_s is approximately unity for fibrous materials; for granular materials, such as soil, $k_s \approx 2$.

5.4.3 Theoretical models

Given the material properties (flow resistivity, porosity, tortuosity and characteristic lengths), it is possible to calculate the characteristic impedance and propagation wavenumber by considering the microscopic propagation within the pores. Attenborough [24] produced a useful review of early methods, but these techniques have been much refined in recent years. Many people have been involved in the development of the models; the description below draws on the work by Johnson *et al.* [25] and summarized by Allard [26] and Allard and Champoux [17]. This is a simple phenomenological model. The absorber frame is assumed to be rigid.

The effective density of the porous material is given by:

$$\rho_e = k_s \rho_0 \left[1 + \frac{\sigma \varepsilon}{j \omega \rho_0 k_s} \sqrt{1 + \frac{4j k_s^2 \eta \rho_0 \omega}{\sigma^2 \Lambda^2 \varepsilon^2}} \right] \quad (5.16)$$

The effective or dynamic bulk modulus of the air in the material is given by:

$$K_e = \frac{\gamma P_0}{\gamma - (\gamma - 1) \left/ \left(1 + \frac{8\eta}{j \Lambda^2 N_p \omega \rho} \sqrt{1 + \frac{j \rho \omega N_p \Lambda^2}{16\eta}} \right) \right.} \quad (5.17)$$

where γ is the ratio of the specific heat capacities (≈ 1.4), P_0 is atmospheric pressure $101,320 \text{ Nm}^{-2}$; N_p is the Prandtl number given by:

$$N_p = \left(\frac{\delta_v}{\delta_h} \right)^2 \quad (5.18)$$

where δ_v and δ_h are the sizes of the viscous and thermal boundary layers. At 1 atmosphere and 20°C the Prandtl number is about 0.77; this can be found from the following formulations. The thickness of the viscous boundary layer is given by:

$$\delta_v = \sqrt{\frac{2\eta}{\rho\omega}} \quad (5.19)$$

Typically the viscous boundary layer is sub-millimetre in size, for example at 100 Hz it is $\approx 0.2 \text{ mm}$. The thickness of thermal boundary layer is given by:

$$\delta_h = \sqrt{\frac{2\kappa}{\rho c_p \omega}} \quad (5.20)$$

where $\kappa \approx 2.41 \times 10^{-2} \text{ Wm K}^{-1}$ is the thermal conductivity of air and $c_p \approx 1.01 \text{ J kg}^{-1} \text{ K}^{-1}$ is the specific heat capacity of air at constant pressure.

Once the effective density and bulk modulus have been determined from Equations 5.16 and 5.17, it is then possible to calculate the characteristic impedance and propagation wavenumber for the porous absorber, which are what are more often used in calculating acoustic properties.

The characteristic impedance z_c is given by:

$$z_c = \sqrt{K_e \rho_e} \quad (5.21)$$

and the propagation wavenumber by:

$$k = \omega \sqrt{\frac{\rho_e}{K_e}} \quad (5.22)$$

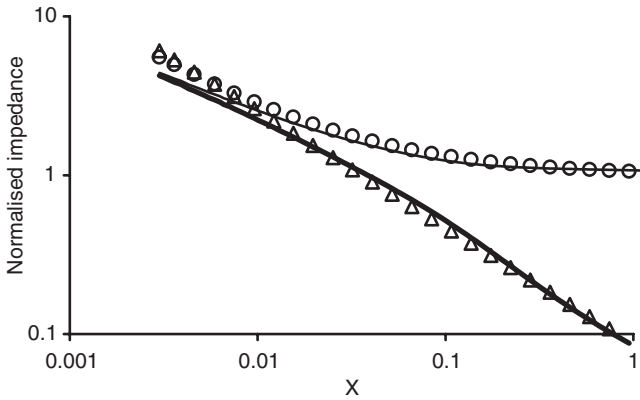


Figure 5.12 Two models for the normalized characteristic impedance (z_c/ρ_0c_0) of a porous absorber compared. The x -axis is $X = \rho_0 f/\sigma$. \circ Re (Delany and Bazley); — Re (Phenomenological); \triangle $-\text{Im}$ (Delany and Bazley); **—** $-\text{Im}$ (Phenomenological).

The formulations in Equations 5.16 and 5.17 give correct high and low frequency asymptotic behaviour, but is only approximately correct at mid-frequencies for complicated pore geometries.

Figures 5.12–5.14 show the normalized characteristic impedance, propagation constant and absorption coefficient for the model from Equations 5.16 to 5.17; these lines are labelled phenomenological. These values are compared to the Delany and Bazley formulations of Equations 5.9–5.10. The following assumptions were made to implement the phenomenological model: $k_s = 1$, $\Lambda' = \Lambda$ and $s = 1$. Both models give very similar results. As stated previously, the Delany and Bazley predictions are known to give inaccurate results at low frequency (the real part of the impedance of the

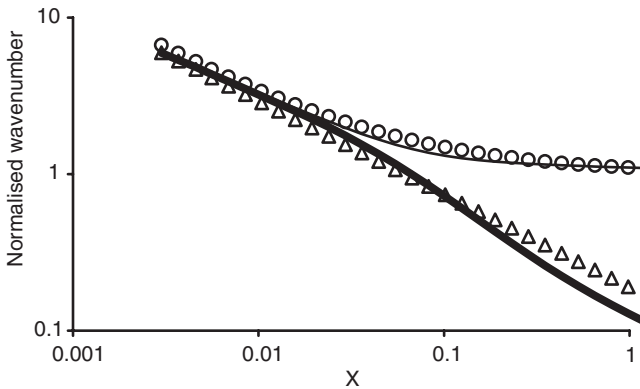


Figure 5.13 Two models for the normalized wavenumber (k/k_0 , where k_0 is the wavenumber in air) for sound propagation through a porous absorber compared. The x -axis is $X = \rho_0 f/\sigma$. \circ Re (Delany and Bazley); — Re (Phenomenological); \triangle $-\text{Im}$ (Delany and Bazley); **—** $-\text{Im}$ (Phenomenological).

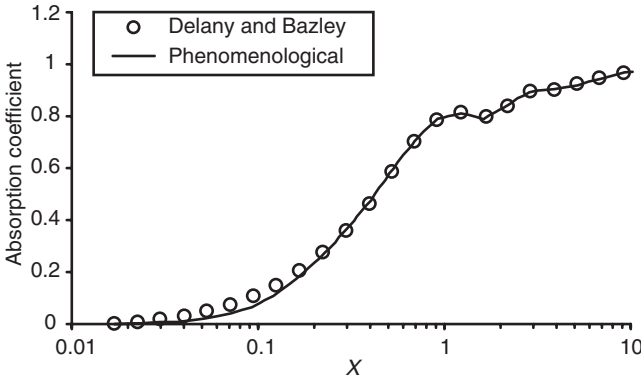


Figure 5.14 Two models for the absorption coefficient of a porous absorber compared. The x-axis is $X = \rho_0 f / \sigma$.

surface of the porous absorber actually goes negative), but these are frequencies at which the absorption from the porous absorber is pretty small anyway.

The comparison in Figure 5.14 showed the absorption coefficient for a given absorber thickness on a rigid backing, rather than the characteristic impedance or wavenumber. How the absorption coefficient and surface impedance are calculated from the characteristic impedance and wavenumber is detailed in the next section.

5.5 Predicting the impedance and absorption of porous absorbers

Once the characteristic impedance and wavenumber for the porous material are known, it is necessary to convert these to the surface impedance and absorption coefficient for a particular thickness of porous absorbent with known boundary conditions. In this case, the most flexible way of predicting the absorption coefficient for porous absorbers is to use the transfer matrix method. Consequently, this section starts by discussing the general case of propagation in one layer of porous absorber in a multi-layered system. Then the specific case of a single layer with a rigid backing will be presented. The prediction model can be extended to multiple layers of absorbent, but the most common situation is the single layer on a rigid backing.

Figure 5.15 shows the system being considered. Only plane wave propagation in the absorbent will be considered, and for now normal incidence only is considered. Section 1.5.1 has already shown how sound behaves when propagating from one medium to another. At each interface between the layers, continuity of pressure and particle velocity is assumed. This allows a relationship between the pressure and particle velocity at the top and bottom of a layer to be produced which is compactly given in matrix format:

$$\begin{Bmatrix} p_{li} \\ u_{li} \end{Bmatrix} = \begin{Bmatrix} p_{xi+1} \\ u_{xi+1} \end{Bmatrix} = \begin{Bmatrix} \cos(k_{xi}d_i) & j \frac{\omega \rho_i}{k_{xi}} \sin(k_{xi}d_i) \\ j \frac{k_{xi}}{\omega \rho_i} \sin(k_{xi}d_i) & \cos(k_{xi}d_i) \end{Bmatrix} \begin{Bmatrix} p_{xi} \\ u_{xi} \end{Bmatrix} \tag{5.23}$$

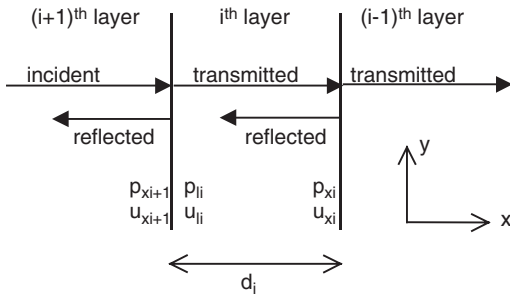


Figure 5.15 Geometry for propagation of sound through a layer of an acoustic medium.

where p_{xi} and u_{xi} are the pressure and particle velocity at the bottom of the i th layer, p_{xi+1} and u_{xi+1} the pressure and particle velocity at the bottom of the $(i + 1)$ th layer, p_{li} and u_{li} the pressure and particle velocity at the top of the i th layer, d_i the thickness of the layer, ρ_i the density of i th layer and k_{xi} the wavenumber for the i th layer.

This formulation can be applied recursively to successive layers, and it is particularly powerful in allowing the calculation of the surface impedance of absorbers, rather than simply a way of gaining specific values for pressure and velocity at the layer boundaries. If the bottom of layer i has an impedance of z_{si} , and the layer i has a characteristic impedance z_i , then the impedance at the bottom of the $i + 1$ layer is:

$$z_{si+1} = \frac{-jz_{si}z_i \cot(k_{xi}d_i) + z_i^2}{z_{si} - jz_i \cot(k_{xi}d_i)} \quad (5.24)$$

Equation 5.24 can be applied repeatedly to calculate the surface impedance of a multi-layered absorber. Next a simple case is considered.

5.5.1 Single layer porous absorber with rigid backing

Consider a single layer of absorber with a rigid backing. The impedance at the surface of layer zero, z_{s0} , which is the backing, is taken to be infinite. Then Equation 5.24 simplifies and gives the impedance on the surface of the absorber as:

$$z_{si+1} = -jz_i \cot(k_{xi}d_i) \quad (5.25)$$

This can then be turned into absorption coefficients using Equations 1.22 and 1.25. Figure 5.16 shows the behaviour of Equation 5.25 as the thickness of the layer increases, using the Delany and Bazley empirical formulations for the porous material properties. As discussed previously, as the porous layer increases in thickness, the absorption increases at lower frequency as expected. Scripts 5.1–5.3 in Appendix B demonstrate the use of these equations.

It is also possible to demonstrate the usefulness of air gaps in increasing absorption. Consider two cases, 2.5 cm of porous absorber mounted on a rigid backing, and 1.25 cm of the same porous absorber mounted 1.25 cm in front of a rigid backing with a 1.25 cm air gap. In the former case Equation 5.25 can be used as before. In the latter

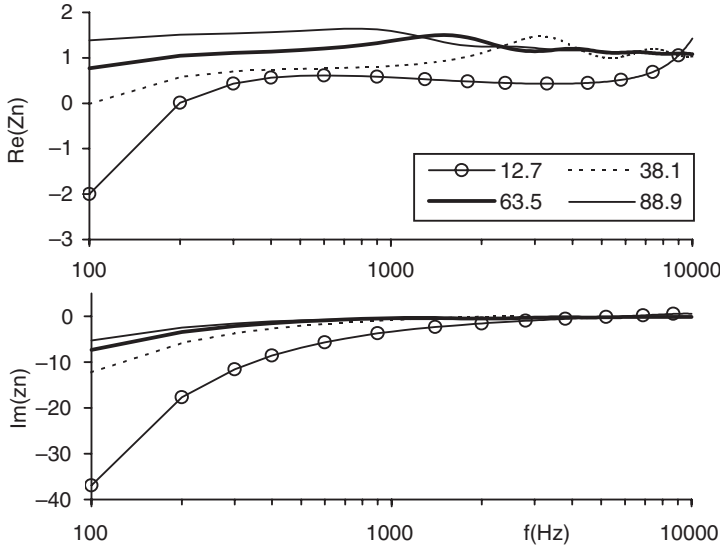


Figure 5.16 Effect of absorber thickness (in mm in legend) on the normalized acoustic impedance using Delany and Bazley model combined with transfer matrix method.

case, Equation 5.24 is applied first to the air layer, and second to the porous absorber layer. For the air layer (layer 1):

$$z_{s1} = -j\rho_0 c_0 \cot(kd_1) \tag{5.26}$$

And for the porous absorber layer (layer 2):

$$z_{s2} = \frac{-jz_{s1}z_2 \cot(k_{x2}d_2) + z_2^2}{z_{s1} - jz_2 \cot(k_{x2}d_2)} \tag{5.27}$$

Figure 5.17 compares the absorption coefficients. It shows that the absorber with the air gap has very similar performance to the thicker absorber alone. This confirms the usefulness of air gaps as discussed in Section 5.1 and elsewhere.

5.6 Local and extended reaction

The propagation direction within many porous absorbers is normal to the surface even for oblique incidence sound because of refraction – see next section. This means that the reaction of the material at any point is independent of the reaction at other points. In this case, the surface is termed locally reacting, as the surface impedance is independent of the nature of the incident wave. This is an extremely useful first order approximation. It means that in multi-layered absorbers the propagation can be assumed normal to the surface and are therefore much easier to evaluate. These assumptions will break down for large sound pressure levels when non-linear propagation is significant. Other common examples of locally reacting materials include

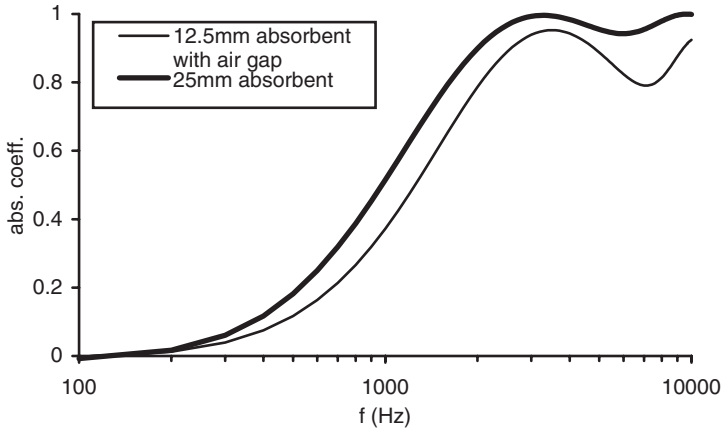


Figure 5.17 Comparison of absorption coefficient for two configurations of porous absorber using transfer matrix methodology.

resonant absorbers whose cavities are partitioned, and for massive walls made of materials like concrete, where the stiffness effect is small enough to be ignored in comparison with the mass effect.

Unfortunately, man-made fibrous materials such as mineral wool often behave as an extended reacting surface because it is anisotropic with the material laid down in layers. The impedance produced is dependent on the incident wave type and angle of incidence. This is one reason why predictions of absorption from the Delany and Bazley model, which are based on normal incidence impedance tube measurements, are difficult to accurately translate into random incidence values measured in the reverberation chamber. A proper model of an extended reacting surface needs to deal with the entire wave field inside the medium. While there are formulations that allow for the anisotropic behaviour of mineral wool [26] – see next section – these formulations produce similar results to the isotropic models because they do not account for the extended reaction.

5.7 Oblique incidence

Consider a sound wave in air incident at an angle ψ to a finite layer of porous material with a rigid backing. The geometry is shown in Figure 5.18. The wavenumber in air is k_0 , and the wavenumber in the material is k . In vector form these are $k_0 = \{k_{0,x}, k_{0,y}, k_{0,z}\}$, $k = \{k_x, k_y, k_z\}$. For simplicity it is assumed that $k_{z,0} = k_z = 0$. Snell's law relates the angles of propagation to the speed of sound in the material as discussed in Chapter 1. In terms of wavenumber this gives:

$$k_y = k_{0,y} = k_0 \sin(\psi) = k \sin(\beta) \quad (5.28)$$

For many porous absorbers, the differences in wavenumber in air and the absorbent are so large that $\beta \rightarrow 0$, and the previous derived normal incident formulae are

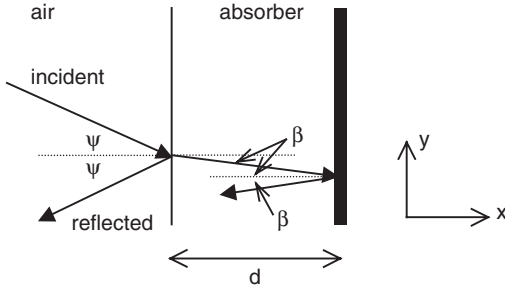


Figure 5.18 Geometry for propagation of sound through a finite layer of a rigid-backed porous absorber.

accurate. For cases where $\beta > 0$, a different formulation can be derived. As $k^2 = k_x^2 + k_y^2 + k_z^2$, this can be combined with Equation 5.28 to give:

$$k_x = \sqrt{k^2 - k_y^2} \tag{5.29}$$

The square root with the positive real part should be chosen. This can then be used to form an alternative form of the surface impedance for a rigidly backed absorber for oblique incident sound.

$$z_{s1} = -jz_c \frac{k}{k_x} \cot(k_x d) \tag{5.30}$$

where z_c is the characteristic impedance of the porous absorber. This is derived using Equation 5.23.

Figure 5.19 shows how the absorption coefficient varies with angle of incidence using the Delany and Bazley formulations. The surface impedance does not vary much with angle of incidence (so these graphs are not shown), but the reflection factor and absorption coefficient vary greatly as the pressure component perpendicular to absorbent drops off with a $1/\cos(\psi)$ relationship, where ψ is the angle of incidence. This was discussed in Chapter 1.

Fibrous porous absorbers can be anisotropic, in other words their acoustic properties vary depending on the angle of the wave to the fibre orientation. In this case, alternative forms for the surface impedance can be deduced. If the effective densities and bulk moduli are measured separately for propagation parallel and perpendicular to the fibres, Equation 5.22 can be applied to obtain the wavenumber parallel and perpendicular to the fibres. The wavenumber perpendicular to the fibres will be denoted k_N and parallel to the fibres k_p . The porous absorber is placed so that the fibres are parallel to the rigid backing, as is most common, then the component of the wavenumber in the x -direction perpendicular to the backing and fibres is given by [26]:

$$k_x = k_N \sqrt{1 - \frac{k_y^2}{k_p^2}} \tag{5.31}$$

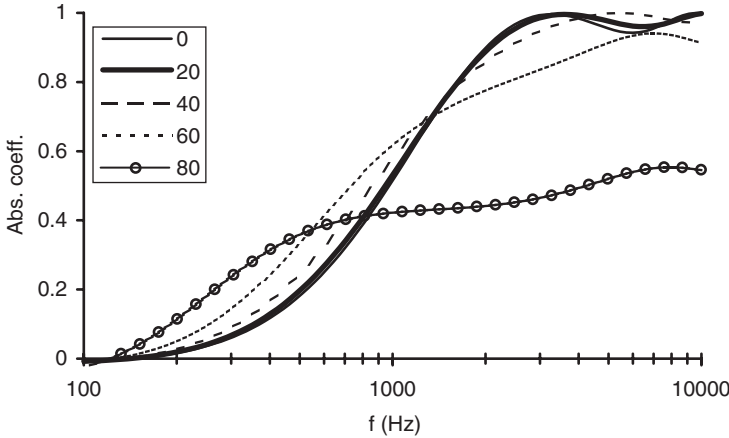


Figure 5.19 Absorption coefficient for different angles of incidence as shown in legend in degrees.

$$k_0 \sin(\psi) = k_y \tag{5.32}$$

$$z_{s1} = -jz_N \frac{k_N}{k_x} \cot(k_x d) \tag{5.33}$$

where z_N is the characteristic impedance for propagation perpendicular to the fibres.

A method for obtaining the parallel and perpendicular propagation wavenumber and characteristic impedance, is to use different flow resistivities in the Delany and Bazley formulations. Typically, the flow resistivities perpendicular (σ_N) and parallel (σ_p) to the fibres are related by [27]:

$$\sigma_N \approx 0.6\sigma_p \tag{5.34}$$

When this formulation is used, it makes some difference to the absorption coefficient and surface impedance, but the change is not that great.

5.8 Biot theory for elastic-framed materials

In the above theories, the frame of the porous absorber was assumed to be rigid and waves only propagated in the air pores. In reality, porous absorbers have elastic frames which can support wave propagation. The consequence of this to the absorption properties of the absorbing material is not as great as might be supposed. For instance, if the porous absorber is anchored to a rigid surface, for example attached to the wall or resting on a floor, this will constrain the motion of the absorber frame. For this reason, the rigid frame models discussed above are used the most, and models that allow for elastic motion of the frame are less commonly used.

Furthermore, as most of the previous models involve some form of empirical fitting, in many cases this fitting can partially compensate for some of the inaccuracies

introduced by not properly modelling the additional wave types which propagate due to the frame being elastic, although strong frame and frame-air resonances cannot be well modelled. If the frame of the porous absorber is not constrained, for example if it is hanging in free air, then resonances of the frame material can be seen in the characteristic impedance of the surface. In this case, a more complete model may be required, and most authors favour using Biot theory [28, 29]. Other models of note are presented by Ingard [2] and Zwicker and Kosten [30].

Biot theory is summarized in more detail in References 5 and 26, where the necessary formulations are given. In this book, only the general principles and concepts will be discussed along with some indications of the relative accuracy of Biot theory and the rigid-framed models discussed earlier in the chapter.

The equations of motion for the displacement and strain tensors of the air in the pores and the frame are defined. These equations of motions include a set of coefficients which detail the coupling between the air and frame. These coefficients can be identified with physical properties such as the bulk modulus of the air in the pores and the elastic frame. The former, the bulk modulus of air in the pores, is taken from the rigid-framed theories detailed earlier. Once these coefficients are determined, the equations of motion can be solved to give the surface impedance of porous layers.

There are now three waves to consider in the structure. There are two compressional waves. In most air-saturated porous materials, the coupling between the frame and air is negligible and these waves can be identified as the frame-borne and airborne waves. Where there is weak coupling, the airborne wave remains mostly within the pores, but the frame-borne wave actually propagates through both the frame and pores. The third wave, the shear wave is also frame-borne, and in most porous absorbents, it is unaffected by the fluid air. (For normal incidence this is not excited and can be ignored.)

Figure 5.20 shows a comparison of theory and experiment from Allard [26]. For many frequencies the rigid-framed model is accurate, but deviations occur around 500 Hz. These inaccuracies are due to the resonances of the frame material which by

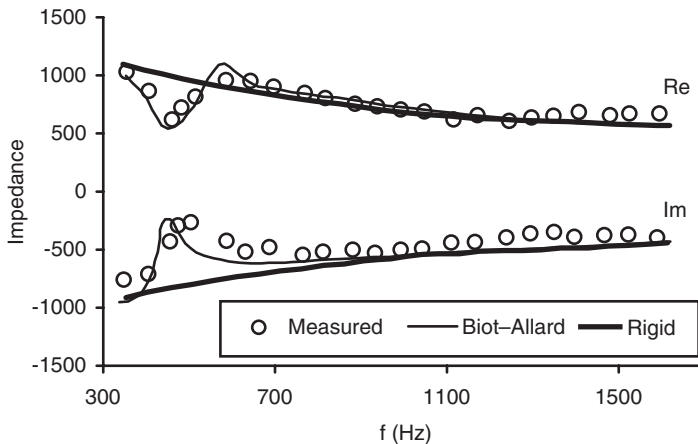


Figure 5.20 Comparison of two prediction models and measurements for a fibrous absorber with a distinct frame resonance (after Allard [26]).

definition cannot be predicted by the rigid-framed model. This is a dense fibreglass material, and so only the quarter wave resonance of the frame is seen. For these frequencies, Biot theory offers better predictions, although it should be noted that some fitting of prediction parameters had to be undertaken to gain this match. So even with Biot theory, the rather circular nature of model verification is still a problem.

5.9 Summary

This chapter has described porous absorbers both qualitatively and quantitatively. There are a large number of possible porous absorbers, and they form an important part of the acoustic palette for acoustic designers both indoors and outdoors. Being able to predict the absorption caused by porous materials, and understanding what causes the absorption, is important to enable materials to be designed with maximum absorption. In the next chapter, resonant absorbers will be discussed, and as many of these use porous absorbers within them, the understanding gained about porous absorber modelling from this chapter will be invaluable in the next.

5.10 References

- 1 L. Cremer and H. A. Müller, *Principles and Applications of Room Acoustics*, Applied Science Publishers trans. by T. J. Schultz (1978).
- 2 U. Ingard, *Notes on Sound Absorption Technology*, Noise Control Foundation (1994).
- 3 P. D'Antonio, *Nestable Sound Absorbing Foam with Reduced Area of Attachment*, US patent 5,665,943 (1997).
- 4 D. A. Bies and C. H. Hansen, *Engineering Noise Control: Theory and Practise*, E&FN Spon, 2nd edn, 42–43 (1996).
- 5 F. P. Mechel, *Formulas of Acoustics*, Springer, Section G (2002).
- 6 National Institute of Occupational Safety and Health, *Criteria for a Recommended Standard: Occupational Exposure to Fibrous Glass*, DHHS (NIOSH) Publication No. 77–152 (1977).
- 7 European Commission Directive 97/69/EC.
- 8 <http://www.hse.gov.uk/lau/lacs/37-3.htm#appendix>.
- 9 J. Pfretzschner, *Rubber Crumb as Granular Absorptive Acoustic Material*, Forum Acusticum, Sevilla, MAT-01-005-IP (2002).
- 10 M. J. Swift and K. V. Horoshenkov, *Acoustic Properties of Recycled Granular Foams*, Euronoise (2001).
- 11 C. M. Harris (ed.), *Handbook of Noise Control*, 2nd edn, McGraw-Hill (1991).
- 12 L. L. Beranek, *Acoustics*, McGraw-Hill (1954).
- 13 F. A. Everest, *Master Handbook of Acoustics*, 4th edn, McGraw-Hill (2001).
- 14 D. A. Bies and C. H. Hansen, “Flow resistance information for acoustical design”, *Appl. Acoust.*, **13**, 357–391 (1980).
- 15 M. Garai and F. Pompili, *Definition and First Validation of a New Mathematical Model of Polyester Fibre Materials*, Forum Acusticum, RBA-03-004-IP, Sevilla (2002).
- 16 M. E. Delany and E. N. Bazley, “Acoustical properties of fibrous absorbent materials”, *Appl. Acoust.*, **3**, 105–116 (1970).
- 17 J. F. Allard and Y. Champoux, “New empirical equations for sound propagation in rigid frame fibrous materials”, *J. Acoust. Soc. Am.*, **91**(6), 3346–3353 (1992).
- 18 J. P. Dunn and W. A. Davern, “Calculation of acoustic impedance of multi-layer absorbers”, *Appl. Acoust.*, **19**, 321–334 (1986).

- 19 Y. Miki, "Acoustical properties of porous materials – modification of Delany-Bazley laws", *J. Acoust. Soc. Jpn.*, **11**, 19–28 (1986).
- 20 Y. Champoux and J. F. Allard, "Dynamic tortuosity and bulk modulus in air-saturated porous media", *J. Appl. Phys.*, **70**, 1975–1979 (1991).
- 21 Y. Champoux and M. R. Stinson, "Propagation in porous materials", *J. Acoust. Soc. Am.*, **92**(2), 1120–1131 (1992).
- 22 K. Attenborough, "On the acoustic slow wave in air filled granular media", *J. Acoust. Soc. Am.*, **81**, 93–102 (1982).
- 23 R. J. S. Brown, "Connection between formation factor for electrical resistivity and fluid-solid coupling factor in Biot's equations for acoustic waves in fluid-filled porous media", *Geophysics*, **45**, 1269–1275 (1980).
- 24 K. Attenborough, "Acoustical characteristics of porous materials", *Phys. Rep.*, **82**, 179–227 (1982).
- 25 D. L. Johnson, J. Koplik and R. Dashen, "Theory of dynamic permeability and tortuosity in fluid-saturated porous media", *J. Fluid Mechanics*, **176**, 379–402 (1987).
- 26 J. F. Allard, *Propagation of Sound in Porous Media: Modelling Sound Absorbing Materials*, Elsevier Applied Science (1993).
- 27 J. F. Allard, R. Bourdier and A. L'Esperance, "Anisotropy effect in glass wool for normal impedance in oblique incidence", *J. Sound. Vib.*, **114**, 233–238 (1987).
- 28 M. A. Biot, "Theory of propagation of elastic waves in a fluid-saturated porous solid. I Low-frequency range", *J. Acoust. Soc. Am.*, **28**(2), 168–178 (1956).
- 29 M. A. Biot, "Theory of propagation of elastic waves in a fluid-saturated porous solid. II Higher frequency range", *J. Acoust. Soc. Am.*, **28**(2), 179–191 (1956).
- 30 C. Zwikker and C. Kosten, *Sound Absorbing Materials*, Elsevier (1949).

6 Resonant absorbers

By using the phenomenon of resonance, it is possible to gain absorption at low to mid-frequencies, where absorption is difficult to achieve with porous absorbers because the thickness and size of the material would be too large. Furthermore, absorbers are often placed at room boundaries where porous absorbers are inefficient as the particle velocity is low. For many resonant absorbers, placing the device at the boundaries will improve their effectiveness. The absorption characteristics of resonant absorbers are a peak of absorption as shown in the dashed line in Figure 6.1. Unlike porous absorbers, wide band absorption is difficult to achieve in one device, and so one of the frequent challenges in the design of resonant structures is to extend the bandwidth.

There are two common forms of the device: the first is the Helmholtz absorber which is named after the German physician and physicist Hermann von Helmholtz (1821–1894) and the second is a membrane or panel absorber. The ideas and concepts of resonant absorption have been known for many decades. In recent years some more specialist devices have been produced, for instance clear absorbers, but these are still based on the same basic physics. While some devices, such as many basic Helmholtz absorbers, can be predicted with reasonable accuracy, others, such as membrane devices,

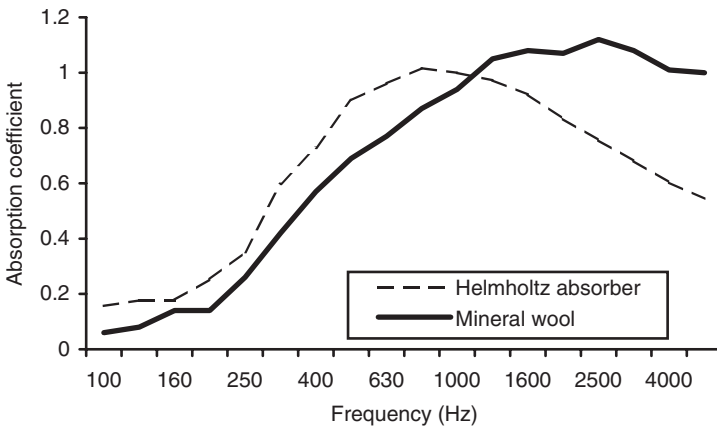


Figure 6.1 Random incidence absorption coefficient for a porous absorber, and a porous absorber covered with a perforated sheet to form a Helmholtz resonant absorber.

are still designed by trial and error. Resonant absorbers are commonly employed to treat low frequency room modes and as parts of silencers within ventilation systems.

6.1 Mechanisms

Resonant absorbers involve a mass vibrating against a spring. The two common types of resonant absorber are illustrated in Figure 6.2. In the case of a Helmholtz absorber, the mass is a plug of air in the opening in the perforated sheet. The resonance is produced by the same mechanism which generates a note when you blow across a beer bottle. To make this into an absorber, losses are provided by a damping mechanism to remove acoustic energy, such as a layer of mineral wool. For a membrane (or panel) absorber, the mass is a sheet of material such as rubber or plywood which then vibrates. The spring in both cases is provided by air enclosed in the cavity. By changing the vibrating mass and the stiffness of the air spring, the resonant frequency of the device can be tuned, and it is at the resonant frequency that absorption is a maximum.

To achieve losses, damping is required. This can be achieved by placing porous absorbent where the particle velocity is large – in the neck of the Helmholtz resonator or behind the membrane in the panel absorber. In the latter case, the absorbent should not be so close as to inhibit movement of the membrane. Alternatively, for Helmholtz devices with small openings, viscous losses within the neck can be used to gain absorption; this is a technique which allows devices without porous absorbent, such

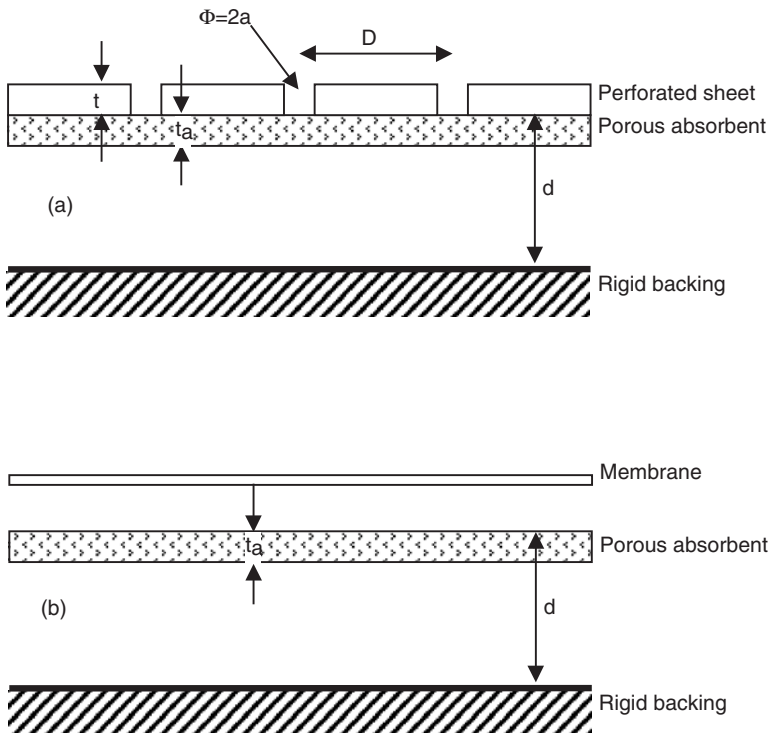


Figure 6.2 Typical constructions for (a) Helmholtz absorber and (b) membrane absorber.

as microperforated absorbers, to be produced. For membrane devices there are also internal losses within the vibrating membrane, but these are usually too small to give high absorption. More significant are the losses that come from the mounting between the membrane and the absorber side walls. Problems arise in predicting performance of membrane absorbers, as the absorption from the boundaries is hard to characterize.

Before discussing the relevant design equations, some example constructions are given to provide a sense of what commercial devices are like. After the design equations, more complex and unusual constructions will be considered.

6.2 Example constructions

6.2.1 Bass trap membrane absorber

Small rooms often exhibit a poor low frequency response with significant emphasis at modal resonances and de-emphasis where modal excitation is small. There is also limited space within which to make acoustic improvements. Porous surface absorption is ineffective at these modal frequencies, because the particle velocity near walls and in corners is essentially zero for these long wavelengths, and also the porous surface would have to be made so deep that significant space within the room would be lost to acoustic treatment. This problem can be solved using a resonant absorber, such as a membrane design. A membrane absorber converts the high sound pressure fluctuations typically found at wall surfaces and in corners into selective absorption in the modal frequency range. As the use of sub-woofers has become more popular in small sound reproduction rooms in recent years, there is a growing need for modal frequency management.

Figure 6.2b shows a membrane absorber using an internally damped membrane. The membrane converts pressure fluctuations into air motion. As the membrane sympathetically vibrates over a selective low frequency range, determined by its mass and the air spring stiffness, it pushes air through an internal porous layer producing low frequency absorption. Simple relationships exist between the design frequency of these resonant systems and the membrane mass, stiffness and cavity depth, and these will be outlined below. Figure 6.3 illustrates the absorption coefficient of this type of device and also shows an example application where the absorbent is placed in the corner where the pressure is a maximum for all room modes. There is also a prediction of the performance using a transfer matrix approach as discussed below. This prediction illustrates, however, that for membrane absorbers the design equations are often inexact in predicting the resonant frequency. There are many reasons for this. For instance the physical mass of the membrane is often different from the vibrating acoustic mass due to mounting conditions.

If the absorber has a sharp resonant peak with a high Q factor, there is a risk of creating a notch at the wrong frequency, thus aggravating rather than ameliorating the modal problems. Consequently, experimental verification of the absorption is necessary, although at these low frequencies this is not easy. The results shown in Figure 6.3 were measured in an unusually large impedance tube.

Specific modal problem frequencies can be addressed with individually tuned absorbers, and while bass membrane absorbers can be designed for a specific frequency and offer a high absorption efficiency, their bandwidth over which they are effectively absorbing is rather limited. One can broaden the absorption by

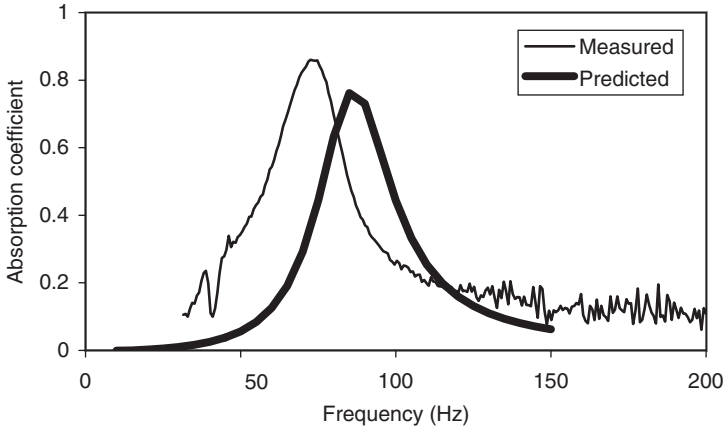


Figure 6.3 Top: Measured and predicted normal incidence absorption coefficient for a commercial membrane absorber (Modex™). Bottom: A typical installation in a small reproduction room; the absorber is in the corner of the room (photo courtesy of RPG Diffusor Systems Inc.).

introducing additional damping in the air cavity, but this often lowers the maximum absorption efficiency. An alternative solution is to use a range of modules, each tuned to work in a different one-third octave band for more general broadband absorption. But a considerable amount of the room boundary must be covered with absorber to get broadband low frequency absorption.

6.2.2 Helmholtz absorption

Currently, wood is more often than not, the preferred surface treatment in general architectural spaces, as well as in critical listening and performance spaces.

However, one of the problems is that flat wooden panels may generate problematic reflections compromising speech intelligibility and music quality. To treat offending reflections, upholstered fibreglass or stretch fabric systems are often used. But it is also possible to use flat attractive wooden panels and also provide absorbers at specified frequencies. Figure 6.4 illustrates such a system and an example application. The grooves are essentially a visual trick to hide the holes if these are not visually desirable. At the base of the grooves there is a single or double diameter hole, providing a sound path through the panel. By varying the groove (i.e. hole) spacing, the hole diameter, and the rear air cavity depth and content, it is possible to obtain absorption over a wide variety of frequencies. The design equations are given later in this chapter and are much more successful than when applied to membrane absorbers.

These Helmholtz absorbers are constructed from class A medium density fibre-board (MDF) cores either painted or surfaced with wood veneers or simulated wood grain melamine. The rear of the panel is covered with a black non-woven glass matt to provide a resistive layer and also to conceal the contents behind the panel. In addition, a fibreglass panel is attached to the back of the glass matt to provide further resistance and losses.

Figure 6.5 shows typical absorption coefficients for different cavity depths and hole sizes. As the holes enlarge, the open area increases leading to greater absorption at higher frequencies; there is also a slight increase in resonant frequency. These trends can be predicted by the design equations given later, but they will not predict the absorption coefficient values greater than 1, shown in Figure 6.5. Predictions give less absorption because the vagaries of reverberation chamber measurements such as edge diffraction are not included in the prediction models – see Chapter 12 for further discussions of this. Increasing the cavity depth causes the stiffness of the spring to decrease, and consequently the peak absorption decreases in frequency. Again this is predictable.

The absorbers shown here are not particularly unusual in terms of the acoustics they exploit. The physics behind the mechanisms has been known for more than a century. The problem with this type of construction is getting the perforated sheet

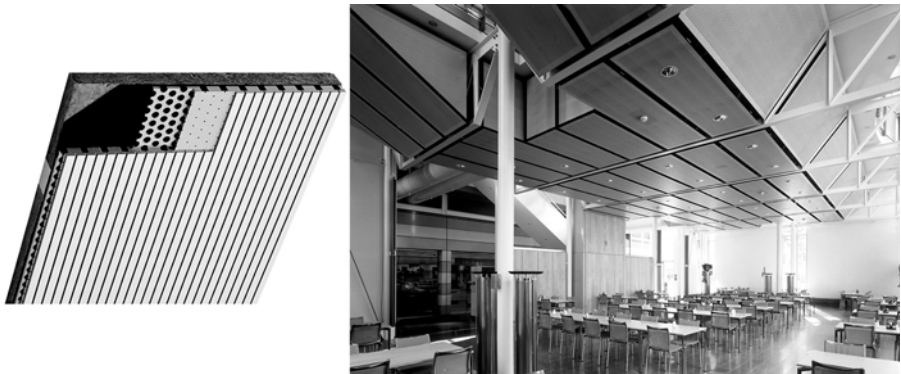


Figure 6.4 A commercial Helmholtz resonator and its application in a cafeteria to reduce reverberance (photo courtesy of n'H Akustik + Design AG).

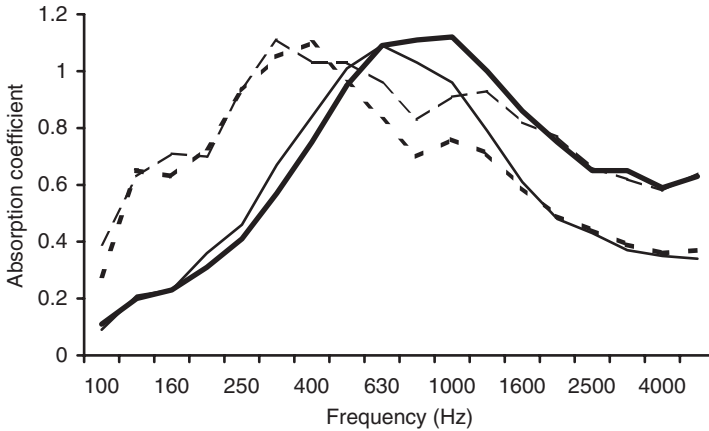


Figure 6.5 Random incidence absorption coefficient for different Helmholtz absorbers. — Small hole, shallow cavity; — Large hole, shallow cavity; ••• Small hole, deep cavity; - - - Large hole, deep cavity (data courtesy of n'H Akustik + Design AG).

with the correct hole size and open area. Standard perforated board, such as peg board, has too small an open area; most perforated metals have too large an open area. Consequently, the perforated sheet often has to be specifically constructed for acoustic purposes, which makes it more expensive than if stock items could be used.

6.2.3 Absorption and diffusion

Figure 6.6 shows a Schroeder style diffuser, which has square holes to provide mid-frequency absorption via a Helmholtz mechanism. These are relatively shallow diffusers and so are only efficient diffusers above ≈ 3 kHz, unless modulation is used to extend the bandwidth as discussed in Chapter 9. Below 3 kHz, absorption is provided by resonant mechanism via the square holes. The diffuser is mounted over porous absorbent with a cavity behind, similar to Figure 6.2a. Consequently, this is a hybrid device providing absorption and diffusion in different frequency ranges. As the frequency ranges are different, it is assumed that the absorption mechanism should not have too much effect on the diffusion performance and vice versa. The frequency of absorption can be varied by choosing the hole size, open area and cavity depth. Although in this case, the amount of variation in these design variables achievable is rather limited because of restrictions imposed by the diffuser surface profile.

This surface is also provided without holes. In Figure 6.7, the absorption for two mounting types is shown. The panel can be mounted with a 1.6 mm gap between the laths (planks) – this is labelled Helmholtz mounts. This gives a small slit opening to the back cavity, which as this contains a porous absorbent generates additional bass absorption via a Helmholtz mechanism. This additional bass absorption can be useful in treating spaces with excess bass reverberation. Similar bass absorption can also be

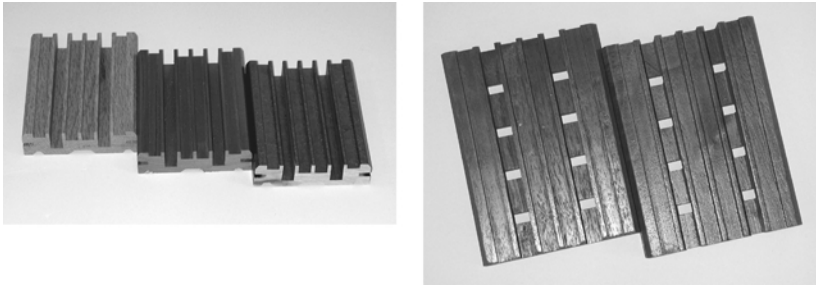


Figure 6.6 A small scale Schroeder diffuser, FlutterFree[®] (left) and a perforated version with square holes (right) forming a Helmholtz resonator.

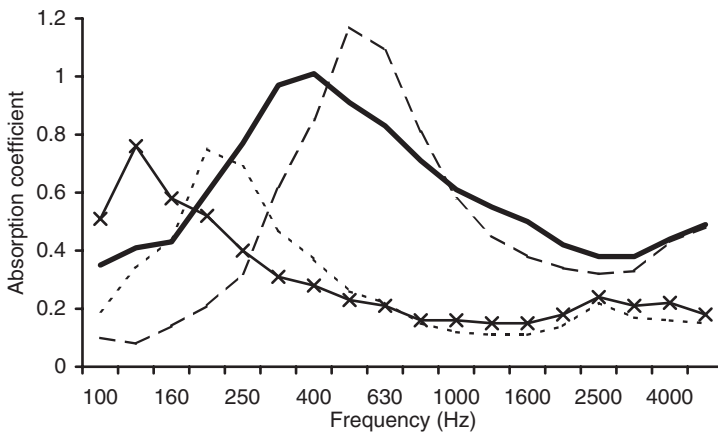


Figure 6.7 Random incidence absorption coefficient for a hybrid absorbing–diffusing system. No holes, Helmholtz mounts, shallow cavity; - - - - Square holes, normal mount, shallow cavity; —X— No holes, Helmholtz mounts, deep cavity; — Square holes, normal mount, deep cavity.

achieved by using tuned membrane absorbers, but a Helmholtz mechanism is generally easier to achieve in a device.

The square holes shown in Figure 6.6 are responsible for the peaks in absorption around 500–600 Hz. The Helmholtz slits provide absorption at a few hundred Hertz or less. Again, the resonant frequency can be easily tuned by choosing an appropriate cavity depth and lath spacing.

6.2.4 Clear absorption

Acousticians have long sought a fully transparent absorptive finish to control reverberation in a room, while maintaining the view through glazing. Glazing is a popular building material, and there are considerable advantages in combining lighting and acoustic function into one device to save on materials and cost. One solution to

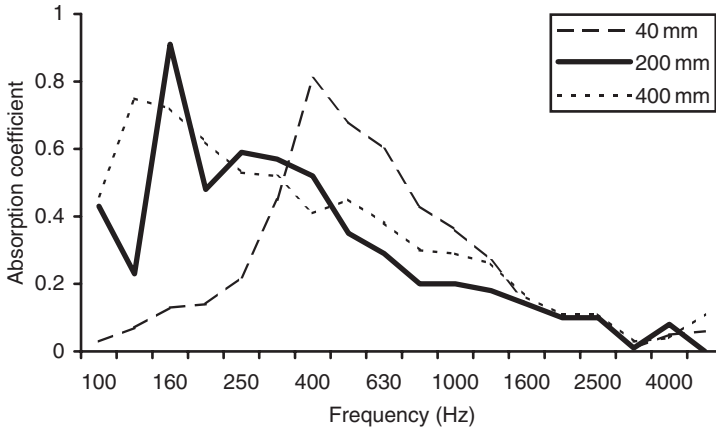


Figure 6.8 Measured random incidence absorption coefficient for three microperforated devices for varying cavity depths as indicated by legend (data courtesy of n'H Akustik + Design AG).

getting a clear absorber is to use microperforation. These are Helmholtz devices, but without the normal resistive material. The device is rather like a double glazing unit, with the first pane being a 5 mm thick panel with sub-millimetre diameter holes spaced 5 mm apart. The holes are drilled mechanically. The device provides absorption through high viscous losses as air passes through the small holes, which are only a bit larger than the boundary layer. This inherent damping eliminates the need for fibreglass or other porous materials in the air cavity between the perforated sheet and the reflective surface behind it. Thus it is possible to provide fibreless, clear absorption. To augment the mid- to low frequency absorption, the device can be curved, tilted or shaped to provide redirection or diffusion in the mid- to high frequency region. The surface is transparent when looked at from straight on, but at oblique angles the holes become more apparent, although the surface is still translucent.

Figure 6.8 shows typical absorption coefficients. The absorption is not as controllable as with Helmholtz devices with resistive material. The requirement for small holes restricts the frequency range over which the resonant absorption can be achieved within manufacturing constraints. So these are useful devices for treating troublesome low to mid-frequency noise and reverberance in spaces such as atria.

Later in this chapter, the design equations for microperforated devices will be outlined and shown to be accurate. Other example constructions will also be discussed, for example the use of elongated orifices and microperforation of membranes.

6.2.5 *Masonry devices*

In 1917, Straub patented the CinderBlox, the first concrete masonry unit (CMU). In 1965, slotted blocks were introduced to provide low frequency absorption. The slots produce a Helmholtz device to provide bass absorption. Figure 6.9 shows a modern



Figure 6.9 A CMU (concrete masonry unit) which uses two slotted Helmholtz absorbers to provide bass absorption, DiffusorBlox[®] (one slot is difficult to see).

equivalent. While the old blocks were useful for noise control, the flat or split face of these blocks can create reflection problems which degrade acoustics. Consequently, a phase grating diffuser is used to break up the reflected sound wavefronts. The design shown in Figure 6.9 utilizes two slotted Helmholtz resonator chambers, as well as the phase-grating pressure gradient absorption mechanism (see Chapter 7). Typical absorption coefficients are shown in Figure 6.10. Painting reduces the high frequency absorption as it seals the porous concrete surface, but does not affect low frequency absorption as would be expected. Good insulation against sound transmission is achieved because of the heavy construction.

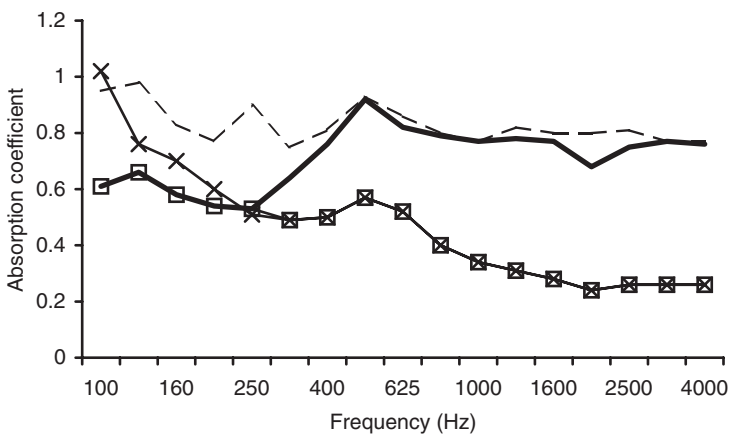


Figure 6.10 Random incidence absorption coefficient for a masonry unit. The slots provide absorption via a Helmholtz mechanism producing low frequency absorption. ----- Slotted, unpainted; _____ Not slotted, unpainted; —x— Slotted, painted; —□— Not slotted, painted.

6.3 Design equations: resonant frequency

Having outlined some example designs, this section outlines the most simple design equations. Consider a simple absorber formed by a cavity with a covering sheet. The sheet could either be perforated to form a Helmholtz design, or solid but flexible to form a membrane absorber (Figure 6.2). It could even be a flexible perforated membrane, which is a combination of the two. In the first two cases, the impedance of the cavity given in Equation 5.25 will simply be altered by the addition of mass ($j\omega m$) and resistance (r_m) terms. These are the acoustic mass and resistance respectively, arising due to the perforated sheet or membrane. The surface impedance of the resonant system is:

$$z_1 = r_m + j[\omega m - \rho c \cot(kd)] \quad (6.1)$$

where $k = 2\pi/\lambda$ is the wavenumber in air, d the cavity depth, m the acoustic mass per unit area of the panel, ω the angular frequency, ρ the density of air and c the speed of sound in air.

For now, the presence of porous absorbent within the cavity is ignored for simplicity. Systems resonate when the imaginary part of the impedance is zero; so to find the resonant frequencies the imaginary terms in Equation 6.1 are set equal to zero. Consider a case where the cavity size is much smaller than the acoustic wavelength, i.e. $kd \ll 1$, so that $\cot(kd) \rightarrow 1/kd$, then the resonant frequency f is:

$$f = \frac{c}{2\pi} \sqrt{\frac{\rho}{md}} \quad (6.2)$$

This is a general formulation; now the specific instance of the Helmholtz resonator will be considered, followed by the case of the membrane absorber.

6.3.1 Helmholtz resonator

The perforated surface is divided into individual cells which are assumed to behave independently with a repeat distance D . D is defined in Figure 6.2, which shows a cross section through the absorber. The absorber is assumed to be perforated in two directions, with the repeat length being the same in both directions. The individual cells will not be entirely independent at low frequency, and consequently physical subdividing of the volume may be required as the wavelength becomes large. This is especially true if good oblique incidence absorption is required, as would be needed for good random incidence absorption, and lateral propagation within the cavity must be suppressed to maximize absorption. When a porous absorbent is placed in the cavity, sound propagation is generally normal to the surface as discussed in Chapter 5, and so the need for subdividing is less critical, except at very low frequencies.

The hole spacing should be large compared to the hole diameter. The acoustic mass per unit area is then $m = \rho D^2 t' / \pi a^2$ where t' is the thickness of the perforated sheet with the end corrections (end corrections allow for the radiation impedance of the orifices and are discussed later) and other variables are as defined in Figure 6.2. The

sheet thickness, t , and hole radius, a , are assumed to be much smaller than the wavelength of sound in air. Under these assumptions, the resonant frequency is:

$$f = \frac{c}{2\pi} \sqrt{\frac{S}{t'V}} \quad (6.3)$$

where $S = \pi a^2$ is the area of the holes and $V = D^2 d$ the volume of each unit cell.

This is the same formulation as derived by other methods, such as lumped parameter equivalent electrical circuit models [1]. The transfer function approach is used here because it can more easily generalize to non-lumped parameter cases, for example when the cavity size is no longer shallow compared to wavelength. It is also consistent with the theories used elsewhere in this book.

An alternative, but entirely equivalent formulation for the Helmholtz resonator, uses the porosity or fraction of open area, ε . This is often more convenient to work with when using perforated sheets and can be derived by considering the geometry in Figure 6.2 to revise Equation 6.3:

$$f = \frac{c}{2\pi} \sqrt{\frac{\varepsilon}{t'd}} \quad (6.4)$$

$$\varepsilon = \frac{\pi a^2}{D^2} \quad (6.5)$$

The vibrating plug of air within the perforations provides the mass of the device. The length of the plug of air is not just the perforated plate thickness. The effect of radiation impedance must be considered, including the mutual interaction between neighbouring vibrating air plugs. Consequently, the vibrating plug of air has a length given by the thickness of the panel plus end corrections to allow for the radiation impedance of the orifice. A full expression for the mass in Equation 6.2 is therefore [2]:

$$m = \frac{\rho}{\varepsilon} \left[t + 2\delta a + \sqrt{\frac{8\nu}{\omega}} \left(1 + \frac{t}{2a} \right) \right] \quad (6.6)$$

The last term in the equation is due to the boundary layer effect, and $\nu = 15 \times 10^{-6} \text{ m}^2 \text{ s}^{-1}$ is the kinematic viscosity of air. This last term is often not significant unless the hole size is small, say sub-millimetre in diameter. δ is the end correction factor which to a first approximation is usually taken as 0.85 and derived by considering the radiation impedance of a baffled piston. A value of 0.85 does not, however, allow for mutual interactions between neighbouring orifices because it is based on a calculation for a single piston. Consequently, other more accurate formulations exist. For a porosity of $\varepsilon < 0.16$, Ingard gives the correction factor as [3]:

$$\delta = 0.8(1 - 1.4\varepsilon^{1/2}) \quad (6.7)$$

In the limit of only one hole in an infinite plane, this is roughly 0.85 as given earlier. An alternative formulation which works for more open structures was developed by

Rschevkin and reported by Cremer and Müller [4]. This reportedly includes the limiting case of $\epsilon = 1$:

$$\delta = 0.8(1 - 1.47\epsilon^{1/2} + 0.47\epsilon^{3/2}) \tag{6.8}$$

For a square aperture, the formulation for $\epsilon < 0.16$, Equation 6.7, changes slightly to [3]:

$$\delta = 0.85(1 - 1.25\epsilon^{1/2}) \tag{6.9}$$

For unusual shapes, the radiation impedance of the plug of air can be numerically evaluated using boundary or finite element models, but the changes this makes to the final resonant frequency are likely to be small. Furthermore, the radiation impedance calculated this way might not allow for mutual interaction.

An added complication with end corrections is that imperfections in constructions, such as burrs, may have an effect which will be ill-defined. For high amplitude sound, turbulence will reduce the acoustic mass and so the resonant frequency will increase.

Figures 6.11 and 6.12 illustrate the effect of changing the open area on the resonant frequency. Figure 6.11 shows the absorption coefficient, with the frequency of peak absorption decreasing as the open area reduces. Figure 6.12 shows the change of resonant frequency in terms of impedance where the frequency of the zero crossing of the imaginary part decreases as the open area reduces. Script 6.1 in Appendix B gives the code to generate the results. As the open area decreases, additional low frequency absorption is generated mainly due to the increased stiffness of the spring in the unit cell as the volume reduces. The high frequency absorption decreases because the proportion of solid parts of the perforated sheet increases, and these parts reflect high frequency sound. Similar results are seen in measurements [5].

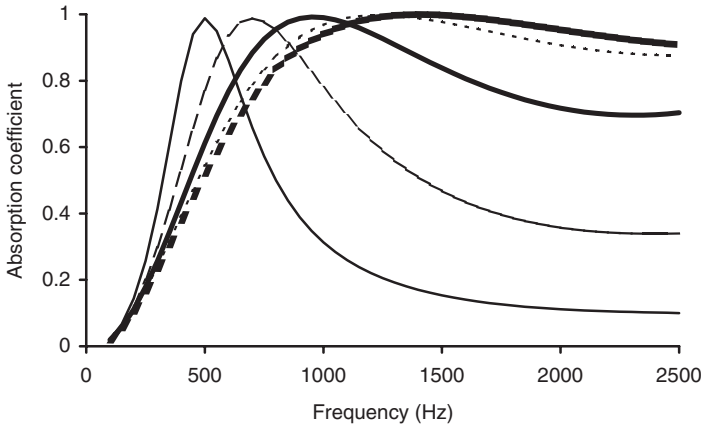


Figure 6.11 Absorption coefficient of a Helmholtz absorber showing the effect of open area. Hole radius 2.5 mm, porous absorbent flow resistivity $20,000 \text{ rayl m}^{-1}$, thickness 2.5 cm, air layer thickness 2.5 cm, perforated sheet thickness 6.3 mm. Open areas: ——— 6%; - - - - - 12.5%; ——— 25%; - - - - - 50%; - - - - - 100%.

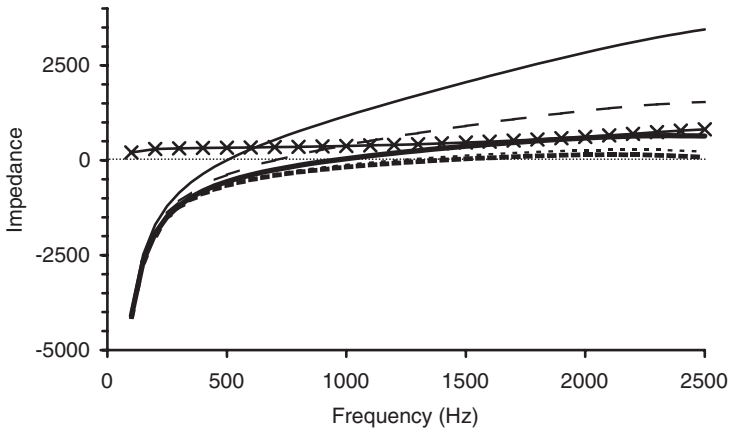


Figure 6.12 Impedance of some Helmholtz absorbers showing effect of open area. Geometry same as Figure 6.11. Only one real impedance is shown, because the variation with open area is negligible. Open areas: — \times — Re, 6%; — Im, 6%; - - - - - Im, 12.5%; — Im, 25%; - · - · - Im, 50%; ····· Im, 100%.

The maximum absorption decreases somewhat as the resonant frequency decreases. If these absorbers were tuned to a lower frequency, this decrease would be more marked. The reason for this is that the impedance of the porous material moves further from the characteristic impedance of air at low frequencies, making the absorption less efficient. The peak absorption can be altered by changing the porous material flow resistivity as illustrated in Figure 6.13. In the case shown in Figure 6.11, the flow resistivity of $25,000 \text{ Nm}^{-4}$ s is such that the resistance is close to the characteristic impedance of air leading to high absorption. An additional effect of changing the flow resistivity is to change the bandwidth over which absorption is effective by altering the Q of the resonance. In this case, a higher flow resistivity would achieve a greater

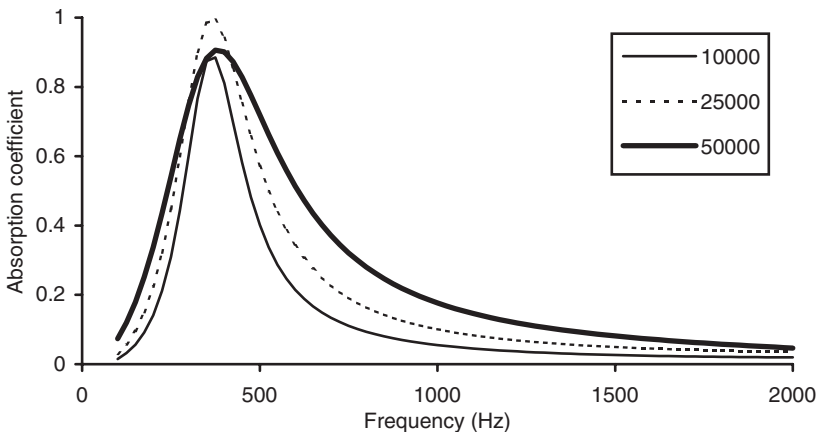


Figure 6.13 Effect of flow resistivity (shown in legend in rayl m^{-1}) on absorption of a Helmholtz resonator.

bandwidth, but will reduce the maximum absorption, as the resistance exceeds the characteristic value. A lower flow resistivity leads to an impedance less than characteristic, which results in a reduction in bandwidth and maximum absorption.

Figure 6.14 shows the trade-off between cavity depth and perforated sheet thickness. The perforated sheet thickness has been varied while keeping the total thickness of the device, cavity plus perforated sheet, constant. Making the covering sheet thicker can generate additional base absorption. But this is at the expense of reduced bandwidth including decreased high frequency absorption.

Another common geometry is a Helmholtz device where slots are used instead of holes, see for example the CMU shown in Figure 6.9. This can have a considerable advantage in some cases, as slots can be easier to make than holes. The orifices can be formed by sawing slots in board or by leaving spaces between parallel planks in wood claddings. For a lath or plank cladding, manufacturers can offer different mounting conditions, with and without spaces between the planks, which enable designers to choose the desired absorption characteristics; see Figures 6.6 and 6.7 for example. The difficulty with slotted Helmholtz devices is deriving the appropriate end correction. Kristiansen and Viglen [6] use a formulation originally derived by Smits and Kosten [7]:

$$\delta = -\frac{1}{\pi} \ln \left[\sin \left(\frac{1}{2} \pi \varepsilon \right) \right] \tag{6.10}$$

This then gives a mass term of

$$m = \frac{\rho}{\varepsilon} (t + 2\delta w) \tag{6.11}$$

where w is the width of the slots. As shall be shown later, this appears to give accurate results.

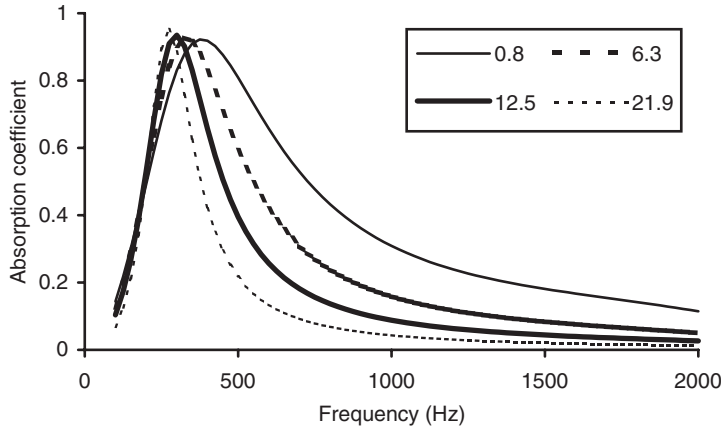


Figure 6.14 Effect of facing thickness (shown in legend in mm) on absorption of a Helmholtz resonator. The total thickness of the device (cavity plus facing) is kept constant.

6.3.1.1 Membrane absorber

For a membrane absorber, m in Equation 6.2 is simply the mass per area of the panel. A common simplification of Equation 6.2 is derived after straightforward algebraic manipulation. This gives the resonant frequency as:

$$f = \frac{60}{\sqrt{md}} \quad (6.12)$$

This is correct when the cavity is filled with air. If the cavity is filled with porous absorbent, then the system is no longer adiabatic, and an isothermal case must be considered below about 500 Hz. In addition, the porosity of the porous absorber should be included although this is a minor effect for more commonly used materials as their porosity is close to unity. Under an adiabatic assumption, Equation 6.12 becomes [8]:

$$f = \frac{50}{\sqrt{md}} \quad (6.13)$$

This formulation holds for oblique incidence when a porous absorbent is in the cavity, because the porous absorbent enforces propagation normal to the front face. For an air cavity without partitions, a new formulation is required for oblique incidence:

$$f = \frac{60}{\cos(\psi)\sqrt{md}} \quad (6.14)$$

where ψ is the angle of incidence.

Unfortunately, these simple formulations for membrane absorbers are often inaccurate. The membrane system is not as simple to model as the perforated absorber. For example, all these assume that the membrane does not support higher order modes at the frequencies of interest. The mass of the membrane is being treated as a single lump mass, and therefore the membrane should move as one like a piston. The effect of bending stiffness is to increase the resonant frequency, but usually Equation 6.2 is dominant. Problems can occur if the membrane is small, because the whole mass may not be able to vibrate freely because it must be secured at the edges. In this case, the actual vibrating mass may be less than expected, and additional losses at the fixings may occur. One solution to this is to attach the edges of the membrane using resilient foam so that the whole membrane can vibrate including the edges. If such a fixing is used, it is important that the cavity remains air tight.

As the angle of incidence increases, there is an increasing chance of bending waves being excited. Consequently, the simple formulations above can breakdown. Unfortunately, the modelling of such bending wave problems is complex as it is very dependent on the construction used.

More complex modelling of panel absorbers does exist [8, 9, 10] but the prediction models presented are not that useful in designing practical surfaces. It is possible to model the plate vibration, and then use a mode matching approach to derive the power absorbed. This is complex, and many parameters concerning real surfaces, such as the mounting conditions of the panel, will not conform to simple conditions that the prediction models use. Consequently, predictions are unlikely to match measurements well. This has already been illustrated in Figure 6.3. For the prediction shown in

Figure 6.3, a transfer function matrix method was used as detailed later. There is a 10 per cent error in the prediction of the peak frequency. In this case, the peak absorption frequency is somewhere between the values given by Equations 6.12 and 6.13.

6.3.2 Losses

So far, the above formulations have only allowed a calculation of the resonant frequency. A proper design method must also allow the absorption coefficient and surface impedance to be determined for all frequencies. To do this, the losses within the device must be modelled. Losses are determined by the resistance term, r_m , in Equation 6.1. For a Helmholtz device with no additional porous absorbent this can be calculated using [2]:

$$r_m = \frac{\rho}{\varepsilon} \sqrt{8\nu\omega} \left(1 + \frac{t}{2a}\right) \quad (6.15)$$

This formulation assumes that the hole radius is not sub-millimetre in size, to ensure it is larger than the boundary layer thickness. An alternative formulation for this resistive term derived by Ingard is often used [3]:

$$r_m = \frac{\sqrt{2\rho\eta\omega}}{2\varepsilon} \quad (6.16)$$

where η is the viscosity of the air, with a value of 1.84×10^{-5} poiseuille. These theoretical equations do not allow for increased resistance that happens if burrs are present. Indeed, Ingard carried out empirical work to show that Equation 6.16 was approximately correct, but taking a value twice as large matches experimental results better. Equation 6.16 is more commonly quoted than Equation 6.15, but for most practical absorbers both are negligible, as is the difference between them! The exception is with devices such as microperforated absorbers where the size of the resistance is critical. For most designs, the losses contributed by Equation 6.15 are very small, and in order to get good absorption it is necessary to add porous material.

Microperforation is rather specialized, so first attention will be focussed on devices with additional porous material and more normal sized holes. The effect of the porous absorbent depends on where it is placed. Ideally, it should be placed where the particle velocity is a maximum. Porous absorption works primarily by viscous losses as sound penetrates the small pores. For this to be maximized, the air motion must be at its greatest, and this is achieved where the particle velocity is largest. For a Helmholtz resonator this means the absorbent being as close to the openings as possible or even in the openings. A balance must be struck, however, as too much absorption in the neck might prevent resonance. The effect of placing an air gap between the perforated sheet and the porous absorbent is to reduce the resistance, and in most cases this will result in a decrease in absorption [5].

For a membrane absorber, the porous absorbent should be just behind the membrane, but it must not touch the membrane. Without the porous absorbent, the primary losses are most likely to come from within the membrane or friction at the fixings between the membrane and the supporting structure. If the porous absorbent behind the membrane is not providing sufficient absorption, perforating the membrane to allow easier access to the porous absorber behind can be done. This then

creates a hybrid Helmholtz-membrane design. Then the design equations should be altered somewhat. The impedance of the membrane alone, z_{mem} , will be a combination of resistance and mass:

$$z_{\text{mem}} = r_{\text{mem}} + j\omega m_{\text{mem}} \quad (6.17)$$

where r_{mem} and m_{mem} are the acoustic resistance and mass of the membrane. Similarly, the impedance of the perforated sheet forming the Helmholtz device, z_{helm} , will be formed from acoustic resistance and mass:

$$z_{\text{helm}} = r_{\text{helm}} + j\omega m_{\text{helm}} \quad (6.18)$$

where r_{helm} and m_{helm} are the acoustic resistance and mass of the perforated sheet. It is necessary to make some assumption about how these impedances interact. The most obvious model is that the impedances act independently and in parallel, then a combined impedance can be derived. The impedance of the device with an air cavity is given by:

$$z = -j\rho c \cot(kd) + \frac{z_{\text{mem}} + z_{\text{helm}}}{z_{\text{mem}}z_{\text{helm}}} \quad (6.19)$$

where d is the cavity depth. To find the resonant frequency of Equation 6.19, the easiest technique is to plot z versus frequency using a numerical tool such as a spreadsheet and inspect for the zero crossing of the imaginary part. Later on, this type of formulation will be discussed in more detail for a microperforated thin membrane. The problem with applying the above formulation is in properly defining the impedance of the membrane.

For a Helmholtz device, the design equations for the case with porous absorbent depend on where the porous layer is located. First some relatively simple formulations are considered, then a more complex treatment using transfer matrixes will be considered. The accuracy of these formulations will be demonstrated later in the chapter.

6.3.2.1 Porous layer right behind perforations

When the porous layer is right in front or behind the perforated plate, then the resistance behaves as though it is actually in the openings. This comes from a consideration of the flow through the device. As sound is squeezed through the holes, the particle velocity is increased. On the other side of the perforated sheet, the flux lines return to a free-field case somewhat gradually; this is shown schematically in Figure 6.15. If the porous layer is within a hole diameter of the perforated sheet, it is assumed that the flux has not yet had time to return to a free field state. Consequently, the resistance added by the porous material, r_m , is altered by fractional open area of the perforated plate (porosity), ε . The resistance is:

$$r_m = \frac{\sigma t_a}{\varepsilon} \quad (6.20)$$

where t_a is the thickness and σ the flow resistivity of the resistive layer. This form is assumed because the volume velocity is reduced by the open area (or porosity) ε , and has not yet had time to recover to a free space value. The key in absorber design is to

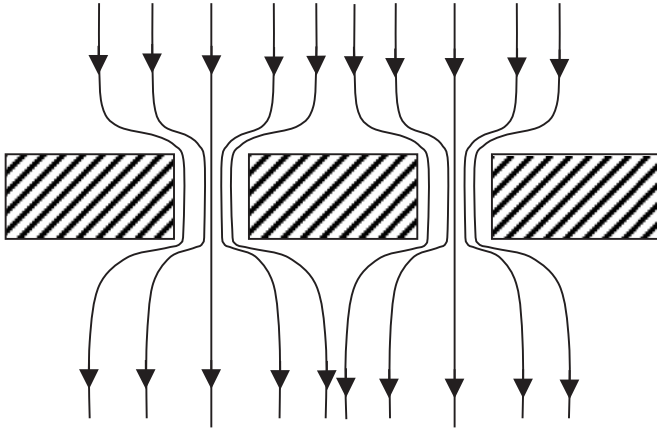


Figure 6.15 Flow through a perforated sheet.

make this resistance in Equation 6.20 as close to the characteristic impedance of air as possible, as this maximizes absorption. If characteristic impedance is achieved at resonance, absorption will be complete. Consequently, a balance between the open area, flow resistivity and absorbent thickness must be struck, while remembering that the resonant frequency of the device is also dependent on the open area of the perforated sheet.

6.3.2.2 Porous layer in the middle of cavity with a perforated covering

It is assumed that the porous material is at least a hole diameter away from the perforated sheet; the materials are not too thick and are also away from the rigid backing. This is not a common situation as it is awkward to construct. As the bulk of the porous layer is away from the perforations, it is assumed that the velocity through the surface is the same as in free space. Consequently, the resistance term is given by:

$$r_m = \sigma t_a \quad (6.21)$$

A more exact formulation would use a full transfer matrix approach as detailed in the following section.

6.3.2.3 More complete solution using transfer matrixes

A full multi-layer solution first calculates the impedance just below the perforated sheet or membrane, and then the effect of the sheet is considered by adding on this impedance. This is a very flexible solution method as it can allow for many different combinations in design. The solution discussed here is split into two forms: the first is when air is immediately behind the perforated sheet and the second when porous absorber backs the perforated sheet.

The first case is shown in Figure 6.16. First, the impedance just behind the perforated sheet is calculated; this can be done to a first approximation using the equations

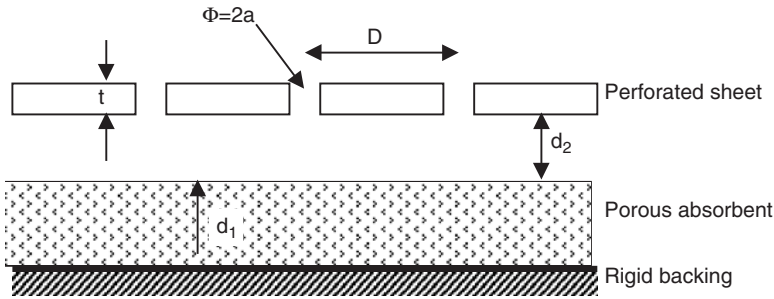


Figure 6.16 Construction for predictions around Equation 6.22.

set out in Section 5.5.1. Consider a simple case of a layer of absorber of thickness d_1 and an air layer of thickness d_2 . The impedance at the top of the absorber is z_1 :

$$z_1 = -jz_i \cot(k_i d_1) \quad (6.22)$$

where z_i is the characteristic impedance and k_i the wavenumber of the porous absorber. The impedance at the top of the air layer and just below the perforation, z_2 , can be found by using a transfer matrix as discussed in Chapter 5.

$$z_2 = \frac{-z_1 j \rho c \cot(k d_2) + \rho^2 c^2}{z_1 - j \rho c \cot(k d_2)} \quad (6.23)$$

The impedance of the Helmholtz absorber, z_3 , is given by using Equations 6.6 and 6.15 [11]:

$$z_3 = \frac{\rho}{\varepsilon} \left(\frac{t}{2a} + 1 \right) \sqrt{8\nu\omega} + (2\delta a + t) \frac{j\omega\rho}{\varepsilon} + z_2 \quad (6.24)$$

where the additional viscous term in Equation 6.6 is ignored as it is generally small.

The second case, with the porous layer next to the perforated sheet was shown in Figure 6.2a. For simplicity, it is assumed that the entire cavity is filled with porous absorber, and the cavity depth is d . This is a common construction because it is simple to make. Two solution methods can be attempted. The most simple is to consider that only plane waves propagating normal to the perforated sheet are present in the porous layer. Then the impedance immediately below the perforated sheet is given by:

$$z_1 = -jz_i \cot(k_i d) \quad (6.25)$$

where z_i is the characteristic impedance and k_i the wavenumber of the porous absorber. Then the mass effect of the perforations can be added, and the effect of open area taken into account to give the surface impedance of the absorber, z_2 , as:

$$z_2 = \frac{1}{\varepsilon} (2\delta a + t) j\omega\rho + z_1 \quad (6.26)$$

The mass and resistance terms due to viscous forces in and around the perforated plate are ignored because they will usually be negligible compared to the term in z_1 .

A more complex solution to this problem allows for the multiple waves propagating in the porous media. The surface is considered in a series of elementary cells of size D by D , each containing one hole. The velocity at the cell boundaries parallel to the perforated sheet is assumed zero. Unless the cavity is actually partitioned, this is only an approximation. This enables the pressure within the cells to be decomposed into a sum of modes within the cell in an analogous way to solving the modes in a room. The impedance below the perforated sheet, z_1 , is then given as a sum over modal terms [11]:

$$z_1 = \frac{z_{0,0} \varepsilon}{\phi} + \frac{4}{\pi} \sum_m \sum_{n, (n \neq 0 \& m \neq 0)} \frac{\nu_{m,n} z_{m,n} J_1^2 \left(\frac{2\pi a}{D} \sqrt{m^2 + n^2} \right)}{\phi(m^2 + n^2)} \tag{6.27}$$

$$z_{m,n} = -j z_i \frac{k_i}{k_{m,n}} \cot(k_{m,n} d) \tag{6.28}$$

$$k_{m,n} = \sqrt{k_i^2 - \frac{4m^2 \pi^2}{D^2} - \frac{4n^2 \pi^2}{D^2}} \tag{6.29}$$

$$\nu_{m,n} = \begin{matrix} 0.5 & m = 0 \text{ or } n = 0 \\ 1 & \text{otherwise} \end{matrix} \tag{6.30}$$

where k_i and z_i are the wavenumber and characteristic impedance of the porous absorber. ϕ is the porosity of the porous absorber, say 0.98 for mineral wool. J_1 is the Bessel function of the first kind and first order. The sum is carried out over all combinations of n and m when both are not equal to zero.

The sum converges as the contributions from higher modes reduce. In fact, in many cases only the plane wave term ($n = 0$ and $m = 1$) need be considered, as the dominant propagation mode in a porous medium will be perpendicular to the perforations due to refraction. This is especially true when high flow resistivity porous materials are used. When only the first term is considered, Equations 6.27–6.30 give similar results to the more simple formulation given in Equation 6.25. Once the impedance, z_1 , immediately below the perforated sheet is known Equation 6.26 can be applied to get the surface impedance of the whole system including the perforated sheet.

6.3.2.4 *Oblique incidence*

For oblique incidence, it can be assumed to a first approximation that the impedance of the Helmholtz absorber will be very similar to the normal incidence value, provided there is a significant amount of porous absorbent in the cavity and/or the cavity is partitioned. With porous material in the cavity, the predominant propagation direction will be normal to the front face due to refraction, and lateral propagation is therefore inhibited. It is the lateral propagation that could change the impedance of the device

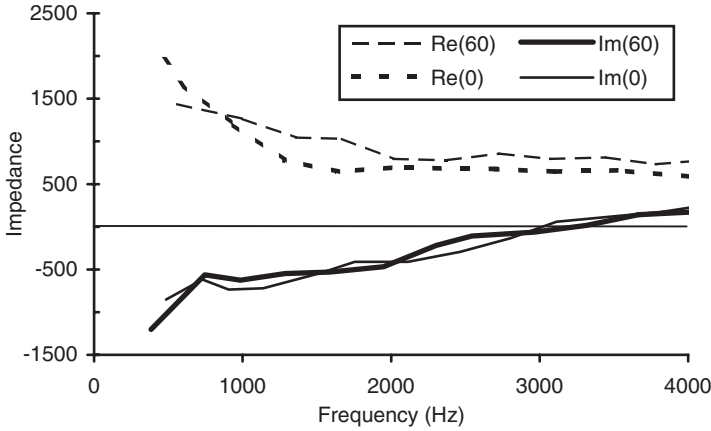


Figure 6.17 Measured impedance for two angles of incidence for a Helmholtz absorber. Angles indicated in legend in degrees (data from Guignouard *et al.* [12]).

at oblique incidences, but this is not normally significant. Figure 6.17 shows the measured impedance for a sample at normal and 60° incidence [12] confirming this assertion. At low frequencies, without partitions, this may become less true as lateral propagation modes become more significant. Any lateral propagation would be expected to decrease the absorption achieved for most angles of incidence.

There is a more complex and complete prediction model for oblique incidence [11]. As the surface is periodic, it is possible to solve the problem with a Fourier decomposition. This method can only produce a solution when the wavelength in air projected onto the surface is an integer multiple of the spacing between the perforations, i.e:

$$ND = \frac{\lambda}{\sin(\psi)} \quad (6.31)$$

where N is a positive integer and ψ the angle of incidence. With this principle, it is possible to carry out a Fourier decomposition into a series of modes within the porous material. Consider the case of a Helmholtz resonator where there the cavity is filled with porous material. The impedance just below the perforated sheet is given by [11, 12]:

$$z_1 = \frac{2}{\pi\phi} \sum_{m=0}^{\infty} \sum_{n=-1, -1 \pm N, -1 \pm 2N, \dots} \nu_{m,n} z_{mn} \frac{J_1^2 \left\{ 2\pi a \sqrt{\frac{m^2}{D^2} + \frac{n^2}{N^2 D^2}} \right\}}{m^2 + \frac{n^2}{N^2}} \quad (6.32)$$

$$z_{mn} = -j\rho c \frac{k_i}{k_{mni}} \cot(k_{mni}d) \quad (6.33)$$

$$k_{mni} = \sqrt{k_i^2 - \chi} \quad (6.34)$$

$$\chi^2 = \left(\frac{2\pi m}{D}\right)^2 + \left(\frac{2\pi n}{ND}\right)^2 \quad (6.35)$$

where the subscript i indicates that the wavenumber and impedance apply to the porous layer. The porous material has a depth d ; ϕ is the porosity of the porous absorber and $\nu_{m,n}$ was defined in Equation 6.30. Once z_1 has been evaluated, Equation 6.26 can be applied to get the impedance of the surface above the perforated sheet at the front face of the absorber.

6.4 Example calculations

6.4.1 Slotted Helmholtz absorber

Kristiansen and Viglen [6] carried out impedance tube measurements on a slotted absorber which allows the accuracy of the above formulations to be partially tested. The absorber had an open area of about 24 per cent; the slots were 15 mm deep and 10 mm wide; the cavity depth was 150 mm and a material with an air flow resistance of 86 Pa s m^{-1} was attached to the bottom of the slotted plate. Script 6.2 predicts the scattering from the slotted absorber, and it is compared with the experimental data in Figure 6.18. Using the transfer matrix method with Equations 6.10, 6.11, 6.20 and 6.1 gives accurate results as shown. Adding the resistance term, Equation 6.15 or 6.16 makes negligible effect to the predictions, changing the absorption coefficient by less than a hundredth.

A simple calculation of the peak of absorption using Equations 6.4 and 6.10 yields a predicted resonant frequency about 100 Hz greater than measured. This shows the power and usefulness of the transfer function matrix procedure for Helmholtz devices. Similar accurate results were also found by Ingard when he examined circular perforations [3] with a thin resistive layer behind the perforated sheet.

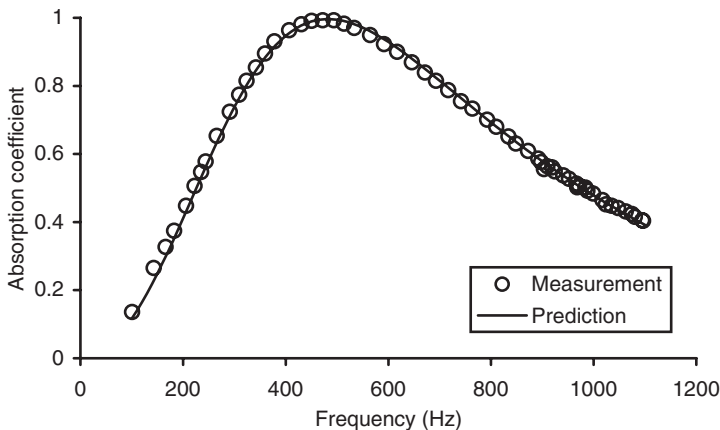


Figure 6.18 Predicted and measured normal incidence absorption coefficient for a slotted Helmholtz absorber (measured data from Kristiansen and Viglen [6]).

6.4.2 Porous absorber filling the cavity

Figure 6.19 compares the predicted and measured normal incidence impedance for a Helmholtz absorber. These use measurements by Guignouard *et al.* [12] using a two-microphone free field method to obtain both normal incidence and 60° incidence results. The two microphone technique is described in Chapter 3. Figure 6.20 shows the predicted absorption coefficients for three arrangements: a porous absorber, a porous absorber faced with a porous sheet with and without an air gap between the porous absorber and the rigid backing. In addition, a measurement for one of the configurations is given. The predictions are for normal incidence, and used a transfer

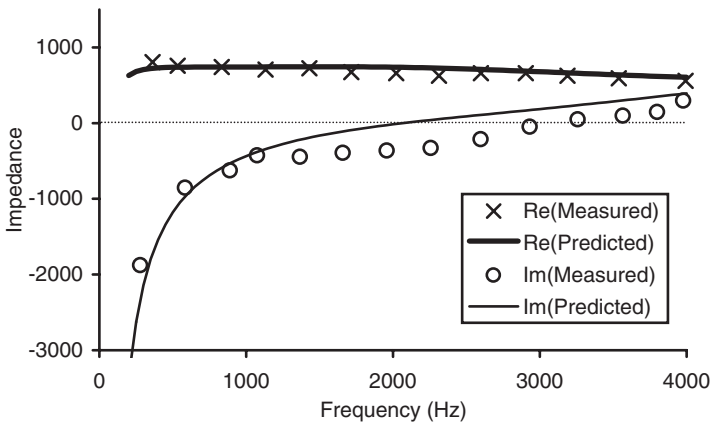


Figure 6.19 Impedance predicted and measured for a Helmholtz absorber (measurements from Guignouard *et al.* [12]).

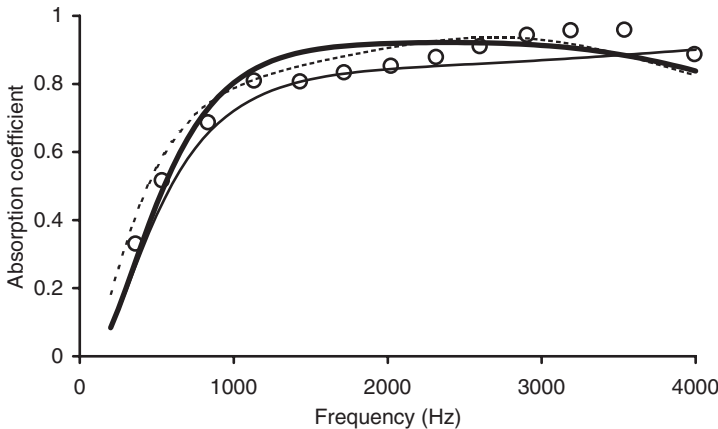


Figure 6.20 Absorption coefficient predicted for three absorbers, plus measurement for one case from Guignouard *et al.* [12] (some interpolation of the measured impedance data was used to obtain the measured absorption coefficient): — Porous absorber only, predicted; — Porous absorber with perforated facing, predicted; - - - Porous absorber with perforated facing and air gap, predicted; o Porous absorber with perforated sheet, measured.

function matrix technique given in Equations 6.22–6.24. The more complex modal decomposition model is unnecessary because the simple model gives satisfactory results. The porous absorber had a flow resistivity of $70,000 \text{ rayl m}^{-1}$ and was 3 cm thick. For the perforated sheet, the holes had a radius of 2.5 mm, the open area was 17.5 per cent and the thickness was 0.75 mm. The prediction model gives reasonable accuracy.

6.5 More complicated constructions

Having set out the design methodology for the most common designs, more complex designs and recent innovations will now be discussed. Much can be gained from application of the simple resonator design as discussed previously, but more complicated designs do exist. In trying to decide whether to use the complex designs, the trade-off lies mainly between acoustic performance and cost of construction. After all, a piece of porous material covered with a perforated sheet is relatively cheap to produce. Once more complex designs are considered, like large-scale microperforation or complex neck plates, the cost of the device will naturally increase. Consequently, the designs discussed in the following sections are only really needed where space is a particular premium, or where special requirements such as transparency need to be achieved.

6.5.1 *Double resonators*

The problem with resonant absorbers is that they have a relatively limited bandwidth. It is common to have to cover a greater frequency range than can be achieved by a single resonator alone. One possibility is to stack a high frequency Helmholtz device in front of a low frequency device. The disadvantage of this is that the surfaces become very deep, and depth is often restricted by non-acoustic constraints. This double system can be most easily modelled as a transfer function matrix. Such a double design was a standard construction used by the British Broadcasting Corporation for many decades in their studios.

6.5.2 *Microperforation*

If the perforations of a Helmholtz resonator are made small enough, then losses will occur due to viscous boundary layer effects in the perforations. To achieve this the perforations must be sub-millimetre in diameter so that they are comparable to the boundary layer thickness. Then it is possible to achieve absorption without using a porous material. This becomes a useful technique because the perforated sheet and the back of the cavity can be made from transparent acrylic or glass and so forming a clear absorber. A commercial realization of this was discussed in Section 6.2.4. From an academic viewpoint, this is a neat device because the physics of the system is very simple and so accurate predictions are readily achieved. A microperforated device was reported by Cremer and Müller [13], where a multi-layer system originally devised by Rschevkin is briefly outlined. It was Maa, however, who appears to have carried out the significant recent development of the concept [14].

The theoretical formulations begin by considering the sound propagation within a cylindrical hole. This problem is well established and is the theoretical foundation of

much work on microscopic propagation in porous absorbents. In fact, the earliest work was probably done by Lord Rayleigh. For a tube which is short compared to wavelength, it can be shown that the specific acoustic impedance of the tube is given by [15]:

$$z_1 = j\omega\rho t \left(1 - \frac{2J_1(k'\sqrt{-j})}{k'\sqrt{-j}J_0(k'\sqrt{-j})} \right)^{-1} \quad (6.36)$$

$$k' = a\sqrt{\frac{\rho\omega}{\eta}} \quad (6.37)$$

where J_0 and J_1 are the Bessel functions of the first kind, of zero and first order respectively, t the tube length and a the tube diameter.

To get the specific acoustic impedance of the perforated sheet, Equation 6.36 must be divided by the plate open area ε . Maa details approximate solutions to the above equation, but with the advent of modern numerical tools on computers, it is as easy to deal with Equation 6.36 directly as to use an asymptotic solution. To deal with the Helmholtz resonator configuration, a transfer matrix must be used to get the surface impedance, z_h :

$$z_h = \frac{z_1}{\varepsilon} - j\rho c \cot(kd) + \frac{\sqrt{2\omega\rho\eta}}{2\varepsilon} + \frac{j1.7\omega\rho a}{\varepsilon} \quad (6.38)$$

The second term is the impedance of the cavity which is assumed to be d deep and to be filled with air. The final term is the end correction to allow for the radiation reactance of the tube. The penultimate term is the radiation resistance for an orifice. Maa uses the formulation from Ingard [3] given in Equation 6.16 for the radiation impedance. Once the impedance is known, the normal incidence absorption coefficient can be readily obtained. These equations are most applicable for common sound intensities; for large intensities the impedance will change due to non-linear effects.

Figure 6.21 compares the prediction according to Equation 6.38 to measurements presented by Maa [15]. The hole separation is 2.5 mm, the hole radius 0.1 mm, the plate thickness 0.2 mm and the cavity depth 6 cm. Reasonable agreement between measurement and prediction is achieved, although not as good as given in the paper. Script 6.3 in Appendix B gives the code for the predictions. The predictions show sharp peaks due to second order resonances. These resonances are relatively narrow in frequency, and so if the results are summed in one-third octave bands, the second order peaks appear less significant.

The problem with these systems is getting broadband absorption. As it relies on resonance, the absorption will be limited to low to mid-frequencies, whereas an ideal clear absorber would probably be one that covered the entire speech frequency range. While in theory the speech frequencies could be covered, in reality the size of holes required is so small as to make the production difficult. To extend the bandwidth, Maa and others have shown that multiple layers can be used. Each layer is then tuned to a different frequency range. This can then be solved by a transfer matrix solution taking each layer in turn. The problem with double layer devices is they increase the

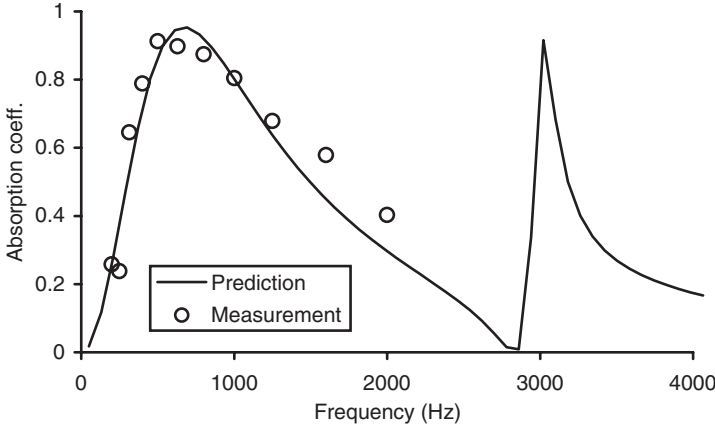


Figure 6.21 Predicted and measured absorption coefficient for a microperforated Helmholtz absorber (measurement data from Maa [15]).

depth and cost of the device, both of which are usually under strict restrictions by non-acousticians.

For oblique incidence, the sound in the cavity travels at an angle to the normal, in fact the same angle as the angle of incidence. Consequently, Equation 6.38 should be altered to:

$$z_h = \left[\frac{z_1}{\varepsilon} - j\rho c \cot(kd) + \frac{\sqrt{2\omega\rho\eta}}{2\varepsilon} + \frac{j1.7\omega\rho a}{\varepsilon} \right] \cos(\psi) \tag{6.39}$$

where ψ is the angle of incidence. The effect of this is to increase the resonant frequency, and so raise the frequency at which absorption is significant. For large angles of incidence, however, the lateral coupling between adjacent holes within the cavity will become significant. This might be expected to lower the absorption for most if not all frequencies. Consequently, in a diffuse field, the absorption would be expected to be broader, but the maximum absorption would be lowered.

As discussed previously, it is possible to combine membrane and Helmholtz mechanisms in a single device. Kang and Fuchs [16] discussed the construction of such a device which was a microperforated plastic membrane; the theory was also applied to glass fibre textiles. This treats the membrane and Helmholtz effects in parallel as discussed previously around Equation 6.19. Good agreement was found between impedance tube and reverberation chamber measurement, and the transfer matrix theory. An example result is shown in Figure 6.22 where random and normal incidence absorption coefficients are compared. The device had a mass per unit area, $m = 0.14 \text{ kg m}^{-2}$; thickness $t = 0.11 \text{ mm}$; hole radius $a = 0.1 \text{ mm}$; hole spacing $D = 2 \text{ mm}$ and a cavity depth of 10 cm. As with the previous microperforated systems, the random incidence absorption is less than the normal incidence absorption, and a shift in frequency is also seen. Using a double layer construction can increase the bandwidth of the device.

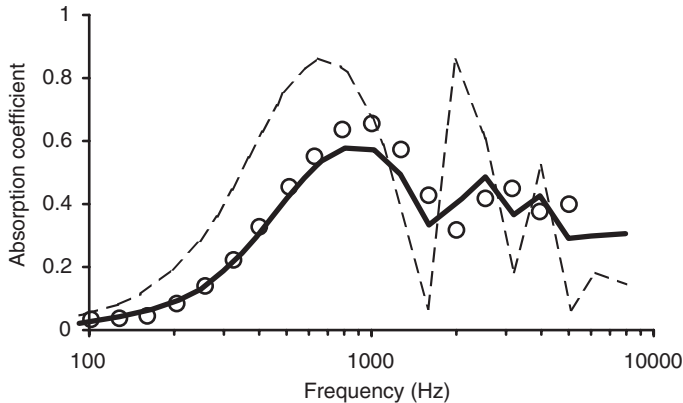


Figure 6.22 Measured and predicted absorption coefficient for a microperforated membrane for different incident sound conditions as shown in legend. \circ Measured, random incidence; — Predicted, random incidence; - - - - Predicted, normal incidence (after Kang and Fuchs [16]).

6.5.3 Lateral orifices

An alternative method to gaining clear absorption is to elongate the neck of the absorber laterally. Again the principle is to exploit viscous boundary layer losses in narrow openings and so remove the need for resistive material. Randeberg developed such a technique [17], and Figure 6.23 shows the device. The front and rear plates are perforated with reasonably large perforations (1–3 mm in diameter), the viscous losses occur in the propagation parallel to and between the plates. Strict control of the plate spacing is required, which must be of the order of the boundary layer thickness, about 0.2 mm. This spacing must be achieved to a high precision, as the results by Randeberg demonstrate that a change in spacing of 0.05 mm makes significant difference to the absorption obtained. Predicting the absorption of the system is complicated and requires a finite difference solution of the Navier–Stokes equation. A simple solution using a calculation of vibrating mass based on the volume of the openings and the elongated orifice does not work.

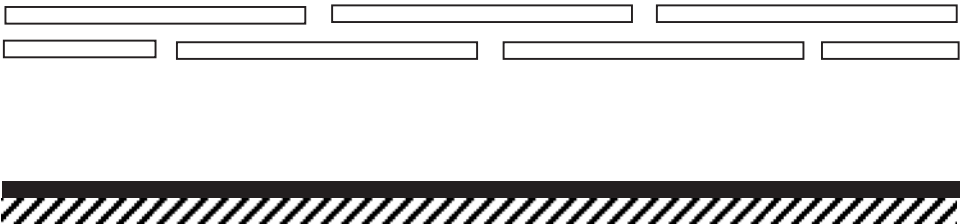


Figure 6.23 A Helmholtz absorber which uses lateral space between two perforated sheets as part of the neck of the device.

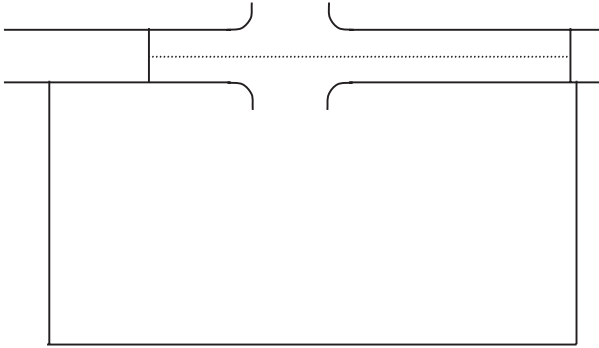


Figure 6.24 A Helmholtz absorber with a slotted neck pate and a resistive foil (shown dotted) freely floating in the slot.

The device gives very similar performance to the microperforated systems discussed previously, and as such offers a different construction rather than improved acoustic performance. Again the absorption is limited to low to mid-frequencies.

Mechel [18] has also suggested the use of lateral orifices, but in a different construction. The type of construction suggested is shown in Figure 6.24. The lateral orifices are narrow enough to have significant viscous and thermal losses, while also creating additional resonances where absorption can be high. The two side branches are made unequal to facilitate a broadening of the absorption bandwidth for normal incidence by generating multiple resonant frequencies. For the orifices to have a significant effect on the system, however, it is necessary to increase the impedance in the neck. Mechel suggests the use of a limp resistive foil. This has the advantage that the perforated sheets do not have to be held very precisely sub-millimetre distances apart, as was the case for Randeberg's design. Disadvantages of the system lie in the complexity of the construction. Measurements are needed to confirm the performance of this type of device.

6.6 Summary

This chapter has outlined the design principles, typical applications and theoretical models for resonant absorbers. Resonant absorbers play a crucial role in improving acoustic conditions exploited for controlling modes, reverberation and noise levels. The next chapter details a couple of absorbers that did not fit neatly into other chapters: seating and absorption from Schroeder diffusers.

6.7 References

- 1 L. E. Kinsler, A. R. Frey, A. B. Coppens and J. V. Sanders, *Fundamentals of Acoustics*, 4th edn, John Wiley & Sons, 284 (2000).
- 2 A. W. Guess, "Result of impedance tube measurements on the acoustic resistance and reactance", *J. Sound Vib.*, **40**, 119–137 (1975).
- 3 U. Ingard, "On the theory and design of acoustic resonators", *J. Acoust. Soc. Am.*, **25**, 1037–1061 (1953).

- 4 L. Cremer and H. A. Müller, *Principles and Applications of Room Acoustics*, Applied Science Publishers translated by T. J. Schultz, 187 (1978).
- 5 W. A. Davern, “Perforated facings backed with porous materials as sound absorbers – an experimental study”, *Appl. Acoust.*, **10**, 85–112 (1977).
- 6 U. R. Kristiansen and T. E. Vigran, “On the design of resonant absorbers using a slotted plate”, *Appl. Acoust.*, **43**(1), 39–48 (1994).
- 7 J. M. H. Smits and C. W. Kosten, “Sound absorption by slit resonators”, *Acustica*, **1**, 114–122 (1951).
- 8 4, op. cit., 191.
- 9 R. D. Ford and M. A. McCormick, “Panel sound absorbers”, *J. Sound Vib.*, **10**, 411–423 (1969).
- 10 F. P. Mechel, “Panel absorber”, *J. Sound. Vib.*, **248**(10), 43–70 (2001).
- 11 J. F. Allard, *Propagation of Sound in Porous Media: Modelling Sound Absorbing Materials*, Elsevier Applied Science, Chapter 10 (1993).
- 12 P. Guignouard, M. Meisser, J. F. Allard, P. Rebillard and C. Depollier, “Prediction and measurement of the acoustical impedance and absorption coefficient at oblique incidence of porous layers with perforated facings”, *Noise Control Engineering Journal*, **36**(3), 129–135 (1991).
- 13 4, op. cit., 204–206.
- 14 D.-Y. Maa, “Microperforated-panel wideband absorbers”, *Noise Control Engineering Journal*, **29**(3), 77–84 (1984).
- 15 D.-Y. Maa, “Potential of microperforated panel absorber”, *J. Acoust. Soc. Am.*, **104**(5), 2861–2866 (1998).
- 16 J. Kang and H. V. Fuchs, “Predicting the absorption of open weave textiles and microperforated membranes backed by an air space”, *J. Sound Vib.*, **220**(5), 905–920 (1999).
- 17 R. T. Randeberg, “A Helmholtz resonator with a lateral elongated orifice”, *Acustica*, **86**, 77–82 (2000).
- 18 F. P. Mechel, “Helmholtz resonators with slotted neck plates”, *Acustica*, **80**, 321–331 (1994).

7 Miscellaneous absorbers

This chapter deals with some absorbers that do not easily fit into categories, but are nevertheless important to airborne acoustics. The first subject is seating and audience absorption. In many auditoria, the seating and audience form the main absorption in the room, and consequently being able to correctly measure and predict the absorption coefficient of the seating and audience is very important. The second subject is how to make efficient absorbers from Schroeder diffusers. Researchers started by looking into why the absorption from Schroeder diffusers could be large, and ended up inventing a new style of absorber.

7.1 Seating and audience

The reverberation time in a hall is dominated by the absorption of the seating and audience; it is essential that these can be measured or predicted accurately in the early stages of design. Section 3.4.1 discussed how the absorption of seating should be measured, and so this discussion concerns the actual values of absorption coefficients that are available in literature and what they mean.

Beranek [1] and Kosten [2] have both produced data for the average absorption coefficients of occupied and unoccupied seating. The data was averaged from measurements in many halls and is useful for estimating reverberation time in the early design stages. The use of average data is not reliable for later design work, however, as there is too much variation in the construction for modern seating and consequently, seating absorption coefficients can vary greatly. Figure 7.1 shows the spread and mean of the absorption coefficients measured by Davies *et al.* [3] for nine seating types. Also shown are the average values from Beranek [1] which are in common use. Considering the range of the current data, the agreement between the mean measured by Davies *et al.* and Beranek's values is quite good up to 1 kHz. At higher frequencies, as Bradley [4] explains, Beranek's absorption data is quite possibly affected by differences in air absorption between the many halls measured. Discrepancies may also arise, because modern theatre seating has slightly more padding than the older ones forming the bulk of Beranek's data.

For occupied seating, measurements by different authors are much more similar [5]. It appears that the absorption of occupied upholstered seats is dominated by the absorption of the occupants and does not vary much over different seat types. Whether occupied or not, the absorption coefficients have the characteristic curve shape of a porous absorber.

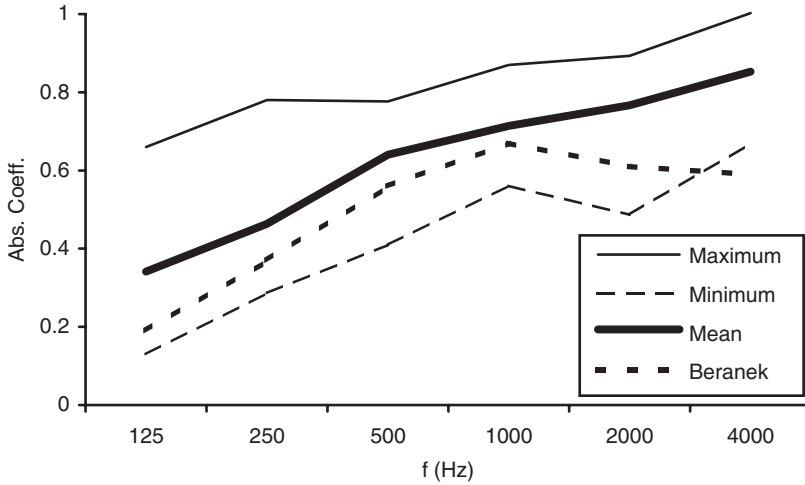


Figure 7.1 The variation in absorption coefficient for audience seating from Davies *et al.* [3] shown as minimum, maximum and mean. Also shown the mean values from Beranek [1].

Figure 7.2 shows the effect of varying the row spacing, over the small range commonly found in auditoria, on the absorption coefficient. Increasing the row spacing decreases the absorption coefficient. Figure 7.3 shows the effect of carpet on the absorption coefficient. The addition of carpet even below seating significantly increases the absorption and so is generally avoided in large concert venues.

Figure 7.4 compares occupied and unoccupied absorption coefficients for two seating types. Although it is normal practice to try and make the absorption of seating the same whether occupied or not, this is not entirely successful as shown in Figure 7.4.

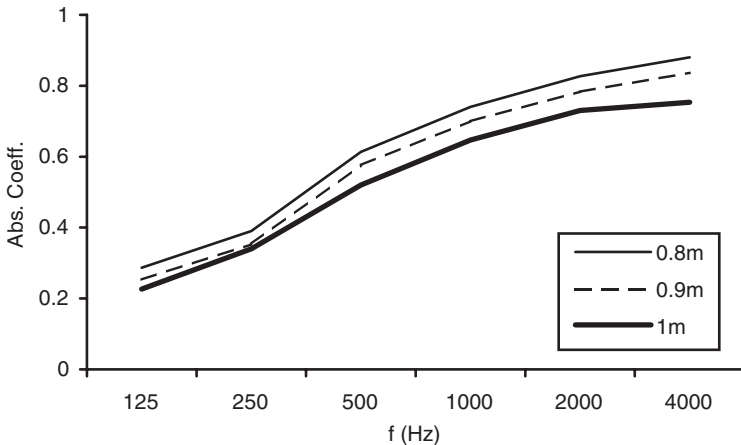


Figure 7.2 Effect of row spacing on the absorption coefficient for a large block of seating (after Davies [5]).

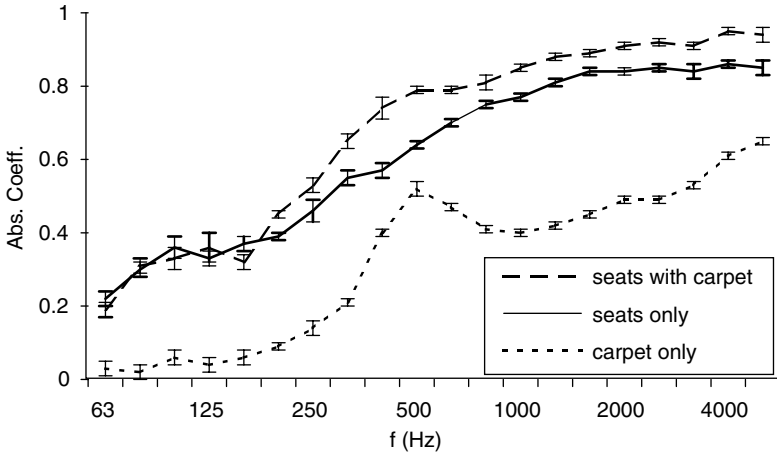


Figure 7.3 Variation of absorption coefficient for seating with and without carpet (data from Davies [5]).

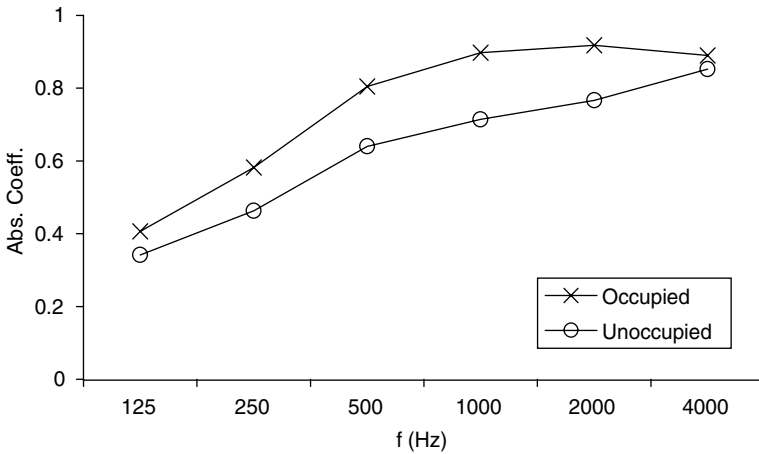


Figure 7.4 Variation in absorption coefficients between occupied and average unoccupied seating (data adapted from Davies *et al.* [3]).

On a related issue, recently Hidaka *et al.* [6] have suggested that draping the seats with felt is a method by which occupied conditions can be simulated during the testing of halls. This appears to be successful at mid-frequencies, but at low frequencies (100–200 Hz) it does not always work because it interferes with the seat dip effect [7, 8].

7.2 Absorbers from Schroeder diffusers

Numerous pictures and sketches of Schroeder diffusers can be found in Chapter 9, for example Figure 9.1. The Schroeder diffuser was designed to diffuse rather than absorb sound, although for sometime there has been anecdotal evidence of absorption. In

recent years, some concerted scientific studies have been able to determine the source of the absorption, and even to show how to turn these diffusers into good absorbers. By changes in geometry and design, it is possible to change a Schroeder surface from a low absorption diffuser to a high absorbing surface. This is of great concern for diffuser installation, as it is very easy to make a high absorbing surface through bad workmanship. Section 9.8 discusses some general principles to achieve low absorption from Schroeder diffusers. What is discussed below, is the mechanism of the absorption, and how this can be exploited to form a good absorber.

When Marshall and Hyde [9] implemented their revolutionary use of Schroeder diffusers in the Michael Fowler Centre, they used rather shallow and wide wells. This was born out of a desire to achieve moderate diffusion, but also because of concern about the diffusers causing excess absorption. Dramatic levels of absorption from Schroeder diffusers were measured by Fujiwara and Miyajima [10] in 1992, the absorption coefficient ranging from 0.3 to 1, and at that time this absorption could not be explained. Fujiwara and Miyajima [11] later reported that the quality of construction was to blame for some of the excess absorption, to achieve low absorption requires good workmanship. Commins *et al.* [12] experimentally investigated the absorption characteristics of a Schroeder diffuser and found values peaking at 0.5. They showed that by slopping the bottom of the diffuser wells, the absorption could be reduced. In 1983, D'Antonio made the first absorption measurements of a commercial QRD[®] with seven 86.4 mm wide wells, with a maximum depth of 196.9 mm. The average absorption coefficient was 0.24 between 125 and 4000 Hz, with a maximum value of 0.35 at 500 Hz.

Although workmanship can explain the excess absorption in many cases, even diffusers constructed to a high standard can have absorption coefficients higher than expected. It was to be anticipated that resonant absorption would occur at the $\frac{1}{4}$ wave resonances in the wells, but the absorption measured is too high to be explained by $\frac{1}{4}$ wave resonance alone. It was Kuttruff [13] who first postulated energy flow between the wells as a probable cause for this excess absorption, although his theoretical model could not predict the high absorption measured by others. Mechel [14] thoroughly discussed the theoretical basis for the absorption effect, and although his studies lacked direct experimental verification, the prediction model developed was shown by others to be accurate. Wu *et al.* [15] brought together measurement and Mechel's prediction model to provide evidence that the energy flow or strong coupling between the wells was indeed responsible for the high absorption. This mechanism is described in the following section.

7.2.1 Energy flow mechanism

Consider a pure tone wave incident onto a Schroeder diffuser. For simplicity consider just two neighbouring wells. Furthermore, consider this to be a frequency where one well is in resonance, and the neighbouring well is not, as illustrated in Figure 7.5. The energy at the mouth of the resonating well will be much greater than that of the non-resonating well. This means that there will be energy flow from the resonating well to the well that is not resonating. Consequently, around the entrances to the wells there is high particle velocity. Indeed, Fujiwara *et al.* [16] showed that the particle velocity is up to 14 times greater at the mouth of Schroeder diffuser wells compared to the incident field. As sound moves around the front of the fins, from one well to the next,

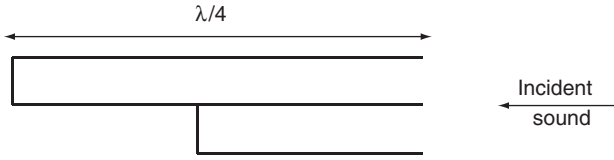


Figure 7.5 Two wells of a Schroeder diffuser.

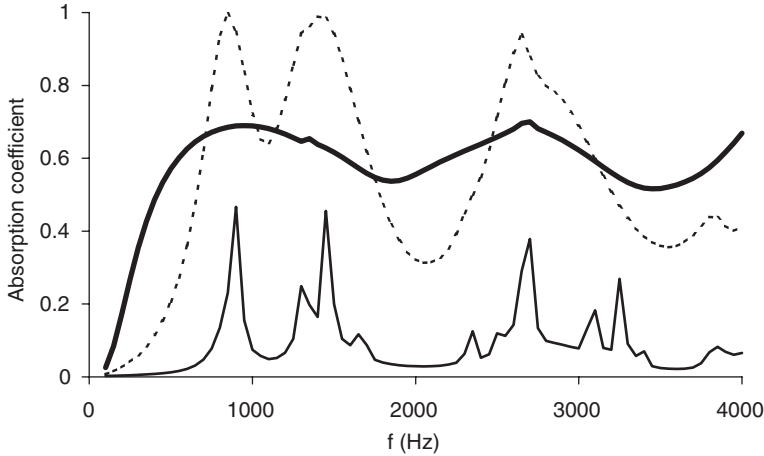


Figure 7.6 Normal incidence absorption coefficient for a quadratic residue diffuser with narrow wells, showing dependence on whether there is a covering at well entrance and what the flow resistance of the covering is. — No covering, Covering of 65 rayls, ——— Covering of 550 rayls.

excess absorption occurs. This is the source of the additional absorption in Schroeder diffusers and occurs even in properly constructed structures.

Knowing that the front face of the diffuser is a region of high particle velocity, it makes sense to place resistive material at the well entrance if the desire is to make an absorber. Mechel [14] demonstrated that resistive layers at the well entrances turn these diffuser structures into potentially useful and practical absorbers. Figures 7.6 and 7.7 show the absorption coefficient and surface impedance for a profiled structure with and without a resistive layer. Two different resistive layers of different flow resistance are illustrated. The effect of the resistive layer is to broaden the resonant peaks, and therefore generating absorption over a greater bandwidth. It also increases the impedance closer to the characteristic impedance for air, and thereby gains more absorption. The resistive layer can be made from wire mesh, cloth or any material with an appropriate acoustic resistance. The advantage of using wire mesh is that the absorber is then washable and durable, which can be useful in some applications.

The resistance of the covering must be such that the total resistance of the wells are close to the characteristic impedance. Too large a resistance leads to an overly damped system and the peaks of absorption are significantly lowered. This is illustrated in Figures 7.6 and 7.7. Too little resistance (no covering) leads to an uneven

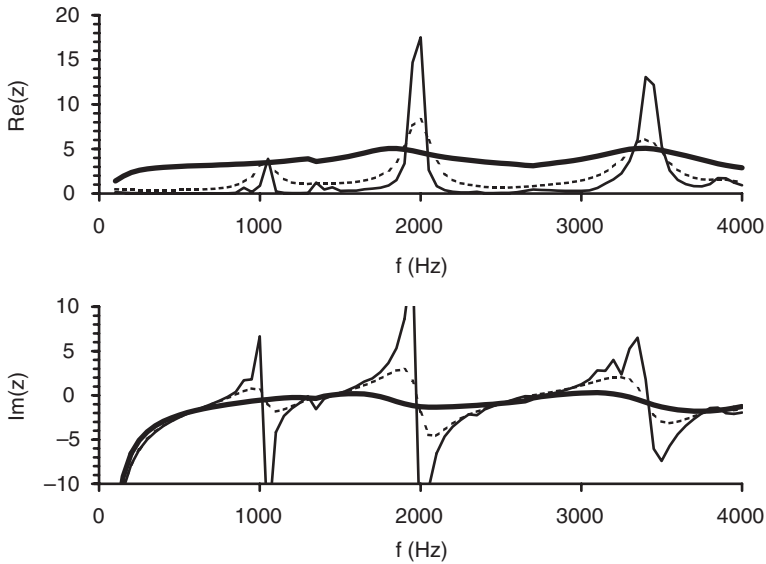


Figure 7.7 Normal incidence surface impedance for a quadratic residue diffuser with narrow wells showing dependence on whether there is a covering at the well entrance and what the flow resistance of the covering is. — No covering; Covering of 65 rayls; ——— Covering of 550 rayls.

performance, too much resistance (550 rayls) leads to over damping, whereas 65 rayls gives the highest peak absorption.

7.2.2 Boundary layer absorption

When the wells of a Schroeder surface become narrow, then the losses at the well walls, due to viscous boundary layer effects can become significant. This absorption can be exploited to produce greater absorption, but the role of the resistive layer must be considered. The key to obtaining a high absorption is that the combination of the resistance of the covering material and the resistance due to losses at the well walls should approach the characteristic impedance of air. If the wells are wide, a high resistance will be needed from the covering material to compensate for the lack of boundary layer absorption. Similarly, if the walls of the wells are rough, then there will be more boundary layer absorption than with a smooth material, and this must be allowed for in the design.

7.2.3 Absorption or diffusion

It is possible to construct Schroeder surfaces to maximize the absorption or maximize the diffusion. Although the surface used to produce high absorption has the same ancestry as those used to disperse sound, crucial design differences result in radically different absorption properties. The two different design remits are contrasted in

Table 7.1. As indicated in Table 7.1, measurements show that 2D surfaces usually absorb more than 1D surfaces as shown in Figure 9.37. The reason for this is probably twofold:

- 1 There are often a greater number of well depths in a 2D diffuser compared to a 1D surface. This means that there are more quarter wave resonances in the 2D surface, leading to more frequencies at which resonance is occurring. This means that the absorption due to quarter wave resonance is significant for more frequencies, and the energy flow between the wells is also greater leading to more losses.
- 2 There is a greater surface area of well boundaries in the 2D diffuser compared to the 1D surface. It is at these boundaries that viscous boundary layer losses occur. Consequently, it is expected that the greater the boundary area, the greater the absorption (unless a high flow resistivity covering is used).

Some of the other features summarized in Table 7.1 are discussed in the following sections.

Table 7.1 Construction differences between Schroeder diffusers and absorbers

	<i>Schroeder surface for absorption</i>	<i>Schroeder surface for diffusion (minimal absorption)</i>
Well width	Usually narrow to exploit viscous boundary layer losses	Usually >2.5 cm to minimize boundary layer losses
Covering	Key to good absorption. Covering should be chosen so surface resistance is $\approx \rho_0 c$ when added to well resistance to maximize absorption	Should not be covered. If covering unavoidable, use low flow resistivity material away from well entrances
1D versus 2D	2D surface often gives more absorption	2D surface gives hemispherical dispersion, 1D surface diffuses in a single plane
Number of different depth wells, N	Determined by the need to have a sufficient number of quarter wave resonances in absorption bandwidth	A larger N usually makes a better diffuser
Depth sequence	Well depths should be chosen to evenly distribute well resonances across absorption bandwidth, best done using numerical optimization	Chosen to maximize dispersion, best done using numerical optimization Narrow period widths should be avoided
Deepest well depth	Determines low frequency limit of absorption	Determines low frequency limit of diffusion, except when period width is small
Construction Mass elements (addition of perforated sheets or membranes)	Well sealed, no slits Can be used to lower bandwidth of absorption	Well sealed, no slits Can be used to lower bandwidth of diffusion
Well sides	Can be rough	Should be smooth

7.2.4 Depth sequence

An optimum depth sequence for diffuse reflections does not necessarily produce the best absorption. It is possible to produce a set of depths that produces a better absorber, than one based on the quadratic residue sequence (see Chapter 9 for definitions of different number sequences). This is done by using a set of well depths which produce more resonance frequencies, distributed more evenly in frequency, and optimally arranging to maximize energy flow between the wells. Mechel [14] was the first to suggest this; he discussed how using a primitive root sequence to determine the well depths of the structure could result in a better absorber than the more common quadratic residue sequence. This is because the primitive root sequence generates more different well depths than a quadratic residue sequence. The simple procedure outlined below works even better, as the primitive root sequence does not evenly space resonant modes in frequency. Another possibility is to use a numerical optimization to find the best well depth sequence. This can follow the principles outlined for diffuse reflection optimization outlined in Chapters 9 and 10. The optimization can be tasked with maximizing the average absorption coefficient across the bandwidth of interest. As with diffuse reflection optimization, this is a slow and moderately complex procedure.

The simple procedure for determining the well depths works by examining the resonant frequencies of the wells. To a first approximation, neglecting viscous boundary layer losses in the well, each well is a quarter wave resonator with resonant frequencies f given by:

$$f = \frac{(2m - 1)c}{4d_n} \quad m = 1, 2, 3 \dots \quad (7.1)$$

where d_n is the depth of the n th well and c the speed of sound.

To maximize the absorption it is necessary to evenly space these resonant frequencies over the design bandwidth avoiding degenerate modes – modes with similar resonant frequencies. This can be simply achieved by a trial and error process using a calculation tool such as a spreadsheet. Once the depths are determined, it is necessary to order them to maximize the losses due to energy flow between the wells. To achieve this, wells causing adjacent in-frequency resonances should not be physically next to each other. This can be done quickly by hand.

Figure 7.8 compares the performance of an absorber made following this simple design method to an absorber produced using a numerical optimization [15]. The performance of the absorber using the simpler design procedure is good. As might be expected the optimization gives slightly better results, but that design involves considerably more computation and encoding effort. The resonant frequencies used during the simple design are also marked as vertical dashed lines. The drop at high frequencies >2.5 kHz occurs due to lack of resonances in the region above 3 kHz (beyond the frequency range shown in the figure). To illustrate that the ordering of the wells is important, Figure 7.8 also shows the results when the absorber is designed using the simple design method, but has the wells stacked in ascending order. There is considerably less absorption at some frequencies, demonstrating the importance of exploiting the scattering by ordering wells properly.

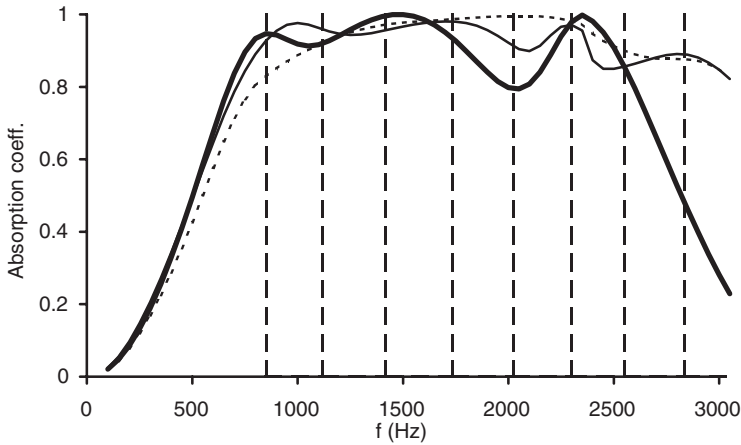


Figure 7.8 Profiled absorbers using different methods to determine the depth sequence. ----- Simple design method; ————— Designed using numerical optimization; ————— Simple design method, ascending well order. Vertical lines indicate resonant frequencies for simple design method (data from Wu *et al.* [15]).

7.2.5 Use of mass elements

High absorption at low frequencies is the most difficult to achieve. Consequently, an important challenge is to get more absorption bandwidth from a given profiled absorber depth. Interestingly, in the paper by Fujiwara and Miyajima [11], it was reported that poorly constructed structures could provide high absorption below the lowest resonant frequency. It is speculated that this additional absorption came from cracks in the well bottoms forming Helmholtz resonators with air cavities behind. This inspired the idea that using perforated plates in some wells could significantly extend the absorption range towards the lower frequencies by adding mass to the system and so lowering the resonant frequency. Another possibility would be to use membranes to act as limp mass elements. A typical construction is shown in Figure 7.9.

Fujiwara *et al.* [16] were the first to publish measurement results on a structure with Helmholtz resonators in the wells, adding mass and so getting better absorption at low frequencies. Wu *et al.* [17] took this work further by producing a prediction model validated against measurement and some basic design methodologies. The simple concept of spacing resonant frequencies, as discussed in Section 7.2.4, can be used again, although predicting the resonant frequencies is more awkward with mass elements. In addition, multiple resonances from each of the wells need to be considered.

Wu *et al.* [17] found that wells with perforations and variable depth wells without perforations are needed to get a wide enough range of resonant frequencies. Both well types are shown in Figure 7.9. The holes of the perforations must be carefully chosen. If they offer significant resistance, it may be necessary to lower the resistance of the resistive material to achieve good absorption. Furthermore, the added mass within the perforations makes it difficult to keep the reactance of the impedance small at high frequencies and so too many wells with perforations make it difficult

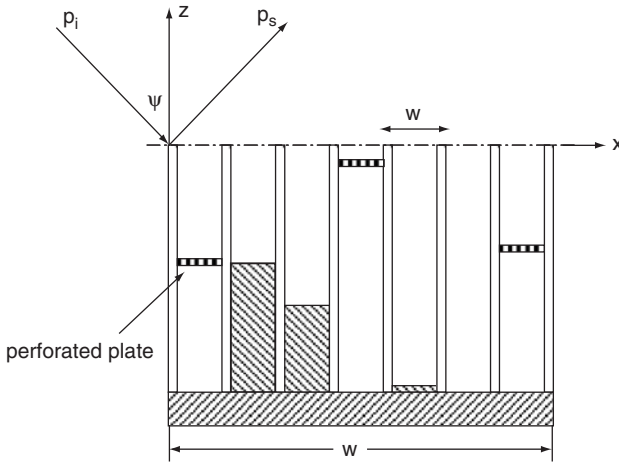


Figure 7.9 One period of a profiled sound absorber with perforated plates (adapted from Wu *et al.* [15]).

to achieve high frequency absorption. These devices can produce greater absorption than a set of standard Helmholtz resonators stacked next to each other, because of the multiple resonances within some of the wells, but they are more expensive to construct.

Figure 7.10 shows a typical result for two optimized designs: one with perforated sheets and one without. Measurements from the impedance tube and predictions are shown. This demonstrates that adding mass elements can extend the low frequency performance of these devices.

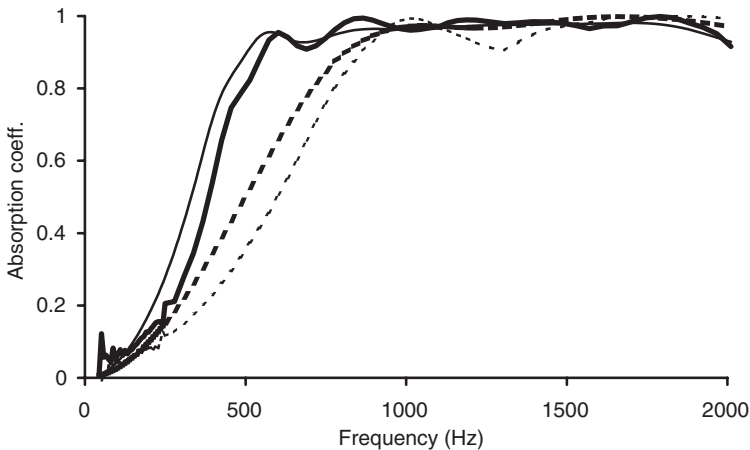


Figure 7.10 Measured and predicted absorption coefficient for two different profiled structures. — With perforated sheets, predicted; — With perforated sheets, measured; - - - - - No perforated sheets, predicted; - - - - - No perforated sheets, measured (after Wu *et al.* [17]).

7.2.6 Number of wells

For a narrow bandwidth, only a few different depth wells are needed. Reducing the number of wells would be useful as it simplifies the design and so reduces manufacturing costs. Wu *et al.* [17] designed a diffuser to work to 3 kHz that only needed three different depth wells. With this small number of wells, however, the density of resonances is insignificant above 3 kHz, and so the absorption becomes less efficient at higher frequencies. Incidentally, the choice of the correct value of the flow resistance for the resistive layer is even more important for absorbers with not many wells.

7.2.7 Theoretical model

Having considered qualitatively the mechanisms behind the absorption of the Schroeder diffusers, a theoretical model for the absorber will be presented. Boundary element methods could be used, but it is also possible to construct a theoretical model using a Fourier decomposition of the infinite periodic surface. This later model could also be used for profiled diffuser scattering. It is applicable to periodic structures and is almost as accurate as a boundary element model, but requires considerably less computation time. Both theoretical approaches divide into two parts: first the admittance of the individual wells must be calculated, then the absorption should be calculated from these well admittances.

7.2.7.1 Admittance of wells

The approach follows similar lines to the transfer matrix approaches used for porous and resonant absorbers in Chapters 5 and 6 and also described in Chapter 1. Consequently, the following is given in brief, and readers are referred to other chapters for more details. The admittance (or impedance) is needed at the entrance of the wells. The well width of a profiled absorber is often narrow compared with diffusers to provide more absorption; therefore the energy losses caused by viscous and thermal conduction in the wells cannot be neglected. Consider the case where the well width, $w \ll \lambda/2$, where λ is the wavelength of the sound, so that only fundamental modes are considered to propagate in each well. The wavenumber in the wells, k_t , is [18]:

$$k_t \approx k + \frac{k}{2w}(1-j)[d_v + (\gamma - 1)d_h] \quad (7.2)$$

where k is the wavenumber in air, γ the ratio of the specific heat $\approx 7/5$ for air and d_v , d_h the thickness of the viscous and thermal boundary layers respectively.

The thickness of the viscous and thermal boundary layers can be found from:

$$d_v = \sqrt{\frac{2\eta}{\rho\omega}} \approx \frac{0.0021}{\sqrt{f}} \quad (7.3)$$

where η is the coefficient of viscosity for air, ω the angular frequency, ρ the density of air and f the frequency.

$$d_h = \sqrt{\frac{2K}{\rho\omega c_p}} \approx \frac{0.0025}{\sqrt{f}} \quad (7.4)$$

where K is the thermal conductivity and c_p the heat capacity per unit mass of air at constant pressure.

For a slit with no perforated sheet present of depth l_n , the impedance at the top of the well is given by:

$$z_1 = r_m - \rho_e c \frac{k}{k_t} \cot(k_t l_n) \quad (7.5)$$

where r_m is the resistance of the covering material and ρ_e the effective density of air in the slit [19]. The effective density can be calculated using:

$$\rho_e = \rho \left[1 + (1 - j) \frac{d_v}{w} \right] \quad (7.6)$$

For a slit with a perforated sheet present at a height d_n from the well bottom, the impedance at the top of the perforated plate is given by:

$$z_p = r_p + j(\omega m_p - \rho_e c \frac{k}{k_t} \cot(k_t d_n)) \quad (7.7)$$

where r_p and m_p are the added resistance and mass due to the perforated sheet. These can be calculated from Equations 6.6 and 6.15 or 6.16. The impedance at the top of the well is:

$$z_1 = \frac{-j\rho c z_p \cot(k_t l_n) + (\rho c)^2}{z_p - j\rho c \cot(k_t l_n)} + r_m \quad (7.8)$$

where l_n is the distance from the perforated plate to the top of the well.

7.2.7.2 From well impedance to absorption: BEM

Once the well impedances are known, a method for gaining the absorption coefficient is needed. One possibility is to apply boundary element methods, which are described in relation to diffuser predictions in Chapter 8. The absorber is treated as a box with an impedance distribution on the front face. A source is placed in the far field and irradiates the absorber. An array of receivers on a sphere measures the far field scattered energy, which is integrated to give the sound power reflected, P_a . A box with an infinite impedance on the front face of the same dimensions is placed in the same set-up. The sound power reflected is calculated, and P_i in this case gives the incident power. From these two powers, the absorption coefficient of the surface can be calculated:

$$\alpha = 1 - \frac{P_a}{P_i} \quad (7.9)$$

Figure 3.3 compares a prediction of the absorption using a boundary element model compared to a multi-microphone free field measurement. Reasonable agreement is achieved. The low frequency discrepancies are as likely to be due to measurement inaccuracies as the BEM model. The BEM is rather laborious, and consequently, a different method can be used exploiting periodicity. This is detailed in the next section.

7.2.7.3 From well impedance to absorption: wave decomposition

Knowing that the surface is periodic, it is possible to decompose the scattered wave according to the periodicity of the surface. This greatly reduces the computation burden compared to a BEM model. There is an assumption that the surface is infinitely wide, and consequently, the prediction accuracy may be compromised at low frequencies for finite samples. The analysis below closely follows the method used by Mechel [14] and Wu *et al.* [15]. The sound field in front of the absorber, shown in Figure 7.9, is decomposed into the incident plane wave $p_i(x, z)$ and scattered field $p_s(x, z)$, which is made up of propagating and non-propagating evanescent waves:

$$\begin{aligned} p(x, z) &= p_i(x, z) + p_s(x, z) \\ p_i(x, z) &= P_i e^{j(-xk_x + zk_z)} \\ p_s(x, z) &= \sum A_n e^{j(-x\beta_n - z\gamma_n)} \end{aligned} \quad (7.10)$$

where $k_x = k \sin(\psi)$, $k_z = k \cos(\psi)$, $\beta_n = k_x + n \frac{2\pi}{W}$, $\gamma_n = -jk \sqrt{(\sin(\psi) + n \frac{\lambda}{W})^2 - 1}$ and $W = Nw$ the width of one period.

To use the above set of equations, the coefficients A_n needs to be obtained for the non-evanescent (propagating) waves. These coefficients represent the magnitude of the grating lobes, and consequently one coefficient needs to be obtained for every grating lobe. The number of grating lobes is usually rather small, and consequently this solution will be much faster than a BEM, where hundreds or thousands of simultaneous equations are common. The corresponding radiating harmonics indices n , which can propagate to the far field must satisfy the following relationship:

$$\left(\sin(\psi) + n \frac{\lambda}{W} \right)^2 \leq 1 \quad (7.11)$$

The outward particle velocity along the positive z -direction and the pressure can be related to the surface impedance as discussed in Sections 1.4.1 and 1.4.2. For this theory, it is more convenient to work with admittance. The relationship between particle velocity u_z and pressure p is thus:

$$\rho c u_z(x, 0) = -\beta(x) p(x, 0) \quad (7.12)$$

where β is the surface admittance, which can be calculated from the well impedance using the transfer matrix approach outlined in Section 7.2.7.1. The relations in Equation 7.10 are differentiated to give the particle velocity, and these are then related to the pressure relations in Equation 7.10 using the admittance relationship in Equation 7.12.

This is imposing the boundary condition of the surface admittance onto the system of equations. This gives:

$$\cos(\psi)p_i - \sum_{n=-\infty}^{\infty} \frac{\gamma_n}{k} A_n e^{-j2\pi xn/W} = \beta(x) \left[p_i + \sum_{n=-\infty}^{\infty} A_n e^{-j2\pi xn/W} \right] \quad (7.13)$$

As the surface is periodic, the surface admittance is also periodic. This enables the surface admittance to be represented by a Fourier analysis. Since the period is W , this gives the admittance as:

$$\beta(x) = \sum_{n=-\infty}^{\infty} B_n e^{-j2\pi xn/W} \quad (7.14)$$

$$B_n = \frac{1}{W} \int_0^W \beta(x) e^{j2\pi nx/W} dx \quad (7.15)$$

Equations 7.13–7.15 are combined to impose the periodicity of the boundary conditions. After multiplication by $e^{j2\pi mx/W}$ and integration over W this gives:

$$\sum_{n=-\infty}^{\infty} A_n \left[B_{m-n} + \delta_{m,n} \left(\frac{\gamma_n}{k} \right) \right] = P_i (\delta_{m,0} \cos(\psi) - B_m) \quad m = -\infty, \dots, +\infty \quad (7.16)$$

$$\delta_{m,n} = \begin{cases} 1 & m = n \\ 0 & m \neq n \end{cases} \quad (7.17)$$

The infinite sum in m can be terminated by monitoring convergence as more terms are added into the sum. On the samples tested so far, the index limits maybe taken as $|m| \leq \pm 2N$, where N is the number of wells in one period.

Equation 7.16 gives a set of simultaneous equations relating the coefficients of the non-evanescent waves A_n to the surface admittance and other known factors of geometry, such as incident angle. These simultaneous equations can be solved using standard solution techniques to get the unknown coefficients.

By considering the energy in the scattered and incident waves shown in Equation 7.10, it is possible to derive an equation for the absorption coefficient. This is given by

$$\alpha = 1 - \left| \frac{A_0}{P_i} \right|^2 - \frac{1}{\cos(\psi)} \sum \left| \frac{A_n}{P_i} \right|^2 \sqrt{1 - (\sin(\psi) + n\lambda/W)^2} \quad (7.18)$$

where the summation runs over radiating spatial harmonics only. The middle term is the specularly reflected energy and the right most term the scattered energy. For a small period width W , the specular reflection is the only non-evanescent reflection. In this case a normalized impedance on the surface of the structure, z_n , can be derived from:

$$z_n = \frac{1 + A_0/P_i}{1 - A_0/P_i} \quad (7.19)$$

Figure 3.3 compares predictions from this Fourier model with the BEM modelling described in the previous section. Free field measurements are also shown. Good agreement is obtained between the prediction models and measurements. Some discrepancies at low frequencies occur between the Fourier and BEM models; this probably occurs because the Fourier model assumes an infinite sample, and the BEM model does not.

Figure 7.10 compared the Fourier theory and impedance tube measurements for two different samples. Again good accuracy is obtained. One of the keys to getting good comparisons between theory and measurement is to get good quality samples. Even apparently small imperfections in the samples can lead to large measurement errors.

This Fourier model can also be applied to periodic diffusers designed for scattering rather than absorption. Although this approach has not been verified, it is assumed that the predictions would be accurate. The advantage in using this method over a BEM model is the reduction in computation time and storage requirements.

7.3 Summary

This chapter has discussed the absorption of seating and Schroeder diffusers/absorbers. Accurate estimations of seating and audience absorption are vital to good room design, especially large concert halls for orchestral music. The absorption of Schroeder surfaces is a more esoteric subject. While the concept of a Schroeder absorber is interesting, and good absorption can be obtained, the cost of constructing such surfaces is rather high, and this limits the commercial exploitation of these concepts.

7.4 References

- 1 L. L. Beranek, "Audience and chair absorption in large halls. II", *J. Acoust. Soc. Am.*, **45**, 13–19 (1969).
- 2 C. W. Kosten, "New method for the calculation of the reverberation time of halls for public assembly", *Acustica*, **16**, 325–330 (1965).
- 3 W. J. Davies, R. J. Orłowski and Y. W. Lam, "Measuring auditorium seat absorption", *J. Acoust. Soc. Am.*, **96**, 879–888 (1994).
- 4 J. S. Bradley, "Predicting theater chair absorption from reverberation chamber measurements", *J. Acoust. Soc. Am.*, **91**, 1514–1524 (1992).
- 5 W. J. Davies, "The effects of seating on the acoustics of auditoria", PhD thesis, University of Salford (1992).
- 6 T. Hidaka, N. Nishihara and L. L. Beranek, "Relation of acoustical parameters with and without audiences in concert halls and a simple method for simulating the occupied state", *J. Acoust. Soc. Am.*, **109**(3), 1028–1042 (2001).
- 7 T. J. Schultz and B. G. Watters, "Propagation of sound across audience seating", *J. Acoust. Soc. Am.*, **36**, 855–896 (1964).
- 8 G. M. Sessler and J. E. West, "Sound transmission over theatre seats", *J. Acoust. Soc. Am.*, **36**, 1725–1732 (1964).
- 9 A. H. Marshall, J. R. Hyde and M. F. E. Barron, "The acoustical design of Wellington Town Hall: design development, implementation and modelling results", *Proc. IoA(UK) Edinburgh* (1982).
- 10 K. Fujiwara and T. Miyajima, "Absorption characteristics of a practically constructed Schroeder diffuser of quadratic-residue type", *Appl. Acoust.*, **35**, 149–152 (1992).

- 11 K. Fujiwara and T. Miyajima, “A study of the sound absorption of a quadratic-residue type diffuser”, *Acustica*, **81**, 370–378 (1995).
- 12 D. E. Commins, N. Auletta and B. Suner, “Diffusion and absorption of quadratic residue diffusers”, *Proc. IoA(UK)*, **10**(2), 223–232 (1988).
- 13 H. Kuttruff, “Sound absorption by pseudostochastic diffusers (Schroeder diffusers)”, *Appl. Acoust.*, **42**, 215–231 (1994).
- 14 F. P. Mechel, “The wide-angle diffuser – a wide-angle absorber?”, *Acustica*, **81**, 379–401 (1995).
- 15 T. Wu, T. J. Cox and Y. W. Lam, “From a profiled diffuser to an optimised absorber”, *J. Acoust. Soc. Am.*, **108**(2), 643–650 (2000).
- 16 K. Fujiwara, K. Nakai and H. Torihara, “Visualisation of the sound field around a Schroeder diffuser”, *Appl. Acoust.*, **60**(2), 225–236 (2000).
- 17 T. Wu, T. J. Cox and Y. W. Lam, “A profiled structure with improved low frequency absorption”, *J. Acoust. Soc. Am.*, **110**(6), 3064–3070 (2001).
- 18 P. M. Morse and K. Ingard, “*Theoretical Acoustics*”, McGraw-Hill, New York, Chapter 6, 285–291 (1968).
- 19 J. F. Allard, “*Propagation of Sound in Porous Media: Modeling Sound Absorbing Materials*”, Elsevier Science, London, Chapter 4, 48–53, 59–62 (1993).

8 Prediction of scattering

To enable the design and characterization of a diffusing surface, it is necessary to be able to predict the reflected pressure from the surface. Currently, this is usually done by considering the scattering from the surface in isolation of other objects and boundaries. The prediction techniques could also be used as part of a whole space prediction algorithm, where all surfaces in a room are simultaneously modelled. At the moment, however, long computation times and storage limitations mean that whole space prediction algorithms are forced to use relatively crude representations of the actual scattering processes. Consequently, when predicting the responses in rooms and semi-enclosed spaces such as street canyons or pavilions, it is more common to use geometric models. The issue of modelling scattering in geometric models is discussed in Chapter 12.

Therefore, the issue for this chapter is predicting the scattering from isolated surfaces. There is a range of choices of models, from the numerically exact but computationally slow, to the approximate but fast models. The prediction methods can also be differentiated as either time or frequency domain models. In diffuser design, frequency domain methods have dominated the development of the modern diffuser. For this reason, this chapter will concentrate on these methods. Table 8.1 summarizes the prediction models which will be considered in this chapter, along with their key characteristics.

The next section will start with the most accurate model, a boundary element method (BEM) based on the Helmholtz–Kirchhoff integral equation. It will then be demonstrated how the more approximate models can be derived from this integral equation, and the relative merits and limitations of the techniques will be discussed. To round off the chapter, an overview of less commonly used techniques will be given.

8.1 Boundary element methods

When BEMs are applied to diffusers, remarkable accuracy is achieved. The accuracy is much better than most acousticians are used to achieving from an acoustics theory. Acousticians are used to using empirical fixes to make measurement match prediction, but that is not often needed when BEMs are used to predict diffuser scattering. The only real disadvantages of BEMs are that the method is prone to human error in meshing the surface, and most importantly, it is slow for high frequencies and large surfaces. Some have attempted to apply the prediction methods to whole rooms for low frequencies, but this is very computationally intense, requiring super computing facilities or a considerable amount of patience while waiting for results.

Table 8.1 Key characteristics of various scattering prediction models detailed in this chapter. The accuracy and computational efficiency columns are indicative; the rank ordering of the top four prediction models might vary depending on surface type being considered and the particular implementation of the algorithm

<i>Model</i>	<i>Accuracy</i>	<i>Computing time</i>	<i>Notes</i>
Standard boundary element method (BEM)	Best	Slowest	Exact provided surfaces are locally reacting and viscous boundary layer losses are small. Slow, especially for large surfaces or high frequencies.
Thin panel BEM			An efficient method for thin surfaces, approximately halving the number of elements in a standard BEM model.
Kirchhoff	↑ ↓	↑ ↓	Uses the Kirchhoff boundary conditions to approximate surface pressures and so is much faster. Less accurate for oblique sources and receivers, low frequencies, rapidly changing surface impedance profiles and surfaces with steep gradients.
Fresnel			Replaces the numerical integration of Kirchhoff model by quicker to compute Fresnel integrals. Requires scattering across width and along length of surface to be orthogonal. Some useful simplifications available for flat and curved surfaces.
Fraunhofer or Fourier	Worst	Quickest	Simplifies numerical integral of Kirchhoff method, only useable in far field. Allows simpler Fourier principles to be applied. Good for understanding physical processes and designs, but least accurate.

8.1.1 The Helmholtz–Kirchhoff integral equation

This integral equation forms the core of many of the prediction models used including BEMs. It is defined below and the following section will then discuss how it is solved. The Helmholtz–Kirchhoff integral equation formulates the pressure at a point, as a combination of the pressure direct from the sources, and a surface integral of the pressure and its derivative over the reflecting surfaces. The single frequency form of the integral equation gives the pressure $p(\mathbf{r})$ at a position \mathbf{r} as [1]:

$$\left. \begin{array}{l} \mathbf{r} \in E \\ \mathbf{r} \in s \\ \mathbf{r} \in D \end{array} \right\} \left. \begin{array}{l} p(\mathbf{r}) \\ \frac{1}{2}p(\mathbf{r}) \\ 0 \end{array} \right\} = p_i(\mathbf{r}, \mathbf{r}_0) + \int_s p(\mathbf{r}_s) \frac{\partial G(\mathbf{r}, \mathbf{r}_s)}{\partial n(\mathbf{r}_s)} - G(\mathbf{r}, \mathbf{r}_s) \frac{\partial p(\mathbf{r}_s)}{\partial n(\mathbf{r}_s)} ds \quad (8.1)$$

where $\mathbf{r} = \{x, y, z\}$ is the vector describing the receiver location, $\mathbf{r}_0 = \{x_0, y_0, z_0\}$ the vector describing the source location, $\mathbf{r}_s = \{x_s, y_s, z_s\}$ the vector for a point on the surface, $p(\mathbf{r}_s)$ the pressure at \mathbf{r}_s , $p_i(\mathbf{r}, \mathbf{r}_0)$ the direct pressure radiated from the source at \mathbf{r}_0 to the receiver at \mathbf{r} , G the Green’s function, n the normal to the surface pointing out the surface, E the external region, s the surface and D the interior of the surface.

The geometry is illustrated in Figure 8.1. $p_i(\mathbf{r}, \mathbf{r}_0)$ is the pressure direct from the source at \mathbf{r}_0 to the receiver point at \mathbf{r} , and so the first term on the right-hand side represents the direct pressure. The integral is carried out over the surface, with \mathbf{r}_s being a point on the surface and $n(\mathbf{r}_s)$ a normal to the surface pointing out of the surface; so the integral gives the contribution of the reflected energy to the pressure at \mathbf{r} . By single frequency, it is meant that the system is in steady state conditions so that the time variation, $\exp(j\omega t)$, can be neglected. G is the Green’s function which gives how the pressure and its derivative propagates from one point in space to another point. Consequently, in 3D the Green’s function is simply a point source radiation equation:

$$G(\mathbf{r}) = \frac{e^{-jkr}}{4\pi r} \quad (8.2)$$

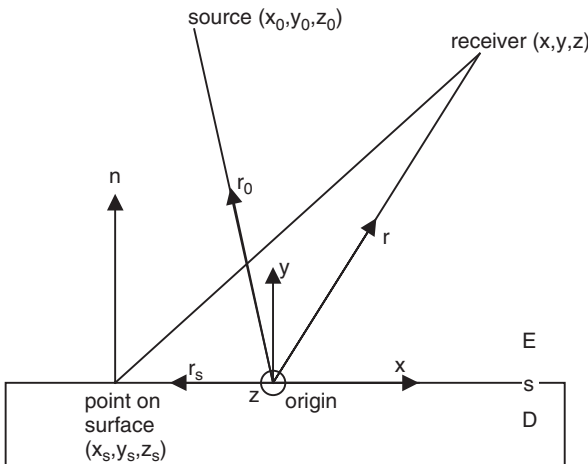


Figure 8.1 Geometry for prediction models.

where $r = |\mathbf{r} - \mathbf{r}_0|$ and k is the wavenumber. Carrying out the solution in two dimensions is extremely useful for diffusers as it can greatly decrease the computational burden in terms of storage and calculation time. In that case the Green's function is given by the Hankel function:

$$G(r) = \frac{-j}{4} H_0^{(2)}(kr) \tag{8.3}$$

where $H_0^{(2)}$ is the Hankel function of the second kind of order zero. The asymptotic version of the Hankel function when kr is large is:

$$\frac{G(r)}{kr \gg 1} = \frac{Ae^{-jkr}}{\sqrt{kr}} \tag{8.4}$$

where A is a constant. So this is a line source radiation equation as would be expected in a 2D world. The Hankel function is most efficiently evaluated using polynomial expansions [2] when kr is small, and using the asymptotic form in Equation 8.4 when kr is large.

There are three possible equations shown in Equation 8.1. The top case is when the point \mathbf{r} is external to the scattering surface ($\mathbf{r} \in E$), the middle case when \mathbf{r} is on a surface ($\mathbf{r} \in s$) and the bottom case when \mathbf{r} is internal to the scattering surface ($\mathbf{r} \in D$). The derivation of Equation 8.1 is well known [1], and so will not be discussed here.

The integral has two terms, one involving the surface pressure $p(\mathbf{r}_s)$ and one involving the surface pressure derivative $\partial p(\mathbf{r}_s)/\partial n(\mathbf{r}_s)$. If the surface is taken to be local reacting, the derivative of the surface pressure will be related to the surface pressure by the surface admittance. In terms of equations:

$$jkp(\mathbf{r}_s)\beta'(\mathbf{r}_s) = \frac{\partial p(\mathbf{r}_s)}{\partial n(\mathbf{r}_s)} \tag{8.5}$$

where β' is the surface admittance. In BEM modelling, it is normal to define quantities in terms of an outward pointing normal. Surface admittances would normally be defined with an inward pointing normal. The prime is used to signify this difference, where $\beta' = -\beta$, where β is the more usual surface admittance. This definition of an outward pointing normal also affects the interrelations between admittance and surface reflection factor, and is relevant when implementing the Kirchhoff solution. The assumption of local reaction means that the surface admittance is independent of the incident and reflected pressure waves. For low absorption surfaces, where $\beta' \rightarrow 0$, the integral equation term using the pressure derivative can be neglected.

8.1.2 General solution method

Having defined the terms and the nomenclature for the integral equation, the general solution technique for a BEM will be presented. The BEM involves the application of Equation 8.1 twice.

- 1 The surface pressures, $p(\mathbf{r}_s)$, on the scattering surfaces are found.
- 2 A numerical integral is carried out over the surface pressures to determine the pressures at the desired external points.

8.1.2.1 *Determining surface pressures*

The determination of the surface pressures is the rate-determining step of a BEM model and so will be described now in detail. The surface pressures depend not only on the incident sound field, but also on each other. This is a statement that there are mutual interactions across the surface, as might be expected. To model the mutual interactions, the usual solution method is to discretize the surface into a number of surface (boundary) elements across which it is approximated that the pressure is constant. The elements must have sufficiently small dimensions to prevent errors in representing the continuous pressure variation by a set of discrete values. This is usually achieved by making elements smaller than a quarter of a wavelength in size for very simple surfaces. As surfaces become more complex, it is safer to use element sizes of $\lambda/8$ or even smaller to ensure proper representation of the pressure variation, where λ is the wavelength of the highest frequency being modelled. Breaking the surface geometry into a series of elements – meshing the surface – can be a difficult process for complicated diffusers, but can be greatly simplified by using specialist meshing programs. This is where human error is most likely to occur. Two-dimensional BEMs not only have computational speed advantages, they are also useful because it is far simpler to mesh a 2D shape.

Once the surface has been discretized, a set of simultaneous equations can be set up with one equation for each boundary element. The equations will be for the surface pressures with \mathbf{r} being taken for positions on the surface in the middle of each of the elements. In matrix form, Equation 8.1 can be rewritten as:

$$\left(\frac{1}{2}\delta + \mathbf{A}\right)\mathbf{P} = \mathbf{P}_i \quad (8.6)$$

$$\begin{aligned} \delta_{nm} &= 1 & m &= n \\ \delta_{nm} &= 0 & m &\neq n \end{aligned} \quad (8.7)$$

$$\mathbf{A}_{mn} = \int_{S_m} \frac{\partial G(\mathbf{r}_n, \mathbf{r}_s)}{\partial n_m(\mathbf{r}_s)} - G(\mathbf{r}_n, \mathbf{r}_s)jk\beta'_m ds_m \quad (8.8)$$

where \mathbf{P} is a $(1 \times N)$ matrix of surface pressures, \mathbf{P}_i a $(1 \times N)$ matrix of incident pressures direct from the source(s) to the surface, N the number of elements, the subscripts n and m refer to the (n, m) element of the matrix or the contribution from the m th element to the n th element surface pressure and s_m is the surface of the m th element.

The calculation of the matrix \mathbf{A} is an important rate-determining step in the BEM. It is roughly an N^2 process, where N is the number of elements. It is relatively slower for 2D processes when compared to 3D models. This is because the Hankel function is slower to evaluate unless it is in-built and optimized for speed by the computing

language used to code the BEM. But then there are great time savings to be had in a 2D model, as Equation 8.8 is only a line integral rather than a surface integration.

The integration of Equation 8.8 can use various algorithms and efficient numerical techniques [3] that can make significant time savings. It is also possible to use more approximate integration for elements that are far away from each other when the mutual interactions are less strong. This has to be done with care, however, because it risks compromising the accuracy of the solution. Evaluating Equation 8.8 when $m = n$, in other words evaluating the influence of an element on itself, requires special consideration. The reason for this is that the integral includes a singularity. The singularity is relatively weak in this case, and so provided care is taken not to consider the case where $\mathbf{r}_n = \mathbf{r}_s$, then the numerical integration will converge to a correct value.

Once the simultaneous equations are constructed, then they can be solved using standard matrix solution techniques which are now commonly available. The BEM method forms full matrixes, so sparse matrix solvers used in techniques such as finite element analysis (FEA) are not directly applicable.

If the set of simultaneous equations were solved alone, it would be possible to get non-unique solutions at certain frequencies. These equate to eigensolutions of the physical body dimensions. There are various methods for overcoming this problem. One solution is to form an overdetermined set of equations, this is the CHIEF method [4]. By placing some receivers in the body of the diffuser, where the pressure must be zero, it is possible to add additional simultaneous equations which help to ensure the correct solution is found. In choosing the receivers inside the body of the surface, often referred to as internal points, it must be remembered that if these internal points are at a node of an incorrect eigensolution, then they do not help force the correct solution. Consequently, several internal points should be used, avoiding lines of symmetry and simple integer relationships between internal point locations. Another remedy to the non-unique solutions problem is to combine Equation 8.1 with its derivative; this is the Burton Miller approach [1]. In reality, most diffuser geometries are such that non-unique solutions are not usually found. Non-unique solutions are most common when the wavelength is small compared to the geometry, but cases with such small wavelength to structural size are not often attempted in diffuser calculations because the computational burden becomes too large. Consequently, at the moment it appears that non-unique solutions are more of a worry for mathematicians than acousticians.

A significant reduction in computation burden can be achieved if there are planes of symmetry in the surface and the source lies on the planes of symmetry. In this case, a simple image source construction can be used to take the place of identical parts of the surface and so greatly reduce the computational burden. This is shown in Figure 8.2. The pressure on identical parts of the surface will be the same; consequently, it is possible to construct a solution using about half the number of elements that would be required to mesh the whole surface. This does not reduce time in setting up the simultaneous equations, but greatly reduces the time required to solve the equations and decreases the memory requirements. The easiest method to exploit the image source construct is to modify the Green's function by an additional term:

$$G(\mathbf{r}) = \frac{e^{-jkr}}{4\pi r} + \frac{e^{-jkr'}}{4\pi r'} \quad (8.9)$$

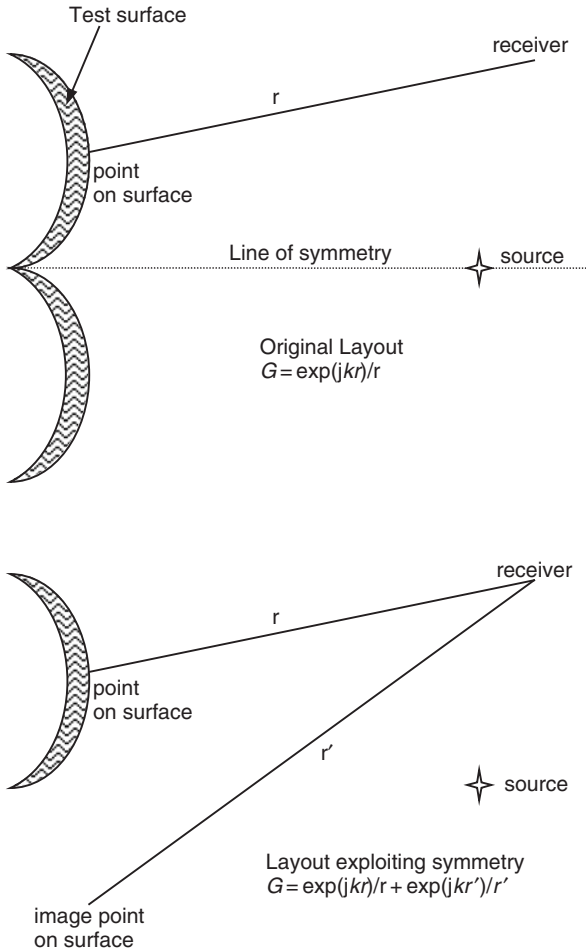


Figure 8.2 Illustration showing the use of an image source for a diffuser made of two arcs. The top illustration shows the original configuration where the source lies on a plane of symmetry. The bottom shows the exploitation of mirror symmetry to half the number of elements required in the BEM model.

where r' is the distance from an image source which is reflected in the plane of symmetry. In 3D cases, multiple symmetry planes may exist, and so multiple image sources may need to be considered. A similar process can also be applied to the 2D Green's function.

It is also possible to assume non-uniform pressure variation across the elements. For instance, it is possible to define the matrixes in terms of the pressures at the element boundaries and assume a linear relationship between these. This reduces the number of elements needed to correctly represent the pressure variation on the surface compared to constant pressure elements. This has potential to make a faster prediction model, but at the cost of a more complex implementation.

8.1.2.2 Determining external point pressures

Once the surface pressures are known, Equation 8.1 becomes a straightforward numerical integration that must be solved. This process is relatively quick and simple as it is just a numerical integration. The use of efficient numerical integration algorithms and asymptotic solutions for the 2D Green's function, when the receivers are far from the surface, can greatly speed up this process.

8.1.2.3 2D versus 3D

Cox [5] examined whether it is possible to predict the scattering from 3D diffusers using a 2D BEM model. The surfaces he tested were single plane surfaces which were extruded in one direction, like 1D Schroeder diffusers and cylinders. This meant that the scattering was roughly orthogonal across the width and along the extruded length. In this case, Cox was able to show that 2D prediction models provided accurate predictions except at low frequencies (for the surfaces Cox tested, this meant below 500 Hz). Cox derived expressions to correct the 2D scattered polar response, so that results matched the real (3D) diffuser scattering. These corrections affect the overall scattered sound power level and not the shape of the polar response.

8.1.3 Thin panel solution

When a surface becomes very thin, then the above solution method will not work. The front and back of surface would have elements which would become rather too close together, and the solution method often becomes inaccurate. It is possible, however, to provide a formulation in terms of the pressure difference and sum across the panel. Not only does this regularize the equations to make them solvable, it approximately halves the number of elements required and so speeds solution times and reduces storage requirements.

The solution method requires both Equation 8.1 and its derivative. Terai [6] showed that with correct regard for the jump relations, the integral equation and its derivative can be given by:

$$\frac{1}{2} \{p(\mathbf{r}_1) + p(\mathbf{r}_2)\} = p_i(\mathbf{r}_0, \mathbf{r}_1) + \iint_s \{p(\mathbf{r}_{s,1}) - p(\mathbf{r}_{s,2})\} \frac{\partial G(\mathbf{r}, \mathbf{r}_{s,1})}{\partial n(\mathbf{r}_{s,1})} - \left\{ \frac{\partial p(\mathbf{r}_{s,1})}{\partial n(\mathbf{r}_{s,1})} - \frac{\partial p(\mathbf{r}_{s,2})}{\partial n(\mathbf{r}_{s,1})} \right\} G(\mathbf{r}, \mathbf{r}_{s,1}) ds \quad (8.10)$$

$$\frac{1}{2} \left\{ \frac{\partial p(\mathbf{r}_1)}{\partial n(\mathbf{r}_1)} + \frac{\partial p(\mathbf{r}_2)}{\partial n(\mathbf{r}_1)} \right\} = \frac{\partial p_i(\mathbf{r}_0, \mathbf{r}_{s,1})}{\partial n(\mathbf{r}_{s,1})} + \iint_s \{p(\mathbf{r}_{s,1}) - p(\mathbf{r}_{s,2})\} \frac{\partial^2 G(\mathbf{r}, \mathbf{r}_{s,1})}{\partial n(\mathbf{r}_1) \partial n(\mathbf{r}_{s,1})} - \left\{ \frac{\partial p(\mathbf{r}_{s,1})}{\partial n(\mathbf{r}_{s,1})} - \frac{\partial p(\mathbf{r}_{s,2})}{\partial n(\mathbf{r}_{s,1})} \right\} \frac{\partial G(\mathbf{r}, \mathbf{r}_{s,1})}{\partial n(\mathbf{r}_1)} ds \quad (8.11)$$

where the 1 and 2 in the subscripts refer to the front and the back of an infinitely thick panel respectively. These are the equations for points on the surface ($\mathbf{r}_1, \mathbf{r}_2 \in s$) and should be used to set up the simultaneous equations which then yield the surface pressures. If the desire is to achieve a reduction in computational burden, further simplifications can be obtained if more assumptions are made. Otherwise, all that these equations achieve is regularization of the thin panel case with no reduction in number of elements. Two simplifications will be considered: first the case of a non-absorbing surface and second the situation of a planar surface with non-zero surface admittance.

8.1.3.1 *Non-absorbing surface*

The surface is assumed to be non-absorbing and thin, then the differentials in the pressures on the front and rear surface are zero as the surface admittance is zero. Under this assumption, Equation 8.10 can be simplified to yield a single equation in terms of the pressure difference across the panel:

$$0 = \frac{\partial p_i(\mathbf{r}_0, \mathbf{r}_{s,1})}{\partial n(\mathbf{r}_{s,1})} + \iint_s \{p(\mathbf{r}_{s,1}) - p(\mathbf{r}_{s,2})\} \frac{\partial^2 G(\mathbf{r}, \mathbf{r}_{s,1})}{\partial n(\mathbf{r}_1) \partial n(\mathbf{r}_{s,1})} ds \quad (8.12)$$

Using this equation, it is possible to discretize the front surface into a set of elements across which the pressure is assumed constant, and set up simultaneous equations in the pressure difference between the front and rear of the panel $\{p(\mathbf{r}_{s,1}) - p(\mathbf{r}_{s,2})\}$. These simultaneous equations can then be solved to give the pressure difference for each element.

Once the pressure difference for each element is known, then the following equation is used to calculate the pressure at external points:

$$p(\mathbf{r}) = p_i(\mathbf{r}_0, \mathbf{r}_1) + \iint_s \{p(\mathbf{r}_{s,1}) - p(\mathbf{r}_{s,2})\} \frac{\partial G(\mathbf{r}, \mathbf{r}_{s,1})}{\partial n(\mathbf{r}_{s,1})} ds \quad (8.13)$$

Incidentally, for a planar surface, it is simple to get the pressures on the front and the rear of the panel if these are wanted (they are not explicitly needed to get the external point pressures). The sum of the pressures on either side of the surface is equal to twice the incident pressure $\{p(\mathbf{r}_{s,1}) + p(\mathbf{r}_{s,2})\} = 2p_i(\mathbf{r}_{s,1})$. This fact can be used with the values for the pressure difference between the front and rear of the panel $\{p(\mathbf{r}_{s,1}) - p(\mathbf{r}_{s,2})\}$ to give the actual surface pressures on either side of the panel.

The matrix form of the integral Equation 8.12 is highly singular when the interaction of an element with itself is considered. To overcome this difficulty, Terai suggested using an asymptotic solution for calculating the contribution of an element's radiation to its own surface pressure. For the 3D case this yields a line integral around the perimeter of the element:

$$\lim_{\mathbf{r} \rightarrow \mathbf{r}_s} \iint_s \frac{\partial^2 G(\mathbf{r}, \mathbf{r}_s)}{\partial n^2} ds = \frac{-1}{4\pi} \left\{ \oint \frac{e^{-jkr(\theta)}}{\mathbf{r}(\theta)} d\theta + 2\pi jk \right\} \quad (8.14)$$

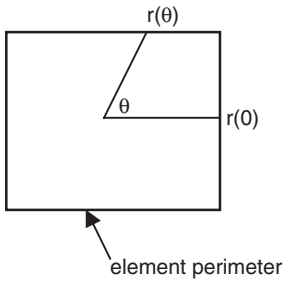


Figure 8.3 Definition θ used for asymptotic form of 3D thin panel BEM.

where θ is defined in Figure 8.3.

For the 2D case the corresponding equation is:

$$\lim_{a \rightarrow 0} \int_0^a \frac{\partial^2 G(\mathbf{r}, \mathbf{r}_s)}{\partial n^2} ds = \frac{1}{2\pi a} \quad (8.15)$$

In many cases, it is possible to set the distance a as being the length of the element, and so the factor above can be used to directly calculate the contribution of the element to itself. For some problems with complex geometries, however, more accurate results are obtained if a smaller value of a is used and the rest of the element is integrated using normal numerical integration procedures.

Apart from this detail, the solution method proceeds in exactly the same way as for the standard BEM model. The thin panel is a particularly useful formulation as it can be used for many scattering surfaces. An overhead canopy above a stage can be treated as a thin rigid surface, and this formulation allows a faster solution than the standard BEM. The accuracy is compromised close to grazing angles, as it does not model the scattering from the finite edges which exist with real surfaces. More details on the accuracy are given later.

The method can also be applied to Schroeder diffusers, which have thin fins as part of the construction. Schroeder diffusers are discussed in Chapter 9, a picture is shown in Figure 9.1. The thin panel solution method allows the Schroeder geometry to be exactly modelled and the scattering predicted for any frequency. This is not true of most prediction methods, which are generally frequency limited as they assume plane wave propagation in the wells.

This method provides unique solutions, provided no enclosed volumes are created out of the elements. Consequently, there is no need to use an overdetermined system in many cases.

8.1.3.2 Planar thin surface with non-zero admittance

By assuming the surface is planar, some of the terms in Equations 8.10 and 8.11 simplify. The aim is to reduce the number of elements involved in the calculation, as unless this is achieved, no improvement in computing effort is achieved. One way of achieving a reduction in the number of elements is to assume that the admittances on

the front and rear of the panel at any point are the same, i.e. $\beta(\mathbf{r}_{s,1}) = \beta(\mathbf{r}_{s,2})$. In room diffuser calculations, this is not going to introduce large errors into the calculation, because it is the bright side scattering which is of primary importance. For all but low frequencies, the pressure is low on the rear of the panel, and consequently what admittance is assumed on the rear is not terribly important. This admittance assumption might not be accurate in all cases. For example if a diffusing roadside barrier is being considered, the scattering in the shadow zone at low frequencies is of interest.

Assuming that $\beta(\mathbf{r}_{s,1}) = \beta(\mathbf{r}_{s,2})$ is a reasonable approximation, and the surface is planar, then for receiver points \mathbf{r}_1 and \mathbf{r}_2 on the front and rear surface, Equations 8.10 and 8.11 can be rewritten as:

$$\frac{1}{2}\{p(\mathbf{r}_1) + p(\mathbf{r}_2)\} = p_i(\mathbf{r}_0, \mathbf{r}_1) - jk \iint_s \beta'(\mathbf{r}_{s,1})[p(\mathbf{r}_{s,1}) + p(\mathbf{r}_{s,2})]G(\mathbf{r}, \mathbf{r}_{s,1})ds \quad (8.16)$$

$$jk \frac{1}{2}\beta'(\mathbf{r}_1)\{p(\mathbf{r}_1) - p(\mathbf{r}_2)\} = \frac{\partial p_i(\mathbf{r}_0, \mathbf{r}_{s,1})}{\partial n(\mathbf{r}_1)} + \iint_s \{p(\mathbf{r}_{s,1}) - p(\mathbf{r}_{s,2})\} \frac{\partial^2 G(\mathbf{r}, \mathbf{r}_{s,1})}{\partial n(\mathbf{r}_1)\partial n(\mathbf{r}_{s,1})} ds \quad (8.17)$$

The surface is again discretized into elements small compared to the wavelength. Then two sets of simultaneous equations can be constructed from Equations 8.16 and 8.17. The first set of equations is in the sum of the pressures, using Equation 8.16, and the second is in the difference pressure across the panel, using Equation 8.17. These simultaneous equations are then separately solved. As two sets of simultaneous equations are being used, with half the number of elements when compared to a standard BEM, then the solution will be quicker by a factor of 4–8 times, depending on the implementation.

The propagation to external receivers is carried out using the following equation:

$$p(\mathbf{r}) = p_i(\mathbf{r}_0, \mathbf{r}_1) + \iint_s \{p(\mathbf{r}_{s,1}) - p(\mathbf{r}_{s,2})\} \frac{\partial G(\mathbf{r}, \mathbf{r}_{s,1})}{\partial n(\mathbf{r}_{s,1})} - jk\beta'(\mathbf{r}_{s,1})[p(\mathbf{r}_{s,1}) + p(\mathbf{r}_{s,2})]G(\mathbf{r}, \mathbf{r}_{s,1})ds \quad (8.18)$$

The accuracy of this technique will be presented later in this chapter.

8.1.4 *Periodic formulation*

When large areas of diffusers are used, BEM models can become too slow to be practical. Consequently, one avenue for research is to find faster methods. For example, fast multipole methods (FMM) are currently attracting considerable attention, although an FMM implementation is extremely complex, and the improvement in computational speed yet to be proven. Another approach to improving BEM predictions is to use information concerning the physical nature of the surface boundary conditions to reduce computational burden. In the case of periodic surfaces, considerable improvements in prediction times can be achieved by exploiting the periodicity.

Diffusers are often applied in a periodic formulation, and this periodicity can be exploited to form a more computationally efficient formulation. Lam [7] developed formulations for periodic 2D hard surfaces. For free waves in a periodic structure, Bloch's theorem [8] states that all field quantities at two points exactly one period apart are related by the same factor. For diffusers and a far field source, the incident pressure for identical parts of the structure will be related by a simple constant phase factor. The relationship between the total pressure at periodic points will be modified by the scattered wave. If the scattering is relatively weak, then it can be assumed that the constant phase factor relating the incident sound pressures between identical parts of the surface will also give the relationship for the total sound pressures. This may appear to be a large leap of faith as diffusers are designed to achieve strong scattering in the far field. Notwithstanding this design remit, it will be shown later in this chapter that the Kirchhoff boundary conditions form the basis of many reasonably good prediction methods, and there is an explicit assumption of weak scattering in applying the Kirchhoff boundary conditions. So this provides some hope that the weak scattering assumption may be fine.

Figure 8.4 illustrates a periodic structure and geometry used. The pressure between identical points on adjacent periods is therefore:

$$A(\mathbf{r}_{s,i=0}, \mathbf{r}_{s,i=j}) = \frac{p_i(\mathbf{r}_{s,i=0})}{p_i(\mathbf{r}_{s,i=j})} \tag{8.19}$$

where $\mathbf{r}_{i=0}$ and $\mathbf{r}_{i=j}$ are vectors for identical points on the surface, where j is an integer and i an index referring to the appropriate period number. This formulation can deal with non-plane wave incidence and so can be used for near field sources and receivers. Given that Equation 8.19 gives the relationship between the pressures on identical parts of the diffuser, it is now possible to produce a new version of Equation 8.1 for periodic surfaces:

$$\left. \begin{array}{l} \mathbf{r} \in E \quad p(\mathbf{r}) \\ \mathbf{r} \in s \quad \frac{1}{2}p(\mathbf{r}) \\ \mathbf{r} \in D \quad 0 \end{array} \right\} = p_i(\mathbf{r}, \mathbf{r}_0) + \int_{S_0} p(\mathbf{r}_{s,0}) \sum_{i=-\infty}^{\infty} A(\mathbf{r}_{s,i}, \mathbf{r}_{s,i+j}) \left[\frac{\partial G(\mathbf{r}, \mathbf{r}_{s,0})}{\partial n(\mathbf{r}_{s,0})} - jk\beta'(\mathbf{r}_{s,0})G(\mathbf{r}, \mathbf{r}_{s,0}) \right] ds \tag{8.20}$$

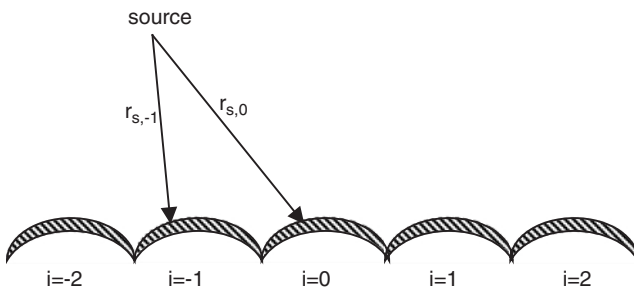


Figure 8.4 Geometry for periodic predictions illustrated for a set of arcs.

where the vector $\mathbf{r}_{s,0}$ is the surface vector for the middle period only. The integration is only carried out over the middle period, surface s_0 , since once the pressure is known on the middle period, it is known for the whole surface (Bloch). Effectively, the Green's function has been modified in a way similar to the image source case discussed previously when symmetry was being exploited. The limits of the infinite sum can be taken as the physical number of periods present in the diffuser. Figure 8.5 shows the scattering from a periodic arrangement of six semicylinders. Measurements are compared to a complete BEM solution (modelling all six semicylinders explicitly), as well as the periodic formulation. Good agreement is obtained between the periodic formulation and the complete BEM solution. Some differences remain. One likely cause is that the number of periods used is relatively small and so edge diffraction effects may have a significant effect on the surface pressures of the outer periods. Alternatively, it may be the weak scattering assumption that is not entirely true.

This technique can also be applied to other structures and in 3D. For example, Figure 8.6 shows the scattering from a planar hybrid surface. This is a flat surface with a complex array of hard and soft patches and is discussed in detail in Chapter 11, and a picture is shown in Figure 11.1. In Figure 8.6, a complete solution where all periods are meshed is compared to a periodic formulation. The case is an array of 4×1 periods at 2 kHz. The two prediction methods produce very similar results, validating the periodic formulation.

The reliance on the weak scattering theory for explaining the relationship between different periods of the device means that it is best to assume that this process works best where the Kirchhoff boundary conditions are accurate. Consequently, it might be expected that the periodic formulations would work less well at low frequencies, and for oblique sources and receivers, especially as these approach grazing angles. It would also be interesting to see how this formulation works for periodic arrangement of strong scattering surfaces, such as pyramids or triangles.

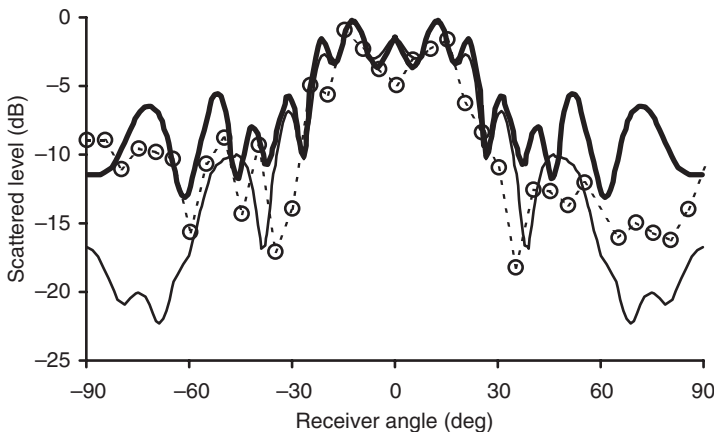


Figure 8.5 Scattering from six semicylinders. Two BEM models compared to measurement. 5 kHz, normal incidence, 1/3 octave band. ---○--- Measured; ——— Standard BEM; ——— Periodic BEM (after Lam [7]).

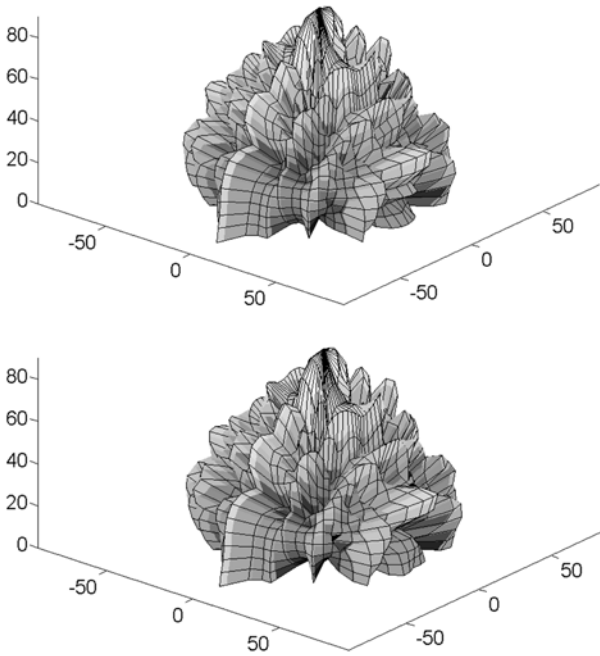


Figure 8.6 Comparison of predictions from complete BEM model (top) and a periodic formulation (bottom) for a planar hybrid surface.

8.1.5 Accuracy of BEM modelling: thin rigid reflectors

Having presented some different BEMs, the next two sections will look at the accuracy these methods achieve. Consider first thin rigid planar and curved surfaces. These commonly occur in indoor and outdoor spaces and are relatively straightforward to mesh and predict using BEMs. It is also relatively easy to construct and measure the scattering from such surfaces, and so enable the accuracy of the prediction methods to be directly compared to scale model measurements (see Chapter 4 for the measurement techniques used).

The full BEM solution based on Equation 8.1 produces accurate predictions of the scattering over a wide range of frequencies [9, 10] for plane and curved surfaces. Figures 8.7 and 8.8 compare predicted and measured results for the total and scattered pressure for a plane thin panel. Good prediction accuracy is achieved for both models. The thin panel model is based on Equations 8.12 and 8.13 and gives very similar results to the full BEM solution (for many angles the lines overlay each other) with a quicker prediction time. The thin panel and full BEM model only deviate for grazing angles and high frequencies. The deviations occur because the thin panel model does not properly represent the finite thickness of the panel, which becomes more critical at grazing angles when the wavelength is not large compared to the panel thickness. Inaccuracies arise because there are no edge elements in the thin panel case and so edge scattering is not properly modelled.

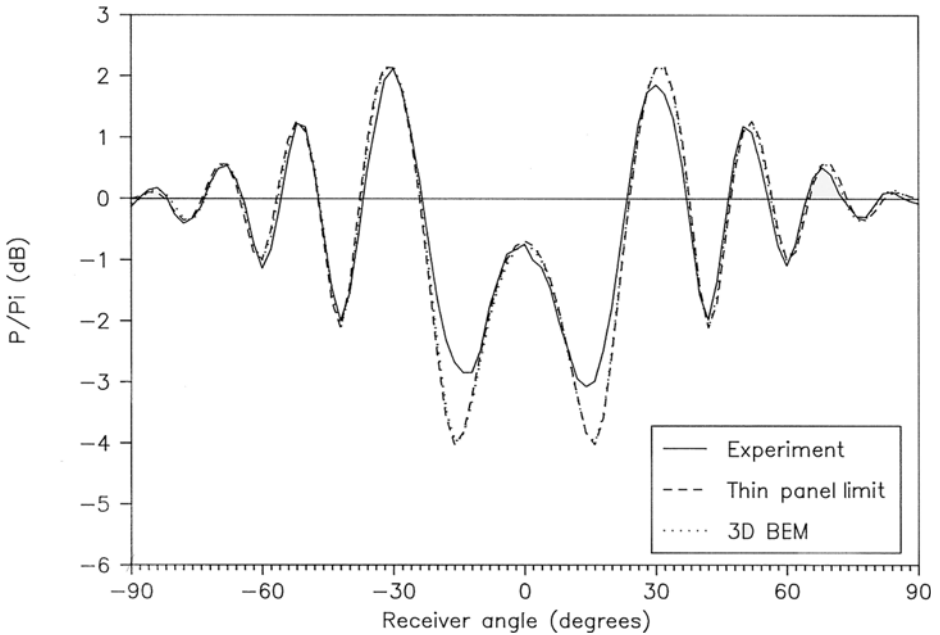


Figure 8.7 Comparison of total field (incident plus scattered) for a plane surface measured and predicted by two boundary element models. Normalized to incident sound at receiver (after Cox [10]).

8.1.6 Accuracy of BEM modelling: Schroeder diffusers

Figure 9.1 left shows a picture of a Schroeder diffuser, and Chapter 9 discusses this design in great detail. The diffuser consists of a series of wells of the same width but different depths. There are two approaches to modelling this surface. The first uses the thin panel solution and allows the diffuser shape to be exactly modelled; the second uses an approximate model of the surface as a box with a variable front face admittance (impedance). These will now be discussed.

The thin panel solution allows explicit representation of the diffuser shape. The complete diffuser can be covered with thin panel elements. Figure 8.9 shows a typical example. The complete enclosure of the diffuser by thin panel elements forces the interior to have zero pressure provided no critical frequencies are found. Two problems could arise from this representation: (1) A large number of thin panel elements with different sizes have to be sealed together, and the technique is therefore prone to human modelling errors. (2) The thin panel limit solutions for a plane panel showed small inaccuracies for scattering at grazing angles, particularly at high frequencies. This could be a problem for Schroeder diffusers with fins, as these are presented edge on to normal incident sources. The main drawback of this method is that it uses a very large number of elements and therefore predictions can exceed available computer power.

The approximate model, using a variable admittance on the front face of a box, is what most authors investigating Schroeder diffusers have used. The admittance

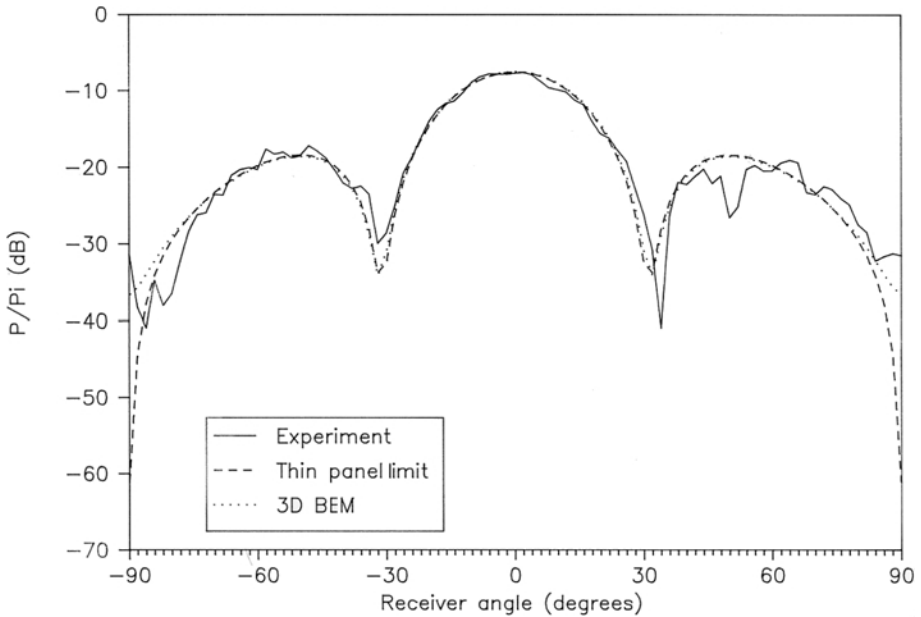


Figure 8.8 Comparison of scattered pressure from a plane surface measured and predicted by two boundary element models. Normalized to incident sound at receiver (after Cox [10]).

on the front face at the entrance of each well is derived from the phase change of plane waves propagating up and down the wells. This representation is expected to work under certain conditions: (1) The frequency must be below the cut-off frequency of the well so plane wave propagation in the wells predominates. (2) The impedance at the opening of the wells must be local reacting. There are two conditions necessary for assumption (2). First, the radiation coupling between the wells has to be small. Second, the radiation impedance of each well must also be small. Fortunately, these conditions seem to hold for practical Schroeder diffusers.

Comparisons with measurement show that the thin panel predictions of Schroeder diffuser scattering are accurate. Figure 8.10 shows an example for the scattered pressure. Similar accuracy is also achieved for the total field. The BEM model based on Equation 8.1 using the box representation with a variable front face admittance is also successful. This demonstrates that the simple phase change local reacting admittance assumption is reasonable – this assumption is discussed in more detail in Chapter 9.

So far, the discussions have been concerned with normal incidence. For oblique incidence sources, there is greater interaction across the front face of the diffuser and the simple phase change model will begin to break down. Figure 8.11 shows an example for a source at 60° , where the thin panel model which is assumed to be correct is compared to the standard BEM model using the variable admittance box. The standard BEM model is most accurate close to the specular reflection angle and

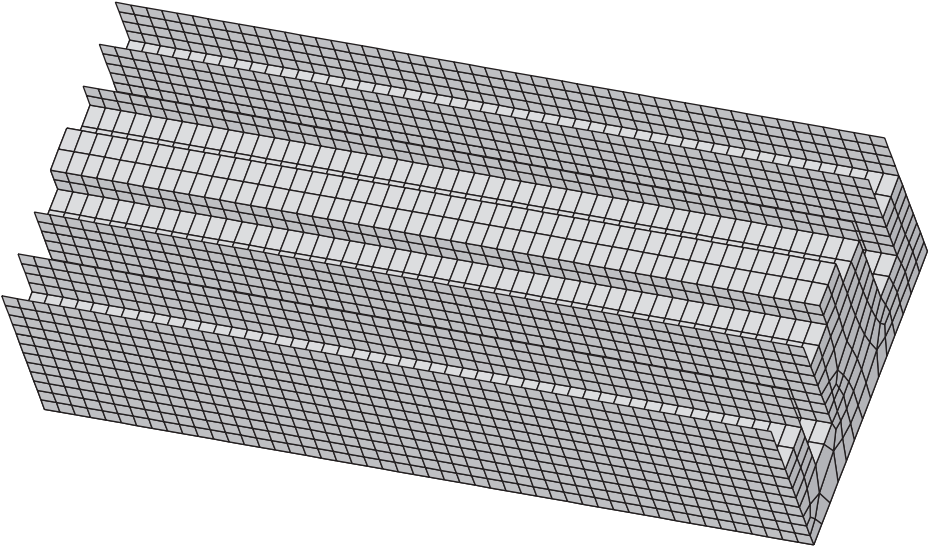


Figure 8.9 An example of a Schroeder diffuser meshed for prediction using a thin panel model.

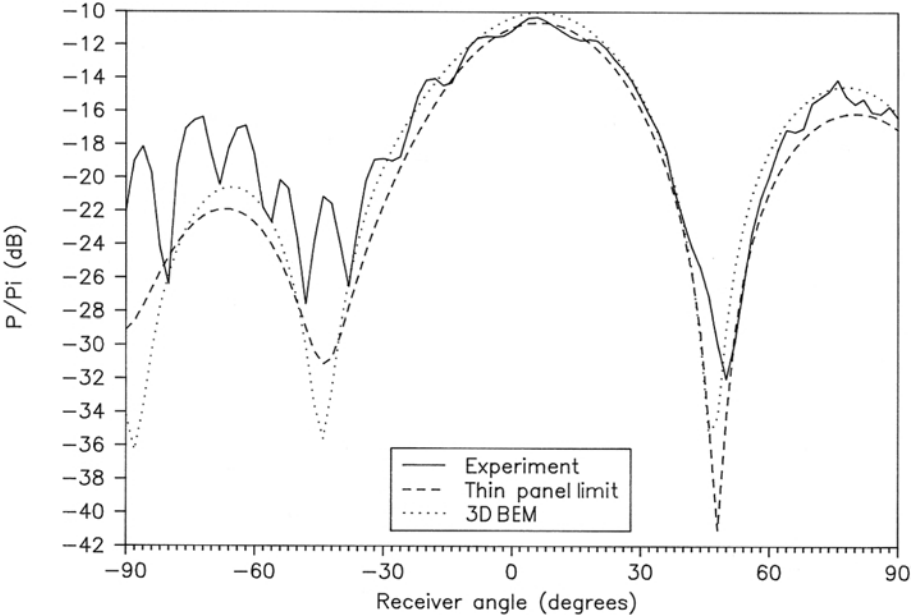


Figure 8.10 Pressure scattering from a Schroeder diffuser measured compared to two prediction models. Normalized to incident pressure at receiver (after Cox [10]).

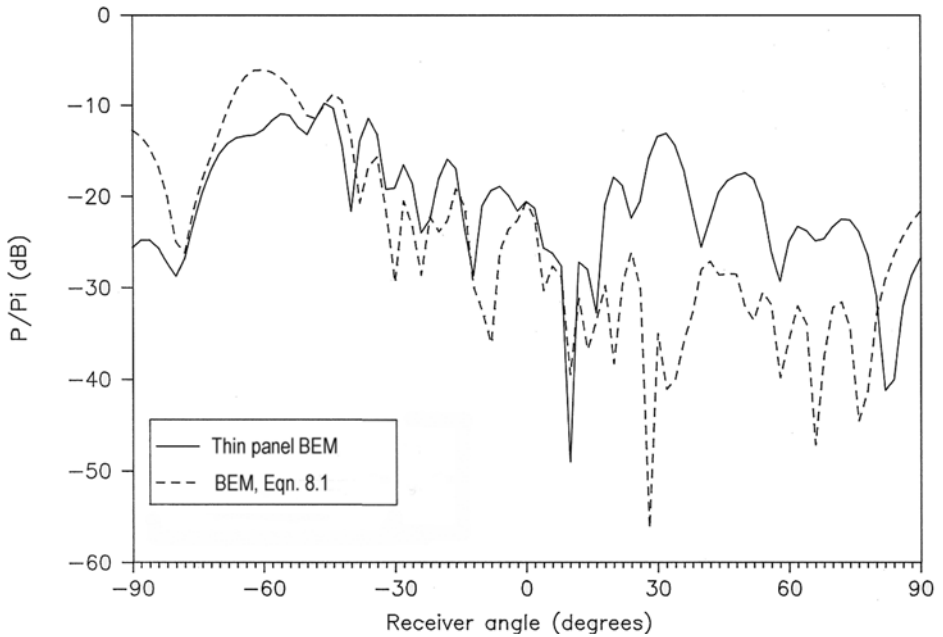


Figure 8.11 Comparison of two prediction models for the scattered pressure for oblique sound incident on a Schroeder diffuser. Normalized to incident pressure at receiver (after Cox [10]).

becomes more inaccurate the further from the specular reflection angle that the predictions are carried out at.

8.2 Kirchhoff

The rate-determining step in carrying out BEM predictions is the time taken to set up and solve the simultaneous equations to determine the surface pressures. Consequently, faster methods for estimating the surface pressures have been derived, as then the solution time can be vastly reduced. For an appropriate approximation, it is possible to turn to optics. Optics uses the Kirchhoff approximation to determine the propagation of light through an aperture. The Kirchhoff approximation gives the wave function and its derivative across the aperture as unaltered from the incident wave. On the surround defining the aperture, both the wave function and its derivative are assumed zero. Adapted for scattering in acoustics, this approximation can be used to obtain the surface pressures and their derivatives for surfaces, and yield reasonably accurate results for far field scattering. There are cases, however, where the method is not accurate, and so the method should be applied with care.

Consider a large planar surface, with constant surface impedance across the whole surface. By considering the definition of pressure reflection factor given in Chapter 1, it would be anticipated that the pressure on the surface $p(\mathbf{r}_s)$ would be given by:

$$p(\mathbf{r}_s) = [1 + R(\mathbf{r}_s)]p_i(\mathbf{r}_s, \mathbf{r}_0) \quad (8.21)$$

where R is the pressure reflection factor of the surface. Equation 8.21 is sometimes referred to as the Kirchhoff boundary condition. If the surface is completely non-absorbing, $R = 1$, then the surface pressure is simply double the incident pressure. When the surface is completely absorbing, $R = 0$, then the surface pressure is just the incident pressure. It is necessary to assume that the diffuser is thin, so that the pressure from the sides of the surface can be neglected. It is also assumed that the surface is large compared to wavelength so that the pressure on the rear of the panel can be assumed to be zero. Then substitution of Equation 8.21 into Equation 8.1 leaves a straightforward numerical integration over the front face which can be rapidly and readily evaluated.

Problems arise when applying the Kirchhoff boundary condition when the actual surface has significant thickness, is small compared to wavelength, or has a rapidly varying surface impedance. Problems also arise for oblique sources and receivers. In the following paragraphs, these problems are highlighted and discussed.

When a surface becomes very deep, then it is possible for second order reflections to occur. These second order reflections are not modelled by the Kirchhoff approximation. This is illustrated in Figure 8.12 for a set of triangles. A simple Kirchhoff model would predict significant grazing energy reflected from this triangular diffuser array, because it only models the first order reflections which result in grazing angle propagation. In reality, however, second order reflections mean that the scattered energy in fact returns back to the source. To prevent this problem, the Kirchhoff boundary conditions should only be applied to surfaces whose surface gradients are not too steep. It is generally assumed that when the surface is steeper than about $30\text{--}40^\circ$, then the prediction method is likely to become inaccurate.

When the surface becomes small compared to wavelength, the surface pressures on the rear of the panel become significant, and the assumption of zero pressure on the rear can be inaccurate. It is the problem of assuming zero pressure on the rear of the panel that can cause the predictions to become inaccurate if the angle of incidence or reflection becomes too large for finite sized surfaces. Furthermore, inaccuracies also appear in some cases because the scattering from the edges is not modelled, as the pressure on the edges is also assumed to be zero. Neglecting edge diffraction will also be more problematical for oblique sources and receivers.

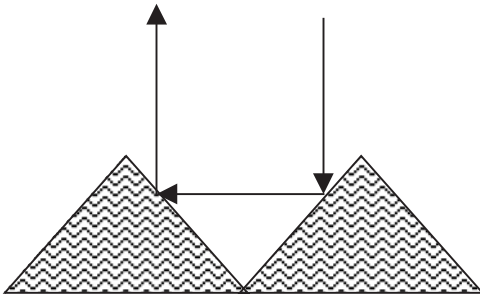


Figure 8.12 Example of a second order reflection from a set of triangles. This reflection will not be properly modelled by the Kirchhoff boundary conditions.

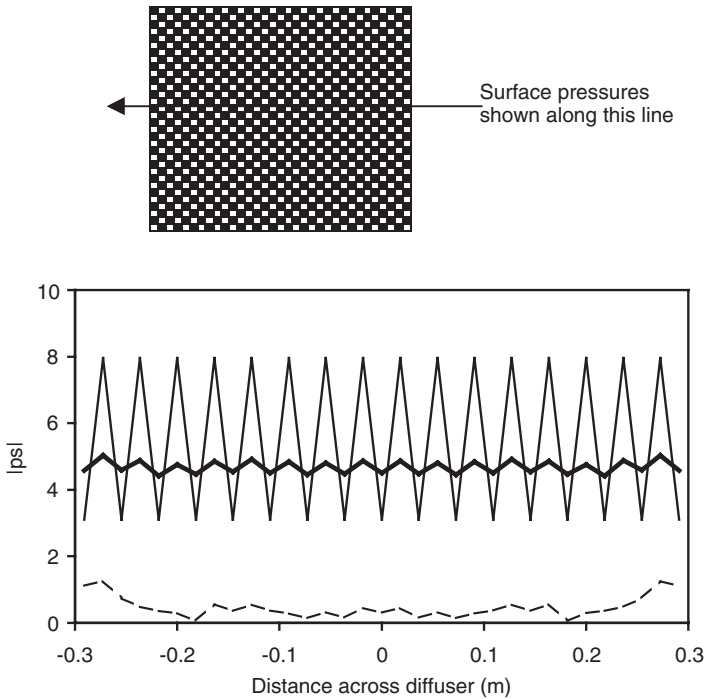


Figure 8.13 Surface pressure distribution for a boundary element model compared to the Kirchhoff boundary conditions. Hybrid surface made up of a periodic arrangement of hard (white) and soft (black) patches as shown. The pressure distribution is shown for a line through the middle of the surface as indicated. ——— Kirchhoff boundary condition pressures; ——— Front pressure, thin panel BEM; - - - - Rear pressure, thin panel BEM.

A surface which has a non-uniform surface impedance, where the impedance variation is rapid, can also cause problems. Consider the hybrid diffuser shown as an insert in Figure 8.13. The dark patches are absorbent ($R = 0$) and the light patches reflective ($R = 1$). Figure 8.13 shows the surface pressure distribution predicted by a BEM model for this surface, and these are compared to the Kirchhoff boundary conditions. The Kirchhoff boundary conditions predict a rapidly fluctuating pressure distribution due to the arrangement of hard and soft patches. The more accurate BEM model shows that mutual interactions across the surface significantly alter the pressure distribution, smoothing out the variation across the surface. This inaccuracy is not only a concern for the surface pressure calculation. If the far field polar response is considered, the Kirchhoff model in this case is most inaccurate.

The surface pressures are inaccurate, because there is an assumption in Equation 8.21 that the surface is large in extent. Consequently, it is necessary to have a surface where the surface impedance variation is large compared to wavelength, i.e. the patches of different impedance should be larger than half a wavelength. This is why the Kirchhoff boundary conditions fail for the case shown in Figure 8.13. This would also appear to rule out the use of the Kirchhoff boundary conditions for Schroeder

diffusers, but fortunately the case of most Schroeder diffusers is less severe than that shown in Figure 8.13, for example the well width is wider for commercial implementations, and good prediction accuracy can be achieved.

Given all the above reservations, the Kirchhoff solution is surprisingly good and useful for many acoustic diffusers. For a plane flat surface, accurate results are achieved because the surface pressures are close to those given by the Kirchhoff boundary conditions. Figure 8.14 shows a typical example. Close to the specular reflection direction, the accuracy of the Kirchhoff solution increases as the frequency increases. As the frequency increases the pressure on the rear of the panel decreases, as does edge diffraction and mutual interactions across the surface. For single curved surfaces, better accuracy is obtained, although there is a tendency for the Kirchhoff solution to incorrectly smooth out local minima in the polar distribution.

To use the Kirchhoff solution for Schroeder diffusers, the model of a box with a variable front face admittance must be used as described in Section 8.1.6. As the Kirchhoff boundary conditions do not allow for mutual interactions across the surface, it is not completely successful in predicting the sound field. This is most obvious at low frequencies. Figures 8.15 and 8.16 contrast the prediction accuracy achieved at low and mid-high frequencies. Again the accuracy is best near the specular reflection angle. The Schroeder diffuser tends to scatter more sound energy to the side than a plane surface, and this tends to mask the decreasing accuracy with an angle that is normally found with the Kirchhoff model. For oblique receivers, the predictions become less accurate as the simple phase change admittance model breaks down.

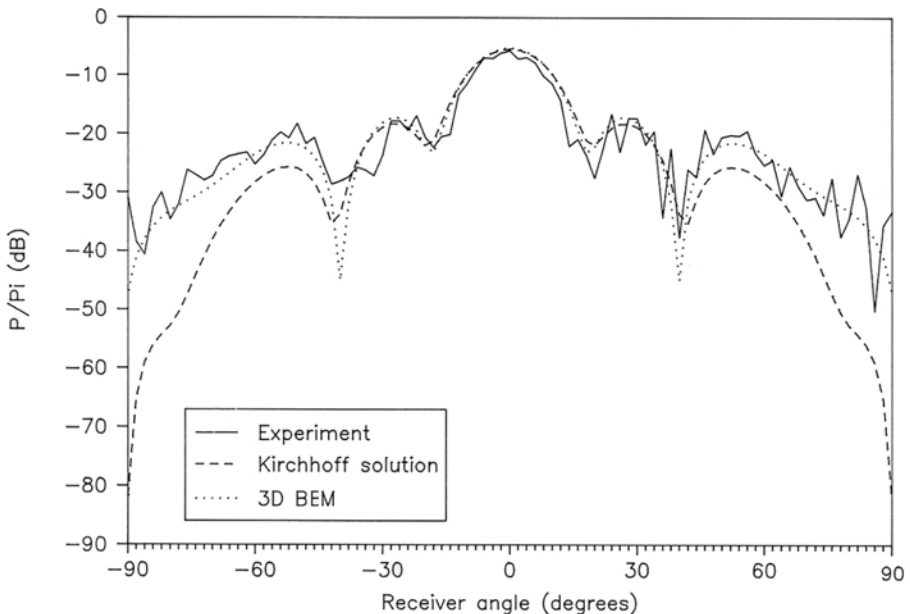


Figure 8.14 Pressure scattering from a plane surface comparing the accuracy of the Kirchhoff solution to BEM and experiment. Normalized to incident pressure at receiver (after Cox [10]).

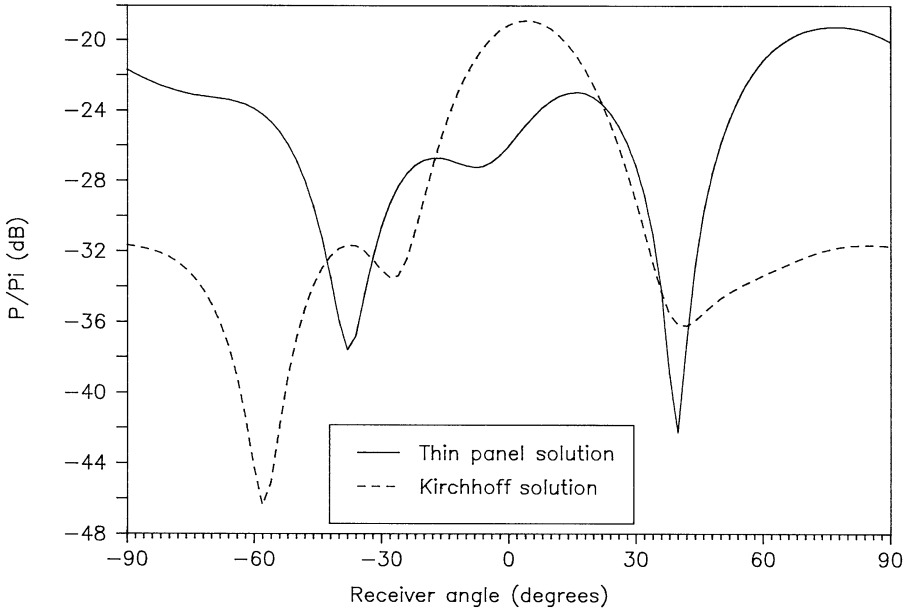


Figure 8.15 Predicted scattering from a Schroeder diffuser at a low frequency using two different prediction models (after Cox [10]).

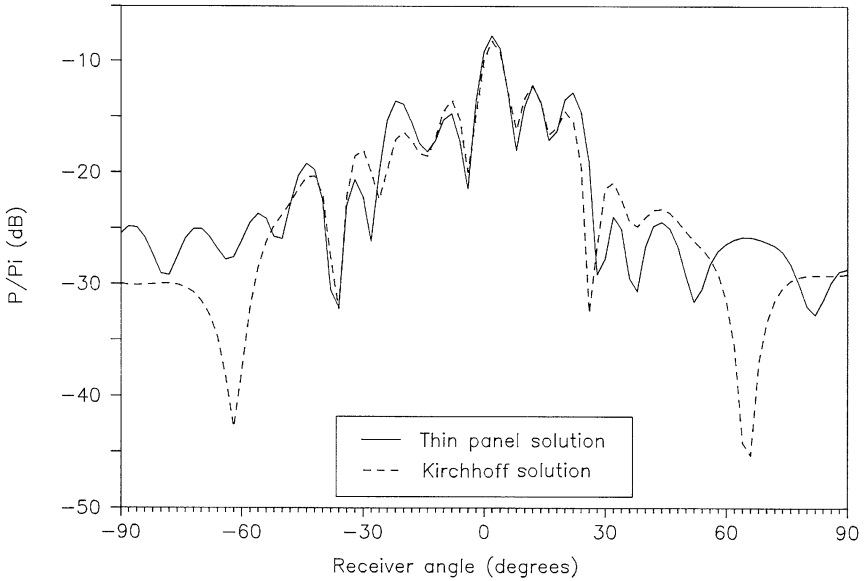


Figure 8.16 Predicted scattering from a Schroeder diffuser at a mid-high frequency using two different prediction models (after Cox [10]).

8.3 Fresnel

Once the Kirchhoff boundary conditions have been assumed, the resulting numerical integration can be simplified further. This can be done either to facilitate faster computation or to enable the derivation and understanding of simpler design principles. The Kirchhoff boundary conditions (Equation 8.21) are substituted into the Helmholtz–Kirchhoff integral equation (Equation 8.1). The usual relationship between surface admittance and pressure reflection factor as given in Chapter 1 is also used. (Remembering that in this case the normal to the surface is pointing outwards, as is usually the case with BEM models, whereas surface admittance is normally defined with an inwardly pointing normal.) Combining these equations gives the following formulation:

$$p(\mathbf{r}) = p_i(\mathbf{r}, \mathbf{r}_0) + \int_s p_i(\mathbf{r}_s, \mathbf{r}_0) [1 + R(\mathbf{r}_s)] \left[\frac{\partial G(\mathbf{r}, \mathbf{r}_s)}{\partial n(\mathbf{r}_s)} - G(\mathbf{r}, \mathbf{r}_s) jk \cos(\psi) \frac{(R(\mathbf{r}_s) - 1)}{(R(\mathbf{r}_s) + 1)} \right] ds \quad (8.22)$$

where ψ is the angle of incidence. It is assumed that the receiver is sufficiently far from the surface so that the differential of the Green's function can be approximately given by:

$$\frac{\partial G(\mathbf{r}, \mathbf{r}_s)}{\partial n(\mathbf{r}_s)} \approx -jkG(\mathbf{r}, \mathbf{r}_s) \cos(\theta) \quad (8.23)$$

where θ is the angle of reflection. This relation is true for both the 2D and 3D Green's function. Combining Equations 8.22 and 8.23 gives:

$$p(\mathbf{r}) = p_i(\mathbf{r}, \mathbf{r}_0) - jk \int_s p_i(\mathbf{r}_s, \mathbf{r}_0) [1 + R(\mathbf{r}_s)] G(\mathbf{r}, \mathbf{r}_s) \left[\cos(\theta) + \cos(\psi) \frac{(R(\mathbf{r}_s) - 1)}{(R(\mathbf{r}_s) + 1)} \right] ds \quad (8.24)$$

Fresnel diffraction is a method normally designed to work with non-absorbing panels, i.e. $R = 1$. In that case Equation 8.24 simplifies further.

$$p(\mathbf{r}) = p_i(\mathbf{r}, \mathbf{r}_0) - 2jk \int_s p_i(\mathbf{r}_s, \mathbf{r}_0) G(\mathbf{r}, \mathbf{r}_s) \cos(\theta) ds \quad (8.25)$$

For simplicity, just the 3D case will be considered, although the findings below are readily translated into a 2D representation. Consider a point source which is not too close to a planar diffuser, then the incident pressure p_i is given by the Green's function. It is necessary to come up with approximations for the distances $|\mathbf{r}_s - \mathbf{r}_0|$ and $|\mathbf{r} - \mathbf{r}_s|$. By considering the geometry shown in Figure 8.1 with the diffuser in the $y = 0$ plane, and a simple binomial expansion, it is possible to show that these distances are given by:

$$|\mathbf{r}_s - \mathbf{r}_0| \approx |\mathbf{r}_0| - \frac{x_0 x_s + z_0 z_s}{|\mathbf{r}_0|} + \frac{x_s^2 + z_s^2}{|\mathbf{r}_0|} \quad (8.26)$$

$$|\mathbf{r} - \mathbf{r}_s| \approx |\mathbf{r}| - \frac{\mathbf{x}\mathbf{x}_s + \mathbf{z}\mathbf{z}_s}{|\mathbf{r}|} + \frac{x_s^2 + z_s^2}{|\mathbf{r}|} \quad (8.27)$$

If Equations 8.26 and 8.27 are substituted into Equation 8.25, the following expression is obtained for the scattered pressure:

$$p_s(\mathbf{r}) \approx -\frac{jk}{8\pi^2} \frac{e^{-jk(r_0+r)}}{rr_0} \cos(\theta) \iint e^{jk(xx_s+zz_s+x_s^2+z_s^2)/r} e^{jk(x_0x_s+z_0z_s+x_s^2+z_s^2)/r_0} dx_s dz_s \quad (8.28)$$

It has been assumed that the variation in $|\mathbf{r}_s - \mathbf{r}_0|$ and $|\mathbf{r} - \mathbf{r}_s|$ in the denominator of the Green's function is negligible compared to the variation in the phase of the complex exponential – an assumption often applied in optics. This enables the denominator of the Green's function to be moved outside the integral. Similar arguments allow the $\cos(\theta)$ to also be moved outside the integration.

The phase terms of the complex exponentials are quadratic in x_s and z_s and so it is not possible to provide an analytical solution to this integration. In the past, this was overcome by using the Fresnel integrals, which were numerical solutions of the above functional form which were readily available in tables. Nowadays, however, there is little point in using Fresnel integrals as computer power has increased to such an extent that the Kirchhoff approximation might as well be used. There are, however, some neat and simple short cuts to calculating the above integration suggested by Rindel [11], which could be used if speed is at a premium. The Fresnel solution does, however, lead the discussion to far field prediction models, which are key to understand Schroeder surfaces and other diffusers. Consequently, the discussion now continues with a far field solution.

8.4 Fraunhofer or Fourier solution

This solution is only valid in the far field, when both source and receiver are some distance from the surface. Then it is possible to neglect the quadratic terms in the integration in Equation 8.28 to obtain:

$$p_s(\mathbf{r}) \approx -\frac{jk}{8\pi^2} \frac{e^{-jk(r_0+r)}}{rr_0} \cos(\theta) \iint e^{jk(xx_s+zz_s)/r} e^{jk(x_0x_s+z_0z_s)/r_0} dx_s dz_s \quad (8.29)$$

For a planar surface, this then gives an analytical equation that can be solved. Assuming the panel is $2a$ long in the x -direction and $2b$ long in the z -direction, the scattering is given by two sinc functions:

$$p_s(\mathbf{r}) \approx -\frac{jkab}{2\pi^2} \frac{e^{-jk(r_0+r)}}{rr_0} \cos(\theta) \operatorname{sinc}\left(k\left(\frac{x}{r} + \frac{x_0}{r_0}\right)a\right) \operatorname{sinc}\left(k\left(\frac{z}{r} + \frac{z_0}{r_0}\right)b\right) \quad (8.30)$$

$$\operatorname{sinc}(x) = \sin(x)/x$$

This is a result familiar from optics and signal processing. The Fourier transform of a rectangular or top hat function gives a sinc() response. (Note that in some numerical

packages and texts sinc() is defined with a π multiplying x .) Equation 8.30 enables quick estimations of the far field scattering from a rigid flat surface and is very fast.

While the above case is interesting, the Fraunhofer solution is arguably going to be most useful in analyzing surfaces which do not have unity reflection coefficient. The most obvious example being the Schroeder diffuser which can be modelled as having a variable phase impedance on the front surface of a box. To carry out this analysis, it is necessary to return to Equation 8.24 and to apply the distance approximations outlined above. For conciseness, consider just the scattered pressure:

$$p_s(\mathbf{r}) = -\frac{jk}{16\pi^2} e^{-jk(r+r_0)} \iint e^{jk(x_0x_s+z_0z_s)/r_0} [1 + R(\mathbf{r}_s)] e^{jk(xx_s+zz_s)/r} \times \left[\cos(\theta) + \cos(\psi) \frac{(R(\mathbf{r}_s) - 1)}{(R(\mathbf{r}_s) + 1)} \right] dx_s dz_s \quad (8.31)$$

To simplify the analysis, just normal incidence sound will be considered; furthermore, it will be assumed that the surface admittance variation is only in the x -direction. It is possible to keep all the terms included, but the equations become rather long and the key points of the analysis lost in a forest of symbols. With these simplifications, it can be shown that the scattering is given by:

$$p_s(\mathbf{r}) = -\frac{jk}{8\pi^2} e^{-jk(r+r_0)} \text{sinc}\left(\frac{kb}{r}\right) \times \left\{ \int_{-a}^a R(\mathbf{r}_s) e^{jkx_s \sin(\theta)} [\cos(\theta) + 1] dx_s \right\} + \left\{ \int_{-a}^a e^{jkx_s \sin(\theta)} [\cos(\theta) - 1] dx_s \right\} \quad (8.32)$$

The term in $[\cos(\theta) - 1]$ is usually less than the term in $[\cos(\theta) + 1]$, especially away from grazing angles. Consequently, it can be ignored. This leads to a scattered pressure of:

$$p_s(\mathbf{r}) = -\frac{jk}{8\pi^2} e^{-jk(r+r_0)} \text{sinc}\left(\frac{kb}{r}\right) [\cos(\theta) + 1] \int_{-a}^a R(\mathbf{r}_s) e^{jkx_s \sin(\theta)} dx_s \quad (8.33)$$

This is essentially the equation used by Schroeder in the design of phase grating diffusers, although he derived his equations following a different philosophy. Furthermore, there are some additional factors outside the integral. Several authors neglect the $[\cos(\theta) + 1]$, and this simplified form is often called a Fourier theory because the integration is essentially a Fourier transform.

8.4.1 *Near and far field*

As the analysis is now considering a far field prediction model, it is expedient to define what the near and far field mean. Unfortunately, with diffusers the location of the near and far field is not as clear cut as for simple piston radiators, which is the case most often cited in acoustic texts. The far field is defined as the region where the difference between minimum and maximum path lengths from the panel to the receiver

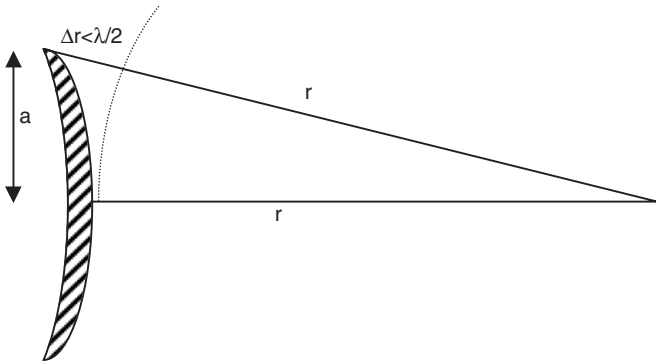


Figure 8.17 Standard construction for determining near field extent.

is small compared to wavelength. In this region, all points on the panel are effectively at the same distance from the receiver [12]. This is illustrated in Figure 8.17. For diffusers, there is an added complication that both the source and receiver need to be considered, but to simplify discussions, it will be assumed that the source is always at infinity. There is also a second requirement for the far field, which is that the receiver distance should be large compared to wavelength. This is, however, not usually the critical requirement for the geometries that occur with diffusers. Frequencies, where the wavelength is long enough for this to be a consideration, are usually below the lower frequency limit at which surface roughness effects are important. When this can be important is when receivers are close to diffusers, as might happen in poorly designed small rooms as discussed in Chapter 2.

In the far field, the polar response is independent of the receiver distance from the surface. This makes it a useful place to test diffusers. By considering the geometry in Figure 8.17 for a planar surface, it is possible to show that the far field is for an on axis receiver radii given by:

$$r > \frac{a^2}{\lambda} \quad (8.34)$$

Unfortunately, this far field formulation is not applicable to the case of oblique sources and receivers. As Figure 4.14 demonstrated, the true far field is only achieved for many diffusers when the receiver radius is many hundreds of metres! For further discussion of this issue, see Section 4.1.1.

8.4.2 Fraunhofer theory accuracy

Provided sources and receivers are in the far field, for plane and Schroeder surfaces, the accuracy of the Fraunhofer theory is similar to the Kirchhoff solution. So if the results in Figure 8.14 were predicted with the Fraunhofer solution, similar results to the Kirchhoff solution would be obtained. Consequently, in the far field the limiting factor for accuracy is the Kirchhoff boundary conditions, so where the Kirchhoff model fails, so does the Fraunhofer method. Consequently, low frequency

predictions, and oblique sources and receivers can cause problems for the Fraunhofer method.

Differences between Kirchhoff and Fraunhofer solutions occur when the receiver is in the near field; this is true for all diffusers. Consequently, high frequency predictions can become inaccurate as the near field extends further at higher frequency – a fact that can often surprise the unwary. Figure 8.18 shows the scattering from an $N = 11$ Schroeder diffuser in the near field. It is assumed the BEM model is accurate, and consequently this shows that the inaccuracies in the Fraunhofer model are significant at this distance. Figure 8.19 shows the same situation, but now the receiver is 50 m from the diffuser, which is safely in the far field. At these distances, the Fraunhofer solution is as accurate as the Kirchhoff model. It is not often, however, that application realistic sources and receivers are this far from the panel. In diffuser design, however, the usual assumption is that a good far field diffuser will also work in the near field, as discussed in Chapter 4.

8.5 Other methods

8.5.1 Transient model

It is possible to use the full time dependent form of the Helmholtz–Kirchhoff integral equation, instead of the constant frequency version, to derive the surface pressures. To solve the time dependent form the surface is again discretized. It can be shown from the time dependent integral equation [13] that the velocity potential and its derivative on the surface can then be represented by the incident velocity potential from the source plus contributions from the other elements at previous times. This is an exact solution and not an iterative method. Problems arise because the convergence of the surface velocity

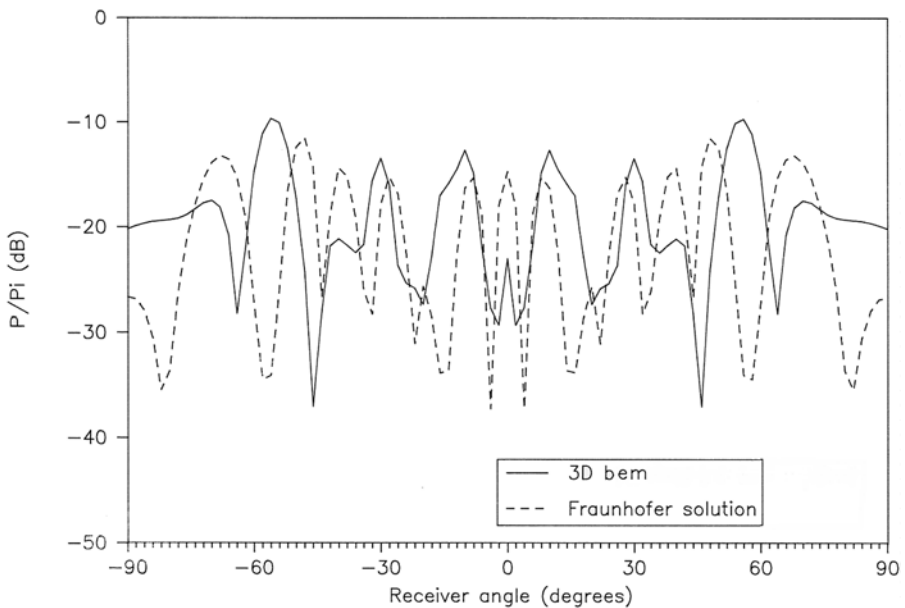


Figure 8.18 Scattered pressure from a surface. Comparison between Fraunhofer solution and BEM model in near field (after Cox [10]).

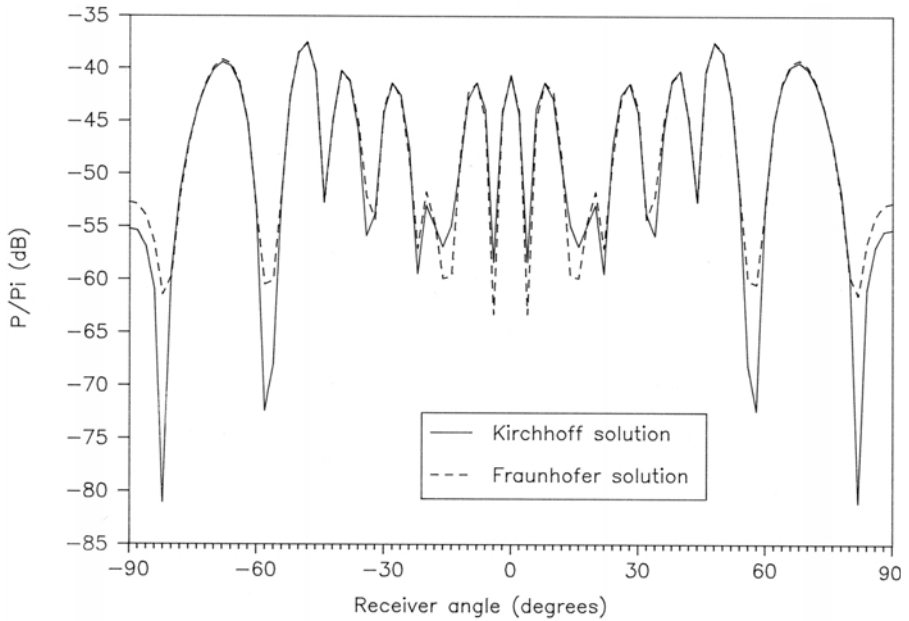


Figure 8.19 Scattered pressure from a surface. Comparison between Fraunhofer and Kirchhoff solutions in the far field (after Cox [10]).

potentials can be very slow. When choosing the elements it is necessary to use elements an eighth of a wavelength or smaller so that the pressure variation is well represented. It is also necessary that any variation within any time step is restricted to be contained within one element. This leads to a very small time step and hence slow convergence. The method has advantages over the constant frequency methods in that once the impulse response has been calculated, the full frequency response can easily be obtained by a Fourier transform. However, the model needs further development, particularly for non-rigid bodies, as the formulation of surface admittance in the time domain is ill defined.

8.5.2 FEA

FEA uses volumetric rather than surface meshes [14]. This makes the technique much slower than boundary element modelling when dealing with exterior domain acoustic problems such as the scattering from diffusers. Where it does have advantages is where there is fluid and structural motion. For example, it can model the behaviour of a non-rigid diffuser which exhibits structural vibration. As this sort of diffuser is currently rare, and structural motion is usually deliberately avoided in diffuser design, the use of FEA for scattering is not the most efficient method.

8.5.3 Edge diffraction models

Edge diffraction models can be used to produce the scattering from wedges and simple shapes. For a plane rigid surface, the total field can be seen as a sum of the direct

sound, specular reflections and edge diffraction components [15]. Consequently, it is possible to solve the scattering problem by integrating over the edges present in a diffuser. This type of method becomes rather slow if high orders of edge diffraction need be considered, as would be the case for complex surfaces. It does, however, directly lead to a sampled impulse response, and consequently is particularly useful where broadband time domain scattering is needed to be calculated or if the results are to be integrated into geometric room acoustic models.

8.5.4 *Wave decomposition and mode-matching approaches*

It is possible to carry out a wave decomposition of the acoustic wave knowing the spatial distribution of the diffuser. Strube [16–18] used this approach to solve the scattering from Schroeder diffusers. In Chapter 7, an example of this type of theory will be used to explain the absorption from Schroeder diffusers. For that reason, this type of theory is only briefly described here. In this theory, it is normal to assume that the diffuser structure is periodic, and then it is possible to decompose the scattered wave into the different diffraction lobes using a Fourier decomposition. It is then possible to set up and solve simultaneous equations into the diffraction lobe scattered amplitudes. These methods offer an alternative approach to boundary element models, but BEMs are considerably more useful as they can be applied to arbitrary surfaces. The modal decomposition models are particularly powerful when predicting the effects of large arrays of periodic structures, as the size of the problem to be solved is considerably smaller under this formulation than with a BEM model.

8.5.5 *Random roughness*

In the theories used so far, a deterministic approach has been taken, with the surface geometry and impedance properties being modelled exactly. For large-scale surfaces with small roughness, this can turn out to be a very inefficient method for carrying out predictions. In that case, it may be advantageous to use a statistical approach, whereby the surface is only determined by some shape statistics (the rms surface height, the slope probability function, etc.) [19]. In diffuser design, these theories are not often useful because the size of the surface roughness is large and the sample of roughness that might be used is small in width, and so a few shape statistics are not sufficient to accurately predict the scattering from the surface. This is illustrated in Figure 8.20. The top shape is meant to generically represent deliberately designed

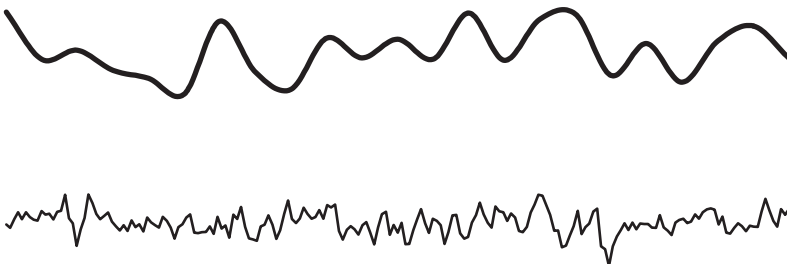


Figure 8.20 Two different randomly generated surfaces.

diffusers, where the scale of the roughness is deep and relatively slow varying. In this case, the small number of bumps on the surface will dominate the scattering in such a way that a statistical approach is not applicable. The bottom line in Figure 8.20, however, represents a more randomly rough surface, for which the theories based on a few shape statistics may be more applicable. To put it another way, there needs to be a sufficient wide sample of the surface roughness for the shape statistics to be properly representative of the surface.

For accidental surface roughness, this statistical approach is more useful, especially as it may be impossible to get the exact geometry of all shapes in existing structures. Random rough theories are probably most commonly used in underwater acoustics, although both Cox and D'Antonio [20] and Embrechts *et al.* [21] have used statistical approaches to diffuser scattering. In the case of Cox and D'Antonio, this was investigated with respect to the design of fractal diffusers. For Embrechts *et al.* a statistical approach was taken to investigate scattering coefficients from surfaces. These approaches usually assume the Kirchhoff boundary conditions, and so an additional limitation is that the surface gradients must not be too steep, otherwise second and high order reflections become important, and the statistical approach breaks down.

8.5.6 Boss models

Boss models are hybrid approaches [19]. They use a deterministic solution for the scattering from a single element – examples include cylinders and hemispheres – and then model the distribution of the elements in a statistical manner. Twersky developed the best known approach [22]. This theory allows high order scattering, across all frequencies, both in 2 or 3D to be considered. Up to date versions of the theory also enable scattering from different sized bosses. One of the problems with applying this model is to represent complex surfaces by a series of regular-sized bosses. In some cases this might be easy; in the case shown at the bottom of Figure 8.20, on the other hand, this would be rather tricky. Rendell *et al.* [23] has applied a boss model to predict scattering by hemispherical surface elements in auditoria.

8.6 Summary

In this chapter, some commonly used prediction models for scattering have been outlined and the necessary equations developed. These theories will be drawn upon in the design of diffusers, which is the subject of next three chapters.

8.7 References

- 1 A. J. Burton, *The Solution of Helmholtz Equation in Exterior Domains Using Integral Equations*, National Physical Laboratory Report NAC30 (1973).
- 2 M. Abramowitz and I. A. Stegun (eds), *Handbook of Mathematical Functions*, Dover Publications Inc., NY (1965).
- 3 W. H. Press *et al.*, *Numerical Recipes*, Cambridge University Press, Cambridge (1989).
- 4 H. A. Schenck, "Improved integral formulation for acoustic radiation problems", *J. Acoust. Soc. Am.*, 55, 41–58 (1968).
- 5 T. J. Cox, "Predicting the scattering from reflectors and diffusers using 2D boundary element methods", *J. Acoust. Soc. Am.*, 96(2), 874–878 (1994).

- 6 T. Terai, "On the calculation of fields around three-dimensional objects by integral equation method", *J. Sound Vib.*, **68**, 71–100 (1980).
- 7 Y. W. Lam, "A boundary integral formulation for the prediction of acoustic scattering from periodic structures", *J. Acoust. Soc. Am.*, **105**(2), 762–769 (1999).
- 8 F. Bloch, "Über die Quantenmechanik der Elektronen in Kristallgittern", *Z. Phys.*, **52**, 555–600 (1928).
- 9 T. J. Cox and Y. W. Lam, "Evaluation of methods for predicting the scattering from simple rigid panels", *Appl. Acoust.*, **40**, 123–140 (1993).
- 10 T. J. Cox, "Objective and Subjective Evaluation of Reflection and Diffusing Surfaces in Auditoria", PhD thesis, University of Salford (1992).
- 11 J. H. Rindel, "Attenuation of sound reflections due to diffraction", *Nordic Acoustical Meeting*, 257–260 (1986).
- 12 L. E. Kinsler, A. R. Frey, A. B. Coppens and J. V. Sanders, *Fundamentals of Acoustics*, 4th edn, John Wiley & Sons (2000).
- 13 Y. Kawai and T. Terai, "A numerical method for the calculation of transient acoustic scattering from thin rigid plates", *J. Sound Vib.*, **141**, 83–96 (1990).
- 14 D. G. Crighton, A. P. Dowling, J. E. Ffowcs Williams, M. Heckl and F. G. Leppington, *Modern Methods in Analytical Acoustics, Lecture Notes*, Springer-Verlag (1992).
- 15 P. Svensson, R. Andersson and J. Vanderkooy, "An analytical time domain model of edge diffraction", *Nordic Acoustical Meeting* (1998).
- 16 H. W. Strube, "Scattering of a plane wave by a Schroeder diffuser: a mode matching approach", *J. Acoust. Soc. Am.*, **67**(2), 453–459 (1980).
- 17 H. W. Strube, "Diffraction by a planar, local reacting, scattering surface", *J. Acoust. Soc. Am.*, **67**(2), 460–469 (1980).
- 18 H. W. Strube, "More on the diffraction theory of Schroeder diffusers", *J. Acoust. Soc. Am.*, **70**(2), 633–635 (1981).
- 19 D. Chu and T. K. Stanton, "Application of Twersky's boss scattering theory to laboratory measurements of sound scattered by a rough surface", *J. Acoust. Soc. Am.*, **87**(4), 1557–1568 (1990).
- 20 T. J. Cox and P. D'Antonio, "Fractal sound diffusers", *Proc. 103rd Convention of the Audio Eng. Soc.*, preprint 4578, Paper K-7, New York (1997).
- 21 J. J. Embrechts, D. Archambeau and G. B. Stan, "Determination of the scattering coefficient of random rough diffusing surfaces for room acoustics applications", *Acta Acustica-Acustica*, **87**, 482–494 (2001).
- 22 V. Twersky, "On scattering and reflection of sound by rough surfaces", *J. Acoust. Soc. Am.*, **29**, 209–225 (1957).
- 23 R. R. Torres, G. Natsiopoulos and M. Kleiner, "Room acoustics auralization with boss-model scattering, compared with a Lambert diffusion model", *Symposium on Surface Diffusion in Room Acoustics*, Liverpool (2000).

9 Schroeder diffusers

One of the most significant occurrences in the design of diffusers, if not the most important event, was the invention of the phase grating diffuser by Schroeder [1, 2]. Apart from very simple constructions, previous diffusers had not dispersed sound in a predictable manner. The Schroeder diffuser offered the possibility of producing so-called optimum diffusion and also required only a small number of simple to use design equations. D'Antonio and Konnert [3] presented one of the most readable reviews of the far field diffraction theory of Schroeder's number theoretic surfaces, experimentally measured their performance and described their application in critical listening environments. Most crucially, they commercialized Schroeder diffusers and so made them widely available. Since the publication of Reference 3, there have been many new developments which have not been brought together and documented in one place. Therefore the intention of this chapter is to tell the whole story of Schroeder diffusers. Much of this chapter featured as a review article in the journal *Building Acoustics* [4].

The chapter will start by outlining a largely qualitative view of the diffuser, how it works and the basic design principles. Following this, a more detailed quantitative and theoretical analysis of the diffuser will be given. In these descriptions, the ingenuity of the original design concept will hopefully become apparent. In addition, more recent developments will be presented, illustrating weaknesses in the original design which can be overcome by modifying the design procedure, sometimes using one of Schroeder's favourite subject area of number theory. Finally, it will be shown that better phase gratings can be made using an optimization procedure.

9.1 Basic principles

Figure 9.1 shows a single plane or 1D Schroeder diffuser. It consists of a series of wells of the same width and different depths. The wells are separated by thin fins. The depths of the wells are determined by a mathematical sequence, such as the quadratic residue sequence. Single plane diffusers cause scattering in one plane, in the other direction, the extruded nature of the surface makes it behave like a plane surface. Because of this it is normal to just consider a cross section through the diffuser (Figure 9.2) which contains the plane of maximum dispersion. Multi-plane diffusers are possible as shown in Figure 9.1 and are discussed later in Section 9.7.

Consider a mid-frequency plane wave incident onto the diffuser. Plane wave propagation within the wells in the y -direction occurs. The plane waves are reflected from the bottom of the wells and eventually re-radiate into the space. For now, it will be assumed



Figure 9.1 Schroeder diffusers: single plane or 1D (left) and 2D (right).

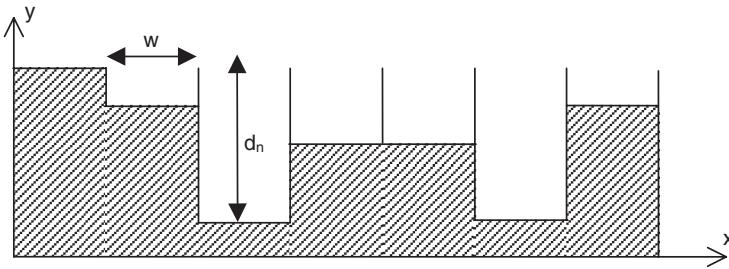


Figure 9.2 A cross section through an $N=7$ quadratic residue diffuser (QRD[®]).

that there is no loss of energy. The pressure at a point external to the diffuser is therefore determined by the interference between the radiating waves from each well. All these waves have the same magnitude but a different phase because of the phase change due to the time it takes the acoustic wave to go down and up each well. Consequently, the polar distribution of the scattering is determined by the choice of well depths. Schroeder showed that by choosing a quadratic residue sequence, the energy scattered into each diffraction lobe direction is the same. In Figure 9.3, an example of the scattering from the surface is given, as calculated by the simplest and most approximate theory at a frequency where optimum diffusion is achieved. Eleven lobes of the same energy are found in this case. These lobes are generated because the surface is periodic.

9.2 Design equations

For the design theory to be correct, plane wave propagation within the wells must dominate. Consequently, an upper frequency for the diffusion to follow the simple design principles can be found from:

$$w = \lambda_{\min}/2 \quad (9.1)$$

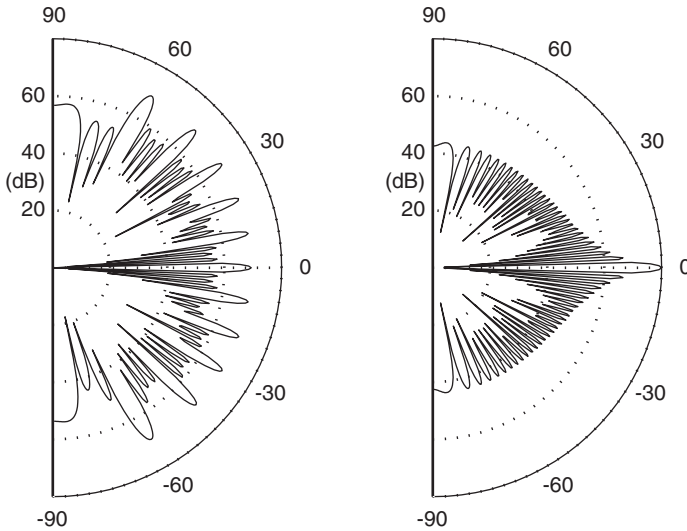


Figure 9.3 Scattered level from a Schroeder diffuser (left) and a plane surface (right) of the same size.

where λ_{\min} is the minimum wavelength before cross modes in the wells appear and w the well width. Above this limit scattering will continue to occur because these are complicated structures. Consequently, this is just a limit of applicability of a theory, and not an upper limit on the diffusion quality.

This need for plane wave propagation explains the need for fins to separate the different depth wells. Even for normal incidence, the lack of wells will cause the scattering not to follow these simple design principles. The fins should be as narrow as possible, but not so narrow that they vibrate and cause significant resonant losses.

A quadratic residue sequence is the most popular mathematical sequence used to form the well depths. The sequence number for the n th well, s_n , is given by:

$$s_n = n^2 \text{ modulo } N \quad (9.2)$$

where modulo indicates the least non-negative remainder and is often written as mod for short. N is the prime number generator which in this case is also the number of wells per period. For example, one period of an $N=7$ QRD has $s_n = \{0, 1, 4, 2, 2, 4, 1\}$.

Schroeder diffusers work at integer multiples of a design frequency, f_0 . The design frequency is normally set as the lower frequency limit. It is more convenient to present formulations in terms of the corresponding design wavelength, λ_0 , and so that will be done here. The depth of the n th well in the diffuser d_n is determined from the sequence via the following equation:

$$d_n = \frac{s_n \lambda_0}{2N} \quad (9.3)$$

The well depths consequently vary between 0 and approximately $\lambda_0/2$. The design frequency is not the lowest frequency at which the surface produces more scattering than a plane surface, it is just the first frequency at which the scattering can have even energy diffraction lobes. It has been shown that Schroeder diffusers scatter differently from a plane hard surface an octave or two below the design frequency [5, 6].

9.3 Some limitations and other considerations

Given the above equations, it is possible to design a diffuser to a desired bandwidth. There are some subtle details in the design that must be heeded to achieve the best possible diffusion.

If the period width (Nw) is too narrow, then at the first design frequency there is only one major lobe, and so this principle of even lobes is rather irrelevant. The period or repeat width is often significant in determining performance, especially when the repeat width is small. This is illustrated in Figure 9.4 where the scattering from diffusers of different period widths is shown. These are both $N=7$ QRDs with a design frequency of 500 Hz. The well widths are 3 and 9 cm, which means that the period widths are 21 and 70 cm respectively. The number of periods for each diffuser is set so that the overall widths of the devices are the same for a fair comparison. For the narrow wells and period width, shown right, the low frequency limit of diffusion is determined by the period width and not by the maximum

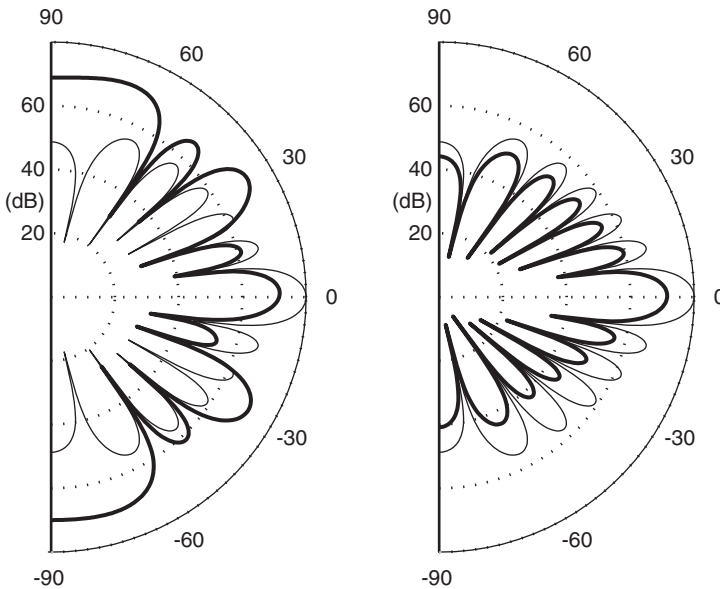


Figure 9.4 The pressure scattered from two quadratic residue diffusers at 1,000 Hz. Left figure ——— QRD well width 9 cm; Plane surface. Right figure ——— QRD well width 3 cm; Plane surface. Overall width kept the same by changing number of periods.

depth. This is illustrated in Figure 9.5 where the diffusion coefficient versus frequency is shown. The narrow well width diffuser only starts causing significant diffusion over and above the plane surface at 1.5 kHz, three times the design frequency. This is roughly the frequency at which the first grating lobe appears for the narrow diffuser and so is the first frequency where significant scattering in oblique directions is achieved. For the wide well width, the first grating lobe appears below the design frequency and so significant diffusion is caused at 500 Hz and above.

For the diffuser to behave optimally, the device must be periodic. The lobes are generated by the periodicity of the surface. Without periodicity, all that the design equations portray is the fact that in certain directions the scattering will have a similar level. This is illustrated in Figure 9.6 where the scattering from one and multiple periods of a diffuser is compared. The directions of similar level are marked. For the periodic cases, the directions of similar level align with the lobes. For the single period case, they are just points of identical level in the polar response; the points do not align with the lobes. Saying the levels are identical in this case is almost a meaningless statement, because in most polar responses there will be angles where the scattering is identical to other angles. Consequently, using one period of the device spoils the point of using the quadratic residue sequence. So using one period causes problems with the mathematical make-up and definition of optimum diffusion for a Schroeder diffuser. However, the scattering from a single period diffuser is often more uniform than a periodic device, as Figure 9.6 shows. This contradiction will be returned to later when modulation is discussed.

If too many periods are included then the grating lobes become rather narrow; this leads to uneven scattering because there are large nulls present, see Figure 9.6. It must be remembered, however, that manufacturing costs are likely to mean that a narrow base shape with a large number of repeats is going to be the cheapest build. Periodicity might also be preferred visually.

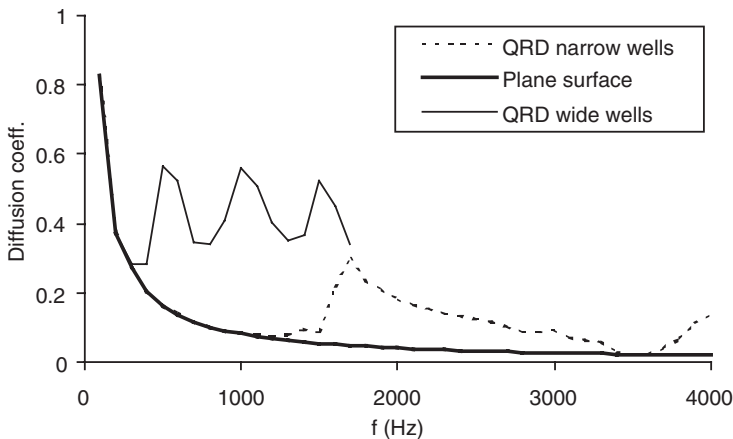


Figure 9.5 Diffusion coefficient spectrum for two QRDs and a plane surface showing the low frequency diffusion limit being determined by period width rather than diffuser depth. The design frequency for the QRDs was 500 Hz.

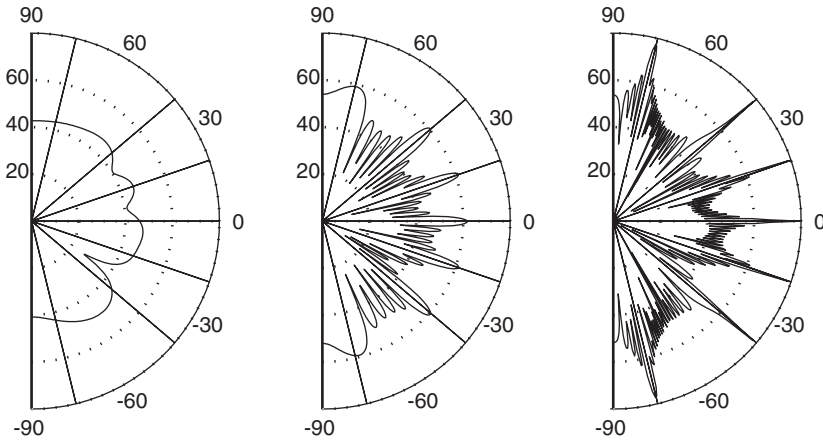


Figure 9.6 The scattering from $N=7$ quadratic residue diffusers at 3,000 Hz for a different number of periods. Left 1 period, middle 6 periods, right 50 periods. Locations of lobes and directions of similar level marked by radial lines at ± 76 , ± 40 , ± 19 and 0° .

The points made in the last three paragraphs mean that the best design is one with a small number of periods, say five, to ensure periodicity, but with the diffraction lobes not too narrow. The period width must be kept large to ensure a large number of grating lobes, which then implies a reasonably large N number. Making the well width wide does not work as it can cause problems with specular-like reflections at high frequencies. Alternatively, modulation schemes can be used as discussed later in the chapter.

From the maximum frequency given in Equation 9.1, it might appear as though a Schroeder diffuser should have the narrowest wells possible to get the widest frequency range, but other considerations limit the width: (1) difficulty and cost of manufacture and (2) absorption. As the diffuser becomes more narrow, then the viscous boundary layer becomes significant compared to the well width and the absorption increases – see Section 9.8. Consequently, practical well widths are at least 2.5 cm, and usually around 5 cm.

The choice of prime number is limited by manufacturing cost, low frequency performance and critical frequencies. For a given maximum depth, d_{\max} , the design frequency achieved is:

$$f_0 = \frac{s_{\max}}{N} \frac{c}{2d_{\max}} \quad (9.4)$$

where s_{\max} is the largest number in the quadratic residue sequence. The ratio of the largest sequence number to the prime number determines the low frequency efficiency of the device [7]. Take two examples: $N=7$, $s_{\max}/N=4/7$; $N=13$, $s_{\max}/N=12/13$. Consequently, an $N=7$ diffuser will have a design frequency nearly an octave below that of an $N=13$ diffuser. It is possible, however, to manipulate some sequences and

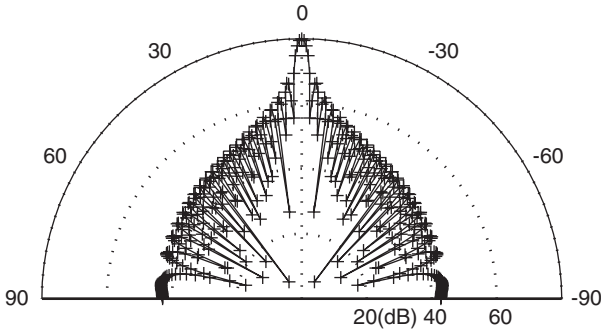


Figure 9.7 The scattering from a quadratic residue diffuser at a critical frequency compared to a plane surface. — Plane surface; + Quadratic residue diffuser. The two lines overlay each other.

increase the bass response. A constant phase shift can be introduced to yield a better bass response:

$$s_n = (n^2 + m) \text{ modulo } N \quad (9.5)$$

where m is an integer constant. Consider two $N = 13$ diffusers:

$$m = 0, s_n = \{0, 1, 4, 9, 3, 12, 10, 10, 12, 3, 9, 4, 1\}, s_{\max}/N = 12/13$$

$$m = 4, s_n = \{4, 5, 8, 0, 7, 3, 1, 1, 3, 7, 0, 8, 5\}, s_{\max}/N = 8/13$$

Consequently, the design frequency has been lowered by two-thirds by this simple manipulation. It must be remembered, however, that this increased performance may not be realized if the repeat width is too narrow.

For a QRD, critical frequencies occur at mNf_0 where $m = 1, 2, 3, \dots$. These are frequencies where the diffuser behaves as a plane surface because all the wells re-radiate in phase. This occurs when all the depths are integer multiples of half a wavelength. Figure 9.5 illustrates such a critical frequency happening at 3.5 kHz in the diffusion spectrum for the narrow diffuser. Figure 9.7 shows the scattering at this frequency. To avoid these critical frequencies, it is necessary to place the first critical frequency above the maximum frequency of the device defined by Equation 9.1, i.e.:

$$N \gg \frac{c}{2wf_0} \quad (9.6)$$

9.4 Sequences

9.4.1 Maximum length sequence diffuser

Schroeder began his work by investigating the scattering from MLS [1]. Figure 9.8 shows one period of such a surface based on the sequence $\{0,0,1,0,1,1,1\}$. Schroeder chose an MLS because it has a flat power spectrum at all frequencies (except DC).

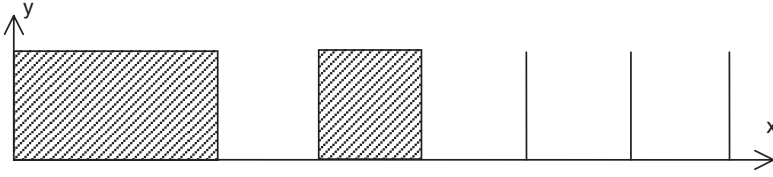


Figure 9.8 A cross section through one period of an $N=7$ maximum length sequence diffuser.

There is a close relationship between the power spectrum and the surface scattering, indeed it is well established in optics that the far field scattering can be found from the Fourier transform of the surface. Equation 8.33 gave the scattering in terms of the pressure magnitude $|p|$ from a surface when the Fraunhofer far field approximations are made:

$$|p(\theta, \psi)| = \left| A[\cos(\theta) + 1] \int_s R(x) e^{jkx[\sin(\theta) + \sin(\psi)]} dx \right| \quad (9.7)$$

where $R(x)$ is the reflection factor, θ the angle of reflection, A a constant, ψ the angle of incidence and k the wavenumber.

This theory is based around representing the complex diffuser shape by a simple box with a variable admittance on the front face – the admittance being determined by considering the plane wave propagation in the wells. This is essentially the same theory used originally by Schroeder, except for the term in $[\cos(\theta) + 1]$. This extra term is an extension that makes the optical Fraunhofer theory more applicable for oblique incidence and reflection. For convenience and compatibility with Schroeder, this term will be ignored:

$$|p(\theta, \alpha)| \approx \left| A \int_s R(x) e^{jkx[\sin(\theta) + \sin(\alpha)]} dx \right| \quad (9.8)$$

Equation 9.8 can be interpreted as a Fourier transform, but the transform is in the variable kx and transforms into $[\sin(\theta) + \sin(\psi)]$ space (rather than the more familiar time to frequency transformation). If the reflection factors $R(x)$ are chosen to have a flat power spectrum with respect to kx , then the amplitude is constant with respect to the transform variable $[\sin(\theta) + \sin(\psi)]$. This does not relate to a constant scattering in all directions, as the transform variable is not a simple function of θ and ψ , but it can be shown that this in fact relates to identical energy lobes, as detailed below.

The device is assumed periodic and then there will be scattering directions where spatial aliasing produces grating (diffraction) lobes. These are directions, where the path length difference from the source to receiver via parts of the panel exactly one period apart is an exact multiple of a wavelength. This is illustrated in Figure 9.9 where periodicity lobes are generated when $|\mathbf{r}_1 + \mathbf{r}_2 - \mathbf{r}_3 - \mathbf{r}_4| = m\lambda$, where m is an

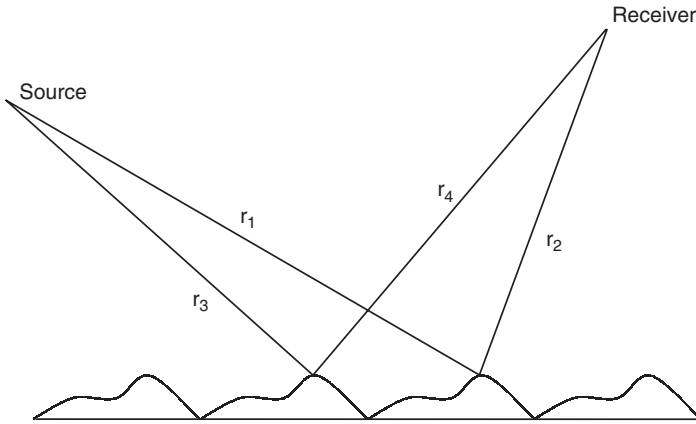


Figure 9.9 Geometry for generation of periodicity lobes.

integer. By considering the geometry of Figure 9.9 further, it is possible to show that these grating lobes appear in the far field at the following angles:

$$\sin(\theta) = \frac{m\lambda}{Nw} - \sin(\psi) \quad m = 0, \pm 1, \pm 2, \dots \quad (9.9)$$

where m is the order of the lobes. If Equation 9.9 is substituted into Equation 9.7 the following results at the design frequency:

$$\begin{aligned} |p_m| &\approx \left| A \int_s R(x) e^{j2\pi xm/Nw} dx \right| \\ &= \left| A \sum_{n=1}^N R_n e^{j2\pi nm/N} \right| \end{aligned} \quad (9.10)$$

where it is assumed that each well radiates as a point source. Strictly speaking a sinc function should be introduced to allow for the piston radiation, but for now the wells will be considered to be relatively narrow compared to wavelength, $w \leq \lambda/4$. Consider a 7-well design. A length 7 MLS is $\{1, 1, 0, 1, 0, 0, 0\}$, so R_n are $\{1, 1, -1, 1, -1, -1, -1\}$. In this case, it can be shown that:

$$\begin{aligned} |p_m| &= A \quad m = 0, \pm N, \pm 2N \\ &= A\sqrt{N+1} \quad \text{otherwise} \end{aligned} \quad (9.11)$$

In other words, the radiating grating lobes ($|m| > 0$ & $|m| < N$) have the same level, whereas the main zeroth order lobe ($m=0$) is lower by $10 \log_{10}(N+1)$. Figure 9.10 shows the scattering from the MLS diffuser where the depth is one-fourth times the wavelength, compared to a hard plane surface of the same size. At this frequency there are five lobes, with the central lobe being suppressed by $10 \log_{10}(8)$ as expected from

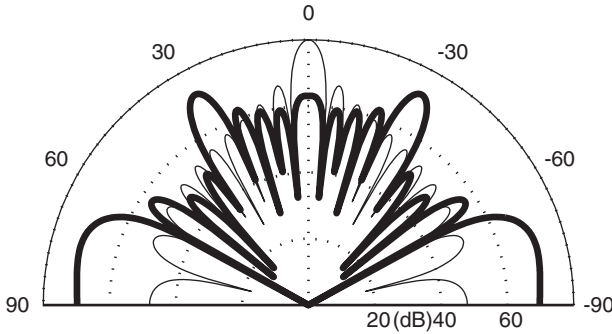


Figure 9.10 The scattering from 5 periods of an $N=7$ MLS sequence at its design frequency. **————** $N=7$ MLS diffuser **————** plane surface.

Equation 9.11. An octave higher, however, at half times the wavelength, the surface behaves like a plane surface because all waves re-radiate with the same phase – this is a critical frequency – the scattering will be rather like that shown in Figure 9.7. Consequently, the MLS diffuser is only useful over an octave. This problem can be overcome, however, by using different number sequences.

9.4.2 Quadratic residue sequence

When a quadratic residue sequence is used, the lobe pressure amplitudes are given by:

$$|p_m| \propto \sqrt{N} \quad m = 0, \pm 1, \pm 2, \dots \tag{9.12}$$

Consequently, all lobes will have the same energy as has been shown in previous polar responses.

9.4.3 Primitive root sequence

A primitive root sequence is generated using the function:

$$s_n = r^n \text{ mod } N \quad n = 1, 2, \dots, N - 1 \tag{9.13}$$

where N is an odd prime, r the primitive root of N and the diffuser will have $N-1$ wells per period. A primitive root is one where s_n for $n = 1, 2, \dots, N - 1$ are all unique [8]. For example $N=7$ has a primitive root of 3, so $s_n = \{3, 2, 6, 4, 5, 1\}$, which generates every integer from 1 to $N-1$. Primitive roots can be found by a process of trial and error, alternatively, tables can be found in texts such as Reference 8. Equation 9.13 can be rewritten as a recursive relationship:

$$s_n = (r \cdot s_{n-1}) \text{ mod } N \tag{9.14}$$

This form is useful because Equation 9.13 can cause overflow problems when being computed for large N .

The primitive root diffuser (PRD) is meant to reduce the energy reflected in the specular reflection direction and so produce a notch diffuser. In addition it should have even energy in the other diffraction lobe directions. As with the QRD, the PRD achieves these performance criteria at integer multiples of the design frequency. At these frequencies, the specular direction amplitudes from the PRD are attenuated by $20 \log_{10}(N-1)$ in comparison with a plane surface. It is noted, however, that virtually any welled surface will achieve a reduced specular energy provided well depths are significant compared to wavelength. Equation 9.10 is a maximum when all radiating waves are in phase, as is the case for a flat surface. As soon as a depth sequence is introduced, partial destructive interference occurs between the waves, leading to a suppressed specular reflection.

The performance of the PRD in suppressing the specular reflection improves as the design prime number, N , increases. This is shown in Figure 9.11 where the pressures scattered from two PRDs are compared to a plane surface. A large number of wells, say greater than 20–30, are needed before a pressure minimum appears at the specular reflection angle.

The levels of the lobes can mathematically be expressed as:

$$\begin{aligned} |p_m| &= A & m = 0, \pm N, \pm 2N \\ &= A\sqrt{N} & \text{otherwise} \end{aligned} \quad (9.15)$$

Although there is an implication of a series of suppressed lobes for $m = \pm N, \pm 2N, \dots$ these are not seen in the far field. The frequencies at which the high order suppressed modes occur will always be greater than the cut-off frequency for plane wave propagation in the wells and so can be ignored.

The specular reflection is attenuated, but it is not a pressure null at integer multiples of the design frequency. Feldman [9] developed a modified primitive root sequence to overcome the problem. The Feldman modified PRD (FMPRD) contains an extra

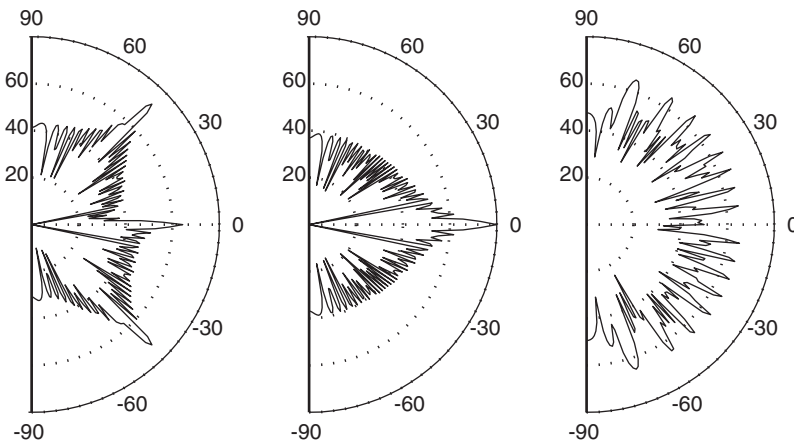


Figure 9.11 Scattering from two primitive root diffusers and a plane surface for normal incidence, showing that a large N number is required to get a significant specular direction notch (0°). From left to right, $N = 7$ PRD, plane surface, $N = 37$ PRD.

zero depth well so the sequence contains all integers from 0 to $N-1$ (instead of from 1 to $N-1$). This spaces the reflection factors evenly around the unit circle for multiples of the design frequency, leading to an exact null in the specular reflection direction. This modification will, however, alter the evenness of the non-zero order lobes.

A PRD does achieve nulls, but not at integer multiples of the design frequency. The nulls appear at frequencies given by $mNf_0/(N-1)$ where $m = 1, 2, 3, \dots$; but it is at the integer multiples that the non-zero order lobes have the same energy. This realization led to Cox and D'Antonio [10] devising a revised formulation for notch diffusers. The technique is to introduce an effective frequency shift to align the reflection factors appropriately around the unit circle at multiples of the design frequency to achieve nulls. This is done by rewriting Equation 9.3 as:

$$d_n = \frac{s_n \lambda_0}{2(N-1)} \tag{9.16}$$

This will be referred to as the Cox and D'Antonio modified PRD (CDMPRD). Figure 9.12 illustrates the two modified PRD compared to a PRD and a plane surface. This demonstrates the introduced nulls that the modified schemes achieve. Also shown is a notch filter designed through optimization, a subject that will be returned to later in this chapter.

It is important to reiterate that these notches are only produced at discrete frequencies. Figure 9.13 shows the scattering from a modified PRD, but not at an integer multiple of the design frequency. No notch is found. While not achieving optimum scattering from a QRD at all frequencies is disappointing, it can be expected that

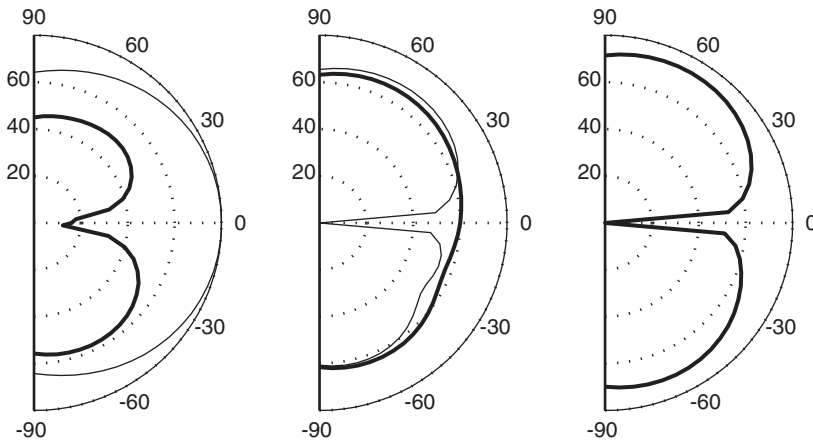


Figure 9.12 Scattering from a primitive root diffuser (PRD), Feldman modified primitive root diffuser (FMPRD), Cox D'Antonio modified primitive root diffuser (CDMPRD), plane surface and optimized surface. $N = 11$. One period, $w = 5$ cm, normal incidence source, at the design frequency of 500 Hz (data from Cox and D'Antonio [10]). Left figure **————** Optimized; **————** Plane. Middle figure **————** PRD; **————** FMPRD. Right figure **————** CDMPRD.

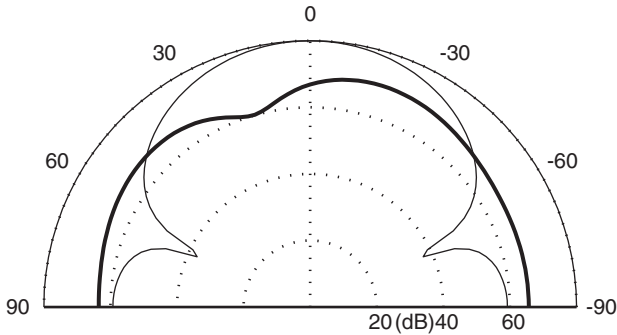


Figure 9.13 Scattering from a modified primitive root diffuser and a plane surface. Design parameters given in Figure 9.12. At 750 Hz, not an integer multiple of the design frequency. — Modified PRD; — Plane surface.

between the frequencies of optimum diffusion, the dispersion from a QRD will still be reasonable. The fact that PRDs only work at discrete frequencies, however, renders the PRDs impractical notch diffusers. This problem can be overcome to a certain extent by optimization [10], to form a broader notch over a wider frequency range. Alternatively, triangles or pyramids may be used to get a more broadband notch as discussed in Chapter 10, but then there are restrictions on the angle of incidence.

9.4.4 Index sequences

Schroeder [11] formed a complex Legendre sequence based on the index function. This has the following reflection factors:

$$R_n = \begin{cases} 0 & \text{for } n \equiv 0 \pmod{N} \\ e^{2\pi i s_n / (N-1)} & \text{otherwise} \end{cases} \quad (9.17)$$

where s_n is the number theoretic logarithm or index function defined by:

$$r^{s_n} = n \pmod{N} \quad n = 1, 2, \dots, N-1 \quad (9.18)$$

where r is a primitive root of N . For example, the $N=7$, $r=3$ sequence is $\{6, 2, 1, 4, 5, 3\}$ as $3^6 = 1 \pmod{7}$, $3^2 = 2 \pmod{7}$, etc. To find a sequence for a given value of N requires a certain amount of trial and error. As the reflection factor for the $n=0$ well is zero, this well should be filled with absorbent. Consequently, the diffuser absorbs a nominal $20 \log_{10}(N-1)$ amount of power. The other wells are fixed depth entities as already seen for other number sequences. Apart from the absorption, the performance of the sequences should be very similar to the PRD.

9.4.5 Huffman and beyond

According to the Wiener–Khinchine theorem, the Fourier transform of an autocorrelation function gives the auto power spectrum. This can be related to diffusers and

enable the use of other sequences to be understood. The Fourier transform of the surface reflection factors approximates to the scattered pressure distribution, although strictly speaking this is in $[\sin(\theta) + \sin(\psi)]$ space. Applying the Wiener–Khinchine theorem to this, if a Fourier transform is applied to the autocorrelation of the surface reflection factors, the scattered energy distribution should result. Consequently, a good diffuser is one which has a delta function autocorrelation function for the reflection factors, as this will lead to an even scattered energy distribution. (Although constant with $\sin(\theta) + \sin(\psi)$, which is not the same as being constant with θ and ψ .)

To demonstrate this, a familiar diffuser sequence can be considered. In Figure 9.14, the autocorrelation function for an $N=13$ quadratic residue sequence is compared to that for a plane surface. It can be seen that the quadratic residue sequence has good autocorrelation properties with small side lobe energy, in other words the autocorrelation for index $\neq 0$ is small. This is one reason that a quadratic residue sequence makes a good diffuser.

Another way of viewing this is as follows. Peaks in an autocorrelation function away from zero indicate a sequence which has some similarity at some displacement. In terms of scattering, there will be angles at which this similarity will lead to lobes due to constructive interference. If all similarities can be removed, then in all directions no complete constructive interference can take place, and so the scattering in all directions will be the same.

Given the above, one approach to finding an appropriate sequence is to look for sequences with good autocorrelation properties. This is not difficult as sequences with optimal autocorrelation properties are a keystone of digital communication systems, whether that is error checking systems for digital audio, code division multiple access (CDMA) systems used in mobile telecommunications or modulating waveforms for radar and sonar. Angus exploited this fact to develop the concept of diffusers based on Huffman sequences [12]. Angus chose Huffman sequences because they are not integer based, and therefore will not suffer from critical frequencies where the surface appears

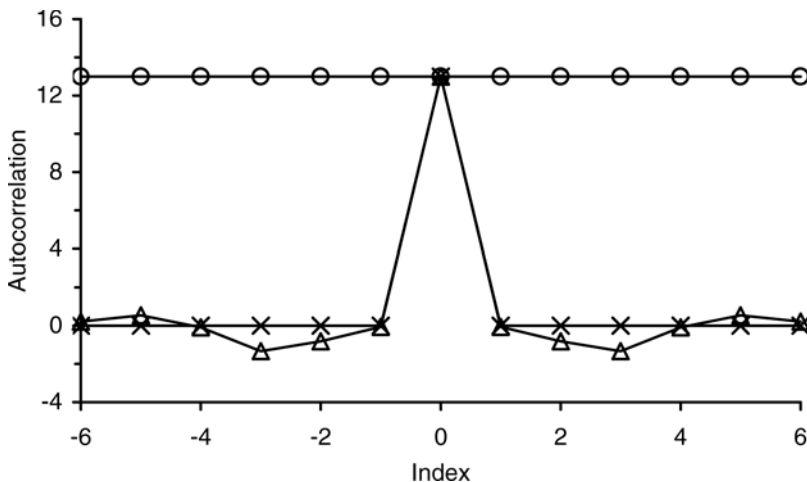


Figure 9.14 The autocorrelation for three different sequences. —△— Quadratic residue; —×— Chu (perfect); —○— Constant (plane surface).

to be a flat plate. A further possible advantage is that Huffman sequences have good aperiodic autocorrelation properties [13] and consequently single periods of the device can be used, and there is no need for periodicity which will generate grating lobes.

Another approach to obtaining a sequence with good autocorrelation properties is to use an optimization algorithm to find sequences with the best autocorrelation properties [8]. The principle of optimization will be discussed in more detail later, but the basic principle is to get the computer to search for a sequence with minimum side lobe energy. This works well for a small number of wells, but when the number of wells becomes large, the number of degrees of freedom in the optimization becomes too large for this to be an efficient process.

A different sequence not considered before will be used to test the principle of choosing sequences with good autocorrelation properties. The Chu sequence is a perfect polyphase sequence, in other words the periodic autocorrelation function is a perfect delta function. Figure 9.14 shows the autocorrelation function for an $N = 13$ case showing that there is no side lobe energy. The elements of a Chu sequence can be generated by [14].

$$s_n = e^{j\varphi_n}$$

$$\varphi_n = \begin{cases} \frac{2\pi}{N} \left[\frac{1}{2}(n+1)n \bmod N \right] & N \text{ odd} \\ \frac{2\pi}{N} \left[\frac{1}{2}n^2 \bmod N \right] & N \text{ even} \end{cases} \quad (9.19)$$

$$0 \leq n \leq N$$

The phase terms φ_n are converted to depths by equating the deepest depth to the design wavelength and maximum phase term, φ_{\max} , i.e.:

$$d_n = \frac{\lambda_0 \varphi_n}{2\varphi_{\max}} \quad (9.20)$$

Figure 9.15 compares the diffusion from an $N = 13$ Chu sequence, with a QRD and a plane surface. The performance from the QRD and the Chu sequence is overall very similar. Consequently, this presents an alternative design method, but not a better one.

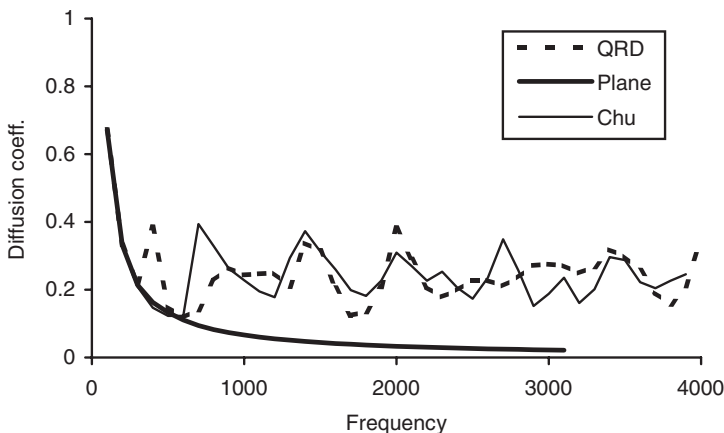


Figure 9.15 Diffusion coefficient spectra for two diffusers and a plane surface.

9.5 The curse of periodicity

The scattered polar responses seen in Figure 9.6 are dominated by grating lobes generated by the fact that the diffusers are periodic. The lobe energy may be constant, but there are large minima between the lobes except at high frequencies when the number of lobes becomes very large. The scattering energy is not even in all directions. For this reason, significantly better performance can be obtained if the periodicity lobes can be removed by making the diffuser aperiodic or increasing the repeat distance. A phase grating diffuser which exploits number theory, such as a QRD, is in many ways cursed by periodicity. A QRD needs periodicity to form its optimum diffusion of even energy lobes, yet the periodicity lobes cause uneven scattering.

One possibility is to use a number sequence with good aperiodic autocorrelation properties. This means that a single period of the number sequence can be generated and used without repetition. There are two problems with this solution, first there are not many large N number aperiodic polyphase sequences known, and second it will usually be cheaper to manufacture a small number of base shapes and use each base shape many times.

Angus [15–20] presented a series of papers outlining methods for using two phase grating base shapes in a modulation scheme to deal with the problems of periodicity. Figure 9.16 shows such a modulation arrangement for two QRDs, one based on $N=7$, the other on $N=5$. The idea is to use two or more base shapes and arrange them according to a pseudorandom arrangement so that there is no repetition.

As discussed previously, the far field scattering distribution is roughly related to the Fourier transformation of the surface reflection factors. For a periodic device, the distribution of surface reflection factors can be expressed as the surface reflection factors over one period, convolved with a series of delta functions.

$$R(x) = R_1(x) * \sum_{n=-\infty}^{n=\infty} \delta(x - nW) \quad (9.21)$$

where $R_1(x)$ is the distribution of reflection factors over one period, n an integer, $*$ denotes convolution, $W = Nw$ is the width of one period of the device and δ the delta function.

Equation 9.21 and the following process are illustrated in Figure 9.17. When a Fourier transform is applied to Equation 9.21 to obtain the scattering in $[\sin(\theta) + \sin(\psi)]$ space, then the convolution becomes multiplication.

$$\text{FT}\{R(x)\} = \text{FT}\{R_1(x)\} \cdot \text{FT}\left\{\sum_{n=-\infty}^{n=\infty} \delta(x - nW)\right\} \quad (9.22)$$



Figure 9.16 A cross section through a modulation scheme using $N=5$ and $N=7$ quadratic residue diffusers and the modulation sequence $\{1,0,0,1,0,1\}$.

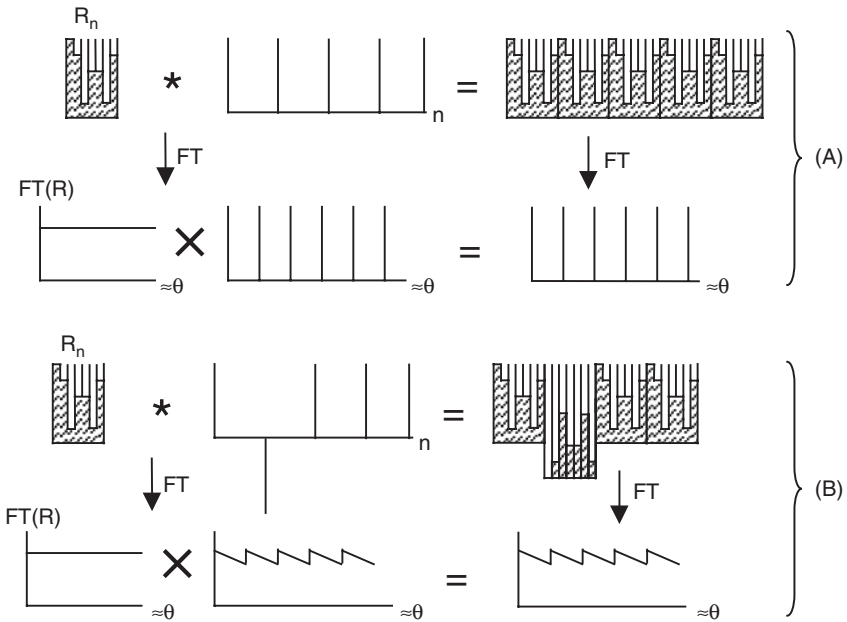


Figure 9.17 A modulation scheme illustrated. In the top case (A), a periodic arrangement is used, and spatial aliasing causes grating lobes even though one period of the diffuser has a flat power spectrum. In the bottom case (B), the inverse of the diffuser is used in a modulation scheme to reduce periodicity effects.

where FT denotes Fourier transform. The Fourier transform of a delta function train is another delta function train, and it is the spikes in this train for $[\sin(\theta) + \sin(\psi)] > 0$ that cause the grating lobes. Consequently, rather than use a delta function chain to form a periodic device, another function should be used which has better Fourier transform properties. Again, what is needed is a sequence with good autocorrelation properties. A good choice is a Barker sequence. This is a binary sequence whose Fourier transform is flattest possible for a binary sequence. Consequently, the response of the whole array of diffusers is closer to the single diffuser alone than if a periodic arrangement is used. If a perfect binary sequence could be found then the single diffuser response would be recovered, but there are no such 1D sequences.

Consider forming a QRD with five periods. The Barker sequence for $N=5$ is $\{1, -1, 1, 1, 1\}$. Consequently, where a 1 appears in the Barker sequence, the normal $N=7$ QRD should appear. Where a -1 appears, an $N=7$ QRD is needed which produces the same scattering except it is 180° out of phase. This can be done by using the rear of the normal $N=7$ diffuser (provided the fins are extended far enough). This is illustrated in Figure 9.17. Consequently, one QRD has a number sequence of $\{0, 1, 4, 2, 2, 4, 1\}$ and the other QRD has a number sequence of $\{7, 6, 3, 5, 5, 3, 6\}$. This second sequence is found by subtracting the first sequence from N . This is equivalent to changing the phase change due to the well depths from φ to $2\pi - \varphi$, i.e. obtaining a 180° out of phase surface.

Figures 9.18 and 9.19 show the scattering from the periodic arrangement of $N=7$ QRDs compared to an arrangement according to the Barker sequence and a single diffuser for two frequencies. One of the frequencies where the diffusion improvement is most dramatic is 2,000 Hz; at other frequencies the improvement is less marked. Figure 9.20 shows the diffusion coefficient versus frequency. A clear improvement is seen in the diffusion, and periodicity lobes are much reduced. As Figure 9.20 shows, the diffusion from the simple periodic array only becomes significant compared to a plane surface at 1–1.5 kHz, an octave or so above the design frequency (500 Hz). This is a case of the diffuser width limiting the low frequency response rather than the diffuser depth. At the design frequency, only one lobe appears in the scattered polar distribution, as shown in Figure 9.19. The Barker sequence means that there is reduced periodicity in the arrangement, and so the low frequency limit of the Barker modulated array is determined by the depth and not the repeat length similar to the periodic case. This is an important result, as it means the low frequency performance of some diffusers can be improved by modulation.

The polar responses show that the scattering from the Barker modulated array is more similar to the single diffuser response, which is as expected from the theory outlined above. A single diffuser response is not recovered because the Barker sequence has good but not perfect autocorrelation properties. Figure 9.21 shows the autocorrelation properties for the diffuser arrangements at the design frequency. The spikes in the side lobes show the repeat distance of 7 for the $N=7$ diffusers. The Barker modulation has lower side lobe energy meaning that the periodicity is reduced. Although the Barker sequence has reduced the periodicity spikes in the autocorrelation

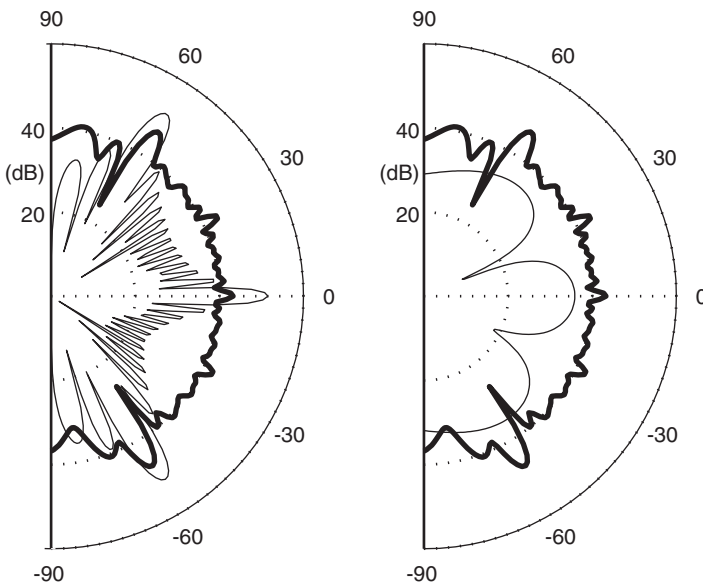


Figure 9.18 Scattered polar distribution from a single QRD, a periodic arrangement and a Barker modulation using the QRD and its inverse. 2,000 Hz = $4f_0$. Left figure: **————** Modulated; **————** Periodic. Right figure: **————** Modulated (same as left figure); **————** One period.

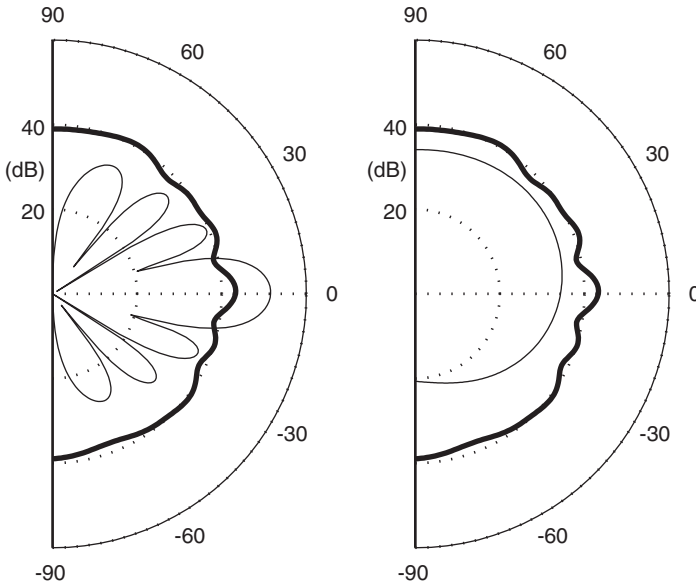


Figure 9.19 Same diffusers as Figure 9.18 but at 500 Hz, the design frequency. Left figure: **—————** Modulated; **—————** Periodic. Right figure: **—————** Modulated (same as left figure); **—————** One period.

function they are not completely eliminated. This is why the single diffuser response is not completely recovered.

There are a variety of number sequences that can be used for the modulation. The Barker sequence is a good choice as it has good aperiodic autocorrelation properties, and it might be expected that the modulation sequence will be used once in a diffuser arrangement. As the modulation sequence does not repeat, a sequence with good periodic autocorrelation coefficient would not be optimal. Barker sequences only analytically exist for certain N numbers $\{2,3,4,5,7,11,13\}$, but computer-based search algorithms have been used to generate number sequences up to length 48 [8]. For larger diffuser arrays, it may be necessary to use other number sequences, such as MLS which strictly speaking are only good with periodic use of the modulation sequence.

The modulation works best at multiples of the design frequency. Only at these frequencies do the diffuser and its inverse create exactly opposite pressures. At other frequencies, the modulation is likely to help with the scattering as it breaks up periodicity lobes, but in a more uncontrolled manner.

At high frequencies, say greater than 5 kHz for the typical geometries used in practical diffusers, the dispersion by a modulated array summed over a one-third octave band is often worse than for a periodic arrangement. This happens because the number of grating lobes in the periodic case saturates, so when the polar responses are summed over a one-third octave band the grating lobes average out. Having said this, the improvements generated by modulation in the more important low-mid frequency ranges far outweigh any slight decrease in performance at higher frequencies.

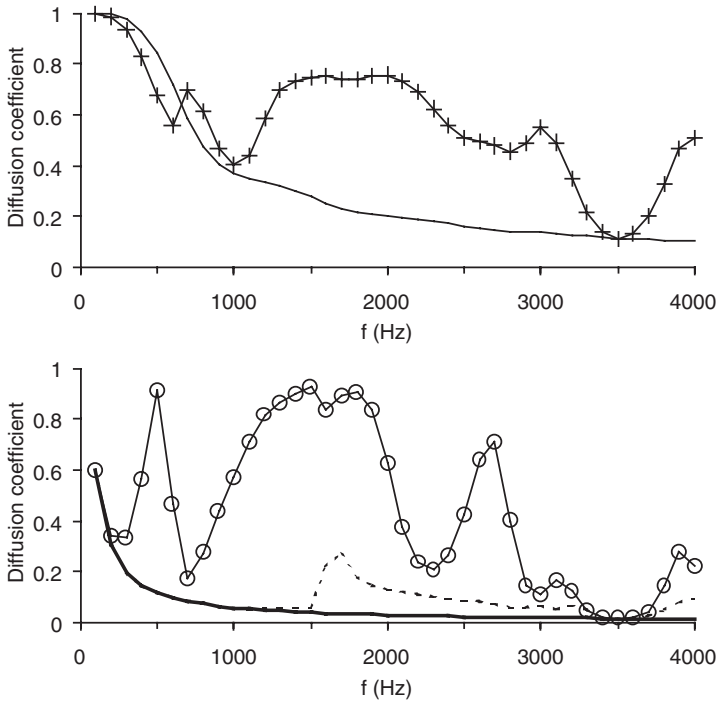


Figure 9.20 Diffusion spectra for three diffuser arrangements and two plane surfaces. Top figure: —+— One period of the QRD; — Plane surface. Bottom figure: - - - - QRD periodic; — Plane surface; —○— QRD Barker modulation.

One other feature of note is that the critical frequency at Nf_0 where the diffusers behave as a flat plate still remains even with the modulation. The flat plate frequency of 3,500 Hz can be seen in the diffusion spectra of Figure 9.20. Both the QRD and its inverse used in the modulation suffer the same critical frequency, and consequently this problem persists. While it is possible to reduce this problem by choosing a larger value for N , it is also possible to use modulation to reduce the effects. To do this, the two diffusers to be modulated must have different critical frequencies. There are further advantages to using two different diffusers. The QRD works at line frequencies based on integer multiples of the design frequency. By using diffusers with two different design frequencies, it is possible to achieve more frequencies with better diffusion [19].

Cox and D'Antonio [10] used a combination of $N=11$ and $N=7$ primitive root diffusers. Figure 9.22 shows the scattering from this arrangement. Not only does the modulated array still achieve a notch at the specular reflection direction, but the two dominant first order lobes are broadened. The notch remains because each period of both diffuser types produces a null in the specular directions, and summing over all periods still leads to nothing scattered in the specular direction.

Angus [20] used a combination of $N=5$ and $N=7$ QRDs in an orthogonal modulation. Figure 9.23 shows the autocorrelation of the reflection coefficients at

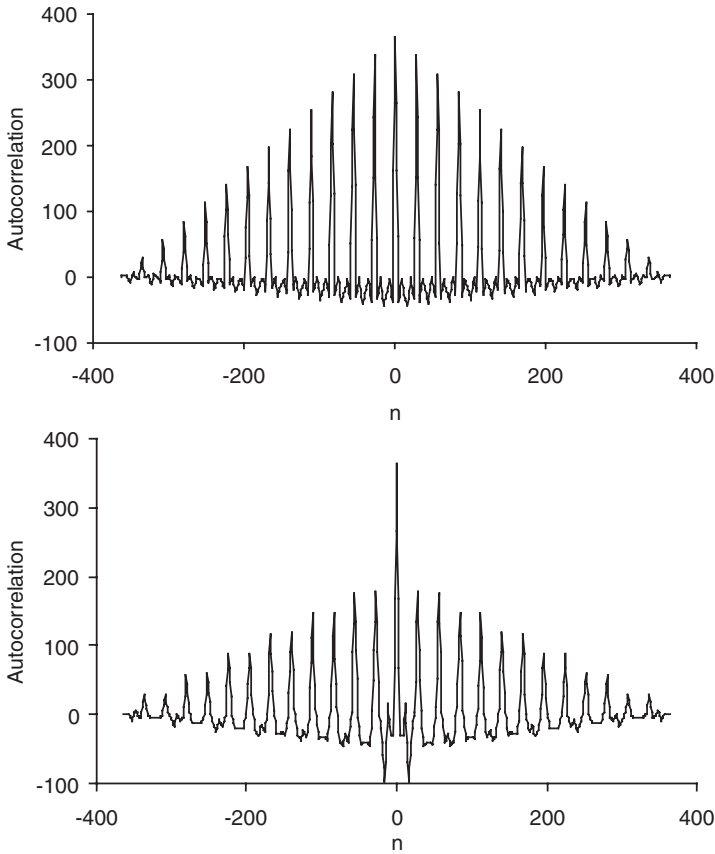


Figure 9.21 Autocorrelation function for two arrangement of quadratic residue diffusers. Top graph, periodic array; bottom graph, Barker modulated array.

the design frequency for a modulation of an $N=5$ and an $N=7$ QRD. It shows that the original periodicity lobes are reduced, but other smaller peaks are produced elsewhere. The locations of the $N=5$ and $N=7$ diffusers can be determined by flipping a coin, or better still by using a pseudorandom sequence with good aperiodic autocorrelation properties such as a Barker sequence. Figure 9.24 shows the diffusion spectrum. The flat plate frequency at 3.5 kHz is removed by the orthogonal modulation, although there is still a decrease in performance around the flat place frequency because at that frequency only the $N=5$ diffusers are creating any dispersion and so a strong specular component still remains. Overall, the performance is not as good as the original Barker modulation using the QRD and its inverse described previously. Consequently, the best choice for modulation is to use a diffuser and its inverse, but choosing a diffuser where the critical frequency is well above the high frequency limit where cross-modes in the wells appear.

The modulation techniques developed by Angus require two or more base shapes. It is possible to achieve modulation using a single asymmetrical base shape. Instead of inverting the diffuser to use the rear, an asymmetrical diffuser can be flipped about its

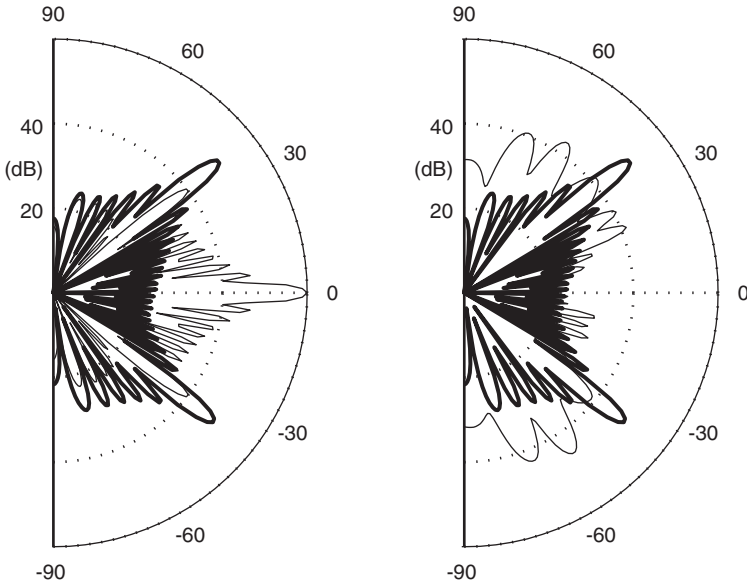


Figure 9.22 Comparison of periodic arrangement of a modified primitive root diffuser (CDMPRD), a modulated sequence of the CDMPRD and a flat plane surface. The periodic surface had 10 periods of $N=11$ diffusers. $w=0.05$ m, frequency is 1,000 Hz, design frequency 500 Hz. The modulated surface was formed from 12 periods of $N=11$ and $N=7$ placed in a random order (data from Cox and D' Antonio [10]). Left figure: **————** Periodic; **————** Plane. Right figure: **————** Periodic (same as left figure); **————** Modulated.

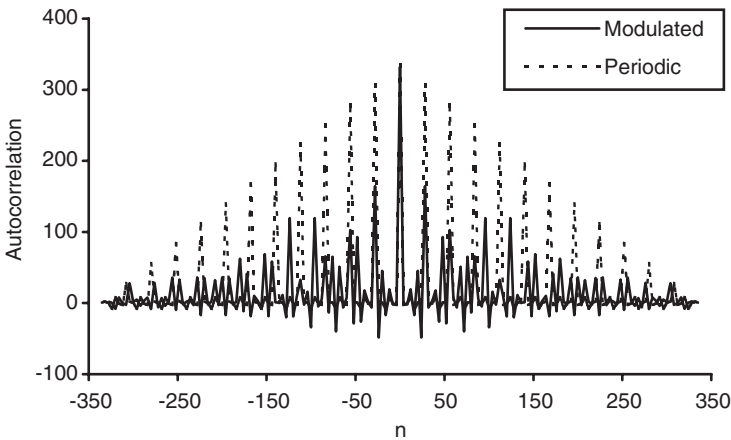


Figure 9.23 Autocorrelation for a periodic arrangement of $N=7$ QRDs and an orthogonal modulation using $N=5$ and $N=7$ QRDs and a Barker sequence.

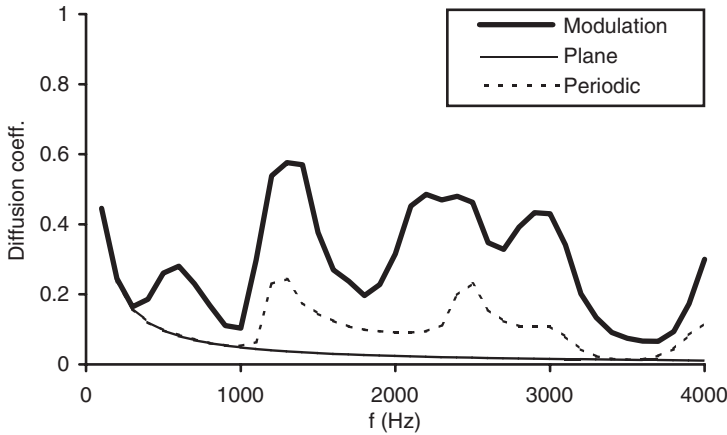


Figure 9.24 Diffusion coefficient spectra for a periodic arrangement of $N=7$ QRDs, an orthogonal modulation using $N=5$ and $N=7$ QRDs and a plane surface.

mid-point. For example, an $N=7$ PRD is $\{1,3,2,6,4,5\}$ and this can be simply flipped to form a new sequence $\{5,4,6,2,3,1\}$. The advantage of this type of modulation is it is cheaper. This modulation will not be successful with quadratic residue sequences or Chu sequences, however, because these are symmetrical. Instead asymmetrical sequences are needed such as primitive root sequences. Figure 9.25 shows the scattering from such a modulation using $N=7$ primitive root sequences. The modulation reduces the non-zero order grating lobes, while still preserving the null in the specular reflection direction.

There is another approach to modulation to reduce periodicity effects and also to improve the base frequency response. The bandwidth of a Schroeder diffuser is limited at high frequencies by the well width and at low frequencies by the maximum depth. Additionally, wide area coverage with periodic arrays focusses energy into certain diffraction directions. To provide full spectrum sound diffusion in a single integrated diffuser, the self-similarity property of fractals can be combined with the

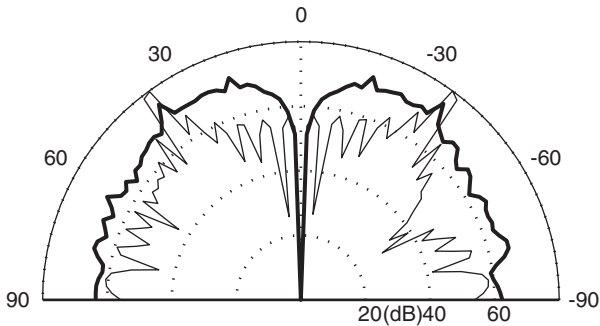


Figure 9.25 Scattering from a periodic and a modulated arrangement of primitive root diffusers, 2.5 kHz. Modulation using one base shape. — Periodic; — Modulated.

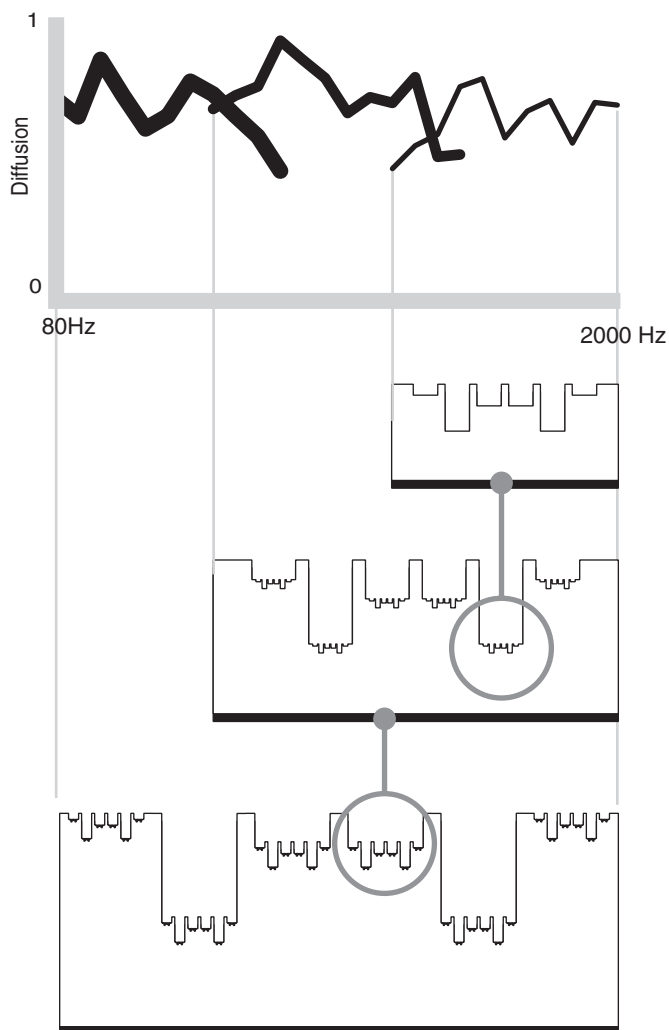


Figure 9.26 A Difractal[®], which imbeds high frequency diffusers within a low frequency diffuser to deal with periodicity, absorption and bandwidth problems (top figure after D'Antonio and Konnert [7]).

uniform scattering property of reflection phase gratings to produce a fractal diffuser. The surface consists of nested self-similar diffusers, each of which covers a specific frequency range and offers wide area coverage, see Figure 9.26. Each diffuser provides uniform scattering over a specific range of frequencies so that the effective bandwidth is extended.

There are numerous natural phenomena exhibiting a macroscopic shape which is repeated microscopically at progressively smaller and smaller scales. At each level of magnification we find a scaled replica of the original. These scaled replications are self-similar, that is they differ only in scale, they are invariant to scaling. The term *fractal* was first coined by Mandelbrot [21] to describe these structures, and hence these diffusing fractals have been termed *Diffractals*. It is possible to carry out the scaling many times; typical commercial implementations use two magnifications of self-similarity. Another way of viewing this is as a two or three way loudspeaker. The construction avoids using narrow deep wells to cover a wide bandwidth, and so decreases the absorption of the device. Figure 2.12 showed an application of this device at the rear of a studio.

At low frequency, the small diffusers at the bottom of the wells will have negligible depth compared to wavelength, and so only the bass diffuser needs to be considered at low frequencies. At high frequencies, the small diffusers will act as a modulated array with phase modulation due to the depth of the deep diffuser. This is illustrated in Figure 9.26. The phases introduced by the large diffuser on the small diffuser are conveniently also quadratic residues, and hence when they sum with the small diffuser phases, the result is still a quadratic residue whose Fourier transform of the exponentiated sequence is still constant. This is a very useful outcome, because it is possible therefore to nest diffusers with overlapping frequency bandwidths. The two layers of magnification appear to operate orthogonally. In reality, however, at mid-frequencies the situation is likely to become very much more complex. The cross-modes of the large wells will affect the scattering from the smaller diffusers. These difficulties make this surface impossible to model with a simple Fraunhofer approach; to properly model this surface requires a full BEM solution or similar.

9.6 Improving base response

The depth of a diffuser usable in design is often limited by non-acoustic factors. Ultimately, the designer or architect will limit the depth available for acoustic treatment. Furthermore, with the wavelength of sound extending to 17 m, it is impossible to construct a practical diffuser which will cover the full audible bandwidth and is also usable in most rooms. Consequently, there is always a need for extending the bandwidth of diffusing devices to a lower frequency.

By using well folding, it is possible to gain a greater bandwidth from a given well depth. Jrvinen *et al.* [22] and Mechel [23] and others have suggested such a modification. The standard Schroeder diffuser, Figure 9.2, has much wasted space at the rear which can be better utilized. Figure 9.27 shows the use of well folding to reduce the depth of an $N = 7$ QRD. The depth of the folded well should be calculated from the mid-line through the well, then predictions can proceed with the simple Fraunhofer theory. For this, an assumption is made that higher order modes in the structure are negligible; a full BEM solution would be needed to account for these effects. Mechel also suggested reordering the wells of the primitive root sequence in ascending order

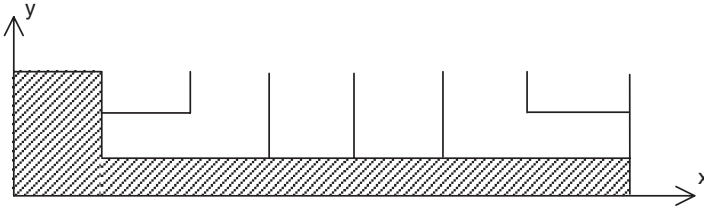


Figure 9.27 A cross section through an $N=7$ quadratic residue diffuser using well folding to reduce depth.

to make the packing more efficient. It should be remembered, however, that this will have a detrimental effect on diffuser performance as the spatial relationship between the different depth wells will have been changed.

An alternative regime is to use perforated sheets to add mass to the impedance of the wells, and so lower the resonant frequency of the wells, and hence the frequency at which the scattering is first optimal. An example of such a device is shown in Figure 9.28, where the use of perforated sheets has enabled the longest wells to be shortened. Such an approach was tried for diffusion by Hunecke [24] using microperforation and for absorption by Fujiwara *et al.* [25] and Wu *et al.* [26] using larger diameter perforations. For a diffuser, it is also important that the perforation size is not made too small otherwise significant losses may result. The principle of the design is that for the first mode, the well reflection factor of a Helmholtz resonator and of a $1/4$ wavelength tube is similar. Consequently, the $1/4$ wave resonator tubes of the Schroeder diffuser can be replaced by Helmholtz devices. This is illustrated in Figure 9.29 where two well reflection factors are compared, one a $1/4$ wave resonator, the other is half the depth with a perforated sheet to create the correct resonant frequency. This reflection factor can be calculated using the transfer function matrix method outlined in Chapter 6. Unfortunately, for higher order modes, the Helmholtz resonator and $1/4$ wavelength tube reflection factor will be dissimilar. Consequently, this design methodology can only work around the design frequency.

Figure 9.30 shows the scattering at the design frequency, showing that the two diffusers behave similarly. The Schroeder diffuser with perforations is about half the depth of the original diffuser, so considerable space savings have been made. A point to note is when carrying out this calculation, it is necessary to include the radiation

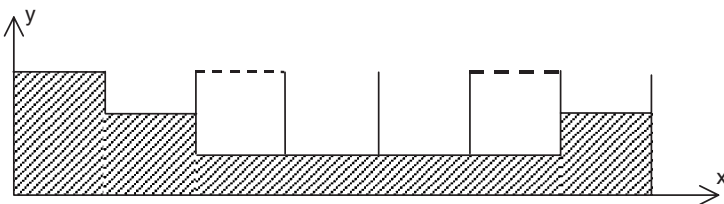


Figure 9.28 A cross section through a Schroeder diffuser using perforated sheets to add mass to the surface impedance of the longest wells and therefore enabling the longest wells to be shortened.

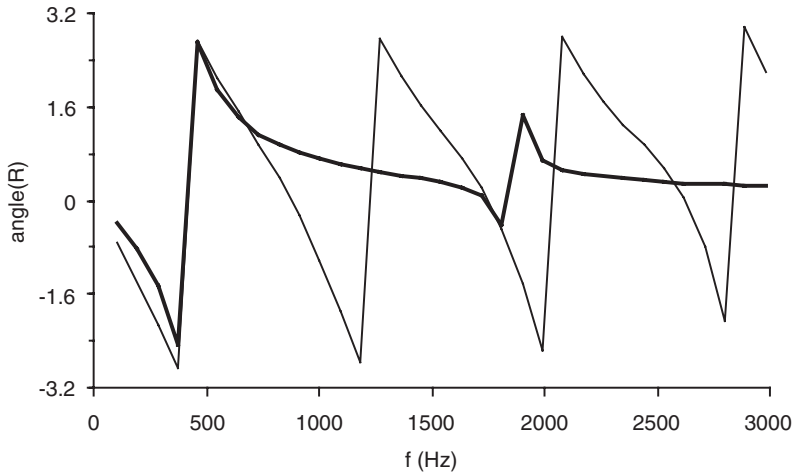


Figure 9.29 Reflection factor phase angle in radians for two wells. — Normal well; — Shorter well with perforated sheet to add mass.

impedance of the 1/4 wave tube. This has been ignored for other Schroeder diffusers because it is a constant term for all wells and therefore does not affect the diffusion. With a mixture of Helmholtz and 1/4 wave devices, however, the correct radiation impedance must be included. Figure 9.31 shows the diffusion coefficient, showing that for many frequencies similar performance is obtained from the perforated device and the normal Schroeder diffuser. At higher frequencies than shown, the scattering from the perforated sheet will become rather specular and so care in design and application is needed. As the principle is to add mass using perforations, mass can also be applied using limp membranes, probably to similar effect, but it may be difficult to reproduce mounting conditions consistently in manufacture.

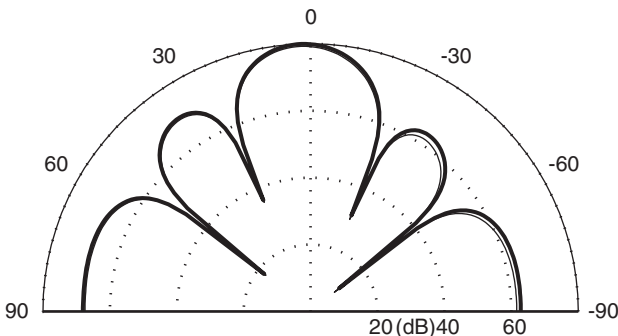


Figure 9.30 Scattering from an $N=7$ QRD at the design frequency and a similar QRD where the longest wells have been shortened and a perforated sheet used to add mass. — QRD; — QRD using perforated wells.

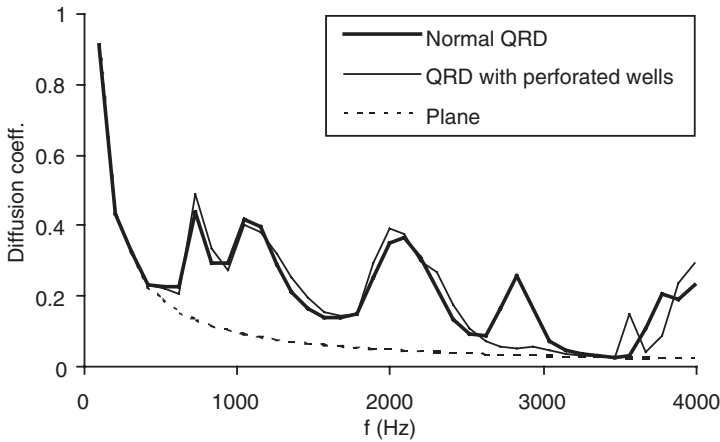


Figure 9.31 Diffusion from a QRD and a QRD using a perforated sheet to enable the deepest well depth to be decreased.

To get a true broadband diffuser using this approach, another design approach must be tried. Later in Section 9.9 an optimization approach will be discussed. This could equally be applied to a diffuser formed from a series of Helmholtz resonators.

9.7 Multi-dimensional devices

So far, the diffusers discussed have been single plane devices. They cause scattering into a hemi-disc, acting as a planar surface in the other directions. While this is probably the most common type of diffuser, there is a need for a diffuser that scatters into a hemisphere. For a Schroeder type diffuser this can be best achieved by forming a two plane device, one that scatters optimally in the x - and z -direction, and therefore gives even lobes on a hemisphere. An example of such a surface was shown in Figure 9.1 right.

As 2D diffusers scatter in multiple planes, for a receiver in the bright zone, the surfaces will cause the scattered energy to be reduced more than a 1D diffuser, provided multiple grating lobes are present. The number of grating lobes is squared if a 1D of width Nw and 2D diffuser of size $Nw \times Nw$ are compared. Therefore the energy in each lobe will reduce by $10 \log_{10}(m)$, where m is the number of grating lobes present for the 1D diffuser.

There are two known processes for forming 2D diffusers. The first, involves forming two sequences, one for the x -direction, one for the z -direction and amplitude modulating the x sequence with the z sequence. For a quadratic residue sequence, this can be expressed as [2]:

$$s_{n,m} = (n^2 + m^2) \text{ modulo } N \quad (9.23)$$

where n and m are integers and give the sequence for the n th and m th wells in the x - and z -directions respectively. A similar procedure can be used for PRDs.

$$s_{n,m} = (r^n + r^m) \text{ modulo } N \quad (9.24)$$

It is even possible to have a quadratic residue sequence in one direction, and a primitive root sequence in the other provided they are based on the same prime number, although it is hard to see why you would chose to do this.

Consider a quadratic diffuser based on $N=7$, a 2D version would be as shown in Figure 9.32. In this case the indexes n and m were started from 4 to place the zero in the middle of the diffuser. As the surface is periodic, it is possible to start the indexes n and m from any integer. 2D number theoretic diffusers will often have less bass diffusion efficiency than a 1D device, as the ratio s_{\max}/N tends to 1 for 2D devices.

Figure 9.32 also illustrates other sequences that can be used. On the diagonal of the diffuser the following sequence appears {4,1,2,0,2,1,4}. This is the original sequence {0,1,4,2,2,4,1} but with every fourth element used. This new sequence has the same Fourier properties as the original sequence due to the shift properties of quadratic residue sequences. This indicates that as well as producing good diffusion in the orthogonal directions x and z , good scattering in the directions along the diagonals should also be obtained.

The second method for making multi-dimensional diffusers is to use the Chinese remainder theorem [27]. This folds a 1D sequence into a 2D array while preserving the Fourier properties of the 1D sequence. The process is described in detail in Chapter 11 where it is applied to hybrid surfaces, but it can equally be applied to polyphase sequences.

The requirement for co-prime factors means that this folding technique cannot be applied to single periods of QRDs, because there is a prime number of wells. This can be overcome by using an odd-number generator N for the quadratic residue sequence which is not prime. For example, a quadratic residue sequence based on $N=15$ will

4	6	3	2	3	6	4	4	6	3	2	3	6	4
6	1	5	4	5	1	6	6	1	5	4	5	1	6
3	5	2	1	2	5	3	3	5	2	1	2	5	3
2	4	1	0	1	4	2	2	4	1	0	1	4	2
3	5	2	1	2	5	3	3	5	2	1	2	5	3
6	1	5	4	5	1	6	6	6	1	5	4	5	1
4	6	3	2	3	6	4	4	4	6	3	2	3	6
4	6	3	2	3	6	4	4	6	3	2	3	6	4
6	1	5	4	5	1	6	6	1	5	4	5	1	6
3	5	2	1	2	5	3	3	5	2	1	2	5	3
2	4	1	0	1	4	2	2	4	1	0	1	4	2
3	5	2	1	2	5	3	3	5	2	1	2	5	3
6	1	5	4	5	1	6	6	6	1	5	4	5	1

Figure 9.32 A sequence array for a 7×7 quadratic residue diffuser, one period is highlighted.

work perfectly well at the design frequency and can be wrapped into a 3×5 array. The problem is that the surface will have flat plate frequencies at three and five times the design frequency (as well as 6,10,9,15 ... times). Consequently, to use a non-prime N , it is necessary to make sure the factors of N are sufficiently large, that the flat plate frequency is above the frequency of interest. For example $N = 143$ has factors of 11 and 13 and so would be a good choice as the flat plate frequencies will be beyond the upper limit of most diffusers. It is also possible to apply the Chinese remainder theorem to some primitive root sequences, or some other mathematical sequences such as the Chu sequence outlined previously.

It has also been suggested by Pollack and Dodds [28] that the wrapping can be carried out in a hexagonal configuration.

$$s_{n,m} = (n^2 + m^2 + nm) \text{ modulo } N \tag{9.25}$$

Figure 9.33 illustrates a hexagonal QRD based on $N = 7$ generated using Equation 9.25.

Figures 9.34 illustrates the scattering from a 2D $N = 7 \times 7$ QRD and a plane surface as a 3D polar balloon, sometimes nicknamed a polar banana [7]. There is a regular set of grating lobes, but these are difficult to see unless the polar response can be animated and rotated. Figure 9.35 shows the data as a contour plot, where the grating lobes become more obvious. These grating lobes form a regular grid, the middle 9 in a 3×3 grid is most obvious in the case shown. These contour plots are effectively the contour on the surface of the hemisphere, looking down onto the hemisphere. Consequently, the x - and z -axis shown are non-linear.

Figure 9.36 illustrates the scattering from a diffuser formed using the Chinese remainder theorem. A Cox D'Antonio modified primitive root sequence based on the prime number $N = 43$ was generated, and so the sequence is 42 elements long. It was folded into a 6×7 array using the Chinese remainder theorem. Figure 9.36 shows the response at four times the design frequency, and the specular lobe which should be present pointing straight up the page is missing. This demonstrates that the folding technique succeeds in preserving the modified primitive root properties. When amplitude modulation is used to form primitive root sequence arrays (Equation 9.24)

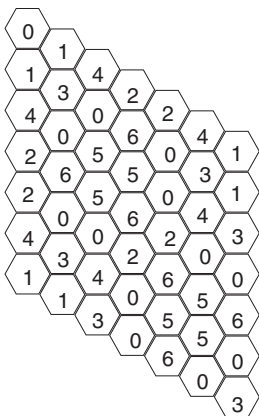


Figure 9.33 One period of a hexagonal quadratic residue diffuser based on $N = 7$.

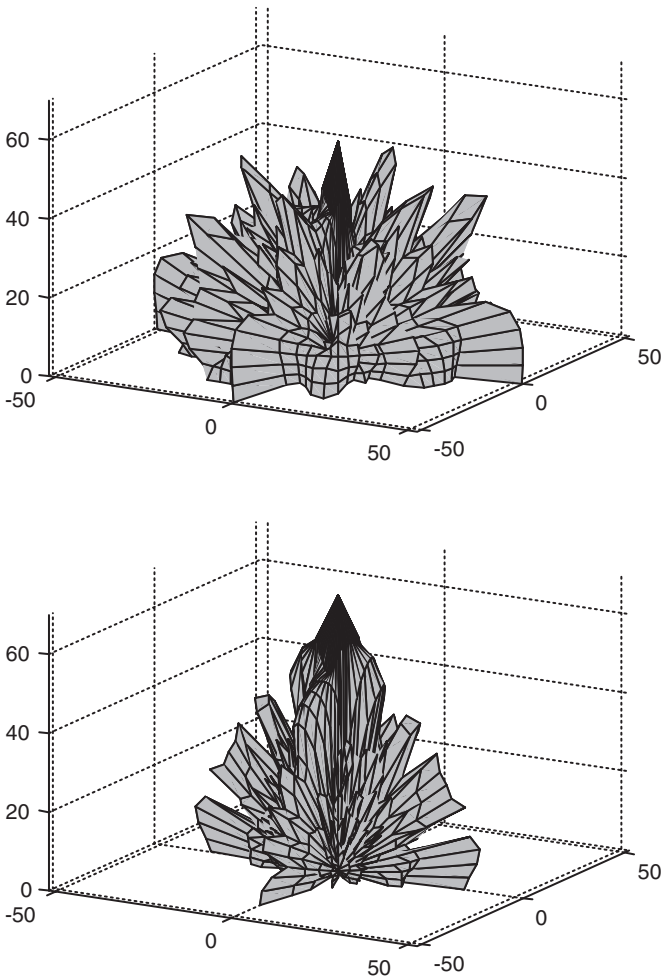


Figure 9.34 Scattering from an $N=7$ QRD at four times the design frequency (top) and a plane surface (bottom).

planes of reduced scattering are produced. All the scattering in the directions given by $\phi = 0, 90, 180, 270^\circ$ will be suppressed.

In general, little measurement or prediction work on multi-dimensional devices has been carried out. It appears, however, that the results learnt from a 1D analysis can be extended to multiple dimensions. The issues of lobes, periodicity, frequency limits, etc. are all similar.

9.8 Absorption

Section 7.2 has discussed in some detail how and why Schroeder diffusers absorb, and how to make a phase grating into an efficient absorber. To recap, Schroeder diffusers primarily absorb because of: (1) energy flows from wells in resonance to wells out of

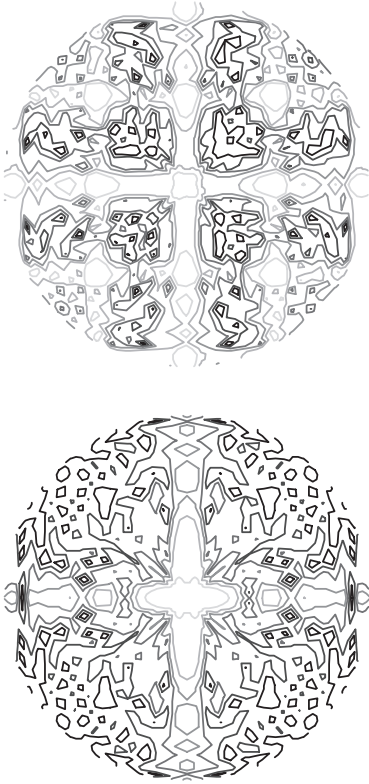


Figure 9.35 Contour plot of polar response shown in Figure 9.34 seen from above. QRD (top) shows 13 grating lobes, where a 3×3 grid of lobes shown in the centre is most clear. Plane (bottom) just has a lobe in the specular reflection direction.

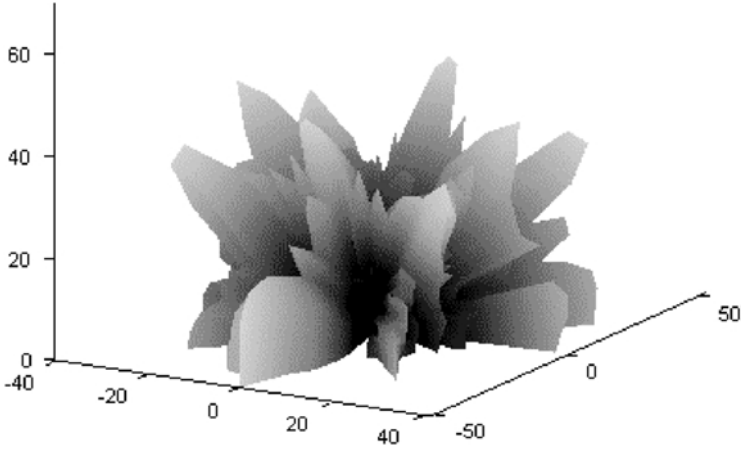


Figure 9.36 Scattering from a modified primitive root diffuser based on the prime 43, and wrapped into a 6×7 array using the Chinese remainder theorem.

resonance, and (2) $1/4$ wave resonant absorption in the wells, especially if the wells are rather narrow. Figure 9.37 shows the random incidence absorption coefficient for 1D and 2D commercial Schroeder diffusers like those shown in Figure 9.1.

The first result of note from Figure 9.37 is to notice how important it is not to cloth cover Schroeder diffusers as this greatly increases the absorption. There is energy flow between wells of the absorber promoted by pressure gradients caused by wells being in resonance and having high energy adjacent to wells not being in resonance and having low energy. Consequently, there is high particle velocity around the front face of a Schroeder diffuser, and any cloth covering will cause excess absorption as might be expected if resistive material is placed in a region of high particle energy flow. Any cloth covering should be placed at least a well width away from the front face. The cloth should have the highest possible flow resistivity; indeed it is better if the cloth is not present at all.

Figure 9.37 also shows the absorption for a 1D Schroeder diffuser compared to a 2D device. The absorption is greater for the 2D diffuser. It is assumed that this is caused because there are a greater number of different depths for the 2D device, leading to more energy flow between the wells as well as a greater density of $1/4$ wave resonances. Furthermore, because there are more well walls present than in a 1D device, more losses due to viscous boundary layer effects can occur.

It is important that the Schroeder diffuser is constructed to a high precision. A little data has been published for Schroeder diffusers showing very high absorption coefficients, but this is generally due to poor construction. Small cracks in the bottom of the wells, between the well sides and bottoms, are difficult to avoid unless care is taken. If any cracks open up to cavities behind, these can cause excess absorption as a Helmholtz absorber/resonator has been formed. Proper sealing with varnish or paint is vital. Construction materials are generally not that important unless rough surfaces are used. Figure 9.38 shows the absorption of a concrete Schroeder diffuser before and after it is sealed with paint. Before being fully sealed, the rough surfaces cause

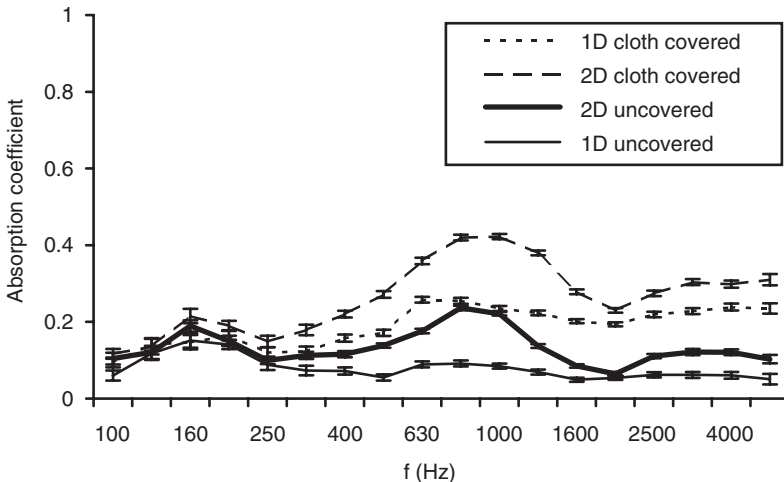


Figure 9.37 Random incidence absorption coefficient measured for one- and two-dimensional Schroeder diffusers based on $N=7$ with and without cloth covering.

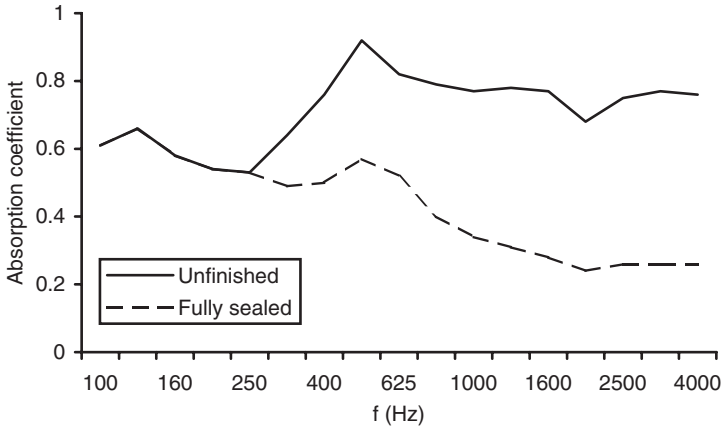


Figure 9.38 Random incidence absorption coefficient measured for a concrete Schroeder diffuser before and after rough surfaces are sealed.

excess losses at the boundary layers and due to the energy flow between wells around the rough edges of the fins. Absorption is greatly reduced by sealing properly.

Commins *et al.* [29] experimentally investigated the absorption characteristics of a Schroeder diffuser. They showed that by slopping the bottom of the diffuser wells, the absorption could be reduced. The effect of the slope is to broaden the resonances of the wells. This will decrease the energy flow within and between wells at resonance. Some early concert hall designs used very wide wells (≈ 30 cm), presumably to avoid the problems of absorption. The problem with such wide well widths is that at high frequencies specular reflections from the bottom of the wells can cause problems [30]. Furthermore, the bandwidth of the device will be greatly reduced. Consequently, if the fear of absorption cannot be overcome, it might be better to use a fractal construction or a surface topology which does not generate strong resonances; the designs described in Chapter 10 could be used.

9.9 But ...

The above analysis has all relied on a simplified model of acoustic scattering, the Fraunhofer type theory. The performance of the Fraunhofer theory can be divided into three frequency ranges, as discussed in Chapter 8. At low frequencies the theory is inaccurate as the mutual interactions across the surface are not correctly modelled by the Kirchhoff boundary conditions. At mid-frequencies, the Fraunhofer theory is most accurate. At high frequencies, the theory becomes inaccurate again because application realistic sources and receivers are not in the far field. Berkhout *et al.* [31] pointed out that the theory used by Schroeder was approximate and concluded that the development of the diffuser should be based on a more complex model. While it is possible to use a more complex theory, it is only with the simplified Fraunhofer theory that the problem can be reduced to the point that the design can be carried out by simple design equations and using basic Fourier concepts. A more complex prediction model can be used in an optimization design solution, and this will be

discussed later. Optimization is, however, a brute force technique which often means the designer learns little about the basic principles of good diffuser design. The optimization produces a set of well depths, but why this is a good set of well depths can often remain a mystery.

Schroeder *et al.*'s [32] reply to Berkhout *et al.* pointed out that measurements and accurate theory were not too different from the approximate theory. It should also be argued that by understanding the Fourier properties one is in a better position to understand and exploit brute force techniques such as optimization, or the inverse problem alluded to by Berkhout *et al.* One probable advantage of working with dispersing surfaces, such as the quadratic residue sequences, is that the laws of physics and the tendency to disorder are going to aid diffusion. The difference between approximate and accurate theories is probably more crucial when exacting results such as notches formed from PRDs are required. Even if the optimum diffusion as defined by Schroeder is not achieved, these are pretty complex surfaces which will create dispersion anyway.

There are other limitations that apply to the Schroeder design, some of which have been touched on before. For instance:

- 1 The design methodology is based on an approximate model.
- 2 Losses are ignored.
- 3 The design is carried out for the far field, whereas most listeners are in the near field.
- 4 The wells are assumed to be local reacting.

Assumption 3 may not be that limiting. There is some evidence that a diffuser that creates good energy dispersion in the far field works well in the near field. In the near field, the path length differences from different points on the surface dominate and cause the scattering to have a large number of minima and maxima. Indeed, the polar plots for different diffusers have similar statistical features in the near field. Some studies have compared periodic and aperiodic arrangements of diffusers either subjectively or objectively [33] using application realistic near field listener positions. In these cases, the aperiodic arrangements, which will create more dispersion in the far field than the periodic cases, are found to be more efficient diffusers in the near field. Consequently, it is assumed that the Schroeder diffuser, which will create good far field dispersion, will also be effective in the near field. A near field polar response normally neglects to show phase, and it is assumed that the phase of the wavefront must contain the information which enables listeners to distinguish between the periodic and aperiodic arrangements.

Schroeder gave an alternative solution to the near and far field problem. He suggested that by bending the diffuser, the far field scattering pattern could be focussed at near field receivers. This means bending the diffuser to follow a parabolic concave mirror. This is not a very useful design because it is rather expensive to execute. A similar effect can be achieved by modulating the well depth phases by the locus of a parabolic mirror. In this case, the varying phases cause the far field beam to be focussed into the near field. It is rather like the use of phase changes in beam steering of transducer arrays. This process has been tested with a boundary element model and shown to work [5].

Assumption 4 concerns whether the well admittances change due to the presence of the neighbouring wells. This assumption has undergone some limited tests. Cox

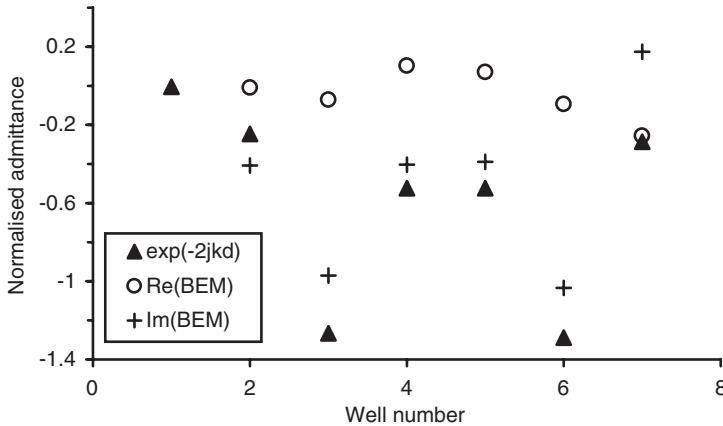


Figure 9.39 Admittance for an $N=7$ QRD at a single mid-frequency. A BEM prediction was used to generate accurate admittances for comparison with the simple phase change calculation ($\exp(-2jkd)$). The first well is zero depth, and so no comparison is possible (after Cox and Lam [5]).

and Lam [5] compared the admittance predicted by a boundary element model which models the surface shape precisely against the simple phase change admittance values derived from a reflection factor of $\exp(-2jkd_n)$. Figure 9.39 shows that reasonable agreement is found, indicating that the surface admittances are indeed local reacting to a reasonable accuracy. Some real parts are seen indicating losses or maybe mathematical inaccuracies in the BEM model. If these are true losses, they are due to evanescent waves as the BEM model did not include any absorption and indicates the small inherent absorption present in these devices. Cox and Lam also looked at the admittance variation along the elongated dimension of a 1D Schroeder diffuser. They again showed that the BEM admittance approximately matched the simple phase change admittance, except for positions close to the ends of the wells.

The most significant limitations of the above number theoretic designs are, however:

- 1 They only work at discrete frequencies.
- 2 Optimum diffusion means the same energy in the diffraction lobes; this is not the same as even energy in all directions.

As the number theoretic Schroeder diffusers are not truly broadband and do not completely disperse to all directions, it is possible to improve on the design. To do this, optimization can be used.

9.10 Optimization

9.10.1 Process

de Jong and van den Berg [34] developed the idea of using an iterative solution method to produce Schroeder style diffusers. It was not until Cox [35] rediscovered

this idea in the early 1990s, however, and D'Antonio [36] provided experimental evidence for the improved performance over traditional number theoretic Schroeder diffusers, that this concept was exploited. de Jong and van den Berg used an approximate prediction model, and narrow deep wells which were rather unrealistic of practical diffuser as the narrow wells would have caused excess absorption. Cox was able to use greater computing power to use more accurate boundary element models, and also used more application realistic geometries.

The concept of optimization is illustrated in Figure 9.40. The idea is to get a computer to go through a trial-and-error process searching for the best well depth sequence possible. First, a starting well depth sequence is randomly chosen. Then the computer predicts the scattering from the surface and evaluates the quality of the scattering in a single figure of merit or error parameter. The computer then adjusts the well depth sequence in an effort to improve the error parameter. When a minimum in the error parameter is achieved the iteration process has completed, and an optimum diffuser has been found. This optimization process is a common technique and has been exploited in a wide range of engineering applications.

To achieve an optimization of diffusers, several key ingredients need to be in place.

- 1 A validated prediction model.
- 2 A figure of merit or error parameter.
- 3 An optimization algorithm to change the well depth sequences.

A validated prediction model is needed and for this a boundary element model can be used. The disadvantage of using a BEM model is that it can be very slow to compute, but as computing power is constantly increasing, this is becoming less of a limitation. For computing power reasons, the diffusers that Cox originally optimized were rather narrow, now it would be possible to carry this out with wider diffusers in periodic arrangements over a wider bandwidth. It is also possible to use the simpler Fraunhofer models, which means the optimization is very fast, but then the accuracy may be compromised. One possibility is to use simple models to carry out a course optimization, and then use the more accurate models to focus on solutions.

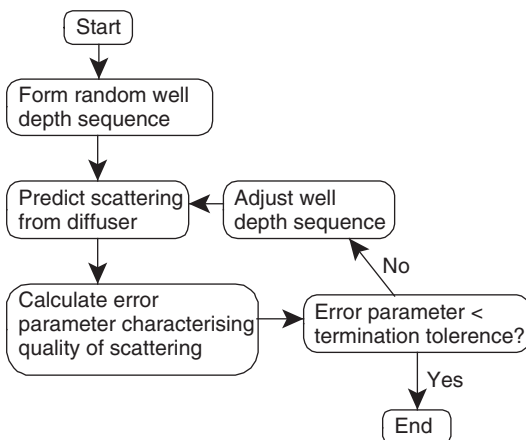


Figure 9.40 Flow diagram for optimizing the well depth sequence of a Schroeder diffuser.

The diffusion coefficient can be used to evaluate the quality of the scattering produced by the surface in a single figure of merit. The diffusion coefficient is evaluated at each frequency band of interest, say each one-third octave band. The diffusion coefficients are then averaged across frequency to obtain a single figure of merit. The risk with this simple averaging process is that the diffusion may be very uneven versus frequency. Frequencies with very good diffusion may compensate for frequencies with very poor diffusion, where a better solution might be moderate diffusion consistent across the whole frequency range. This problem is most easily solved by subtracting a standard deviation of the diffusion coefficients from the mean value across frequencies. This then penalizes cases with very uneven diffusion coefficient spectra.

An optimization algorithm is used to adjust the well depth sequence during the search. It is needed so that the different well depth sequences can be tried and tested in a logical manner rather than on a completely random trial-and-error basis. A usual analogy for a 2D optimization is finding the lowest point on a hilly landscape (while blindfolded). If a human was to carry out such a search, they would start by going downhill on the presumption that this will lead them to a lower point. The optimization algorithm must make similar decisions. It is vital that the solution is found in the fewest steps as otherwise the optimization process becomes rather tedious. The landscape is a 2D optimization, in other words only two well depths. Practical optimization involves many more degrees of freedom, and as the number of degrees of freedom increases, finding the minima becomes more difficult.

There are a variety of algorithms available for optimization [37]. The key decision is whether the optimization is to take place with only the figure of merit known, or with the figure of merit and its derivative. Knowledge of the derivative greatly speeds optimization processes and the derivative should always be used if available. To continue with the landscape analogy, it is much quicker if the person is told the downhill direction, rather than they having to stagger around for a while trying to decide which way is downhill. The problem with diffuser optimization is that the derivative is not often known. With the Fraunhofer theory and a simple figure of merit, such as minimizing the specular zone energy, it is possible to derive the derivative of the figure of merit [10]. This greatly speeds the optimization.

For most work on diffuser optimization, only function values are known. A downhill simple algorithm has been often used, which is rather slow. It is, however, extremely robust to non-linear constraints, something which will become important for the non-welled constructions discussed in Chapter 10. There are other techniques like genetic algorithms or quasi-Newton gradient descent methods. The disadvantage of a genetic algorithm is that it requires tuning by appropriately choosing population sizes, mutation rate, etc. Methods which calculate gradients with finite differences such as quasi-Newton methods can cause problems with solution techniques such as BEM models which often have small numerical inaccuracies which can greatly affect the estimated gradient. A downhill simplex method may not be trendy, but it just needs plugging in and it works.

When carrying out the optimization for a Schroeder diffuser, it is most efficient to use a BEM model where the diffuser is modelled as a box with a variable admittance on the surface. Then all that changes during the optimization is the surface admittance and not the surface profile. This means that the time consuming processes of carrying out the Green's function integrations can be done once at the start of the optimization.

This greatly reduces optimization time. In fact, it should be possible to get the derivatives of the figure of merit in this case [38]. Time spent speeding up the prediction algorithm is time well spent; in a typical optimization process the scattering is typically evaluated a thousand times, so unless each individual case takes a matter of seconds, the optimization process will become very slow.

In any optimization problem there will be a large number of local minimum, but somewhere there will be the numerically lowest point called the global minimum. To return to the landscape analogy. The blindfolded person might find a valley bottom and think the best point has been found, not realizing that over the next mountain ridge there is a lower valley. The key to a good optimization algorithm is not to be trapped in poor local minima, but to continue to find deep local minima. Provided a good optimization algorithm is chosen, this should not be a problem. Especially if the optimization is tried many times from different starting points as is customary good practice.

When there are a large number of degrees of freedom in an optimization problem, i.e. a large number of well depths to be optimized, the surface describing the variation of the figure of merit with the well depths becomes very complex. There will be a very large number of minima. It is virtually impossible to find the global minimum unless a large amount of time is used with the optimization algorithm being started over and over again from a wide variety of places on the error surface. Fortunately, as the number of degrees of freedom increases, the need to find the numerical global minimum becomes less important. Experience has shown that there are a large number of good local minima solutions available, and although the scattering will be different in each case, there is often negligible difference in performance between the good local minima. There is usually no magical global minimum where the quality of scattering produced is significantly better than good local minima.

9.10.2 Results

When testing the results of an optimization, it is important to look at frequencies, source and receiver positions different to that used during the optimization. This checks to see whether the optimization process has found a robust solution. There is always a risk that the optimizer will overfit a poor solution; this is where the solution is good only for the geometries and frequencies used during the optimization.

Figure 9.41 shows the scattering from two optimized diffusers compared to an $N = 7$ QRD. One of the optimized diffusers had fins; the other had a stepped profile, essentially a Schroeder diffuser with the fins removed. Both the optimized diffusers produce more even scattering than the QRD at this and other frequencies.

Cox [35] found that the optimized $N = 7$ diffuser with fins outperforms the QRD over a wide variety of frequencies. When the number of wells was increased to about 36 and compared to two periods of an $N = 17$ QRD, however, the gains were less marked. The scattering from the QRD was already fairly uniform at the low frequencies, and so the room for improvement was relatively small. This was not, however, particularly due to the use of a quadratic residue sequence, even a diffuser with randomly determined well depths gave reasonable diffusion.

Removing the constraints on geometry imposed by a Schroeder style diffuser and forming a stepped diffuser produce better diffusion. The magic in the Schroeder diffuser geometry is not that it produces diffusion, but that it enables simple design

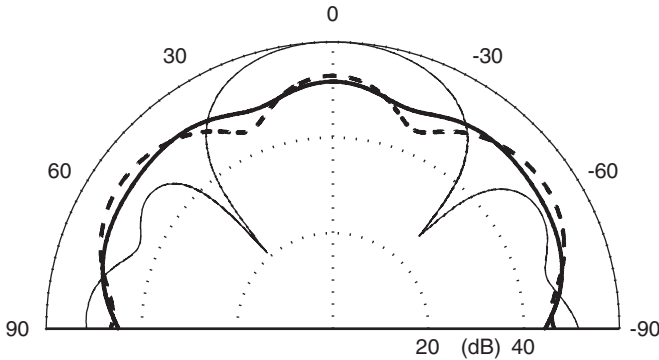


Figure 9.41 The scattering from an ——— $N=7$ Schroeder diffuser, - - - an optimized Schroeder diffuser, ——— an optimized stepped diffuser at 1,050 Hz (data from Cox [35]).

methods to be brought to bear on the problem. Removing the fins enables a simpler geometry, which is cheaper to make. It has also removed the resonant wells and so will have lower absorption. The improved performance was seen for both the $N=7$ and $N=36$ cases. Interestingly, the $N=7$ optimized stepped diffuser looked rather like a faceted semicylinder.

D'Antonio [36] carried out a thorough experimental evaluation of the work of Cox. The measurements confirmed that optimization produced better diffusers than number theory sequences. D'Antonio also looked at the performance of the diffusers outside the domain of optimization; at higher frequencies, at oblique angles of incidence, for different receiver radii and for a periodic arrangement. Outside the domain of optimization, the optimized diffusers were found to give roughly the same diffusion as the Schroeder diffusers – sometimes worse, sometimes better. The solution to this problem is to carry out the optimization including all frequencies, angles of incidence and source and receiver radii of interest. With modern computing power, this is not a problem.

The original optimization work was limited to narrow single diffusers because of computing power. Now, this optimization process can be applied to larger area diffusers. Figure 9.42 compares the diffusion from an $N=7$ QRD to an optimized modulated arrangement of phase grating diffusers. The improvement in diffusion is quite marked.

It is also possible to optimize for a non-even scattering distribution. For example, Cox and D'Antonio [10] tried to minimize the energy in a particular direction, to produce a notch in the specular reflection direction to create an improved PRD. In Figure 9.43 the results from trying to optimize a diffuser to work from 500 to 3,000 Hz for an angular range of $\pm 5^\circ$ about the specular reflection direction are shown. The diffuser is labelled *optimized* and is compared to a plane surface and a modified PRD. Across the optimization range, the specular reflection is reduced by about 25 dB compared to a plane surface and 10 dB when compared to the PRD. This was for a single period of the diffuser. When multiple periods were attempted, the results were far less dramatic. Over the bandwidth 500–3,000 Hz, the best-optimized diffusers could achieve was an extra 4 dB attenuation of the specular and near

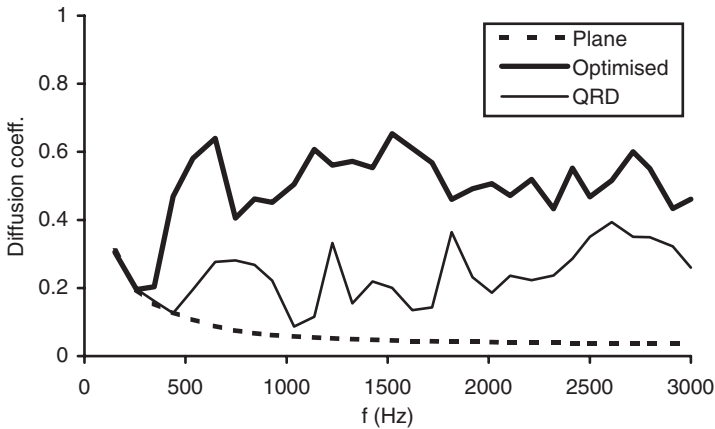


Figure 9.42 Diffusion coefficient for multiple periods of a Schroeder diffuser and an optimized phase grating diffuser.

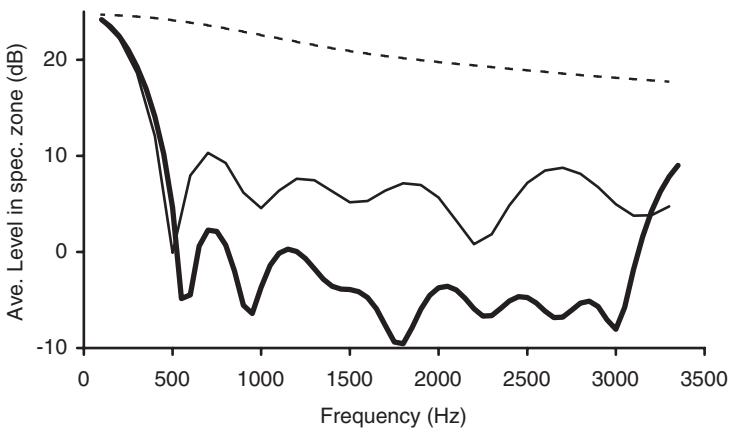


Figure 9.43 The average energy in the specular zone for three surfaces as indicated in the legend. ----- Plane; ——— Optimized; ——— Modified PRD (after Cox and D'Antonio [10]).

specular energy when compared to the modified primitive root. Although the reduction would probably be audible in certain applications, the improvement could hardly be termed dramatic. It is impossible to prove a negative with optimization techniques, but experience has shown that using optimization to shape polar responses or creating notches is fraught with difficulty. Optimization is most successful when trying to create uniform dispersion.

9.11 Summary

Schroeder diffusers have been hugely successful thanks to their simple concept and design, and their commercial exploitation. There has always been a certain reticence

among designers to use this type of diffusers. The rumours of absorption have continued since their inception, with high absorption coefficients being published for poorly constructed surfaces. But now with a proper understanding of the absorption mechanisms, this should no longer be a problem. A few people have claimed to hear strange artefacts from Schroeder diffusers, but the designs they have been listening to have not followed some of the important design principles discussed in this chapter. Following proper design principles, applying all the current knowledge, results in high quality sound from Schroeder diffusers. One of the main stumbling blocks to their use is, however, their visual appearance which is either loved or loathed. Consequently, new diffusers were needed which had defined acoustical properties but with different visual aesthetics. This will be addressed in the next chapter.

9.12 References

- 1 M. R. Schroeder, "Diffuse sound reflection by maximum-length sequences", *J. Acoust. Soc. Am.*, 57(1), 149–150 (1975).
- 2 M. R. Schroeder, "Binaural dissimilarity and optimum ceilings for concert halls: more lateral sound diffusion", *J. Acoust. Soc. Am.*, 65, 958–963 (1979).
- 3 P. D'Antonio and J. Konnert, "The reflection phase grating diffuser: design theory and application", *J. Audio Eng. Soc.*, 32(4) (1984).
- 4 T. J. Cox and P. D'Antonio, "Schroeder diffusers: a review", *Building Acoustics*, 10(1) 2003.
- 5 T. J. Cox and Y. W. Lam, "Prediction and evaluation of the scattering from quadratic residue diffusers", *J. Acoust. Soc. Am.*, 95(1), 297–305 (1994).
- 6 W. R. T. Tenkate, "On the bandwidth of diffusers based upon the quadratic residue sequence", *J. Acoust. Soc. Am.*, 98(5), 2575–2579 (1995).
- 7 P. D'Antonio and J. Konnert, "The QRD diffractal: a new one- or two-dimensional fractal sound diffuser", *J. Audio Eng. Soc.*, 40(3), 113–129 (1992).
- 8 P. Fan and M. Darnell, *Sequence Design for Communications Applications*, John Wiley & Sons, 49 (1996).
- 9 E. Feldman, "A reflection grating that nullifies the specular reflection: a cone of silence", *J. Acoust. Soc. Am.*, 98(1), 623–634 (1995).
- 10 T. J. Cox and P. D'Antonio, "Acoustic phase gratings for reduced specular reflection", *Appl. Acoust.*, 60(2), 167–186 (2000).
- 11 M. R. Schroeder, "Phase gratings with suppressed specular reflections", *Acustica*, 81, 364–369 (1995).
- 12 J. A. S. Angus, "Non-integer-based diffusers", *Proc. Audio Eng. Soc. 107th Convention* NY, preprint 5064 (1999).
- 13 Op. cit., 269–298.
- 14 Op. cit., 187–188.
- 15 J. A. S. Angus, "Large area diffusers using modulated phase reflection gratings", *Proc. Audio Eng. Soc.*, 98th Convention, preprint 3954 (D4) (1995).
- 16 J. A. S. Angus, "Using modulated phase reflection gratings to achieve specific diffusion characteristics", *Proc. Audio Eng. Soc.*, 99th Convention, preprint 4117 (1995).
- 17 J. A. S. Angus and C. I. McManmon, "Orthogonal sequence modulated phase reflection gratings for wideband diffusion", *Proc. Audio Eng. Soc.*, 100th Convention, preprint 4249 (1996).
- 18 J. A. S. Angus and A. Simpson, "Wideband two dimensional diffusers using orthogonal modulated sequences", *Proc. Audio Eng. Soc. 103rd Convention*, preprint 4640 (1997).
- 19 J. A. S. Angus and C. I. McManmon, "Orthogonal sequence modulated phase reflection gratings for wide-band diffusion", *J. Audio Eng. Soc.*, 46(12), 1109–1118 (1998).

- 20 J. A. S. Angus, "Using grating modulation to achieve wideband large area diffusers", *Appl. Acoust.*, **60**(2), 143–165 (2000).
- 21 B. B. Mandelbrot, "The fractal geometry of nature", Freeman, San Francisco (1983).
- 22 A. Jrvinen, L. Savioja and K. Melkas, "Numerical simulations of the modified Schroeder diffuser structure", *J. Acoust. Soc. Am.*, **103**(5), 3065 (1998).
- 23 F. P. Mechel, "The wide-angle diffuser – a wide-angle absorber?", *Acoustica*, **81**, 379–401 (1995).
- 24 J. Hunecke, "Schallstreuung und Schallabsorption von Oberflächen aus Mikroperforierten Streifen", University of Stuttgart, PhD thesis (1997).
- 25 K. Fujiwara, K. Nakai and H. Torihara, "Visualisation of the sound field around a Schroeder diffuser", *Appl. Acoust.*, **60**(2), 225–236 (2000).
- 26 T. Wu, T. J. Cox and Y. W. Lam, "A profiled structure with improved low frequency absorption", *J. Acoust. Soc. Am.*, **110**, 3064–3070 (2001).
- 27 M. R. Schroeder, "Chaos, power laws: minutes from an infinite paradise", W.H. Freeman & Co. (1991).
- 28 J.-D. Pollack and G. Dodd, *Personnel communication*.
- 29 D. E. Commins, N. Auletta and B. Suner, "Diffusion and absorption of quadratic residue diffusers", *Proc. IoA (UK)*, **10**(2), 223–232 (1988).
- 30 T. J. Cox and Y. W. Lam, "The performance of realisable quadratic residue diffusers (QRDs)", *Appl. Acoust.*, **41**(3), 237–246 (1994).
- 31 A. J. Berkhout, D. W. van Wulfften Palthe and D. de Vries, "Theory of optimal plane diffusers", *J. Acoust. Soc. Am.*, **65**(5), 1334–1336 (1979).
- 32 M. R. Schroeder, R. E. Gerlach, A. Steingrube and H. W. Strube, "Response to 'theory of optimal planar diffusers'", *J. Acoust. Soc. Am.*, **65**(5), 1336–1337 (1979).
- 33 T. J. Hargreaves, "Acoustic Diffusion and Scattering Coefficients for Room Surfaces", PhD thesis, University of Salford (2000).
- 34 B. A. de Jong and P. M. van den Berg, "Theoretical design of optimum planar sound diffusers", *J. Acoust. Soc. Am.*, **68**(4) 1154–1159 (1980).
- 35 T. J. Cox, "Optimization of profiled diffusers", *J. Acoust. Soc. Am.*, **97**(5), 2928–2941 (1995).
- 36 P. D'Antonio, "Performance evaluation of optimized diffusors", *J. Acoust. Soc. Am.*, **97**(5), 2937–2941 (1995).
- 37 W. H. Press *et al.*, "Numerical Recipes, the Art of Scientific Computing", Cambridge University Press, 289–292 (1989).
- 38 R. D. Ciskowski and C. A. Brebbia (eds), "Boundary Element Methods in Acoustics", Kluwer Academic Publishers (1991).

10 Geometric reflectors and diffusers

Cylinders, pyramids and plane surfaces are common items in rooms, in this chapter the performance and design of these geometric surfaces will be considered as well as fractal and optimized curved surfaces. While most diffuser design is about breaking up wavefronts by surface roughness or impedance changes, it must be remembered that even a plane surface can cause diffraction from its edges, provided the surface has a similar size to the acoustic wavelength or smaller.

Triangles or pyramids can produce dispersion, redirection and specular reflection depending on the geometry used. Applied correctly, triangles and pyramids can form notch diffusers, where the energy in certain directions is much reduced. Curved surfaces are more obviously diffusers and more universally used; indeed a simple sphere or cylinder is very effective at spatially spreading reflections in a hemisphere or a single plane respectively, but this is not the only ingredient to a good diffuser. Furthermore, a single sphere or cylinder on its own is not very useful, and so many spheres or cylinders next to each other are needed. Then the scattering is as much about how the objects are arranged, periodically or randomly, as about the scattering characteristic of a single item. Well-designed curved surfaces can be a less obvious acoustical treatment, and so will often blend into modern architectural designs.

This chapter will first consider the role of plane surfaces, as an understanding of scattering from finite-sized plane surfaces is fundamental to an understanding of diffraction and diffuse reflection.

10.1 Plane surfaces

Understanding the reflection effects of finite-sized plane surfaces is important. With no surface roughness, any scattering generated is by edge scattering. Consequently, understanding plane surfaces enables finite size effects from more complex surfaces to be partly or fully explained. Whether by accident or design, plane surfaces are probably the most common architectural surface.

10.1.1 *Single panel response*

Consider the geometry shown in Figure 10.1, where a source and receiver are near a finite-sized plane surface. The surface is assumed rigid, hard and non-absorbing. If the source and receiver are chosen so that the geometric reflection point, the point at which the angle of incidence equals the angle of reflection, lies on the panel, then the scattered pressure as a function of frequency, as shown in the top line in Figure 10.2,

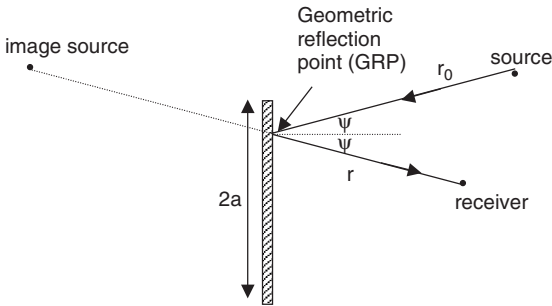


Figure 10.1 Geometry for sound reflecting from a plane surface.

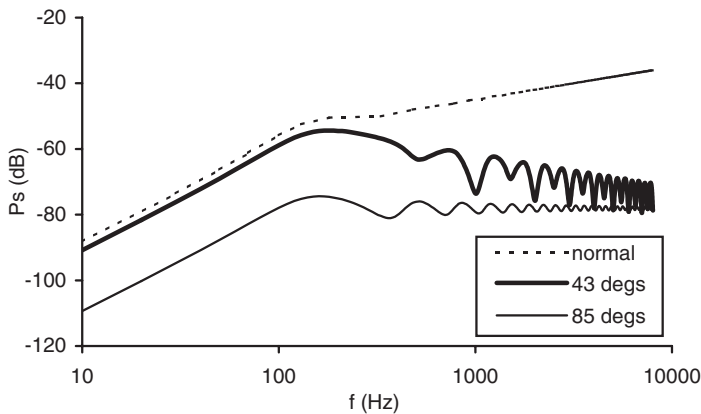


Figure 10.2 Scattered pressure from a plane surface for normal incidence sound, for three different receiver angles as shown in legend.

resembles an approximate high pass filter. At very low frequencies, when the wavelength is very large compared to panel size, little or no sound is scattered from the surface. At very high frequencies, when the wavelength is small compared to the surface size, strong specular reflection results.

It is useful to define the cut-off frequency for the plane reflector and the transition frequency between specular reflection and significant diffraction. To continue with the filter analogy, the transition frequency can be taken as the -3 dB point of the high pass filter [1–4]. This gives acousticians an approximate frequency below which the panel most effectively scatters sound in all directions and above which the panel produces more specular-like reflections. Rindel has derived a simple and useful formulation for the cut-off frequency. Rindel [4] used a simplified Fresnel solution method for the scattering from a plane surface, with the Fresnel integrals approximated by simple mathematical functions. Using this solution method, Rindel found a transition frequency above which the Fresnel integrals remain roughly constant. He defined this point as the cut-off frequency. For a plane panel it is given as:

$$f_{-3\text{dB}} = \frac{cr^*}{8a^2 \cos^2(\psi)} \quad (10.1)$$

where r^* is given by:

$$r^* = \frac{2rr_0}{r + r_0} \quad (10.2)$$

where r_0 is the distance from the source to the panel centre, r the distance from the receiver to the panel centre, $2a$ the panel width, c the speed of sound, and ψ the angle of incidence.

The use of a cut-off frequency is most valid for receivers close to the specular reflection direction. Figure 10.2 also shows predictions for the scattering at two oblique reflection angles. This shows that representing the scattered pressure by a simple high pass filter does not work for every direction. In this case, there is often a complicated pattern of minima and maxima. When the geometric point of reflection lies on the surface of the panel, it is reasonable to assume that the scattered pressure at high frequencies is going to be dominated by specular type reflection. When the geometric reflection point does not lie on the panel, however, the scattered pressure is entirely due to diffraction. In this case, the diffracted energy reaching the receiver will decrease as the frequency increases. Consequently, the frequency response for these receivers is more likely to follow something closer to a band pass filter response. This is illustrated by the 43° receiver in Figure 10.2. This is not always true, however, as shown at the grazing reflection angle case. A rough guide to the region over which the cut-off frequency representation works is therefore the region over which the geometric reflection point lies on the panel. Incidentally, to simplify the calculation of these angles, an image source construction is a good idea as it greatly reduces the complexity of the trigonometry – this is shown in Figure 10.1.

For a plane panel, the case of scattering close to the specular reflection direction is usually of most interest, as this will have the largest amount of the scattered energy at high frequencies. Nevertheless, with significant energy scattered into other angles at low frequencies, the use of a cut-off frequency should be done with caution. Equation 10.1 has either assumed a square panel where the azimuth and elevation incident angles are the same or a 2D world. For rectangular panels, and arbitrary incidence angles with square panels, there will be two different cut-off frequencies to consider. For circular or odd-shaped panels, the transition will be more complicated, but similar general principles to that shown in Figure 10.2 apply.

Figure 10.3 shows the total sound field impulse response – incident plus reflection sound – for plane wave scattering. The direct and reflected sound are clearly distinguishable, as is the edge scattering wave which has a negative magnitude. Figure 10.4 shows the frequency response of the total sound field in Figure 10.3. The reflected sound from a plane panel is very similar to the incident sound field unless the panel is small. This means that the frequency response shows distinct comb filtering. Comb filtering is characterized by minima and maxima at a regular spacing in frequency. The ear is particularly sensitive to this emphasis and de-emphasis of frequency components, and when audible, listeners will complain of harshness or glare from these reflections.

In diffuser design, the ability of a surface to disperse the sound spatially is often monitored. Figure 10.5 shows the scattering from a plane thin rigid surface as a polar response. The scattering is shown for several frequencies and is in the far field. For the largest wavelengths (lowest frequencies), the scattered response is exactly the same as that produced by a dipole, following a $|\cos(\psi)|$ function typical



Figure 10.3 Time response for incident and scattered sound from a plane surface (not the same case as Figure 10.2).

of a low frequency dipole approximation. At grazing angles there is zero pressure. This only happens for the infinitesimally thin surface, since surfaces with finite thickness produce finite pressure. In fact, the pressure for all angles is relatively low for large wavelengths, as destructive interference is the dominant phenomenon, as is true of dipoles. To put this in a less technical language, when the wavelength is much larger than the panel size, the wave does not 'see' the panel and propagates largely undisturbed.

As the frequency increases and the wavelength becomes comparable and then smaller than the panel size; eventually a specular reflection becomes apparent. Energy is concentrated in the specular reflection direction obeying Snell's law, where the angle of incidence equals the angle of reflection. This is a special case of Fermat's principle, where the specular reflection direction is the shortest possible path length and so is preferred.

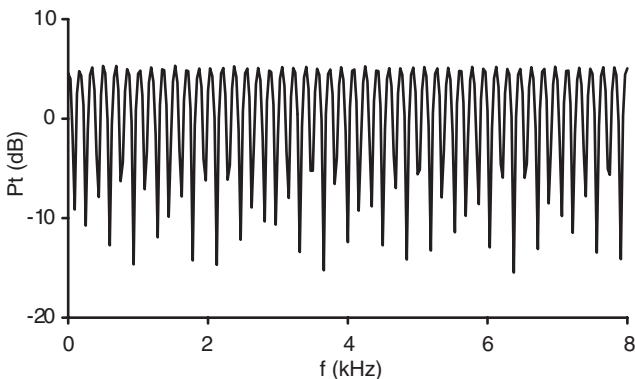


Figure 10.4 Total field frequency response for plane surface scattering.

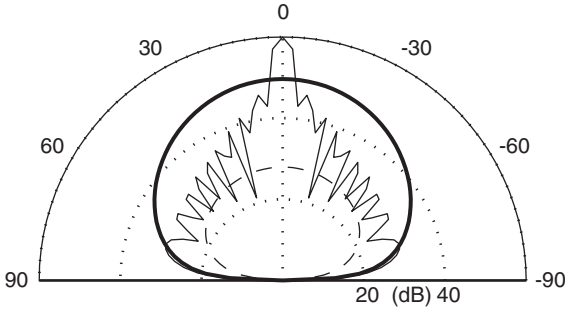


Figure 10.5 Polar response for scattered pressure from a plane panel for three different frequencies. - - - - $\lambda = 20a$; ——— $\lambda = 2a$; ——— $\lambda = 0.2a$. Thin panel boundary element method (BEM) prediction.

Figure 10.5 presents the far field response. In real spaces, however, listeners and sources can be quite close to surfaces. Figure 10.6 shows how the scattered pressure distribution varies for a high frequency, as the receiver approaches the panel. At 0.8 m from the panel, the receiver arc diameter is actually smaller than the panel width. For all receivers on the 0.8 m arc, the scattered pressure is high, because for every receiver there is a geometric reflection point on the panel giving a strong specular reflection. As the receiver arc moves further from the panel, fewer receivers get a strong reflection, eventually the far field response is achieved.

Figure 10.6 implies that, close to the panel, the flat surface is good at dispersing sound. In particular, good coverage is achieved because all receivers get similar energy in the reflection. Does this imply that a plane surface is a good diffuser as it is dispersing scattered energy evenly to all receivers? In reality, the plots in Figure 10.6 are only telling a part of the story. The polar plots of scattered energy do not show how the direct and reflected sounds interfere, or the effect this has on the sound heard by the listener. In fact, a comb filter response would result, and this is likely to

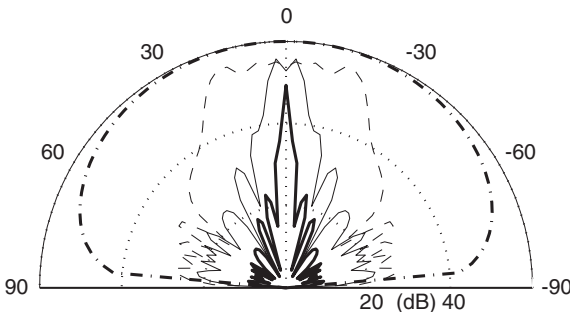


Figure 10.6 High frequency scattering from a plane surface 1 m wide ($=30\lambda$) for four different receiver radii: - · - · - 0.8 m; - - - - 1.2 m; ——— 5.0 m; ——— 1000 m.

colour the sound due to changes in emphasis of different frequency components as discussed in Chapter 2.

10.1.2 Panel array response: far field arc

When multiple plane panels in an array are used, then the response is a combination of both the response of a single panel and the periodic arrangement of the array. Figure 10.7 shows a sketch of an array which will be used to demonstrate the response. For simplicity, scattering in one plane predicted using a 2D model will be used. The findings can be generalized to a 3D array, as the general principles are the same. Using the simple Fourier theory detailed in Chapter 8, it is possible to represent the array response, p_a , as a multiplication of the single panel response and a set of delta functions:

$$p_a(\beta) = p_1(\beta) \sum_{n=-\infty}^{n=\infty} \delta\left(\beta - \frac{m\lambda}{W}\right) \quad (10.3)$$

$$\beta = \sin(\psi) + \sin(\theta) \quad (10.4)$$

where β is the transform variable, as discussed in Chapter 9, ψ and θ are the incidence and reflection angles, respectively, p_a the pressure from the array, p_1 the pressure from a single panel, m an integer, λ the wavelength, $2a$ the single panel width, W the repeat distance, and δ the delta function.

This formulation is for the far field. It is an approximate representation, and so the graphs which are being shown are actually generated by an accurate BEM model described in Chapter 8. Equation 10.3 is being used purely to aid understanding of the physical processes. This formulation is using similar arguments as was used for modulated forms of Schroeder diffusers in Chapter 9, where the concept is given in a little more detail.

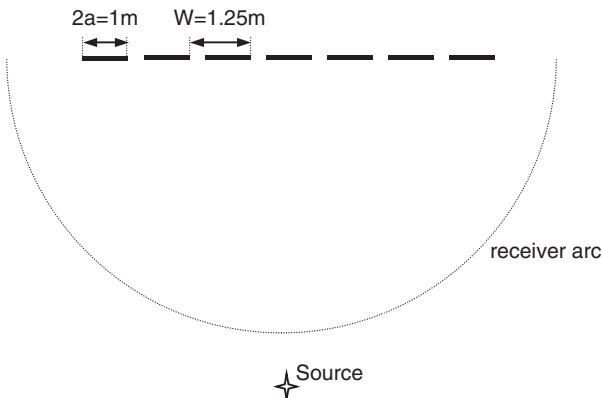


Figure 10.7 Sketch of an array of plane tested (source and receiver position not to scale).

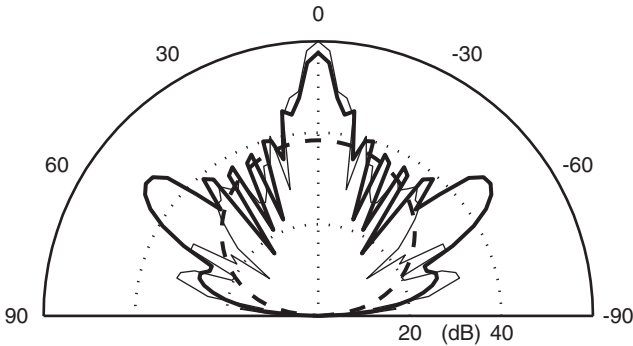


Figure 10.8 Scattering from array of plane panels for three different frequencies.
 - - - 34 Hz ($\lambda = 10.2a$); — 340 Hz ($\lambda = 2a$); — 10 kHz ($30\lambda = 2a$). The $1/\sqrt{f}$ variation which naturally occurs with line sources has been removed by normalization.

Figure 10.8 shows the scattering for three contrasting frequencies. The last term in Equation 10.3 means that it would be expected that whenever:

$$\beta = \sin(\psi) + \sin(\alpha) = \frac{m\lambda}{W} \quad (10.5)$$

there should be a reflection similar to the single panel alone. For the middle frequency in Figure 10.8, Equation 10.5 predicts lobes at $0, \pm 53^\circ$ and this is borne out by the prediction of the grating lobes. Consequently, at mid-frequencies, periodicity effects will often dominate, and Equation 10.5 will predict their location.

At low frequencies, the scattering from a single panel is rather small (20 dB less in the specular reflection direction) and follows a dipole response as the wavelength is large compared to panel size. In this case, the single panel response $p_1(\beta)$ dominates the scattered level. The array produces a polar response which is very similar to a single panel, albeit with an increased power due to the greater surface area of the array of panels compared to a single panel. There are no periodicity lobes, because the wavelength is so large, that only the zeroth order mode ($m = 0$) can exist in the far field.

At the highest frequencies, the scattering is dominated by a strong specular reflection. Equation 10.5 predicts a large number of side lobes (≈ 70), but these are not seen. The reason for this is that the response of the single panel, p_1 is highly directional as was shown in Figure 10.5. Consequently, most of the side lobes are of very low level. In fact, the scattering from the array of panels is not too dissimilar to that of a single panel, except for a change in radiated power due to the greater surface area in the array.

10.1.3 Panel array response: near field

One of the commonest occurrences of simple reflector arrays is above stages and audiences in auditoria. In this case, it is not just the response on a far field arc that should be considered, but also the response at application-realistic source and receiver positions. In many cases, this will be along a straight line 5–12 m below the reflector

array. This produces a scattered response that is quite different in characteristic to the far field arc. Figure 10.9 shows the scattering from the same array as shown in Figure 10.7, with a far field source and a line of receivers 8 m below the array running parallel to the array. (A far field source is used to simplify matters, but in reality both sources and receivers would probably be 5–12 m below the array.) Figure 10.9 also indicates the panel locations.

At high frequencies, the specular reflection from each panel is apparent. The scattered pressure is uneven with minima where the geometric reflection point for a receiver is between panels, and maxima where the geometric reflection point lies on the panels. For most designs of overhead canopies, this uneven response is

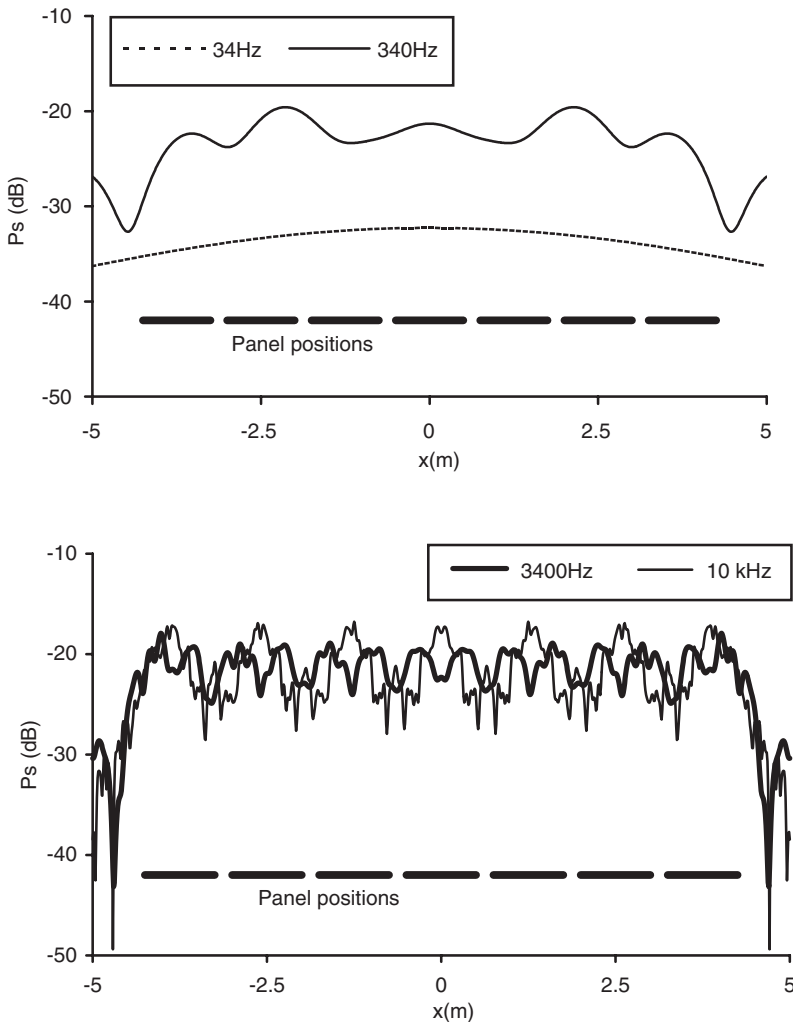


Figure 10.9 Near field scattering from an array of plane panels along a straight line for various frequencies. The panel positions in the x -direction are shown at the bottom of the picture.

undesirable. Due to these absences between reflectors at high frequency, and the strong specular reflections between, it would be normal to use shaped elements, such as arcs, instead of plane panels to scatter energy more evenly to all receivers. This will be discussed in more detail later in this chapter.

For the middle two frequencies (340 and 3,400 Hz), the response is a complex mix of minima and maxima. These are near field effects (the 10 kHz case was also in the near field, but the high directivity of the individual panel response weakened the near field effects). The rapidly changing path length differences from the array to the receiver, as the receiver location is moved along the x -axis, cause a multitude of minima and maxima. The lowest frequency is in the far field, so something like the dipole response seen previously for the far field arc is obtained.

Rindel [5] used Fresnel theory to investigate arrays of ceiling reflectors. He used square reflectors and investigated the effect of reflector density on the frequency response. He found that if the geometric reflection point lay on a panel, a high pass characteristic with some similarity to the single panel response was obtained. Due to the fact that the reflections come from multiple panels, the actual frequency response had many more local minima and maxima than was the case for the single panel alone.

If the geometric reflection point was between panels, however, the scattering had a low pass filter response. In the latter case, the energy is greatest when the scattering is greatest, and this occurs at the low frequencies. At high frequencies, the energy is concentrated in specular directions and so the scattered energy for these receivers is small. Rindel showed that using smaller panels was advantageous, as it reduced the roll-off at high frequencies for receivers away from the geometric reflection point.

Either the size of the reflectors or the panel density determines the low frequency performance of an array. It is possible to imagine cases where it is a combination of these effects which is important. The mid- and high frequency performance is dominated by strong local variations, due to the size of the reflectors and the repeat distance between them. The solution to this is to use non-plane surfaces, as shall be discussed later in this chapter. Alternatively, maybe a pseudorandom arrangement of different panel sizes and spacings could be used.

10.2 Triangles and pyramids

Moving on from plane surfaces, a variety of geometric shapes will be considered in the following sections. Triangles and pyramids can display a wide variety of scattering behaviour from a good diffuser, to a surface that generates specular reflections, depending on the geometry. Indeed, the scattering performance from an array of triangles or pyramids is very much determined by the steepness of the side slopes. For simplicity, the analysis below only considers a 2D case with triangles, but the arguments can easily extend to 3D surfaces such as pyramids.

A simple ray tracing yields much information about how a triangle reflects sound. Figure 10.10 shows some simple ray tracing examples. As the angle (χ) of the triangle varies, the reflection characteristic shifts between a notch response, diffuse reflection and a specular response. To understand a triangular arrangement, very simple prediction theories based on the Kirchhoff method will not always work because they do not model the second and high order reflections (see Chapter 8). Consequently, it is safer to use a BEM model or similar. Initially, only high frequencies will be considered

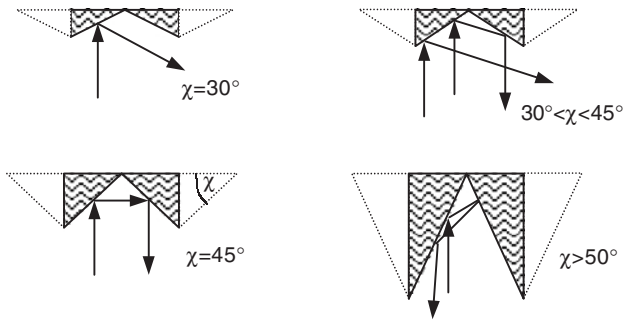


Figure 10.10 Ray tracing of the sound reflecting from the centre of a pair of triangles.

at normal incidence. This makes the pattern of scattering clear. A further simplification is that the response for only the centre portion of two triangles will be considered, as this is more representative of what happens when an array of triangles is used.

For shallow angles, $\chi < 30^\circ$, only a single reflection occurs from each side in the ray tracing shown in Figure 10.10. This results in two distinct lobes being generated at angles of $\pm 2\chi$. An example of the far field scattering is shown in Figure 10.11. This then forms a notch response, with the energy returned to the specular direction being minimized. This is effectively a redirecting surface, which generates two strong reflections in different distinct directions. Unlike primitive root diffusers discussed in Chapter 9, this surface forms a notch over a relatively wide frequency range, although the performance will be compromised at low to mid-frequencies, when finite-sized panel effects become important. Equation 10.1 could be used as a guide as to when each side will produce specular like reflections and so produce a notch response, and when the scattering will be more dominated by edge diffraction. This finite panel effect is true for all the discussion below, but these comments will not be repeated again. With a

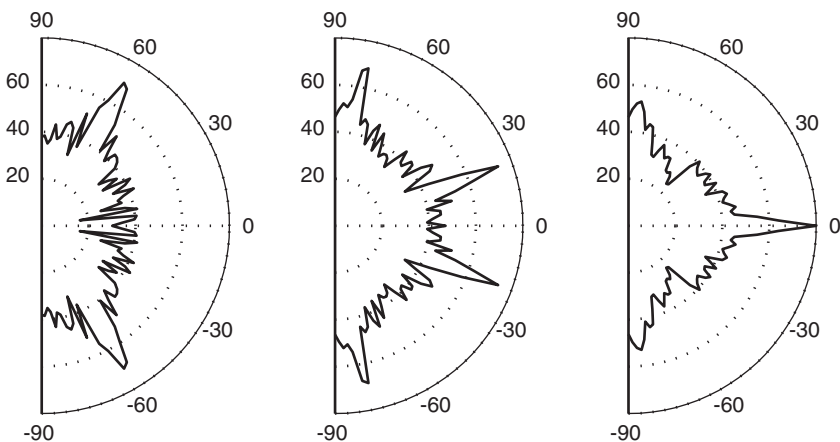


Figure 10.11 Scattering from the centre of two triangles for three side angles, from left to right: $\chi = 30^\circ, 40^\circ, 45^\circ$.

$\chi < 30^\circ$ triangle, there is only a notch for certain incident angles, whereas a primitive root diffuser worked for any angle of incidence but only at a few distinct frequencies.

For $30^\circ < \chi < 45^\circ$ a mixture of single and double reflections is seen in Figure 10.10. The single reflections will again form lobes in the directions of $\pm 2\chi$, the double reflection directions will be in the directions of $\pm(180 - 4\chi)$. Figure 10.11 shows the scattered polar response, with four distinct lobes. By choosing an appropriate triangle angle, it is possible to have a notch in the specular reflection direction, but now the scattered energy is spread over four lobes which is probably more desirable.

$\chi = 45^\circ$ is a special case because the energy is returned back into the specular reflection direction, as shown in Figures 10.10 and 10.11. This is sometimes termed a corner reflector. The ability of a corner reflector to return energy back to sources is relatively well known and has been exploited in some auditoria as a way of returning energy back onto a stage to give reflections which help musicians and actors hear themselves and others.

For $45^\circ < \chi < 54^\circ$ double reflections occur, but these only generate two lobes. An example is shown in Figure 10.12 for $\chi = 50^\circ$. As χ increases beyond 54° the number of reflections a ray undertakes before escaping the surface increases. A varying number of clear distinct lobes are still generated, and simple ray tracing techniques can still be used to locate the directions of the most significant lobes. The relative level of the lobes varies, however, depending on the reflection paths. When the angle becomes very large $\chi > 85^\circ$, then a single fairly broad lobe appears. The surface is in many ways acting like a horn loudspeaker in that a highly directional response is obtained. This occurs because the escape angles for the rays are limited to $\pm(90 - \chi)$. This then returns the energy back to the source, but in a more diffuse manner than occurs with a $\chi = 45^\circ$ surface. The simplistic analysis used here needs to be read with a little caution. Once these devices become very narrow and a great number of reflections occur, then a resonant structure has been formed. Consequently, there is a risk of resonant absorption as is seen for Schroeder diffusers.

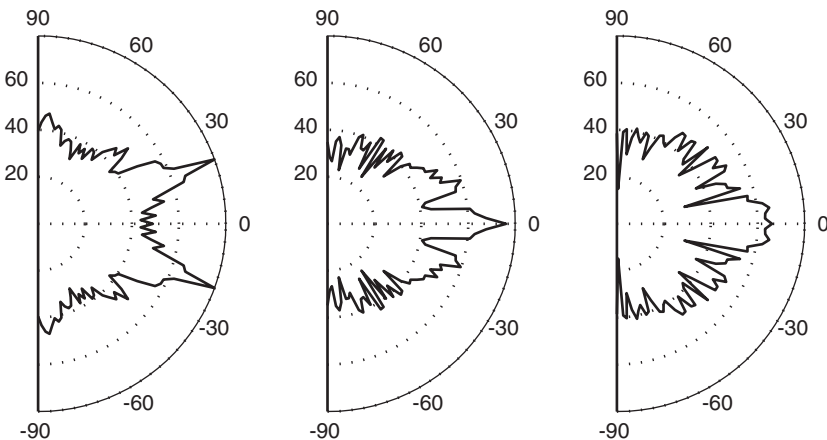


Figure 10.12 Scattering from the centre of two triangles for three side angles, from left to right: $\chi = 50^\circ, 80^\circ, 85^\circ$.

10.2.1 Arrays of triangles

The single triangle response is not that useful because usually large areas are needed to be covered, and then the surface will become too deep, unless this is incorporated into the overall room shape in some way. Consequently, arrays of triangles need to be considered. Figure 10.13 shows the scattering from an array of $\chi = 15^\circ$ triangles compared to a single triangle of the same size. Also shown is the response of two plane panels. An impressively large notch of almost 30 dB is generated for the array case compared to the plane surface. Additional lobes are also seen and these are the effects of periodicity. The location of these can be predicted from Equation 10.5, however, not all the lobes appear. The $m = 0$ and $m = 3$ lobes are attenuated because the single triangle response is weak in those directions. These periodicity lobes can be reduced by using modulation, similar to that used for Schroeder diffusers and discussed in Chapter 9. For example, two different triangle sizes could be chosen and arranged according to a pseudorandom number sequence.

Figure 10.13 actually represents a frequency where the notch diffuser is working well. Figure 10.14 plots the drop in the specular direction level as a function of frequency for the single triangle and the array. This shows that at other frequencies the attenuation is not as good, for example at 1,500 Hz the attenuation is only 13 dB. While this is a drop in level which is likely to be audible, it would be better if the performance could be improved. For example, the reflection free zone concept for small room design [6] would typically be trying to achieve a 20 dB drop in the first order specular reflection level.

A brief parametric study looking at different triangle sizes shows that the peaks and dips in Figure 10.14 relate to the triangle depth. The maximum attenuation occurs when the depth is a multiple of $\lambda/2$. Unfortunately, if the χ is increased further, say to 30° , this

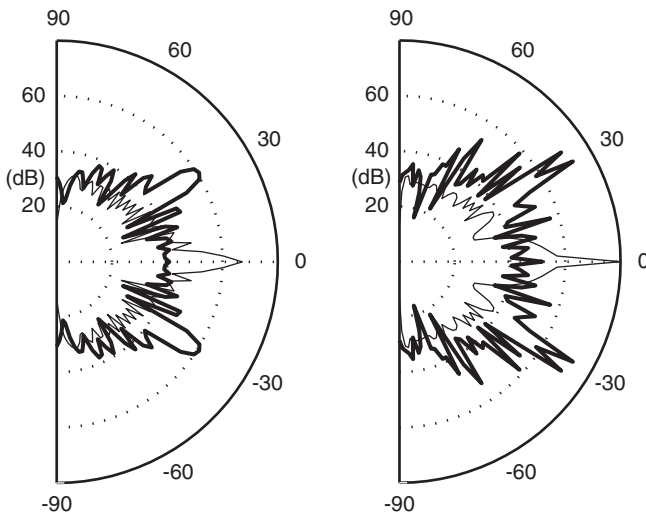


Figure 10.13 Scattering from triangles and plane surfaces. Left figure: — Plane surfaces same size as one triangle; — One triangle. Right figure: — Plane surfaces same size as five triangles; — Five triangles.

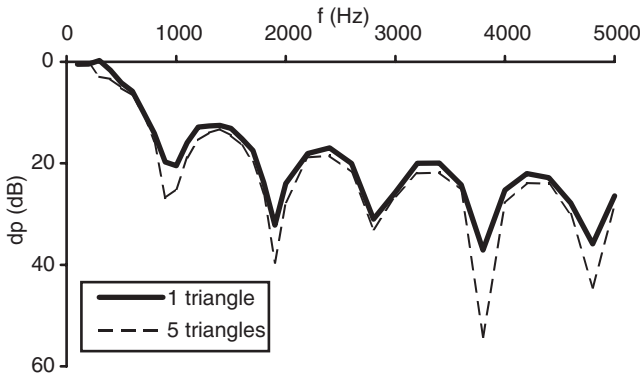


Figure 10.14 Drop in specular zone level when a triangle diffuser replaces a plane surface for different number of triangles (note y-axis plotted in reverse order).

neat story relating the depth of the triangle to the wavelength of the minima and maxima is no longer true. Nevertheless, these results again lead to the thought that orthogonal modulation could solve the problem, following the ideas developed by Angus for Schroeder diffusers and outlined in Chapter 9. By using two or more different depth triangles, so that their frequency bands of higher specular reflection energy are different, it should be possible to improve the notch generated. By using two different depth triangles, it might be expected that the improvement would be of the order of 3 dB, so a large number of different triangles would need to be used. Another solution to the problem is just to make the triangles much deeper, although overly deep surfaces are often not possible for non-acoustic reasons such as cost, weight and visual appearance.

10.3 Concave arcs

Concave surfaces such as domes are often an acoustician's nightmare. Used wrongly they lead to focussing effects that generate strong reflected energy in certain places. This can lead to uneven energy distribution across the room, and also echoes and colouration of timbre.

Whether an arc causes problems depends on the positions of the sources and receivers, and the radius of the arc. Figure 10.15 shows the scattering from a concave arc at a mid-high frequency for different receiver radii. Figure 10.16 schematically shows a ray tracing of the surface scattering. Figures 10.15 and 10.16 show that the focussing effect of the curved surface is only a problem for some receiver distances, close to the focal length of the arc. Consequently, it is possible to use a curved surface provided the focus of the surface is away from the listeners. For example, a concave ceiling in an auditorium is not a problem provided the curved surface focusses the sound well above or below the audience. If the focus is well above the audience, then the concave surface can paradoxically cause dispersion, but not as well as many other surface shapes. On the other hand, if the focus is below the audience, although the focussing may not be heard, the concentration of non-lateral sound from above may not be desirable for other acoustic reasons.

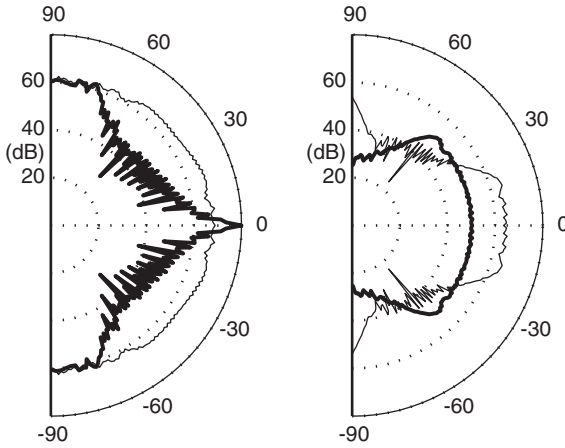


Figure 10.15 Scattering from a concave arc for various receiver radii, r . r_f is the focal length of the concave surface. Left figure: ——— $r < r_f$; ——— $r = r_f$. Right figure: ——— $r > r_f$; ——— $r \gg r_f$.

If a concave arc with a focus on listeners is inevitable, there are two possible solutions, absorbers or diffusers. Absorbers can be placed in front of the surface to remove the reflection, although this must be considered alongside reverberation time requirements in the room. There might also be a desire to produce some reflected energy from the concave surface for reasons of ensemble reflections to musicians, or early reflections to audiences to improve spaciousness or clarity. Diffusers can be used to break up the reflected wavefront and so disperse the focus, while still maintaining the acoustic energy

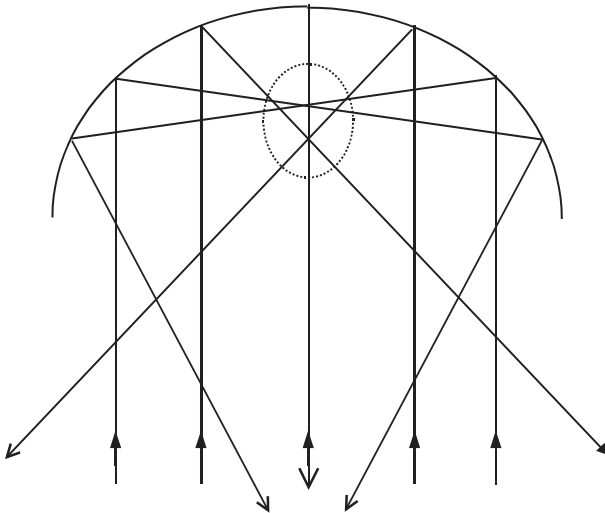


Figure 10.16 Ray tracing for scattering from a concave arc. The region marked with a dashed line will receive higher reflection levels than elsewhere.

and avoiding absorption. Figure 2.29 showed a scattered polar distribution for a concave arc before and after treatment with an optimized curved diffuser. Figure 2.30 showed the curved surface used. The reduction in focussing is dramatic.

10.4 Convex arcs

A single cylinder is an efficient disperser of sound in one plane, and a single sphere is efficient at dispersing hemispherically. They generate responses that mimic the behaviour of radiating line and point sources, respectively. Figure 10.17 shows the scattering from a semicylinder as a function of frequency. The radial axis range of this graph is only 20 dB, so at all frequencies, the response from the semicylinder is fairly omnidirectional. The 400 Hz line is where the wavelength is roughly the width of the semicylinder, and so some finite width diffraction lobing effects are seen. The lowest frequency, 40 Hz, is not omnidirectional because the rear of the semicylinder becomes important – it would be omnidirectional if a cylinder had been modelled. At the two highest frequencies, the scattered level only varies by 2–3 dB over the receiver arc.

It might appear that the cylinder is the ideal diffuser – the Holy Grail of diffuser designs – but this unfortunately is not the case. A single cylinder on its own is rarely of much use. The example given in Figure 10.17 was 0.5 m deep, already deeper than many architects allow, and it was only 1 m wide, not wide enough for most applications. One solution is to use multiple cylinders in an array. Then the response of the cylinder array is dominated by how the cylinders are arranged, and the perfect response from a single cylinder becomes a secondary and less important issue. Another solution is to flatten the cylinder, but then the perfect angular dispersion will be lost for oblique sources.

There are also issues with cylinders and the total sound field response. Figure 10.18 shows the pressure impulse response for a direct sound and a reflection from a large semicylinder. The semicylinder has the same width as the plane panel used for Figure 10.3 to allow direct comparison between the surface types. The reflected sound is attenuated because of spatial dispersion, but the time signature is still very similar to the reflection from the plane surface. Consequently, large cylinders and semicylinders produce comb filtering similar to that from plane surface, as shown in Figure 10.19,

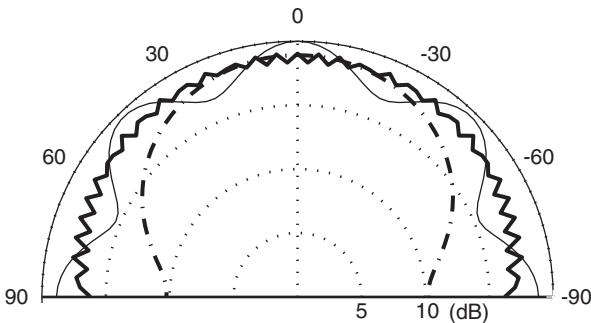


Figure 10.17 Scattering from a 1 m diameter semicylinder for various frequencies. (The $1/\sqrt{f}$ variation with frequency due to Green's function has been removed by normalization.) — · — · — · — 40 Hz ($\lambda = 8.5d$, $d = \text{cylinder diameter}$); ——— 400 Hz ($\lambda = 0.85d$); ——— 4000 Hz ($\lambda = 0.085d$).

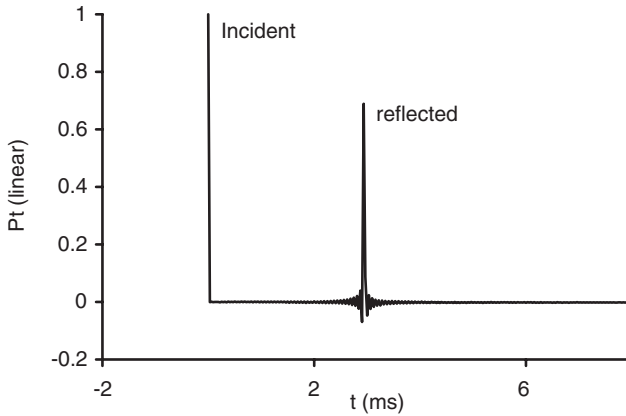


Figure 10.18 Incident and reflected time response for a semicylinder the same width as the plane surface case of Figure 10.3.

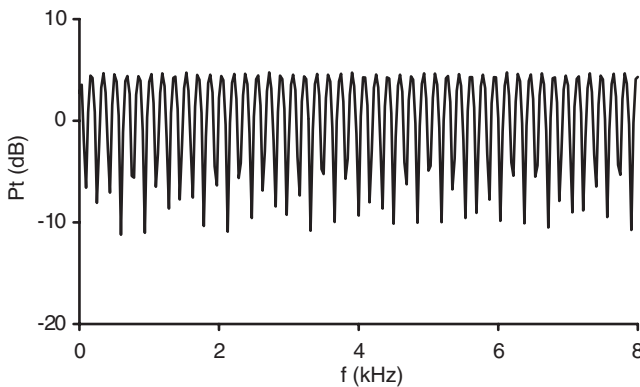


Figure 10.19 Total field frequency response for large semicylinder scattering.

albeit that the comb filtering variation is now over a slightly smaller magnitude range. The comb filtering is thought to give rise to the harsh sound that large semicylinders generate, although a more detailed set of subjective tests would be interesting and could clarify the situation. Certainly, semicylinders are an enigma, they appear to be a near perfect diffuser from dispersion graphs, but they do not sound like a perfect diffuser.

10.4.1 Geometric scattering theory and cut-off frequencies

One method that has been proposed to predict the scattering from a curved surface is geometric theory [3, 7]. The scattering processes are split into two, first the diffraction from the finite-sized panel is considered and then the effect of curvature added. The finite size effect is predicted using Fraunhofer or Fresnel theory. The effects of curvature are accounted for by a simple beam tracing method. If a curved surface is illuminated by a beam with parallel sides, the reflected beam will diverge due to the

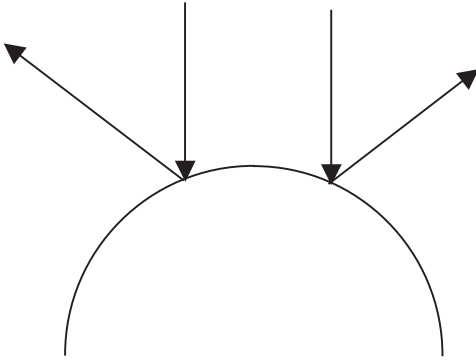


Figure 10.20 Effect of curvature on a sound beam.

curvature of the surface as shown in Figure 10.20. If the wavelength is assumed to be small compared to panel size, then simple geometric constructions can be used to calculate the attenuation due to curvature. For plane waves, this is given by [3]:

$$\text{Attenuation} = \left| 1 + \frac{r^*}{R_c \cos(\psi)} \right| \quad (10.6)$$

where the composite radius r^* is defined in Equation 10.2, R_c is the radius of curvature of the panel and ψ the angle of incidence and reflection. It is also possible to produce a formulation for spherical waves [7]. Figure 10.21 shows the scattered pressure versus frequency for the specular reflection direction for the two theories and the 3D BEM model. It is assumed that the 3D BEM gives accurate results and so this indicates that the geometric model works to a certain degree – the magnitude is approximately right but the ripples are not predicted. Figure 10.22 shows a scattered polar response. The geometric theory of scattering is not successful for receivers where the geometric reflection point is not on the panel. For these receivers, the effect of adding curvature should be to increase the scattered pressure, as energy is moved

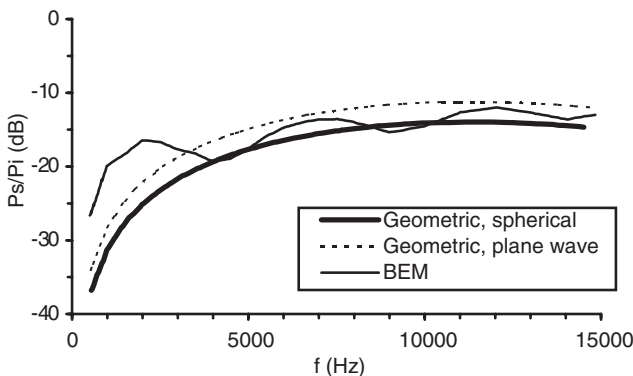


Figure 10.21 Prediction of scattering from a curved surface using three theories (after Cox [9]).

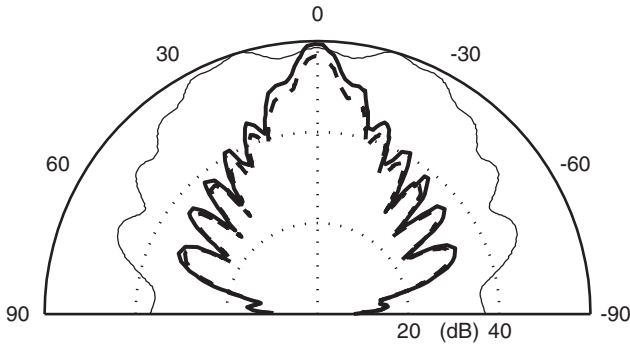


Figure 10.22 Prediction of polar response from curved surface using three theories (data from Cox [9]). — BEM; ——— Geometric, plane wave; - - - Geometric, spherical wave.

away from specular reflection angles to others. The geometric formulation incorrectly applies an attenuation whatever the angle of reflection.

The cut-off frequency for plane panels was a simple concept that readily allows some rough and ready design principles to be applied. Can this concept also apply to curved surfaces? Investigations have shown [8, 9] that Equation 10.1 also works for curved surfaces, provided the receivers are close to the specular reflection direction, which was a necessary stipulation for plane surfaces also.

10.4.2 Performance of simple curved diffusers

For normal incidence, diffusers based on part of an arc of a circle have good dispersion performance. Figure 10.23 compares the predicted scattering from a semicylinder and a flattened semicylinder (ellipse) for normal and oblique incidence. For normal incidence the semicylinder disperses the sound well, as it generates a virtual line source. For oblique incidence, however, the performance is poorer for the flattened semicylinder. The flattened semicylinder has poorer performance for both oblique and normal incidence. Incidentally, the trends are similar if a section of a circle is used instead of a flattened circle, only a complete semicylinder at normal incidence produces the very good dispersion. Consequently, if a whole semicylinder cannot be used in an application, a better solution than flattening the semicylinder or taking part of a circle is needed. There are two possibilities, first to use an array of semicylinders, and second to use optimization to construct a more complicated curved shape. Arrays are considered below, and complicated curved shapes later in this chapter.

10.4.2.1 Arrays of semicylinders

Once cylinders are arranged in an array, the performance is dominated by a combination of the single cylinder response and the periodicity. If the simple analysis surrounding Equation 10.3 is considered, then the key to gaining good diffusion from a set of cylinders is mainly down to how they are arranged. The scattered pressure

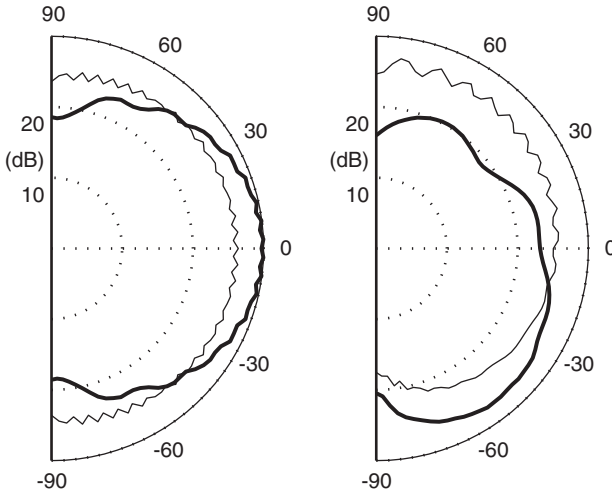


Figure 10.23 Scattering from two surfaces for normal (left graph) and oblique (right graph) incidence. In the latter case the incidence angle is 60° . — Semicylinder; - - - Flattened semicylinder.

distribution from one cylinder, $p_1(\beta)$ is constant if second-order reflections are not considered. Consequently, the sum of the delta functions in Equation 10.3 dominates the scattered pressure distribution. Once again a modulation technique, where the cylinders are not arranged periodically, is needed to change the functional form of the last term in the Equation 10.3 to give more even scattering.

The simplest method to follow is the modulation techniques described for Schroeder diffusers outlined in Chapter 9. For cylinders, this means using two or more semicylinders and arranging them randomly or pseudorandomly on the wall. This will reduce periodicity and so improve dispersion. Figure 10.24 shows this by comparing an array of semicylinders to a random array of semicylinders. At mid-frequencies, where there are some grating lobes, but not too many, the aperiodic arrangement helps to

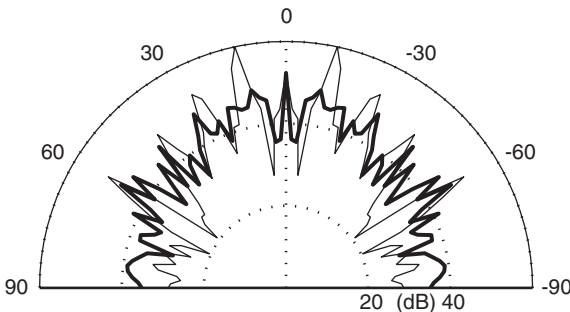


Figure 10.24 Scattered pressure distribution for a periodic and aperiodic arrangement of semicylinders. For the periodic set, $4\lambda \approx d$, where d is the diameter (chord) of the semicylinder. — Periodic; - - - Aperiodic.

create extra lobes, so improving dispersion. In this case, it is surprising how dominated the scattering is by lobing. A simple diffraction grating with one point source in the middle of each diffuser can produce reasonably accurate predictions of the scattering. At mid-frequencies, simple geometric base shapes very much mimic point sources.

The overall envelope shows some reduction for reflection angles far from the specular reflection direction. This tailing off is presumed to occur due to second and higher order reflections from the array – neighbouring semicylinders get in the way and prevent near grazing scattering. Similar results are seen for oblique incidence.

At high frequency, however, the modulation of the cylinders does not affect dispersion significantly for normal incidence. An example is shown in Figure 10.25. At high frequencies the grating lobes are so close together spatially, that the local variation in minima and maxima is similar for periodic, modulated and random arrangements. Again, as in the mid-frequency range, there is a gradual tailing off at the edges of the overall envelopes of the polar responses. In the example shown in Figure 10.25 there is roughly a 15 dB drop from normal to grazing receivers. At oblique incidence (result not shown), the modulated arrangement is better at controlling the overall envelope, and a clear improvement on a periodic arrangement is achieved.

As previously discussed, dispersion is only one aspect of diffuser performance, although possibly the most important one. The total field response, incidence plus reflection, should also be considered. Figure 10.26 shows the total field for a periodic set of four cylinders. Only two arrivals are shown because the array was set up symmetrically and so there are only two unique arrival times. Figure 10.27 shows the frequency response for the total sound field. This can be compared to previous graphs in this chapter for plane and single curve surface scattering. Using an array of cylinders has not destroyed the comb filtering, but has somewhat reduced it. It might be expected that comb filtering aberrations such as colouration may well still be present, but may not be so noticeable. Figures 10.28 and 10.29 show the total field time and frequency responses for a complicated arrangement of many different-sized semicylinders. The use of a random arrangement of cylinder sizes and shapes has further broken up the frequency response, making it much less likely that colouration will be heard.

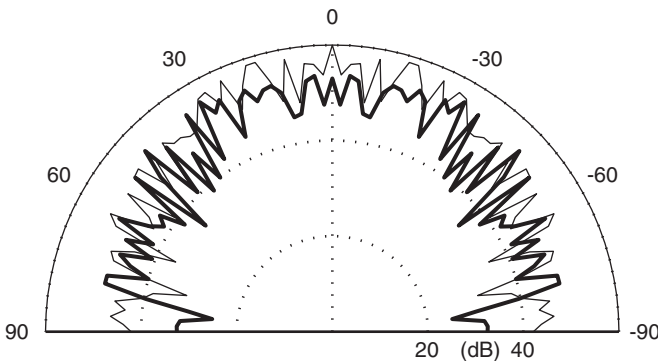


Figure 10.25 Scattered pressure distribution for a periodic and aperiodic (modulated) arrangement of semicylinders. For the periodic set, $15\lambda \approx d$, where d is the diameter (chord) of the semicylinder. — Periodic; - - - Aperiodic.

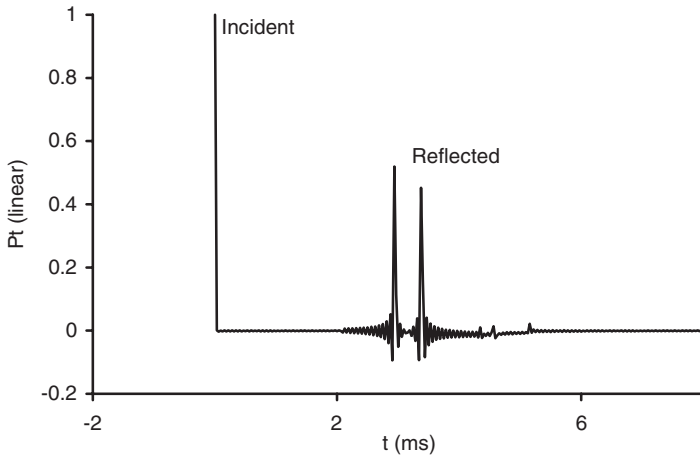


Figure 10.26 Scattering from an array of four cylinders symmetrically arranged about source.

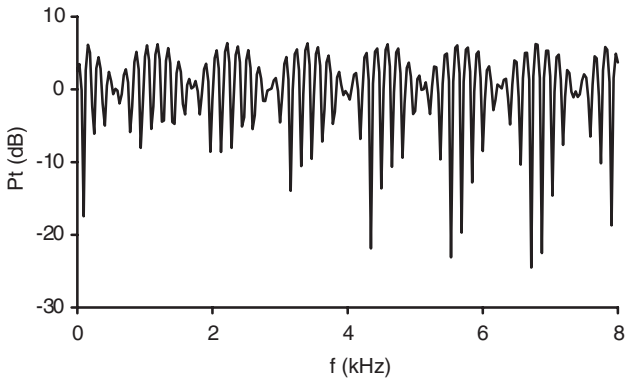


Figure 10.27 Frequency response for four periodic cylinders.

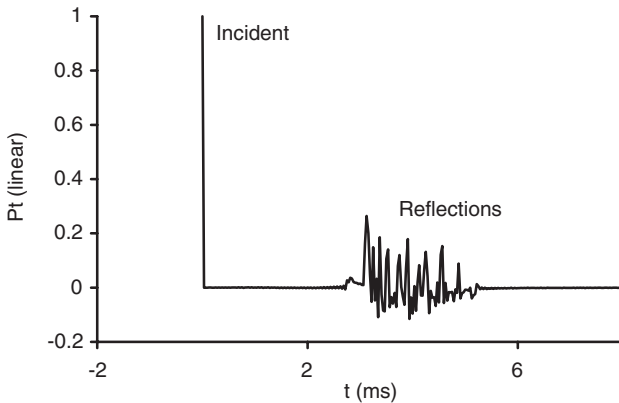


Figure 10.28 Total sound field for a complicated random array of many different sized semicylinders.

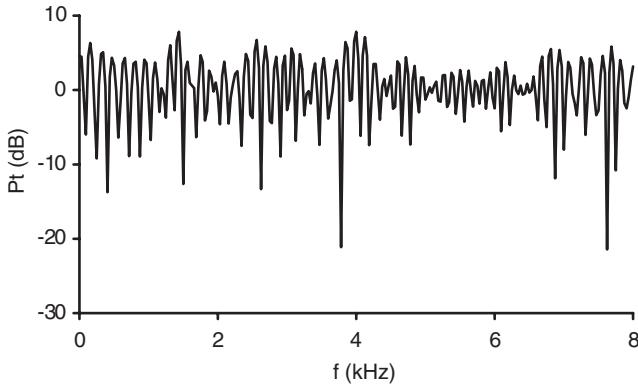


Figure 10.29 Frequency response of total sound field for a complicated random array of many different sized semicylinders.

In conclusion, several key features will determine the performance of semicylinder arrays. The low frequency limit of the diffuser will either be determined by the repeat distance or the diffuser depth. Multiple grating lobes need to be present for dispersion and hence repeat distance is important (see also Chapter 9). The issue of depth has not been discussed before for semicylinders, and unfortunately is as likely as not to be set by non-acoustic requirements. If the depth is the determining feature, then empirical results have shown that curvature produces significantly more scattering than a plane panel when the depth is greater than $\approx \lambda/10$. The mid-frequency performance is dominated by the semicylinder arrangement. The key to good performance is to avoid periodicity, or to ensure that the repeat distance is as large as possible. The high frequency performance, when the number of grating lobes is very large, seems difficult if not impossible to control.

10.5 Optimized curved surfaces

10.5.1 Example application

When designing a diffuser, the requirements of visual aesthetics and acoustics must be considered, and these are often in conflict. Schroeder diffusers may have well-defined acoustic performance, but they do that with a very specific visual appearance which it seems is either loved or loathed. Unless diffusers are visually acceptable to the architect, they are unlikely to be used. Curved surfaces are common in modern architecture. Spurred on by the availability of new materials and computer aided design, architects are increasingly designing prestigious buildings where large flat surfaces appear to be outlawed in principle.

Curved diffusers are therefore appealing because they can complement modern architectural trends. They can have a form which blends with other structures in a modern building and they do not have to look like an obvious add-on. The Hummingbird Centre in Toronto is an interesting example [10] shown in Figure 2.2. Diffusers were required on the side walls of the auditorium because a sound enhancement

system was being installed which would generate echoes across the room, unless some surface treatment was applied. The original design specification was for Schroeder diffusers, which were to be cloth wrapped to hide their visual appearance. After much persuasion, a curved surface designed by optimization was accepted instead, and because this fitted the visual appearance of the room, there was no need to hide the diffusers. The curved diffusers blended with the room design while having good acoustic performance. Other examples of optimized curved surface were previously shown in Figures 2.30 and 2.21.

10.5.2 *Design process*

Section 9.10 described how it is possible to get a computer to search for the best possible depth sequence for a Schroeder diffuser. It is also possible to get a computer to search for the best curved shape to generate dispersion [11]. For those unfamiliar with optimization, it may be necessary to read Section 9.10 before the description below, because the background details of how optimization works will not be repeated.

As with any diffuser optimization process, it is necessary to have a set of numbers that describe the surface shape. These shape parameters can then be changed by the optimizer to allow the computer to search through possible surface shapes. In the case of Schroeder diffusers this was straightforward – the shape parameters were the well depths. For a curved surface, a different regime is needed. Any surface shape can be represented by a Fourier series and so the surface displacement, y , can be represented by:

$$y(x) = \sum_{n=1}^N a_n \cos(k_x x) + b_n \sin(k_x x) \quad (10.7)$$

where a_n and b_n are the shape parameters which are altered to change the surface shape. k_x is usually set so that the harmonic for $n = 1$ corresponds to half a wavelength across the panel in the x -direction. N is the number of harmonics used. This gives a single plane diffuser which has modulation in the y -direction only. It is also possible to use 2D Fourier transforms to form the shape in multiple dimensions, the only cost is computation time as the number of shape parameters to be optimized increases.

From Fourier theory, if an infinite series was used, any diffuser shape can be produced. In reality it is necessary to truncate the series at some point as every extra element in the series gave a new dimension to the optimization process. Too many dimensions and the minimization became too slow. Furthermore, one advantage of curved diffusers over more complex surfaces, is their simpler construction leading to potentially lower costs and lower absorption. An increase in the number of harmonics in the series increases the complexity of the diffuser shape, which may cause excess absorption and increased cost. For these reasons, 4–6 harmonics are typically used. Once a surface shape is formed, it is necessary then to scale the shape to fit the maximum displacement in the y -direction required (i.e. fixing the maximum diffuser depth).

There are other mathematical representations of curved surfaces which can be used. For example, it is possible to define a number of variable points on the surface shape

and use a cubic spline algorithm in one plane or a bicubic spline algorithm [12] in two planes to form a smooth curved surface between the variable points. It is possible to construct a harmonic series not based on sinusoidal basis functions. Frequency and amplitude modulation processes can also be used to generate many different shapes. Although there are many possibilities, the essential principle that one needs parameters that define the shape remains.

Problems sometimes arise when the best surface found by the computer does not meet the visual requirements of the architect. A curve was wanted, but the solutions produced were not quite what the designer originally envisaged. In addition, it is often necessary to ensure that the surface avoids other objects in the room, or has appropriate breaks to allow for lighting. In this case, non-acoustic constraints must be used in the optimization process to force the shape to meet visual and physical constraints. This can be done via a set of fuzzy coordinates through which the surface must pass. Figure 10.30 illustrates how such a system can be used to force a surface to pass through particular points. The error parameter in the optimization becomes a combination of the diffusion coefficient that measures the scattering quality and a penalty value that measures how close the surface is to the constraint points (this can be an additive or multiplicative penalty). This is often used to ensure that edges of diffusers meet walls as illustrated in Figure 10.30c. In addition, this technique can be used to ensure that:

- cusps are not formed between adjacent periods of periodic diffusers;
- the left and right edges of diffusers are at the same displacement so that periodic diffuser edges will meet without a discontinuity;
- obstructions, such as pillars, are avoided.

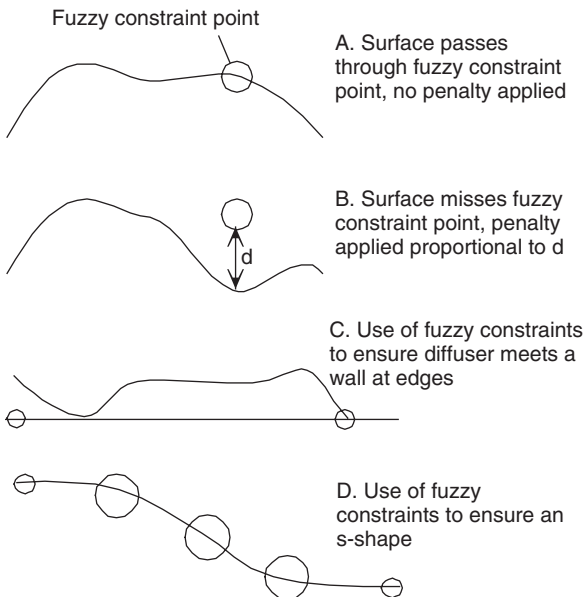


Figure 10.30 Use of fuzzy constraints to ensure that optimized curved diffuser meets visual and physical constraints (after Cox and D'Antonio [13]).

While using such a constraint system is straightforward for physical problems, such as avoiding cusps, it is more problematic when trying to force the shape of the curve into the visual aesthetic demanded by the designer. Often during room design the interior designer has a definite idea about the general shape required for the diffuser – ‘we would like an s-shaped diffuser’. Trying to come up with a suitable set of constraint points for this is possible, but involves some trial and error. For example, the points shown in Figure 10.30d will work for sometime, but not all of the time. In addition, the constraint point system lacks elegance and will slow down the optimization process, by increasing the complexity of the error function surface to be searched. One partial solution is to use the spline construction, as then the constraints can often be linear constraints on the shape parameters.

A superior system is one where the surface is designed from shape variables in such a way that the only surfaces generated are ones that satisfy the visual constraints. One way to do this is distortion [13]. The architect supplies a base shape, and distortion is used to change the acoustical performance of the shape, while retaining the visual integrity. Such a process is familiar in image processing as a technique for adding effects to photographs. This is illustrated in Figure 10.31. In the distorted pictures, it is still possible to recognize the picture as being a person; the rough visual appearance



Figure 10.31 Distortion in image processing (after Cox and D'Antonio [13]).

is maintained, yet radically different pictures are obtained. The idea behind diffuser distortion is to alter the surface shape using image processing and other techniques in such a way that the general visual appearance is maintained, and yet a different acoustic performance is obtained. To achieve this compression, modulation and warping techniques are used.

10.5.3 Performance for un baffled single optimized diffusers

Initial work on curved diffusers examined whether they could perform better than arcs of a circle [11]. It was found that for all depths and widths tested that optimized diffusers were as good or better than the arc of a circle. An interesting trend in the solutions from the optimization process was that when the maximum allowable depth and width of the surface were similar, so allowing a rough semicircular surface to be formed, this was the surface shape found by the optimization process. This near semicircle was similar to the arc of a circle and so for these geometries the optimization process could only produce diffusers which matched the performance of the circle arc. When the geometric constraints meant that a semicircle was not a possible solution, then the optimized surface found different more complex shapes that were better at generating spatial dispersion than the standard curved surface.

The failure to improve on the simple arc does not show a fundamental weakness in the optimization process, it can be argued that it illustrates how well it works! What has been shown is that for the geometries tested here, approximately semicircular diffusers have near optimal spatial dispersion and there is little room for improvement. (Remembering that spatial dispersion is not the only consideration for diffusers, time dispersion should also be considered.) This is illustrated in Figure 10.32 where the scattered pressures from two arcs and one optimized surface are shown. For the wide

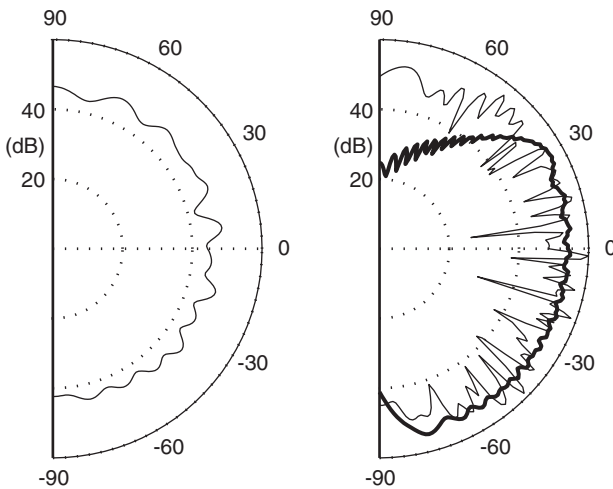


Figure 10.32 Scattering from three surfaces at 2.8 kHz, 30° incident source. Left figure: Standard curved diffuser (same as optimized diffuser) 1 × 0.4 m. Right figure: **————** Standard curved diffuser, dimensions 4 × 0.4 m; **————** Optimized diffuser 4 × 0.4 m (data from Cox [11]).

arc (right graph), the scattered pressure shows a noticeable fall off at large angles of incidence. The optimized diffuser provides more uniform scattering and does not suffer from such a fall off in pressure. For the narrower surface (left graph), the arc is nearly semicircular; the diffusion is fairly uniform, and it would be difficult for any surface to improve on the scattering produced in terms of spatial redistribution. The optimized diffuser shape is also a rough semicircle, indicating that this is almost certainly the best shape possible within the geometric constraints. Note that this assumes the philosophical limitation that the best diffuser is determined by spatial dispersion only.

Typical examples of a standard deviation diffusion parameter as a function of incident angle for an arc and optimized surfaces are shown in Figure 10.33. The

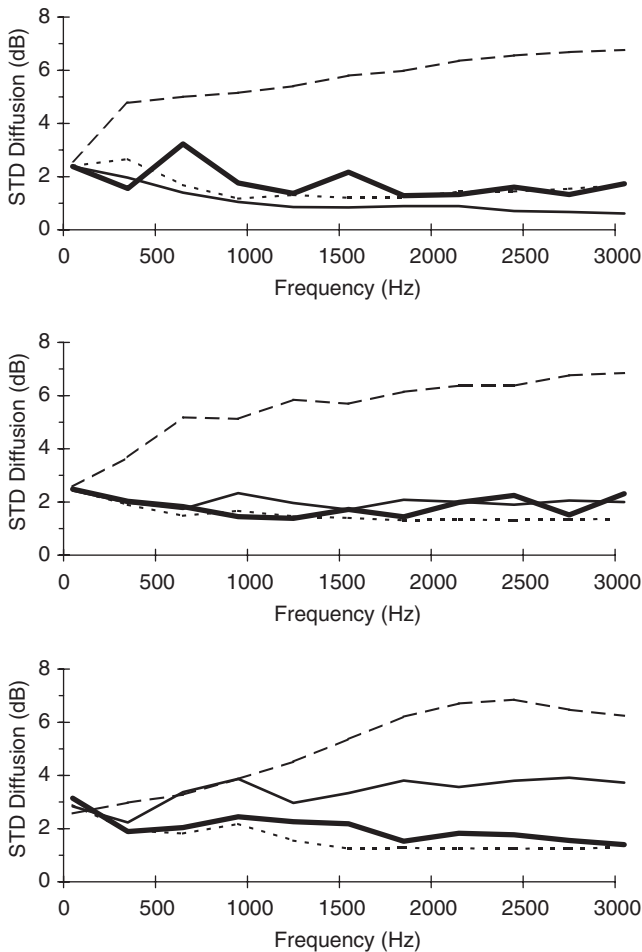


Figure 10.33 Diffusion from four surfaces, incidence sound angles different for each graph: top normal, middle 30° and bottom 60° incidence sound. This uses an old standard deviation measure, where complete diffusion is when the standard deviation is zero. ----- Plane surface; — Arc of a circle; — Optimized fractal; Optimized curved surface (after Cox and D'Antonio [17]).

figure is using an old diffusion evaluation technique, and the lower the value of diffusion the greater the spatial dispersion. In this case, the optimized diffuser has sacrificed a little performance for normal incidence sound, to improve the scattering for oblique sources. This shows the ability of the new surface to produce more uniform scattering for random incident sound.

10.5.4 Periodicity and modulation

When placed in a periodic arrangement, the quality of scattering at low to mid-frequencies is dominated as much by the periodicity effects (primarily grating lobes), as by the actual surface shape. One solution to grating lobes (spatial aliasing) is to remove the periodicity completely by using a very large surface. Unfortunately, this is likely to be an expensive solution, and consequently a modulation scheme like that devised for Schroeder diffusers and discussed in Chapter 9 can be used.

Consider a single asymmetrical diffuser base shape shown in Figure 10.34 in bold. If this base shape was arranged in a periodic fashion, grating lobes will arise. If, however, some of the periods are rotated, then the periodicity can be removed. In the case shown in Figure 10.34, the repeat distance has been doubled by this modulation. In general this will improve the diffusion. A key to this type of modulation is to form a shape which is sufficiently asymmetrical, so that flipping the shape produces completely different scattering. A further complication is ensuring that neighbouring

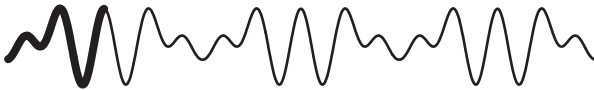


Figure 10.34 A curved diffuser (not optimized for acoustics). The base shape is shown in bold. By changing the orientation between periods, it is possible to increase the repeat length of the diffuser.

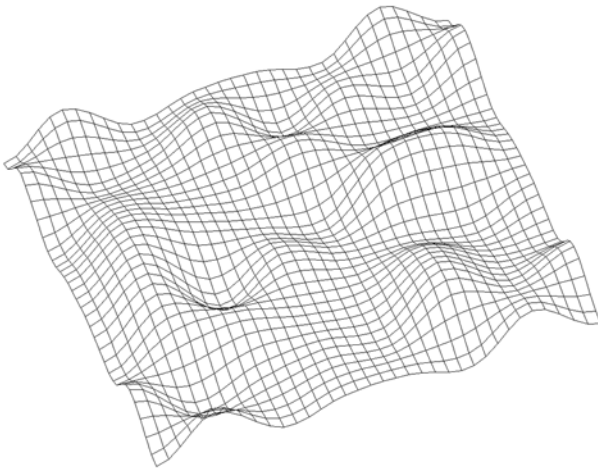


Figure 10.35 An asymmetric single base shape used in modulation (after D'Antonio and Cox [14]).

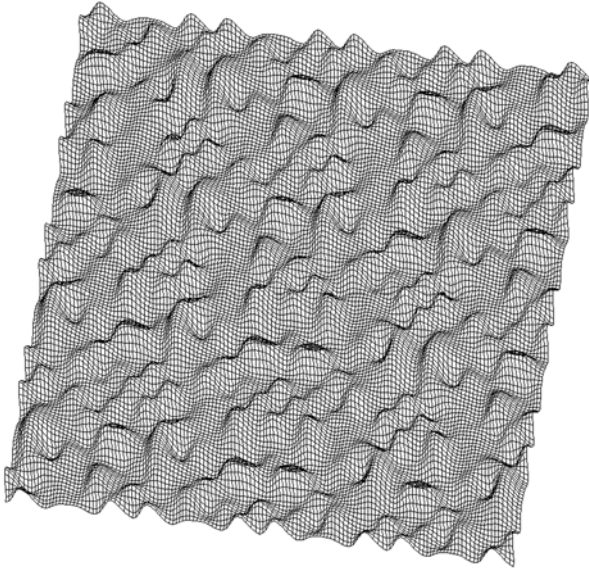


Figure 10.36 Modulated 4×4 array of base shape shown in Figure 10.35 (after D’Antonio and Cox [14]).

diffusers tile together without discontinuity in surface displacement or gradient. By forming surfaces with zero end gradients and with the same surface displacement on both ends, it is possible to form a surface that will tile in any orientation. Then the architect can decide what pattern to form. More importantly, pseudorandom arrays enable diffusers of considerable extent to be created from small base shapes.

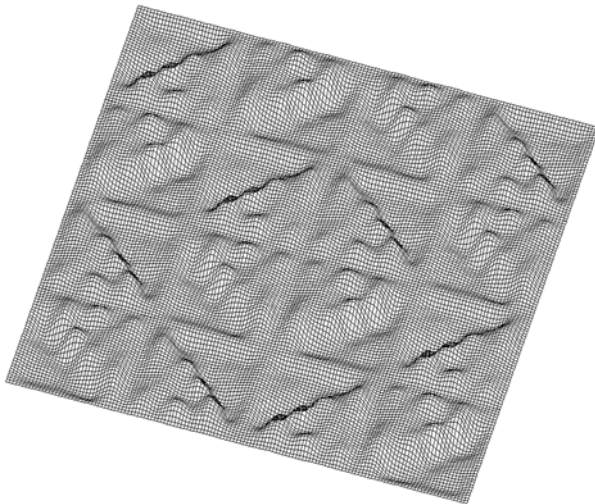


Figure 10.37 Modulated array inspired by log cabin quilt pattern (after D’Antonio and Cox [14]).

In its extreme, this modulation can result in a surface where the individual base shape is not clearly distinguishable [14]. Figure 10.35 shows a single period of a curved surface, and Figure 10.36 shows the same shape in a modulated array. The single period device has the same symmetrical shape on each edge, and the gradient around the perimeter is zero. This allows the surface to be tiled in any orientation. When placed in a modulated array, the base shape disappears in a complex pattern of minima and maxima. This allows the use of one base shape and reduces manufacturing costs.

Unfortunately, a periodic look is often favoured, whereas a modulation forms a random appearance. It seems that a periodic object enables the eye to more easily decode the design. A completely random surface can be too difficult to interpret and hence not pleasing to the eye. This is, of course, a bland generalization, there are successful architectural designs where randomness is embraced, but it is more common for a periodic entity to be specified. Using this asymmetrical base shape gives designers control over the appearance, it can be made to look random or periodic, but the designers have to remember that short repeat distances will result in worse dispersion. For example, Figure 10.37 shows a modulated array where a distinct pattern has been formed which follows the well-known log cabin quilt pattern. Again only a single base shape is being used.

10.5.5 Stage canopies

Overhead stage canopies are often designed with arrays of curved panels. The primary role of a stage canopy is usually to provide reflections back to the musicians or actors to allow them to hear themselves and others. Canopies may also be used to distribute some energy to the audience. The delay times between the direct sound and the overhead canopy reflection can be short in the audience area, however, and care should be taken to avoid colouration due to comb filtering. If a completely flat large surface is used above the stage, plenty of energy will return to the musicians. Unfortunately, the energy will be too strong and likely to cause colouration. Consequently, a canopy often needs to be shaped to create temporal diffusion to reduce colouration. This is often done with curved surfaces. Figure 2.22 showed an example of a curved canopy designed using optimization.

Canopies appear to fall into two rough categories, the categories being determined by the amount of open area in the canopy. Sometimes canopies completely cover the stage (virtually no open area). For instance, these are common where the canopy is being used to block sound entering a fly tower. Other canopies use elements sparsely with plenty of open area between the canopy diffusers or reflectors.

A diagram of the front to back section of a stage canopy used in an optimization study [15] is shown in Figure 10.38. The stage occupies $0.5 < x < -9$ m, and the audience to the right of the section is shown in the positive x -direction. The canopy is such that there is a little open space between each of the reflectors to allow some energy into the void above. The canopy is about 7 m above the stage so that the reflections are delayed by an amount known to give a good chance of reflections aiding ensemble and support [16]. The five diffusers are arranged on the arc of a large circle. The design criterion in the study was that for any source position on the stage, as even as possible energy distribution would be created to all positions on the stage. In other words, each musician has an equally good chance of hearing each other as far as the stage canopy

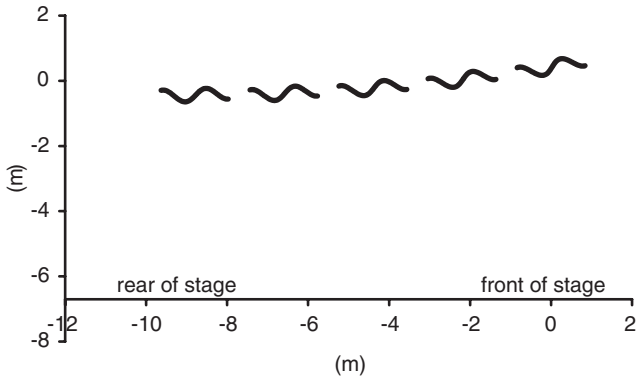


Figure 10.38 Cross-section of canopy used in optimization study (after Cox and D'Antonio [15]).

reflections are concerned. This is a criterion that can be used in an optimization process described previously.

The optimized design was compared to several other reflector shapes, such as a plane surface and arcs of circles. The optimized surface outperformed the other diffuser shapes in producing the most even energy distribution across the stage area. Figure 10.39 shows the scattering coverage plot from the plane reflector canopy at 2 kHz for a source in the middle of the stage. The variation in pressures across the width is small because this was modelled as a large flat surface; any variation is due to spherical spreading and path length differences. There is a large reflection level directly below the source – much of the energy is being reflected straight back to

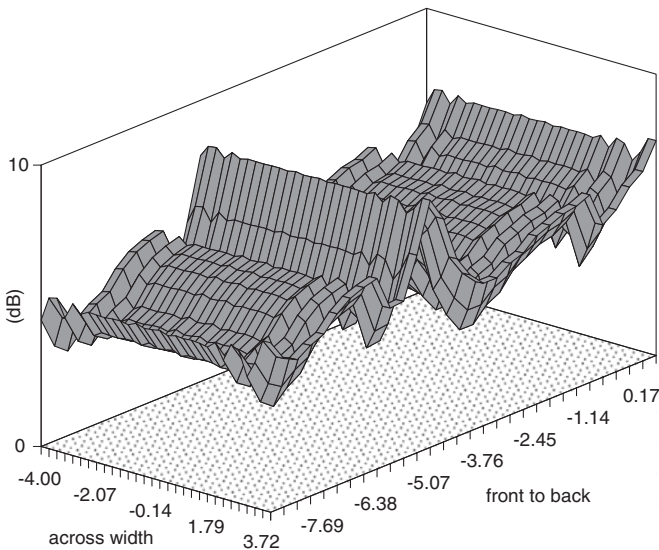


Figure 10.39 Scattering from stage canopy with plane reflectors (after Cox and D'Antonio [15]).

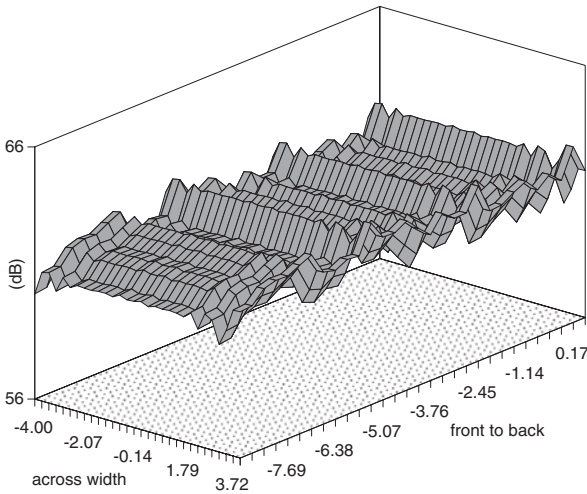


Figure 10.40 Scattering from stage canopy with optimized curved diffusers (after Cox and D'Antonio [15]).

the musician who is playing the instrument. Dips in the reflected pressures occur where there is no geometric reflection point on one of the reflectors due to the spaces in the canopy design. As discussed previously, shaping the reflectors can reduce the effects of pressure minima; this is often done by forming convex arcs [5].

The effect of using a more complex optimized curved surface is shown in Figure 10.40. The effect of the surface diffusers is to mask the lack of energy for certain receivers where pure specular energy is lacking. It also greatly reduces the strong specular energy being directed straight back to the musician. The reflected energy is more evenly distributed across the stage – all pressure levels along the front to back axis lie within 3 dB of each other.

A couple of details concerning the optimization are worthy of note. First, during the optimization it is possible to also get the optimizer to look at the best locations and angles of the canopy elements. Second, the criterion given of even energy across the stage is now considered not to be the best for all cases. Consider a canopy with a small open area, in other words a large surface with the same width and depth as the stage. A flat surface will give very good coverage on the stage, as noted before. The desire here is to promote temporal diffusion to minimize the effects of harsh overhead reflections, which are strong and similar to the direct sound. Consequently, it is better in this case to design a stage canopy to promote maximum dispersion across a complete arc from -90 to $+90^\circ$, in other words asking for maximum dispersion not just on the stage. If simple arcs are avoided, this maximizes the temporal dispersion from the overhead canopy, and it is presumed this will minimize colouration effects.

10.6 Fractals

Fractal construction techniques are used to create natural objects in computer-generated graphics, for example to generate landscapes for animated films. Fractals

are surfaces with a different visual aesthetic to common sound diffusers and so offer the possibility of expanding the pallet of surfaces available to designers [17].

There is reason to believe that fractal surfaces may have good acoustic properties. Fractals are self-similar or self-affine; as a surface is magnified a similar looking surface is found. Consequently, the different surfaces at different magnifications can be used to scatter different frequency ranges, in an analogous way to the use of different sized drivers to radiate different frequency ranges from multi-way loudspeakers. This is the principle of the Diffractal [18] as discussed in Chapter 9 and shown in Figure 9.26, which imbeds small-scaled copies of an $N=7$ QRD at the bottom of a larger $N=7$ QRD. The small QRDs scatter mid-high frequencies, and the large QRDs the bass frequencies. The construction is precisely self-similar; the exact shape is found upon magnification. This will not be true for surfaces considered here, where the surfaces are simply statistically self-similar or self-affine.

There are many established techniques for generating finite sample approximations to mathematically pure fractal shapes [19, 20]. Single plane diffusers are described and are made from extruded 1D fractals. Construction methods for higher dimensioned surfaces are also available, but are ignored for conciseness.

10.6.1 *Fourier synthesis*

Fractal surfaces can be constructed from spectral shaping of a Gaussian white noise source. Figure 10.41 is a schematic showing how the surfaces can be generated, such a scheme is more familiar in digital signal processing as a time signal filtering process. The Gaussian white noise is passed through a filter which is implemented using simple Fourier techniques. The shaping of the spectrum is a linear roll-off with a defined number of dB per octave. The decrease in spectral content per octave is characterized by the gain of the filter at each spatial frequency. The filter gain $A(X)$ is given by:

$$A(X) = \frac{1}{X^{\beta/2}} \quad (10.8)$$

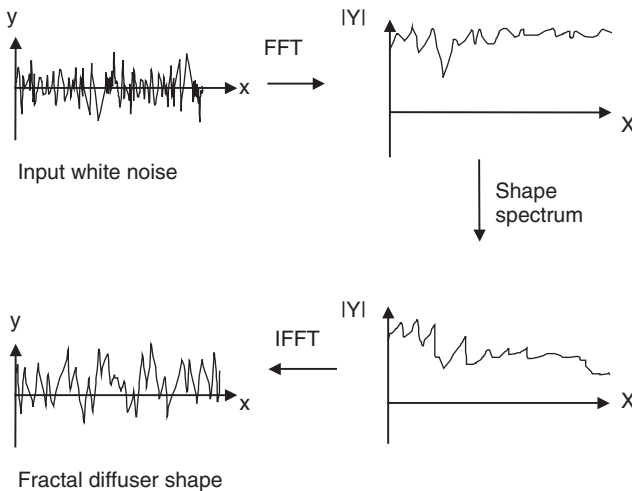


Figure 10.41 Schematic diagram showing Fourier synthesis construction technique (after Cox and D'Antonio [17]).

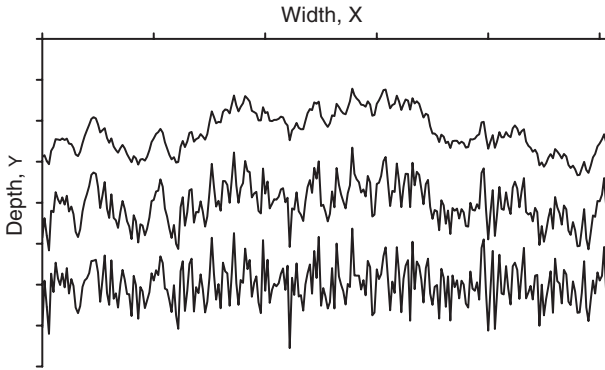


Figure 10.42 Different fractal surfaces generated by Fourier synthesis. Bottom line, input white noise; middle line, pink noise; top line, brown noise (after Cox and D'Antonio [17]).

where X is the spatial frequency and β the spectral density exponent which takes values between 1 and 3. This then insures that the dimension lies between 1 and 2 as might be expected for a 1D fractal shape. Figure 10.42 illustrates some typical surface shapes that are generated by such a scheme. The bottom line is the input Gaussian white noise. The middle line was generated with a roll-off of 3 dB/octave ($\beta = 1$) and gives $1/f$ noise, which in acoustics is termed pink noise. It is also a commonly occurring spectrum in other natural phenomena, for example in the pitch variations found in music. The top line is formed by a steeper roll-off of 6 dB/octave ($\beta = 2$) and is characteristic of Brownian motion, random walk or brown noise.

The shapes given in Figure 10.42 can be made into diffusers by extrusion, and will be termed fractional Brownian diffusers (FBD), as the functions represent fractional Brownian motion. By varying the spectral density exponent, the spikiness of the surface shape can be altered. In the most general terms, to get the best low frequency scattering performance, the spectral density exponent should be large leading to a smooth shape. To get the best high frequency performance, however, a low spectral density exponent is needed as this makes a spiky shape. The story is, however, more complicated. It has been found that although the spectral density exponent does determine the scattering quality at low and high frequencies to a certain degree, the correct choice of white noise sequence is most important. Unfortunately, it is not possible to optimize these surfaces, as there are too many governing shape parameters.

10.6.2 Step function addition

Brownian motion can also be simulated by a series of randomly displaced step functions. Although this is not always as mathematically pure as a Fourier synthesis technique, it facilitates a reduction in the number of parameters required to represent the surface shape.

To get proper Brownian motion requires the addition of an infinite number of step functions. Each step function has a random amplitude, and the position of the step

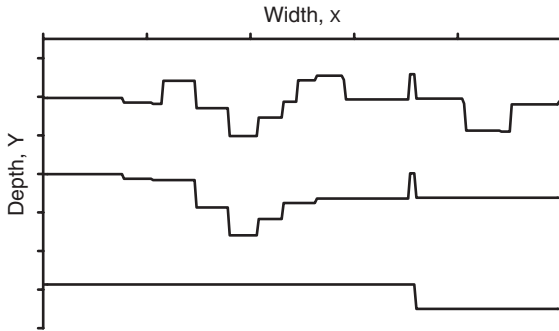


Figure 10.43 Fractal generation by step function addition. Bottom line, 1 step function; middle line, 10 step functions; top line, 20 step functions (after Cox and D'Antonio [17]).

is a random position somewhere along the width of the diffuser. The displacement of the diffuser from a flat surface y at a distance x along the diffuser is given by:

$$y(x) = \sum_{i=1}^{\infty} A_i f(x - x_i) \quad \text{where} \quad f(\alpha) = \begin{cases} 0, & \alpha < 0 \\ 1, & \alpha \geq 0 \end{cases} \quad (10.9)$$

where A_i are a set of Gaussian distributed random amplitudes and x_i a uniformly distributed random set of positions on the diffuser with $-a \leq x_i \leq a$, where $2a$ is the diffuser width. Figure 10.43 illustrates the random addition of step functions for a few terms.

To utilize this generation method efficiently the infinite sum in Equation 10.9 needs to be truncated. In acoustics the difference in wavelength from the highest to the lowest frequency of interest is not so great that a sound diffuser requires self-similarity over a large range of magnifications. Instead of an infinite sum of terms, a finite number, N , has been used, with each successive term having a decaying amplitude.

$$y(x) = \sum_{i=1}^{\infty} B_i f(x - x_i) \quad \text{where} \quad B_i = \frac{1}{i^\alpha} \quad 0 \leq \alpha \leq \infty \quad (10.10)$$

The decaying amplitude function produces a similar probability distribution of values as the original Gaussian random values A_i , except at the most extreme values of A_i . The other difference is that the amplitudes can now only be regularly spaced values, rather than being truly random. This reduces the number of independent parameters to $N + 1$, the set of displacements x_i and the amplitude decay rate α , and enables optimization to be used.

Using only a few step functions can lead to flat areas which might be prone to producing specular reflections at high frequencies, or sharp spikes which are undesirable. This can be seen in the 20 step function surface shown in Figure 10.43. Consequently, rather than step functions, $f(x)$ can be replaced with functions with more graceful transitions. For example, a hyperbolic tangent function can be used for this:

$$f(x) = \tanh(\gamma_i x) \quad (10.11)$$

The effect of using a hyperbolic tangent function is to round the top and the bottom of the step functions. The γ_i value changes the rate of transition from the top to the bottom of the step and the amount of rounding. γ_i may either be a constant for all terms in Equation 10.10, or alternatively may be allowed to decay or increase:

$$\gamma_i = \frac{1}{j\xi} \quad 0 \leq \xi \leq \infty \quad (10.12)$$

The ‘fractal’ shape is now determined by $N+2$ parameters. These are known as random addition diffusers (RAD).

When optimizing and testing these surfaces, it was surprising to find that this generation technique can make semicylinders when the depth was roughly half the width. As discussed previously in connection with curved surface optimization, the semicylinder is very good at dispersing sound provided it is not in an array. This demonstrates that the optimization is working, but does raise the question as to whether the optimized shape can really be called a fractal.

When a more application realistic wide diffuser is optimized, the arc of a circle is no longer optimal, and better fractal diffusers are found. Figure 10.33 compared different diffusers using a standard deviation diffusion parameter (small is best). The fractal is better than the arc of a circle for random incidence sound. It seems that optimized fractal surfaces do produce reasonable diffusers; however, optimized curved surfaces often have better dispersion. Consequently, fractal construction techniques may produce different visual aesthetics to an optimized curved surfaces, but not better diffusers.

10.7 Summary

This chapter has covered a wide range of different diffuser types. Starting with plane surfaces, it looked at the effects of edge diffraction. The performance of arcs, triangles, pyramids, fractals and curved surfaces was then considered. Current state of the art is to use numerical optimization to allow the surface shape to meet both the acoustic and visual requirements. With good design, there are many shapes that can make good diffusers, but only a few of these will ever be visually acceptable in a particular project. The next chapter looks at the use of absorption to promote diffuse reflections.

10.8 References

- 1 L. Cremer, “Early reflections in some modern concert halls”, *J. Acoust. Soc. Am.*, **85**, 1213–1225 (1989).
- 2 L. Cremer, “Fresnel’s methods of calculating diffraction fields”, *Acustica*, **72**, 1–6 (1990).
- 3 J. H. Rindel, “Attenuation of sound reflection from curved surfaces”, *25th Conference on Acoustics* (1985).
- 4 J. H. Rindel, “Attenuation of sound reflections due to diffraction”, *Nordic Acoustical Meeting*, 257–260 (1986).
- 5 J. H. Rindel, “Design of new ceiling reflectors for improved ensemble in a concert hall”, *Appl. Acoust.*, **34**, 7–17 (1991).
- 6 P. D’Antonio and J. Konnert, “The RFZ/RPG approach to control room monitoring”, *Proc. Audio Eng. Soc. Convention*, preprint 2157 (I–6) (1984).
- 7 A. D. Pierce, *Acoustics, an Introduction to its Physical Principles and Applications*, McGraw-Hill Inc. (1981).

- 8 T. J. Cox and Y. W. Lam, "Evaluation of methods for predicting the scattering from simple rigid panels", *Appl. Acoust.*, **40**, 123–140 (1993).
- 9 T. J. Cox, "Objective and Subjective Evaluation of Reflection and Diffusing Surfaces in Auditoria", PhD thesis, University of Salford (1992).
- 10 J. P. O'Keefe, T. J. Cox, N. Muncy and S. Barbar, "Modern measurements, optimized diffusion, and electronic enhancement in a large fan-shaped auditorium", *J. Acoust. Soc. Am.*, **103**(5), 3032–3033, also *Proc. 16th ICA* (1998).
- 11 T. J. Cox, "Designing curved diffusers for performance spaces", *J. Audio Eng. Soc.*, **44**(5), 354–364 (1996).
- 12 W. H. Press *et al.*, *Numerical Recipes, the Art of Scientific Computing*, Cambridge University Press, 289–292 (1989).
- 13 T. J. Cox and P. D'Antonio, "Holistic diffusers", *Proc. IoA(UK)*, **21**(6), 201–206 (1999).
- 14 P. D'Antonio and T. J. Cox, "Embodiments of aperiodic tiling of a single asymmetric diffusive base shape", patent pending.
- 15 T. J. Cox and P. D'Antonio, "Designing stage canopies for improved acoustics", *Proc. IoA(UK)*, **19**(3), 153–160 (1997).
- 16 M. Barron, *Auditorium Acoustics and Architectural Design*, E&FN Spon, 55 (1993).
- 17 T. J. Cox and P. D'Antonio, "Fractal sound diffusers", *Proc. 103rd Convention of the Audio Eng. Soc.*, preprint 4578, Paper K-7, New York (1997).
- 18 P. D'Antonio and J. Konnert, "The QRD DIFFRACTAL: a new 1 or 2-dimensional fractal sound diffusor", *J. Audio Eng. Soc.*, **40**(3), 117–129 (1992).
- 19 H.-O. Peitgen and D. Saupe (eds), *The Science of Fractal Images*, Springer-Verlag (1988).
- 20 J. Feder, *Fractals*, Plenum Publishing Corporation (1988).

11 Hybrid surfaces

A diffuser needs to break up the reflected wavefront. While this can be achieved by shaping a surface, it can also be achieved by changing the impedance of the surface. Indeed, the Schroeder diffuser is often interpreted as a variable impedance surface. In this chapter, variable impedance is achieved by patches of absorption and reflection. Unlike the Schroeder diffuser, these cannot be designed for minimum absorption. These surfaces are hybrids somewhere between pure absorbers and non-absorbing diffusers. Partial absorption is inherent in the design, and any reflected sound is dispersed.

Using patches of absorption to generate dispersion is not particularly new. In studio spaces people have been arranging absorption in patches rather than solid blocks for many years. In recent times, however, a new breed of surface has been produced, where the absorbent patches are much smaller, and the arrangement of these patches is determined by a pseudorandom sequence to maximize the dispersion generated. This chapter will start by discussing some implementations of these surfaces to give a sense of how they can be constructed. Then a more detailed theoretical basis for their design will follow.

11.1 Planar hybrid surface

The binary amplitude diffuser, also known as a BADTM panel [1], is a flat hybrid surface having both absorbing and diffusing abilities. The panel simultaneously provides sound diffusion at high and mid-band frequencies, and crosses over to absorption below some cut-off frequency. Figure 11.1 shows a typical construction. Mineral wool is faced with a complex perforated mask, and the panel is fabric wrapped for appearance. The white patches on the mask are holes, and the black patches hard reflecting surfaces.

Figure 11.2 shows the random incidence absorption coefficient for a hybrid surface compared to the mineral wool alone, the effect of changing the backing depth is also shown. The additional vibrating mass within the holes of the mask causes the absorption curve to shift down in frequency generating additional low to mid-frequency absorption. At high frequency, the hard parts of the mask reflect some of the sound, preventing absorption happening in some parts of the mineral wool, and so causing the absorption coefficient to reduce. It is at these high frequencies, where the absorption is reduced, that the surface should start to generate significant amounts of diffuse reflections.

To accomplish mid- to high frequency dispersion, a 31×33 2D array of absorptive and reflective areas is used. The reflective areas map to the 1 bit and the absorptive areas map to the 0 bit in a binary pseudorandom number sequence. The distribution of these binary elements is based on an optimal binary sequence with a flat power spectrum as this maximizes dispersion. For example, this could be based on an maximum length sequences.

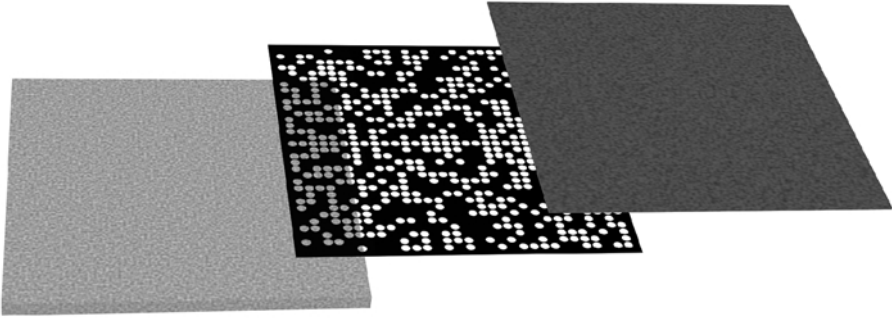


Figure 11.1 Construction of a hybrid surface, left porous absorber, middle the mask and right fabric.

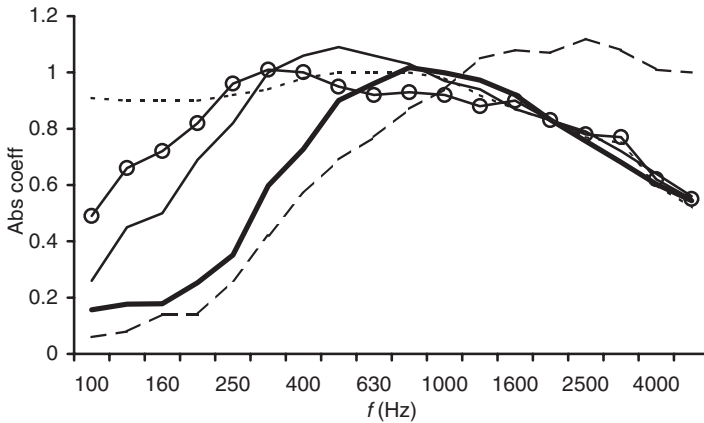


Figure 11.2 Random incidence absorption coefficient for a hybrid surface (BAD™ panel) compared to mineral wool. Four different backing depths for BAD panel shown.
 — 2.5 cm BAD; — — — 5.1 cm BAD; —○— 7.6 cm BAD;
 - - - - 10.2 cm BAD; - - - - 2.5 cm Fibreglass.

Hybrid surfaces extend the acoustical performance of traditional fabric wrapped absorbers, and allows wide area coverage without excessive deadening at mid- to high frequencies. The surface is used in facilities that need reflection control, and provides it from a simple inexpensive construction. Furthermore, the acoustic function can be hidden which can lessen the conflict between visual aesthetics and acoustic requirements. Alternatively, many architects have expressed interest in seeing the mask, due to its unique appearance and the fact that it offers an alternative to the traditional periodic perforated metal patterns. Figure 11.3 shows a home theatre installation in which a black anodized aluminium mask was used.

11.2 Curved hybrid surface

Flat hybrid surfaces such as the BAD panel still generate a coherent specular reflection, albeit attenuated, because it is partially absorbed. The hard parts of the mask



Figure 11.3 Example application of planar hybrid surface (BAD panel) in a home theatre (left). The BAD panels are to the left of the seating and are also shown magnified in the right picture.

still generate reflected waves that arrive in phase in the specular direction. The solution to this is to shape the surface as then the specular scattering can be significantly reduced to offer even more uniform diffuse reflections. Figure 11.4 illustrates such a construction. In the case shown, the surface is upholstered in fabric to hide the mask. The absorption performance of curved hybrid surfaces will be similar to the planar surfaces, but as shall be shown later in this chapter, the dispersion will be

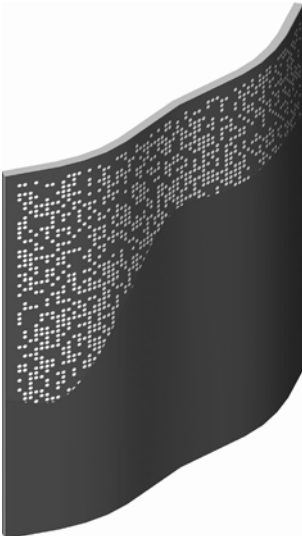


Figure 11.4 Construction of a curved hybrid surface (DigiWave™).



Figure 11.5 A curved hybrid diffuser (Digiwave), applied to the ceiling and side walls of SonyM1, New York (photo by Paul Ellis of The M Network Ltd courtesy of Harris Grant Associates).

greatly increased. This curved construction has found favour in recording studios as it allows treatment away from the extremes of complete absorption, specular reflection or diffuse reflection. This enables the sweet spot, the place where the room acoustics are best, to be spatially expanded. Figure 11.5 shows an application of a curved hybrid surface [2] on the ceiling of a post production studio.

As mineral wool has a lower speed of sound than air, hybrid surfaces also have the ability to perturb the sound field more when compared to hard diffuser of the same depth. In theory, these can produce diffuse reflections at a lower frequency, although at low frequency the effect of these surfaces can be dominated by absorption. Nevertheless, it appears that hybrid surfaces can make efficient use of a limited depth. As absorption is inevitable in these devices, they are not useful in spaces, such as large auditoria for symphonic music, where absorption must be minimized.

11.3 Simplest theory

In this section, a discussion of the design of hybrid surfaces using the simplest Fourier theory will be given. As with Schroeder diffusers, much can be learned by considering the simplest construct, but ultimately, more exact theories will be necessary to match the experiment. Consider a simple Fourier theory as discussed in Chapter 8, and for

simplicity consider a 2D world so that predictions in one plane only are considered. The pressure amplitude, $|p_s|$, reflected from a planar, variable impedance surface is given by:

$$|p_s(\theta, \psi)| \approx \left| A \int_s R(x) e^{jkx[\sin(\theta) + \sin(\psi)]} dx \right| \quad (11.1)$$

where ψ and θ are the angles of incidence and reflection, $R(x)$ the surface reflection factor a distance x along the surface, k the wavenumber, A a constant, and s the diffuser surface.

This is an approximate far field theory, which forms the basis of the hybrid surface design. This simple prediction theory and the subsequent design process are only applicable at mid- to high frequencies. At low frequencies, the mutual interactions across the surface make the prediction model inaccurate, as shall be discussed later. Equation 11.1 is a Fourier transform in kx and transforms the reflection factors into $[\sin(\theta) + \sin(\psi)]$ space. To a first approximation, the absorptive parts of the hybrid surface will have a reflection factor of $R(x) = 0$ and the reflective parts have $R(x) = 1$. A pseudorandom number sequence with good autocorrelation properties is used to determine the spatial distribution of the hard and soft patches. For example, the number sequence might be $\{0, 1, 0, 1, 0, 1, 0, 0, 0, 0, 1, 0, 1, 0, 0, 0, 0, 0, 0\}$, and where there is a 1 in the sequence a patch of absorption is used, where this is a 0 in the sequence the surface is reflective. Figure 11.6 illustrates a surface where the impedance variation is in one plane only, and the strips of absorption or reflection are extruded in one direction. Surfaces which scatter hemispherically, such as those shown in Figure 11.1, are formed from number sequence arrays. The number sequence arrays are formed by applying a folding technique to a 1D sequence. Schroeder named the folding technique the Chinese remainder theorem [3] after a famous mathematical problem involving modular arithmetic. This is discussed in Section 11.4.2.

A number sequence with good autocorrelation properties will have a flat power spectrum with respect to kx . This means the pressure amplitude scattered is constant with respect to the transform variable $[\sin(\theta) + \sin(\psi)]$, which means good dispersion is generated in a polar response. If the surface is periodic, this will relate to grating lobes all having the same level except for the zeroth order lobe, in many ways similar to the theories behind Schroeder diffusers and discussed in Chapter 9.

Consequently, the choice of number sequence is crucial to obtaining diffuse reflections. The initial development of this diffuser was carried out by Angus [4] who began by looking at MLS. Maximum length sequences are a good starting point as they have desirable Fourier properties. There are many other bipolar sequences which have flat Fourier transforms, but MLS are the best documented and known. The issue of sequences is discussed in more detail in the next section.



Figure 11.6 A 1D hybrid surface. The cross-hatched patches are absorptive and the clear patches reflective (or vice versa).

11.4 Number sequences

To gauge the quality of a number sequence for a hybrid surface, the autocorrelation function can be examined. This is because the autocorrelation function directly relates to the scattering performance of the surface, see Section 9.4.

11.4.1 One-dimensional sequences

The reflection factors for the hybrid surface are 0 (absorption) and 1 (reflection), consequently the number sequence used should have optimal autocorrelation properties for 0s and 1s, which means a good unipolar sequence is needed. Most pseudorandom binary sequences, on the other hand, have autocorrelation properties designed with a bipolar sequence composed of +1s and -1s. The autocorrelation side lobe performance of a unipolar and bipolar sequence can be very different. Figure 11.7 demonstrates this for a maximum length sequence of length 15. When a sequence can be bipolar (positive and negative), the autocorrelation function side lobes, on either side of zero delay, include cancelling effects, which enable a low side lobe energy to be created as desired. When the sequence is unipolar, no cancellation can occur, and the autocorrelation side lobe levels are higher. Consequently, it would be anticipated that the scattering performance would be worse for a unipolar sequence. The consequence of no cancellation is that the d.c. component in the power spectrum is large, as shown in Figure 11.8. This means that the energy in the specular reflection direction, when $\sin(\theta) + \sin(\psi) = 0$, will be attenuated less for a unipolar surface in comparison to a bipolar surface.

In a bipolar maximum length sequence, the mean value of the reflection factors is close to zero, and consequently, the d.c. value of its power spectrum is close to zero (Figure 11.8). This means that suppression of the zeroth order lobe in the polar response, when $[\sin(\theta) + \sin(\alpha)] = 0$ occurs – see Figure 11.7. The construction of diffusers based on bipolar MLS was discussed in Section 9.4.1; these are a type of Schroeder diffuser.

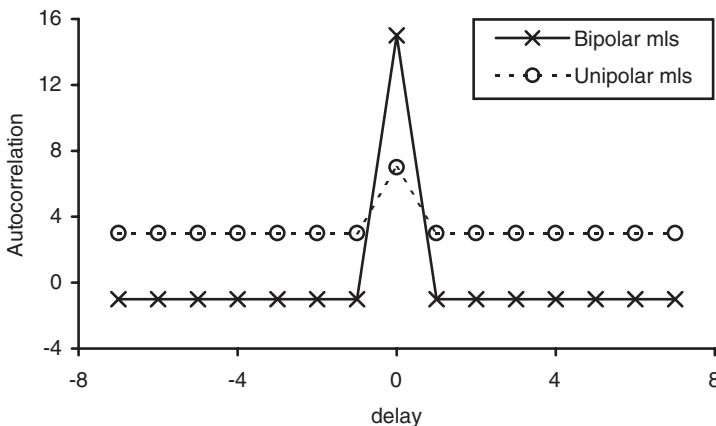


Figure 11.7 Autocorrelation function for a bipolar (+1s and -1s) and unipolar (+1s and 0s) MLS. The former is like a phase grating diffuser, the latter is like a hybrid surface.

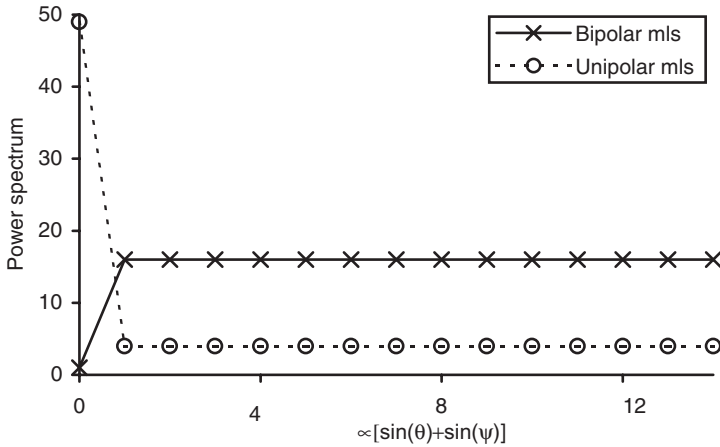


Figure 11.8 Comparison of power spectra for the reflection coefficients of surfaces formed from bipolar and unipolar MLS.

With a unipolar maximum length sequence, a hybrid diffuser is being constructed. The mean value of the reflection factors is no longer close to zero. Indeed the d.c. value is actually higher than the other spectrum values, and consequently the zeroth order lobe is significantly greater than other lobes. Figure 11.8 illustrates this by comparing the power spectra of a unipolar and bipolar maximum length sequence. Figure 11.9 shows the polar response for a diffuser constructed from bipolar and unipolar maximum length sequences. This is evidence that the planar hybrid surfaces will have a significant specular energy lobe, with the zeroth order lobe being about $10 \log_{10}(N)$

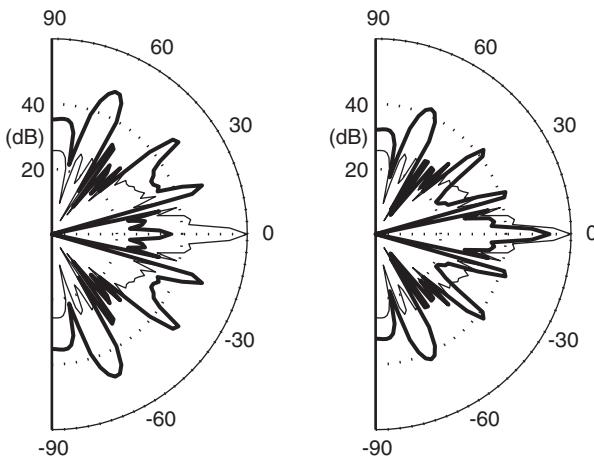


Figure 11.9 Scattering from diffusers constructed using bipolar and unipolar MLS. — Plane surface, shown in both figures; — Maximum length sequence, either bipolar (left figure) or unipolar (right figure).

times larger than the other lobe energies, where N is the size of the maximum length sequence. The specular reflection lobe will be attenuated by about 6 dB compared to a plane hard surface (as expected for a surface which is 50 per cent absorptive by surface area). The scattering lobes are not even for the hybrid surface, but the scattering in the specular energy is reduced.

When the open area of the panel is about 50 per cent then the maximum length sequence is a good choice. The performance of the maximum length sequence when composed of unipolar elements is worse than when it is bipolar as shown above, but the maximum length sequence will still be the best possible sequence achievable; there are no better unipolar sequences, although there are some which are just as good. Problems arise if the open area of the panel needs to be reduced, as common optimal binary number sequences usually have a similar number of 0s and 1s.

There are a set of sequences, called optical sequences [5], which are unipolar and have a different number of 1s and 0s. Angus [6] suggested that these could be used to overcome some of the problems associated with MLS. For instance, they can be used to form a surface with a non-50 per cent open area. Optical sequences were developed for use in fibre optical code division multiple access (CDMA) processes. CDMA systems enable multiple users to use a single digital transmission line efficiently. Fibre optic CDMA sequences, where the light intensity is either on or off cannot have cancellation, and hence unipolar sequences are needed. They use an optimal sequence defined as one where the maximum of the side lobes of the autocorrelation function has the smallest possible value.

The problem with optical sequences is that the typical construction methods available result in a very low number of 1s in a long sequence. For example, a typical length 20 sequence is {0, 1, 0, 1, 0, 1, 0, 0, 0, 0, 1, 0, 1, 0, 0, 0, 0, 0, 0, 0} which only contains five 1s and so would give a nominal open area of 25 per cent. This occurs because of the application the optical sequences were devised for. Optical fibre systems require very low side lobe performance which necessitates a low occupancy of 1s, as this is the only way to achieve low side lobe energy in the autocorrelation function when no cancellation can occur. Unfortunately, from a diffuser designer's point of view, this makes the sequences, especially the very long sequences, not that useful. The surface will either be very reflective (if the 1s are associated with absorption) or very absorptive (if the 1s are associated with reflection). Incidentally, the above sequence can also be written as (2, 4, 6, 11, 13) where the index number gives the location of the 1s. For low occupancy cases, this is a much more compact representation of the sequences and so will be used below.

Optical sequences are usually generated in families. These are a set of sequences which not only have good autocorrelation properties, but have low energies for the cross correlation between family members. In an optical sequence, five parameters are used to specify their performance. ξ is the number of 1s in the sequence, N the length, M the family size (the number of sequences in the family), S_{xxm} the maximum side lobe value in the autocorrelation function, and S_{xym} the maximum value in the cross correlation function between sequences in the same family. These parameters can be stated in an abbreviated form $(\xi, N, M, S_{xxm}, S_{xym})$. For the length 20 sequence given above this would be expressed as $(5, 20, M, 3, S_{xym})$.

There are some sequences with a reasonable occupancy, for example (3, 7, 1, 1, 1), but the length of these sequences is too short to be of much use for diffusers. As with phase grating diffusers, a designer should always look to maximize the repeat length

to minimize periodicity effects. This means that large N sequences are required, and then the number of 1s becomes too small using the normal optical sequence generation technique. Consequently, when N is large, three construction techniques are suggested, as outlined below. In reality, a combination of techniques might be needed.

1 This technique involves starting with a sequence with too few 1s and increasing the number of 1s. Given a $(\xi, N, M, S_{xxm}, S_{xym})$ family of sequences, it is possible to increase the number of 1s, but at the penalty of increasing the maximum value of the autocorrelation and cross correlation. This is best illustrated with an example:

A set of optical sequences (3, 25, 4, 1, 1) are: (1, 2, 7), (1, 3, 10), (1, 4, 12), (1, 5, 14). The sequences are taken in pairs, and a bit-wise OR taken between the pairs to form new sequences. So if both sequences have a zero bit, then the new sequence has a zero bit, otherwise the new sequence has the bit set to one. In the above case there are six unique combinations, as sequences are not combined with themselves. The new sequences are: (1, 2, 3, 7, 10), (1, 2, 4, 7, 12), (1, 2, 5, 7, 13), (1, 3, 4, 10, 12), (1, 3, 5, 10, 13), (1, 4, 5, 12, 13). These form a new family of sequences with the property $(\xi' = 5, N' = 25, M' = 6, S'_{xxm} = 2, S'_{xym} = 3)$, where the prime is used to denote the new sequence. The number of 1s has increased from three to five, but both the autocorrelation and cross correlation properties have degraded. The maximum side lobe value in the autocorrelation has increased from 1 to 2.

The above process in general produces new sequences where the number of 1s is $\xi' \geq 2^* \xi - S_{xym}$, where ξ, S_{xym} are the values for the original sequences. If too many 1s are generated after the OR operations, some 1s are randomly chosen to be changed to 0s. This was not necessary in the above example. The autocorrelation and the cross-correlation of the new sequences will be $S'_{xxm} \leq 2S_{xxm} + 2S_{xym}$ and $S'_{xym} \leq \xi + 3S_{xym}$ respectively. In the construction example above, the new sequences are considerably better than the worst case given by these upper bounds. For diffuser design, repeated application of this process is likely to be needed.

2 A very similar approach to (1) would be to take a sequence with too many 1s and reduce the number of 1s. For example, it should be possible to start from a family of MLS, and via logical operations reduce the number of 1s to the desired value.

3 The last technique involves constructing a family of optical sequences and then concatenating these together. As the family will have mutual low correlation, they should work well in a concatenated longer sequence.

For short sequences, it is possible to use a computer search to find the best sequence. For a small sequence length, say $N \leq 20$, it is possible to do an exhaustive search of every possible combination to find the best sequences. Every possible combination of bits with the correct number of 1s is tested by first constructing the autocorrelation function for each case, and then finding the sequence or sequences which have the smallest maximum value for the autocorrelation sidelobes. This is simple to encode, but as N increases it rapidly becomes very time consuming process to carry out. The number of unique combinations to search is given by:

$$N_c = \frac{N!}{\xi!(N - \xi!)} \quad (11.2)$$

where ξ is the number of 1s in the sequence and ! indicates factorial. Consequently, for $N=20$, $\xi=10$ there are nearly 200 thousand combinations, and this roughly doubles for every additional bit.

For say $20 < N < 48$ a numerical optimization [7] can be used to search for the best sequence. In this case optimization algorithms are used to avoid the need to test every possible combination, but even so this is still going to be a slow process. As computing power increases, this will be applicable to larger sequence lengths. Even with increasing computing power, the length of sequence over which optimization can be carried out is not going to rapidly expand. For an $N=48$ sequence with 24 1s and 24 0s, there are about 10^{13} unique sequence combinations to search.

Unlike the numerical optimization of Schroeder well depths discussed in Chapter 9, this is a discrete function optimization. In other words, the values of the optimization parameters, which are the locations of the 1s in a binary sequence can only take discrete values. This means the best algorithm for tackling this problem is a genetic algorithm as it can explicitly represent the discrete sequences as genes.

A genetic algorithm is a technique for searching for optimum configurations in engineering problems. Figure 11.10 illustrates how a typical genetic algorithm works. It essentially mimics the process of evolution that occurs in biology. A population of individuals is randomly formed. Each individual is determined by their genes, in this case the genes are simply the binary sequence indicating where hard and soft patches should be placed on the surface. Each individual has a fitness value that indicates how good they are. In this case, it is the largest energy in the autocorrelation side lobes.

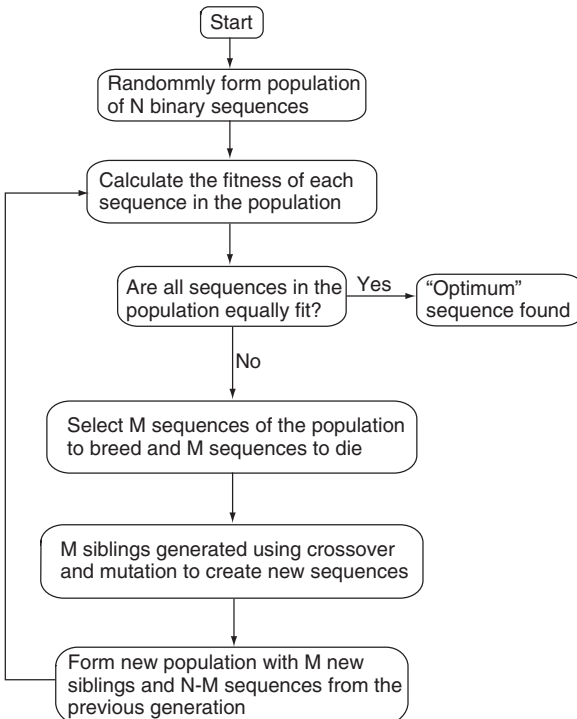


Figure 11.10 Optimization of numerical sequences using a genetic algorithm.

Over time, new populations are produced by breeding and the old populations die. Offspring are produced by pairs of parents breeding. An offspring has a gene sequence that is a composite of the sequences from the parents. A common method for doing this is multiple point cross over. For each bit in the sequence, there is a 50 per cent chance of the child's bit coming from parent A and a 50 per cent chance of the bit being from parent B. Mutation is also used. This is a random procedure whereby there is a small probability of any bit in the child sequence flipping during breeding. Mutation allows sequences outside the parent population to be searched.

Selecting sequences to breed and die can be done randomly. As with conventional evolution theory, the fittest are most likely to breed and pass on their genes, and the least fit the most likely to die. By these principles, the fitness of successive populations should improve. This process is continued until the population becomes sufficiently fit, so that the sequence produced can be classified as optimum.

An additional advantage of using a numerical optimization is that it gives complete control over the reflectivity of the diffuser. This can be specified as a desirable characteristic; any individual not having the desired reflectivity will be scored as less fit. Consequently, the trait of undesired reflectivity will die off.

Figure 11.11 shows the diffusion coefficient for a hybrid surface formed from an optimized sequence, compared to a hybrid surface formed from a random sequence. An improvement in performance is seen for most frequencies, although the improvement is not vast. The main problem with this technique is that it is impossible to find long optimal sequences because the number of possible sequences to search becomes too large. One solution to this problem is to generate a family of good sequences of relatively low N with low mutual cross correlation, and to concatenate them together to get a longer sequence. This is possible because during the optimization both the autocorrelation and cross correlation properties can be considered at the same time.

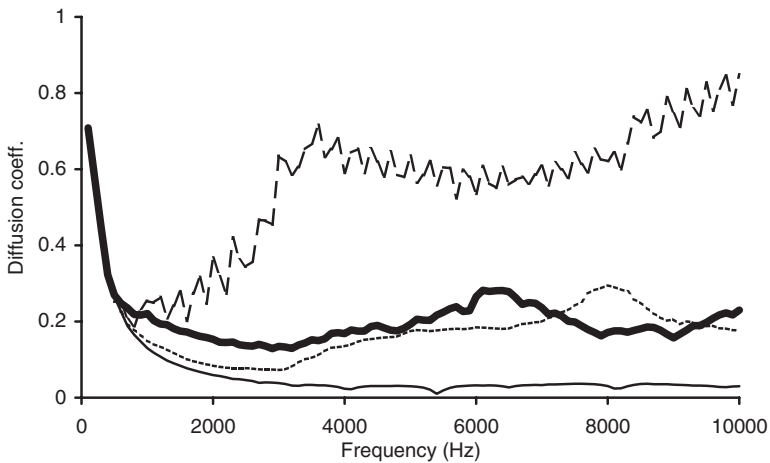


Figure 11.11 Diffusion coefficient for four surfaces showing how an optimized sequence can improve on a random sequence. — Flat non-absorbing surface; - - - - - Hybrid surface formed using a typical random sequence; ——— Hybrid surface formed using an optimized sequence; - · - · - 25 cm fibreglass (after Cox and D'Antonio [7]).

11.4.2 Two-dimensional sequences

Obtaining a 2D sequence to apply to a hemispherical scatterer such as that shown in Figure 11.1 can be achieved by two methods. The first method is the so-called perfect array construction method [5], which could be applied as they have roughly 50 per cent absorptive and 50 per cent reflective surfaces. These are called perfect because they have zero side lobe energy in the bipolar autocorrelation. These generate rectangular grids of holes, but it is also possible to construct optimal binary sequences on a hexagonal array pattern as well. The second method for forming an array is to apply the Chinese remainder theorem to a 1D sequence with good autocorrelation properties. The Chinese remainder theorem is a process that wraps a 1D sequence into a 2D array and yet preserves the good autocorrelation and Fourier properties.

Consider a length 15 sequence which will be wrapped into a 3×5 array. The elements are sequentially labelled $a_1, a_2, a_3 \dots a_{15}$. The sequence has two co-prime numbers, 3 and 5. By co-prime, it is meant that for the two numbers the only common factor is 1. The 1D sequence is written down the diagonal of the array, and as it is periodic, every time the edge of the array is reached the position is folded back into the base period. The process is illustrated in Figure 11.12.

Figure 11.13 shows another way of viewing this process. The coordinates (column, row) of the elements $a_1 \dots a_{15}$ are determined by modulo indexing. The subscript is called the index, n . The column for element a_n is determined by n modulo 5 and the row is determined by n modulo 3.

This folding technique still maintains the good autocorrelation properties of the sequence. For example, Figure 11.7 shows the autocorrelation for a length 15 unipolar maximum length sequence. Figure 11.14 shows the autocorrelation for the same sequence wrapped into a 3×5 array using the Chinese remainder theorem. The same autocorrelation properties are achieved in terms of the side lobe energy values. The Chinese remainder theorem can be applied before or after the Fourier transform as illustrated in Figure 11.15. Consequently, the folding technique preserves the ideal Fourier properties. Once the array is formed, any periodic section can be chosen. For example, it is possible to start filling anywhere in the array and so move the pattern around. This will not change the acoustic performance, but may change the visual aesthetic. The mask shown in Figure 11.1 was formed doing this.

11.5 Designing curved hybrid surfaces

The principles of optimization used to design rigid curved surfaces in Chapter 10 can also be applied to hybrid curved surfaces. A binary sequence with good autocorrelation properties is chosen, then the computer is tasked to find the best shape. Figure 11.4 showed part of a typical surface produced. The advantage of curving the surface is that it will break up the coherent wavefront reflected from the rigid parts of the planar mask. Consequently, the curved surface will have improved spatial and temporal dispersion.

11.6 Absorption

Figure 11.2 above showed the random incidence absorption coefficient for a planar surface with and without the perforated mask. This shows that the hybrid surface is

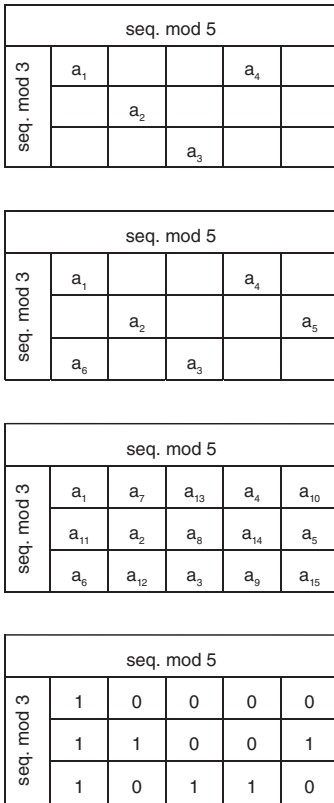


Figure 11.12 Folding a length 15 sequence, $a_1 \dots a_{15}$ into a 2D array using the Chinese remainder theorem. The last table shows the wrapping of the MLS sequence $\{1, 1, 1, 0, 1, 1, 0, 0, 1, 0, 1, 0, 0, 0, 0\}$.

index, n	0	1	2	3	4	5	6	7	8	9	10	11	12	13	14
Column coordinate = n modulo 5	0	1	2	3	4	0	1	2	3	4	0	1	2	3	4
Row coordinate = n modulo 3	0	1	2	0	1	2	0	1	2	0	1	2	0	1	2

Figure 11.13 The Chinese remainder theorem expressed as modulo indexing.

behaving like the Helmholtz absorbers discussed in Chapter 6. It is possible to predict the absorption characteristics using the transfer function matrix method. Problems arise, however, because the hole spacing is not regular and many holes are too close together for the normal assumptions of sound propagation through a perforated sheet. Nevertheless, it seems possible to at least predict the trends of the absorption.

The amount of added mass in the holes determines the increase in absorption at bass frequencies. For the BAD panel, if additional bass absorption is required, it is possible to reduce the open area (this will not be true for all geometries), as shown in

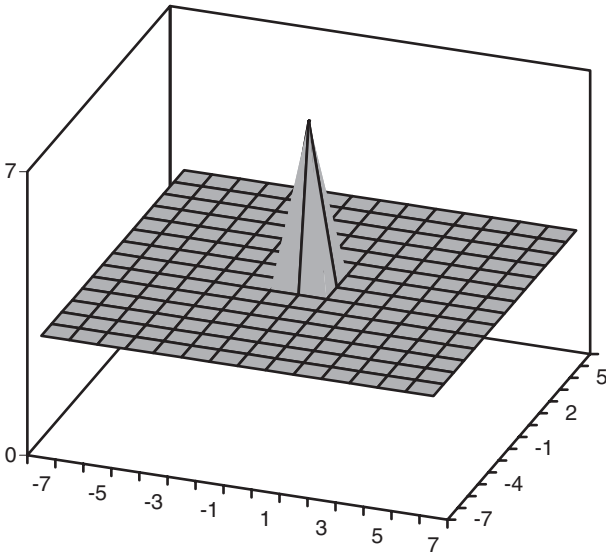


Figure 11.14 The autocorrelation function for a unipolar $N=15$ maximum length sequence folded using the Chinese remainder theorem.

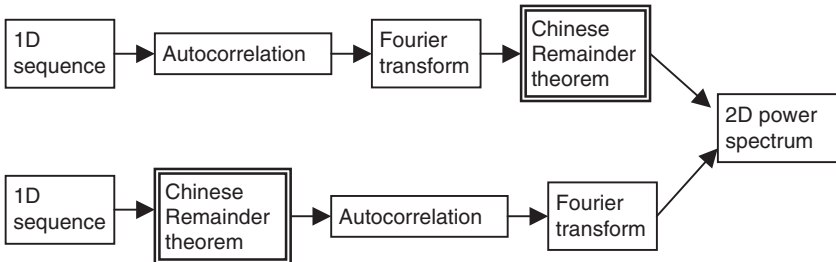


Figure 11.15 The Chinese remainder theorem can be applied before or after the Fourier transform, and consequently, it preserves good autocorrelation properties when used to fold 1D sequences into 2D arrays.

Figure 11.16. Alternatively, thicker mineral wool layers can be used, or the panel can be spaced from the backing wall to effectively increase the backing depth and so lower the resonant frequency of the system. The effect of changing the backing depth is shown in Figure 11.2 giving the expected trends.

The drop-off in high frequency absorption is due to the per cent open area of the panel. In a simplistic analysis, a 50 per cent open area panel would be expected to have an absorption coefficient of 0.5 at high frequency. Figure 11.16 shows the effect of reducing the open area, on the absorption coefficient. Similar absorption results would be expected for curved hybrid surfaces, but these have not been measured.

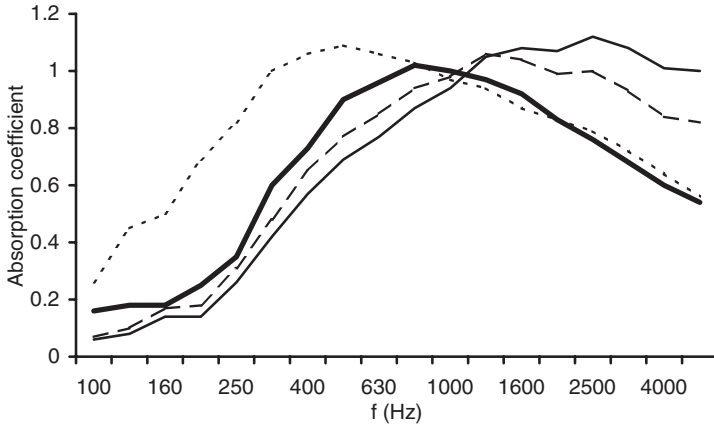


Figure 11.16 Random incidence absorption coefficients for various planar hybrid surfaces (BAD panels). — 25 mm fibreglass; - - - BAD 16 mm hole, 25 mm fibre glass backing; ——— BAD 13 mm hole, 25 mm fibre glass backing; ····· BAD 13 mm hole, 51 mm fibre glass backing.

11.7 Accuracy of simple theories

The absorption coefficient measurements also give information about the likely accuracy of the design principles based on the simple Fourier theory of Equation 11.1. Some of the key assumptions behind the theory are:

- 1 The absorption coefficient of the soft patches is 1 and there is no phase change on reflection.
- 2 The Kirchhoff boundary conditions are true.

The absorption coefficient of the soft patches is not 1 at low frequency because there is insufficient depth of mineral wool to cause complete absorption. At mid- and low frequencies mutual interactions across the panel render the Kirchhoff boundary conditions inaccurate. The Kirchhoff boundary conditions assume that the pressure on the hard patches is twice the incident pressure and on the soft patches is just the incident pressure. This is only true, when the soft and hard patches are large in extent compared to wavelength. It is only at high frequency, when the wavelength becomes millimetre in magnitude, that it might be expected that the Kirchhoff boundary conditions will be accurate. Consequently, the discussions above are really only true for the highest frequencies of interest. To put this another way, for a 50 per cent open area sample predicted with the simple Fourier theory, the absorption should be 0.5. Figure 11.2 shows that this is not achieved, for instance at mid-frequencies the absorption is around 1.

Despite these problems, it is still possible to learn something by considering the simple Fourier theories. For instance the Fourier theory shows that as with all diffusers, periodicity is a problem as energy gets concentrated in the lobe directions. Consequently, the repeat distance of the diffuser should be made as large as possible. This can be done using a modulation scheme, as discussed for Schroeder diffusers in Chapter 9 and curved surfaces in Chapter 10, or by designing the diffuser based on a larger number sequences.

Consider using a modulation scheme where two different hybrid surfaces are used. One of these is denoted A, the other B. A wall is filled by arranging the hybrid surfaces according to a pseudorandom sequence, for example if a length 5 Barker sequence is used, the arrangement of the surfaces would be: A A A B A. This is a method for reducing periodicity effects.

Modulation schemes pose problems for diffusers based on unipolar sequences. The most successful modulation scheme for Schroeder diffusers was to modulate a surface with a phase inverted version of the diffuser. In a unipolar environment, it is difficult to see how exact broadband phase inversion can be achieved. It is possible to go some way to achieve the inversion and therefore good performance. Consider a unipolar maximum length sequence a , an approximate inverse sequence can be found by adding 1 modulo 2, so the inverse sequence is given by $a + 1$ modulo 2. These two base shapes can then be arranged in a pseudorandom order to form a modulated array to reduce periodicity effects.

For example, consider the top three graphs in Figure 11.17. The top graph shows the autocorrelation properties for a periodic sequence of 13 $N = 127$ unipolar MLS.

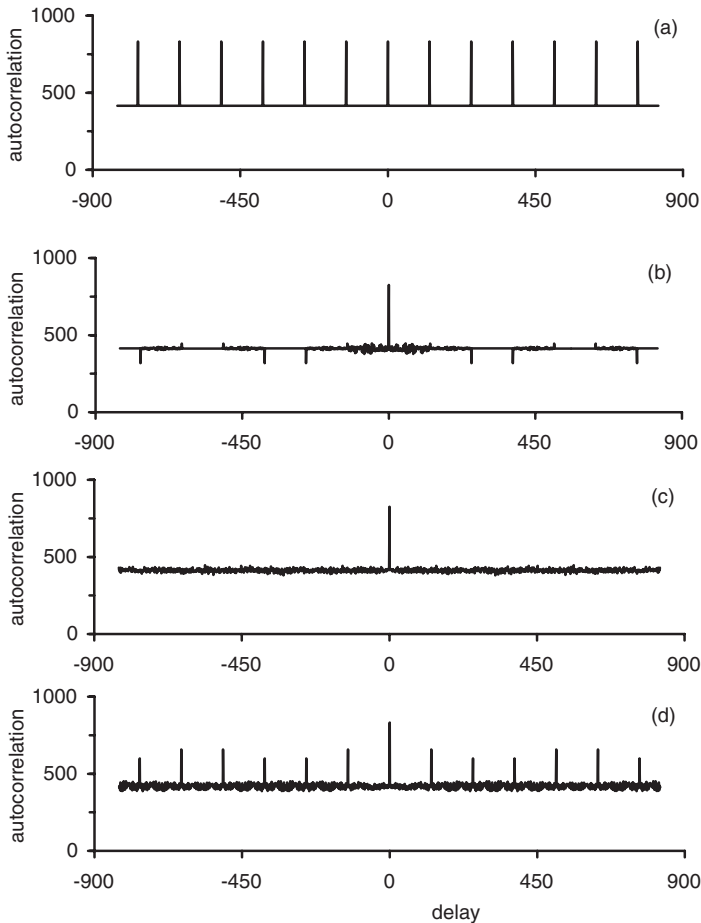


Figure 11.17 Autocorrelation properties for four sequences: (a) Periodic (b) Modulated using inverse (c) Random length 1651 and (d) One base shape modulation.

As expected, there are periodicity lobes every 127 units. This is compared in the third graph down to a random sequence of length 1651 ($= 13 \times 127$) showing no periodicity lobes. A modulated arrangement is shown in the second graph using a hybrid surface and its inverse. The ordering of the two surfaces was determined by the length 13 pseudorandom sequence with the best unipolar aperiodic autocorrelation properties. The effects of periodicity have been greatly reduced. Figure 11.18 shows the effects of the modulation in terms of a scattered polar distribution. The modulation has removed the periodicity effects for the non-zero order lobes. In that respect the modulation has been successful, but the dominant characteristic of the polar response is still the zero order specular lobe. The only way to deal with this is to introduce some possibility of phase cancellation, for example by curving the surface.

Another technique would be to use two sequences from the same family with mutually good crosscorrelation properties. Although this does not appear to work as well as the inverse process described above. It would also be possible to modulate using number sequences of different lengths – a similar process was described for Schroeder diffusers in Chapter 9 where it was called orthogonal modulation.

As with Schroeder diffusers, it is possible to modulate a single asymmetrical base shape. The mask shown in Figure 11.1 could be rotated by 90° and arranged with the original mask in a random arrangement. Brief tests on 1D sequences show this to be less successful than using two or more different base shapes. The bottom graph in Figure 11.17 shows the autocorrelation coefficient for a 1D asymmetric single base shape modulation. In this case the sequence order is just reversed to give the second base shape. While not as good as the modulation using two base shapes discussed previously, one base shape modulation still gives a better result than the periodic arrangement. The advantage of this technique is that it only needs one type of mask to be made.

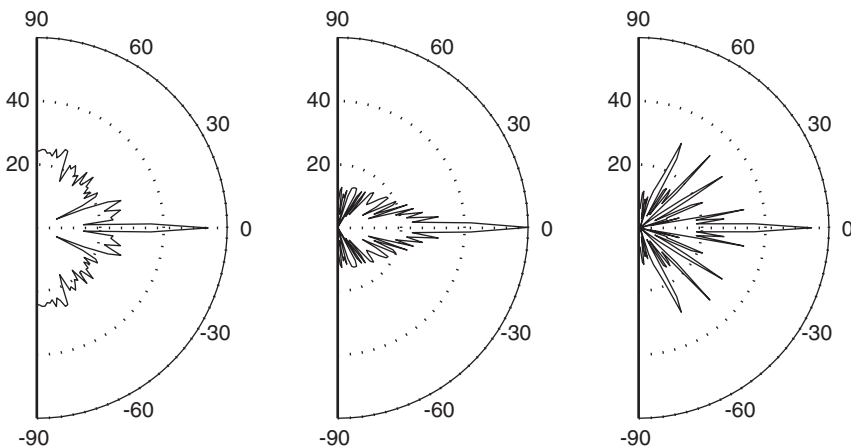


Figure 11.18 Scattering from three surfaces showing how modulation can improve the performance of hybrid surfaces: (left) maximum length sequence hybrid surface using modulation, (middle) planar non-absorbing reflector, and (right) maximum length sequence hybrid surface periodic.

11.8 Diffuse reflections

Measuring these surfaces to get the scattering performance is awkward. The normal measurement techniques described in Chapter 3 have used scale models of diffusers because of the problems of getting far enough away from full scale surfaces. For hybrid surfaces, accurate scale models of these surfaces cannot be easily produced because the impedance properties of porous materials do not scale in the same way as the wavelength in air. It would be possible to empirically find a substitute material to use in the scale models which has the appropriate impedance properties, but this is a rather tedious process. Nevertheless, diffusion measurements have been carried out on full scale samples, even though the receivers and source are rather too close to the panel. For example, Figure 11.19 shows the scattered polar response from a BAD panel and the porous material for the 1.25 kHz one-third octave band. The energy in the specular zone is attenuated by 6 dB. This is exactly as would be expected for a 50 per cent open area panel. Additional side lobe energy is produced compared to the flat hard surface.

Consider an analysis now based on the simple Fourier model. (There is a need for analyses based on a more accurate model, but these are not yet completed.) The diffusion coefficient is shown in Figure 11.20 and the polar distribution for one example frequency in Figure 11.21. For this comparison, five surfaces were predicted: a curved hybrid surface with a binary sequence of hard and soft patches, a plane hybrid surface based on the length 31 maximum length sequence, a plane hard surface, an $N=7$ QRD, and an optimized rigid curved surface. This last surface was 30 cm deep which is typical of the non-absorbing diffusers used in performance spaces and so is useful for comparison. The hybrid curved surface is much shallower, about 7 cm deep.

The diffusion coefficient spectra shows that moving from a flat hard surface to a hybrid plane surface increases the dispersion, as was also found in the measurements reported in Figure 11.19. Curving the hybrid surface produces more dramatic improvement in the diffusion coefficient. There appears to be much to be gained from curving hybrid surfaces. Interestingly, the quality of diffusion for the curved hybrid surface is only a little worse than the rigid optimized curved surface, which is four times as deep. This seems to indicate that a hybrid curved surface is a good method for generating more diffuse reflections from a restricted depth. Although, this

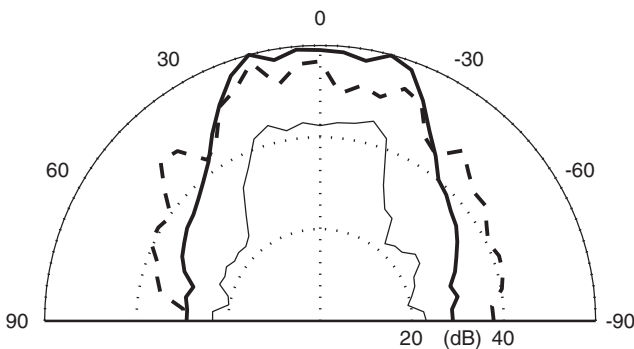


Figure 11.19 Measured scattering from a binary amplitude diffuser compared to a hard surface and a piece of absorbent. - - - BAD; — Non-absorbing flat reflector; ···· 25 mm fibreglass (data from Angus and D'Antonio [6]).

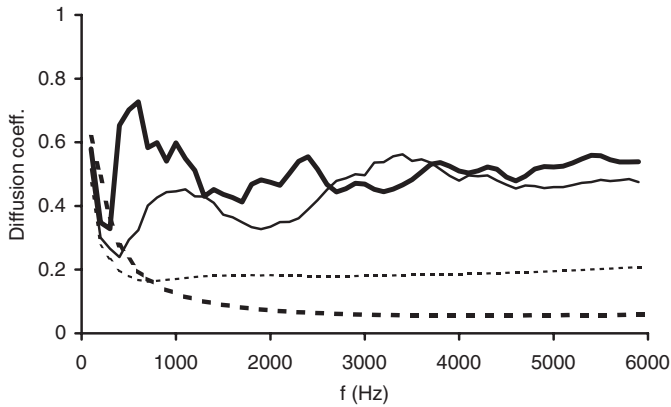


Figure 11.20 Diffusion coefficient for four surfaces. Flat non-absorbing reflector; - - - - - Flat hybrid surface; — Curved hybrid surface; ——— Non-absorbing optimized curved diffuser (after Cox and D’Antonio [7]).

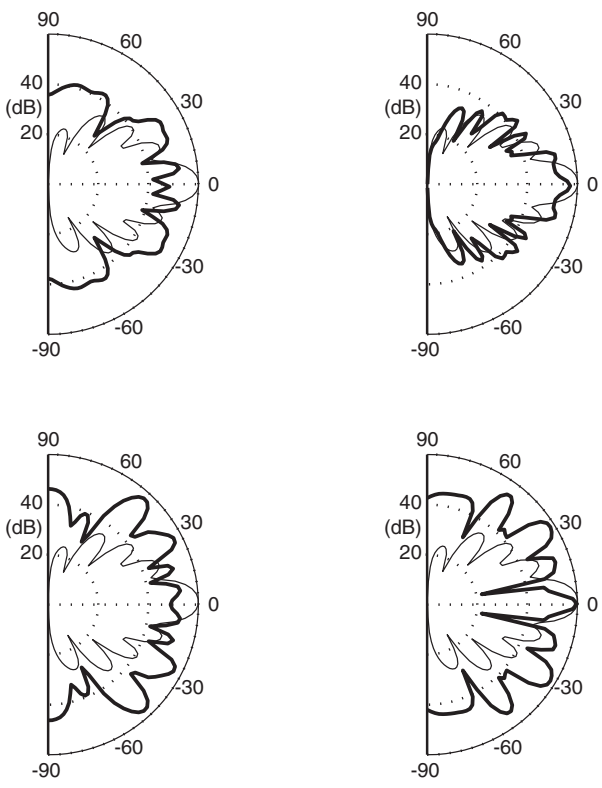


Figure 11.21 Scattering for five surfaces, in each case the thin line represents a planar non-absorbing surface of the same size as the diffusers. Top left: curved hybrid surface. Bottom left: curved hard diffuser; Top right: flat hybrid surface; Bottom right: $N = 7$ QRD.

is only useful where absorption is also wanted. Indeed, the problem with this analysis is that Fourier theory assumes an absorption coefficient of 0.5 across all frequencies, whereas practical surfaces appear to be mainly absorbing up to about 2 kHz. Consequently, for practical surfaces, it is only the right side of the diffusion coefficient graph which is most accurate.

11.9 Boundary element modelling

The above analysis has only considered a single plane device, but the findings should extend to surfaces designed to scatter hemispherically. In the case of the measurement, it was only possible to measure a hemispherical diffuser in a single plane and then the sources and receivers were rather too close. Furthermore, it is known that the Kirchhoff boundary conditions are not accurate at low to mid-frequencies and so simple models are rather unreliable. Using boundary element modelling (BEM) it is possible to calculate the scattering over a hemisphere including interactions across the surface, provided the absorbent patches remain locally reacting. The only other limitation is that a periodic arrangement of the surfaces must be tested, and the BEM model becomes rapidly too slow. Consequently, a thin panel, periodic formulation must be used as outlined in Chapter 8.

Figure 11.22 top left shows the scattering from a 4×4 array of the BAD panel at 3 kHz which is an MLS-based hybrid planar surface shown in Figure 11.1. This is

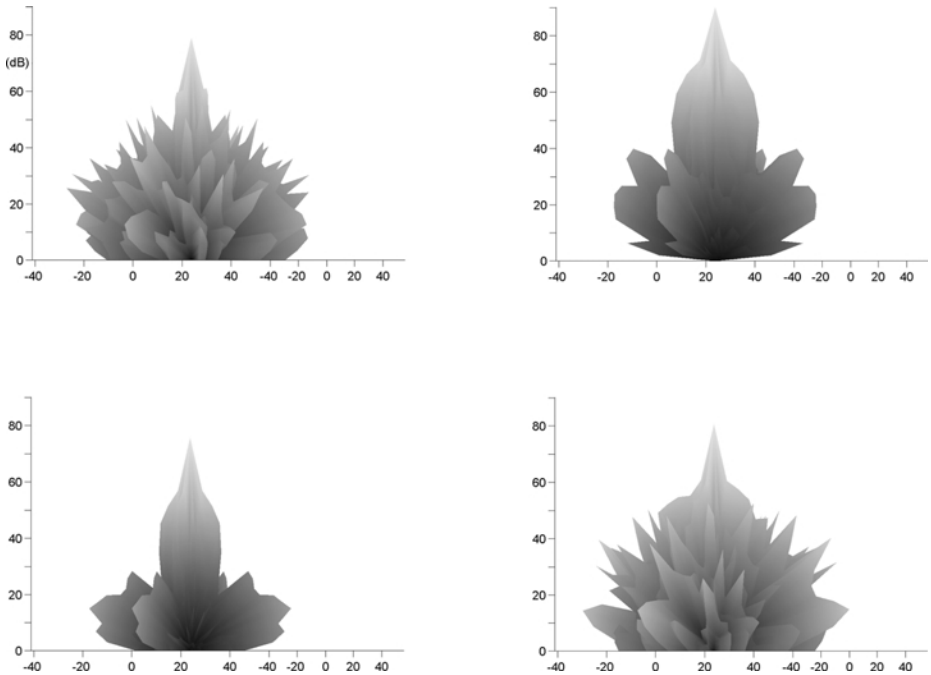


Figure 11.22 Scattering from arrays of surfaces at 3 kHz. Top left: BAD panel; Top right: plane surface. Bottom left: A perforated mask with regular hole spacing. Bottom right: A random perforated mask. 3D polar balloons viewed from side.

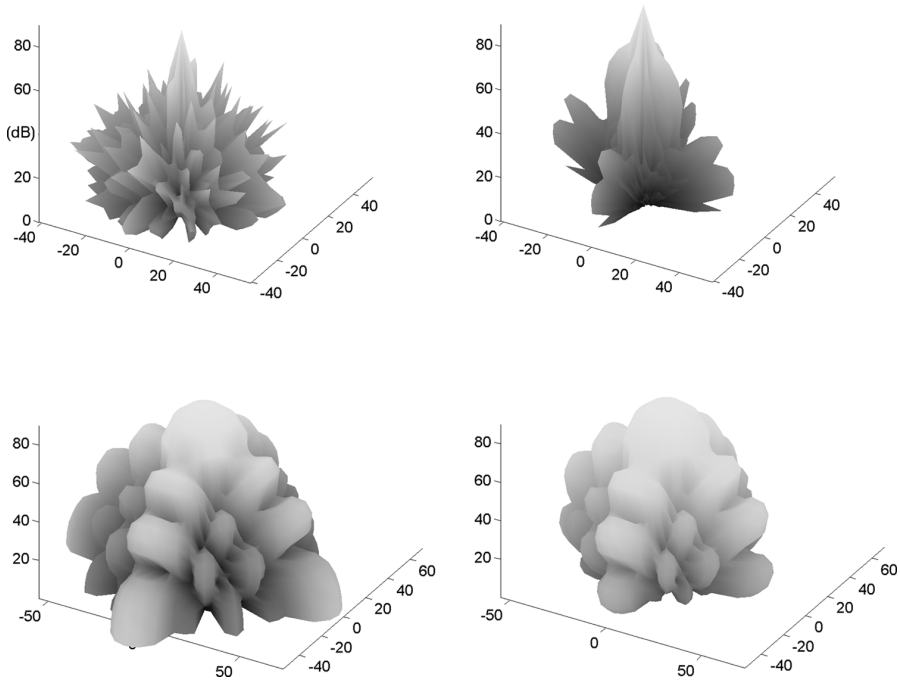


Figure 11.23 Hemispherical polar balloons, top 3 Hz, bottom 400 Hz. Left: BAD hybrid surface. Right: Plane hard surface.

compared to a planar hard surface top right. The polar balloon is shown side on and it illustrates the drop in specular reflection energy as was found with the simpler theories. It also shows that a strong specular component still exists from the hybrid surface. The bottom left graph is for a perforated mask where the holes are regularly spaced. This shows that the side lobe performance is better for the BAD panel, confirming the usefulness of a pseudorandom hole arrangement for getting more diffuse reflections. The bottom right graph is for a perforated mask where the hole locations are determined randomly. The performance is similar but slightly worse than the BAD panel. This shows the superiority of using pseudorandom number sequences rather than a random hole arrangement.

Figure 11.23 compares the scattering from the BAD panel to a plane surface at two contrasting frequencies. At the low frequency shown at the bottom of the chart, the mineral wool is not providing much absorption and so the BAD panel behaves similar to the planar hard surface, although a little additional dispersion is achieved. At the higher frequency shown in the top charts, the difference between the surfaces is marked, as would be expected.

11.10 Summary

Hybrid surfaces offer a new solution to room designers who want both reverberation control and diffuse reflections in a single surface. Flat hybrid surfaces have a

considerable advantage in being cheap and the treatment being hidden. More work is needed, however, to look at how this technology can be exploited further both in making better designs and in understanding where they are best applied.

11.11 References

- 1 P. D'Antonio, *Planar Binary Amplitude Diffusor*, Patent no. US 5,817,992 (1998).
- 2 P. D'Antonio and T. J. Cox, *Acoustical Treatments with Diffusive and Absorptive Properties and Process of Design*, US patent 6112852 (2000).
- 3 M. R. Schroeder, *Chaos, Power Laws: Minutes From an Infinite Paradise*, W. H. Freeman & Co. (1991).
- 4 J. A. S. Angus, "Sound diffusers using reactive absorption grating", *Proc. 98th Convention Audio Eng. Soc.*, preprint 3953 (1995).
- 5 P. Fan and M. Darnell, *Sequence Design for Communication Applications*, John Wiley & Sons Inc. (1996).
- 6 J. A. S. Angus and P. D'Antonio, "Two dimensional binary amplitude diffusers", *Proc. Audio Eng. Soc.*, preprint 5061 (D-5) (1999).
- 7 T. J. Cox and P. D'Antonio, "Optimized planar and curved diffusers", *Proc. 107th Convention Audio Eng. Soc.*, preprint 5062, New York (1999).

12 Absorbers and diffusers in rooms and geometric models

So far, this book has discussed how to design diffusers and absorbers, but mostly in isolation of where and how they are applied. The chapter starts by presenting some of the issues arising from the application of absorbers in rooms, especially the issue of the translation of absorption coefficients from free field measurements to reverberation chamber measurements or to full room application. The chapter then proceeds to discuss how absorption and diffuse reflection properties are represented in geometric room acoustic models and the problems this presents to obtaining accurate room predictions.

12.1 Absorption coefficients: from free field to random incidence

In Chapter 3, various methods for measuring absorption were outlined. These included free field and random incidence techniques. Unfortunately, it is not easy to translate between free field and random incidence values for a variety of reasons which will be discussed in the following paragraphs. Being able to translate from the free field measurements to random incidence values is extremely useful, because the free field measurements are done in a controlled environment which is ideal for validating prediction models, but to make these measured coefficients useful to practitioners they need converting into random incidence values.

The translation from a set of angle dependent free field absorption coefficients to a random incidence value is normally carried out using Paris' formula [1]:

$$\alpha_s = \int_0^{\pi/2} \alpha(\psi) \sin(2\psi) d\psi \quad (12.1)$$

where α_s is the random incidence absorption coefficient and $\alpha(\psi)$ the absorption coefficient in the free field at an incident angle ψ .

This formula is derived by considering the sound incidence on a surface in a diffuse space, the $\sin(2\psi)$ term arising because of solid angle considerations. If the surface is locally reacting, then it is possible to just measure the normal incidence impedance, apply the formulations given in Equations 1.22 and 1.25 to get the angle-dependent absorption coefficient and from Equation 12.1 the random incidence value. For a locally reacting surface a single measurement at 55° will suffice as this is the same as the random incidence value. Many surfaces, however, are not locally reacting as discussed in Section 5.6.

Makita and Hidaka [2] examined the problem of translating from free field to random incidence coefficients for homogeneous and isotropic sound absorbing porous materials. They measured different polyurethane foams in the impedance tube and the reverberation chamber and compared the random incidence absorption coefficients derived from the impedance tube measurement using Paris' formulation and the reverberation chamber measurements. Discrepancies arise because:

- The reverberation chamber is not completely diffuse leading to the Paris' formula being inaccurate and some angles of incidence being emphasized over others.
- Diffraction at the edges of the sample creates excess absorption in the reverberation chamber measurements. The impedance discontinuity at the edges of the sample causes additional sound to bend into the sample as this has a lower speed of sound.
- The mounting conditions are different which may affect how the frame of the absorbent vibrates.
- The assumption of local reaction, so that small sample measurements in the impedance tube can be translated to the large sample measurement in the reverberation chamber, may not be correct.

Makita and Hidaka carried out a series of reverberation chamber measurements on the foams with different sizes to get the absorption coefficient of an infinite size array using extrapolation. Figure 12.1 shows the inferred absorption coefficient for an infinite sample, compared to the finite-sized 12 m² sample, which is the recommended size in ISO 354 [3]. These absorption coefficients are shown for one typical sample of the six different foams tested. The average difference in the absorption coefficient between the finite and infinite samples for all six foams is also shown. Figure 12.1 illustrates that great differences in the absorption due to edge effects can be obtained, even if the edges of the samples are covered with a reflective frame as is normal practice and required by the ISO 354.

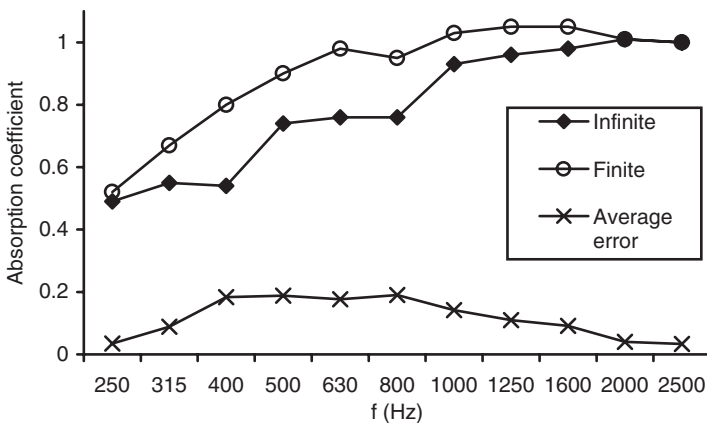


Figure 12.1 Comparison of measured random incidence absorption coefficients for finite and infinite samples for one material. Also shown is the average error between the finite and infinite sample absorption coefficients for six materials (data from Makita and Hidaka [2]).

Bartel [4] examined the extrapolation from finite to infinite area absorption. The paper also contains a useful and comprehensive literature review of previous work in this area. The simplest model for the absorption coefficient extrapolation assumes a linear relationship. This can be represented by:

$$\alpha_{\infty} = \alpha_s + mE \quad (12.2)$$

where α_{∞} is the absorption coefficient for an infinite sized sample, α_s the absorption coefficient for a finite sized sample, for example a 12 m² sample in a reverberation chamber measurement, m a constant, and E the perimeter of the finite sized sample.

The sensitivity of the absorption coefficient to the perimeter varies with material type and frequency. Figure 12.2 shows a plot of the absorption coefficient for different perimeter sizes measured in the reverberation chamber, showing that the edge diffraction effects can be very significant. This is with the edges of the sample covered with a reflective strip as required by the standard. Figure 12.3 shows how the value of the constant m varies with frequency and material type. Bartel also investigated the effect of sample shape. Sample shape only affected the absorption coefficient by at most 3 per cent, so the size of the perimeter is much more important than the shape of the sample edge.

To derive the constant m requires a series of measurements on different sample sizes in the reverberation chamber. Consequently, Equation 12.2 does not help derive random incidence absorption coefficients from impedance tube measurements, because impedance tube measurements do not give values for m . Bartel [4] reports, however, a formulation attributed to Norwood [5] to allow the perimeter effect to be predicted, and so allow the translation from impedance tube to random incidence values. The normalized admittance β of the sample is measured in the impedance tube and is given by:

$$\beta = \frac{\rho c}{z} = g - jb \quad (12.3)$$

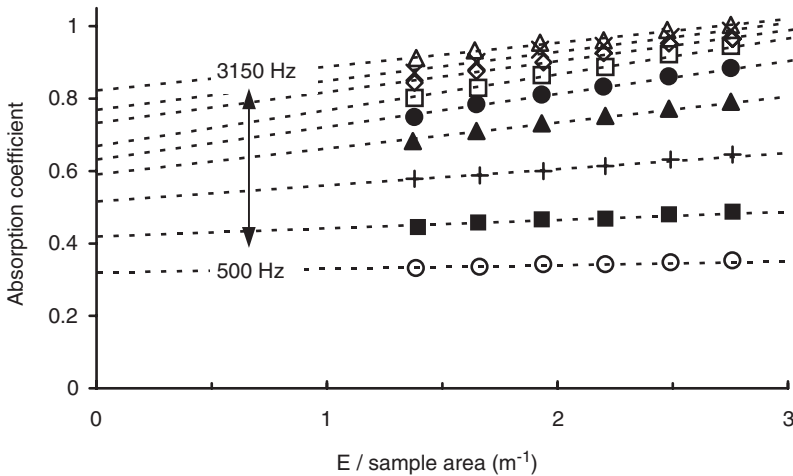


Figure 12.2 Random incidence absorption coefficient as a function of perimeter divided by sample area. Shown for different one-third octave bands. ○ 500; ■ 630; + 800; ▲ 1000; ● 1250; □ 1600; ◇ 2000; × 2500; △ 3250 Hz (data from Bartel [4]).

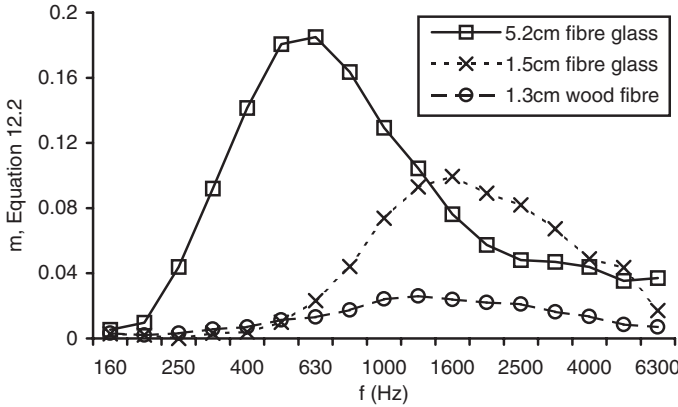


Figure 12.3 Variation of constant m in Equation 12.2 which measures the perimeter effect for random incidence absorption coefficient. Results for three different materials given as indicated (data from Bartel [4]).

where z is the surface impedance, ρ the density and c the speed of sound in air.

The average absorption coefficient for a finite rectangular sample is then given by:

$$\alpha = \frac{16g}{\pi} \int_0^{\pi/2} \int_0^{\pi/2} \frac{\sin^3(\phi) d\phi d\theta}{|\beta|^2(A^2 + B^2) + 2(gA + B) \sin(\phi) + \sin^2 \phi} \quad (12.4)$$

where

$$A = \int_0^{ka \sin \phi} \cos(x \sin(\theta)) J_0(x) dx - \frac{1}{ka \sin \phi} \int_0^{ka \sin \phi} x \cos(x \sin(\theta)) J_0(x) dx \quad (12.5)$$

$$B = \int_0^{ka \sin \phi} \cos(x \sin(\theta)) N_0(x) dx - \frac{1}{ka \sin \phi} \int_0^{ka \sin \phi} x \cos(x \sin(\theta)) N_0(x) dx \quad (12.6)$$

where $a = 2/E$, and J_0 and N_0 are the Bessel functions of the first and second kind, respectively. These formulations can also be used to gain random incidence predictions of absorbers based on the formulations derived in Chapters 5–7.

Makita *et al.* [6] presented a revised Paris' formula which accounts for inaccuracies in the cosine law formulation. The formulations derived are rather complex, but enable the effects of the boundary layer on the absorption to be accounted for. The boundary layer effect is not normally as big as the perimeter effect, but can still be significant.

12.2 From the reverberation chamber absorption coefficients to room predictions

The problem of projecting from reverberation chamber measurements to whole room design has already been discussed in Chapter 3 with respect to seating. While seating

is a rather specialized case, it is generally true that there are often problems making whole room predictions of objective parameters based on reverberation chamber measurements of absorption. Even when the inaccuracies in the absorption coefficient are numerically small, the inaccuracy in the resulting reverberation time in a space can be quite significant, if large areas of the absorbent are used, as the inaccuracy in the total absorption will be large. The problems centre on two issues, edge diffraction and non-diffuseness.

1 *Edge diffraction*: The sample size tested in the reverberation chamber is often smaller than that applied in the real space. Consequently, there is greater edge diffraction effects in the reverberation chamber than in the real space. This can lead to significantly different absorption coefficients between the two spaces. The solution to the edge effect problem could be to determine the absorption of the edges, as was done for seating in Chapter 3. Alternatively, it is possible to test different sample sizes in the reverberation chamber, and from there extrapolate to the sample size used in the real room. The formulations given in the previous section for the influence of sample perimeter can also be used to extrapolate the absorption of large sample sizes from the smaller reverberation chamber samples.

2 *Non-diffuseness*: The acoustic conditions in the reverberation chamber and the real room may be very different. The reverberation chamber may be diffuse, while the real room is not diffuse. This could lead to the random incidence absorption coefficient measured in the reverberation chamber not matching the absorption coefficient in application. Actually, a more common scenario is that both the reverberation chamber and real room are non-diffuse, but they are non-diffuse in different ways.

The effect of the diffuseness of the space is difficult to account for. If the non-diffuseness is generated in a simple manner, for instance all the absorption on one surface of the room, then there are reverberation time formulae that can deal with these cases. (Gomperts carried out a comprehensive review of reverberation time formulations [7].) A modern solution would be to use a geometric room acoustic model, to properly model the sound distribution in both spaces rather than assume a diffuse field. This is an appealing solution, but as shall be discussed in the next section, the application of absorption coefficients in computer models is not necessarily straightforward. For instance, what should be done with absorption coefficients greater than one which commonly occur with reverberation chamber measurements? If a geometric model is used, it is best if both the reverberation chamber and the real room are modelled, rather than making the assumption that the reverberation chamber is diffuse. This requires the modeller to have access to the reverberation times with and without the sample in the reverberation chamber, and these are not usually available.

12.3 Absorption in geometric room acoustic models

Geometric models are becoming a core tool for practitioners and researchers designing or investigating the propagation of sound within a space. To gain accurate predictions from these models, it is necessary for the geometric models to correctly model absorption effects, but this is not as straightforward as might first have been thought.

Geometric room acoustic models calculate the sound propagation within a space using a ray tracing [8], beam or cone tracing [9], image source [10, 11] or hybrid approaches [12]. (A hybrid approach meaning a combination of some of the other three methods [13].) They are high frequency approximations to the true sound propagation and do not properly deal with the wave nature of sound.

For readers unfamiliar with geometric models, it is necessary to describe how the sound might be modelled, but for brevity only one type of modelling will be described, and readers are directed to the literature for further reading. Here ray tracing will be considered, as this is the easiest to describe. In ray tracing, the sound energy is modelled as rays that propagate around the room like rays of light. When the ray hits a surface in the room, it is reflected from the surface, and if no scattering is considered, the angle of reflection equals the angle of incidence. There is a receiver in a room, usually a sphere, and every time a ray passes through the sphere, the reflection contributes to the energy impulse response. This process is illustrated in Figure 12.4.

Every time a ray reflects from the surface, the energy of the ray is decreased by a factor of $1 - \alpha$, where α is the absorption coefficient of the surface. One problem is that absorption coefficient tables published in the literature often contain values greater than 1. How should these be translated into use in the geometric model, where values greater than 1 are meaningless? Furthermore, many geometric models are now producing auralizations of the sound field within the space to allow designers to hear the effect of design changes. To get a natural rendition of the sound field, a wide audio bandwidth is required, yet absorption coefficient data is normally only available for a restricted bandwidth of 100 Hz–5 kHz [14]. These and other issues are discussed below.

Although a geometric room acoustic model has knowledge of the angle of incidence that a ray strikes a surface, it is usual for a random incidence absorption coefficient to be applied to every reflection. If local reaction is assumed, and the normal incidence impedance of surfaces is known, it would be possible to predict the absorption coefficient as a function of incident angle and use these in computer models instead. Nijs *et al.* [15] examined this and found that for simple room geometries, in their case a reverberation chamber, angular-dependent absorption coefficients made little difference to calculated levels and reverberation times. For a coupled room, however, Nijs *et al.* found that using an angular-dependent absorption coefficient enhanced prediction accuracy. Using just random incidence absorption coefficients, inaccuracies of 15–20 dB in predicted level were found between prediction and measurement in the

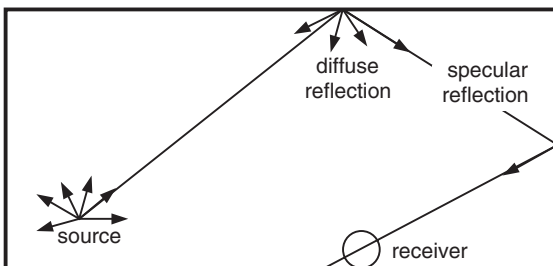


Figure 12.4 Picture of ray tracing in a room.

coupled space; using angular-dependent absorption coefficients, this error dropped to 4–7 dB. It would be interesting to know how sensitive the parameters which are highly dependent on correct modelling of early reflections, like early lateral energy fraction [16], are to angular dependent absorption, even in rooms with simple geometries.

One cause for the absorption coefficients to be greater than 1 in reverberation chamber measurements is that Sabine's formulation [17] becomes inaccurate when the absorption is high ($\alpha > 0.2$ – 0.4). According to Sabine's formula, a room constructed from completely absorbing walls still has a reverberation time greater than zero. A couple of authors have suggested that alternative reverberation time formulations should be used to calculate the absorption coefficients from the reverberation time measurements, as these absorption coefficients then give more accurate predictions in real spaces with geometric models. Nijs *et al.* [15] used the Eyring [18] equation to deal with some of the problems of excess absorption that occurs when using Sabine's formula. Dance and Shield [19] favoured the use of the Millington [20] reverberation time formulation. These formulations can be found in Chapter 1.

The problem with using alternative reverberation time formulations to get absorption coefficients from reverberation chamber measurements is that the geometric room acoustic modellers need access to the reverberation times measured in the reverberation chambers to re-derive the absorption coefficients. The data that is generally available in literature is just the calculated absorption coefficients using Sabine's formulation. Consequently, using other reverberation time formulations can be rather awkward to implement. Dance and Shield overcame this to a certain extent, however, by publishing a conversion chart to get from the Sabine absorption coefficients to the Millington values by carrying out some geometric room predictions which simulated typical reverberation chamber measurements. This chart is shown in Figure 12.5.

Figure 12.6 shows the reverberation times predicted for a concert hall from Dance and Shield. The top graph shows that classical reverberation time formulations are inaccurate in non-diffuse spaces, and using a geometric model can improve prediction

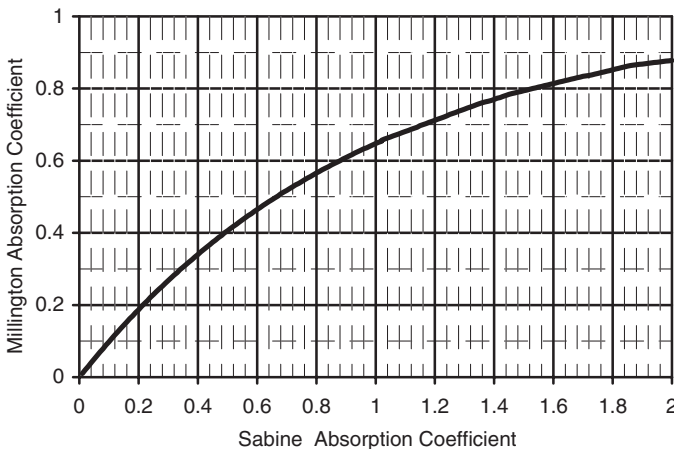


Figure 12.5 Chart to translate from Sabine measurements in reverberation chambers, to Millington values to be used in real space predictions in geometric models (modified from Dance and Shield [19]).

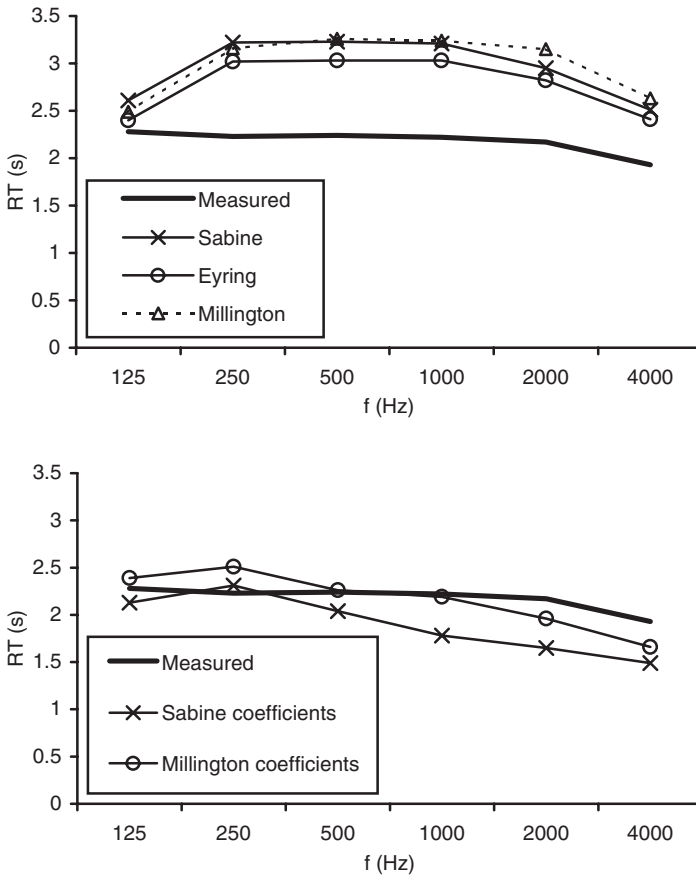


Figure 12.6 Predicted reverberation times compared to measurement for a concert hall. Top: Predictions using various reverberation time formulations. Bottom: Predictions using a geometric model with different absorption coefficient formulations (data from Dance and Shield [19]).

accuracy – a finding by Antonio *et al.* [21] and many others. The bottom graph shows that using absorption coefficients derived using a Millington formulation in geometric models gives more accurate results. However, in some cases not shown here, the findings are less clear cut.

Using more exacting reverberation time equations may help predictions, but it does not prevent measured absorption coefficients often exceeding 1 due to edge effects and the non-diffuse nature of the reverberation chamber. Nijs *et al.* [15] state that in the reverberation chamber the absorption is overestimated as the sound field is non-diffuse with the sample present; furthermore the overestimation is greater if volume diffusers are present; They therefore recommend a 20 per cent reduction of the measured values from the reverberation chamber as a good first guess for the input into a ray tracing program and hard limiting coefficients, so they do not exceed 1. Summers [22] points out, however, that there is a great variation in measured absorption coefficients between different reverberation chambers, a point borne out

by the results shown in Figure 3.4. Consequently, the 20 per cent rule suggested by Nijs *et al.* is unlikely to generalize.

The work could be extended to include the effects of edge diffraction, which previously in this chapter have been shown to cause significant estimation errors in the absorption coefficients. The work also needs to consider inter-laboratory variation in random incidence absorption coefficient measurement. An alternative solution to the problem of mapping from the reverberation chamber to the real room is empirical fitting. As a surface treatment is used over time, an understanding of how the absorption coefficient varies between the reverberation chamber and real rooms is developed. If the reverberation time was underestimated this time, next time the modeller might put in a smaller absorption coefficient. This is obviously not very satisfactory, but is the reality of applying many scientific models to engineering problems. This is why experienced geometric modellers usually produce better predictions than novices. This also creates problems in verification of computer models. Too often, the absorption coefficients for surfaces are found by fitting predictions to match measurements, and then the same measurements are used to show that the numerical method works!

So far, the issue of phase change on reflection has not been discussed. The true reflection from a surface should include changes in magnitude and phase, and consequently the pressure reflection factor or impedance is needed. This is problematical for many reasons. Impedance data for surfaces is not available as the random incidence absorption coefficient only gives information on energy. Furthermore, many building surfaces have non-local reacting behaviour which creates problems in measuring and implementing the phenomena in geometric models. For many predictions it is probably unnecessary to go into this detail, which is fortunate as it would pose some difficult or impossible problems to overcome.

In recent years, there have been round robin trials of geometric room acoustic models comparing the accuracy of the different techniques [23]. One of the key findings from this process has been that the accuracy of the prediction models is highly dependent on the quality of the input data, including the absorption coefficient of surfaces. So to summarize, defining absorption coefficients (and impedance) for geometric room acoustic models appears to be a tricky problem. Fortunately, experienced practitioners can usually produce estimations of absorption coefficients that are good enough using previous knowledge. This is not an entirely satisfactory situation as subjectivity should not be part of a prediction model.

12.4 Diffuse reflections in geometric room acoustic models

Early work on geometric models concentrated on the issue of modelling absorption. In recent years much attention has been focussed on the modelling of scattering or dispersion from surfaces, often referred to as diffuse reflections. Geometric models inherently cannot precisely model the wave nature of sound. They approximate the sound to have a short wavelength, much shorter than any dimension within the room; this enables sound to be modelled as particles, rays, beams or as coming from image sources. Unfortunately, the wavelength of sound is relatively large at low to mid-frequencies, and consequently geometric models that do not attempt to predict the effects of surface and edge scattering are liable to produce inaccurate results. In real life, an incident sound will inevitably be scattered into angles other than the specular reflection direction upon reflection from most surfaces.

The problems of diffuse reflection modelling in geometric models are well established. For example, Hodgson [24] used a ray tracing model that took diffuse reflections into account by redistributing diffuse energy according to Lambert's law [1]. He concluded that in simple empty rooms, the effects of diffuse surface reflections are negligible in small or proportionate rooms, while in large disproportionate rooms the effects can be considerable. To take another example, in the first round robin study of room acoustic models [25], three prediction models were found to perform significantly better than others. These three prediction models produced results approximately within one subjective difference limen, while the less successful computer models produced predictions inaccurate by many difference limen. What differentiated the three best models from the others was the inclusion of a method to model surface scattering.

If the overall room shape and sizes and orientations of surfaces are such that they will cause reflections to be well mixed for purely geometrical reasons, a diffuse field may be created even if no rough or scattering surfaces are used. In this context, mixing means that the reflection paths involve all the surfaces of the room. For mixing room shapes the reverberation time can be well predicted even without diffuse reflection modelling, even if predictions of finer parameters such as clarity may suffer [26]. However, as it is difficult to know in advance if a room shape is mixing, it is best to always include diffuse reflection modelling in a geometric model, as otherwise unnecessary uncertainty is generated and potentially inaccurate estimations of acoustic parameters result.

The most obvious error created by a lack of diffuse reflection modelling is an over prediction of reverberation time [27, 24]. This is especially true in enclosed spaces where absorption is concentrated on one surface, such as in concert halls, or when the room shape is highly disproportionate, such as in large factories. In some halls, the choice of scattering coefficients has a greater impact on the estimated reverberation times than the uncertainty in the absorption coefficients [28]. Torres and Kleiner [29] found that changes in the scattering coefficient in geometric models are audible in auralizations, and that the diffuse reflections should be modelled with frequency dependence. Gomes and Gerges [30] also found that using correct scattering coefficient values in a diffuse reflection model was important for gaining accurate predictions for an auditorium. The most recent round robin on geometric models [23] found that the biggest errors with geometric models were consistently at low frequencies, presumably because of their inability to model diffraction effects correctly as these are most prominent at low frequencies.

There are many different methods for incorporating diffuse reflections into a geometric room acoustic model. Dalenbäck *et al.* [28] give a comprehensive survey of the techniques. Many of the techniques are similar or just variants. Consequently, only a few of the most important and commonly used techniques are outlined here, and readers are referred to Dalenbäck *et al.* for a more comprehensive review. While there are many possible methods, there is a problem that it is not known which modelling technique, if any, is intrinsically more accurate. It is known that a diffuse reflection model is needed for accurate predictions, but it is not known if one model is better than any of the others. One key determining factor is, however, the computing time. Accurate diffuse reflection models are relatively simple for low orders of reflections, but often become increasingly computationally expensive as the reflection order increases.

12.4.1 Ray re-direction

This method is a ray scattering process as suggested by Kuttruff [1]. A wall is considered to reflect a proportion of all the incident sound energy diffusely. The proportion of diffusely reflected energy is given by the scattering coefficient s , and this is distributed according to Lambert's law. The remaining energy $(1 - s)$ is reflected in a specular manner. The direction of the diffuse reflection is determined by two random numbers. The angle of azimuth is chosen by a random number in the interval $[-\pi, \pi]$, and the elevation angle is given by the inverse cosine of the square root of a random number that is chosen from the interval $[0, 1]$.

Concentrating all the diffusely reflecting energy into one direction is not true to reality, but this method is fine for the reverberant sound field, as there are a large number of reflections to average out the response. For the early sound field where there are fewer reflections, however, the method is not so good. Instead of giving many weak reflections from a diffusing surface spread over time, a receiver gets a few stronger reflections. This can, to a certain effect, be solved by generating multiple rays from the diffuser in multiple directions, but this then becomes very computationally expensive.

12.4.2 Transition order using particle tracing

The reflection calculation method is separated by a user-defined transition order [31]. Reflections with orders lower than the transition order are purely specular. After the transition order, sound rays are treated as energy packets similar to a normal ray tracing method. At each subsequent wall reflection after the transition order, a secondary impulse source is created at the reflection point, which radiates into the room as an elemental area source. The energy is then re-grouped into a ray and traced forward in a direction given by a random process in which either a purely specular or a diffuse direction will be chosen depending on whether the value of a random number generated by the program is greater or smaller than the wall's scattering coefficient. If the reflection is diffuse, then its direction is determined by a second random process based on Lambert's diffusion law.

The choice of transition order is dependent on the hall shape rather than size [32]. In rectangular rooms, a transition order of 0 in low frequency bands, and 1–3 in the high frequency bands was found to be appropriate. In the fan shaped halls, where correct modelling of the specular reflections is important to account for the influence of the hall geometry, a higher transition order was also required in the low frequency bands. Generally, the choice of transition order should be based on the importance of the specular components in the early reflections in defining the acoustic characters of the hall. An order of 1 or higher should be used only when the sound field is significantly affected by the specular components, such as at high frequencies or with strong reflecting surfaces. In real halls where the sound field is expected to be more diffuse, lower transition orders should be used.

The main problem with this method of diffuse reflection modelling is that the concept of a transition order is not physically satisfactory, since diffuse reflections should occur even at the very first reflection rather than suddenly being switched on at the transition order.

12.4.3 *Diffuse energy decays with the reverberation time of the hall*

Upon each reflection, the scattering coefficient is used to define the fraction of energy diffusely scattered into non-specular angles, while the remaining energy is reflected specularly in the usual way. The diffuse energy is ambient energy spread throughout the room volume. This energy is assumed to decay exponentially, the decay constant being determined by Eyring's formulation. A visibility check is used to ensure that the right surfaces contribute to the received sound [33].

The problem with this is that it assumes that the Eyring's formulation is correct, which is not necessarily true, especially if the space is non-diffuse. Some have used an iterative procedure to gradually improve the estimated reverberation time, but this slows computation as it requires multiple passes through the algorithm.

12.4.4 *Radiosity and radiant exchange*

The diffuse part of a reflection is stored and the specular ray tracing continued. When the stored diffuse energy is emitted, all subsequent surface reflections are assumed to be diffuse. These methods use a stochastic radiative exchange process to propagate sound from surface to surface. This radiosity can be modelled by integral equations, but more commonly uses simple heat exchange formulations. The radiant exchange takes place at time intervals given by multiples of the mean free time between reflections.

12.4.5 *Early sound field wave model*

Another suggestion is to use wave based models, such as a time domain Fourier approach, to model the early sound field, before resorting to a ray tracing with randomized ray redirection for the later sound field. This has the advantage of potentially being more accurate in modelling the early sound field which is more important from a psychoacoustic standpoint, while allowing ray tracing to take over where it is computationally more efficient and sufficiently accurate.

12.4.6 *Distributing the diffuse energy*

Having described some of the models used, it is apparent that they have many common features. One of these is that the diffusely reflected energy from a surface is modelled as radiating from the surface with a particular spatial distribution, and in most current models, Lambert's law is used to determine this distribution.

Another possibility is to base the dispersion function for a surface on the polar response measured or predicted in the free field. Problems would arise because the polar response would be from a surface of significant finite extent, whereas many geometric models would require the correct dispersion from a point on the surface. This needs consideration in designing the model, and a method to reverse engineer the point reflectivity function from the finite-sized polar response is needed. This can be done using Farina's method for characterizing diffusers, which was discussed in Chapter 4. The situation is more complex with beam tracing, as the beam may interact with part of a surface, and so the reflectivity function would neither be the point reflectivity function or the finite-sized polar response. There is a further problem in dealing with situations where only part of the surface is illuminated, as might happen when

objects cast shadows on surfaces, or with directional sources. Polar responses are usually measured or predicted using complete illumination by omnidirectional sources.

The most common dispersion law for computer models is Lambert's law, also referred to as the cosine law. It states that the intensity scattered by a surface follows a cosine distribution with respect to the incident and reflected sound angle to the wall. This is illustrated in Figure 12.7 for a normal incident source. Stated in terms of equations for a ray tracing case [1]:

$$I_r = \frac{I_0 dS \cos(\psi) \cos(\theta)}{\pi r^2} \quad (12.7)$$

where I_r is the reflected intensity at the surface, I_0 the incident intensity at the surface, θ the angle of the receiver to the surface normal, ψ the angle of the source to the surface normal, dS the area of the surface being considered, and r the receiver radius.

This formulation is a simple statement of solid angle projections. For instance, the solid angle is zero for sources and receivers close to grazing. If the surface is partly absorbing, then the intensity should be attenuated by the corresponding intensity reflection factor, but to simplify discussions the surface will be assumed non-absorbing in this discussion.

True rooms are not purely specular and neither purely diffuse following Lambert's law. They are somewhere between. For the reverberant field, however, the evidence is that the sound field more closely matches a diffuse case than a specular one [1].

Figure 12.8 shows the scattering distributions for a surface with 1, 50 and 99 per cent diffuseness, where the diffuse reflection is modelled using Lambert's law. Also included for comparison in Figure 12.9 are the polar distributions for a periodic diffuser, a single cylinder, a plane surface and a randomly rough surface with small roughness. Each surface is 2 m wide and the source and receiver are in the far field. The scattered distribution using the Lambert model does not match many of the real surfaces very well for many cases. The closest is the random rough surface, which approximately

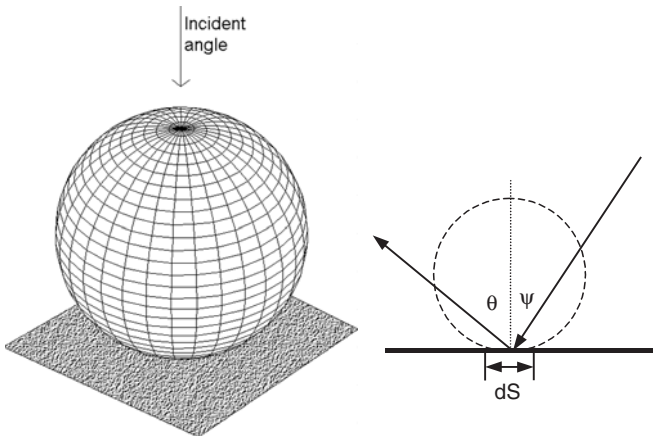


Figure 12.7 Two views of the Lambert distribution of intensity, left 3D view, right cross-section.

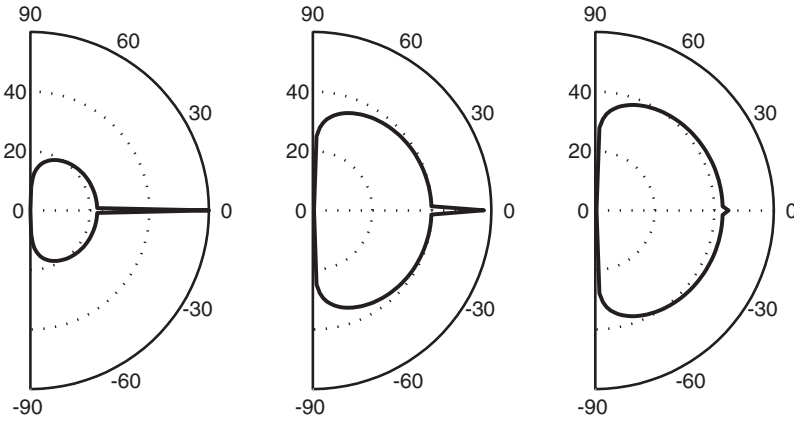


Figure 12.8 Typical far field energy distributions in a geometric model for different values of scattering coefficient s and a normal incident source. Left to right $s = 0.01, 0.5, 0.99$.

matches the $s = 0.99$ case. Consequently, room acoustic models are not producing scattering distributions close to real diffuser scattering. However, this is probably not that important for the reverberant field where there are a large number of reflections over which the errors in any one diffuse reflection tend to average out, or at least mask the problem. It is more of a problem, however, for the early sound field where precise modelling of first order reflections is needed.

Lambert's law is a natural choice for room acoustic modellers, because it is the asymptotic high frequency case, which is intrinsically the frequency range where the geometric models are most correct. Furthermore, it deals with scattering from a point,

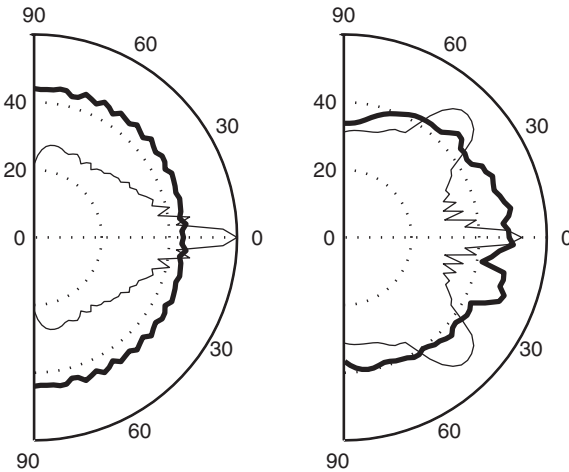


Figure 12.9 Some typical far field one-third octave polar response patterns for different surfaces. Left figure: — Plane surface; — Single semi-circle. Right figure: — Random rough surface; — Periodic diffuser.

which fits with the philosophy of most models. Lambert's law deals with high frequency incoherent scattering, but in acoustics the wavelength is often comparable to surface roughness. Indeed, diffusers such as Schroeder diffusers would not function as designed if the scattering was incoherent. In rooms, incoherence is not achieved, just complication. It is true to say, however, that at very high frequencies, the scattering from surfaces will approximate Lambert's law. At the key frequencies for room design, and for first order reflections, some believe that it is better to approximate the scattering from specialist diffusers according to a uniform energy distribution rather than Lambert's law in geometric room acoustic models.

There is a further problem with Lambert's law with single plane diffusers. Single plane diffusers produce dispersion in one plane and are very common in spaces: pipe work, balcony fronts, 1D Schroeder diffusers, columns, etc. Yet most current computer models disperse reflections according to Lambert's law, scattering the sound in all directions over a hemisphere. This has the potential to cause prediction errors, again particularly acute for the early sound field. It might be thought that this prediction inaccuracy is less important for the later sound field, and indeed the averaging effect of multiple numerous reflections probably makes the model less sensitive to incorrect modelling of the reflections. In recent years, however, attention has been drawn to the importance of late lateral energy in auditoria [34] and the role of spatial impression. Consequently for a correct auralization of large music spaces, it may be important to correctly model the spatial distribution of late sound, and correct modelling of anisotropic scatterers is probably needed to achieve this.

12.4.7 Scattering coefficients

In Chapter 4, methods for measuring and characterizing the scattering from surfaces were given, including characterization in terms of a scattering coefficient. It is intended that this coefficient should be used as an input to geometric room acoustic models. At the time of writing, the success of the new scattering coefficient appears to be mixed, with some suggesting that it works well within geometric room acoustic models, and others reporting problems. Hopefully, over the next few years, as the scattering coefficient becomes more established, the position will be clarified.

Gomes and Gerges [30] found that errors greater than 20 per cent in early decay time can occur if the scattering coefficients are incorrect, and 30 per cent if the absorption coefficients are incorrect. In contrast, Nijs *et al.* [15] found that varying scattering coefficients had relatively small effect on predicted levels (3–4 dB) in a complex coupled set of rooms, although Summers [22] has questioned whether diffraction can be so insignificant in the coupled rooms modelled.

In the past, there has not been a defined way to gain scattering coefficients for surfaces, so researchers have adopted an empirical approach to investigations. They have examined what scattering coefficients are needed to gain accurate predictions in rooms by a trial-and-error process. The results from these investigations are presented below, as they give some guidelines as to what scattering coefficients might be used. One problem with getting the correct scattering coefficient this way, however, is the interrelationship between the absorption and scattering coefficients used in the geometric model, and the predicted acoustic parameters. The reverberation time predicted in a space will depend on both the absorption and scattering coefficients. The effect is most marked for disproportionate spaces or ones where the absorption is

unevenly distributed. It is not correct, therefore to determine the scattering coefficient by simply adjusting the reverberation time prediction until it matches measurement, as there is usually considerable uncertainty as to what the absorption coefficient of surfaces should be and this also affects reverberation time.

As the theoretical basis of different methods of modelling diffuse reflections is not the same, it is likely that different prediction models will require different values of the scattering coefficient even for the same wall under the same room conditions. Lam [33] investigated the scattering coefficients required for three different diffuse modelling algorithms, using scale models with largely smooth walls. In simple proportionate rooms, where the room dimensions are comparable, the predictions were similar whatever the method of modelling diffuse reflections and the scattering coefficient used. In a highly disproportionate room, however, the scattering coefficient required to gain accurate results varied with the diffuse reflection modelling algorithm. The required scattering coefficient varied between 0.25 and 1 for the three geometric models considered. It was also found that different scattering coefficients were required to give accurate predictions of different acoustic parameters within the same prediction model. Out of the three models tested, the models presented in Sections 12.4.2 and 12.4.3 were most robust and so were favoured by Lam.

Lam further investigated the effect of scattering coefficients in a concert hall. The trend with scattering coefficients is that going from a zero coefficient to a low value, say $s=0.1$ or 0.2 , can make a large difference to predicted acoustic parameters. Increases in the scattering coefficient from these low values create a much smaller effect [33]. Consequently, the sensitivity of the scattering coefficient to affect volumetric acoustic parameters is not linear. Figure 12.10 shows the early lateral energy fraction (ELEF) for different scattering coefficients in a real concert hall. Measurements are compared with various predictions. The difference limen for ELEF is about 0.075 [35], so differences bigger than this value are significant. ELEF is chosen because it is probably the parameter most affected by the diffuse reflection modelling

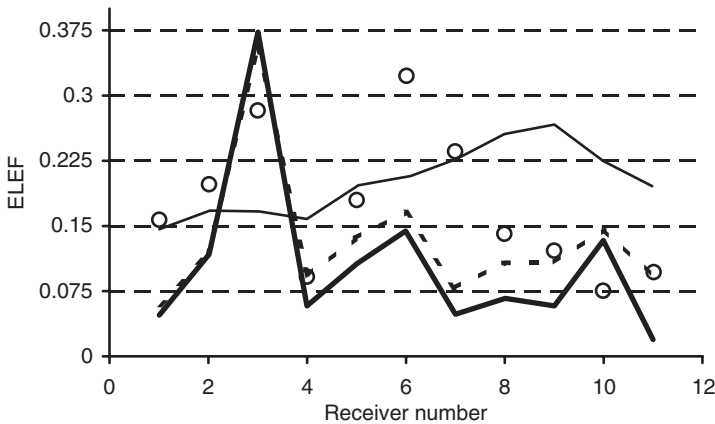


Figure 12.10 Variation of early lateral energy fraction (ELEF) with different scattering coefficients. The horizontal grid lines are spaced at the subjective difference limen. ○ Measured; — $s=0$; $s=0.1$ for walls, 0.7 for seats; — $s=1$ (after Lam [32]).

algorithm, as it depends purely on the early sound field. This shows that the predictions are sensitive to getting the correct scattering coefficients.

There will be cases, however, where accurate predictions cannot be achieved whatever the values of the scattering coefficients. This will be particularly noticeable for acoustic parameters which are very sensitive to the early sound field, such as clarity and early lateral energy fraction [16]. The early sound field contains only a few reflections, and consequently inaccuracies in the modelling of sound field are most apparent. These cases show that the diffraction effects present in real life reflections are far more complicated than the simple scattering assumed in geometric models – as already indicated by Figures 12.8 and 12.9. It is only by summing over a large number of reflections that the simple scattering assumptions can be regarded as valid approximations. Fortunately, in many situations there are enough reflections that inaccuracies tend to average out, but in some cases such as coupled rooms and under deep balconies this will not be true. Certainly, a geometric room acoustic model should not be used to evaluate first-order reflection paths, unless surfaces are simple large and planar or generate diffuse hemispherical dispersion.

Lam recommends that a good starting point for scattering coefficients at mid-frequencies is to set the value to 0.1 for planar walls, as the value remains largely constant at around 0.1 in rooms of sizes ranging from 5,000 to 30,000 m³ and shapes ranging from rectangular to hexagonal [32]. Certainly, the scattering coefficient should never be set to zero, because even with smooth walls edge diffraction is important. Nijs *et al.* [15] recommend lower scattering coefficients for plane walls of at most 0.02, although Summers [22] could not get accurate predictions using such a low value with a different geometric model. Dalenbäck [36] recommends 0.1–0.2 as a minimum value on all surfaces, except in very large planar surfaces where 0.08–0.1 is recommended.

Gomes and Gerges [30] found that in cases where early reflections are few, a higher scattering coefficient (as high as 1) can be used to improve the accuracy of the predictions of early decay time. In the lower frequency bands the correct scattering coefficient can change from 0.1 in smaller auditoria (volumes less than 10,000 m³) to over 0.4 in larger concert halls (volumes about 30,000 m³). A slight increase was also observed in models with more complicated shapes, but this is not great.

Lam set the scattering coefficient to 0.7 for seating [33], whereas Dalenbäck [36] recommends 0.4–0.7 for 125–4 kHz on audience areas. For generally rough surfaces, Dalenbäck suggests high values of 0.8 where the roughness is of the order of, or higher than the wavelength, and gradually lower below. For example, if the roughness scale is 0.3 m, set 0.8 for 1–4 kHz, 0.6 at 500 Hz, 0.3 at 250 Hz and 0.15 at 125 Hz. He notes that generally, there is greater risk associated with underestimating scattering coefficients than with overestimating them.

As an additional approach to estimating scattering coefficients, Dalenbäck suggests testing for the sensitivity to diffusion settings. This is done by calculating acoustic parameters with an initial reasonable guess of scattering coefficients, and with diffuse modelling switched off. The modeller can then examine if the resulting acoustic parameters differ substantially. If the parameters vary, then scattering coefficient has to be more carefully estimated, and it can be wise to include in the room design some options for final fine tuning of the reverberation time.

Appendix C gives a table of scattering coefficients for a variety of surfaces. These are correlation scattering coefficients calculated using a method outlined in Chapter 4.

These were calculated using a 2D boundary element model and so represent single plane surfaces such as cylinders. The use of the table values within a geometric model will take a little interpretation. It has already been shown that the scattering coefficient required in geometric models varies between different diffuse reflection modelling algorithms. One deficiency in the table data is the raised values for random incidence scattering coefficients at low frequencies. This arises because the scattering from the edge and the rear of the test sample is different from a flat surface; an empirical fix might be required to gain lower values at low frequencies. Furthermore, the predictions are for the plane of maximum scattering, whereas most diffuse reflection algorithms will interpret these values as being for hemispherically scattering devices and distribute the scattered energy according to Lambert's law. So, although the predictions were produced using single plane scatterers, they will probably be better matched to hemispherical scatter values in many geometric models. The values in the table for semicylinders will probably better match the required values for hemispheres; the table values for 1D Schroeder diffusers will probably better match the required values for 2D Schroeder diffusers. When modelling a single plane device (cylinder, 1D Schroeder diffuser), it may be necessary to reduce the scattering coefficient table values, if the geometric model distributes energy according to Lambert's law using a single scattering coefficient.

This section has summarized the current state of knowledge on using scattering coefficients in geometric models. There are many gaps in understanding and knowledge, and many problems still remain and need further research.

12.5 Summary

This chapter has presented some of the problems associated with going from isolated predictions or measurements of acoustic surface properties, to whole room predictions. It has considered the problems associated with the use of absorption coefficients in simple statistical models, as well as the role of absorption and scattering coefficients in geometric room acoustic models. The next and final chapter will look at how active technology can provide absorption and diffuse reflections.

12.6 References

- 1 H. Kuttruff, *Room Acoustics*, 4th edn, Spon Press (2000).
- 2 Y. Makita and T. Hidaka, "Comparison between reverberant and random incident sound absorption coefficients of a homogeneous and isotropic sound absorbing porous material – experimental examination of the validity of the revised $\cos \theta$ law", *Acustica*, **66**, 214–220 (1988).
- 3 ISO 354:1985, "Acoustics – measurement of sound absorption in a reverberation room".
- 4 T. W. Bartel, "Effect of absorber geometry on apparent absorption coefficients as measured in a reverberation chamber", *J. Acoust. Soc. Am.*, **69**(4), 1065–1074 (1981).
- 5 T. D. Northwood, "Absorption of diffuse sound by a strip or rectangular patch of absorptive materials", *J. Acoust. Soc. Am.*, **35**, 1173–1177 (1963).
- 6 Y. Makita, T. Hidaka, J. Kaku and J. Yoshimura, "Re-examination of the set of numerical values of the functions which the revised $\cos \theta$ law and the revised Paris' formula comprise", *Acustica*, Research note, **74**, 159–163 (1991).
- 7 M. C. Gomperts, "Do the classical reverberation time formulas still have the right to existence?", *Acustica*, **16**, 255–268 (1965).

- 8 A. M. Ondet and J. L. Barbry, "Modeling of sound-propagation in fitted workshops using ray tracing", *J. Acoust. Soc. Am.*, **85**(2), 787–796 (1989).
- 9 I. A. Drumm and Y. W. Lam, "The adaptive beam-tracing algorithm", *J. Acoust. Soc. Am.*, **107**(3), 1405–1412 (2000).
- 10 J. B. Allen and D. A. Berkley, "Image method for efficiently simulating small room acoustics", *J. Acoust. Soc. Am.*, **65**, 943–950 (1979).
- 11 H. Lee and B. Lee, "An efficient algorithm for the image model technique", *Appl. Acoust.*, **24**, 87–115 (1988).
- 12 M. Vorländer, "Simulation of the transient and steady-state sound propagation in rooms using a new combined raytracing/image-source algorithm", *J. Acoust. Soc. Am.*, **86**, 172–178 (1989).
- 13 U. Stephenson, "Comparison of the mirror image source method and the sound particle simulation method", *Appl. Acoust.*, **29**, 35–72 (1990).
- 14 M. Kleiner, B.-I. Dalenbäck and P. Svensson, "Auralization – an overview", *J. Audio. Eng. Soc.*, **41**(11), 861–875 (1993).
- 15 L. Nijs, G. Jansens, G. Vermeir and M. van der Voorden, "Absorbing surfaces in ray-tracing programs for coupled spaces", *Appl. Acoust.*, **63**, 611–626 (2002).
- 16 ISO 3382:1997, "Acoustics – measurement of the reverberation time of rooms with reference to other acoustical parameters".
- 17 W. C. Sabine, *Collected Papers on Acoustics*, Cambridge (MA), Harvard University Press (1922).
- 18 C. F. Eyring, "Reverberation time in 'dead' rooms", *J. Acoust. Soc. Am.*, **1**, 217–226 (1930).
- 19 S. M. Dance and B. M. Shield, "Modelling of sound fields in enclosed spaces with absorbent room surfaces. Part I: performance spaces", *Appl. Acoust.*, **58**, 1–18 (1999).
- 20 G. Millington, "A modified formula for reverberation", *J. Acoust. Soc. Am.*, **4**, 69–81 (1932).
- 21 J. Antonio, L. Godinho and A. Tadeu, "Reverberation times obtained using a numerical model versus those given by simplified formulas and measurements", *Acta Acustica united with Acustica*, **88**, 252–261 (2002).
- 22 J. E. Summers, "Comments on 'Absorbing surfaces in ray-tracing programs for coupled spaces'", *Appl. Acoust.*, submitted for publication (2002).
- 23 I. Bork, "A comparison of room simulation software – the 2nd round robin on room acoustical computer simulation", *Acustica*, **86**, 943–956 (2000).
- 24 M. Hodgson, "Evidence of diffuse surface reflections in rooms", *J. Acoust. Soc. Am.*, **89**, 765–771 (1991).
- 25 M. Vorländer, "International round robin on room acoustical computer simulations", *Proc. 15th ICA*, **II**, 689–692 (1995).
- 26 B.-I. Dalenbäck, "The importance of diffuse reflection in computerized room acoustic prediction and auralization", *Proc. IoA(UK)*, **17**, 24–34 (1995).
- 27 Y. W. Lam, "On the parameters controlling diffusion calculation in a hybrid computer model for room acoustics prediction", *Proc. IoA(UK)*, **16**(2), 537–544 (1994).
- 28 B. Dalenbäck, M. Kleiner and P. Svensson, "A macroscopic view of diffuse reflection", *J. Audio Eng. Soc.*, **42**, 793–807 (1994).
- 29 R. R. Torres and M. Kleiner, "Audibility of 'diffusion' in room acoustics auralization: an initial investigation", *Acustica/Acta Acustica*, **86**, 919–927 (2000).
- 30 M. H. A. Gomes and S. N. Y. Gerges, "On the accuracy of the assessment of room acoustics parameters using MLS technique and numerical simulation", *Acustica/Acta Acustica*, **86**, 891–895 (2000).
- 31 G. Naylor, "Treatment of early and late reflections in a hybrid computer model for room acoustics", *124th Acoust. Soc. Am. Meeting*, Paper 3aAA2, New Orleans (1992).

- 32 Y. W. Lam, “The dependence of diffusion parameters in a room acoustics prediction model on auditorium sizes and shapes”, *J. Acoust. Soc. Am.*, **100**, 2193–2203 (1996).
- 33 Y. W. Lam, “A comparison of three diffuse reflection modelling methods used in room acoustics computer models”, *J. Acoust. Soc. Am.*, **100**(4), 2181–2192 (1996).
- 34 J. S. Bradley, R. D. Reich and S. G. Norcross, “On the combined effects of early- and late-arriving sound on spatial impression in concert halls”, *J. Acoust. Soc. Am.*, **108**(2), 651–661 (2000).
- 35 T. J. Cox, W. J. Davies and Y. W. Lam, “The sensitivity of listeners to early sound field changes in auditoria”, *Acustica*, **79**(1), 27–41 (1993).
- 36 <http://www.rpginc.com/research/reverb01.htm>.

13 Active absorption and diffusion

The absorber and diffuser technologies discussed in previous chapters have difficulty with low frequency sound. Low frequency waves have long wavelengths, which means the absorbers and diffusers have to be large to perturb or absorb the wavefronts. This can be overcome to a certain extent by the use of resonant structures, most often used in bass absorber design, but in the recent years there has been growing interest in the use of active control technologies to absorb or diffuse low frequency sound.

Active control offers the possibility of bass absorption or diffuse reflections from relatively shallow surfaces, as well as the possibility of variable acoustics. An example application for active absorption is the control of modes in small rooms. The cost and difficulties of implementation are, however, considerable, and this is the major reason why this technology has not been more widely applied.

Active absorption has much in common with active noise control, indeed in many ways it is the same concept just re-organized behind a slightly different philosophy. Olson and May carried out pioneering active control experiments and they suggested an active noise control method based on interference [1]. In their method, an electro-acoustic feedback loop was used to drive the acoustic pressure to zero near an error microphone placed close to a secondary loudspeaker. This is illustrated in Figure 13.1.

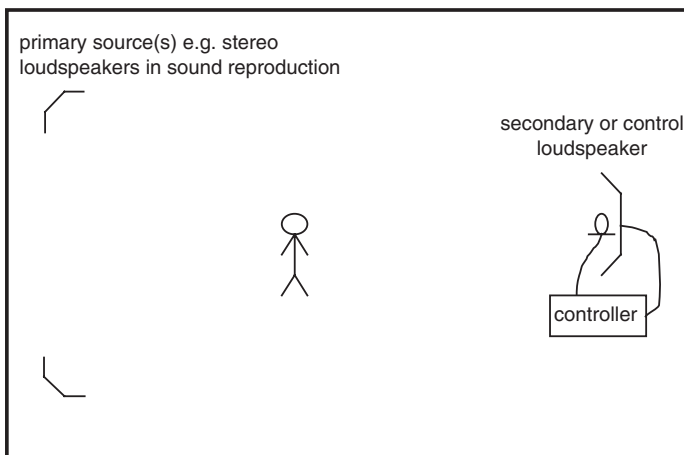


Figure 13.1 Schematic of active absorption in a small room. In this case, a microphone close to the secondary loudspeaker is used to provide an error signal for the controller to minimize.

This was the first active absorber. More sophisticated active absorption systems specifically alter the surface impedance of the control loudspeaker, towards a user-specified target value. They may be configured as feedforward or feedback devices and often constructed around single channel filtered-x LMS adaptive filter algorithms. Recent developments have moved away from the use of superposition (interference), and resistive material is used in combination with active controllers to gain actual dissipation. For instance, by using the active controller to maximize the particle velocity through the resistive material and so maximize absorption, this concept was also first suggested by Olsen and May [1].

13.1 Some principles of active control

In writing about this subject, it is necessary to go through some basic principles of active control, as it is assumed that many readers will not be familiar with concepts of adaptive filtering and active control.

The particular form of a control system is dictated by the physics of the environment in which it operates and the control task to which it is set. However, broad classifications of control systems exist which are useful in differentiating between certain very different approaches to the control problem. These classifications distinguish feedforward from feedback control systems, which may or may not be adaptive to changes in their operating environment.

Consider the system in Figure 13.2. The signal s is corrupted by the addition of the noise signal n at the first summing node, generating the observable signal d . At the second summing node, a signal y is subtracted from d . The result of this subtraction is the error signal, e .

- If $y = n$, then the noise corruption on the signal s is removed, $e = s$; this is the ideal.
- If y is a reasonable approximation of n , then some of the noise contamination is removed, $e \approx s$; this is more realistic of what happens with active control systems.
- If y is largely uncorrelated with n , then the second summing node represents an additional source of noise, further corrupting the signal s in e ; this is to be avoided.

The cancelling signal y is derived by filtering operations – through the filter block W which is an adaptive filter, i.e. a filter that can change its coefficients to achieve the required control – on the reference signal x . The optimal configuration of the adaptive

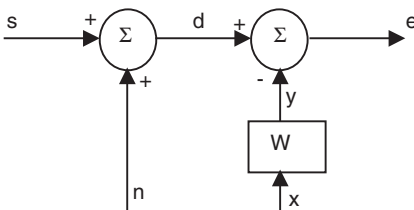


Figure 13.2 A basic active noise control system to remove noise n from signal s .

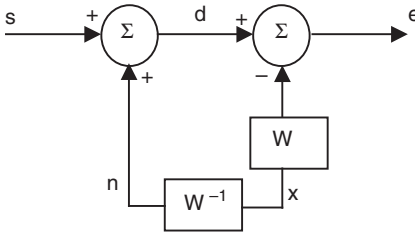


Figure 13.3 A basic active noise control system to remove noise n from signal s .

cancelling filter, W , is the inverse of the filter relating n to x . This case is illustrated in Figure 13.3 in which the transfer function e/s is seen by inspection to be 1. The noise added at the first summing node is perfectly cancelled at the second summing node. Such perfect performance is never achieved in practice for several reasons, most important among which are the imperfect implementation of the cancelling filter and the imperfect correlation between the noise n and the reference x .

Consider the problem of imperfect correlation. The attenuation of the noise component in d is a function of the coherence between noise and reference signal. The attenuation increases as the coherence increases, and useful levels of noise attenuation can only be achieved with high coherence between the reference and the noise signal; this can pose problems in electroacoustic applications.

Ideally, an analytical solution for the necessary filter W would be derived; however, computing the coefficients of the filter W is usually a non-trivial problem. Fortunately, a computationally efficient iterative approach to the identification of necessary filter coefficient exists; this is an adaptive filter running under the least mean square (LMS) algorithm.

The technique uses an iterative search process to find the filter W that minimizes the error e . The LMS algorithm discovered by Widrow and Hoff [2] has been found to be robustly stable in many practical applications. It is also a clear, simple and computationally efficient approach to identifying W . There are other techniques for solving minimization problems, but the LMS approach forms the basis of most contemporary adaptive noise cancelling systems.

The weights of the filter W are updated using the following equation. The coefficients of the adaptive filter at the $k + 1$ iteration is given by:

$$W_{k+1} = W_k + 2\alpha e_k x_k \quad (13.1)$$

where subscript k refers to iteration number, W_k is the vector of adaptive filter coefficients at iteration k , e_k the error at iteration k , α the update rate and x_k is input to the adaptive filter at iteration k .

The performance of the LMS algorithm is illustrated below by an example which is also supplied in the MATLAB script *simple_lms.m*. A simulation of a discrete time implementation of Figure 13.2 was coded, in which:

$$n_k = 0.5x_k + 0.2x_{k-1} \quad (13.2)$$

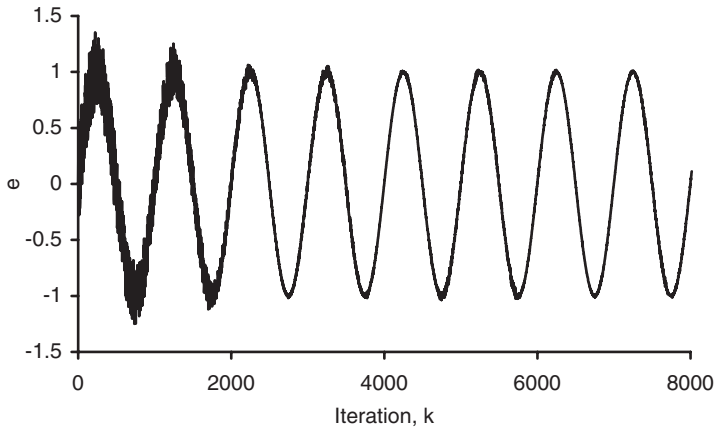


Figure 13.4 Removing noise from a sine wave using active control.

A length 2 adaptive filter W was updated using the LMS algorithm (Equation 13.1) in a signal environment in which s was a simple sinusoid and x a random process.

The error signal is shown in Figure 13.4. The initial noise is seen to be quickly cancelled leaving a pure sinusoidal wave, the signal s . The decay of the noise follows a roughly exponential form, which is due to the convergence behaviour of the LMS algorithm approximating the first-order convergence of a steepest descent algorithm.

The convergence of the two coefficients of the adaptive filter W is shown in Figure 13.5. The weights are seen to approach the optimal values implied by Equation 13.2. This is very similar to the system shown in Figure 13.2, except that the white noise signal is fed direct to x and then filtered to get the signal n .

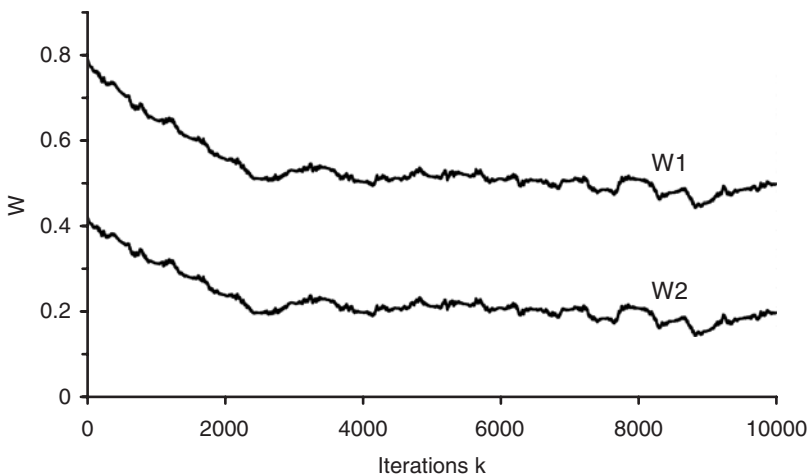


Figure 13.5 Filter coefficients for filter W during training.

Having studied some fundamentals of noise cancelling, it is now possible to consider the practicalities of active impedance systems.

13.2 An example active impedance system and a general overview

Figure 13.6 shows a possible feedforward controller for an active impedance system [3–6]. While there are other possible set-ups, this system allows some of the general principles to be explained. A signal generator is driving the primary source in the top left of the diagram. The role of the primary source is to generate acoustic waves for the controller to operate on. In the diagram shown, this is constrained within a pipe (shown dotted), but it could be within other spaces. The sound from the primary source then propagates to the control surface (secondary loudspeaker) shown top right.

The control surface is instrumented to sense pressure and velocity. Consequently, the impedance at the surface of the controller is known. Using an LMS algorithm, it is possible to alter how the control loudspeaker moves so that the surface impedance is some desired value.

The velocity v_k at the control surface is sensed by integrating the output from a miniature accelerometer mounted on the cone surface. An alternative technique would use two closely spaced microphones [7, 8]. The pressure is measured using a surface microphone. This pressure is then passed through the filter F_d . F_d is the desired admittance, and consequently, the signal d_k is the desired velocity. The desired and actual velocities are subtracted to give an error signal, e_k . If this error was zero, then the surface admittance is as desired. If the error is non-zero, then the LMS algorithm is used to change the weights of the adaptive filter W , to reduce the error. Consequently, there is an adaptation time over which the error gradually converges to a small value, preferably zero. Setting the correct value for the update rate given in Equation 13.1 is crucial to achieving training, too large a value and the system never converges, too small a value, and the convergence is very slow. There can be problems with instability during training.

The input to the adaptive filter is a signal x_k which must correlate with the primary source signal. The correlation is required otherwise all that the control surface will do

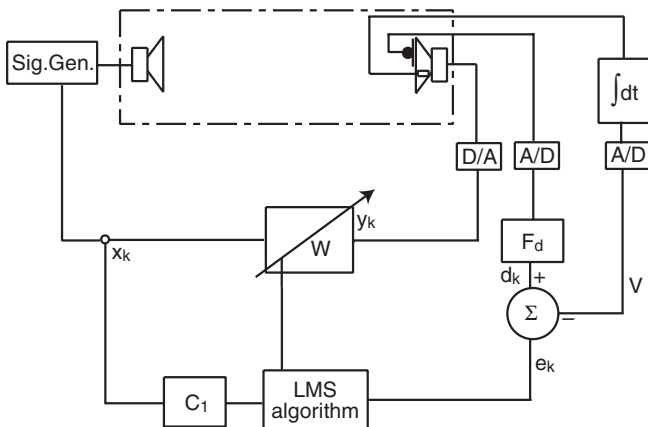


Figure 13.6 A feedforward active impedance control system.

is add additional noise. This signal can be derived from two places, forming either a feedback or feedforward system. In a feedforward case, the signal x_k is an electronic feed from the primary signal source. This is the case shown in Figure 13.6. The great advantage of feedforward is that it forms a stable system and no unstable feedback can occur. The disadvantage is that an electronic feed of the source signals is required, which means the active surface could be used with electroacoustic sound reproduction systems such as stereo systems but not sound production systems such as acoustic musical instruments or speech.

In the feedback case, a microphone picks up the signal from the primary source (Figure 13.7). This can actually be the miniature microphone on the surface of the control loudspeaker. With this system, however, there is potential for instability, as a loop is formed which will become unstable if the gain of the loop exceeds 1. The solution to this problem is to insert a feedback compensation filter F_1 which is designed to cancel the feedback path. The feedback cancellation is awkward; however, and if not entirely successful the system will go unstable. Alternatively, highly directional loudspeakers and microphones can be used to steer energy from the control source away from the microphone connected to the reference input, but performance is frequency dependent.

The usual system is to train the coefficients of the adaptive filter, and once the error is sufficiently low, to fix the coefficients. In this example, adaptation is used purely as an efficient method for obtaining the filter coefficients W which may not be analytically derivable.

In order that the impedance converges to the correct value, the measurements on which the control signal derivation is based must provide a true and accurate measurement of the actual ratio of pressure and particle velocity. Any error in these measurements will result in convergence to a value other than that desired by the user. Transduction will introduce non-flat frequency responses onto the signals; these components in the circuits will filter and change the signal response. The role of the plant model, C_1 , is to compensate for the frequency responses of the transducers and other components. The filter which models the plant is that referred to in the phrase ‘filtered-x’.

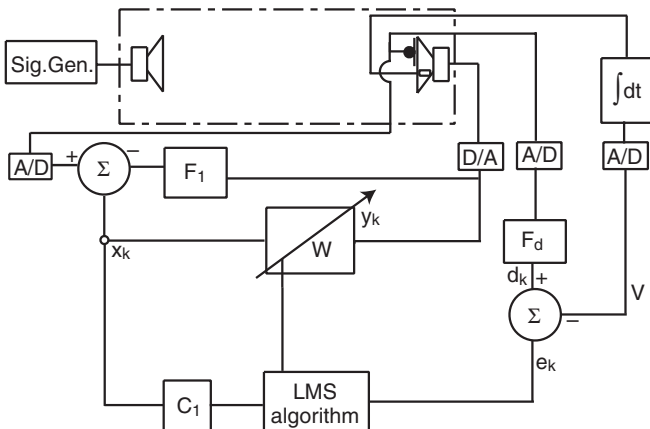


Figure 13.7 A feedback active impedance control system.

The design of the plant model presents significant problems. It may be sufficient to measure the frequency response of the plant off-line with a noise or impulsive test signal, and fit this with a finite impulse response (FIR) filter providing a reasonable estimate of the actual plant response. The accuracy of the plant model appears to determine whether or not convergence of the filter will be achieved, and over what timescale adaptation may take place without the risk of instability [9].

There is some tolerance of plant model errors, which is fortunate since the object of employing an adaptive active control system is to enable a controller to track changes in its environment during operation. Any such changes will introduce errors between the assumed and the current plant response. Where gross run-time alteration of the plant response is anticipated, a run-time measurement of the plant which continually updates filter C_1 may be employed. This has been attempted using maximum length sequence (MLS) signals at very low levels presented simultaneously with program material [10]. Eriksson also reports techniques for on-line modelling [10].

In fact, while people may refer to the active absorption systems as adaptive, this is a rather misleading name in many cases. The system might be adaptive during the training of the system, but are most often used with the adaptation turned off, to do otherwise risks instability in operation. But without adaptation ability, the system is vulnerable to changes in the physical acoustics such as temperature changes and room occupancy.

A theoretical analysis of the significance of transduction errors for active impedance control in a 1D waveguide is presented by Darlington *et al.* [11], along with measured results derived from the intentional perturbation of pressure and velocity control signals. It is concluded that the transducers and associated signal-conditioning circuits should be calibrated to within 1 dB magnitude error and 5° phase error in order to achieve better than 95 per cent acoustic absorption. This analysis is helpful in that it identifies the significance of transduction errors, but a discussion of the measurement method itself and its relation to a theoretically modelled ratio of pressure and velocity at the surface of a loudspeaker cone is not attempted. This relationship is important in two ways.

Physical measurements of the impedance at the loudspeaker cone depend on two factors – the correct transduction of cone velocity and a suitable measurement of the pressure at the cone surface. Velocity measurement can be done via a two-microphone method or an accelerometer, but the position of the accelerometer is shown to be crucial. Nicholson reports [3] that at frequencies as low as 150 Hz, significant differences appear in the magnitude and phase of velocity between accelerometers mounted at different points on the cone, as the local mass load encourages the onset of non-piston motion. Accelerometer locations where the dust cap meets the cone are most suitable. Nicholson also investigated microphone locations immediately adjacent to the control source cone and found that a frame mounting 5 mm from the dust cap was best. It is important that the microphone does not pick up the effects of the cone vibration (the velocity) as otherwise the system becomes unstable.

Having given some sense of how an adaptive system might work in principle, the following sections detail the application of these types of controllers.

13.3 Active absorption in ducts

When the system described in Section 13.2 is constrained to one-dimensional plane waves, the controller is very successful. This would be the case for low frequency

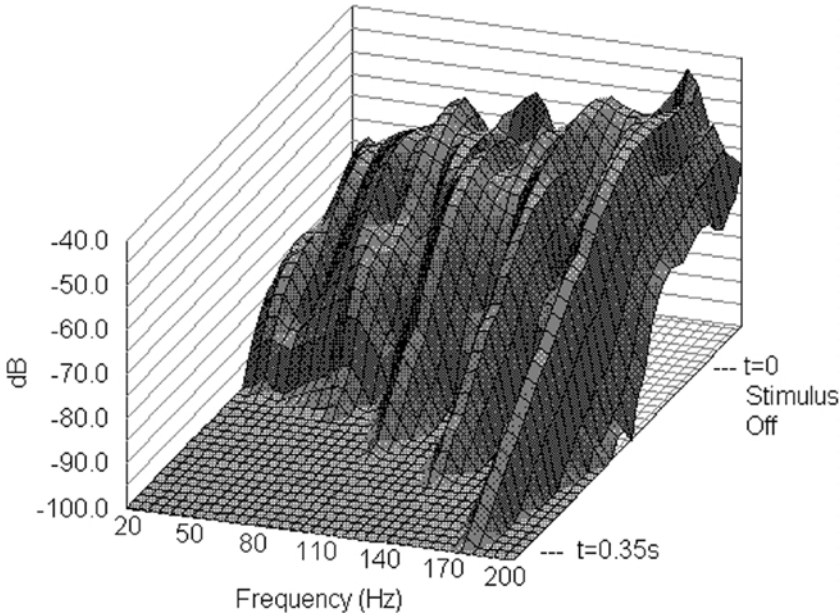


Figure 13.8 Waterfall plot of decay of modes in a 4 m duct, controller off (after Avis [5]).

control within ducts. Figure 13.8 shows the modes in a duct with the controller turned off (so the termination is the control loudspeaker, which is not being driven, the termination impedance being dictated by the mechanical characteristics of the loudspeaker). The plot shows the steady state response ($t = 0$) and the resulting decay when the primary source is turned off. Figure 13.9 shows the same situation but with the controller in operation. The ability of the controller to add damping to the modes and therefore make them decay faster is evident. The active absorber in this case had been trained to achieve an impedance equal to the characteristic impedance of air for plane waves.

13.4 Active absorption in three dimensions

It is possible to train the active absorber in a duct to a characteristic impedance, turn the adaptation off, and then use the system within a room. Unfortunately, in this case only small reductions in pressure are obtained. The controller surface does achieve high absorption coefficients. Furstoss *et al.* [12] report absorption coefficients of about 0.9, but the area over which this absorption is achieved is only in the region of the loudspeaker cone. Consequently, while a high absorption coefficient is achieved, the total absorption added to the room is small and so the effect on the room is small.

In a 3D environment, the relationship between the control source surface impedance and the modal behaviour of the room is not simple. The sound field in the room is not plane, although it can be considered to result from the sum of a number of

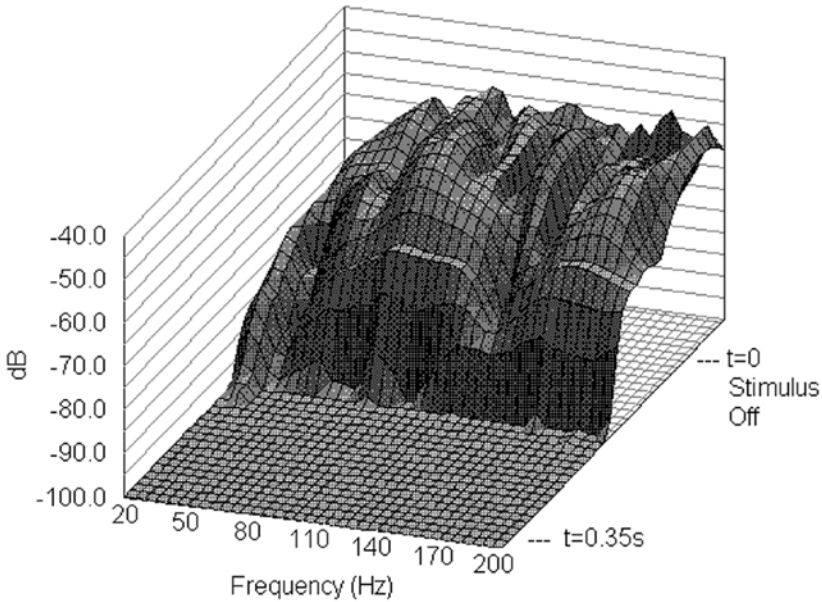


Figure 13.9 Waterfall plot of decay of modes in a 4 m duct, controller on (after Avis [5]).

normal modes which individually are plane waves [13]. There exist three orthogonal coordinate axes for particle velocity rather than the single axis within the duct, and the velocity of the controlling driver may lie in the plane of one coordinate or perhaps none of the three. The meaning of a characteristic impedance is therefore no longer clear, and hence it follows that the characteristic impedance solution for the duct is unlikely to result in optimal control of the modal behaviour of the room. Consequently, a different target function is required. For instance, it might be possible to train the system to minimize the pressure at one or more points in a room. This is then a traditional active control system, and more on these can be found in Nelson and Elliot [14].

Alternatively, it is possible to consider the relationship between surface pressure and velocity in terms of the power radiated by the source. It can be shown that in certain circumstances the power radiated becomes negative, corresponding to absorption of energy by the source. When a pistonic sound source radiates acoustic power at low frequency, the power radiated is proportional to $p\nu^*$, where ν is the velocity, p the total pressure and $*$ indicates a complex conjugate. If the velocity of the source can be controlled to minimize the power radiated, which is equivalent to maximizing the ingoing intensity, the source is then absorbing acoustic power. This has, however, rather simplified the situation, as the pressure across the cone is not constant, and the total pressure at the cone will contain direct and reflected components from primary and secondary sources. The risk with maximizing the ingoing intensity is that the controller will achieve this by maximizing the pressure, and so the sound pressure levels within the room will increase. For this reason, this control target is rather problematical.

Another problem with this system is that there is no energy dissipation. The active absorption is generated by superposition or interference. In effect, the active control system works by changing the radiation impedance of the primary and secondary sources in the room rather than by absorbing energy from waves radiated by the primary source. Consequently, what these active absorption systems achieve is a reduction in radiated power [15]. To really achieve, absorption requires a proper dissipation mechanism – this can be achieved through hybrid designs discussed in Section 13.5. In the following two sections, however, some experimental results from modal control using adaptive and non-adaptive techniques are presented.

13.4.1 *Low frequency modal control – example results*

Consider the system described in the previous section. This system will be used to try and deal with low frequency modes that are present in a room. Figures 13.10 and 13.11 compare the pressure distribution of the primary axial mode in a room with the controller on and off. In this example, the controller reduces the steady state pressure in the mode by about 6 dB. In this case, a single 8 inch loudspeaker is capable of almost halving the decay time of the first axial mode, which is at ≈ 44 Hz.

These systems work for single modes well isolated in frequency. As soon as modes become degenerate, the active controller has problems. If many modes need to be controlled, many control loudspeakers need to be used. There is probably a need for one control loudspeaker per mode. Consequently, a full control system is going to be expensive to implement.

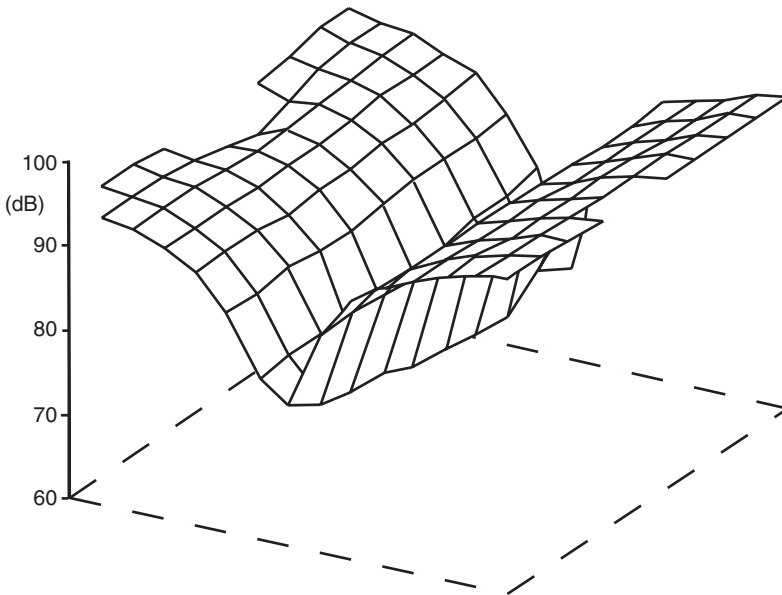


Figure 13.10 Distribution of pressures in a small room for the main axial mode (about 44 Hz). Controller off (after Avis [5]).

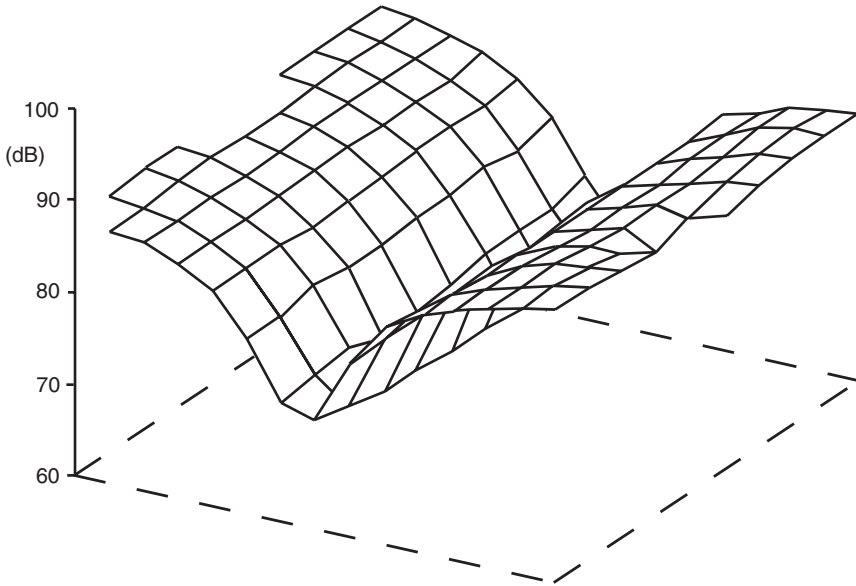


Figure 13.11 Distribution of pressures in a small room for the main axial mode (about 44 Hz). Controller on (after Avis [5]).

13.4.2 Low frequency modal control – alternative control regime

Adaptive systems incur significant cost, both in terms of hardware and in terms of constraints on operation due to stability and convergence issues. This has motivated several authors to look for other non-adaptive control regimes for modal control [16–19]. Below is a short description of one of these. Avis [17] examined an analytical modal decomposition to derive a control filter which acts to reduce the modal quality factor by the user-defined relocation of system poles. The aim was to go further than conventional steady state equalization, since the psychoacoustic cues for the detection of resonance have been shown to be related to time domain rather than frequency domain modal artefacts [20]. Additionally, this has potential for controlled equalization across the whole sound field.

A standard expression for the sound field in a room is in terms of a modal decomposition [21]. The modal decomposition implies that the sound field may be considered as the sum of a large number of second-order functions; these functions can be implemented as infinite impulse response (IIR) biquad filters. The coefficients of these filters are determined by fitting responses to measurements in the physical sound field. Figures 13.12 and 13.13 show an example of the fitting of magnitude and phase for two modes in a small room.

A secondary source is used to radiate pressures, which combine with the natural sound field of the room to generate modes with smaller Q factors, i.e. ones that decay faster. Figures 13.14 and 13.15 show a typical result. The controller is formulated such that the poles of the controlled sound field are relocated further away from the unit circle than the uncontrolled case. The controller works well at the measurement

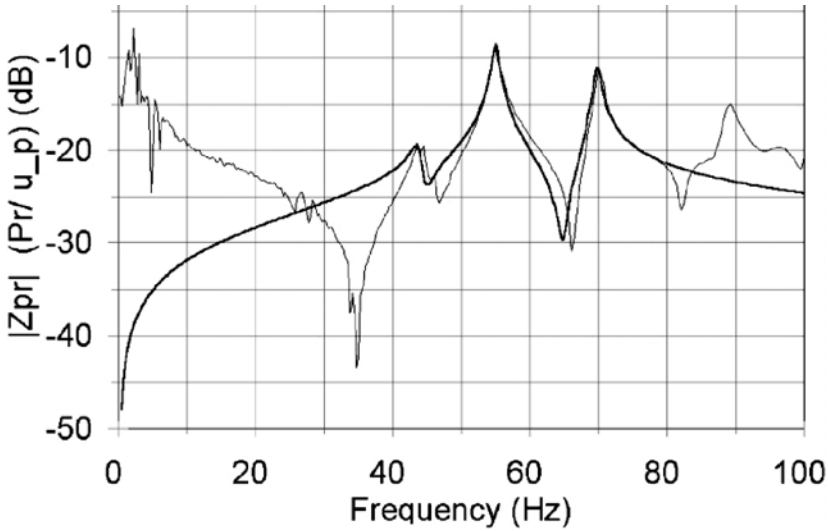


Figure 13.12 Example fitting of measured magnitude of modal response (————) to biquad model (————) (after Avis [17]).

point used to fit the IIR filters, but operates less effectively at locations remote from that point.

This system can be used to control multiple modes simultaneously. Because the control technique mimics the action of the addition of damping, the time, frequency and spatial aspects of the modal nature of the sound field are all addressed simultaneously and in

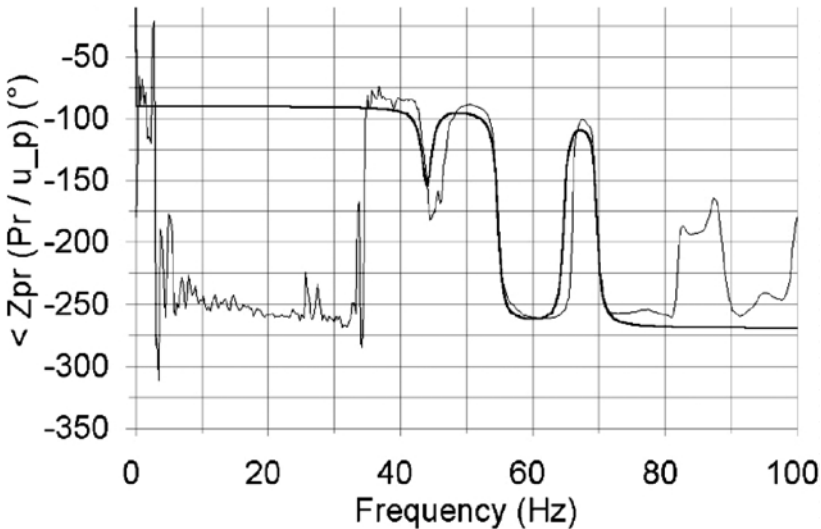


Figure 13.13 Example fitting of measured phase of modal response (————) to biquad model (————) (after Avis [17]).

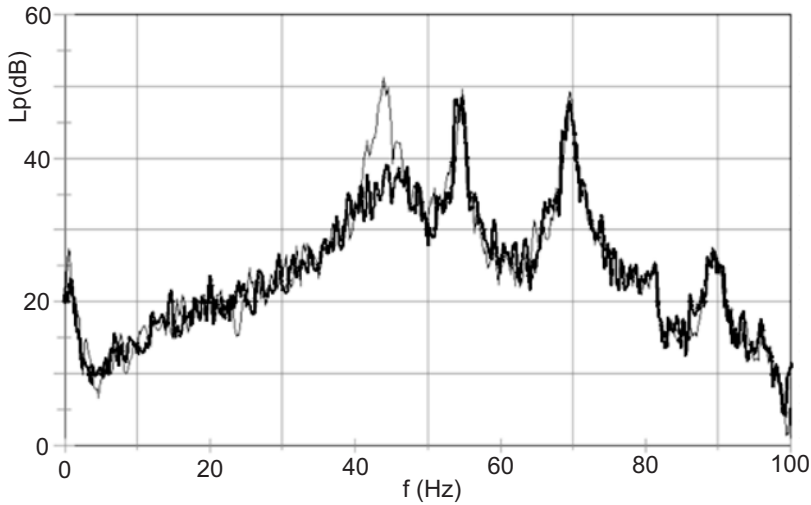


Figure 13.14 Effect of biquad controller designed for a single mode at 44 kHz (after Avis [17]).

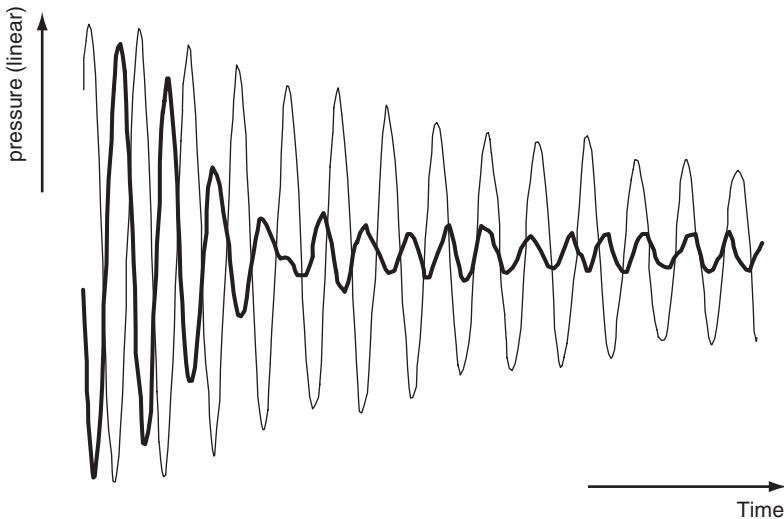


Figure 13.15 Effect of biquad controller designed for a single mode at 44 kHz (after Avis [17]). — Controller off; — Controller on.

sympathy. The effectiveness of control is again limited to situations where the modes are widely spaced and not degenerate. The sensitivity of this control regime to changes in room conditions is unknown. Presumably it would be necessary to regularly recalibrate the system for the damping to remain efficient.

13.5 Hybrid active–passive absorption

The above adaptive systems have not had explicit dissipation mechanisms included; they have worked by a process of interference or superposition. It makes sense to try to include some form of real resistance as better performance can be achieved. Consequently, this is a hybrid approach involving the combination of absorbent material with an active controller. Indeed, Olson and May [1] considered the possibility of using their secondary loudspeaker to absorb sound by placing it behind acoustically resistant cloth and to use the active controller to maximize the dissipation of energy in the cloth. A concise summary of the development of the hybrid approach is given by Smith *et al.* [22].

Furstoss *et al.* [12] picked up the hybrid concept in the 1990s and made it into a useable device. It is mostly their work which is reported below. A piece of resistive material is placed in front of the active element, and the absorber is made efficient by creating a virtual quarter wavelength resonator behind (as though the resistive material is a quarter of a wavelength from a rigid wall). A typical set-up is shown in Figure 13.16. In the example shown, the surface of the control loudspeaker is instrumented to measure velocity and pressure, and this is used as inputs to an active controller, which drives the control loudspeaker. The controller is tasked with setting the appropriate backing impedance condition. The active control system avoids the need for a large air gap as would be required for a passive resonant absorber at low frequency. Furthermore, it can produce broadband efficiency rather than the limited bandwidth achieved by the passive quarter wave resonant absorbers.

At low frequency the pressure drop across the resistive material can be given by the flow resistivity and particle velocity:

$$\frac{p_2 - p_1}{\nu} = \sigma d \quad (13.3)$$

where p_2 and p_1 are the pressures at the front and the rear of the resistive material, ν the particle velocity, σ the flow resistivity, and d the material thickness.

If the active element renders the backing pressure to be zero (like a quarter wavelength tube), the impedance of the layer is:

$$z = \frac{p_2}{\nu} = \sigma d \quad (13.4)$$

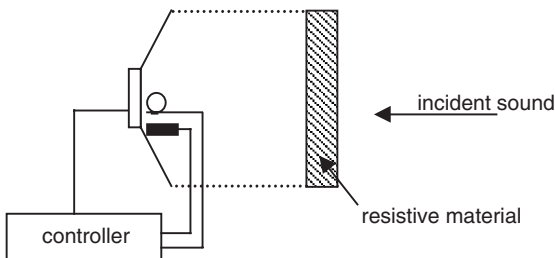


Figure 13.16 A hybrid active–passive absorber.

This is the flow resistance of the resistive material, which should be set to the characteristic impedance to maximize absorption.

Therefore, an alternative set-up to Figure 13.16 is to place a microphone at the rear of the porous material, and a controller is then tasked with minimizing the pressure at microphone. Figure 13.17 shows the results from such an arrangement. High absorption across a relatively wide frequency range is achieved. Absorption is not as high for oblique incident sound, averaging around 0.6–0.7 for an angle of incidence, $\psi = 60^\circ$, because for that case the optimal backing pressure for maximum absorption is no longer zero – see below. When used in an array of active absorbers, good performance is achieved although transduction problems currently limit the useful frequency range to 1 octave around 280 Hz.

While this above regime works for low frequencies, this anechoic termination becomes less successful as the frequency increases. Furstoss *et al.* [12] showed that a better termination criteria is obtained by considering the optimal backing impedance more completely. Consider a porous layer between two fluids as shown in Figure 3.18. The impedance at the front face can be found using the transfer matrix approach described in Chapters 1 and 5. The impedance at the back face is:

$$z_b = \frac{z_c k}{k_x} \cdot \frac{-jz_f \cot(k_x d) + z_c k/k_x}{z_f - jz_c k/k_x \cot(k_x d)} \quad (13.5)$$

where z_f is the impedance on the front face and k_x is the component of the wavenumber in the porous layer in the x -direction (which can be found from Equations 5.9 and 5.10). The wavenumber k and characteristic impedance z_c in the porous medium can be found using the porous absorber models given in Chapter 5. By considering

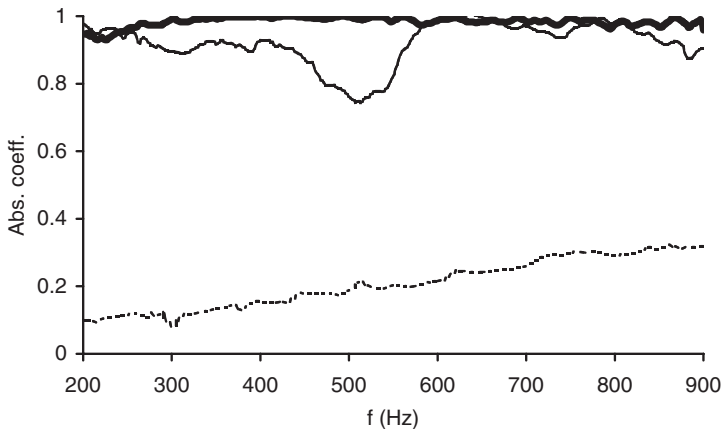


Figure 13.17 Absorption coefficient for a resistive material with and without an active controller backing minimizing the pressure at the rear of the material. The distance r refers to the distance of the microphone from the centre of the control loudspeaker. Material with rigid backing; — Hybrid absorber, $r=10$ cm; — Hybrid absorber, $r=0$ cm (after Furstoss *et al.* [12]).

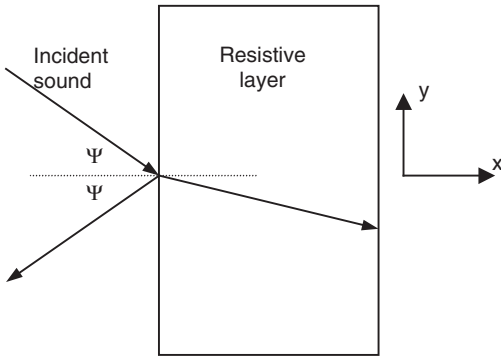


Figure 13.18 Geometry under consideration when determining optimal backing impedance for hybrid active-passive absorption.

Equation 13.5, the optimal backing impedance for maximum absorption can be found for a particular angle of incidence by setting $z_f = p_0 c_0 / \cos(\psi)$.

Figure 13.19 shows the optimal backing impedance for a particular situation, where the porous material is offering a resistance close to $p_0 c_0$. At low frequency, the optimal backing impedance is zero similar to a zero pressure condition, as indicated before, but as the frequency increases, the optimal backing impedance also changes. It will also change with the porous material's resistance and the angle of incidence. Consequently, minimizing the backing pressure does not necessarily produce optimal absorption, although in the case shown it will be fairly effective below 1 kHz. This impedance matching approach requires pressure and velocity transducers on the active control surface.

Smith *et al.* [22] compared the impedance matching exemplified by Equation 13.5 and pressure release control conditions. They found that the impedance matching approach was superior, requiring less control effort and achieving higher absorption coefficients. Absorption coefficients ranged from 0.8 to 1 from 100 to 1 kHz.

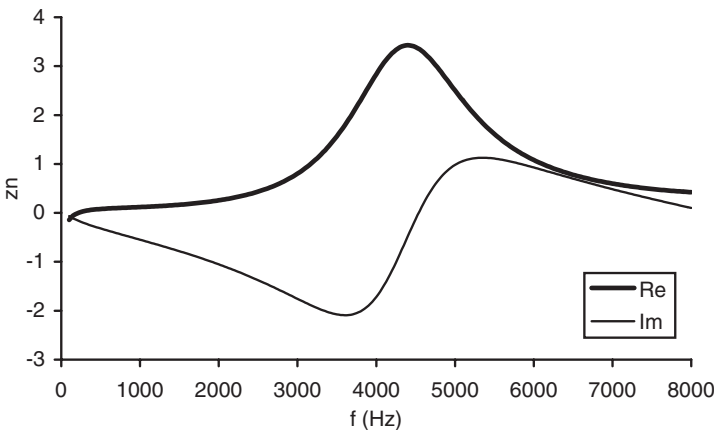


Figure 13.19 Optimal normalized backing impedance for a hybrid active-passive absorber.

An alternative approach to hybrid absorption was developed by Guigou and Fuller [23]. They used a smart foam design which integrated a lightweight distributed piezoelectric PDVF actuator – the active component – between individual layers of sound absorbing foam – the passive component – such that the control can efficiently operate over a broad range of frequencies. The foam providing absorption passively at high frequencies, and the active element in collaboration with the foam providing absorption at low frequencies. In this case, the active surface is being used to reduce the radiated power from a vibrating surface.

13.6 Active diffusers

Although passive diffusers have found a wide range of applications, difficulties arise due to non-acoustic constraints. For example, the space available for diffusers is usually limited. To achieve diffuse reflections, a passive diffuser must be significantly deep compared to the wavelength of sound, and at low frequencies building space costs generally limit the depth of the diffuser and the performance is compromised. An active device offers the possibility of producing a diffuser that works at a lower frequency from a given available depth when compared to a passive device.

Another limitation in diffuser design comes from the visual requirements set by interior designers or architects [24]. A good diffuser must be a unified part of the architectural design, rather than an obvious add-on. While it is possible to achieve rough surfaces that are pleasing to many, there is an appeal in having a flat surface that creates diffuse reflections. Potentially, active surfaces could form surfaces that appear to be visually flat and uniform, but are actually dispersing sound. A final advantage that an active surface has over a passive device is that variability can be easily achieved. Many rooms have to be multi-purpose, and active elements have the potential to enable the acoustics of a space to be changed.

The structures and control regimes described for active absorbers can be adapted to make active diffusers. Instead of absorption, the surface will aim to break up wavefronts and so create dispersion without adding damping. This work is currently in its early stages [25], so only concepts are presented here.

Figure 13.20 shows a possible structure for actively diffusing surfaces. A Schroeder diffuser profile is used with active elements substituting for one or more of the wells.



Figure 13.20 Artist's impression of an active diffuser (after Cox *et al.* [25]).

Passive Schroeder diffusers break up the reflected wavefront using phase changes. These phase changes are introduced by the wells of differing length on which the sound is incident – plane waves propagate within the wells and take different times to propagate up and down the wells because of the different depths. Consequently, the simplest model for an active diffuser uses the active elements to produce additional low frequency dispersion by controlling the well termination impedance to simulate a deeper well.

A Schroeder style device is appealing for many reasons as the active element is constrained within a pipe, simplifying the modelling and measurement of termination impedance. Only plane wave radiation and propagation needs to be considered at the frequencies of interest. The disadvantage is that the surface is always going to look like a diffuser.

The high frequency diffusion is provided by the passive elements in the Schroeder diffuser, and the active elements deal with the low frequencies. There is a complementary relationship between the passive and active elements, as there was with hybrid active absorbers, which is again exploited.

Initial simulations of the active diffuser using the control structures shown in Figures 13.6 and 13.7 have investigated the use of an active diffuser to replace the longest wells within a Schroeder diffuser. The task of the active elements is to make the wells look longer than they physically are. Consequently, the desired admittance will be a $j \tan(kd)$ function, where k is the wavenumber and d the additional depth required for the active well. As this function has a series of singularities within it, it is necessary to introduce a small amount of resistance to make the filter F_d in Figure 13.6 or 13.7 stable.

Figure 13.21 shows a simulation of the diffusion coefficient for a passive diffuser, and an active diffuser where the deepest wells have been replaced by shorter active wells, very similar performance is achieved. Many practical problems associated with the active diffuser still remain to be overcome.

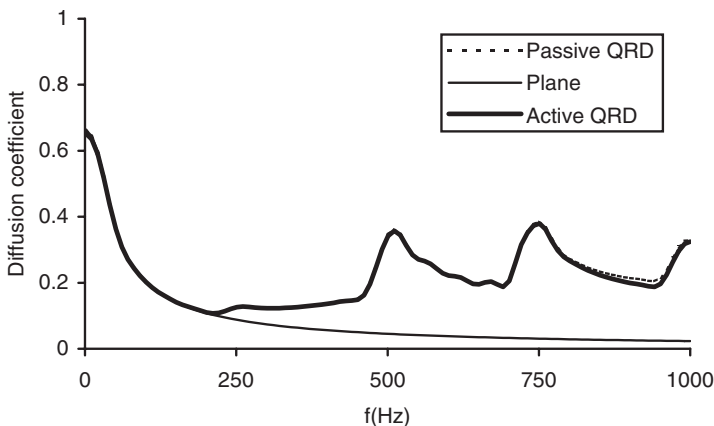


Figure 13.21 The diffusion coefficient from an active and passive diffuser, and a plane surface. For most frequencies, the passive and active diffuser results are the same and the lines overlay each other (after Cox *et al.* [25]).

13.7 Summary

This chapter has discussed the use of active elements to achieve improved absorption or greater dispersion. The main advantage of active control is that it overcomes the need for large passive surfaces which are needed at low frequencies where sound wavelengths are long. Unfortunately, the cost and practical difficulties associated with this technology have meant that its use is not widespread. Some believe, however, that active systems are the future of low frequency absorber and diffuser technology.

13.8 References

- 1 H. F. Olson and E. G. May, "Electronic sound absorber", *J. Acoust. Soc. Am.*, **25**, 1130–1136 (1953).
- 2 B. Widrow and S. D. Stearns, *Adaptive Signal Processing*, Prentice Hall, Englewood Cliffs (1985).
- 3 G. C. Nicholson and P. Darlington, "Active control of acoustic absorption, reflection and transmission", *Proc. IoA(UK)*, **15**(3), 403–409 (1993).
- 4 G. C. Nicholson, "The Active Control of Impedance", PhD thesis, University of Salford, UK (1995).
- 5 M. R. Avis, "The Active Control of Low Frequency Room Modes", PhD thesis, University of Salford, UK (2000).
- 6 G. C. Nicholson and P. Darlington, "Smart surfaces for building acoustics", *Proc. IoA(UK)*, **13**(8), 155–164 (1991).
- 7 F. Orduna-Bustamante and P. A. Nelson, "An adaptive controller for the active absorption of sound", *J. Acoust. Soc. Am.*, **91**, 2740–2747 (1992).
- 8 J. Y. Chung and D. A. Blaser, "Transfer function method of measuring in-duct acoustic properties", *J. Acoust. Soc. Am.*, **68**, 907–921 (1980).
- 9 C. C. Boucher, S. J. Elliot and P. A. Nelson, *The Effects of Modelling Errors on the Performance and Stability of Active Noise Control Systems*, Recent Advances in Active Control of Sound and Vibration, Virginia State University, Technomic Publ. (291–301).
- 10 L. J. Ericksson and M. C. Allie, "Use of random noise for on-line transducer modelling in an adaptive active attenuation system", *J. Acoust. Soc. Am.*, **85**(2), 797–802 (1989).
- 11 P. Darlington, G. C. Nicholson and S. E. Mercy, "Input transduction errors in active acoustic absorbers", *Acta Acustica*, **3**, 345–349 (1995).
- 12 M. Furstoss, D. Thenail and M. A. Galland, "Surface impedance control for sound absorption: direct and hybrid passive/active strategies", *J. Sound Vib.*, **203**(2), 219–236 (1997).
- 13 H. Kuttruff, *Room Acoustics*, 4th edn, Spon Press (2000).
- 14 P. A. Nelson and S. J. Elliott, *Active Control of Sound*, Academic Press (1993).
- 15 R. D. Ford, "Where does the power go?", *Proc. 11th ICA*, **8**, 277–280 (1983).
- 16 P. Herzog, A. Soto-Nicola and F. Guery, "Passive and active control of the low-frequency modes in a small room", *Proc. Audio Eng. Soc.*, *98th Convention*, Paris, preprint 3951(D1) (1995).
- 17 M. R. Avis, "Q-factor modification for low-frequency room modes", *Proc. Audio Eng. Soc.*, *21st Conference*, St Petersburg (2002).
- 18 J. Mourjopoulos, "Digital equalisation of room acoustics", *J. Audio Eng. Soc.*, **42**(11), 884–900 (1994).
- 19 Y. Haneda, S. Makino and Y. Kaneda, "Multiple-point equalisation of room transfer functions by using common acoustical poles", *IEEE Transactions on Speech and Audio Processing*, **5**(4), 325–333 (1997).
- 20 S. E. Olive, P. L. Schuck, J. G. Ryan, S. L. Sally and M. E. Bonneville, "The detection thresholds of resonances at low frequencies", *J. Audio Eng. Soc.*, **45**(3), 116–127 (1997).

- 21 P. M. Morse and K. U. Ingard, *Theoretical Acoustics*, McGraw-Hill, 555–572 (1968).
- 22 J. P. Smith, B. D. Johnson and R. A. Burdisso, “A broadband passive–active sound absorption system”, *J. Acoust. Soc. Am.*, **106**(5), 2646–2652 (1999).
- 23 C. Guigou and C. R. Fuller, “Adaptive feedforward and feedback methods for active/passive sound radiation control using smart foam”, *J. Acoust. Soc. Am.*, **104**(1), 226–231 (1998).
- 24 T. J. Cox and P. D’Antonio, “Holistic diffusers”, *Proc. IoA(UK)*, **21**(6), 201–206 (1999).
- 25 T. J. Cox, M. R. Avis and L. Xiao, The potential for room acoustic active diffusers, Forum Sevilla (2002).

Appendix A

A.1 Table of absorption coefficients

Material	Frequency (Hz)					
	125	250	500	1000	2000	4000
<i>Curtains or drapes</i>						
Light velour 0.338 kg/m ² hung straight in contact with wall [1]	0.04	0.05	0.11	0.18	0.30	0.35
Medium velour 0.475 kg/m ² , hung straight [1]	0.05	0.07	0.13	0.22	0.32	0.35
Medium velour 0.475 kg/m ² , draped to half area [1]	0.07	0.31	0.49	0.75	0.70	0.60
Heavy velour 0.61 kg/m ² , hung straight [1]	0.05	0.12	0.35	0.48	0.38	0.36
Heavy velour 0.61 kg/m ² , draped to half area [1]	0.14	0.35	0.55	0.77	0.70	0.60
<i>Variation with draping</i>						
Hung straight [2]	0.04	0.16	0.19	0.17	0.20	0.25
Draped to half area [2]	0.15	0.25	0.30	0.28	0.35	0.40
Draped to 40% of area [2]	0.19	0.31	0.35	0.34	0.44	0.50
Curtains in folds against wall [3]	0.05	0.15	0.35	0.40	0.50	0.50
<i>Cotton curtains, 0.475 kg/m²</i>						
Draped to 7/8 area [4, 5]	0.03	0.12	0.15	0.27	0.37	0.42
Draped to 3/4 area [4, 5]	0.04	0.23	0.40	0.57	0.53	0.40
Draped to 1/2 area [4, 5]	0.07	0.37	0.49	0.81	0.65	0.54
<i>Carpet</i>						
Carpet heavy, on concrete [2]	0.02	0.06	0.14	0.37	0.60	0.65
Heavy carpet (same as line above) on foam rubber or 1.35 kg/m ² hair felt [2]	0.08	0.24	0.57	0.69	0.71	0.73
Heavy carpet (same as two lines above) with latex backing on foam rubber or 1.35 kg/m ² hair felt [2]	0.08	0.27	0.39	0.34	0.48	0.63
Haircord on felt [6]	0.10	0.15	0.25	0.30	0.30	0.30
Pile and thick felt [6]	0.07	0.25	0.50	0.50	0.60	0.65
No underlay (pad), woven wool loop, 1.2 kg/m ² 2.4 mm pile height [2]	0.10	0.16	0.11	0.30	0.50	0.47
No underlay (pad), woven wool loop, 1.4 kg/m ² 6.4 mm pile height [2]	0.15	0.17	0.12	0.32	0.52	0.57
No underlay (pad) woven wool loop, 2.3 kg/m ² 9.5 mm pile height [2]	0.17	0.18	0.21	0.50	0.63	0.83
Loop pile tufted carpet, 1.4 kg/m ² , hair underlay 1.4 kg/m ² [2]	0.03	0.25	0.55	0.70	0.62	0.84

A.1 Table of absorption coefficients (*Continued*)

<i>Material</i>	<i>Frequency (Hz)</i>					
	125	250	500	1000	2000	4000
Loop pile tufted carpet, 1.4 kg/m ² , hair underlay 3.0 kg/m ² [2]	0.10	0.40	0.62	0.70	0.63	0.88
Loop pile tufted carpet, 1.4 kg/m ² , hair and jute underlay 3 kg/m ² [2]	0.20	0.50	0.68	0.72	0.65	0.90
Loop pile tufted carpet, 1.4 kg/m ² , no underlay [2]	0.04	0.08	0.17	0.33	0.59	0.75
Loop pile tufted carpet, 0.7 kg/m ² , 1.4 kg/m ² hair underlay pad [2]	0.10	0.19	0.35	0.79	0.69	0.79
16 mm wool pile with underlay [1]	0.20	0.25	0.35	0.40	0.50	0.75
9.5 mm wool pile no underlay on concrete [1]	0.09	0.08	0.21	0.26	0.27	0.37
Cord carpet [3]	0.05	0.05	0.10	0.20	0.45	0.65
Thin (6 mm) carpet on underlay [7]	0.03	0.09	0.20	0.54	0.70	0.72
6 mm pile carpet bonded to closed-cell foam underlay [7]	0.03	0.09	0.25	0.31	0.33	0.44
Thick (9 mm) carpet on underlay [2]	0.08	0.08	0.30	0.60	0.75	0.80
Needle felt 5 mm stuck to concrete [8, 9]	0.01	0.02	0.05	0.15	0.30	0.40
Thin carpet cemented to concrete [11]	0.02	0.04	0.08	0.2	0.35	0.4
<i>Other floors</i>						
Wood block/lino/rubber flooring [6]	0.02	0.04	0.05	0.05	0.1	0.05
Parquet fixed with asphalt, on concrete [1]	0.04	0.04	0.07	0.06	0.06	0.07
Wood on solid floor [1]	0.04	0.04	0.03	0.03	0.03	0.02
Floors, wood [2]	0.15	0.11	0.10	0.07	0.06	0.07
Wood platform, large airspace below [1]	0.40	0.30	0.20	0.17	0.15	0.10
Floor boards on joist floor [6]	0.15	0.20	0.10	0.10	0.10	0.10
Floors, concrete or terrazzo [2, 10]	0.01	0.01	0.015	0.02	0.02	0.02
Concrete floor [11]	0.01	0.02	0.02	0.02	0.02	0.02
Linoleum or vinyl stuck to concrete [12, 9]	0.02	0.02	0.03	0.04	0.04	0.05
Linoleum, asphalt tile or cork tile on concrete [2, 5, 13]	0.02	0.03	0.03	0.03	0.03	0.02
Layer of rubber, cork, linoleum and underlay or vinyl and underlay, stuck to concrete [18, 9]	0.02	0.02	0.04	0.05	0.05	0.10
Cork, lino or rubber tile on solid floor [1]	0.04	0.03	0.04	0.04	0.03	0.02
2.5 mm cork on solid backing	0.05	0.1	0.2	0.55	0.6	0.55
Slate [1]	0.01	0.01	0.01	0.02	0.02	0.02
<i>Theatre seating, unoccupied</i>						
Beranek's values [14]	0.19	0.37	0.56	0.67	0.61	0.59
Average of nine modern seating designs, 0.9 m row spacing [15]	0.34	0.46	0.64	0.71	0.77	0.85
One seat type, 0.8 m row spacing [15]	0.29	0.39	0.61	0.74	0.83	0.88
Same seat as line above, 0.9 m row spacing [15]	0.25	0.35	0.58	0.70	0.78	0.84
Same seat as two lines above, 1 m row spacing [15]	0.23	0.34	0.52	0.65	0.73	0.75
Upholstered seating [6]	0.45	0.60	0.73	0.80	0.75	0.64
Upholstered seating, well upholstered [16]	0.44	0.60	0.77	0.89	0.82	0.70
Upholstered seating, leather covered [16]	0.40	0.50	0.58	0.61	0.58	0.50
<i>Seating, occupied</i>						
Occupied theatre seating average from References 1 and 15	0.41	0.58	0.80	0.90	0.92	0.89
Audience on timber seats (1/m ²) [2]	0.16	0.24	0.56	0.69	0.81	0.78
Audience on timber seats (2/m ²) [2]	0.24	0.4	0.78	0.98	0.96	0.87

<i>Material</i>	<i>Frequency (Hz)</i>					
	125	250	500	1000	2000	4000
Orchestra with instruments (1.5 m ² /person) [2]	0.27	0.53	0.67	0.93	0.87	0.8
Wooden pews (100% occupancy) [16]	0.57	0.61	0.75	0.86	0.91	0.86
Wooden chairs (100% occupancy) [16]	0.60	0.74	0.88	0.96	0.93	0.85
Wooden pews (75% occupancy) [16]	0.46	0.56	0.65	0.75	0.72	0.65
<i>Miscellaneous</i>						
Water surface in swimming pool [17]	0.01	0.01	0.01	0.01	0.02	0.02
Water surface in swimming pool [2]	0.008	0.008	0.013	0.015	0.02	0.025
Marble or glazed tile [2]	0.01	0.01	0.01	0.01	0.02	0.02
Solid wooden door [18, 9]	0.14	0.10	0.06	0.08	0.10	0.10
Ventilation grille [8, 9]	0.60	0.60	0.60	0.60	0.60	0.60
<i>Wood</i>						
Plywood panelling, 1 cm thick [2, 10]	0.28	0.22	0.17	0.09	0.1	0.11
22 mm chipboard, 50 mm cavity filled with mineral wool [18, 9]	0.12	0.04	0.06	0.05	0.05	0.05
3–4 mm plywood sheets, >75 mm cavity with 25–50 mm mineral wool [8, 9]	0.50	0.30	0.10	0.05	0.05	0.05
Plywood/hardwood, air space [6]	0.32	0.43	0.12	0.07	0.07	0.11
6 mm wood fibreboard on laths, cavity >100 mm deep [18, 9]	0.30	0.20	0.20	0.10	0.05	0.05
Fibreboard, solid backing [6]	0.05	0.1	0.15	0.25	0.3	0.3
Fibreboard, 25 mm air space [6]	0.3	0.3	0.3	0.3	0.3	0.3
9.5–12.7 mm wood panelling, 5–10 cm air space behind [1]	0.30	0.25	0.20	0.17	0.15	0.10
Wood, 50 mm thick	0.01	0.05	0.05	0.04	0.04	0.04
<i>Concrete</i>						
Rough concrete [19]	0.02	0.03	0.03	0.03	0.04	0.07
Smooth unpainted concrete [18, 9]	0.01	0.01	0.02	0.02	0.02	0.05
Smooth concrete, painted or glazed [18, 9]	0.01	0.01	0.01	0.02	0.02	0.02
Concrete block, coarse [2]	0.36	0.44	0.31	0.29	0.39	0.25
Concrete block, painted [2, 5, 13]	0.10	0.05	0.06	0.07	0.09	0.08
Porous concrete blocks without surface finish, 400–800 kg/m ³ [9]	0.05	0.05	0.05	0.08	0.14	0.20
Clinker concrete, no surface finish, 800 kg/m ³ [8, 9]	0.10	0.20	0.40	0.60	0.50	0.60
<i>Bricks and blocks</i>						
Brick, unglazed [2]	0.03	0.03	0.03	0.04	0.05	0.07
Brickwork, plain painted [6]	0.05	0.04	0.02	0.04	0.05	0.05
Smooth brickwork with flush pointing, painted [17]	0.01	0.01	0.02	0.02	0.02	0.02
Brick, unglazed, painted [2]	0.01	0.01	0.02	0.02	0.02	0.03
Smooth brickwork with flush pointing [18, 9]	0.02	0.03	0.03	0.04	0.05	0.07
Smooth brickwork, 10 mm deep pointing, pit sand mortar [8, 9]	0.08	0.09	0.12	0.16	0.22	0.24
Breeze block [6]	0.2	0.3	0.6	0.6	0.5	0.5
<i>Plaster</i>						
Lime cement plaster [18]	0.02	0.02	0.03	0.04	0.05	0.05
Glaze plaster [18, 9]	0.01	0.01	0.01	0.02	0.02	0.02
Painted plaster surface [8, 9]	0.02	0.02	0.02	0.02	0.02	0.02
Plaster with wallpaper on backing paper [18, 9]	0.02	0.03	0.04	0.05	0.07	0.08
Plaster, gypsum or lime, rough finish on lath [20, 10]	0.02	0.03	0.04	0.05	0.04	0.03

A.1 Table of absorption coefficients (*Continued*)

<i>Material</i>	<i>Frequency (Hz)</i>					
	125	250	500	1000	2000	4000
Plaster, gypsum or lime, smooth finish on lath [2]	0.14	0.1	0.06	0.04	0.04	0.03
Plaster, gypsum or lime, smooth finish on lath [20, 10]	0.02	0.02	0.03	0.04	0.04	0.03
Plaster, on laths/studs, air space [6]	0.3	0.1	0.1	0.05	0.04	0.05
Plaster, gypsum or lime, smooth finish on tile or brick [2]	0.013	0.015	0.02	0.03	0.04	0.05
Plaster, lime of gypsum on solid backing [6]	0.03	0.03	0.02	0.03	0.04	0.05
Acoustic plaster [6]	0.30	0.35	0.5	0.7	0.7	0.7
Acoustic plaster, 40 mm thick [21]	0.31	0.55	0.84	0.78	0.71	0.54
Acoustic plaster, 68 mm thick [21]	0.47	0.74	0.76	0.65	0.62	0.49
<i>Plasterboard</i>						
Gypsum board, 1.27 cm nailed to studs with 4.1 m c-t-c [2]	0.29	0.1	0.05	0.04	0.07	0.09
Plasterboard on frame, 9.5 mm boards, 10 cm empty cavity [22, 9]	0.11	0.13	0.05	0.03	0.02	0.03
Plasterboard on frame, 9.5 mm boards, 10 cm cavity filled with mineral wool [22, 9]	0.28	0.14	0.09	0.06	0.05	0.05
Plasterboard on frame, 13 mm boards, 10 cm empty cavity [22, 9]	0.08	0.11	0.05	0.03	0.02	0.03
Plasterboard on frame, 13 mm boards, 10 cm cavity filled with mineral wool [22, 9]	0.30	0.12	0.08	0.06	0.06	0.05
2*13 mm plasterboard on steel frame, 5 cm mineral wool in cavity, surface painted [12, 9]	0.15	0.10	0.06	0.04	0.04	0.05
<i>Glazing</i>						
Glass, ordinary window glass [2, 10]	0.35	0.25	0.18	0.12	0.07	0.04
Single pane of glass, 3–4 mm [6]	0.2	0.15	0.1	0.07	0.05	0.05
Single pane of glass, >4 mm [6]	0.1	0.07	0.04	0.03	0.02	0.02
Single pane of glass, 3 mm [22, 9]	0.08	0.04	0.03	0.03	0.02	0.02
Double glazing, 2–3 mm glass, 1 cm gap [8, 9]	0.10	0.07	0.05	0.03	0.02	0.02
Double glazing, 2–3 mm glass, >3 cm gap [22, 9]	0.15	0.05	0.03	0.03	0.02	0.02
Glass, large panes, heavy glass [2, 5, 13]	0.18	0.06	0.04	0.03	0.02	0.02
<i>Mineral wools and foam</i>						
2.5 mm fibreglass, rigid backing [23]	0.08	0.25	0.45	0.75	0.75	0.65
2.54 cm fibreglass, 24–48 kg/m ³ [2]	0.08	0.25	0.65	0.85	0.8	0.75
2.5 cm fibreglass, 2.5 cm airspace [2]	0.15	0.55	0.8	0.9	0.85	0.8
5 cm fibreglass, rigid backing [23]	0.21	0.50	0.75	0.90	0.85	0.80
7.5 cm fibreglass, rigid backing [23]	0.35	0.65	0.80	0.90	0.85	0.80
10 cm fibreglass, rigid backing [23]	0.45	0.90	0.95	1.00	0.95	0.85
5 cm mineral wool (40 kg/m ³), glued to wall, untreated surface [8, 9]	0.15	0.70	0.60	0.60	0.85	0.90
5 cm mineral wool (40 kg/m ³), glued to wall, surface sprayed with thin plastic solution [8, 9]	0.15	0.70	0.60	0.60	0.75	0.75
5 cm mineral wool (70 kg/m ³), 30 cm in front of wall [8, 9]	0.70	0.45	0.65	0.60	0.75	0.65
5 cm wood-wool set in mortar [8, 9]	0.08	0.17	0.35	0.45	0.65	0.65
5.1 cm fibreglass, panels with plastic sheet wrapping and perforated metal facing [2]	0.33	0.79	0.99	0.91	0.76	0.64
5.1 cm fibreglass, 24–48 kg/m ³ [2]	0.17	0.55	0.8	0.9	0.85	0.8
Acoustic tile, 1.27 cm thick [5]	0.07	0.21	0.66	0.75	0.62	0.49

<i>Material</i>	<i>Frequency (Hz)</i>					
	125	250	500	1000	2000	4000
Acoustic tile, 1.9 cm thick [5]	0.09	0.28	0.78	0.84	0.73	0.64
Polyurethane foam, 2.5 cm thick	0.16	0.25	0.45	0.84	0.97	0.87
<i>Ballast</i>						
Ballast or other crushed stone, 3.18 cm, 15.2 cm deep [2]	0.19	0.23	0.43	0.37	0.58	0.62
Ballast or other crushed stone, 3.18 cm, 30.5 cm deep [2]	0.27	0.58	0.48	0.54	0.73	0.63
Ballast or other crushed stone, 3.18 cm, 45.7 cm deep [2]	0.41	0.53	0.64	0.84	0.91	0.63
Ballast or other crushed stone, 0.64 cm, 15.2 cm deep [2, 10]	0.22	0.64	0.7	0.79	0.88	0.72
<i>Microperforated absorber</i>						
4 cm cavity [21]	0.08	0.27	0.70	0.35	0.11	0.04
40 cm cavity [21]	0.64	0.56	0.41	0.28	0.13	0.06
<i>Diffusers</i>						
Hybrid absorber–diffuser (BAD™ panel mounted on 2.5 cm fibreglass) [21]	0.17	0.40	0.86	1.00	0.84	0.61
2D $N=7$ QRD™, design freq. = 500 Hz [21]	0.14	0.12	0.14	0.20	0.09	0.12
2D $N=7$ QRD as line above, with cloth covering [21]	0.16	0.17	0.28	0.41	0.26	0.3
1D $N=7$ QRD, design freq. = 500 Hz [21]	0.11	0.1	0.07	0.08	0.06	0.06
1D $N=7$ QRD as line above, with cloth covering [21]	0.13	0.14	0.2	0.24	0.20	0.23

A.2 References

- 1 L. L. Beranek, *Acoustics*, McGraw-Hill (1954).
- 2 C. M. Harris (ed.), *Handbook of Noise Control*, 2nd edn, McGraw-Hill (1991).
- 3 D. Templeton (ed.), *Acoustics in the Built Environment*, 2nd edn, Architectural Press (1997).
- 4 V. S. Mankovsky, *Acoustics of Studio and Auditoria*, Focal Press (1971).
- 5 F. Alton Everest, *Master Handbook of Acoustics*, 4th edn, McGraw-Hill (2001).
- 6 A. Fry (ed.), *Noise Control in Building Services*, Pergamon Press (1988).
- 7 P. H. Parkin, H. R. Humphreys and J. R. Cowell, *Acoustics, Noise and Buildings*, Faber and Faber (1979).
- 8 J. Kristensen, *Sound Absorption Coefficients – Measurement, Evaluation, Application*, note #45, Statens Byggeforskningsinstitut, Hørsholm (1984, in Danish).
- 9 C. Lynge, *ODEON Room Acoustics Program, User manual*, DTU, Denmark (2001).
- 10 Physikalisch-Technische Bundesanstalt, <http://www.ptb.de/en/index.html>
- 11 L. L. Beranek and T. Hidaka, “Sound absorption in concert halls by seats, occupied and unoccupied, and by the hall’s interior surfaces”, *J. Acoust. Soc. Am.*, **104**(6), 3169–3177 (1998).
- 12 J. Petersen, *Rumakustik*, SBI-anvisning 137, Statens Byggeforskningsinstitut, Hørsholm (1983).
- 13 R. W. Young, “Sabine reverberation and sound power calculations”, *J. Acoust. Soc. Am.*, **31**, 912–921 (1959).
- 14 L. L. Beranek, “Audience and chair absorption in large halls. II”, *J. Acoust. Soc. Am.*, **45**, 13–19 (1969).

- 15 W. J. Davies, R. J. Orłowski and Y. W. Lam, “Measuring auditorium seat absorption”, *J. Acoust. Soc. Am.*, **96**, 879–888 (1994).
- 16 D. A. Bies and C. H. Hansen, *Engineering Noise Control: Theory and Practice*, E&FN Spon, 2nd edn (1996).
- 17 V. O. Knudsen and C. M. Harris, *Acoustical Designing in Architecture*, John Wiley (1953).
- 18 H. W. Bobran, *Handbuch Der Bauphysik*, Verlag Ulstein, Berlin (1973).
- 19 ISO/TR 11690-3, “Acoustics – recommended practice for design of low-noise workplaces containing machinery – Part 3: Sound propagation and noise predictions in workrooms” (1997).
- 20 D. Davis and C. Davis, *Sound System Engineering*, Focal Press (1997).
- 21 RPG Diffusor Systems Inc., www.rpginc.com
- 22 W. Fasold and H. Winkler, “Bauphysikalische entwurfslehre, band 4: bauakustik”, VEB Verlag für Bauwesen, Berlin (1976).
- 23 L. E. Kinsler, A. R. Frey, A. B. Coppens and J. V. Sanders, *Fundamentals of Acoustics*, 4th edn, John Wiley & Sons (2000).

Appendix B

MATLAB scripts

B.1 Chapter 5: script_5_1

```
%Absorption of a rigid backed porous absorber
%Using Delany and Bazley formulations
%Normal incidence absorption coefficients

close all
clear all

c = 340;           %speed of sound
rho = 1.21;       %density of air
Z0 = c*rho;       %characteristic impedance of air

sigma = 50000;    %flow resistivity
l = 0.0254;       %thickness
f = [100:50:10000]; %frequency
nf = length(f);

%Delany and Bazley
X = rho*f/sigma; %dimensionless quantity for Delany and Bazley
zc = rho*c*(1 + 0.0571*(X.^ - 0.754) - j*0.087*(X.^ - 0.732)); %characteristic
    impedance
k = (2*pi/c).*f.*(1 + 0.0978*(X.^ - 0.700) - j*0.189*(X.^ - 0.595)); %complex
    wave number

gamma = j*k;      %propagation constant
z = zc.*coth (gamma*l) %surface impedance

figure
semilogx(f, real(z), 'b', f, imag (z), 'g');
title('Impedance of rigid backed porous absorber')
xlabel('Frequency(Hz)')
ylabel('Impedance')
legend('Real','Imaginary')
R = (z - Z0)/(z + Z0); %reflection factor
figure
semilogx(f, abs(R), 'b', f, angle(R), 'g');
title('Reflection factor of rigid backed porous absorber')
xlabel('Frequency(Hz)')
```

```

ylabel('Reflection factor')
legend('Magnitude','Phase')
anormal = 1 - abs(R).^2;    %absorption coefficient
figure
semilogx(f, anormal);
title('Normal incidence abs. coeff. of rigid backed porous absorber')
xlabel('Frequency(Hz)')
ylabel('alpha')

```

B.2 Chapter 5: script_5_2

```

%Absorption of a rigid backed porous absorber
%Using Delany and Bazley formulations
%Normal incidence absorption coefficients
%Demonstrating effects of thickness
close all
clear all
c = 340;           %speed of sound
rho = 1.21;       %density of air
Z0 = c*rho;       %characteristic impedance of air
sigma = 20000;    %flow resistivity
f = [100:50:10000]; %frequency
nf = length(f);
%Delany and Bazley
X = rho*f/sigma; %dimensionless quantity for Delany and Bazley
zc = rho*c*(1 + 0.0571*(X.^ - 0.754) - j*0.087*(X.^ - 0.732)); %characteristic
impedance
k = (2*pi/c).*f.*(1 + 0.0978*(X.^ - 0.700) - j*0.189*(X.^ - 0.595)); %complex
wave number
figure(1)
hold on
for il = 1:4           %thickness loop
    l = (il - 0.5)*0.0254; %thickness
    z = -j*zc.*cot(k*l) %surface impedance
    R = (z - Z0)/(z + Z0); %reflection factor
    anormal = 1 - abs(R).^2; %absorption coefficient
    str = dec2bin(il, 3)
    semilogx(f, anormal, 'color', [str2num(str(1)) str2num(str(2)) ... str2num(str(3))]);
    title('Abs. coeff., rigid backed porous absorber')
    xlabel('Frequency(Hz)')
    ylabel('alpha')
    strlegend(il, 1:6) = char(num2str(l,4));
end
legend(strlegend)
axis([100, 10000, 0, 1])

```

B.3 Chapter 5: script_5_3

```

%Absorption of a rigid backed porous absorber
%Using Delany and Bazley formulations
%Normal incidence absorption coefficients

close all
clear all
c = 340;          %speed of sound
rho = 1.21;      %density of air
z0 = c*rho;      %characteristic impedance of air

%Frequency
f = [100:50:10000];
nf = length(f);

%Consider absorbent layer alone

%Delany and Bazley
sigma = 20000;   %flow resistivity
X = rho*f/sigma; %dimensionless quantity for Delany and Bazley
zc = rho*c*(1 + 0.0571*(X.^ - 0.754) - j*0.087*(X.^ - 0.732)); %characteristic
    impedance
k = (2*pi/c).*f.*(1 + 0.0978*(X.^ - 0.700) - j*0.189*(X.^ - 0.595)); %complex
    wave number
l = 0.0254;      %thickness
z = -j*zc.*cot(k*l) %surface impedance

figure(1)
semilogx(f, real(z), 'b', f, imag(z), 'g');
title('Effect of air gap')
xlabel('Frequency(Hz)')
ylabel('Impedance')
legend('Real', 'Imaginary')
R = (z - z0)/(z + z0); %reflection factor
anormal = 1 - abs(R).^2; %absorption coefficient

figure(2)
semilogx(f, anormal);
title('Effect of air gap')
xlabel('Frequency(Hz)')
ylabel('alpha')

%Consider absorbent with air layer behind
l = l/2; %depth of air layer
kair = 2*pi*f/c;
zs1 = -j*z0*cot(kair*l); %impedance at top of air layer
zs2 = (-j*zs1.*zc.*coth(k*l) + zc.^2)/(zs1 + zc.*coth(gamma*l)); %impedance
    at surface of absorber

figure(1)
hold on
semilogx(f, real(zs2), 'c', f, imag(zs2), 'm');
title('Effect of air gap')

```

```

xlabel('Frequency(Hz)')
ylabel('Impedance')
legend('Real 25mm', 'Imaginary 25mm',...
'Real 12.5mm air gap', 'Imaginary 12.5mm air gap')
R = (zs2 - z0)/(zs2 + z0); %reflection factor
anormal = 1 - abs(R).^2; %absorption coefficient
figure(2)
hold on
semilogx(f, anormal, 'r');
title('Effect of air gap')
xlabel('Frequency(Hz)')
ylabel('alpha')
legend('25mm absorbent', '12.5mm absorbent and air gap')

```

B.4 Chapter 6: script_6_1.m

```

%Absorption of a perforated absorber
%Normal incidence
close all
clear all
c = 340; %speed of sound
rho = 1.21; %density of air
Z0 = c*rho;
viscosity = 15e - 6; %kinemetric viscosity of air
sigma = 20000; %flow resistivity of mineral wool
l1 = 0.025; %backing thickness air
l2 = 0.025; %backing thickness porous absorber
f = [100:50:2500]; %frequency
nf = length(f);
kair = 2*pi*f/c;
w = 2*pi*f;
%Impedance at top of air layer
z1 = -j*Z0.*cot(kair*l1);
%Calculate impedance of porous material (Delany and Bazley)
X = rho*f/sigma; %dimensionless quantity for Delany and Bazley
zc = rho*c*(1 + 0.0571*(X.^ - 0.754) - j*0.087*(X.^ - 0.732)); %characteristic
impedance
k = (2*pi/c).*f.*(1 + 0.0978*(X.^ - 0.700) - j*0.189*(X.^ - 0.595)); %wavenumber
%Impedance at top of porous absorbent
z2 = (-j*z1.*zc.*cot(k*l2) + zc.^2)/(z1 - j*zc.*cot(k*l2));
%Loop over different open areas
eta = [0.0625, 0.125, 0.25, 0.50, 1.00]
ne = length(eta);
for m = 1: ne
    a = 2.5e - 3; %hole radius

```

```

D = sqrt(pi/eta(m))*a;    %hole spacing
delta = 1.6 * (1 - 1.47*eta (m)^0.5 + 0.47*eta (m)^3/2);    %end correction
t = 6.3e - 3;    %plate thickness
rm = (rho/eta (m))*sqrt (8*viscosity*w) * (1 + t/(2*a));    %surface resistance
z3 = (j/eta (m)) * (2*delta*a + t)*w*rho + z2 + rm;    %impedance of resonant
    absorber
R = (z3 - rho*c)/(z3 + rho*c);    %reflection factor
alpha = 1 - abs(R).^2;    %absorption coefficient
figure(1)
hold on
str = dec2bin(m, 3)
plot(f, real(z3), 'color', ...
[str2num(str(1)) str2num(str(2)) str2num(str(3))] ... , 'LineStyle', '-');
plot(f, imag(z3), 'color', ... [str2num(str(1)) str2num(str(2)) str2num(str(3))] ... ,
'LineStyle', ':');
figure(2)
hold on
plot(f, alpha, 'color', ... [str2num(str(1)) str2num(str(2)) str2num(str(3))]);
end

```

B.5 Chapter 6: script 6_2.m

```

%Absorption of a slotted absorber
%Normal incidence
close all
clear all
c = 340;    %speed of sound
rho = 1.21; %density of air
r0 = 32;    %air flow resistance of porous material =
    %flow resistivity*thickness
l = 0.1;    %backing thickness
f = [100 : 10 : 1100]; %frequency
nf = length(f); %number of frequency terms
k = 2*pi*f/c; %wavenumber
w = 2*pi*f; %angular frequency
z1 = rho*c*coth(j*k*l); %impedance at top of air cavity
t = 15e - 3; %plate thickness
d = 0.01; %slot width
eta = (0.0465*4*d)/(pi*0.05^2); %open area
delta = -(d/pi)*log (sin(pi*eta/2)); %end correction
z2 = (j/eta)*(2*delta + t)*w*rho + z1 + r0/eta; %impedance of resonant absorber
figure %plot impedance
plot(f, real(z2), 'b', f, imag(z2), 'g');
title('Impedance')
xlabel('Frequency(Hz)')
ylabel('Impedance')
legend('Real', 'Imaginary')

```

386 Appendix B

```
R = (z2 - rho*c)/(z2 + rho*c); %reflection factor
anormal = 1 - abs(R).^2; %absorption coefficient
figure %plot absorption coefficient
plot(f, anormal);
title('Normal incidence absorption coefficient')
xlabel('Frequency(Hz)')
ylabel('alpha')
```

B.6 Chapter 6: script 6_3

```
%Microperforated
%Helmholtz absorber

close all
clear all

D = 2.5e - 3; %hole separation
d = 0.2e - 3; %hole diameter
a = d/2; %hole radius
t = 0.2e - 3; %sheet thickness
l = 0.06; %cavity depth

f = linspace(50, 8000, 100);
nf = length(f);
w = 2*pi*f;
c = 340;
k = w/c;
rho = 1.21;
viscosity = 1.85e - 5;
eta = pi*a^2/(D^2); %open area
z1 = -j*rho*c*cot(k*l); %impedance, top of cavity;
%Impedance of covering sheet
kd = a*sqrt(rho*w/viscosity);
s = kd*sqrt(-j);
z2 = j*w*rho*t./(1 - 2*besselj(1, s)/(s.*besselj(0, s)));
z2 = z2/eta + j*w*0.85*2*rho*a/eta + sqrt(2)*kd*viscosity/(2*a*eta);
z = z1 + z2;

R = (z - rho*c)/(z + rho*c); %reflection factor
anormal = 1 - abs(R).^2; %absorption coefficient

hold on
plot(f, anormal, 'g')
xlabel('f (Hz)')
ylabel('abs. coeff')
```

B.7 Chapter 13: simple_lms.m

```
%LMS demo

close all
clear all
```

```

N = 10000;    %number of time iterations
k = [1:N];    %this is inefficient for storage, but allows graphs to be plotted
s = sin(2*pi*k*10/N);    %input signal
figure
plot(k, s)
title('Input signal s')
xlabel('Time k')
ylabel('(linear)')
x = (rand(N,1) - 0.5)*2;    %noise signal
figure
plot(k, x)
title('Noise signal x')
xlabel('Time k')
ylabel('(linear)')
W_1 = ([0.5,0.2]);    %this is W^1 - 1 in Figure 13.2
W = rand(1,2);    %starting adaptive filter weights (assigned randomly)
alpha = 0.001;    %update rate
e = zeros(N,1);
Wstore = zeros(N, 2);
n(1,1) = 0;
for j = 2 : N
    n(j, 1) = W_1*x(j - 1 : j);    %this is convolution in matrix format
    %Note that W_1(2) is actually the first coefficient
    %and W_1(1) is actually the second coefficient
    d = s(j) + n(j);
    y = W*x(j - 1 : j);    %output from adaptive filter
    e(j - 1) = d - y;    %error
    W = W + 2*alpha*e(j - 1)*rot90(x(j - 1 : j), 1);    %update weights
    Wstore(j - 1, :) = W;    %store weights for future plotting
end
figure
plot(e)
title('Error')
xlabel('Time k')
ylabel('(linear)')
figure
plot(Wstore(:, 1))
hold on
plot(Wstore(:, 2), 'r')
title('Adaptive filter coefficients')
xlabel('Time k')
ylabel('(linear)')

```

Appendix C

C.1 Diffusion coefficient table

Surface	Angle of incidence ($^{\circ}$)	Frequency (Hz)																	
		100	125	160	200	250	315	400	500	630	800	1000	1250	1600	2000	2500	3150	4000	5000
1 Effect of changing diffuser width and periodicity																			
<i>1.1 Planar non-absorbing surfaces, infinitesimally thin</i>																			
0.62 m wide	0	0.63	0.62	0.61	0.60	0.58	0.54	0.50	0.44	0.36	0.27	0.22	0.17	0.13	0.10	0.08	0.06	0.04	0.02
	56.9	0.63	0.62	0.61	0.60	0.58	0.56	0.53	0.46	0.42	0.37	0.33	0.28	0.23	0.19	0.15	0.12	0.09	0.07
	random	0.63	0.62	0.61	0.60	0.58	0.55	0.52	0.45	0.40	0.34	0.29	0.25	0.20	0.17	0.14	0.11	0.09	0.07
1.22 m wide	0	0.60	0.58	0.55	0.50	0.44	0.37	0.27	0.22	0.17	0.13	0.10	0.08	0.05	0.04	0.02	0.00	0.01	0.01
	56.9	0.60	0.57	0.54	0.51	0.45	0.42	0.36	0.32	0.27	0.23	0.19	0.15	0.12	0.09	0.07	0.05	0.03	0.03
	random	0.60	0.57	0.54	0.51	0.45	0.40	0.34	0.29	0.24	0.20	0.16	0.13	0.11	0.08	0.06	0.05	0.04	0.03
2.44 m wide	0	0.50	0.44	0.36	0.27	0.22	0.17	0.13	0.10	0.07	0.05	0.04	0.02	0.00	0.01	0.01	0.00	0.00	0.00
	56.9	0.47	0.43	0.39	0.35	0.31	0.27	0.22	0.18	0.15	0.12	0.09	0.07	0.05	0.03	0.03	0.03	0.01	0.02
	random	0.48	0.43	0.38	0.33	0.28	0.24	0.20	0.16	0.13	0.10	0.08	0.06	0.05	0.04	0.03	0.03	0.03	0.02
3.66 m wide	0	0.37	0.29	0.23	0.18	0.14	0.11	0.08	0.06	0.04	0.02	0.01	0.01	0.01	0.00	0.01	0.00	0.01	0.01
	56.9	0.38	0.34	0.31	0.27	0.23	0.19	0.16	0.13	0.10	0.07	0.05	0.04	0.03	0.03	0.02	0.02	0.03	0.04
	random	0.38	0.33	0.28	0.24	0.20	0.17	0.14	0.11	0.09	0.07	0.05	0.04	0.04	0.03	0.03	0.02	0.02	0.02
7.32 m wide	0	0.18	0.14	0.11	0.09	0.07	0.05	0.04	0.03	0.04	0.04	0.04	0.04	0.07	0.07	0.05	0.05	0.06	0.06
	56.9	0.25	0.22	0.18	0.15	0.12	0.09	0.07	0.05	0.04	0.04	0.04	0.02	0.03	0.03	0.02	0.02	0.02	0.01
	random	0.23	0.19	0.16	0.13	0.11	0.09	0.07	0.06	0.05	0.05	0.05	0.05	0.04	0.04	0.04	0.03	0.03	0.03

Surface	Angle of incidence (°)	Frequency (Hz)																	
		100	125	160	200	250	315	400	500	630	800	1000	1250	1600	2000	2500	3150	4000	5000
1.2 Semicylinder(s) non-absorbing surfaces, radius 0.3 m (1 cm flat section between each period)																			
1 period, 0.61 m wide	0	0.72	0.77	0.83	0.91	0.98	0.99	0.97	0.98	0.98	0.93	0.95	0.95	0.94	0.96	0.97	0.98	0.98	0.98
	56.9	0.70	0.72	0.75	0.79	0.83	0.85	0.88	0.87	0.87	0.80	0.79	0.80	0.80	0.82	0.83	0.84	0.86	0.87
	random	0.74	0.76	0.80	0.85	0.89	0.91	0.89	0.89	0.89	0.86	0.85	0.86	0.86	0.86	0.86	0.87	0.87	0.88
2 periods, 1.22 m wide	0	0.66	0.66	0.64	0.57	0.47	0.46	0.71	0.70	0.76	0.51	0.55	0.74	0.66	0.78	0.77	0.73	0.77	0.80
	56.9	0.61	0.57	0.60	0.78	0.73	0.73	0.56	0.51	0.77	0.77	0.73	0.74	0.76	0.76	0.77	0.77	0.81	0.83
	random	0.65	0.62	0.61	0.68	0.64	0.65	0.60	0.54	0.73	0.65	0.69	0.73	0.74	0.75	0.76	0.76	0.79	0.80
4 periods, 2.44 m wide	0	0.51	0.43	0.35	0.30	0.24	0.20	0.25	0.62	0.37	0.21	0.26	0.39	0.32	0.48	0.44	0.42	0.43	0.54
	56.9	0.47	0.52	0.52	0.48	0.52	0.52	0.32	0.21	0.57	0.39	0.40	0.52	0.53	0.55	0.65	0.67	0.64	0.66
	random	0.48	0.46	0.43	0.40	0.40	0.39	0.37	0.34	0.47	0.37	0.40	0.49	0.50	0.51	0.56	0.60	0.62	0.63
6 periods, 3.66 m wide	0	0.36	0.28	0.23	0.19	0.16	0.12	0.13	0.25	0.25	0.12	0.20	0.22	0.27	0.39	0.33	0.39	0.49	0.73
	56.9	0.41	0.43	0.41	0.35	0.37	0.45	0.23	0.15	0.45	0.24	0.29	0.45	0.44	0.48	0.59	0.59	0.62	0.67
	random	0.38	0.35	0.31	0.27	0.31	0.31	0.27	0.24	0.35	0.25	0.30	0.39	0.43	0.44	0.49	0.56	0.61	0.66
12 periods, 7.32 m wide	0	0.18	0.14	0.11	0.09	0.07	0.06	0.05	0.06	0.18	0.11	0.20	0.51	0.40	0.65	0.60	0.74	0.68	0.82
	56.9	0.29	0.27	0.23	0.18	0.16	0.38	0.19	0.12	0.32	0.13	0.24	0.42	0.44	0.51	0.56	0.58	0.69	0.68
	random	0.23	0.20	0.17	0.14	0.18	0.21	0.18	0.16	0.26	0.17	0.27	0.42	0.44	0.48	0.58	0.66	0.67	0.71
2 Effect of surface depth, 6 semi-ellipses, non-absorbing, each 0.6 m width, total width 3.66 m (1 cm flat section between semi-ellipses)																			
1 cm deep	0	0.37	0.29	0.23	0.18	0.14	0.11	0.08	0.06	0.04	0.02	0.01	0.01	0.01	0.01	0.01	0.01	0.02	0.04
	56.9	0.38	0.34	0.31	0.27	0.23	0.19	0.16	0.12	0.10	0.07	0.05	0.04	0.04	0.03	0.02	0.03	0.06	0.07
	random	0.38	0.33	0.28	0.24	0.20	0.17	0.14	0.11	0.09	0.07	0.05	0.05	0.04	0.03	0.04	0.03	0.03	0.04
2 cm deep	0	0.37	0.29	0.23	0.18	0.14	0.11	0.08	0.06	0.04	0.03	0.01	0.02	0.02	0.02	0.02	0.04	0.09	0.14
	56.9	0.38	0.34	0.31	0.27	0.23	0.19	0.16	0.13	0.10	0.07	0.05	0.04	0.04	0.04	0.03	0.05	0.11	0.13
	random	0.38	0.33	0.28	0.24	0.21	0.19	0.15	0.12	0.10	0.08	0.06	0.06	0.05	0.05	0.06	0.07	0.08	0.10
5 cm deep	0	0.37	0.29	0.23	0.18	0.14	0.11	0.08	0.07	0.07	0.06	0.05	0.08	0.11	0.15	0.25	0.24	0.35	0.36
	56.9	0.38	0.34	0.31	0.27	0.23	0.23	0.19	0.15	0.13	0.10	0.08	0.07	0.08	0.09	0.12	0.14	0.18	0.18
	random	0.38	0.33	0.29	0.25	0.24	0.21	0.17	0.14	0.13	0.11	0.10	0.11	0.12	0.15	0.17	0.17	0.22	0.27
10 cm deep	0	0.37	0.29	0.23	0.18	0.14	0.11	0.08	0.11	0.30	0.24	0.20	0.33	0.27	0.32	0.57	0.51	0.70	0.74
	56.9	0.38	0.34	0.30	0.27	0.24	0.37	0.29	0.24	0.23	0.20	0.20	0.20	0.22	0.26	0.32	0.41	0.43	0.42
	random	0.39	0.35	0.32	0.29	0.26	0.26	0.21	0.19	0.23	0.22	0.24	0.27	0.29	0.32	0.41	0.42	0.49	0.52

C.1 Diffusion coefficient table (Continued)

Surface	Angle of incidence (°)	Frequency (Hz)																	
		100	125	160	200	250	315	400	500	630	800	1000	1250	1600	2000	2500	3150	4000	5000
20 cm deep	0	0.36	0.28	0.23	0.18	0.14	0.11	0.10	0.32	0.44	0.20	0.03	0.17	0.29	0.27	0.57	0.58	0.58	0.55
	56.9 random	0.36	0.34	0.31	0.29	0.30	0.49	0.29	0.16	0.29	0.32	0.37	0.33	0.31	0.40	0.48	0.48	0.54	0.55
30 cm deep (semicylinder)	0	0.37	0.34	0.30	0.28	0.29	0.30	0.26	0.23	0.28	0.32	0.28	0.34	0.35	0.39	0.47	0.51	0.57	0.62
	56.9 random	0.36	0.28	0.23	0.19	0.16	0.12	0.13	0.25	0.25	0.12	0.20	0.22	0.27	0.39	0.33	0.39	0.49	0.73
3 Triangles, non-absorbing, 3.66 m wide (0.01 cm flat section between each period)	0	0.41	0.43	0.41	0.35	0.37	0.45	0.23	0.15	0.45	0.24	0.29	0.45	0.44	0.48	0.59	0.59	0.62	0.67
	56.9 random	0.38	0.35	0.31	0.27	0.31	0.31	0.27	0.24	0.35	0.25	0.30	0.39	0.43	0.44	0.49	0.56	0.61	0.66
15 periods, angle 60°	0	0.34	0.27	0.22	0.17	0.13	0.10	0.08	0.06	0.04	0.03	0.01	0.01	0.06	0.01	0.01	0.01	0.01	0.02
	56.9 random	0.42	0.39	0.34	0.31	0.30	0.25	0.22	0.22	0.16	0.22	0.10	0.08	0.26	0.20	0.16	0.24	0.27	0.27
9 periods, angle 45°	0	0.32	0.27	0.23	0.20	0.17	0.15	0.15	0.19	0.15	0.16	0.11	0.09	0.17	0.14	0.18	0.17	0.16	0.16
	56.9 random	0.37	0.28	0.23	0.18	0.14	0.11	0.08	0.06	0.05	0.05	0.04	0.01	0.03	0.02	0.02	0.01	0.02	0.02
6 periods, angle 30°	0	0.38	0.35	0.32	0.28	0.23	0.21	0.38	0.29	0.14	0.19	0.30	0.18	0.24	0.22	0.16	0.08	0.09	0.11
	56.9 random	0.37	0.33	0.29	0.24	0.20	0.18	0.27	0.23	0.17	0.21	0.22	0.18	0.22	0.23	0.19	0.16	0.17	0.12
3 periods, angle 18°	0	0.37	0.28	0.23	0.18	0.14	0.11	0.09	0.13	0.42	0.23	0.23	0.36	0.41	0.33	0.36	0.33	0.23	0.18
	56.9 random	0.37	0.34	0.31	0.28	0.30	0.46	0.29	0.21	0.29	0.24	0.20	0.23	0.18	0.20	0.17	0.15	0.11	0.09
3 periods, angle 18°	0	0.38	0.33	0.30	0.28	0.27	0.28	0.24	0.22	0.26	0.25	0.25	0.26	0.27	0.27	0.25	0.22	0.18	0.14
	56.9 random	0.37	0.29	0.23	0.19	0.20	0.32	0.39	0.32	0.37	0.33	0.30	0.30	0.29	0.23	0.20	0.15	0.12	0.11
4 Semi-ellipses mounted on 3.63 m wide flat baffle, non-absorbing, each semi-ellipse 0.6 m wide, 0.2 m deep	0	0.39	0.43	0.53	0.48	0.38	0.35	0.30	0.29	0.24	0.22	0.20	0.20	0.21	0.19	0.14	0.11	0.12	0.06
	56.9 random	0.42	0.40	0.38	0.35	0.30	0.29	0.30	0.30	0.28	0.27	0.26	0.25	0.24	0.20	0.17	0.14	0.12	0.09
1 semi-ellipse in middle of baffle	0	0.36	0.27	0.24	0.25	0.23	0.19	0.24	0.19	0.12	0.04	0.03	0.05	0.03	0.03	0.03	0.02	0.02	0.05
	56.9 random	0.44	0.50	0.45	0.48	0.47	0.43	0.38	0.36	0.30	0.22	0.16	0.12	0.10	0.12	0.16	0.17	0.11	0.10
3 semi-ellipses with 0.6 m flat sections between	0	0.43	0.42	0.41	0.41	0.41	0.38	0.36	0.34	0.29	0.24	0.20	0.19	0.19	0.19	0.20	0.16	0.13	0.12
	56.9 random	0.37	0.29	0.23	0.19	0.24	0.55	0.38	0.32	0.33	0.12	0.12	0.17	0.17	0.10	0.09	0.16	0.17	0.26
flat sections between	0	0.41	0.53	0.60	0.48	0.41	0.51	0.36	0.41	0.37	0.44	0.54	0.44	0.23	0.25	0.45	0.42	0.29	0.68
	56.9 random	0.41	0.42	0.40	0.37	0.37	0.42	0.37	0.40	0.38	0.35	0.30	0.37	0.36	0.34	0.36	0.38	0.36	0.36

Surface	Angle of incidence (°)	Frequency (Hz)																	
		100	125	160	200	250	315	400	500	630	800	1000	1250	1600	2000	2500	3150	4000	5000
5 Optimized curved surfaces, 3.6 m wide, modulated arrays																			
3 periods, 30 cm deep	0	0.42	0.35	0.27	0.29	0.60	0.55	0.34	0.43	0.56	0.29	0.36	0.52	0.63	0.42	0.74	0.75	0.32	0.79
	56.9 random	0.50	0.67	0.65	0.51	0.39	0.37	0.26	0.27	0.37	0.63	0.61	0.53	0.60	0.60	0.57	0.57	0.56	0.49
6 periods, 20 cm deep	0	0.40	0.31	0.24	0.19	0.14	0.12	0.10	0.33	0.54	0.37	0.36	0.30	0.19	0.38	0.15	0.31	0.34	0.55
	56.9 random	0.42	0.37	0.33	0.27	0.30	0.50	0.35	0.22	0.38	0.48	0.55	0.61	0.53	0.65	0.57	0.55	0.53	0.60
6 periods, 10 cm deep	0	0.44	0.37	0.32	0.27	0.28	0.31	0.30	0.29	0.37	0.47	0.43	0.48	0.50	0.57	0.51	0.54	0.57	0.57
	56.9 random	0.40	0.30	0.23	0.20	0.15	0.11	0.11	0.10	0.09	0.08	0.06	0.41	0.56	0.31	0.64	0.30	0.63	0.63
6 periods, 5 cm deep	0	0.43	0.40	0.36	0.34	0.31	0.25	0.25	0.22	0.48	0.48	0.52	0.49	0.53	0.48	0.47	0.37	0.44	0.43
	56.9 random	0.42	0.39	0.36	0.32	0.29	0.28	0.27	0.23	0.30	0.34	0.38	0.47	0.50	0.46	0.48	0.47	0.49	0.52
6 periods, 5 cm deep	0	0.41	0.31	0.24	0.19	0.14	0.11	0.08	0.07	0.05	0.03	0.02	0.11	0.17	0.30	0.45	0.56	0.52	0.64
	56.9 random	0.43	0.38	0.33	0.27	0.24	0.20	0.16	0.14	0.21	0.21	0.17	0.13	0.13	0.16	0.19	0.30	0.31	0.36
6 Hybrid surfaces, 3.6 m wide, modulated arrays	0	0.42	0.36	0.31	0.25	0.23	0.20	0.17	0.16	0.19	0.19	0.16	0.15	0.17	0.24	0.32	0.37	0.40	0.46
	56.9 random	0.41	0.30	0.24	0.19	0.14	0.11	0.08	0.06	0.05	0.03	0.01	0.02	0.02	0.01	0.01	0.01	0.02	0.03
3 periods of a flat hybrid surface	0	0.46	0.39	0.34	0.28	0.24	0.20	0.17	0.14	0.10	0.08	0.07	0.06	0.09	0.12	0.10	0.15	0.31	0.39
	56.9 random	0.47	0.40	0.34	0.28	0.23	0.19	0.16	0.12	0.09	0.08	0.07	0.07	0.11	0.13	0.14	0.15	0.15	0.17
3 periods of a curved hybrid surface, 2.5 cm deep	0	0.40	0.30	0.24	0.19	0.14	0.11	0.08	0.07	0.05	0.03	0.02	0.04	0.06	0.06	0.06	0.15	0.22	0.29
	56.9 random	0.46	0.39	0.33	0.28	0.23	0.22	0.18	0.16	0.15	0.12	0.12	0.14	0.22	0.23	0.21	0.29	0.31	0.51
3 periods of an curved hybrid surface, 7.5 cm deep	0	0.47	0.39	0.33	0.28	0.23	0.22	0.18	0.16	0.15	0.12	0.11	0.14	0.19	0.19	0.21	0.26	0.29	0.34
	56.9 random	0.40	0.30	0.24	0.19	0.14	0.11	0.09	0.09	0.09	0.10	0.25	0.40	0.53	0.53	0.25	0.32	0.67	0.57
3 periods of an curved hybrid surface, 7.5 cm deep	0	0.45	0.39	0.31	0.28	0.23	0.28	0.24	0.26	0.46	0.35	0.36	0.46	0.45	0.43	0.41	0.41	0.44	0.42
	56.9 random	0.47	0.39	0.32	0.27	0.24	0.26	0.23	0.22	0.31	0.28	0.29	0.39	0.44	0.42	0.36	0.42	0.50	0.48

C.1 Diffusion coefficient table (Continued)

Surface	Angle of incidence (°)	Frequency (Hz)																	
		100	125	160	200	250	315	400	500	630	800	1000	1250	1600	2000	2500	3150	4000	5000
7 Schroeder diffusers, 3.6 m wide																			
N = 7 QRD, 6 periods, 0.2 m deep	0	0.40	0.28	0.24	0.18	0.15	0.11	0.10	0.12	0.20	0.23	0.13	0.11	0.09	0.23	0.39	0.04	0.19	0.28
	56.9	0.46	0.41	0.37	0.31	0.32	0.21	0.25	0.33	0.43	0.33	0.36	0.16	0.33	0.47	0.44	0.33	0.39	0.62
	random	0.43	0.36	0.30	0.23	0.22	0.19	0.21	0.32	0.33	0.29	0.28	0.14	0.26	0.37	0.38	0.25	0.26	0.43
Optimized diffuser, modulated array, 6 periods, 8 wells/period, 0.17 m deep	0	0.40	0.29	0.23	0.18	0.19	0.17	0.15	0.35	0.60	0.41	0.41	0.50	0.59	0.39	0.34	0.39	0.30	0.34
	56.9	0.45	0.39	0.41	0.34	0.30	0.31	0.43	0.41	0.54	0.57	0.42	0.48	0.58	0.50	0.58	0.55	0.59	0.57
	random	0.43	0.37	0.34	0.27	0.23	0.27	0.32	0.37	0.49	0.51	0.42	0.44	0.54	0.45	0.45	0.49	0.43	0.47
N = 7 PRD, 6 periods, 6 wells/period, 0.2 m deep	0	0.40	0.28	0.23	0.17	0.15	0.13	0.12	0.09	0.10	0.34	0.13	0.15	0.21	0.27	0.10	0.35	0.21	0.07
	56.9	0.47	0.42	0.38	0.32	0.29	0.39	0.42	0.34	0.29	0.31	0.19	0.23	0.37	0.36	0.21	0.28	0.34	0.22
	random	0.44	0.36	0.30	0.23	0.20	0.29	0.29	0.27	0.28	0.26	0.22	0.24	0.26	0.34	0.25	0.31	0.34	0.26
Diffractional, 1 period, 3 orders of size, N = 7, 0.5 m deep	0	0.39	0.46	0.30	0.41	0.41	0.43	0.60	0.35	0.42	0.42	0.43	0.52	0.57	0.49	0.49	0.40	0.47	0.54
	56.9	0.61	0.53	0.56	0.56	0.53	0.61	0.79	0.63	0.68	0.68	0.57	0.43	0.62	0.67	0.66	0.56	0.16	0.69
	random	0.48	0.42	0.45	0.47	0.45	0.50	0.64	0.48	0.53	0.52	0.49	0.40	0.54	0.53	0.50	0.48	0.36	0.53
Optimized diffuser, 6 modulated periods, 12 wells/period, 0.17 m deep	0	0.40	0.29	0.23	0.18	0.18	0.15	0.27	0.63	0.60	0.52	0.59	0.33	0.31	0.49	0.37	0.30	0.42	0.54
	56.9	0.43	0.39	0.38	0.32	0.42	0.62	0.53	0.77	0.59	0.47	0.68	0.54	0.62	0.54	0.49	0.42	0.50	0.73
	random	0.40	0.35	0.30	0.24	0.29	0.42	0.46	0.64	0.55	0.47	0.59	0.44	0.46	0.50	0.44	0.41	0.47	0.54

C.2 Correlation scattering coefficient table

	<i>Angle of incidence</i> (°)	<i>Frequency</i> (Hz)																	
		100	125	160	200	250	315	400	500	630	800	1000	1250	1600	2000	2500	3150	4000	5000
Plane surfaces, non-absorbing, any size	All/any	0.00	0.00	0.00	0.00	0.00	0.00	0.00	0.00	0.00	0.00	0.00	0.00	0.00	0.00	0.00	0.00	0.00	0.00
1 Effect of changing diffuser width and periodicity, semicylinder(s) non-absorbing surfaces, radius 0.3 m (1 cm flat section between each period)																			
1 period, 0.61 m wide	0	0.06	0.09	0.13	0.20	0.29	0.38	0.43	0.45	0.59	0.78	0.82	0.80	0.92	0.89	0.92	0.94	0.95	0.96
	56.9	0.27	0.24	0.23	0.26	0.32	0.45	0.69	0.79	0.80	0.92	0.88	0.91	0.90	0.90	0.91	0.92	0.94	0.96
	random	0.24	0.21	0.21	0.25	0.32	0.43	0.62	0.73	0.74	0.82	0.86	0.88	0.90	0.91	0.94	0.95	0.96	0.96
2 periods, 1.22 m wide	0	0.04	0.05	0.05	0.04	0.02	0.11	0.65	0.87	0.64	0.56	0.87	0.79	0.90	0.89	0.92	0.93	0.94	0.91
	56.9	0.13	0.12	0.18	0.40	0.43	0.71	0.85	0.93	0.80	0.71	0.81	0.87	0.90	0.89	0.93	0.92	0.94	0.96
	random	0.16	0.16	0.21	0.32	0.34	0.52	0.80	0.93	0.76	0.67	0.88	0.87	0.91	0.91	0.93	0.94	0.95	0.95
4 periods, 2.44 m wide	0	0.01	0.00	0.02	0.06	0.02	0.08	0.35	0.74	0.55	0.49	0.87	0.77	0.87	0.84	0.80	0.86	0.83	0.88
	56.9	0.14	0.19	0.24	0.34	0.36	0.82	0.87	0.96	0.76	0.52	0.77	0.86	0.90	0.88	0.92	0.92	0.95	0.98
	random	0.21	0.22	0.24	0.29	0.30	0.53	0.78	0.93	0.71	0.56	0.87	0.86	0.90	0.88	0.90	0.93	0.94	0.94
6 periods, 3.66 m wide	0	0.00	0.01	0.01	0.04	0.03	0.05	0.25	0.55	0.53	0.45	0.86	0.72	0.80	0.81	0.79	0.85	0.82	0.95
	56.9	0.15	0.20	0.23	0.26	0.24	0.84	0.89	0.97	0.74	0.48	0.75	0.85	0.89	0.87	0.94	0.95	0.97	0.98
	random	0.22	0.23	0.24	0.26	0.26	0.52	0.76	0.91	0.68	0.51	0.86	0.85	0.89	0.88	0.90	0.94	0.94	0.95
12 periods, 7.32 m wide	0	0.00	0.00	0.01	0.02	0.02	0.03	0.13	0.33	0.48	0.40	0.86	0.76	0.84	0.87	0.83	0.81	0.87	0.90
	56.9	0.16	0.15	0.10	0.08	0.12	0.81	0.89	0.97	0.71	0.40	0.74	0.88	0.93	0.90	0.94	0.91	0.93	0.94
	random	0.23	0.22	0.21	0.20	0.19	0.48	0.73	0.87	0.64	0.46	0.86	0.86	0.89	0.87	0.89	0.92	0.92	0.91
2 Effect of surface depth, 6 semi-ellipses, non-absorbing, each 0.6 m width, total width 3.66 m (1 cm flat section between semi-ellipses)																			
1 cm deep	0	0.00	0.00	0.00	0.00	0.00	0.00	0.00	0.00	0.01	0.01	0.01	0.02	0.02	0.04	0.04	0.10	0.14	0.37
	56.9	0.00	0.00	0.00	0.00	0.00	0.01	0.00	0.00	0.01	0.01	0.01	0.01	0.01	0.02	0.03	0.07	0.21	0.20
	random	0.00	0.00	0.00	0.00	0.00	0.02	0.01	0.01	0.02	0.01	0.02	0.02	0.03	0.04	0.06	0.10	0.13	0.20
2 cm deep	0	0.00	0.00	0.00	0.00	0.00	0.00	0.00	0.01	0.03	0.04	0.05	0.07	0.09	0.15	0.17	0.36	0.47	0.80
	56.9	0.00	0.00	0.00	0.00	0.00	0.02	0.02	0.02	0.02	0.03	0.03	0.04	0.05	0.08	0.13	0.27	0.53	0.54
	random	0.00	0.00	0.00	0.00	0.01	0.05	0.04	0.04	0.06	0.05	0.07	0.08	0.10	0.15	0.22	0.33	0.41	0.53

C.2 Correlation scattering coefficient table (Continued)

	Angle of incidence (°)	Frequency (Hz)																	
		100	125	160	200	250	315	400	500	630	800	1000	1250	1600	2000	2500	3150	4000	5000
5 cm deep	0	0.00	0.00	0.00	0.00	0.00	0.00	0.01	0.06	0.20	0.23	0.33	0.40	0.51	0.67	0.77	0.86	0.84	0.92
	56.9	0.00	0.00	0.00	0.00	0.01	0.12	0.11	0.11	0.15	0.16	0.19	0.24	0.29	0.39	0.54	0.85	0.93	0.94
	random	0.00	0.00	0.01	0.01	0.06	0.16	0.16	0.18	0.22	0.25	0.31	0.38	0.47	0.59	0.71	0.80	0.82	0.85
10 cm deep	0	0.00	0.00	0.00	0.00	0.00	0.01	0.03	0.26	0.64	0.71	0.85	0.82	0.73	0.80	0.88	0.86	0.93	0.96
	56.9	0.00	0.00	0.00	0.01	0.05	0.38	0.35	0.37	0.46	0.51	0.56	0.65	0.72	0.81	0.92	0.93	0.94	0.95
	random	0.02	0.04	0.06	0.09	0.15	0.31	0.36	0.44	0.54	0.64	0.73	0.78	0.80	0.84	0.89	0.91	0.93	0.94
20 cm deep	0	0.00	0.00	0.00	0.01	0.01	0.03	0.12	0.66	0.91	0.61	0.26	0.78	0.86	0.76	0.91	0.88	0.87	0.86
	56.9	0.03	0.04	0.06	0.09	0.19	0.75	0.76	0.88	0.87	0.81	0.70	0.72	0.85	0.92	0.91	0.96	0.97	0.98
	random	0.14	0.16	0.18	0.20	0.25	0.47	0.64	0.87	0.90	0.76	0.62	0.80	0.90	0.87	0.92	0.93	0.94	0.95
30 cm deep (semicylinder)	0	0.00	0.01	0.01	0.04	0.03	0.05	0.25	0.55	0.53	0.45	0.86	0.72	0.80	0.81	0.79	0.85	0.82	0.95
	56.9	0.15	0.20	0.23	0.26	0.24	0.84	0.89	0.97	0.74	0.48	0.75	0.85	0.89	0.87	0.94	0.95	0.97	0.98
	random	0.22	0.23	0.24	0.26	0.26	0.52	0.76	0.91	0.68	0.51	0.86	0.85	0.89	0.88	0.90	0.94	0.94	0.95
3 Triangles, non-absorbing, 3.66 m wide (0.01 cm flat section between each period)																			
15 periods, 60°	0	0.01	0.01	0.00	0.00	0.00	0.01	0.02	0.03	0.04	0.06	0.05	0.06	0.37	0.12	0.06	0.12	0.13	0.17
	56.9	0.49	0.60	0.68	0.71	0.58	0.19	0.18	0.33	0.25	0.45	0.23	0.27	0.68	0.65	0.95	0.92	0.93	0.98
	random	0.34	0.35	0.35	0.34	0.32	0.28	0.24	0.30	0.27	0.32	0.24	0.34	0.50	0.53	0.67	0.69	0.72	0.75
9 periods, 45°	0	0.00	0.00	0.00	0.00	0.01	0.04	0.03	0.07	0.16	0.29	0.30	0.17	0.23	0.22	0.22	0.19	0.23	0.28
	56.9	0.03	0.04	0.06	0.07	0.08	0.20	0.54	0.95	0.99	0.75	0.93	0.97	0.99	0.99	0.99	0.99	1.00	1.00
	random	0.15	0.17	0.19	0.21	0.23	0.28	0.37	0.59	0.80	0.79	0.69	0.82	0.83	0.87	0.89	0.90	0.90	0.91
6 periods, 30° 3.66 m wide	0	0.00	0.00	0.00	0.00	0.01	0.02	0.06	0.36	0.96	0.98	0.81	0.99	0.89	0.97	0.97	0.99	1.00	0.99
	56.9	0.01	0.02	0.02	0.04	0.18	0.81	0.76	0.72	0.70	0.83	0.90	0.94	0.99	1.00	0.99	0.99	1.00	1.00
	random	0.11	0.13	0.14	0.17	0.26	0.47	0.61	0.72	0.81	0.90	0.93	0.95	0.95	0.97	0.97	0.98	0.98	0.98
3 periods, 18°	0	0.00	0.01	0.01	0.02	0.17	0.49	0.66	0.78	0.90	0.99	0.98	0.95	0.99	0.99	0.99	0.99	0.99	0.99
	56.9	0.01	0.10	0.37	0.42	0.37	0.39	0.43	0.51	0.59	0.71	0.82	0.94	0.98	0.94	0.94	0.99	0.97	0.98
	random	0.07	0.17	0.31	0.38	0.41	0.48	0.56	0.67	0.78	0.88	0.93	0.94	0.97	0.98	0.99	0.99	0.99	0.99
4 Semi-ellipses mounted on 3.63 m wide flat baffle, non-absorbing, each semi-ellipse 0.6 m wide, 0.2 m deep																			
1 semi-ellipse in middle of baffle	0	0.01	0.02	0.03	0.09	0.20	0.22	0.36	0.40	0.35	0.22	0.19	0.27	0.20	0.19	0.14	0.18	0.21	0.30
	56.9	0.09	0.17	0.24	0.29	0.37	0.39	0.43	0.48	0.52	0.47	0.44	0.43	0.37	0.48	0.67	0.74	0.77	0.60
	random	0.15	0.22	0.28	0.32	0.38	0.42	0.47	0.51	0.53	0.48	0.44	0.46	0.48	0.49	0.50	0.53	0.52	0.54

	<i>Angle of incidence</i> ($^{\circ}$)	<i>Frequency</i> (Hz)																	
		100	125	160	200	250	315	400	500	630	800	1000	1250	1600	2000	2500	3150	4000	5000
3 semi-ellipses with 0.6 m flat sections between	0	0.00	0.01	0.03	0.05	0.26	0.72	0.88	0.89	0.70	0.46	0.53	0.65	0.63	0.58	0.51	0.66	0.68	0.76
	56.9	0.03	0.17	0.52	0.62	0.56	0.66	0.78	0.80	0.90	0.95	0.94	0.72	0.54	0.72	0.90	0.80	0.91	0.91
	random	0.13	0.22	0.38	0.50	0.57	0.67	0.79	0.85	0.85	0.76	0.69	0.75	0.77	0.75	0.79	0.85	0.81	0.78
5 Optimized curved surfaces, 3.6 m wide, modulated arrays																			
3 periods, 30 cm deep	0	0.00	0.03	0.06	0.16	0.59	0.95	0.99	0.95	0.88	0.71	0.88	0.89	0.92	0.79	0.92	0.93	0.82	0.95
	56.9	0.05	0.31	0.74	0.76	0.70	0.68	0.85	0.88	0.92	0.95	0.94	0.89	0.94	0.96	0.95	0.99	0.97	0.99
	random	0.15	0.30	0.50	0.64	0.74	0.79	0.90	0.94	0.89	0.86	0.91	0.93	0.95	0.94	0.94	0.95	0.96	0.97
6 periods, 20 cm deep	0	0.00	0.00	0.00	0.01	0.02	0.04	0.14	0.61	0.81	0.94	0.80	0.78	0.68	0.84	0.60	0.84	0.78	0.86
	56.9	0.01	0.02	0.02	0.04	0.23	0.73	0.79	0.88	0.98	0.86	0.78	0.92	0.94	0.94	0.98	0.98	0.96	0.96
	random	0.09	0.11	0.14	0.16	0.27	0.48	0.68	0.85	0.94	0.89	0.80	0.86	0.90	0.93	0.89	0.94	0.95	0.94
6 periods, 10 cm deep	0	0.00	0.00	0.00	0.01	0.01	0.02	0.07	0.15	0.23	0.30	0.38	0.82	0.86	0.80	0.89	0.73	0.90	0.89
	56.9	0.00	0.01	0.01	0.03	0.11	0.15	0.20	0.24	0.67	0.71	0.77	0.81	0.82	0.89	0.96	0.97	1.00	0.99
	random	0.01	0.03	0.04	0.09	0.15	0.20	0.25	0.31	0.50	0.62	0.73	0.84	0.89	0.92	0.95	0.94	0.95	0.96
6 periods, 5 cm deep	0	0.00	0.00	0.00	0.00	0.00	0.00	0.01	0.02	0.03	0.04	0.13	0.49	0.62	0.80	0.90	0.93	0.90	0.91
	56.9	0.00	0.00	0.00	0.01	0.01	0.02	0.02	0.04	0.31	0.39	0.42	0.42	0.43	0.52	0.69	0.81	0.93	0.95
	random	0.00	0.01	0.01	0.02	0.05	0.06	0.06	0.12	0.29	0.36	0.43	0.50	0.58	0.70	0.82	0.88	0.91	0.92
7 Schroeder diffusers, 3.6 m wide																			
N = 7 QRD, 6 periods, 0.2 m deep	0	0.00	0.01	0.02	0.05	0.08	0.07	0.04	0.35	0.51	0.67	0.57	0.52	0.44	0.73	0.85	0.39	0.71	0.86
	56.9	0.04	0.06	0.12	0.26	0.41	0.17	0.16	0.71	0.75	0.84	0.71	0.51	0.74	0.91	0.83	0.79	0.67	0.93
	random	0.12	0.15	0.19	0.27	0.36	0.30	0.25	0.69	0.78	0.72	0.69	0.51	0.66	0.86	0.82	0.69	0.70	0.88
Optimized diffuser, modulated array, 6 periods, 8 wells/period, 0.17 m deep	0	0.00	0.01	0.02	0.04	0.20	0.21	0.27	0.65	0.78	0.80	0.85	0.86	0.95	0.92	0.95	0.82	0.88	0.96
	56.9	0.03	0.07	0.11	0.22	0.40	0.43	0.55	0.58	0.76	0.90	0.74	0.89	0.95	0.96	0.94	0.96	0.96	0.97
	random	0.09	0.14	0.18	0.25	0.36	0.48	0.55	0.68	0.82	0.89	0.83	0.87	0.93	0.94	0.93	0.90	0.91	0.94
N = 7 PRD, 6 periods, 6 wells/period, 0.2 m deep	0	0.00	0.01	0.02	0.05	0.04	0.14	0.19	0.14	0.32	0.81	0.65	0.69	0.88	0.88	0.97	0.98	0.97	0.42
	56.9	0.04	0.09	0.18	0.38	0.41	0.47	0.66	0.59	0.61	0.83	0.96	0.93	0.88	0.94	0.92	0.89	0.95	0.96
	random	0.11	0.15	0.20	0.29	0.34	0.47	0.52	0.52	0.62	0.88	0.85	0.82	0.88	0.92	0.92	0.90	0.93	0.75
Diffraction, 1 period, 3 orders of size, N = 7, 0.5 m deep	0	0.16	0.45	0.28	0.39	0.70	0.85	0.87	0.83	0.73	0.79	0.89	0.86	0.96	0.96	0.89	0.84	0.91	0.90
	56.9	0.30	0.74	0.76	0.63	0.67	0.64	0.84	0.70	0.77	0.87	0.92	0.77	0.89	0.93	0.92	0.95	0.89	0.96
	random	0.33	0.56	0.66	0.61	0.72	0.80	0.88	0.80	0.78	0.85	0.91	0.80	0.91	0.92	0.91	0.91	0.90	0.91
Optimized diffuser, 6 periods modulated array, 12 wells/period, 0.17 m deep	0	0.00	0.01	0.01	0.03	0.14	0.20	0.50	0.78	0.82	0.84	0.92	0.81	0.89	0.87	0.84	0.92	0.92	0.94
	56.9	0.04	0.08	0.13	0.24	0.50	0.70	0.67	0.90	0.92	0.92	0.95	0.88	0.91	0.96	0.97	0.99	0.98	0.98
	random	0.14	0.17	0.21	0.27	0.40	0.61	0.69	0.90	0.90	0.91	0.92	0.87	0.87	0.90	0.91	0.93	0.94	0.94

Index

- 1D diffuser 89–90
- absorbers and absorbent materials:
 - bass traps/bins 13
 - granulated rubber 134
 - ground 4
 - measurement of 58–85
 - impedance tube 58–64
 - in situ* 74–7
 - multi-microphone, free field 65–8
 - reverberation chamber method 68–71
 - two microphone, free field 64–5
 - see also* flow resistance or resistivity; impedance, characteristic; pore: shape factor and characteristic dimensions; porosity; tortuosity; wavenumber
 - phase grating absorber 188–200
 - optimized 193–4
 - properties:
 - basic principles 6–22
 - characteristics of 1–2
 - hybrid absorber-diffuser 163
 - internal 78–84
 - seating and audience 71–4, 186–8
 - see also* active absorbers; carpet, absorption from; curtain absorption; foam; Helmholtz absorber; hybrid absorber-diffuser; membrane absorber; microperforated absorber; mineral wool; plaster, acoustic; porous absorber; resonant absorbers; seating absorption
- absorbers and diffusers 33–6
 - comparison of 4–5
 - in rooms and geometric models 335–52
- absorption coefficient 1
 - active absorber 369
 - carpet 135
 - concrete masonry unit 164
 - coustone/quietstone 137
 - curtains 134–5
 - definition 9–12, 18
 - different angles of incidence 153
 - foam 131
 - geometric room acoustic models 339–43, 349
 - granulated rubber 134
 - Helmholtz absorber 157, 160, 168–70, 178–9
 - hybrid absorber-diffusers 163, 313–14, 324, 327
 - measurement of 58–77
 - membrane absorber 159
 - microperforated absorber 164–5, 180–3
 - mineral wool 130
 - periodic profiled absorber 68
 - plaster 135
 - porous absorber using transfer matrix methodology 148–51
 - profiled absorber 190, 194–5
 - random incidence 9, 58, 68–71
 - finite and infinite sample 336–8
 - from free field 335–40, 343
 - reverberation chamber 338–9
 - scattering coefficient measurement 113, 115, 122, 125
 - Schroeder diffuser 265–6
 - seating 186–8
- absorption versus diffusion reflection 4–5
- active absorbers 13, 131, 369, 371, 372
- active absorption:
 - in a small room 355
 - control system 359–60
 - control, principles of 356–9
 - in ducts 361–2
 - energy dissipation in 364
 - feedback/feedforward 360
 - hybrid with passive absorption 368–71
 - LMS 357
 - overview 359–61
 - in three dimensions 362–4
 - alternative control regime 365–8
 - example results 364–5
 - modal control 364–8
 - using biquad filters 365–8

- active diffusers 44, 371–3
- active impedance *see* active absorption;
active diffusers
- active noise control 356
- admittance 16–18, 196–7, 205, 267–8,
359
- AES-4id-2001 *see* diffusion coefficient
- air absorption 9
- apparent specular absorption coefficient 113
- audience absorption 186–8
- audience canopy 47
- auralisation 340, 344, 349
- autocorrelation:
diffusion coefficient 106–7
hybrid absorber-diffusers 317–18, 320–1,
323–4, 327, 328–9
modulation/periodicity 248–51, 253
Schroeder diffusers 245–47
- Barker sequence 249, 328
modulated diffuser array 250–4
- bass traps/bins 13
- beam tracing *see* geometric room acoustic
models
- BEM *see* boundary element method
- Bessel function 176, 181, 338
- Biot theory 153
- Bloch theorem 213
- boss models 231
- boundary element method (BEM) 202–30,
257
2D versus 3D 209
example predictions 68, 98–102, 280–4,
292–3, 332
external point pressures 209
Fast Multipole Method (FMM) 212
general solution method 205–19
Helmholtz–Kirchhoff integral
equation 204–5
non-unique solutions 207
Burton Miller method 207
CHIEF method 207
periodic formulation 212–15
scattering and diffusion coefficients 118,
121
Schroeder diffusers/absorbers 196–200,
216–19, 268–70
surface pressures 206–9
thin panel solution 209–12
accuracy 215–16
non-absorbing surface 210–11
planar thin surface with non-zero
admittance 211–12
transient 228–30
- boundary plane measurement 89, 91–2,
98, 111
- bulk modulus 16, 144–6, 154
- canopy design *see* audience canopy; stage
canopy
- carpet, absorption from 129, 135–6, 187–8
- CDMPRD *see* Cox and D’Antonio modified
PRD
- ceiling tile, acoustic 7
- characteristic impedance *see* impedance,
characteristic
- characteristic lengths 21, 144–5
- Chinese remainder theorem 317
method 324–6
Schroeder diffusers 261–2, 264
- Chu sequence 247, 255, 262
- Cinerama Theatre 45–6
- clear absorber 164
- Cleveland Institute of Music 50
- coherence 30–1
- colouration, reducing 45–6
music practice rooms 39–43
sound reproduction 32–9
- comb filtering 29, 35, 37–8, 103–4, 279,
291, 295, 305
- compressibility 16
- concave arc 288–90
focusing effects 52–3
polar responses 53, 102, 123, 289
- concrete masonry unit (CMU) 164–5, 170
- convex arcs 290–7
see also semicylinders
- corner reflector 286
- Corning Glass Centre 52
- correlation scattering coefficient 109, 119,
120–4, 351
- coustone/quietstone 137, 138
- Cox and D’Antonio modified PRD
(CDMPRD) 244, 254, 272–3
- curtain absorption 134–6
for different weight material 135
with different fullness of draping 134
- curved diffuser 293
application of 24, 25, 45–7, 53–4, 297–8
cut-off frequencies 291–3
hybrid absorber-diffuser 324, 330–1
modulation 303–5
optimized 297–307
design process 298–301
results 301–3
polar responses 290, 293–5, 301
stage canopy 305–7
see also concave arc; convex arc;
semicylinders
- cylinders *see* semicylinders
- damping 13, 158, 160, 164, 191, 362, 366
- Delany and Bazley empirical model 58,
141–3, 147, 150–3
- density, effective 16, 146, 152

- Diffractal 256
- diffraction 32
 - grating 294
- diffsorption *see* hybrid absorber-diffuser
- diffuse reflections:
 - from absorbers *see* hybrid absorber-diffusers
 - geometric room acoustic models 104–7, 112, 124, 230, 340–1, 343–52
 - measurement and characterization of 87–126
 - other methods for characterizing 124–6
 - in situ* measurement of 124
- diffuse sound field 11–12, 43, 69, 74, 118, 125, 336, 339, 341–2, 346
- diffusers:
 - application, compared to absorption 4–5
 - applications and basic principles of 23–56
 - colouration, reducing 32–9, 45–6
 - echo control 23–32
 - focusing effects of concave surfaces 52–3
 - music practice room with 39–56
 - noise barriers 55
 - position of a listener from 36–7
 - reverberation chambers 43–4
 - road side barriers 53–5
 - sound reproduction 32–9
 - spaciousness 44–5
 - speech intelligibility in underground (subway) stations 44
 - stage and audience canopies/shell 46–52
 - street canyons 55
 - surface/volume diffusers 43
 - visual appearance 25
 - wavefronts reflected from 26–8, 32
 - see also* active diffusers; convex arcs; curved diffuser; fractal diffusers; geometric reflectors and diffusers; hybrid absorber-diffuser; optimized, diffusers; primitive root diffuser; quadratic residue diffuser; Schroeder diffuser; semicylinders; triangular diffusers
- ‘diffusor’ 32
- diffusion coefficient 87, 91, 98, 100–13, 118–20, 122–4, 270, 299
 - compared to scattering coefficient 32, 104–5, 120–2, 124
- diffuser manufacturer and application 105–6
- geometric room acoustic models 106–7
- obtaining polar responses 109–10
- principle 107–9
- Schroeder diffuser 87–8, 102
- spectra 120–3, 247, 250, 302
 - active and passive diffusers 372
 - arrays of semicylinders 103
 - hybrid absorber-diffusers 323, 330–3
 - Schroeder diffusers 237, 252, 255, 260, 273
 - various diffusers 111
 - table 111–12
- diffusorBlox 165
- drapes *see* curtain absorption
- early lateral energy fraction (ELEF) 106, 341, 350–1
- echo 13–15, 23–32, 109
 - absorption verses diffuse reflection 4
- edge diffraction 214, 221, 222, 229–30, 285, 343, 351
 - absorbers 64, 65, 77, 161, 337, 339
 - models 230
- Edwina Palmer Hall 53
- ellipses 112
- end correction 167–8, 170
- energy attenuation coefficient 9
- envelopment *see* spatial impression
- extended reaction 61, 150
- Eyring formulation 10, 69, 126, 341, 346
 - Eyring–Norris equation 10
- far field 99–102, 240, 267, 280–2, 317
 - see also* near field
- Fast Multipole Methods (FMM) 212
- Feldman modified primitive root diffuser (FMPRD) 243, 244
- Fermat’s principle 279
- fibreglass *see* mineral wool
- fibrous absorbers *see* porous absorber
- finite element analysis (FEA) 207, 229
- flow impedance measurement 81–2
- flow resistance or resistivity 21
 - active absorbers 368–9
 - defined 138–40
 - empirical formulations 139–40
 - measurement 78–81
 - alternating airflow method 79
 - direct airflow method 78
 - flow impedance 81–2
 - Ingard’s method 80
 - in models of porous absorbents 141–3, 146, 153
 - resonant absorption 169–70, 173–4
 - Schroeder diffusers/absorbers 190, 192, 196
 - units 138
- flow through a perforated sheet 174
- flutter echoes 14–15, 23, 39
- FlutterFree 117, 163
- FMPRD *see* Feldman modified primitive root diffuser
- foam 21, 129–33, 140–1, 336, 371
 - flow resistivity 139–40

- focussing *see* concave arc
- Fourier synthesis *see* fractal diffusers
- Fourier theory 122, 200, 226, 298
array, response of 281
hybrid absorber-diffusers 316, 327, 332
Schroeder diffuser 226, 228
- fractal diffusers 231, 302, 308–11
Fourier synthesis 308–9
Fractional Brownian Diffusers (FBD) 309
random addition diffusers (RAD) 311
Schroeder diffuser (DiffRACTal) 255–7
step function addition 309–11
- Fraunhofer prediction model 203, 225–9, 291
BEM model, comparison between 228–9
Kirchhoff solutions, comparison between 229
Schroeder diffusers 240, 257, 266, 269–70
- frequency response 97, 124–5, 159, 229, 284, 360–1
comb filtering 35, 37–8, 103
curved surfaces 291, 297
flat surface and a diffuser 28–31
music practice room 42
plane surface 277–9
room, low frequency 12–14
see also total sound field
- Fresnel prediction model 203, 224–5, 277, 284, 291
- genetic algorithm 77, 270, 322–3
- geometric reflection point 36, 48, 278, 280, 283–4, 307
- geometric reflectors and diffusers 276–311
see also convex arcs; curved diffuser; optimized, diffusers; semicylinders; triangular diffusers
- geometric room acoustics models:
diffusion coefficients 106–7
modelling of scattering:
diffuse energy decays with reverberation time of the hall 346
distributing the diffuse energy 346–8
early sound field wave model 346
radiosity and radiant exchange 346
ray re-direction 345
scattering coefficients 349–52
transition order using particle tracing 345
user-defined transition order 345
polar responses 348
scattering coefficients 106–7, 344–52
- glass fibre *see* mineral wool
- glazing 163–4
- global minimum 271
- goniometer 89, 121
- grating lobes 237–8, 241, 247–9, 251, 255, 260, 262, 282, 294, 297, 303, 317
- Green's function 204–5, 208–9, 214, 224–5, 270, 290
- Hankel function 205–6
- Helmholtz absorber 157–8, 194–5
absorption versus diffuse reflection 5
application 13, 161–5
clear absorber 164
design equations 166–70, 172–8
double resonators 180
end correction 167–8, 170
example calculations 178–80
example constructions 164
facing thickness, effect of 170
flow resistivity, effect of 169–70
hybrid absorber-diffuser 162–3
lateral orifices 183
measured impedance for 177–9
open area, effect of 168–9
random incidence absorption coefficient 162
slotted 170, 178
slotted neck pate and a resistive foil 184
see also microperforated absorber; resonant absorber
- Helmholtz mount 162
- Helmholtz resonator 258, 260
- Helmholtz–Kirchhoff integral equation 202, 204–5, 224, 228
- Hemispherical diffuser 90
- Hit Factory 36, 38
- Huffman sequence 245–7
- Hummingbird Centre 24–5, 297
- Huygen's construct for reflection from:
cylinder 27
flat surface 26
hybrid surface 30, 32
Schroeder diffuser 28
- hybrid absorber-diffuser 38, 112, 163, 221, 313–34
1D 317
absorption 324–6
accuracy of simple theories 327–9
boundary element modelling 214–15, 332–3
construction of a 314–15
curved hybrid surface 314–16
designing curved hybrid surfaces 324
diffuse reflections 330–2
diffusion coefficient spectra 323, 330–3
number sequences 318–24
optimized 322–4
planar 313–14
polar responses 221, 319, 329–33

- hybrid absorber-diffuser (*Continued*)
 - random incidence absorption
 - coefficient 314
 - simplest theory 316–17
 - wavefronts (Huygen's construct) 30, 32
- hybrid active-passive absorber 368
- hybrid curved diffuser (Digiwave) 316
 - see also* hybrid absorber-diffuser
- hybrid room models *see* geometric room
 - acoustic models
- image processing, distortion in 300
- image shift 4, 33, 48
- image source modelling *see* geometric room
 - acoustic models
- impedance:
 - active 359–61, 368–70
 - characteristic:
 - definition 15–16
 - empirical models for 141–3
 - measurement 82–3
 - phenomenological model 147
 - normalized 18
 - propagation constant and
 - characteristic 142
 - radiation 258–9
 - surface impedance 335–7, 340
 - admittance, reflection and absorption coefficient 17–18
 - anisotropic materials 152–3
 - in situ* measurement 74–7
 - measurement 60–8
 - measurement and prediction
 - compared 143, 151, 154, 179
 - resonant absorber 166, 173, 175–8, 181
 - rigid backed porous absorbent 20, 152
 - transfer matrix modelling 20, 148–53
- impedance tube measurement 68, 76–7, 141, 151, 159, 178, 182, 200, 336–7
 - flow impedance 81
 - overview 60–1
 - standing wave method 61–2
 - transfer function method 62–4
 - wavenumber 82
- impulse response 89, 93–4, 103, 113–14, 124, 229–30, 340
 - in a room 8, 10, 34
 - flat surface and a diffuser 28–31
 - music practice room before and after treatment 41
 - scattered 92, 94
 - in situ* measurement of absorption 74–5
 - see also* total sound field
- index sequences 245
- infinite impulse response (IIR) 365–6
- intelligibility *see* speech intelligibility
- Kath and Kuhl method 71–4
- Kirchhoff:
 - boundary conditions 213–14, 220–24
 - Fraunhofer solution, difference between, 228
 - predicted polar responses 221–3
 - prediction model 203, 208, 219–24, 225, 228–9, 284, 327, 332
- Kresge Auditorium 46–7
- Lambert's cosine law 105, 107, 344–9, 352
- lateral reflections 44–5
- Live End Dead End (LEDE) 33
- local reaction 151, 267–8
- Man Made Mineral Fibres (MMMFs) 132–3, 140
- Masonry units 42, 164–5
- maximum length sequences (MLS) 44, 70, 89, 115, 251, 313, 317–19, 320–1, 324, 329, 332, 361
 - sequence diffuser 239–42
 - polar responses 242, 319
- measurement of:
 - absorbent materials 58–86, 78–84
 - polar responses 88–103
 - scattering/diffusion 87–128
- membrane absorber 13, 61, 163
 - design equations 166, 171–2
 - losses 172–78
 - example construction 158–61
 - isothermal 171
 - mechanisms 158–9
 - microperforation 182
- microperforated absorber 164, 180–3
- Millington equation 10, 69, 341, 342
- mineral wool 129
 - in a partition 19
 - absorption mechanism 15
 - application 7, 11, 136, 140, 176
 - characteristic lengths 145
 - flow resistivity 140
 - in hybrid absorber-diffusers 313–14, 316, 326–7
 - local and extended reaction 151
 - manufacture 132–3
 - modelling 21
 - porosity 140
 - in resonant absorbers 13, 158
 - see also* porous absorbent; porous absorber
- MLS *see* maximum length sequence
- modal control 12–13, 40
 - active 364–7
- mode matching prediction of scattering 230
- modulation 162, 237–8, 262, 287–8, 294–5, 298–9, 301, 327–9

- curved surfaces 303–5
- polar responses showing effects of 250–1, 254–5, 294–5, 329
- Schroeder diffusers 248–55
- modulo 235
- Mommertz and Vorländer method *see*
 - scattering coefficient
- multi-microphone measurement of
 - impedance and absorption:
 - free-field 64, 66, 198
 - for non-isotropic, non-planar surfaces 65–6
 - for periodic surfaces 66–8
- music practice rooms 39–43
- Navier–Stokes equation 183
- near field:
 - acoustic holography 101
 - diffusers 36–7, 267
 - measurement 98–102
 - multi-microphone measurement 66
 - prediction models, and 213, 226
 - scattering 283
 - see also* far field
- noise control 2–3, 11, 13, 165
 - barriers 55
 - factories 11
 - porous absorbers 11
- non-diffuse sound field 11–12, 43, 69, 74, 118, 125, 336, 339, 341–2, 346
- non-environment 36
- notch diffuser 244–5
- number sequences:
 - optimized 247, 322–3
 - perfect array construction method 324
 - see also* Barker sequence; Chu sequence; Huffman sequence; index sequences; maximum length sequences (MLS); primitive root sequence; quadratic residue sequence
- optimized:
 - curved surface 276
 - application of 24–5, 46–7, 53–4, 297–8
 - design process 298–301
 - modulation 303–5
 - results 301–3
 - stage canopy 305–7
 - diffuser 112, 124, 330–1
 - diffusion coefficient 105
 - fractals 311
 - hybrid absorber-diffuser 322–4
 - notch diffuser 244–5
 - number sequences 247, 322–3
 - phase grating absorber 193–4
 - Schroeder diffusers 267, 268–73
 - procedure 268–71
 - results 271–3
 - optimizing to obtain absorber
 - properties 76–7
 - optimum diffusion 233–4, 237, 245, 248, 267–8
 - panel absorbers *see* membrane absorbers
 - Paris' formula 118, 335–6, 338
 - particle velocity of plane wave 15
 - periodicity of diffusers 248–9
 - see also* modulation
 - phenomenological model of porous
 - absorbents 147–8
 - pipes and ducts, absorption in 20
 - planar hybrid absorber-diffuser 112, 221, 313–34
 - BEM model 214–15
 - polar responses 221, 319, 329, 330–1, 332–3
 - see also* hybrid absorber-diffuser
 - plane surface 276–85
 - cut-off frequencies 291–3
 - far field arc 281–2
 - frequency response 277
 - Huygen's construct 26
 - near field 282–4
 - polar responses 99, 280, 282
 - single panel response 276–84
 - plaster, acoustic 7, 129, 135, 137
 - polar banana 262
 - polar responses:
 - calculating scattering coefficients
 - from 120–4
 - concave arc or prism 53, 102, 123, 289
 - curved diffusers 290, 294–5, 301
 - for diffusion coefficients 109–10
 - fibreglass 330
 - geometric models 348
 - hybrid surfaces 215, 319, 329–33
 - Lambert distribution 347
 - measurement 88–104
 - MLS diffuser 242, 319
 - modulation, showing effects of 250–1, 254–5, 294–5, 329
 - near and far fields 95–103
 - plane surfaces 99, 280, 282
 - plane, random rough, semi-circle and periodic surfaces 348
 - prediction accuracy, demonstrating 97, 214–18, 221, 222–3, 227–9, 293
 - primitive root diffuser 243–5, 250
 - quadratic residue diffuser 235–6, 238–9
 - redirecting surface 109
 - sample considerations 102–3
 - Schroeder diffusers 250–1, 254–5, 259, 262–3, 272
 - triangles 284–8

- pore:
 - shape factor and characteristic dimensions 144–5
 - structures, differences 130
- porosity 21, 58, 78, 83–4, 133, 138–9, 140–2, 144, 167, 171, 173, 176, 178
 - definition 140
 - measurement of 83–4
 - table of typical values 141
- porous absorber 5, 11–21, 59, 61, 64, 78, 82–3, 129–41, 143–5, 157, 171–2, 174, 176, 178–80, 186, 369
 - comparison of models 154
- porous absorption 129–55
 - anisotropic materials 152–3
 - backing distance, effect of 130–1
 - basic material properties 137–40
 - characteristic dimensions 144–5
 - flow resistivity 138–40
 - porosity 140
 - tortuosity 21, 137, 145–6
 - Biot theory for elastic-framed material 153
 - characterizing 21
 - covers 131–2
 - external lagging 21
 - impedance and absorption of 148–51
 - single layer with rigid backing 149–51
 - local and extended reaction 150
 - material types 132–38
 - absorbent plaster 135–6
 - carpets 135
 - coustone 137
 - curtains (drapes) 134–5
 - mineral wool and foam 132–3
 - recycled materials 133–4
 - mechanisms and characteristics 129–32
 - models 21
 - oblique incidence 151–3
 - open and closed pore 129–30
 - porous absorbents:
 - macroscopic empirical models 141–3
 - material properties 144
 - modelling propagation within 141–6
 - theoretical models 145–8
 - treatment to reduce break out noise 20
 - see also* foam; Man Made Mineral Fibres (MMMFs); mineral wool
- prediction of scattering 202–32
 - mode matching 230
 - polar responses demonstrating
 - accuracy 98, 214–18, 220, 222–3, 228–9, 293
 - random roughness 203–31
 - transient BEM 229–30
 - wave decomposition 198–200, 230
- see also* boundary element method; Fourier; Fraunhofer; Fresnel; Kirchoff
- pressure:
 - of a plane wave 15
 - pressure reflection coefficient *see* reflection coefficient
- primitive root:
 - diffuser (PRD) 119, 120–1, 243–5, 254–5, 264, 285–6
 - polar responses 243–5, 250
 - sequence 242–5
- profiled absorbers 188–200
 - different methods to determine the depth sequence 194
- propagation constant 15, 82, 142
- pyramids 284
- quadratic residue:
 - diffuser (QRD) 23, 253, 258, 261–2
 - 1D and 2D 234
 - absorption 263, 265–6
 - admittance at well entrance 268
 - critical frequencies 239
 - cross section 234
 - design equations 234–6, 238–9
 - diffusion coefficient spectra 237, 247, 252, 255, 260, 273
 - improving bass response 257–60
 - multi-dimensional devices 260–3
 - periodicity and modulation 248–55
 - polar responses 235–6, 238–9, 250–1, 259, 262–4, 272
 - see also* Schroeder diffusers
 - sequence 193, 235, 242
- random addition diffusers (RAD) 311
- random incidence absorption coefficient *see* absorption coefficient
- random rough surfaces:
 - polar response 348
 - prediction models 230–1
- ray tracing 10, 284–9, 340–7
 - in a room 340
 - scattering from a concave arc 289
 - sound reflecting from a pair of triangles 285
 - see also* geometric room acoustic models
- reactance 16
- receiver arc radius, effect of:
 - diffusion coefficient 101
 - diffusion coefficient boundary measurement technique 91
- recycled materials 133–4
- redirecting surface 109
- reflection:
 - coefficient (factor) 219, 224, 240, 244–6, 248, 258–9, 268, 317–18, 343, 347

- absorber measurements 61–3, 65, 76–7
- angle of incidence 152
- definition 16–18,
- free zone (RFZ) 91–2, 287
 - sound reproduction room 2–3, 33, 35, 159
- from a flat and diffusely reflecting hall 49
- from a plane surface 277
- in large spaces 45–6
- phase grating 24, 28–9, 49, 112, 257
- polar response 99, 102
- spatial and temporal dispersion 31, 324
 - see also* Schroeder diffusers
- resistance 16
- resonant absorbers 157–84
 - calculations 178–80
 - porous absorbent filling the cavity 179–80
 - slotted Helmholtz absorber 178
 - construction examples 159–65
 - absorption and diffusion 162–3
 - bass trap membrane absorber 159–60
 - clear absorption 163–4
 - Helmholtz absorption 160–2
 - masonry devices 164–5
 - damping 13
 - design equations 166–78
 - double resonators 180
 - Helmholtz-membrane absorber,
 - combined 173
 - lateral orifices 183
 - slotted neck plate 184
 - see also* Helmholtz absorber; membrane absorber; microperforated absorber
- reverberation:
 - in a music practice room 42
 - chamber:
 - controlling modes in 43–4
 - measuring absorption coefficients 21, 43, 68, 73, 104
 - control 6–11
 - statistical model of 7–11
 - enhancement system 24
 - time 4, 44, 106, 186, 289
 - absorption measurement 69–71, 339–44
 - definition and formulations 8–12
 - geometric room acoustic models 340–4, 346, 349–51
 - scattering coefficient
 - measurement 114–15, 124, 126
- Rivercenter for the Performing Arts 46–7
- road side barriers 53–5
- room acoustic models *see* geometric room acoustic models
- room diffuseness, measuring scattering coefficients 125–6
- Royal Albert Hall 52
- Royal Festival Hall 14
- Sabine's formulation 1, 8–9, 12, 69, 341
 - conversion to Millington values 341
- scattering:
 - centre of two triangles 285
 - plane surface scattering, frequency
 - response for 279–80
 - prediction of 202–31
 - other methods 228–30
 - semicylinder 291
 - surface 37
 - theory 214, 291–3
 - cut-off frequencies 291–3
 - see also* polar response; specific diffuser types
- scattering coefficients 87–8, 112–20, 231
 - anisotropic surfaces 116–18
 - compared to diffusion coefficient 32, 104–5, 120–2, 124
 - correlation scattering coefficient 109, 119, 120–4, 351
 - definitions 112
 - free field 119
 - from polar responses to scattering coefficients 120–4
 - from room diffuseness 125–6
 - in geometric room acoustic models 106–7, 344–52
 - inverse problem 124–5
 - measurement set-up 114
 - non-circular samples 116
 - prediction of 118–20
 - principle 112–13
 - rationale and procedure 113–16
 - sample considerations 116
 - Schroeder diffuser 87–8, 107, 118–20, 122
 - table 123–4
- Schroeder diffuser 102, 107, 112, 233–74, 286–8, 297–8, 313, 316–18, 327–9, 349, 352
 - 1D 89, 233–4, 265, 349, 352
 - 2D 260–3
 - absorption coefficient 265–6
 - active diffusers 371–2
 - admittance of narrow wells 196–7
 - applications 44, 52
 - basic principles 233–4
 - bass response, improving 257–60
 - critical (flat plate) frequencies 239, 242, 252–3, 262
 - depths 194
 - design equations 234–6
 - design for diffusion and absorption compared 192

- Schroeder diffuser (*Continued*)
- Diffractal 256
 - diffusion coefficient 87–8, 104
 - spectra 237, 252, 255, 260, 273
 - folded wells 257–8
 - fractal 255–7
 - hexagonal 262
 - Huygen's construct 28
 - hybrid absorber-diffuser 163
 - limitations and other considerations 236–9
 - modulation 248–55
 - multi-dimensional devices 260–3
 - optimization 268–73
 - perforated sheets 258
 - periodicity, curse of 248–9
 - polar responses 238–9, 250–1, 254–5, 259, 262–3, 272
 - predicted scattering 218, 223
 - oblique sound incident on 220
 - predicting scattering from 209, 211
 - boundary element model 216–19
 - Fraunhofer or Fourier model 226, 229
 - Kirchhoff boundary conditions 222–4
 - wave decomposition models 230
 - profiled absorbers 188–200
 - absorption or diffusion 191
 - boundary layer absorption 191
 - depth sequence 193
 - energy flow mechanism 189–91
 - number of wells 196
 - theoretical model 196–9
 - use of mass elements 194–5
 - scattering coefficient 87, 88, 104, 118–20, 122
 - sequences 239–7
 - Chu 247
 - Huffman 245–7
 - index 245
 - maximum length 239–42
 - primitive root 242–5
 - quadratic residue 233, 239, 242
 - single plane *see* Schroeder diffusers, 1D
 - see also* primitive root diffuser; quadratic residue diffuser
- Schroeder frequency 11
- seating absorption 186–8
 - measurement 71–4
- semicylinders 102–3, 110, 290–1, 297, 311, 352
 - arrays of 293–7
 - diffusion coefficient spectra 103
 - frequency response 291, 297
 - Huygen's construct 27
 - incident and reflected time response 291
 - polar response 214, 348
 - total sound field 296
- sequences *see* number sequence; Schroeder diffusers: sequences
- in situ* measurement of:
 - absorption 74–7
 - diffuse reflections 124
- Skyline diffuser 40, 88
- Snell's law 17, 20, 151, 279
- sound beam, effect of curvature 292
- sound insulation and porous absorbers 18–19
- sound production rooms 1–3
- sound propagation:
 - mathematical constructs 15–16
 - through a finite layer of a rigid-backed porous absorber 152
 - transmission and reflection at a surface 16–18
 - transmission through an acoustic medium 149
- sound reproduction rooms 2, 32–9
- spatial dispersion 27, 109
 - see also* diffuse reflections
- spatial impression 44–5, 349
- specular reflection 2–3, 27–30, 33, 36, 39, 48, 52, 310
 - bottom of wells 265–6
 - diffuse reflection evaluation 108, 110
 - flat surface and plane panel arrays 277, 279–80, 282–4
 - geometric room acoustic models 345
 - hybrid absorber-diffuser 314–15, 318, 320, 333
 - primitive root diffusers 243–4, 252, 255, 272
 - scattering coefficient 113, 118–20
 - triangles and pyramids 276, 284, 287–8
- specular zone 101–2, 107
 - definition 100
 - hybrid absorber-diffuser 330
 - level for notch diffusers 272–3
 - level for triangles 288
- speech intelligibility 2, 4, 23, 161
- underground (subway) stations 44
- stage canopy 47–8, 305–7
- stage shells (enclosures) 48–52
- standing wave:
 - ratio 61
 - tube method 58–64
 - see also* impedance tube measurement
- stepped diffuser 271
- street canyons 55
- structural form factor *see* tortuosity
- subway stations *see* underground stations
- surface impedance *see* impedance, surface
- surface pressures 206–9
- surround sound and diffusers 33, 39

- temporal dispersion 27–9, 36, 103, 307, 324
- thermal boundary layer 146
- tortuosity 21, 137, 145–6
 - effect on sound propagation 145
 - measurement 144
- total sound field 36–9, 103–4, 279, 291, 295
 - for periodic and random cylinders 296
 - see also* frequency response; impulse response
- transfer function measurement of absorbers
 - free field 64
 - impedance tube 62–4
 - see also* multi-microphone method; two-microphone method
- transfer matrix modelling:
 - active absorbers 369
 - basic formulations 19–20
 - Helmholtz absorbers 173–5, 178
 - membrane absorbers 159, 173–5
 - microperforated absorbers 181
 - multi-layer absorbent 18–20
 - for pipes and ducts 19–21
 - porous absorbents 148–53
 - Schroeder diffuser wells 196, 198
 - techniques 132
 - theory 182
- transient BEM 229–30
- triangular diffusers 276
 - arrays of 287–8
 - polar responses 286–7
- ray tracing of reflection 285
- triangles and pyramids 284–8
- two microphone measurement methods 62–5
- two port model *see* transfer matrix modelling
- underground stations 44
- velocity of a plane wave 15
- viscous boundary layer 146
- visual aesthetics 105, 297, 311, 314
- volumetric diffusers 43
- wave decomposition prediction of
 - scattering 198–200, 230
- wavefronts reflected from diffusers and reflectors 26–8, 32
- wavenumber 20, 61, 66, 76, 78, 175
 - definition 15–16
 - measurement:
 - direct 82
 - indirect 82–3
 - in narrow wells 196
 - within porous absorbents 141–2, 146–8, 152–3
 - anisotropic materials 152–3
 - Delany and Bazley model 141–2
 - other empirical models 142–4
- Wiener–Khinchine theorem 245–6